NCHRP

Web-Only Document 190:

Structural Design of Culvert Joints

I.D. Moore
D. Becerril García
Queen's University
Kingston, Ontario

H. Sezen
T. Sheldon
Ohio State University
Columbus, OH

Contractor's Final Report for NCHRP Project 15-38
Submitted April 2012

National Cooperative Highway Research Program
TRANSPORTATION RESEARCH BOARD
OF THE NATIONAL ACADEMIES

ACKNOWLEDGMENT

This work was sponsored by the American Association of State Highway and Transportation Officials (AASHTO), in cooperation with the Federal Highway Administration, and was conducted in the National Cooperative Highway Research Program (NCHRP), which is administered by the Transportation Research Board (TRB) of the National Academies.

THE NATIONAL ACADEMIES

Advisers to the Nation on Science, Engineering, and Medicine

The **National Academy of Sciences** is a private, nonprofit, self-perpetuating society of distinguished scholars engaged in scientific and engineering research, dedicated to the furtherance of science and technology and to their use for the general welfare. On the authority of the charter granted to it by the Congress in 1863, the Academy has a mandate that requires it to advise the federal government on scientific and technical matters. Dr. Ralph J. Cicerone is president of the National Academy of Sciences.

The **National Academy of Engineering** was established in 1964, under the charter of the National Academy of Sciences, as a parallel organization of outstanding engineers. It is autonomous in its administration and in the selection of its members, sharing with the National Academy of Sciences the responsibility for advising the federal government. The National Academy of Engineering also sponsors engineering programs aimed at meeting national needs, encourages education and research, and recognizes the superior achievements of engineers. Dr. Charles M. Vest is president of the National Academy of Engineering.

The **Institute of Medicine** was established in 1970 by the National Academy of Sciences to secure the services of eminent members of appropriate professions in the examination of policy matters pertaining to the health of the public. The Institute acts under the responsibility given to the National Academy of Sciences by its congressional charter to be an adviser to the federal government and, on its own initiative, to identify issues of medical care, research, and education. Dr. Harvey V. Fineberg is president of the Institute of Medicine.

The **National Research Council** was organized by the National Academy of Sciences in 1916 to associate the broad community of science and technology with the Academy's purposes of furthering knowledge and advising the federal government. Functioning in accordance with general policies determined by the Academy, the Council has become the principal operating agency of both the National Academy of Sciences and the National Academy of Engineering in providing services to the government, the public, and the scientific and engineering communities. The Council is administered jointly by both Academies and the Institute of Medicine. Dr. Ralph J. Cicerone and Dr. Charles M. Vest are chair and vice chair, respectively, of the National Research Council.

The **Transportation Research Board** is one of six major divisions of the National Research Council. The mission of the Transportation Research Board is to provide leadership in transportation innovation and progress through research and information exchange, conducted within a setting that is objective, interdisciplinary, and multimodal. The Board's varied activities annually engage about 7,000 engineers, scientists, and other transportation researchers and practitioners from the public and private sectors and academia, all of whom contribute their expertise in the public interest. The program is supported by state transportation departments, federal agencies including the component administrations of the U.S. Department of Transportation, and other organizations and individuals interested in the development of transportation. **www.TRB.org**

www.national-academies.org

CONTENTS

ABSTRACT

Findings and conclusions of experimental and computational studies are presented regarding the effect of longitudinal bending on joints in rigid (reinforced concrete) and flexible (corrugated steel and thermoplastic) culverts. Two joint types are examined – those releasing the longitudinal bending moments (denoted ‘moment-release joints’) like gasketted bell and spigot joints, and those transferring them (denoted ‘moment-transfer joints’) such as band connections. Structural design requires evaluation of the ability to transfer vertical shear force across moment-release and moment-transfer joints, longitudinal bending moments across moment-transfer joints, and for moment-release joints to accommodate rotations.

Both field performance and laboratory experiments are used to evaluate the behavior of jointed pipe systems for four different diameters, two different cover depths, and response to surface loads in a variety of positions. Different approaches are investigated for analysis of the structural behavior of joints to determine thrust, moment and rotation across joints. One considering two beams supported by elastic springs is used to develop a simplified design procedure. A second design approach involves finite element analysis using beam-on-elastic-spring modeling. Design examples are presented, and preliminary tests of the capacity of three of the test pipes indicate that these products satisfy the structural design requirements being proposed.

EXECUTIVE SUMMARY

This report presents the findings and conclusions of experimental and computational studies of the effects of longitudinal bending on joints in rigid (reinforced concrete) and flexible (corrugated steel and thermoplastic) culverts. Two kinds of culvert joints are examined – those that release the longitudinal bending moments (denoted 'moment-release joints') such as gasketted bell and spigot joints, and those that transfer the longitudinal bending moments (denoted 'moment-transfer joints') such as band connections. Structural design requires evaluation of the joint's ability to support the vertical shear force acting across moment-release and moment-transfer joints, longitudinal bending moments that develop across moment-transfer joints, and the ability of moment-release joints to accommodate rotations.

Field performance was assessed by reviewing the literature, surveying State DOTs, and undertaking six field tests on a variety of rigid and flexible culverts. Extensive physical data was collected during six laboratory test series on different jointed pipe systems featuring four different diameters, two different cover depths, and response to surface loads in a variety of positions. Experiments were also performed to assess the joint characteristics for some of the test pipes under rotation and shear prior to burial.

The laboratory tests demonstrated that the response under surface load of shallow buried concrete pipes with moment-release joints can be approximated as stiff links undergoing rigid body rotation, with joints acting as hinge points. Response of shallow buried structures to surface loads is primarily localized to the two pipe segments on either side of the joint closest to the surface load, so deflections in those particular pipes are small at their other ends. Response of shallow buried flexible pipes to surface load attenuates rapidly away from the joint closest to the surface load. This attenuation means that surface loads in the vicinity of a joint connecting two particular pipes cause little deflection or rotation at the other two ends of those pipes, so a simplified approach for the structural design of moment-release or moment-transfer joints connecting either rigid or flexible culverts was developed by considering just two pipes interacting across a joint.

While structural design requires considerations of forces, and moments or rotations, the laboratory and field testing primarily provided measurements of deformations, given the challenges of designing experiments where the forces and moment acting across joints are measured directly. Therefore, evaluation of the forces and moments that occurred during the tests requires the jointed pipe system to be modeled. Three alternative approaches were

investigated. First, the behavior of the jointed pipe system was analyzed using beam-on-elastic-spring modeling, where deformations around the pipe circumference are neglected, deflections along the pipe springlines are used to represent the longitudinal pipe response, and the pipe is considered as a beam with circular cross-section. This modeling approach then uses a series of uniformly spaced vertical elastic springs to represent the restraint against vertical movements provided by the soil. Second, beam-on-elastic-spring analysis considering just two beams was used to develop equations for thrust, moment and rotation across a joint. Third, some analyses were undertaken using full three-dimensional finite element modeling. The laboratory experiments on buried jointed pipes were used to assess the performance of these calculation approaches. Nonuniform bedding conditions are required before earth loads lead to shear forces, moments or rotations across joints. While efforts to define nonuniform bedding in the laboratory tests did not provide clear guidance on the nonuniform bedding conditions to consider in design, analysis of these pipe systems lead to development of solutions for earth load effects on shear force and moment or rotation across joints associated with changes in soil stiffness. The concept proposed is to double the soil stiffness on one side of the joint relative to the other side, a situation where weather events or changes in construction practice occur between placement of one pipe segment and the next.

Proposals are included for modifications to the AASHTO LRFD Bridge Design Specifications. First, a simplified design method is proposed based on the interactions of two beams on elastic springs connected by a joint. A second method based on finite element analysis of the beam-on-elastic-spring approximation is also proposed. Design examples are presented, and preliminary tests of the capacity of two of the test pipes indicate that these products satisfy the structural design requirements being proposed.

CHAPTER 1 BACKGROUND

Traditional methods for the structural design of buried culverts and storm drains (culverts) ignore longitudinal stresses, transverse stresses, and circumferential stresses at the joint. The structural design of the culvert joint assumes only in-plane loading of the pipe's cross-section, that is, in-plane bending and in-plane thrust. Current practice does not consider longitudinal bending moments and shear resulting from nonuniform loading and/or variations in the bedding support along the length of the pipe.

Field observations show that longitudinal effects such as variation in bedding stiffness may be the cause of many culvert failures. Failure of the joint may allow water and soil to seep through the joint, potentially resulting in loss of soil support, and ultimately, collapse of the pipe and pavement damage.

Longitudinal distress resulting from poor bedding alignment and stiffness is a problem that may be solved using tighter standards for construction/installation. Nevertheless, experience shows that most pipe installations are less than perfect. A structural design process that considers longitudinal effects will improve the performance of joints.

The objective of this research is to develop structural design requirements for joints in flexible and rigid culverts to withstand variations in construction, support, and loading conditions. These requirements shall be suitable for consideration for adoption by the AASHTO Highway Subcommittee on Bridges and Structures.

CHAPTER 2 RESEARCH APPROACH

The project was divided into the following two phases:

Phase 1 – Tasks 1 to 6 involved a review of relevant practices, literature, existing guidance, and research findings, assembly of data on in-service performance and structural failure modes of various joints for all types of culverts. Activities included field testing and field-scale laboratory testing of joints in representative culverts, development of preliminary structural design criteria, and analysis conducted using finite element modeling.

Phase 2 - Tasks 7 to 9 featured further laboratory testing to investigate the expected loads and strength of culvert joints, development of simplified design equations based on analysis of the effects of longitudinal bending using beam-on-elastic-spring modeling, preparation of specifications and commentary suitable for inclusion in the AASHTO LRFD Bridge Design Specifications, and preparation of example design calculations.

The research agencies were Queen's University (QU) and Ohio State University (OSU).

CHAPTER 3 FINDINGS AND APPLICATIONS

The research findings are presented in the six following areas:

- Overview of joint types and the key quantities required for structural design;
- Information regarding the field performance of culvert joints; this was undertaken by collecting information from State DOTs, and through field testing six culverts in Ohio;
- Laboratory testing was undertaken of six representative buried pipe joint systems to capture culvert joint performance under surface live load, to assess the influence of surface load position, and to investigate different levels of construction quality; laboratory testing was also undertaken to assess the strength of joints in three representative pipe systems;
- Computer analyses were conducted to examine the potential for exploring local effects in pipe joints and the potential for using beam-on-elastic-spring analysis of joint behavior;
- Simplified design equations were developed using beam-on-elastic-spring analysis of two pipes interacting at a joint, for both rigid and flexible culverts responding to earth loads and surface live loads;
- Design specifications were developed for a simplified design method based on approximate equations and an alternative approach based on finite element analysis of pipes represented as beams on elastic springs; example calculations are provided based on the simplified design method.

Overview of joint types and structural design requirements

There are essentially two kinds of joints, which differ in how they treat the longitudinal bending that arises from surface loads and variations in bedding stiffness along the pipes:

- those designed to permit rotation of one end of the pipe relative to the next, thereby releasing the longitudinal bending moments; these are designated throughout this report as ‘moment-release joints’; examples include gasketted bell and spigot joints, gasketted tongue in groove joints, and those two joint types used without gaskets;
- those designed to limit rotation of the two pipe ends relative to each other, and transfer longitudinal bending moments from one pipe to the next; these are designated throughout this report as ‘moment-transfer joints’; examples include band joints and welded connections.

The structural design of culvert joints includes assessment of

- the vertical shear force that acts across moment-release and moment-transfer joints;

- the bending moment that acts across moment-transfer joints;
- the axial force that acts across moment-transfer joints (it is assumed that moment-release joints have very limited ability to transfer axial tensions); and
- the expected rotation of one pipe relative to the other across moment-release joints.

Procedures to calculate shear force and bending or rotation quantities during design need to consider a range of different pipe geometries and stiffness, joint types, burial conditions, and loading geometries. Evaluation of design performance requires measurement of the ability of the joints to support those quantities (shear force, longitudinal bending moment or rotation, and axial force). Load and resistance factor design will involve evaluation of whether factored resistance exceeds factored loads. This project examined reinforced concrete culverts with bell and spigot or tongue in groove joints, corrugated steel pipes with band connections, and thermoplastic (high density polyethylene (HDPE) and polyvinyl chloride (PVC)) pipes with gasketted bell and spigot connections. However, in principle the design methods could be used for other cases (e.g. mortared joints in reinforced concrete pipes, welded connections in metal or thermoplastic pipes, or band connections in thermoplastic culverts).

This project focuses primarily on the effects of longitudinal bending on joints, and does not explicitly study the mechanisms leading to axial forces across joints. While axial load capacity is discussed in the proposed material for inclusion in the AASHTO standard and situations leading to axial load capacity are discussed elsewhere in the report, no laboratory and computational contributions are reported here on methods for estimating expected axial loads.

Further background on joint types and structural design requirements is found in the literature review presented in Appendix A.

Field performance

A survey of state highway engineers was conducted, as detailed in Appendix B. This survey identified the most common types of culverts and joint systems being used, and experience regarding the performance of those systems. One important objective of the survey was to gather data to inform the choice of culverts to be tested in the field and in the laboratory. Input from that survey and the panel overseeing the project lead to the following choices for laboratory testing presented in Appendix C:

- 24 inch (0.6 m) diameter reinforced concrete pipe (RCP) with gasketted bell and spigot joint, the commonest joint configuration for reinforced concrete pipes

- 48 inch (1.2 m) diameter reinforced concrete pipe with bell and spigot joint, tested without a gasket, representing the performance of joints assembled without seals
- 36 inch (0.9 m) diameter corrugated steel pipe (CSP) with hugger band connection (the commonest form of connection for these pipes), but without seals
- 36 inch (0.9 m) diameter corrugated steel pipe with hugger band connection and two O-rings (the commonest system for these pipes)
- 36 inch (0.9 m) PVC pipe with gasketted bell and spigot joint (the commonest system for these pipes)
- 60 inch (1.5 m) HDPE pipe with gasketted bell and spigot joint (the commonest system for these pipes)

Six culverts were tested in the field at various locations in Ohio, measuring the response of the joints in five of those structures as they responded to a test truck (two reinforced concrete culverts, two corrugated steel culverts, and one high density polyethylene culvert), and another HDPE culvert during construction, Figure 1. Details of this fieldwork are presented in Appendix D. Corrugated steel pipes were instrumented with strain gages, the reinforced concrete and thermoplastic culverts were instrumented with reflective surveying prisms and monitored with a servo-controlled total station, and all culverts were fitted with linear displacement transducers to measure movements across the joint as well as changes in pipe diameter. Response was measured for a truck in various locations relative to the pipe joint, and at various magnitudes.

These tests and those examined in Appendix C demonstrate that movements during culvert installation are significantly larger than movements measured during any of the surface loading tests examined in the field. Installation plays an important role in creating permanent deformations in pipes and in causing potential problems such as leakage at the joints, and soil stiffness increases after years of service, and this leads to substantial reductions in incremental response under repeated vehicle loads. In all cases, movement measured during dynamic loading was less than or equal to movement measured during static loading (on average movements under moving loads were 73% of those under static loads), though the dynamic tests did not incorporate bumps over the culvert equivalent to bridge expansion joints or other perturbations associated with the enhancement typically being captured by dynamic load allowances.

Laboratory testing

Buried pipe tests

Laboratory tests on culvert joints consisted of two testing programs. The objective of the first was to examine the six different jointed culvert systems selected for testing (as discussed in the previous section) when shallow buried and responding to simulated vehicle loads, Figure 2. Tests were conducted in one half of the large scale buried infrastructure test pit at Queen's University, featuring length 25 ft (8 m), width 25 ft (8 m) and depth 10 ft (3 m). Two common configurations were examined for each pipe, where well graded sandy gravel was placed in accordance with AASHTO practice, i.e. a minimum dry unit weight equal to 90% of the maximum from a standard Proctor test (i.e. Sn-90). The first test featured burial to 4 ft (1.2 m), Figure 3, while the second featured burial to 2 ft (0.6 m) (Figure 3 with 2 ft (0.6 m) of soil removed).

Tests on the rigid pipes featured two complete pipe lengths, and two additional smaller pipe segments attached at either end. Tests on the flexible pipes featured two pipe segments. In all cases, the joint being tested was located at the mid-point across the test pit, as per Figure 2.

All surface loading experiments were conducted using an actuator (loading cylinder) acting on a steel plate with the standard AASHTO geometry for a wheel pair at the end of an axle, Figure 4. Figure 3a illustrates the three surface load positions used, one directly over the joint, and the second and third distances of 3 ft (0.9 m) along the pipe on either side of the joint. Figure 4b shows the arrangement of the centrally positioned loading experiment, as well as a steel load plate placed at one of the other load positions.

Figure 4 also shows the end-treatment ('flexible retaining wall') on either side of the embankment illustrated earlier in Figure 3a. This earth retaining system improves the strength of the end soil and permits the near-vertical geometry, but otherwise does little to enhance the stiffness of the soil.

Top left (first CSP), Top Middle (first RCP), Top right (first HDPE pipe)
Bottom left (second CSP) Middle (second RCP), Bottom Right (second HDPE pipe).
Figure 1 Images of the six culverts in Ohio tested under vehicle loads.

a. 24 inch (0.6 m) diameter reinforced concrete pipe with gasketted bell and spigot joint

b. 36 inch (0.9m) diameter corrugated steel pipe with unsealed band joint

c. 60 inch (1.5 m) diameter high density polyethylene pipe with bell and spigot joint

d. 36 inch (0.9m) diameter PVC pipe with gasketted bell and spigot joint

e. 48 inch (1.2 m) diameter reinforced concrete pipe with unsealed bell and spigot joint

Figure 2. Five of the six laboratory test pipes placed prior to burial (the sixth test pipe was similar to the second, but was fitted with O-rings).

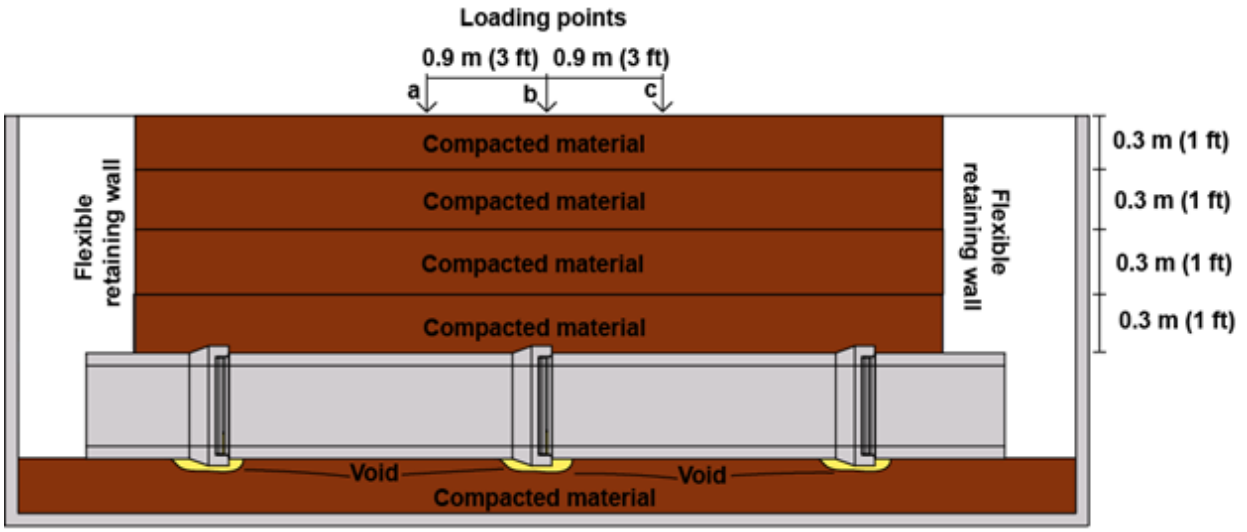

a. Longitudinal cross-section showing three surface load positions (compacted bedding excavated and filled with loose material to accommodate protruding bells, denoted ‘void’ here).

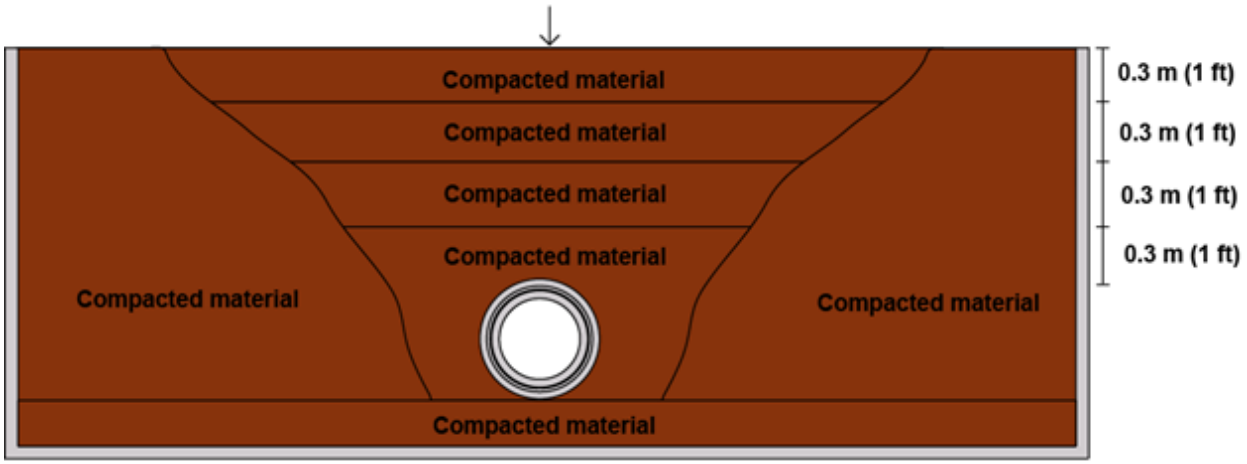

b. Cross-section normal to pipe axis, illustrating pipe placement within a temporary trench excavated in compacted material, and backfilled with the same compacted material.

Figure 3. Configuration of tests involving 24 in (0.6 m) diameter reinforced concrete pipes at 4ft (1.2 m) of cover and buried in accordance with AASHTO LRFD Bridge Construction Specifications.

In most cases the performance of the culvert joint was tested up to 22.5 kips (100 kN), slightly more or slightly less than the full service load for a wheel pair associated with a single axle AASHTO design truck, 16 kips (71 kN), increased by multiple presence factor of 1.2, and dynamic load allowances of 25% at 2 ft (0.6 m) burial and 17% at 4 ft (1.2 m) burial. Ultimate strength tests were also performed once for each culvert system, at 2 ft of cover with load at the central position b shown in Figure 3a.

a. 24 in. (0.6 m) RCP at 4 ft (1.2 m) cover b. 36 in. (0.9 m) CSP at 2 ft (0.6 m) cover

Figure 4. Live load testing of two of the jointed culvert systems tested in the laboratory.

Typical results from these tests are provided in Figure 5, where vertical deformation profiles are shown along the pipe (the average of readings taken at both springlines, though in all cases the movements of opposite springlines were almost identical). These and other results provided in Appendix C indicate that:

- Deformations when load is over the joint are almost symmetric about the joint, and those with offset 3 ft (0.9 m) from the joint are almost a reflected version of those with the load offset 3 ft (0.9 m) on the other side of the joint (shown as a negative offset)
- Deformations along the shallow buried rigid (reinforced concrete) pipes feature approximately rigid body rotation of the pipe segments; movements occur along the whole of each pipe on either side of the joint being examined
- Deformations along the shallow buried flexible (corrugated steel, and lined corrugated PVC and HDPE) pipes are more localized under the loading point, and attenuate within a distance of from one to two pipe diameters along the pipe axis; for shallow buried pipes of these lengths, the vertical movements of the springlines are small once the other ends of the pipes are reached.

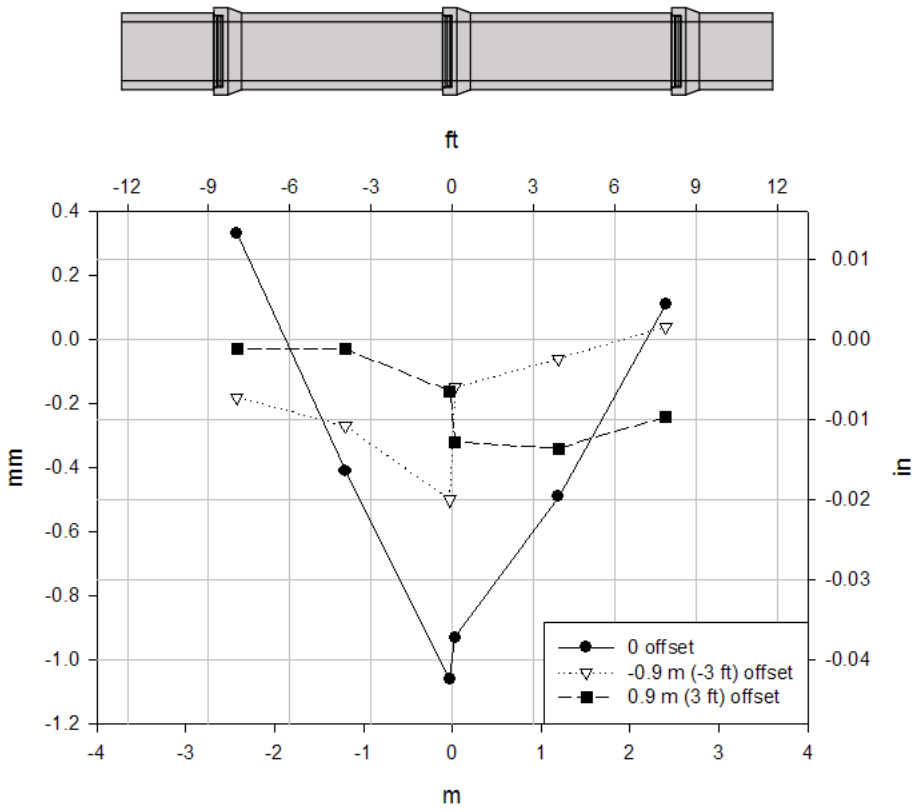

(a) 24 in. (0.6 m) diameter reinforced concrete pipe; poor backfill; load of 18 kips (80 kN)

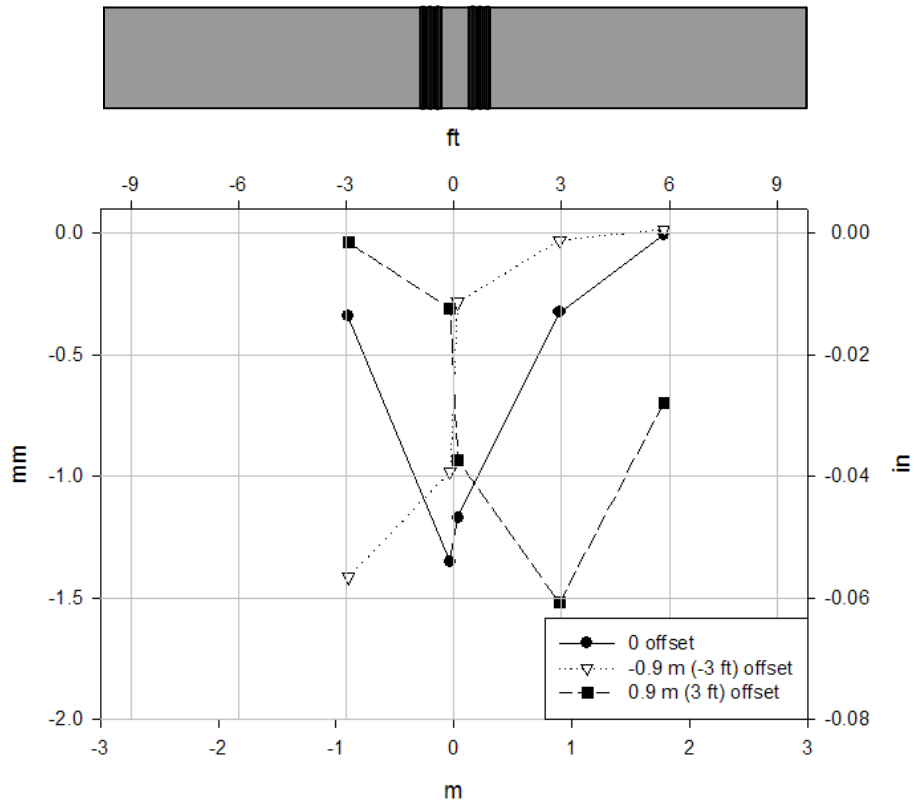

(b) 36 in. (0.9 m) diameter corrugated steel pipe with O-rings under the hugger band; good backfill; load of 22.5 kips (100 kN).

Figure 5. Vertical deformations along four of the test pipes at 2 ft (0.6 m) cover.

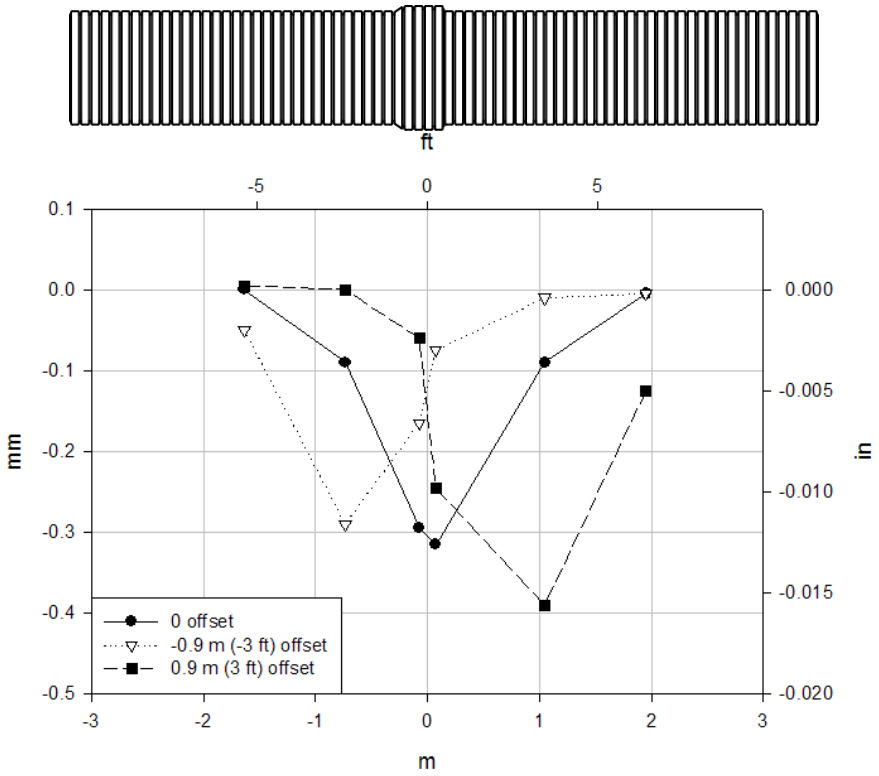

(c) 36 in. (0.9 m) diameter PVC pipe; good backfill; load of 22.5 kips (100 kN)

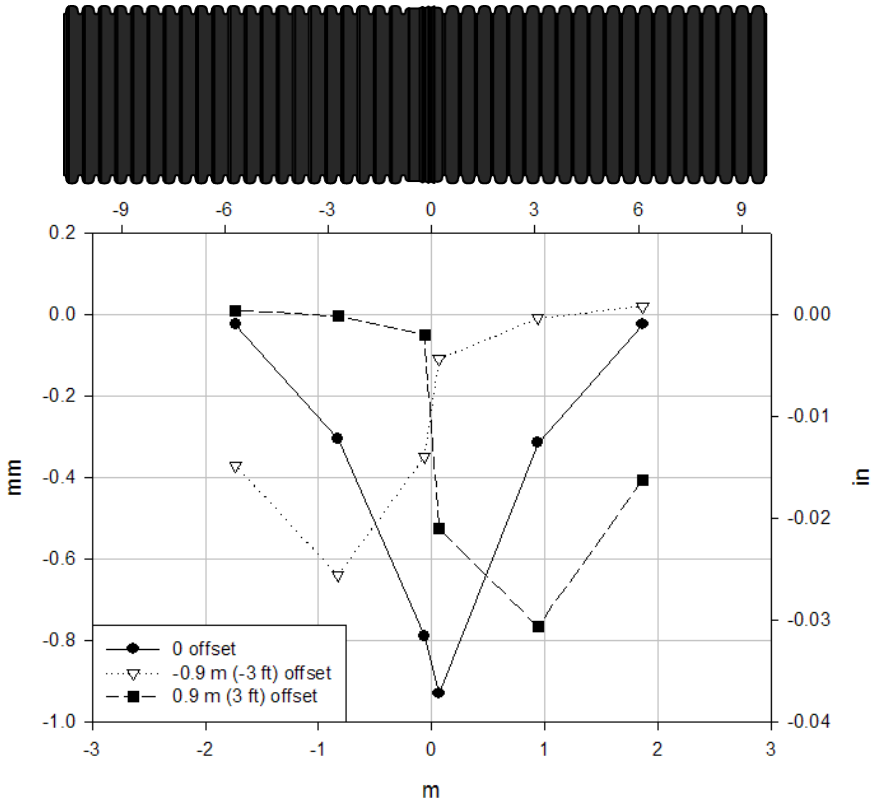

(d) 60 in. (1.5 m) diameter HDPE pipe; good backfill; load of 22.5 kips (100 kN)

Figure 5. continued

These experimental results are for vehicle loads, and earth loads are also important. While it is not straightforward to simulate deep burial in the large scale testing facility at Queen's, earth load effects on joints are important nevertheless. Earth loads cannot produce longitudinal effects across culvert joints unless there are variations in soil support along the pipes, since otherwise the pipes settle uniformly under the earth loads and no shear or bending occurs across the joint. Tests were therefore performed simulating various kinds of imperfect bedding conditions. While these are detailed in Appendix C, the use of voids under certain sections of the pipe invert was not found to produce very distinct behavior, and these tests did not provide clear guidance on imperfections that could reasonably be considered during design. Therefore, an alternative approach for design due to earth loads was developed after the experimental results were interpreted using beam-on-elastic spring analysis, as explained in a later section.

Measurements were also taken of the circumferential response of the joints in each of the test culverts. Data included:

- Ovaling deformations of all of the flexible pipes
- Hoop and axial strains in the corrugated metal pipes and the hugger band
- Circumferential strains in the bell and spigot of the 24 in. (0.6 m) diameter reinforced concrete pipe

These measurements are discussed together with design of joints for circumferential behavior in a subsequent section.

Other tests on pipe joints

Figures 6 and 7 illustrate the two kinds of tests used to quantify the performance of joints connecting unburied pipes.

The first tests featured bending tests on the 24 in. (0.6 m) diameter concrete, 36 in. (0.9 m) diameter corrugated steel, and 36 in. (0.9 m) diameter PVC pipes, prior to burial. Figures 6a and 6b show the test configuration used for the concrete pipe. This test was first performed with the extreme ends of the pipeline open (i.e. with atmospheric pressure acting inside and outside the pipe). These ends were then sealed with steel plates and those plates anchored to the side walls of the test pit. The experiment was carried out with internal pressure of 6.4 psi (45 kPa) and then -12 psi (-85 kPa) to quantify the effect of differential pressure on the gasket (the end plates were tied to the side walls to ensure the large axial forces resulting from pressure differences on those plates do not pass along the pipe and through the joints, since such forces would pull the joint apart or compress the joint, forces that do not occur in the field).

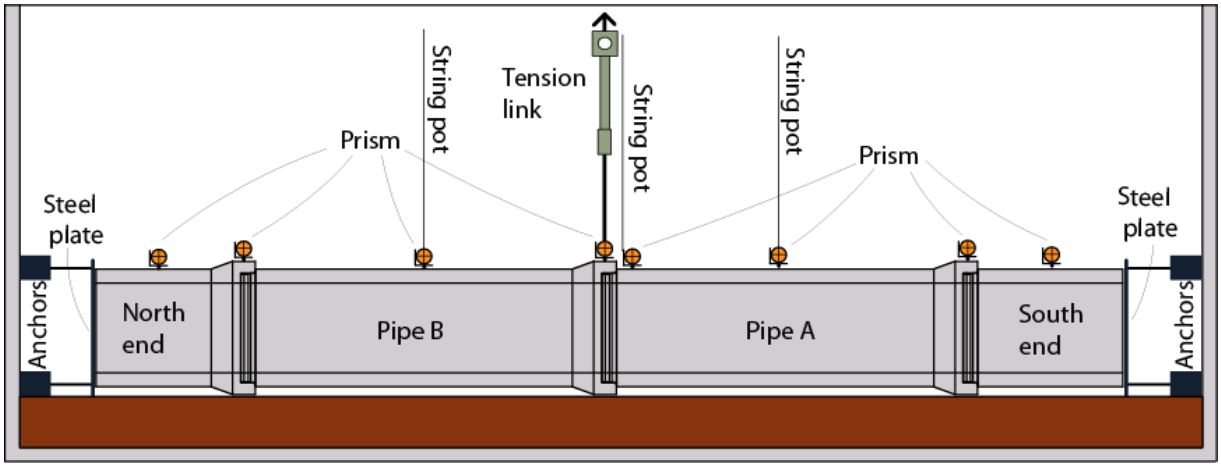

a. Illustration of the experimental configuration

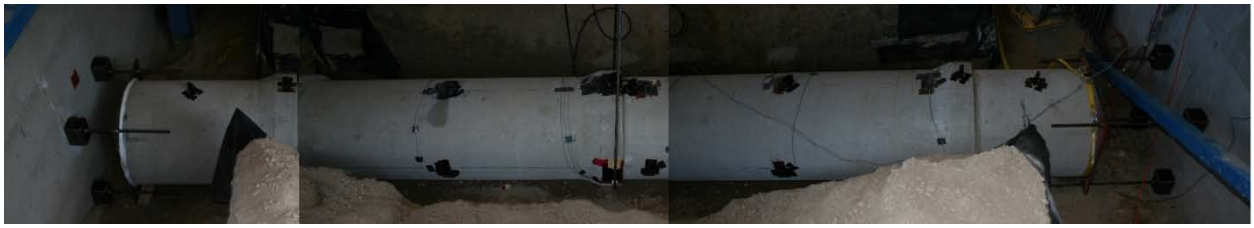

b. Photograph of experiment showing end plates anchored to the walls of the test pit

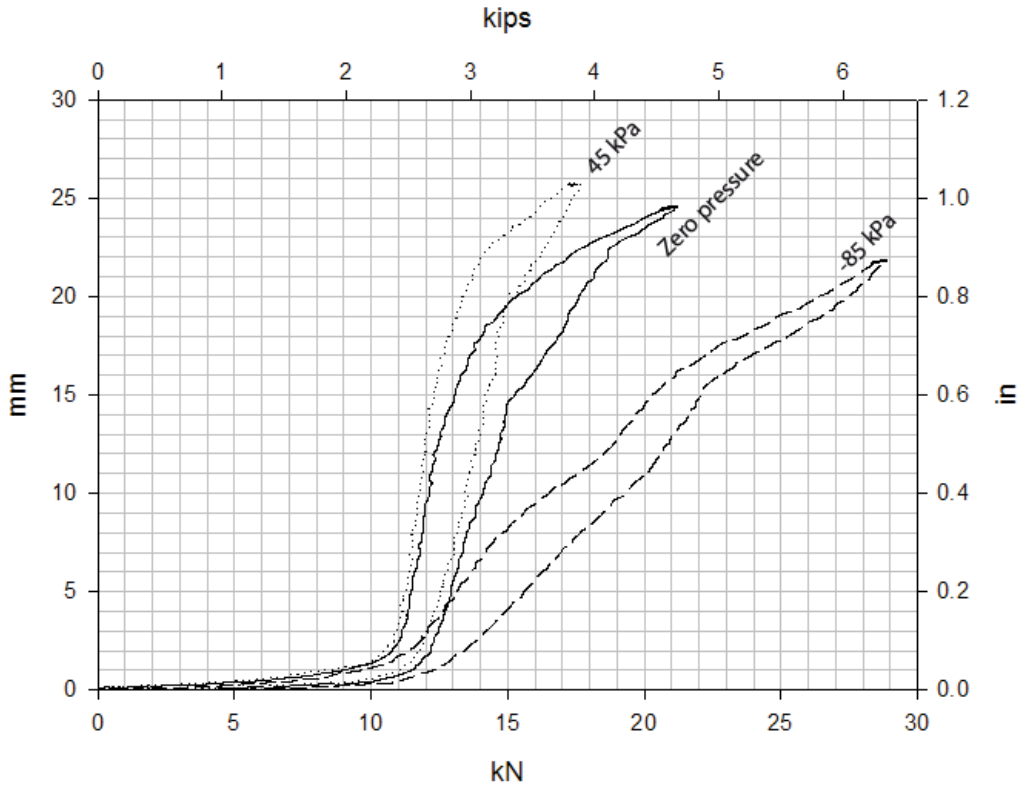

c. Vertical lifting force versus vertical deflection for three internal pressures (1 kPa = 6.4 psi).

Figure 6. Bending test on the 24 in (0.6 m) reinforced concrete pipe.

Rotations commenced once the vertical force reached about 2.5 kips (12 kN), the load needed to support the pipe weight. The nonlinear loading and unloading curves illustrates the complex interactions occurring between the gasket, the bell, and the spigot during rotation.

It is not likely practical to use this approach to characterize the performance of the joint in bending, and this particular configuration would need to be modified to provide performance under shear. Therefore, a dedicated joint testing frame was designed for use in measuring joint strength in shear and bending. Two steel frames are used, with one pipe segment strapped to each. Figure 7a shows the frame being used to test the bending capacity of the joint. The two frames are connected together with hinges located adjacent to the joint invert. The right hand frame (as illustrated in Figure 7) is anchored to the floor of the laboratory, so it cannot move vertically or rotate. The left hand end of the left frame is lowered to induce bending. Measurements of the changes in vertical force used to hold that left hand end are used to calculate bending moment applied across the joint. Figure 7b illustrates the configuration used to test the shear capacity of the joint. For shear testing, the hinges connecting the two frames are removed so the frames are completely separate. The left hand end of the left hand frame is supported on the laboratory floor using a wooden block, so that end in this configuration is stationary. Vertical force is applied through the curved steel loading fixture (colored blue in Figure 7b), and since this load is adjacent to the joint and the pipe joint is the only connection between the two frames, most of that applied vertical force passes as a shear force across the joint.

The testing frame has been designed so that bending and shear tests can also be performed with internal and external fluid pressures acting. Those tests are not part of the current project which focuses on the structural design of culvert joints. However, they can be undertaken in the future to investigate the hydraulic performance of joints (the potential for joint leakage).

Computer analyses of culvert joints

Finite element analysis of the beam-on-elastic-spring approximation

Finite element analysis can be used in a variety of ways to model the longitudinal behavior of buried pipes and develop design estimates of the magnitudes of shear force and rotation or bending moment across joints. Appendix J provides details of beam-on-elastic-spring modeling undertaken using finite element analysis. This approach represents the pipe as a beam with circular cross-section. Instead of modeling the details of the wall geometry and explicitly

representing the circular shape of the pipe, total section properties A (the total area of the cross-section) and I (the second moment of area of the cross-section) of the whole pipe cross-section are employed. Thin beam theory is then employed to characterize the longitudinal bending characteristics of the pipe. The resistance to deformation provided to the pipe by the soil is then represented using a series of vertical elastic springs distributed along the pipe.

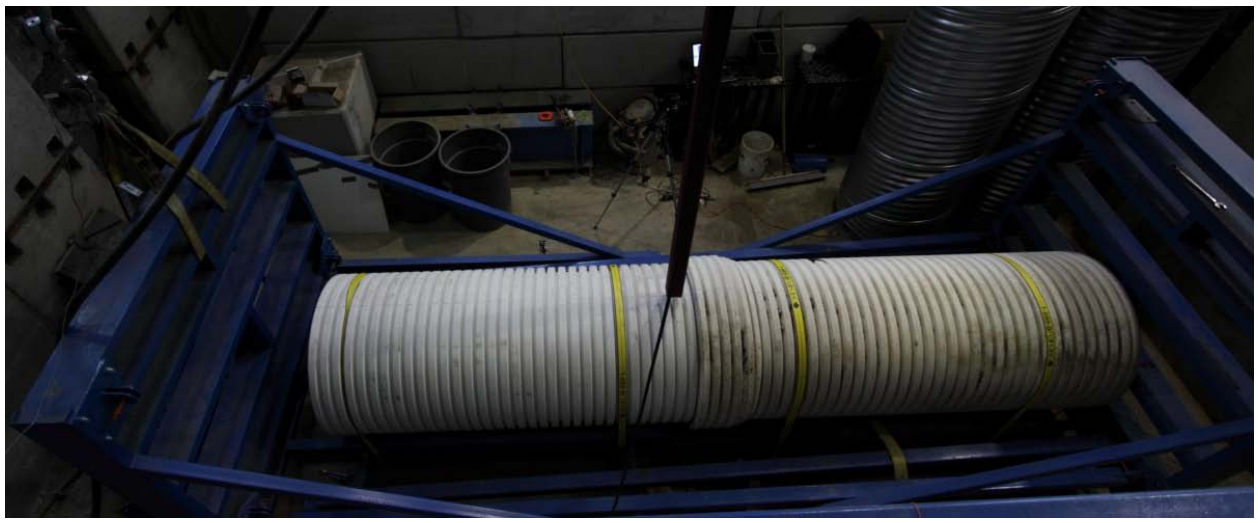

a. Configuration of the bending test on the PVC pipe; hinges are installed connecting the two frames under the joint and the left hand end is held and lowered to induce bending.

b. Configuration of the shear test on the CSP; hinges are removed to disconnect the frames and the left end of the left frame sits on a wooden support; shear force is applied immedately left of the joint.

Figure 7. Load testing system to establish strength of pipe joints in bending and shear.

The assumptions associated with beam-on-elastic-spring analysis greatly simplify the analysis, and make it straightforward to consider situations involving just two pipes interacting across a joint, or a whole series of pipes connected by joints. However those approximations:

- Mean that the analysis provides no input on changes in shape or stresses and strains around the circumference of the joint
- Violate the normal restrictions for use of thin beam theory where beam (i.e. pipe segment) length must generally be more than 10 times the beam depth (i.e. pipe diameter); typical pipe segments have length that is less than 6 diameters, and often four diameters or less
- Feature elastic spring stiffness representing the soil resistance to vertical movement of the pipe that is a complex function of the geometry and material properties of the soil envelope; this makes the rational assessment of the spring stiffness challenging
- Lead to elastic spring stiffness that is also a function of the structural characteristics of the pipe, since issues like the wavelength of longitudinal deformations influence the volume of soil that is responding to resist deformations, so the elastic spring stiffness is also a function of structural as well as soil properties
- Involve estimations of A and I for profiled or corrugated walls that must account for axial compression and extension of the corrugated or profiled wall (as discussed in Appendix I); they are not simple functions of diameter and wall thickness at one axial position.

Appendix J illustrates how finite element analysis of the beam-on-elastic-spring model can capture the behavior of the 24 in. (0.6 m) diameter reinforced concrete test pipe, the 36 in. (0.9) diameter corrugated steel test pipe, and the 60 in. (1.5 m) diameter HDPE test pipe. For each analysis, however, the stiffness values for the soil springs were back-calculated so computed deformations fit the test observations as effectively as possible (i.e. the soil stiffness was chosen so calculations matched observations). The Appendix also includes other discussion on methods available for estimating the spring stiffness for use in the analysis.

Three-dimensional finite element analysis

Appendix J presents calculations for the three-dimensional response of the 24 in. (0.6 m) diameter reinforced concrete test pipe, and compares calculated response to measurements of deformation and strains. This illustrates how three-dimensional analysis can be an effective tool for modeling the complex distributions of strains in these components of the jointed pipe system. However, analysis of this kind is challenging, and it is not yet considered suitable for use in design of joint components.

Simplified design equations

Simplified design equations have been developed for rigid and flexible pipes based on the observations made in the earlier section reporting on vertical deformation patterns along the springlines of buried culverts as a result of surface live load. Appendix E summarizes background concepts for the simplified design, and Appendix F provides details of the derivation of the equations. The simplified design methods are presented here in three groups – equations for rigid pipes connected by moment-release joints, those for flexible pipes connected by moment-release joints, and those for flexible pipes connected by moment-transfer joints. Situations where moment-transfer joints are used with rigid pipes (e.g. where mortar is used to seal joints between concrete pipes) might also be analyzed using the equations for flexible pipes, though there is no experimental evidence to demonstrate the equations are effective for those systems).

The formulations for moment-release joint are based on the assumption that the joint has no rotational stiffness (i.e. there is negligible moment-transfer from one pipe to the next). This should be a conservative approximation, since any non-zero rotational stiffness at the joint will reduce the magnitude of displacements that the shear force has to make compatible.

The formulations for moment-transfer joint are based on the assumption that the joint has the same longitudinal bending stiffness as the pipe barrels. Again, this should be a conservative approximation, since joints of lower stiffness would lead to reduce values of bending moment, and joints with higher stiffness would have no affect on the behavior, since the response of a pipe with a short length featuring higher stiffness should be controlled by the stiffness of the barrels (that is, the rest of the pipe structure).

Simplified design of moment-release joints connecting rigid culverts

Measurements of buried reinforced concrete pipe response to surface load indicate that the high stiffness pipe segments act almost like rigid links, with their vertical movement and rotation dependent on the magnitude of the applied loads, the eccentricity of the loads on each pipe (the distance from its centerline), and the stiffness of soil support. The two pipes interact across the moment-release joint that connects them, and a shear force develops across that joint sufficient to ensure that the vertical deformations of the two pipes at the joint are the same. Appendix F presents the formulation of the solutions for shear force and pipe deformations (including rotation across the joint). Since there are only two pipes involved, exact algebraic solutions can be derived. The two-pipe approximation is conservative because it considers just one pipe on

either side of the joint being considered, and neglects the resistance provided by all the other pipe segments beyond those two adjacent pipes. Appendix F includes additional discussion of the conservative nature of the 'two beam'-on-elastic-spring approximation compared to finite element solutions for beam-on-elastic-springs involving more pipe segments.

Design is based on considerations of two rigid beams of length L_p, sitting on soil modeled as a series of linear elastic springs, Figure 8. Earth loads are uniformly distributed along the two pipes with force per unit length along the pipe of magnitude W_E, Figure 8a,

$$W_E = \gamma_E VAF\, H\, \gamma_S\, OD \qquad [1]$$

for earth load factor γ_E, vertical arching factor VAF, burial depth to the springline H, unit weight of the soil $\gamma_S$and external pipe diameter OD.This simplifies the calculation of the earth load contributed by the soil between the crown and springline, though this is balanced by the weight of the pipes themselves (which are not explicitly included in the calculation).

Now, consider the situation where weather effects or changes in construction practice (as a result of personnel changes on site, for example) lead to one pipe resting on soil characterized by spring stiffness k_{soil} (having units of vertical stress per unit of vertical deformation, i.e. lbf/ft^3 or kN/m^3), and the next having stiffness of twice that value. This change in stiffness of the soil support then results in shear force and rotation across the joint connecting them. Considerations of vertical force equilibrium and compatibility of displacements at the joint can be used to determine shear force across the joint of

$$V_J = W_E L_P / 12 \qquad [2]$$

and joint rotation given by

$$\theta_J = -\frac{W_E}{4\, L_P k_{soil} OD} \qquad [3]$$

The shear force is, therefore, 1/12th of total vertical force acting on each pipe $W_E L_P$, and is dependent on the ratio of soil stiffnesses on either side of the joint rather than the actual stiffness magnitude. Other ratios of soil stiffness have been examined in Appendix F, and shear force increases to a maximum value of 1/4th of the total force acting on each pipe if one of the pipes rests on rigid ground. However, rigid support under one of the pipes is not likely reasonable, so a factor of two is proposed for use in design.

Surface force of total magnitude P_L is spread over a distance L_0+LLDF.H along the pipe based on the normal AASHTO use of live load distribution factor LLDF at depth H and tire pressure

length L_0 along the pipe and width W_0 across the pipe. As with earth load, the depth considered here is that to the springline of the pipes (since use is being made of beam-on-elastic spring theory, and the springline is the location equivalent to the beam 'centroid').

Now maximum rotation under the live load develops when the load is located directly above the joint, Figure 8b, and a solution for rotation can be derived,

$$\theta_J = \frac{6\ w\ P_L}{k_{soil} L^3\ OD}\{L - (L_0 + LLDF\ .\ H)/2\} \qquad [4]$$

where w given by

$$w = \frac{\min\{OD, W_0 + LLDF.\ H\}}{(W_0 + LLDF.\ h)} \qquad [5]$$

accounts for load spreading across the pipe at depth H (a value of w=1 corresponds to a wide pipe or very shallow burial leading to lateral load spreading distance that is less than the pipe diameter and all of the lateral load acting on the pipe; a value of w<1 corresponds to a narrow pipe or deeper burial, where some load falls outside the external diameter of the pipe OD).

Maximum shear force results when all of the load along the pipe at depth H falls on one pipe and just reaches the joint, Figure 8c, and considerations of vertical force equilibrium and compatibility of displacements at the joint can be used to derive a solution for shear force resulting from live load

$$V_J = w\ P_L\{0.5 - \frac{3(L_0 + LLDF\ .\ H)}{8L_P}\} \qquad [6]$$

Simplified design of moment-release joints connecting flexible culverts

Measurements of buried flexible pipes to surface load indicate that there is rapid attenuation of deformations away from the location of the surface load. Therefore, simplified design equations can be developed considering a joint connecting two very (infinitely) long flexible pipes, and employing the solutions reported by Hetényi (1948).

The principles for calculating the response of flexible pipes interacting across a joint are illustrated in Figure 9. Considerations of compatibility of vertical deformation at the joint can be used to derive an expression for the maximum shear force across the joint and the joint rotation resulting from earth load, Figure 9a,

$$V_J \approx 0.157 \frac{W_E}{\lambda} \quad [7]$$

and

$$\theta_J \approx 0.0918 \frac{W_E \lambda}{k_{soil} OD} \quad [8]$$

where

$$\lambda = \sqrt[4]{\frac{k_{soil} OD}{4\,EI}} \quad [9]$$

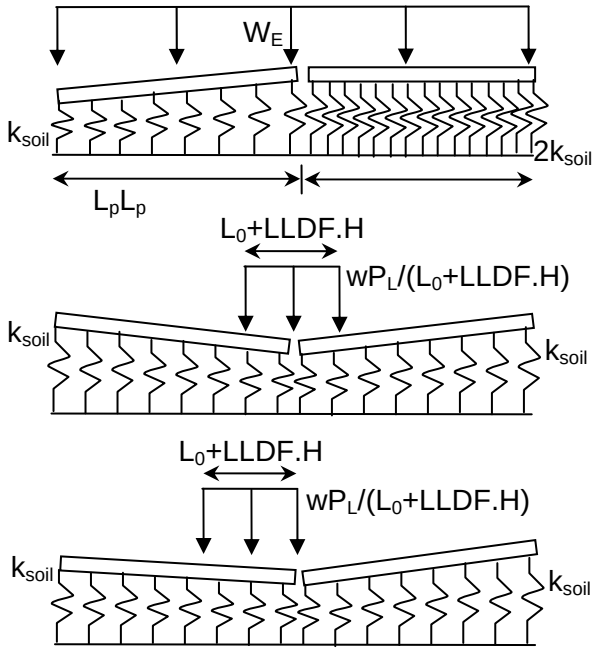

a. Uniform earth load on two pipes resting on soil of two different stiffnesses.

b. Live load on the ground surface centered over the joint and causing peak rotation.

c. Live load on the ground surface to the left of the joint and causing peak shear force.

Figure 8. Design principles for two rigid pipes connected by a moment-release joint.

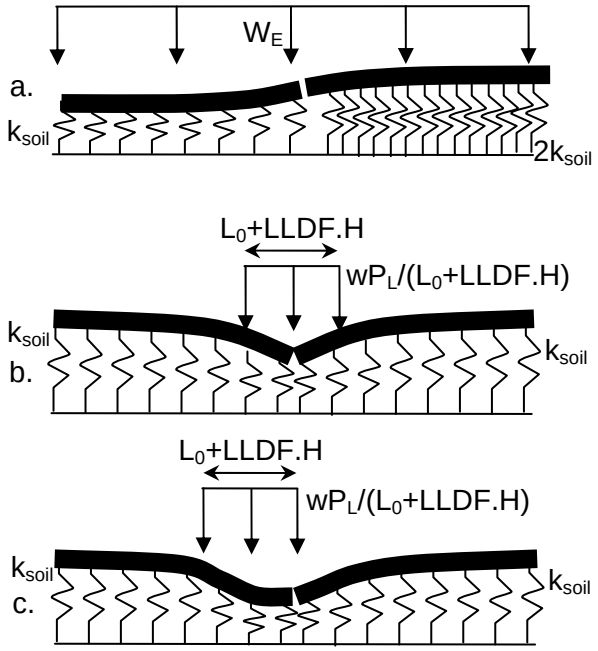

a. Uniform earth load on two pipes resting on soil of two different stiffnesses.

b. Live load on the ground surface centered over the joint and causing peak rotation.

c. Live load on the ground surface to the left of the joint and causing peak shear force.

Figure 9. Design principles for two flexible pipes connected by a moment-release joint.

introduces a characteristic length of the bending deformation associated with a beam (i.e. pipe) of flexural rigidity *EI* resting on soil of stiffness k_{soil}. Parameter *OD* is the average diameter of contact surface between the pipe and the soil. It would be the external diameter of a plain (e.g. concrete) pipe, but the average diameter of a corrugated or profiled structure.

As before, the maximum rotation under the live load develops when the load is located directly above the joint, Figure 9b, and is found to be

$$\theta_J = -\frac{4\mathrm{F_H}\lambda}{\mathrm{k_{soil}OD}}\mathrm{e}^{-0.5\lambda L_H}\sin 0.5\lambda L_H \qquad [10]$$

where force per unit length along the pipe due to live load F_H is given by

$$\mathrm{F_H} = \frac{\mathrm{w\ P_L}}{\mathrm{L_0 + LLDF\,.H}} \qquad [11]$$

w is defined as before, and to simplify the expression, spreading length L_H is defined as

$$\mathrm{L_H} = \mathrm{L_0 + LLDF\,.H} \qquad [12]$$

As before, maximum shear force develops when the load is on one pipe but just remains on one side of the joint, Figure 9c, and the solution is found to be

$$\mathrm{V_J} = \left|\frac{\mathrm{F_H}}{4\lambda}[1 + \mathrm{e}^{-\lambda L_H}(\sin\lambda L_H - \cos\lambda L_H)]\right| \qquad [13]$$

Simplified design of moment-transfer joints connecting flexible culverts

The development of design equations for flexible pipes connected by a moment-transfer joint is very similar to the process used for moment-release joint. Now, however, earth loads lead to expressions for shear force and bending moment which must consider compatibility of both vertical deformation and rotation at the point connecting segments of pipe resting on soil with changing stiffness. Maximum shear force resulting from earth load can be derived

$$V_J \approx 0.154 \frac{W_E}{\lambda} \qquad [14]$$

whereas the maximum longitudinal bending moment resulting from earth loads is

$$M_J \approx 0.0580 \frac{W_E}{\lambda^2} \qquad [15]$$

This expression takes into consideration the fact that the change in soil stiffness may not occur directly under the joint (it is the maximum moment along the pipe caused by the stiffness change).

Further analysis reveals that surface loads having the same magnitude and spreading characteristics as those considered earlier produce maximum shear force of

$$V_J = \left| \frac{F_H}{4\lambda} [e^{-\lambda L_H} (\cos \lambda L_H - \sin \lambda L_H) - 1] \right| \qquad [16]$$

(the same as that for moment-release joints) and maximum bending moment that is given by

$$M_J = \left| \frac{F_H e^{-(\frac{\lambda L_H}{2})} \sin(\frac{\lambda L_H}{2})}{2\lambda^2} \right| \qquad [17]$$

Design using finite element analysis

Finite element analysis modeling a series of pipes connected by joints as beams on elastic springs was found to provide effective estimates of observed behavior. Three of the laboratory test series on buried pipes described earlier in the report were examined, and spring stiffness values were back-calculated to produce deformations to fit the laboratory observations. Use of conservative estimates of the elastic spring stiffness for the soil would provide larger values of shear forces across joints, and rotations or moments across the joint. Specifications describing this kind of analysis have been drafted and appear after the material drafted for simplified design in Appendix G. Finite element modeling of this kind might then be used to consider other more complex conditions, such as depth of burial that varies along the pipeline, more severe soil stiffness changes than those considered in the simplified design, or changes in pipe

diameter. However, at present there are no experimental data to demonstrate that this modeling approach works successfully for these cases.

Three-dimensional finite element analyses were found to provide useful estimates of local strains in components of pipe joints (like the bell and spigot of reinforced concrete pipes). However, at present, full three-dimensional finite element analysis is a complex and demanding exercise, and is therefore considered to be a research tool, and not suitable for structural design of culvert joints in the AASHTO LRFD Bridge Design Specifications.

Empirical value of soil stiffness for use in design

Now, the force values for use in the structural design of joints connecting reinforced concrete pipes are independent of the stiffness of the soil springs (see equations [2] and [6] for rigid pipes). The force and moment values for use in structural design of flexible pipes are dependent on λ which is a function of the fourth root of that stiffness (equations [7], [13 to 17]). Design values of k_{soil} are also required for all calculations of rotation (though all example calculations for joint rotation are consistent with what was observed in the laboratory and in the field, producing rotations that are much smaller than the rotational capacity of conventional moment-release joints).

The use of elastic spring models greatly simplifies the modeling of the soil around and above the pipe, and the spring stiffness k_{soil} might be expected to be a function of soil modulus and the geometry of the soil envelope around and above the pipe (as discussed earlier). However, it is also a function of the structural characteristics of the problem (the pipe properties). The approach chosen for assessing the magnitude of this parameter is to use measurements obtained during the six sets of laboratory experiments, to back-calculate k_{soil}. These calculations are presented in Appendix E. Figure 10 presents each of these values, and this shows that k_{soil} is not clearly correlated with burial depth, pipe diameter, or pipe stiffness. The proposed approach then is to choose a reasonable lower bound value for design, i.e. 191,000 pcf (30,000 kN/m^3).

The variations in soil spring stiffness shown in Figure 10 might also be considered to support the concept of examining earth load effects associated with consecutive pipes that have soil spring stiffness that changes.

The data in Figure 10 is back-calculated using the tests reported in Appendix C for pipes placed in sandy gravel backfill. Terzaghi (1955) provided guidance on spring modeling for beams resting on sand at three densities, Table 1, and his proposed values for dry/moist or submerged sand in loose, medium and dense states are included in Figure 10 (plotted at zero depth). The design proposal of 191 kips/ft^3 (30 MN/m^3) is also illustrated, and corresponds to a value between loose and medium density. Coarse grained soils like sand exhibit wide stiffness variations when at low levels of earth pressures, as seen in the AASHTO design recommendations for constrained modulus developed by McGrath et al. (2002). The design recommendation falls between the loose and medium density values of Terzaghi (1955).

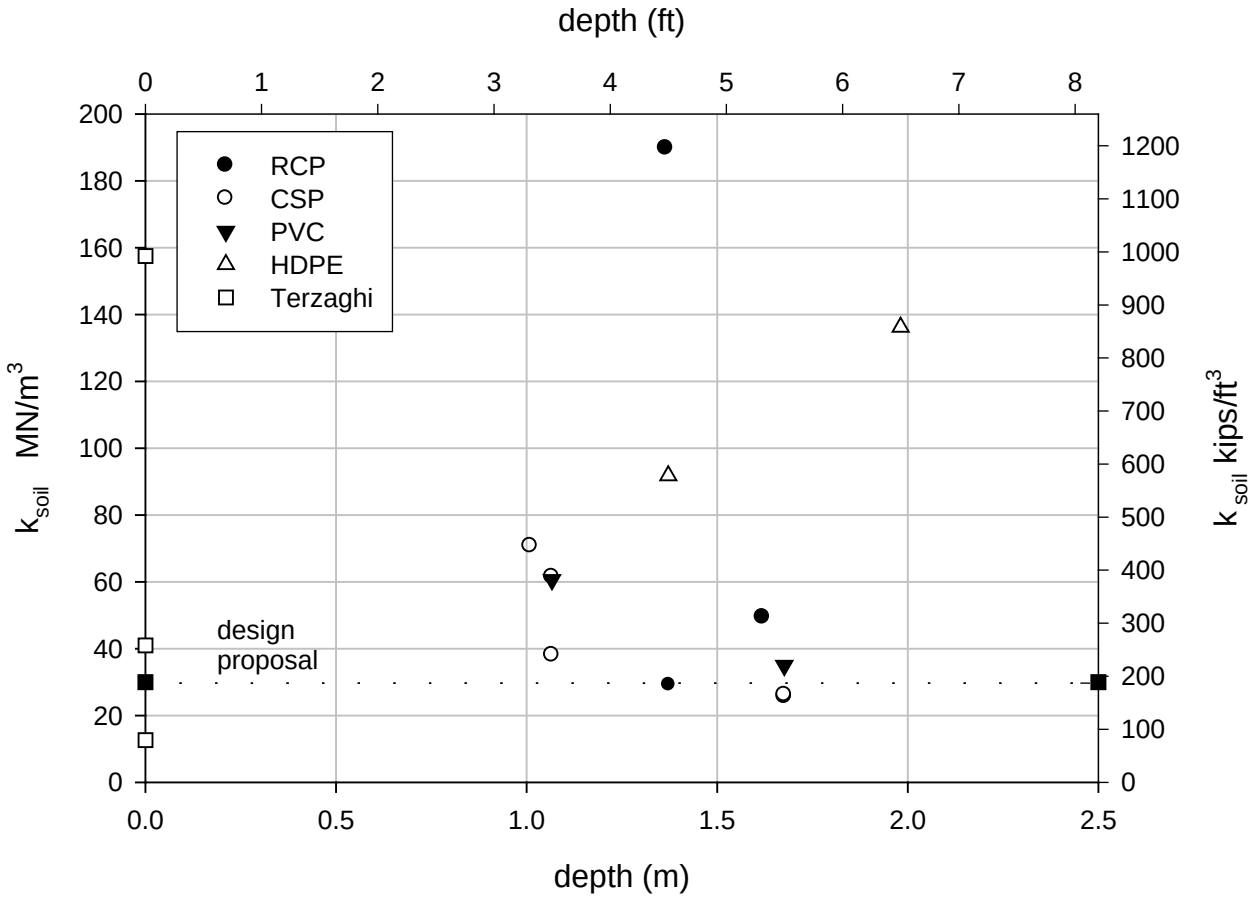

Figure 10. Values of back-calculated soil stiffness k_{soil} for all six sets of buried pipe experiments shown relative to the depth of the pipe springlines; the proposed value for use in design is also shown, together with Terzaghi (1955) values for sand in loose, medium and dense states.

Table 1. Values of for beams 1 ft (0.3 m) wide, resting on sand (from Terzaghi, 1955).

Relative Density of Sand	Loose		Medium		Dense	
	kips/ft^3	MN/m^3	kips/ft^3	MN/m^3	kips/ft^3	MN/m^3
Dry/moist, limiting values	40-120	6.2 - 19	120-605	19 - 95	605-2000	95 - 311
Dry/moist, proposed values	75	12	260	41	1000	157
Submerged, proposed values	50	7.8	160	25	605	95

Spring stiffness can also be back-calculated for use with beam-on-elastic-spring analysis based on the finite element method, and this provides opportunities for more detailed curve-fitting to match observed pipe deformations. This is illustrated in Appendix J. The range of values obtained is presented in Appendix E, and this is found to be similar to those resulting from the simplified design equations. The same design value of 191 kips/ft^3 (30 MN/m^3) is therefore proposed for use in design based on finite element analysis.

Circumferential response of pipe ends at joints

The use of the current provisions of the AASHTO LRFD Bridge Design Specifications to design the pipe ends (including bells and spigots in reinforced concrete and thermoplastic pipes, and the ends of corrugated steel pipes under a band connection) is investigated in Appendix E. It is demonstrated that:

a. bending moments calculated from measured values of circumferential strain on the inner and outer surfaces of the 24 in. (0.6 m) diameter reinforced concrete pipe at the crown and invert (the critical location) are less than those that would be estimated using conventional design theory developed for the pipe barrels; design based on existing provisions for the barrels would then be conservative

b. design calculations of deformations in the flexible tests pipes were generally higher than measured values; this implies that circumferential design of the ends of these flexible pipes would be conservative based on existing AASHTO provisions for the barrels.

Estimation of flexural rigidity of flexible pipes

Whether undertaking structural design of joints for flexible pipes using the simplified design equations or finite element analysis of the beam-on-elastic-spring approximation, the flexural rigidity (EI) of the pipe responding in longitudinal bending is required. It is necessary, therefore, to estimate or measure that stiffness. Appendix I provides guidance on how the flexural rigidity can be estimated for corrugated steel and profiled thermoplastic structures. Appendix I includes comparisons of measured and calculated values of EI.

Design specifications and design examples

Draft revisions for the AASHTO LRFD Bridge Design Specifications are provided in Appendix G. This includes the following material:

- Strength limit states in 12.5.2 are augmented to include joint failure
- Values of resistance factors in 12.5.5 are augmented to include values for joint failure; resistance factors of 0.67 are suggested to match those already present for the longitudinal seam strength of corrugated steel structures; this relatively low resistance factor also reflects the fact that pipes are joined in the field (without the control associated with pipe manufacturing), though experimental evidence could be developed using statistical analysis of strength tests
- Provisions regarding settlement in 12.6.2.2 are augmented to modify references to differential movements along the pipe axis
- A new section 12.15 is drafted to cover the calculation of shear force across the joints, and bending moment or rotation (for moment-transfer and moment-release joints, respectively)
- Section 12.15 is primarily focused on the simplified design equations based on the interaction of two pipes across a joint (presented in an earlier section)
- Section 12.15 includes guidance on design based on finite element analysis modeling using beams on elastic springs; this material could be omitted if AASHTO prefers to incorporate less new material into the LRFD Specifications.

Example calculations for the simplified design method are provided in Appendix E. These illustrate design for

- 24 in. (0.6 m) and 48 in. (1.2 m) diameter reinforced concrete pipes at cover depths of 2 ft (0.6 m), 4 ft (1.2 m), 8 ft (2.4 m) and 20 ft (6 m); these examples are for pipes with moment-release (e.g. gasketted bell and spigot) joints
- 36 in. (0.9 m) diameter corrugated steel pipe with moment-transfer (e.g. hugger band) joints at cover depths of 2 ft (0.6 m), 4 ft (1.2 m), 8 ft (2.4 m) and 20 ft (6 m)
- 36 in. (0.9 m) diameter corrugated steel, 36 in. (0.9 m) diameter PVC, and 60 in. (1.5 m) diameter HDPE pipes with moment-release (e.g. gasketted bell and spigot) joints at cover depths of 2 ft (0.6 m), 4 ft (1.2 m), 8 ft (2.4 m) and 20 ft (6 m)

Table 2 provides maximum values of shear, moment or rotation calculated for each of the jointed pipe systems.

These specifications will:

- provide product manufacturers with the requirements for structural capacity of joints (so they can ensure their jointing systems have adequate capacity to transfer shear force and longitudinal moment), or so they can determine what restrictions on burial depths are needed for specific products and joint systems (minimum and maximum burial depths that ensure factored demand is less than factored resistance)
- enable DOTs and consultants designing specific culvert installations to assess demand, and check whether particular joint systems are suitable for specific projects
- provide design values of shear force and longitudinal moment that can be used in subsequent work to ensure that hydraulic performance of joints is adequate (that gaskets do not leak under these imposed loads)

Table 2. Maximum values of shear force and moment or rotation for design examples.

Pipe	Joint	Shear force across the joint		Moment across the joint		Joint rotation
		lbf	kN	ft.lb	kN.m	degrees
24 in. (0.6 m) RCP	Release	8700	39	-	-	0.18
48 in. (1.2 m) RCP	Release	17000	77	-	-	0.12
36 in. (0.9 m) CSP	Transfer	5100	23	3500	4.8	-
36 in. (0.9 m) CSP	Release	5100	23	-	-	0.25
36 in. (0.9 m) PVC	Release	5100	23	-	-	0.25
60 in. (1.5 m) HDPE	Release	11000	49	-	-	0.13

As might be expected, these calculations indicate that:

- Larger diameter structures need to be designed to transfer greater shear forces;
- Larger diameter structures have smaller requirements for rotation capacity in moment-release joints;
- Joints for flexible pipes are required to transfer smaller shear forces than those for rigid pipes;
- All calculated requirements for joint rotation are small compared to the rotation angles that can be accommodated by most conventional moment-release joints; design of rotational capacity of the joint is likely dominated by considerations of assembly in the field, rather than the rotational capacity that is needed once the pipes are installed.

Measurements reported in Appendix H undertaken for the 24 inch (0.6 m) diameter reinforced concrete and PVC test pipes with moment-release joint, as well as corrugated steel test pipe

with moment-transfer joint, indicate that these existing systems have joints satisfying the structural design requirements being proposed.

CHAPTER 4 CONCLUSIONS AND SUGGESTED RESEARCH

This report presents the findings and conclusions of experimental and computational studies of the effects of longitudinal bending on joints in rigid (reinforced concrete) and flexible (corrugated steel and thermoplastic) culverts. Two kinds of culvert joints were examined – those that release the longitudinal bending moments (denoted 'moment-release' joints) such as gasketted bell and spigot joints, and those that transfer the longitudinal bending moments (denoted 'moment-transfer' joints) such as band connections. Structural design requires evaluation of the joint's ability to support the vertical shear force acting across moment-release or moment-transfer joints, longitudinal bending moments that develop across moment-transfer joints, and the ability of moment-release joints to accommodate rotations. Axial loads can also develop which need to be carried by moment-transfer joints. The current project focuses on longitudinal bending so does not provide input on expected values of axial forces. Therefore, current requirements to ensure the joint has a proportion of the axial load capacity of the pipes it is connecting may be employed until procedures are available for estimating axial force.

First, the project featured a literature review and a survey of DOTs to determine current usage and past experience with culvert joints. Field performance was also assessed using six field tests on a variety of rigid and flexible culverts. Those tests indicated that movements (rotations and deformations) across joints in culverts that have long been in service are small, and that response during construction is substantially greater. Extensive physical data was collected during six laboratory test series on different jointed pipe systems covering four different diameters, two different cover depths, and response to surface loads in a variety of positions. Experiments were also performed to assess the joint characteristics for some of the test pipes under rotation and shear prior to burial. The laboratory tests demonstrated that under surface loading:

- the response of shallow buried concrete pipes with moment-release joints can be approximated as rigid links undergoing rigid body rotation, with joints acting as hinge points; response of shallow buried structures to surface loads is primarily localized to the two pipe segments on either side of the joint closest to the surface load, so deflections in those particular pipes are small at their other ends;
- the response of shallow buried thermoplastic pipes with moment-release joints rapidly attenuates away from the joint closest to the surface load, with the joint acting as a hinge point; this attenuation means that surface loads in the vicinity of a joint connecting two particular pipes result in small deflections and rotations at the other two ends of those pipes;

- the response under surface load of shallow buried corrugated steel pipes with moment-transfer joints rapidly attenuates away from the joint closest to the surface load; this attenuation means that surface loads in the vicinity of a joint connecting two particular pipes also results in negligible deformations at the other two ends of those pipes;
- longitudinal bending influencing two particular shallow buried pipes connected by a joint is barely affected by the presence of other pipe segments or the joints that connect them;
- nonuniform bedding conditions are required before earth loads can cause forces, moments or rotations across joints; efforts to define nonuniform bedding in the laboratory tests did not lead to clear guidance on what kinds of non-uniformity to consider in design.

It was concluded that a simplified approach for the structural design of moment-release or moment-transfer joints connecting either rigid or flexible culverts could be developed by considering just two pipes interacting across a joint.

While structural design requires considerations of forces and moments, the laboratory and field testing primarily provided measurements of deformations, given the challenges of designing experiments where the forces and moment acting across joints are measured directly. Therefore, evaluation of the forces and moments that occurred during the tests requires the jointed pipe system to be modeled. Three alternative approaches were investigated. First, the behavior of the jointed pipe system was analyzed using beam-on-elastic-spring modeling, where deformations around the pipe circumference are neglected, deflections along the pipe springlines are used to represent longitudinal bending, and the pipe is represented as a beam with circular cross-section. This modeling approach then uses a series of uniformly spaced vertical elastic springs to represent the restraint against vertical movements provided by the soil. Second, beam-on-elastic-spring analysis was used to develop equations for thrust, moment and rotation across a joint connecting just two beams (the two-beam analysis). Third, some analyses were undertaken using full three-dimensional finite element modeling. The laboratory experiments on buried jointed pipes were used to assess the performance of these calculation approaches. The computational studies lead to the following conclusions:

- while full three-dimensional finite element analysis provides superior estimates of local effects in the joint, the analysis is challenging and is not suitable for use in the structural design of culvert joints

- the design equations for two rigid or flexible pipes interacting across a moment-release or moment-transfer joint provide a basis for a simplified design process that is suitable for implementation in the AASHTO LRFD Bridge Design Specifications
- back-calculated values for the stiffness of the elastic soil springs varied widely, but fell within the range identified by Terzaghi for sands at various densities
- a value of soil spring stiffness suitable for use in design calculations based on the simplified (i.e. two-beam) equations or finite element analyses of more extensive beam-on-elastic-spring systems is 191,000 pcf (30 MN/m^3)
- the effect of earth loads on shear force and moment or rotation across joints can be assessed using an imperfect bedding case featuring the recommended soil spring stiffness on one side of the joint, and twice that value on the other side of the joint; this might correspond to a situation where weather effects or changes in personnel on site lead to a change in soil stiffness between placement of one pipe segment and the next.

Changes have been proposed to the AASHTO LRFD Bridge Design Specifications to address the structural design of culvert joints. These include a simplified design method based on the two-beam equations, and a second method based on finite element analysis of the beam-on-elastic-spring approximation. Design examples were presented, and preliminary tests of the capacity of three of the test pipes indicate that these products satisfy the structural design requirements being proposed.

This project has developed procedures for estimating expected shear force, moment and rotation values across joints as a result of longitudinal bending. Physical evidence is based on six sets of laboratory experiments for shallow buried culverts responding to surface loads. It would be valuable to evaluate the performance of the procedures proposed for earth load effects using tests simulating deep burial. This might provide evidence that soil spring stiffness values are dependent on burial depth.

It would be helpful to extend the research to examine circumstances that generate axial loads across joints. For example, tests could be performed on pipes buried with high gradients (pipes installed down slopes is a common cause of axial tensions in joints).

The project focuses on the structural design of culverts. However, inadequate performance is often associated with joint leakage. It would be valuable to extend the work to examine how shear force and moment or rotation across joints influences gasket performance (the ability of the gasket to prevent leakage). Short and long term gasket performance should be studied,

since gaskets are generally fabricated from time-dependent materials like natural and synthetic rubbers. This could be undertaken using the pipe joint testing system developed for this project. Development of a standard AASHTO joint strength and leakage test would also be valuable.

The measurements of pipe response were conducted using sandy gravel backfills. It would be useful to conduct tests in other backfills permitted by AASHTO, to obtain soil spring values for those materials.

Work could be performed to determine resistance factors for joints, replacing the current proposal to employ a factor of 0.67. This would involve statistical analysis of a series of many resistance (strength) tests on specific pipe joint systems. Ideally, this would be undertaken in conjunction with work to develop a standard AASHTO test for the structural and hydraulic performance of culvert joints (the joint strength and leakage test mentioned above).

REFERENCES

American Association of State and Highway Transportation Officials (AASHTO). 2006. AASHTO LRFD Bridge Design Specifications 3rd Edition with 2005 and 2006 Interim Revisions. Washington D.C.

Hetényi, M. 1946. *Beams on elastic foundations*. University of Michigan Press, Ann Arbor, Mich.

McGrath, T.J.; Moore I.D.; Selig, E.T.; Webb, M.C. and Taleb,B. 2002. Recommended Specifications for large span culverts, *NCHRP Report 473*, Transportation Research Board, Washington D.C.

Terzaghi, K. 1955. Evaluation of Coefficients of Subgrade Reaction. *Géotechnique*. 5, No. 4:297-326.

.

Literature Review

Table of Contents

A.1 Introduction

This literature review covers
a. existing standards including joint design and joint testing protocols
b. published articles on design or performance of joints
c. other related literature for this project:
    - studies of longitudinal pipe response for nonuniform ground support
    - three-dimensional analyses of pipe behavior
    - 'beam-on-elastic-spring' and related analyses

The joint systems being examined include:
a. band-type systems, Figure A.1a (these are either flat, or profiled to conform to the outside of corrugated or profiled pipe products
b. tongue and groove systems (Figure A.1b) or bell and spigot systems (Figure A.1c)
c. placement end – to – end and wrapping with external seal

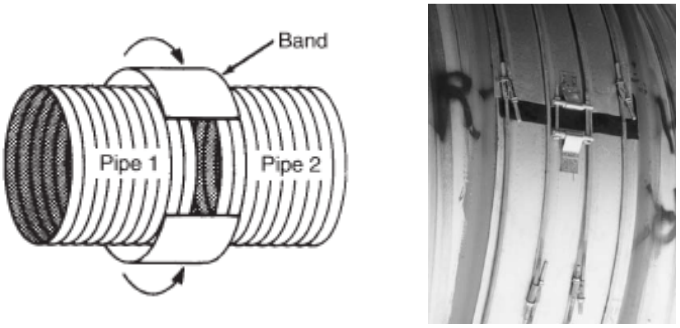

a. band-type systems

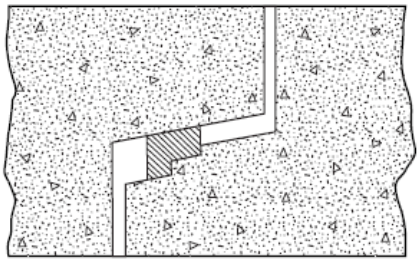

b. tongue and groove systems

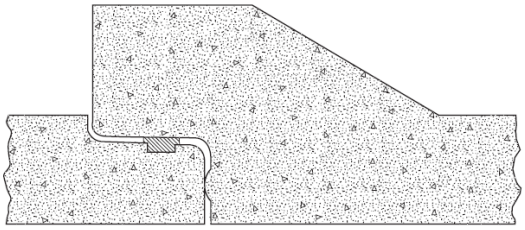

c. bell and spigot

Figure A.1 Pipe connection systems

Sealing systems for joints include:

i. O ring, sleeve gaskets, strip gaskets and wraps, Figure A.2a and Figure A.2b
ii. Profiled rubber gaskets, Figure A.2c
iii. Mastic or other sealants, Figure A.2d

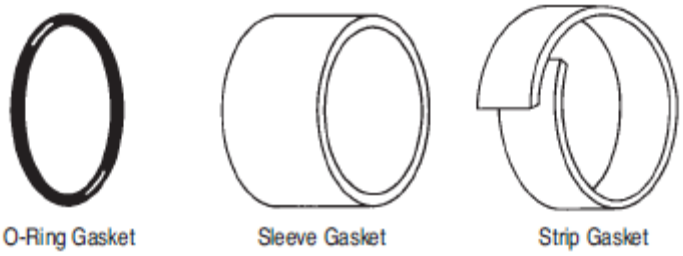

a. O rings, sleeve gasket, strip gasket

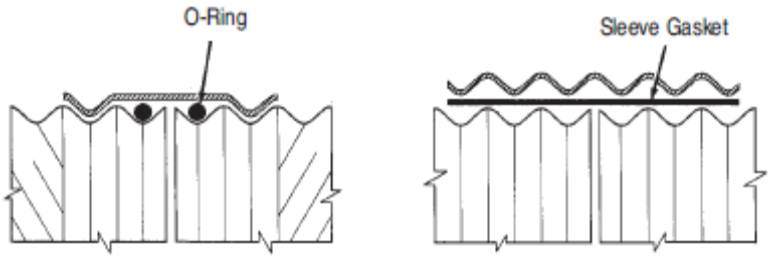

b. Use of O rings and sleeve gasket (corrugated steel pipe examples, CSPA, 2002)

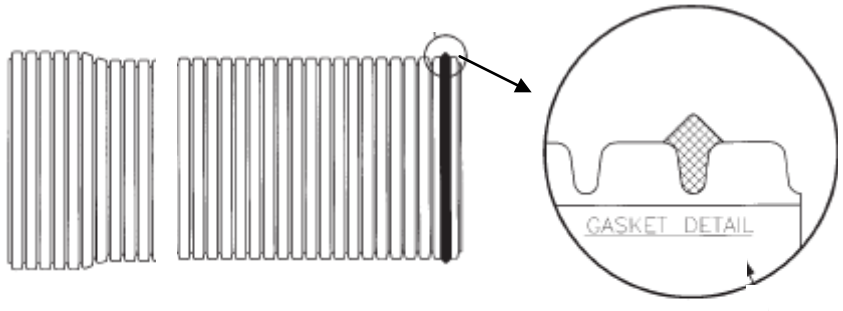

c. Profiled rubber gasket (A2000, PVC pipe example, http://www.westernprecast.com/downloads/pipeproducts/bro_A2000D.pdf)

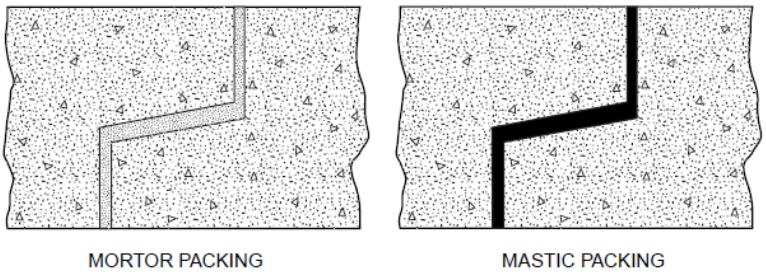

d. Mortar or Mastic sealants (ACPA, 2009)

Figure A.2 Sealing systems at joints

A.2 Pipe joint standards.

A.2.1 Introduction

A series of ASTM standards exist providing specifications for design, geometry and testing of jointed culvert and pipe products. Table A.1, Table A.2, and Table A.3 provide summaries of these standards for concrete, corrugated steel and polymer pipe structures, respectively. The tables provide the standard numbers, titles, pipe types, joint types, and brief details of other relevant information such as standard joint tests, joint materials. The standards for concrete, steel and polymer pipes are listed in each of the next three subsections. More details of these testing and other requirements are discussed with related literature in Section A.3. Specifications for joints given in the 2nd edition of the *AASHTO LRFD Bridge Construction Specification* are also briefly summarized.

A.2.2 Concrete pipe standards

Concrete pipe design standards ASTM C 14 (AASHTO M 86) and ASTM C 76 (AASHTO M 170) feature some minor discussion of their jointing systems.

Joints specifications are guided by ASTM C 443-05a (AASHTO M 315) for joints with rubber gasket between the bell or groove, and the spigot or tongue, ASTM C 877 for external sealing bands, and ASTM C 990 for bell or groove with spigot or tongue sealed by bitumen or butyl rubber.

Standard test methods for pipe are described in ASTM C 497. Infiltration and exfiltration testing is covered by ASTM C 969, low-pressure air testing is covered by ASTM C924, and vacuum testing is covered in ASTM C1214. Larger diameter pipes are discussed in ASTM C1103, including air and water testing after installation.

Joints for concrete, gravity flow pipes sealed using rubber O rings or profile gaskets are covered by ASTM C 1628, and this standard includes guidance on pressure testing.

A.2.3 Steel pipe standards

Corrugated steel pipe product standard specification ASTM A760 – 09 (similar to AASHTO M36) is supported by the design standard ASTM A796 (similar to the AASHTO LRFD bridge design standard), and installation practice ASTM A 798. Roberts (2002) provides further description of joint options and the requirements in the 2nd edition of the *AASHTO LRFD Bridge Construction Specification*.

A.2.4 Polymer pipe standards

Joints for polymer pipes with elastomeric gasket between bell and spigot or mechanical connections are discussed in ASTM D3212. This standard describes both pressure and vacuum tests for these systems.

Gasket requirements for polymer pipes are described in ASTM F 477.

The standard for large diameter corrugated HDPE pipe and fittings includes the description of an ‘elongation test’, to test whether the joint pulls apart.

Field testing of joint leakage is described in ASTM F 1417, based on air pressure. Joint assembly is covered in ASTM F 1668, the standard guide to polymer pipe burial (construction) practice.

A.2.5 AASHTO Bridge Specifications

The 2nd edition of the *AASHTO LRFD Bridge Construction Specification* provides requirements for pipe joints in Section II (subsection 26.4). CSPA (2002) indicates that work was conducted in the early 1980s by California Transportation (CALTRANS) and the Bridge Design Code Committee of the American Association of State Highway and Transportation Officials (AASHTO) to develop mechanical and structural performance requirements for field joints in corrugated steel pipe. Subsection 26.4 provides joint property requirements for both erodible and non-erodible soils. The requirements for joint properties are specified in six categories:

1. Shear strength which is expressed as a percentage of calculated shear strength of the pipe on a transverse cross-section remove from the joint (2% normally, and 5% in special cases)
2. Moment strength which is expressed as a percentage of calculated moment strength of the pipe on a transverse cross-section remove from the joint (2% normally, and 5% in special cases)
3. Tensile strength is required if longitudinal loads may develop that could separate adjacent pipes. Requirement is resistance of 5000 lb (22kN) for pipes under 42 in. diameter, and 10000 lb (44 kN) for pipes over 42 in. diameter.
4. Joint overlap can be specified if the standard joint does not meet the moment strength (essentially the joint permits movement given that moment will exceed capacity)
5. Soil tightness is specified by limiting openings to 1 in. (25mm), and lengths of channels wider than 1/8 in. (3mm) must be four times the opening size. Furthermore, for all soils, the ratio of D85 soil size to opening size must be greater than 0.3 for medium to fine sand and 0.2 for uniform sand (ratios that do need not to be met for cohesive backfills plasticity index exceeds 12). Alternatively, if a joint passes a 14kPa (2 lb/in.2) hydrostatic test without leakage, it is considered soil tight.
6. Water-tightness is controlled by using the soil tightness criteria, and adding dimensional tolerances for the pipe ends (less than 0.5 in. (13 mm) diameter or 1.5 in. (38 mm) in circumference for watertight joints.

Table A.1 Summary of relevant concrete pipe standards.

Standard	Title	Pipe types	Joint type	Joint design, testing or other requirements
ASTM C 76-08 (AASHTO M 170)	Reinforced Concrete Culvert, Storm Drain, and Sewer Pipe	Reinforced concrete	All	Provides details of steel reinforcement for joints (distinguishing between non-rubber gasket joints and rubber gasket joints).
ASTM C 443-05a (AASHTO M 315)	Joints for Circular Concrete Pipe and Manholes, Using Rubber Gasket	Reinforced concrete (some provisions also used for corrugated steel pipes)	Bell or groove, and spigot or tongue, with rubber gasket	Water test under internal pressure; straight pipe uses 13psi (90kPa) internal pressure for 10min (or up to 24 hrs); pressure is 10psi (70kPa) for bent joint over 10 minutes (one side at outside of joint opened 0.5in (13mm) from assembled position. Gasket not stretched more than 30% when in position. Bell and spigot are designed to withstand fracture from gasket forces when joined or when tested. Bell and spigot have maximum 3.5o taper angle (up to 5o permitted if the configuration passes the leakage tests). An annular space no more than 75% of uncompressed gasket dimension; the width of that annular space shall not vary by more than 10 % of the uncompressed gasket thickness.
ASTM C 497-05	Test Methods for Concrete Pipe, Manhole Sections, or Tile	Concrete	Joints sealed with gaskets.	The hydrostatic test is described for assessing leakage at joints. Gasket lubricant tests are described. The joint shear test is described. The off-center hydrostatic joint test.
ASTM C 877-08	External Sealing Bands for Noncircular Concrete Sewer, Storm Drain and Culvert Pipe	Concrete	Pipe ends abut External sealing bands	Type I: Rubber & mastic band; Type II Plastic film and mesh reinforced mastic band & steel straps; Type IIIA. HDPE band or Type IIIB. Rubber band; both have butyl rubber adhesive. Property requirements for each band type are specified in detail.
ASTM C 924-02	Standard Procedure for Testing Concrete Pipe Sewer Lines by	Concrete	Any	Air test applies 4 psi i.e. 27 kPa, then record time for 1 psi i.e. 7kPa pressure drop, and compared to requirement (e.g. 3.6 min per 100ft of pipe). Pump rate requirements are also specified.

	Low-Pressure Air Test Method			
ASTM C 969-02	Standard Practice for Infiltration and Exfiltration Acceptance Testing of Installed Precast Concrete Pipe Sewer Lines	Precast concrete	Any preformed flexible joint sealants to prevent solid (soil) flow through joint	Water infiltration of exfiltration tests of joints: infiltration rate is measured or exfiltration rate (after filling pipe with water to specific head and measuring water loss). Pipe larger than 24in diameter can be accepted on visual inspection. Infiltration testing used where groundwater > 2ft above crown. Allowable infiltration is 200 gal/(in. of internal diameter) (mile of sewer) (24 h) for average head on test section ≤6 ft; exfiltration limit is 200 gal/(in. of internal diameter) (mile of sewer) (24 h) for average head on test section ≤ 3 ft.
ASTM C 990-09 (similar to AASHTO M 198)	Joints for precast concrete pipe and box, and other sections using preformed flexible joint sealants for use in storm sewers and culverts	Concrete	Bell or groove on one end and spigot or tongue on end of joining section	Assembled in straight alignment to develop a pressure of at least 10 psi (70 kPa) for 10 minutes Bitumen or butyl rubber sealants. Minimum properties for both materials are specified in detail. Design to withstand fracture from gasket forces when joined or when tested; maximum 10o orientation error permitted; larger orientation errors are permitted if the joint passes the tests and is accepted by the owner.
ASTM C 1103–03	Joint Acceptance Testing of Installed Precast Concrete Pipe Sewer Lines	Concrete – diameter over 27inch	Rubber gasket	Air and water tests after installation; similar to C924 but for larger diameter pipes.
ASTM C 1214-02	Test Method for Concrete Pipe Sewerlines by Negative Air Pressure (Vacuum)	Concrete	Gasketted 4in to 36in sewer lines.	Vacuum test after construction: test time measured for vacuum to drop from 7 to 5 in. of mercury. Minimum time depends on diameter and length e.g. 24 inch diameter time is 3.6 minutes per 100 ft.
ASTM C 1628-06	Joints for Concrete Gravity Flow		Bell and spigot with rubber	Straight configuration test: internal pressure 13 psi (90 kPa) for 10 min; up to 24 hours if leakage occurs.

	Sewer Pipe, Using Rubber Gaskets		gaskets – either O rings or profile gaskets.	Deflected position test: deflect to create 1⁄2-in. (13mm) wider than assembled position on one side of outside perimeter; pressure of 10 psi for 10 min. Structural Test: joint shear tests according to ASTM C 497. Gives tolerances on manufactured geometry, and bell and spigot geometries. Gasket deformation must be between 15% and 50% (60% for noncircular gaskets) of dimension difference between bell and spigot. Maximum 35% (30% noncircular gasket) circumferential stretch. Maximum taper of 2o (3o if proven and accepted by owner).
CSA A257.3-03	Joints for circular concrete sewer and culvert pipe, manhole sections, and fittings using rubber gaskets		Bell (or groove) and spigot (or tongue) with rubber gasket	Similar to ASTM but higher testing pressures: 13 psi (90kPa) or 15 psi (103kPa) for straight alignment; maximum 3.5^{o} taper angle; no leakage when one side of outside of joint is opened 13mm than assembled position Gasket not stretched more than 30% of original circumference

Table A.2 Summary of relevant corrugated metal pipe standards.

Standard	Title	Pipe types(s)	Joint type(s)	Joint design, testing or other requirements
ASTM A760– 09 (AASHTO M36)	Corrugated Steel Pipe, Metallic-Coated for Sewers and Drains	Corrugated steel	All	Difference in diameter of two pipes that are butted together is limited to 0.5in. (13mm). Gives minimum thicknesses of bands, sleeves and bells used in joints. Specifies shear, moment and tensile force capacity of joint as a function of the pipe barrel (see further details in relation to the AASHTO Specifications in Section A.2.5). Defines gasket geometries to be used.
ASTM A796 / A796M - 06	Structural Design of Corrugated Steel Pipe, Pipe-Arches, and Arches for Storm and Sanitary Sewers and Other Buried Applications	Corrugated steel	Not specified	Contains no explicit mention of joints
ASTM A 798 A 798M – 07	Practice for Installing Factory-Made Corrugated Steel Pipe for Sewers and Other Applications	Corrugated steel	All	Provides construction guidelines for joints: gasket installation, coupling bands, sleeve couplers and bell and spigot joining, and finally joint backfill.

Table A.3 Summary of relevant polymer pipe standards

Standard	Title	Pipe types(s)	Joint type(s)	Joint design, testing or other requirements
ASTM D 3212 – 07	Joints for Drain and Sewer Plastic Pipes Using Flexible Elastomeric Seals	HDPE and PVC	Elastomeric gasket between bell (or socket) and spigot; or mechanical joint to develop the pressure seal	Do pressure and vacuum when straight and then when deflected to 5% of outside diameter pressure of 10.8 psi (74 kPa) for 10 min; vacuum of 10.8 psi (74 kPa) for 10 min (pressure change < 3 kPa, and again 10 min later change < 17 kPa).
ASTM F 477 – 08	Elastomeric Seals (Gaskets) for Joining Plastic Pipe	Polymer pipes (Gravity flow and pressure pipes)	Gasketted	Requirements for gaskets (elastomeric and thermoplastic elastomeric seals); includes deformation test for polymer-gasket compatibility. Not stretched more than 30% when in position.
ASTM F 667 – 06	Large Diameter Corrugated Polyethylene Pipe and Fittings	HDPE	All	Elongation test to examine resistance to joint separation under axial load; weight of 5 lb/in. of inside diameter (maximum 50 lb) on bottom end of pipe hanging vertically.
ASTM F 1417 – 05	Standard Test Method for Installation Acceptance of Plastic Gravity Sewer Lines Using Low-Pressure Air	Polymer pipes	All	The low-pressure air test is described. The test is conducted either at internal pressure of 3.5 psi (24 kPa) and the flow rate monitored to maintain this pressure, or the test starts at internal pressure of 3.5 psi (24 kPa) and time required for pressure to drop to 2.5 psi (17 kPa) is recorded.
ASTM F 1668 – 08	Standard Guide for Construction Procedures for Buried Plastic Pipe	Polymer pipes	All	No

A.3 Design and performance of jointed pipes

A.3.1 Design requirements for joints

Kurdziel (2002, 2004), Romer and Kienow (2004), Rahman and Watkins (2005) and Dittel and Quasada (2008) all discuss the design requirements for pipe joints. Design considerations include:

- geometry of the bell, spigot, and groove left for the gasket (including limits on taper angles and other geometrical tolerances between the inner and outer surfaces)
- capacity of the joint to withstand the compression load when the spigot is inserted into the bell (codes mention that design must withstand fracture from gasket forces when joined or tested)
- geometrical limits to ensure the space left for the gasket is some fraction of the gasket height (e.g. an empirical value like 75%)
- ability to maintain water-tightness after joint rotation (that is rotation of the axis of the pipe contributing the spigot relative to the axis of the pipe contributing the bell); in reinforced concrete pipe, this rotation is specified as 0.5in (13mm) of opening at one point on the external circumference relative to the initial installed position of the spigot within the bell
- limits on how much the gasket is stretched (e.g. an extension limited to 30% is typical) and
- pressure testing at some standard value when the pipes are in straight alignment e.g. 13psi (90 kPa) and when they are rotated e.g. 10psi (70kPa)

Kurdziel (2004) examined joint response without lubricants, and provided a variety of force-deformation measurements for different joint systems. He indicated that lubricants used to facilitate assembly can cause the gasket to swell, and *"can have a substantial impact on gasket swell… Gasket swells of greater than 100 percent are not uncommon and such diameter increases can induce forces great enough to crack the pipe"*. He also concluded that during joint design, there is a need to consider sealing force, gasket deformation, and stresses induced in the bell.

Other considerations outlined by Romer and Kienow (2004):

– Need for the bell to support the spigot acting as a cantilever.
– Need for adequate shear and tensile strength to support one-half the adjacent pipes weight and other construction loads anticipated.
– Need for adequate circumferential strength in the bell to support earth loads, based on the specified load and support conditions.
– Need for adequate circumferential strength in the bell to resist gasket pressure (hoop stress) plus hydrostatic pressure plus hydrodynamic (surge) pressure.
– Need for adequate gasket size and stiffness to center the joint and to support the joint without loss of compression and leakage at the pipe crown.
– Need for adequate rotational capability, specified as either magnitude of deflection within a specified length or in degrees.
– Need for adequate and realistic tolerances to reflect actual manufacturing processes.

Rahman and Watkins (2005) indicate that joints should have

- ability to tolerate thermal effects
- ability to resist over-insertion

- consideration of the Reissner effect (ovaling that occurs in the cross-section due to longitudinal bending)
- ability to resist prying open (lever action) which can occur when the rotation angle is exceeded across a joint and the spigot comes in contact with the bell

Kurdziel (2002) indicates that gasketted joint design should consider both minimum and maximum contact pressures between the gasket and the spigot and bell. He notes correctly that the pressures that develop depend on the stiffness of the pipe components (the tendency of the bell to open and the spigot to close will influence contact pressures).

Dittel and Quasada (2008) further indicate that gasket design to develop optimal sealing performance depends on dimensioning based on geometric interference, seal stability during installation and assembly, avoidance of assembly-locking tendencies, adequate seal reaction to pressure, and the allowable stress and strain for the pipe materials (to avoid pipe damage due to seal contact pressures).

ACPA (2009) discusses hydraulic requirements such as

- Resistance to infiltration of ground water and/or backfill material.
- Resistance to storm water.
- Control of leakage from internal or external heads.
- Hydraulic continuity and a smooth flow line.
- Flexibility to accommodate lateral deflection or longitudinal movement without creating leakage problems.
- Resistance to shear stresses between adjacent pipe sections without creating leakage problems.

Other issues discussed by ACPA (2009) include ease and effectiveness of installation. While field performance can be expected to depend on the care with which the jointed pipe systems is installed, the design of jointing systems that facilitate reliable installation can help to alleviate potential problems.

While not concerned directly with design, installation guides provide details on joint assembly and placement of bedding and other soil plays an important role in the resulting joint performance. For example, section 11 of ASTM F 1668 – 08 *Standard Guide for Construction Procedures for Buried Plastic Pipe* describes recommended procedures to maintain joint integrity during construction of polymer culverts and sewers. A 798/A 798M – 07 *Standard Practice for Installing Factory-Made Corrugated Steel Pipe for Sewers and Other Applications* and A 807/A 807M – 02e *Standard Practice for Installing Corrugated Steel Structural Plate Pipe for Sewers and Other Applications* also deal with these issues.

Specific joint systems will have particular characteristics that can render them unsuitable for all or some installations. For example, joints sealed with rubber gaskets and mastic joint fillers can provide some flexibility (reducing moments across the joint and elsewhere in the pipe) without impairing water-tightness. However, mortar joints will be rigid, and can be expected to crack and leak if deformations are imposed, ACPA (2009). Joint systems featuring external wraps can resist external groundwater pressure if properly installed, but ability to resist internal pressure will be very limited.

A.3.2 Testing procedures

A.3.2.1 Concrete pipe testing

ASTM C443 (2005) specifies requirements for hydrostatic pressure testing of joints in concrete pipes. First, hydrostatic pressure testing is conducted on joints when two pipe sections are fitted together in a straight configuration with the gasket or gaskets in place. The assembly is subjected to an internal hydrostatic pressure of 13 psi (30 ft) (89 kPa) pressure head for 10 minutes. After completing the test for pipes in straight alignment, the test sections are deflected to create a position 1⁄2 in. (13mm) wider than the assembled position on one side of the outside perimeter of each joint. This is subjected to an internal hydrostatic pressure of 10 psi (68 kPa) for 10 minutes. One outcome of the specification of a deflection to create a position 1⁄2 in. (13mm) wider, is that this corresponds to different rotation angles for pipes with different external diameter, and consideration should be given in the testing and design procedures to whether a constant angle or rotation to produce constant joint opening should be specified or accommodated. Now, substantial axial forces are needed to resist the pressures on the seals used at the open ends of the pipes. The normal testing arrangement involves clamping of the compression of the two pipes together to transfer these axial forces, and this means very substantial axial compressions are generated across the joint, forces that would not be expected in the field. This is a major shortcoming of these tests, and a testing arrangement is needed where these resisting forces are not transferred across the joint.

ASTM C497 (2005) describes the joint shear test, where shear force, normal to the longitudinal axis of the pipes, is applied across the assembled joint between two concrete pipes. The test is a proof-of-design test to evaluate structural “capability” (not capacity) of the pipe joint under shear.

ASTM C497 (2005) also describes the off-center hydrostatic joint test. In this test, an assembled concrete pipe joint sealed with a gasket is hydrostatically tested while the bell and spigot of the test joint assembly are placed in the maximum off-center position (compressing the gasket to its fullest extent on one side of the joint, and relaxing (unloading) the gasket to its fullest extent on the diametrically opposed position around the joint. The test configuration is shown in Figure A.3. Again, this arrangement suffers from the same problem discussed in the earlier paragraph regarding C443 – the test can feature a compressive axial force being transferred across the joint being tested.

ASTM C924 (2002) features test requirements for vacuum testing of small diameter concrete pipes (24 in. or less). A pressure of 4 psi (27 kPa) is employed.

ASTM C 1103 (2003) describes air and water tests after installation, tests that are similar to those described in ASTM C924 (2002) but for larger diameter pipes.

A number of the pressure testing standards state directly or indirectly that pressure tests are not necessarily reproducible. This is a reflection of their development as ‘pass or fail’ tests that do not provide specific details of the joint condition (except whether they provide an effective seal). If possible, it would be useful to relate the performance of pipe systems in these tests to more specific information about the joint conditions (contact pressures between bell and pipe elements and the gasket, for example), though this is not likely possible for field conditions, given the wide range of possible pipe configurations (pipe volumes, numbers of joints, pipe saturation levels, joint types, backfill conditions, and water levels).

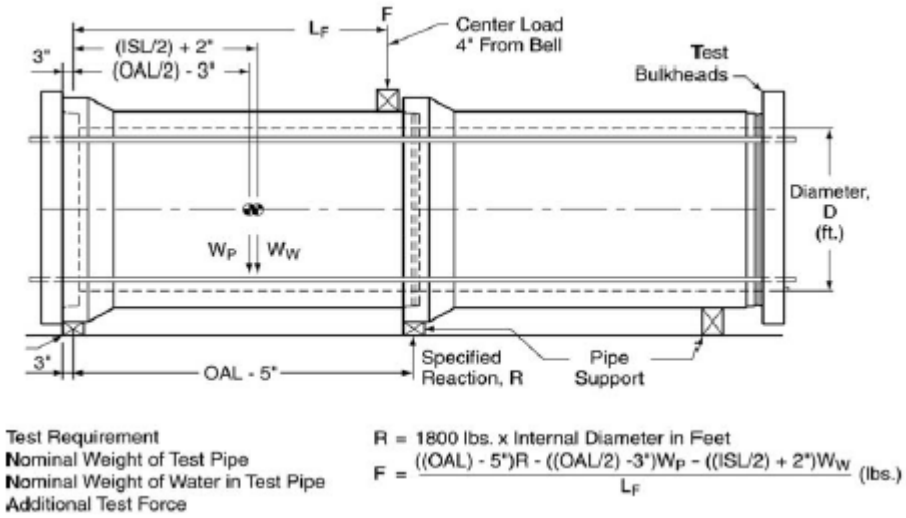

Figure A.3 Configuration of the off-center hydrostatic joint test (from ASTM C 497, 2005).

ASTM C497 (2005) describes gasket lubrication tests:

- Durometer and Volume Change Tests (to evaluate change in volume); and a
- Wash Test for Subaqueous Lubricants (to evaluate loss of lubricant after washing).

ASTM C443 (2005) also specifies the requirements for gaskets in concrete pipes. Gasket tests feature:

- tension test in accordance with ASTM D 412
- hardness test in accordance with ASTM D2240
- compression test in accordance with ASTM D395 (22 hrs at 70^o C)
- accelerated aging in accordance with ASTM D 573 (96 hrs at 70^o C)
- water absorption in accordance with ASTM D 471 (48 hrs at 70^o C); distilled water is used

The required gasket properties are specified in ASTM C 1619.

A.3.2.2 Corrugated steel pipe testing.

While ASTM A760 and the AASHTO bridge specifications define limits of moment, shear force and tensile force across an assembled joint, there is no guidance provided on how to measure these. These standards also define requirements for soil and water-tightness, but again do not define test methods for undertaking those tests. However, some of the test procedures for pressure testing concrete pipe could potentially be employed.

A.3.2.3 Polymer pipe testing

Standard pipe pressure testing for polymer pipes includes

a. leakage assessment in the laboratory for two pipes connected at the joint and in straight alignment (according to ASTM D 3212), Figure A.4.
b. Leakage assessment in the laboratory for two pipes connected at the joint after distortion by 5% diameter decrease (according to ASTM D 3212), Figure A.5

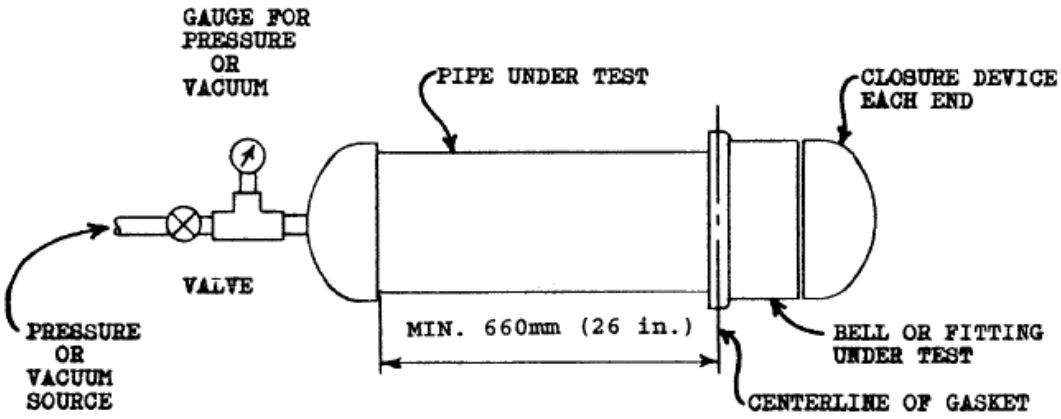

FIG. 1 Test Specimen

Figure A.4 Pressure test for polymer pipes in straight alignment according to ASTM D 3212.

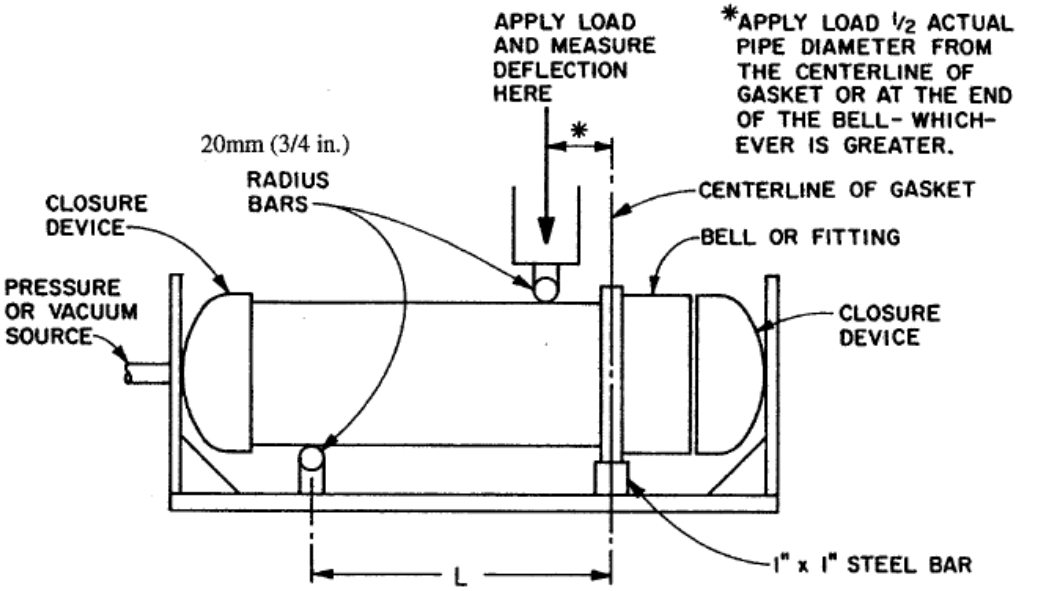

NOTE—L = actual pipe diameter or 610 mm (24 in.), whichever is greater.

FIG. 2 Shear Deflection Test

Figure A.5 Pressure test for polymer pipes after distortion with a 5% decrease in vertical diameter, ASTM D 3212.

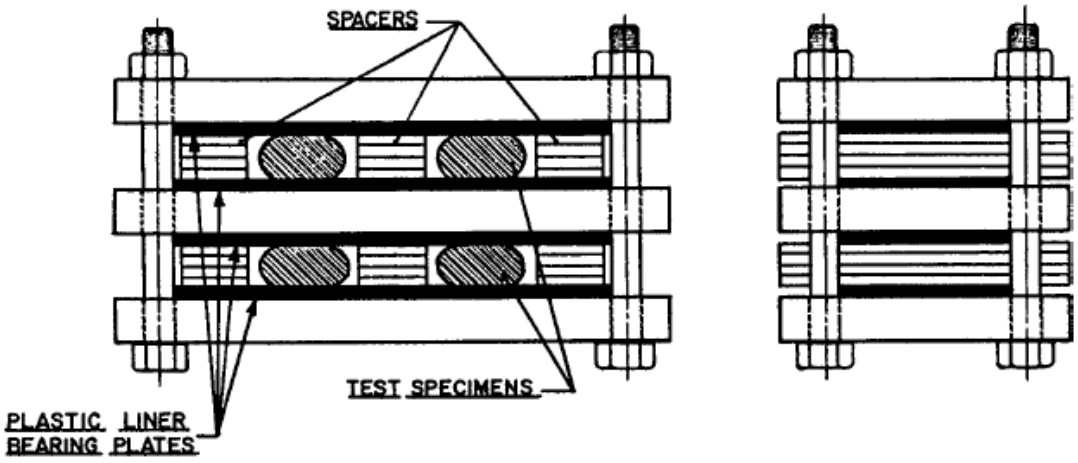

Figure A.6 Compatibility test for polymer and gaskets ASTM F 477-08.

Issues of compatibility between the polymer used to manufacture the pipe and the gasket material are examined using a compatibility test for polymer and gaskets defined by ASTM F 477-08. The test fixture is illustrated in Figure A.6.

A.3.2.4 Laboratory measurement of joint stiffness characteristics

Workers such as Vipulanandan and Liu (2005) and Buco et al. (2008) have developed laboratory test concepts examining the response of two pipes interacting across a joint. Figure A.7 illustrates the configuration of their laboratory test. The rig permits axial and vertical loading across two pipes connected at a central joint. The rig allows the rotational characteristics of the central joint to be assessed (as the pipes are raised and lowered near the central point), under different levels of axial force. Axial characteristics of the joint could be assessed by monitoring axial response as loads are applied by the horizontal jack. This configuration does not permit measurements where shear force is applied across the joint.

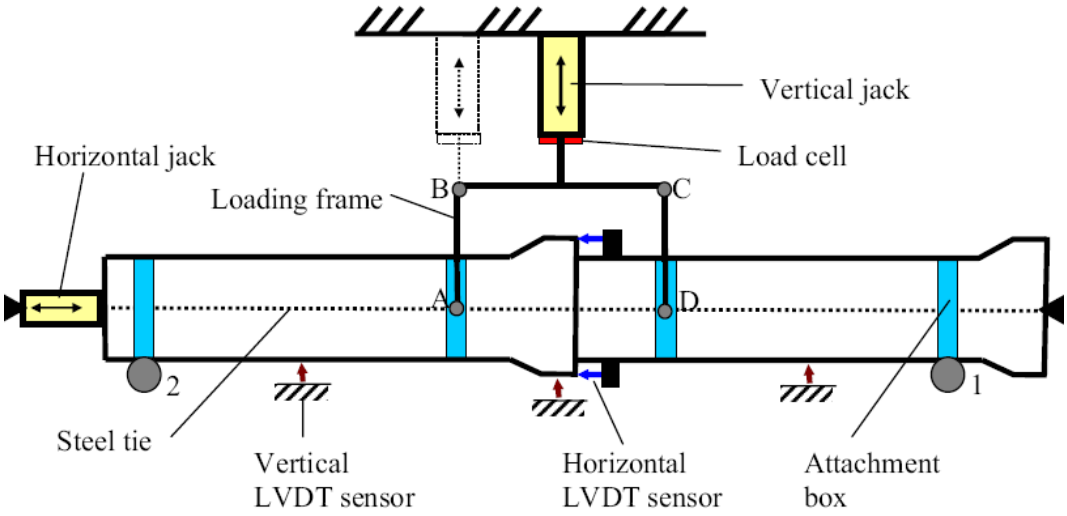

a. Test arrangement

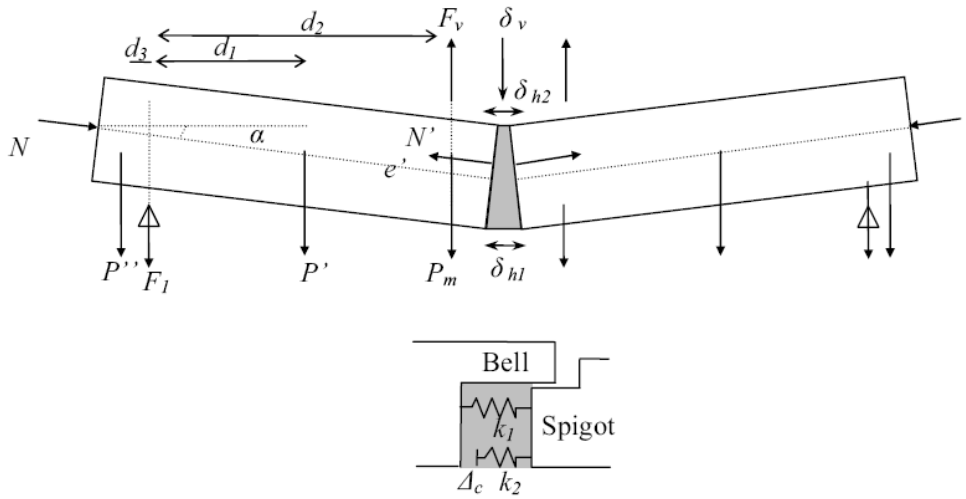

b. Definition of joint statics and kinematics

Figure A.7 Laboratory test arrangement of Buco et al (2006) to characterize joint stiffness under force and moment.

A.3.3 Longitudinal bending in buried pipes and culverts

Jeyapalan and Abdel-Magid (1987) studied failures in reinforced polymer mortar pipes using finite element analysis. A number of nonuniform bedding conditions were examined, Figure A.8. The primary focus of their study was a beam-on-elastic-spring analysis which will be discussed subsequently in Section A.4.4 Analysis of beams on elastic springs.

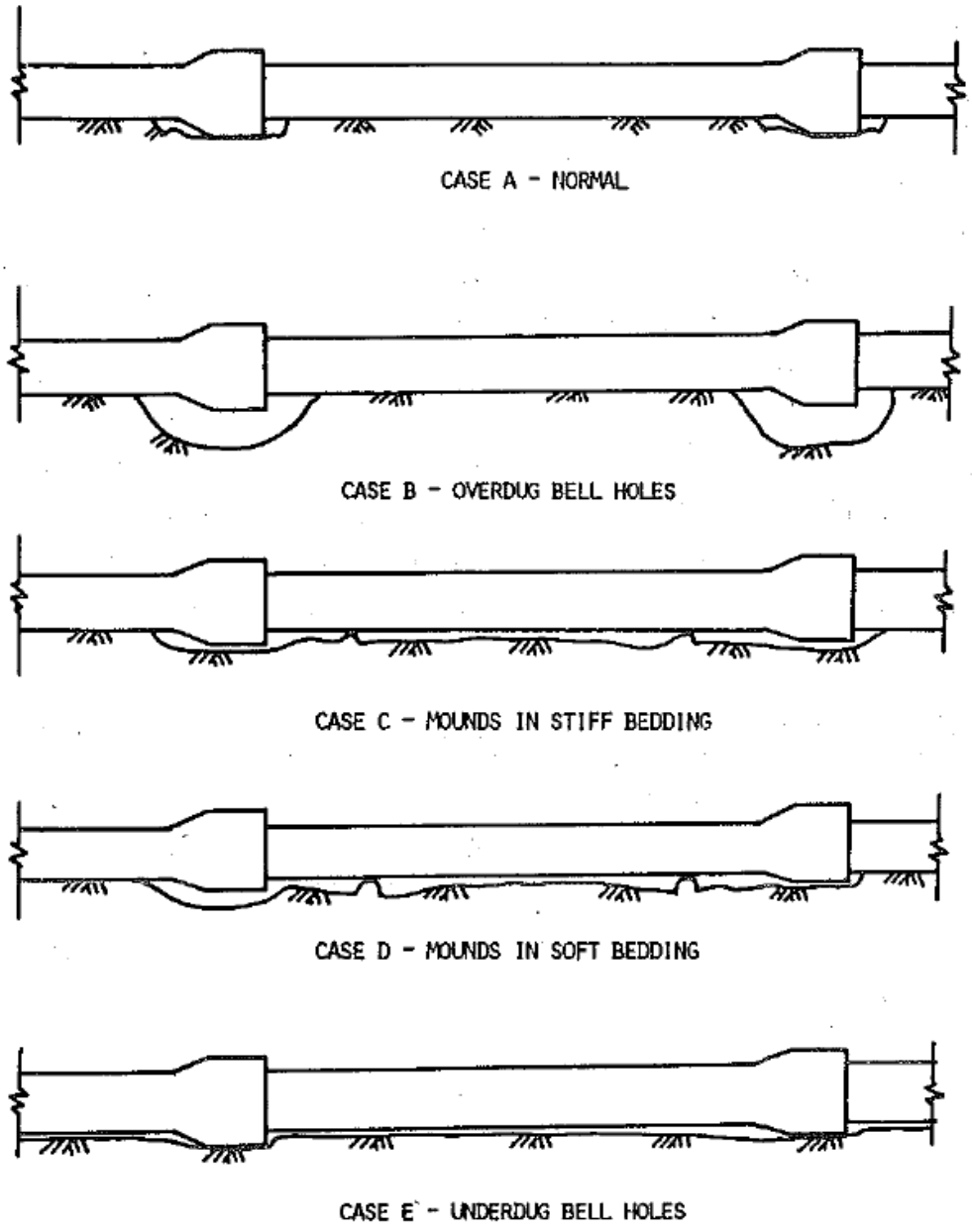

Figure A.8 Nonuniform ground support conditions defined by Jeyapalan and Abdel-Magid (1987).

Benmansour et al. (1997) used beam-on-elastic-spring analysis to study the influence of three different nonuniformities in support under the invert of jointed pipes:

- A hard point under the invert, Figure A.9a;
- Pipeline passing between regions with different soil stiffness, Figure A.9b (see also Elachachi et al. 2004);
- Pipeline passing over a void, Figure A.9c.

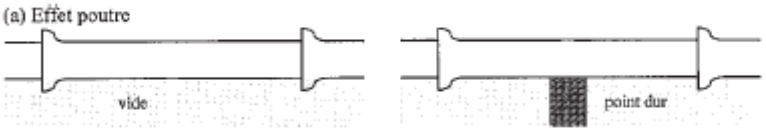

a. Effect of a hard point under the pipe invert.

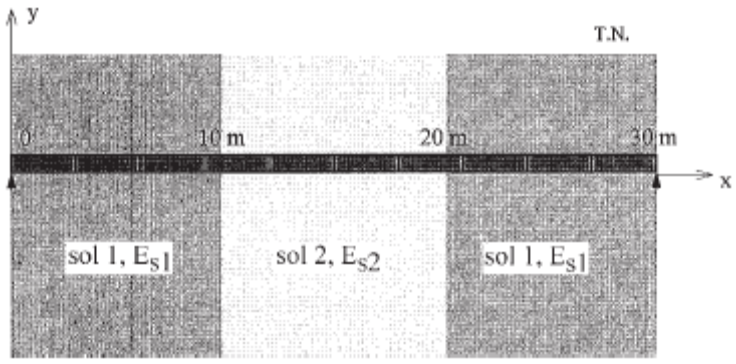

b. Pipeline passes between soils with different stiffness characteristics

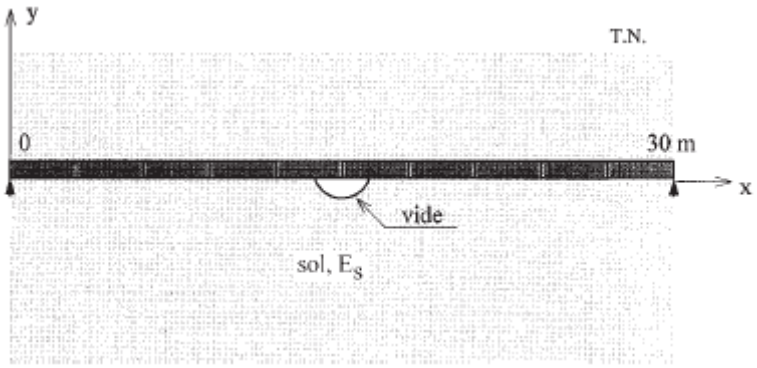

c. Presence of a void under the pipeline.

Figure A.9 Changes in soil support along the pipeline studied by Benmansour et al. (1997)

Rajani and Tesfamariam (2004) examined longitudinal bending in water pipes where scour at water leaks produces a region where bedding is absent under the pipe, Figure A.10. This study for pressure pipes is primarily computational in nature, and employs a beam-on-elastic-foundation modeling. Further discussion will be left until a subsequent section.

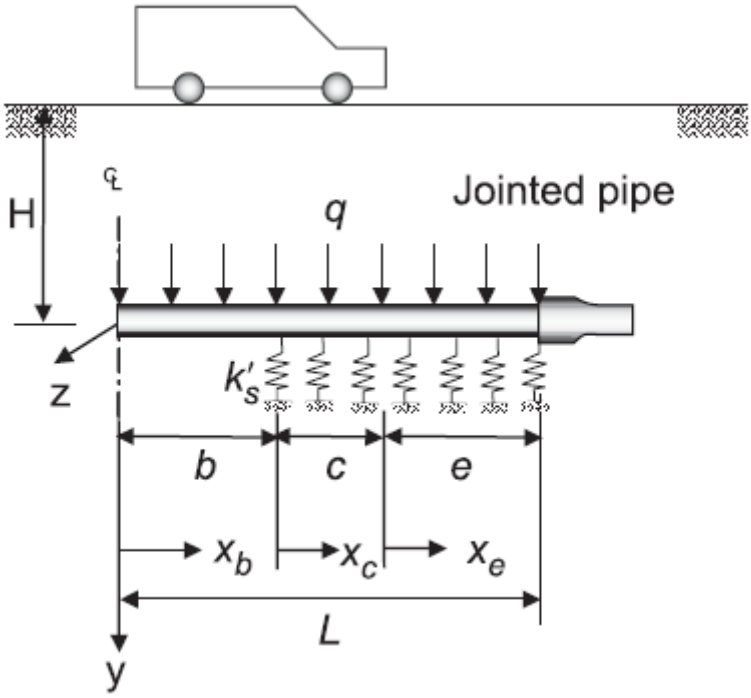

Figure A.10 Analysis of jointed water pipe with region of scour (void) under the pipe, Rajani and Tesfamariam (2004).

Buco et al. (2006) studied failures in unreinforced concrete sewers using stochastic analysis of field data as well as three-dimensional finite element analysis. The nonuniform bedding conditions are shown in Table A.4 .

Table A.4 Embedment cases considered by Buco et al. (2006)

Case		Joint	Bedding condition	
1	A_1	E_{joint}=40GPa	Reference: uniform bedding along the pipe. E_{soil}=50MPa	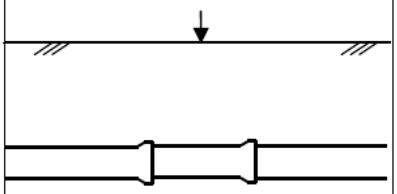
	B_1	E_{joint}=300kPa		
2	A_2	E_{joint}=40GPa	Spread heterogeneity L=3.4m: bedding under central pipe (from invert to springline, 12 cm thick) less compacted. E_{bed}=5 MPa	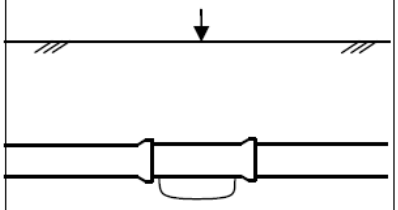
	B_2	E_{joint}=300kPa		
3	A_3	E_{joint}=40GPa	Local heterogeneities L=0.2m: over dug holes around pipe bells. E_{hole}=1MPa. Patch load applied above pipe centre.	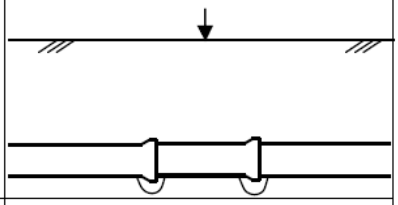
	B_3	E_{joint}=300kPa		
4	A_4	E_{joint}=40GPa	Ditto A_3 with patch load applied above pipe joint.	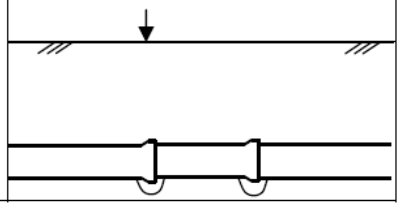
	B_4	E_{joint}=300kPa		

Balkaya et al. (2012) have recently completed a study examining the effect of nonuniform bedding on PVC water pipes. This three-dimensional finite element study used elastic-plastic soil modeling and explicit representation of the culvert joint to study the effect of a void left under the pipe during construction, or a void that develops due to soil erosion at a water leak during the service life of the pipe, Figure A.11, either under the joint, or adjacent to the joint (under the spigot or the bell).

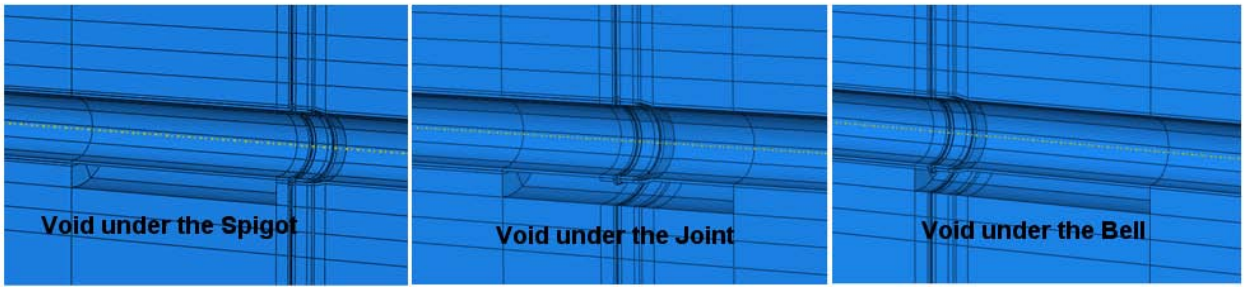

Figure A.11 Nonuniform bedding around and along PVC pipe, Balkaya et al. (2012).

These four different studies can guide choices made during testing and analysis for the current project.

A.4 Methods of analysis

A.4.1 Analysis of jointed pipes

While Kurdziel (2004) concluded that "there does not appear to be any means for mathematically estimating this performance without using physical testing similar to that used in this study", recent finite element analyses have demonstrated the ability to provide effective representations of joint behavior.

Toliver (2002) describes finite element calculations of a redesigned joint for large diameter HDPE pipe. Deformed shapes are examined, and implications drawn for improved joint performance. The analysis appears to model the bell and spigot in detail, but the approach taken to modeling the gasket is not clear. Furthermore, the conference paper does not discuss the modeling process in detail, nor are the comparisons of calculated behavior to measurements.

Buco et al. (2006) and Buco (2007) developed a three-dimensional finite element analysis of a jointed pipe system, Figure A.12. The approach involved a simplified model of a gasketted bell and spigot joint. The purpose of their analysis was not to develop an explicit representation of the individual components of the joint system, or to calculate the stresses and deformations in these components, or to study the contact and shear stresses between them. Instead, the goal was to have an approximate model with the correct joint stiffness characteristics (e.g. axial deformation under axial load and rotation under moment). The stiffness characteristics were measured using their test fixture (seen earlier in Figure A.7) and the computer model was developed on that basis.

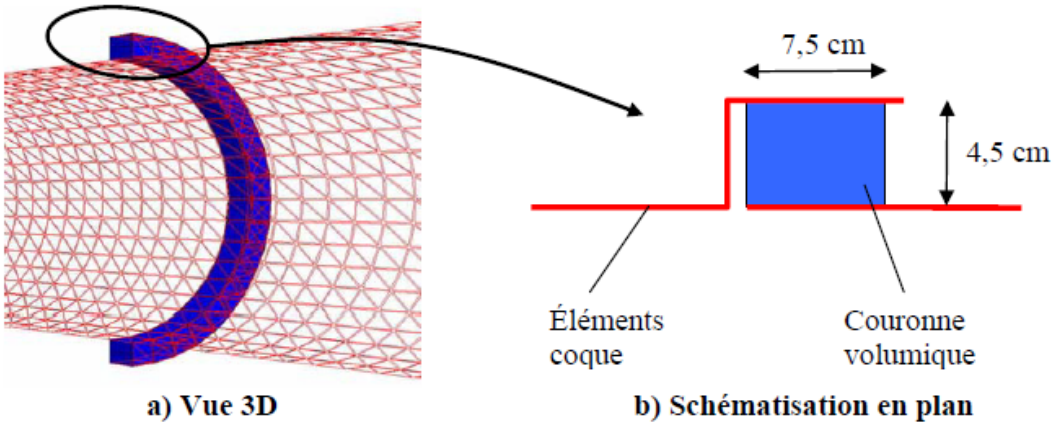

Figure A.12 Joint model of Buco (2007) used in analysis reported by Buco et al. (2006)

Balkaya and Moore (2009) have developed three-dimensional finite element analysis to permit calculations of the influence of gasket modulus, rubber-pipe friction, insertion length and joint rotation on the overall performance of a pipe-joint system. The numerical analyses are performed using ABAQUS. Figure A.13 shows details of a gasketted joint modeled by Balkaya and Moore (2009). This analysis explicitly considers the bell, the spigot, and the gasket. Analysis includes direct modeling of the joint assembly process where the spigot is inserted into the bell (where the gasket is already in position within the bell). The analysis calculates the stiffness of the joint relative to axial movement of the two components (additional insertion or partial removal), as well as the relationship between bending moment and rotation across the joint. Once the available joint compliance is expended (rotation brings the inner surface at the end of the bell into contact with the outside surface of the spigot), the analysis can calculate the increased stiffness and the

effect of that local contact on the stresses in the thermoplastic structure. This type of analysis is able to study the local behavior (distributions of stress, for example) and overall behavior (relationships between force and deformation, and moment and rotation) of the joints.

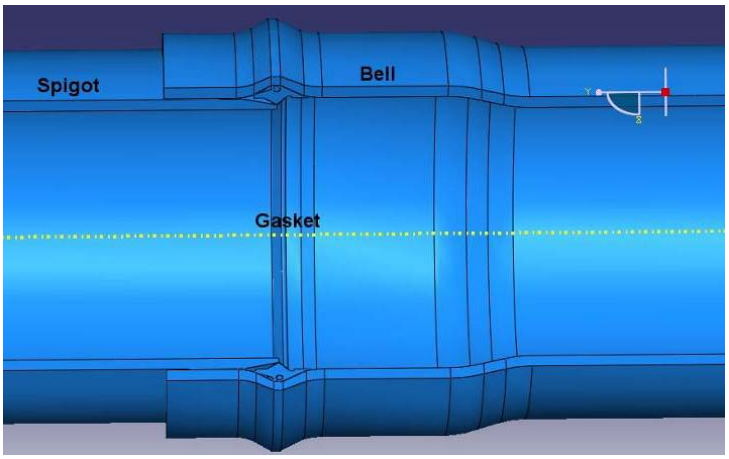

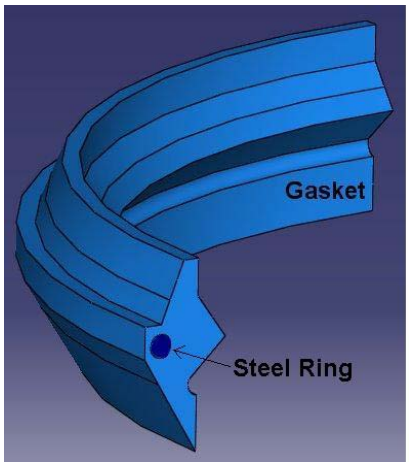

(a) The Gasketted PVC Pipe-Joint Assembly, (b) Rieber Gasket Details.

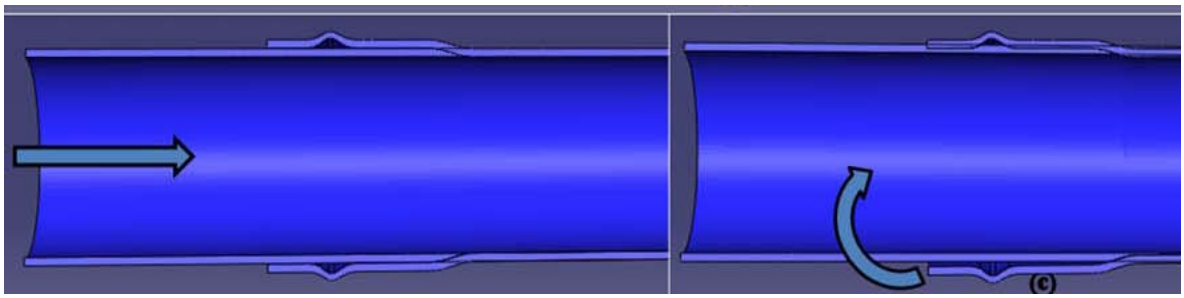

(c) Relative movements during insertion and rotation

Figure A.13 Three-dimensional analysis of a PVC pipe joint using ABAQUS (Balkaya and Moore, 2009).

For example, Dittel and Quasada (2008) have described their experience in analysis of gasketted joints, together with a commentary of a number of joint performance issues that need consideration during design (e.g. overlap of the undeformed gasket relative to the outer wall of the spigot and/or the inner wall of the bell). These analysts offer a joint analysis service, their analysis procedures are essentially proprietary, and most details are not available for direct review or imitation.

A.4.2 Analysis of buried pipe response

Considerable advances have been made over the past fifty years modeling the behavior of buried pipes to earth pressures and surface load. These include the two dimensional finite element analyses of culvert behavior of Katona (1978) and Duncan (1979), approaches which are now used regularly in the design of large span and other culvert structures. These plane strain analyses represent vehicle load as equivalent line loads running parallel to the culvert axis. Some use of plane strain modeling has been reported in assessments of the influence of longitudinal seams in corrugated plate structures affecting circumferential behavior (thrusts, moments and deformations in the horizontal plane perpendicular to the culvert axis). For example, Katona and Akl (1987)

modeled slip at specially designed joints in corrugated metal culverts, which compress when hoop thrust across the joint reaches some thresh-hold, promoting positive arching in deeply buried structures (redistribution of earth loads away from the culvert as a result of decreases in the circumference or perimeter of the metal culvert). However, since the primary focus of the current study is the influence of circular joints connecting whole-pipe segments, the primary focus of this part of the literature review is longitudinal bending and its influence on those joints. Longitudinal bending cannot be captured in the plane strain analyses.

Three-dimensional finite element analyses have been used to calculate circumferential and longitudinal response to live loads, like the semi-analytic approaches of Moore and Brachman (1994), Fernando et al. (1996) and Moore and Taleb (1999) and the full three-dimensional elastic analyses of Arockiasamy et al. (2006) and the fully nonlinear 3D analysis of Brachman et al. (2012). Comparisons by Moore and Brachman (1994) and Moore and Taleb (1999) to metal culvert response measured in the field demonstrate the advantages of three-dimensional calculations:

- Better modeling of load dissipation in the ground in the longitudinal direction
- Modeling of the much lower flexural and axial stiffness of corrugated metal plate in the axial direction (much lower than circumferential properties)
- Better calculations of displacement, thrust and moment
- Ability to determine moments, thrusts and stresses in the longitudinal direction.

There are also disadvantages to use of full three-dimensional finite element analysis:

- Need for use of specialized ‘research’ and other high level analysis programs (e.g. ABAQUS)
- Greater difficulty in developing the finite element mesh, modeling soil placement and compaction, and more difficulty obtaining successful calculations of nonlinear soil-pipe interaction across the interface
- Higher computational cost
- Greater difficulty modeling nonlinear soil behavior and its effects, including the effect of soil compaction.

Buco et al. (2006) have used three-dimensional finite element analysis to model unreinforced concrete sewer pipes responding to earth loads and live loads associated with nonuniform bedding. His analysis includes explicit modeling of the pipe joints (discussed further later in the report).

Trickey and Moore (2007) have recently used ANSYS to examine longitudinal bending in a buried pipe responding to a circular pressure distribution applied at the ground surface, Figure A.14.

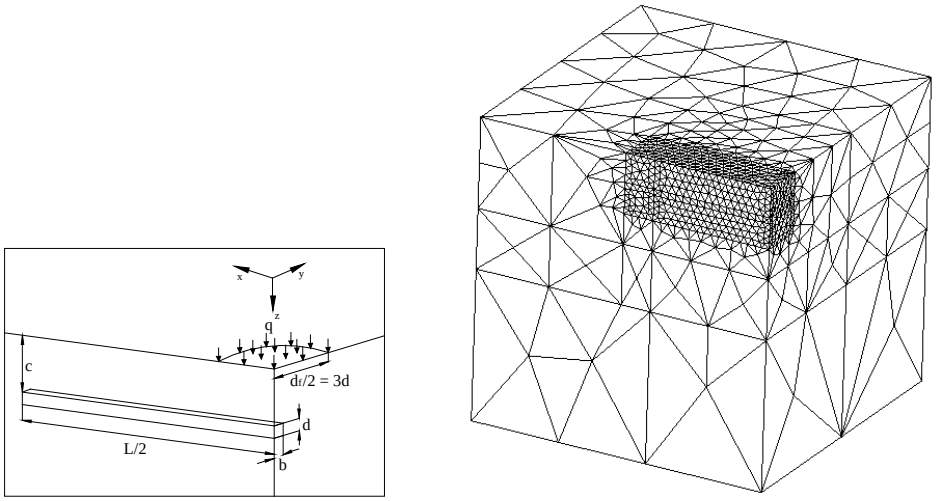

a. Problem geometry b. 3D Finite element mesh

Figure A.14 Problem examined by Trickey and Moore (2007)

Solutions for maximum deflection ρ_{max} and maximum longitudinal bending moment M are presented in Figure A.15 for a pipe with length L equal to 25 times its diameter d, and a range of burial depths c. These illustrate results for a range of pipe flexibility ratios K_r defined by elastic soil modulus E_s and structural properties

$$K_r = \frac{EI}{E_s L^4}$$

This figure also includes the solutions of Poulos, which are discussed in a subsequent subsection in relation to 'beam-on-elastic-spring' models.

Figure A.15 serves to illustrate the roles of both the burial depth and the dimensionless ratio of longitudinal pipe stiffness to soil stiffness, and how these influence both deflections and peak bending moments (for this particular case of surface loading and continuous elastic pipes). The expected behavior for jointed pipes will have some similarities. However, significant differences include

a. joints of reduced rotational stiffness that increase the peak deflections and reduce the peak moments
b. different ground support conditions instead of the continuous uniform soil support considered in these solutions
c. different loading conditions associated with dead load, and more concentrated wheel loads
d. the need to determine joint rotation, and both shear and bending moments across the joints.

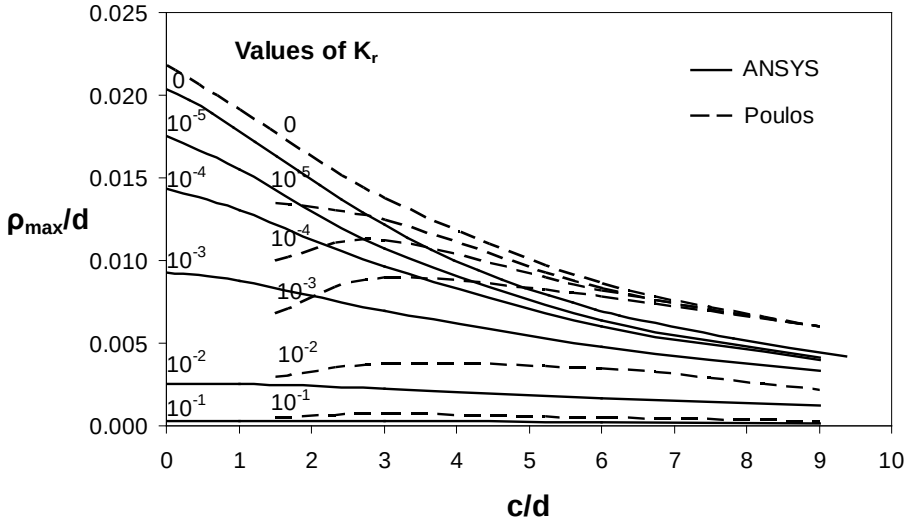

a. Maximum deflection: L/d=25, ν_s=0.3

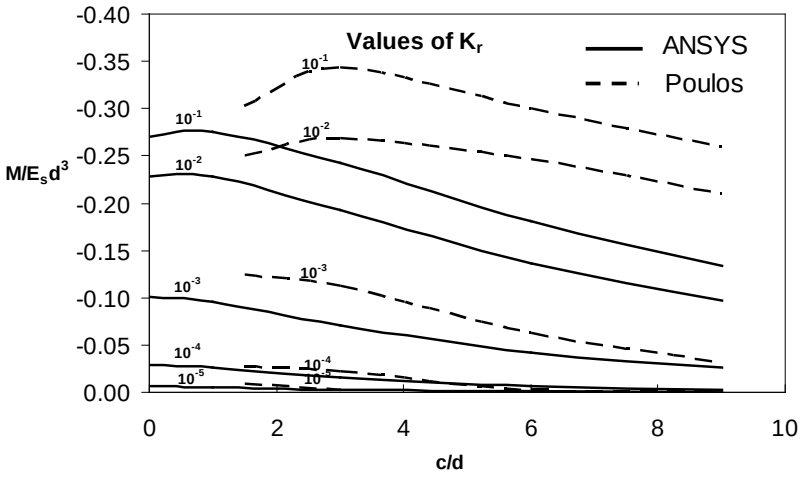

b. Maximum moment: L/d=25, ν_s=0.3

Figure A.15 Comparison of 3D finite element solutions and the beam on elastic foundation solutions of Poulos (1976) as presented by Trickey and Moore (2007).

A.4.3 Finite element analysis of pipe with nonuniform ground support

Buco et al. (2006) and Buco (2007) describe three-dimensional finite element analyses conducted for buried jointed pipe systems. They simplified the joint modeling so that the global stiffness characteristics were captured (axial force versus axial displacement, shear force versus shear displacement, and bending moment versus rotation). The analysis explicitly represents the surrounding soil. Buco et al. (2006) considered a number of cases involving different levels of bedding non-uniformity for concrete pipes, Table A.4.

Buco (2007) then employed this joint model in calculations of buried pipe behavior, as illustrated in Figure A.16. This figure shows the vertical cross-section of the pipe placed within a trench dug in native soil, and one of the three-dimensional meshes used in his calculations.

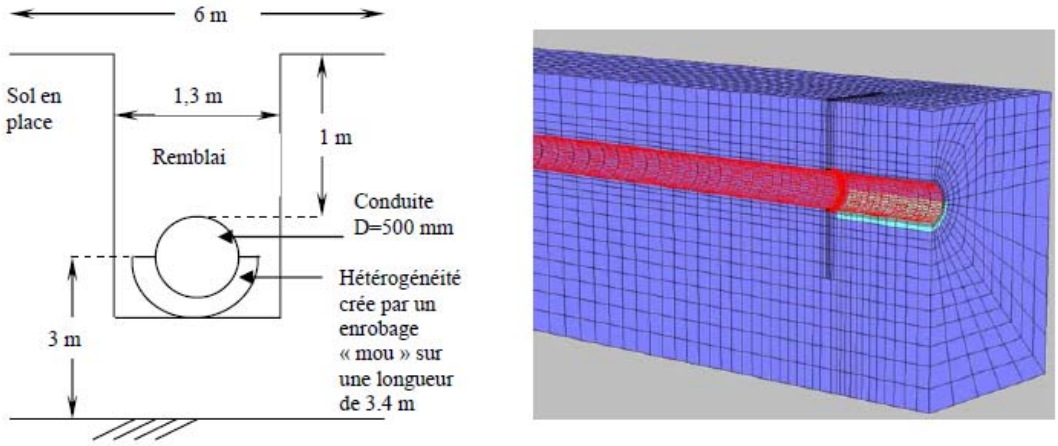

a. vertical cross-section b. three-dimensional finite element mesh

Figure A.16 Details of the buried jointed pipe analysis of Buco (2007)

Examples include completely uniform soil support, a barrel spanning between bells, and bedding with over-excavation at the bells. They compared their calculations of longitudinal stresses associated with these different embedment conditions, and compared these to observations of pipe performance from the Greater Lyon region. This study concluded that:

- "the major part of the observed defects might be related to the longitudinal behavior
- "if the load is located above the center of a pipe section, this behaves as a vertically loaded beam supporting most of the applied load"
- "if the load is situated above the joint the axial force distribution is entirely transferred to the adjacent pipes
- "the amount and the extent of this transferred effort is dependent of the barrel length
- "As expected, the size of the soil heterogeneity produces an opposite influence on the axial force compared to that found for vertical displacements
- "Small scale soil variability does not generate any negative effect: it reduces the level of the internal effort….and may be at the origin of the pipe differential movements
- "On the other hand, larger scale modification of bedding properties increases the overall flexion and may result in circumferential cracks"

As discussed earlier, Balkaya et al. (2012) have studied the effect of voids in the bedding under PVC pressures pipes. Using ABAQUS, the jointed PVC pipe described earlier in Section A.3.4.1 was modeled, for bedding conditions featuring a void at some point along the pipe, Figure A.17. This work demonstrates that the circumferential tensions in the wall of the pressure pipe remain the largest, but that the presence of the void can double those circumferential stresses in the pipe wall where it spans across the void.

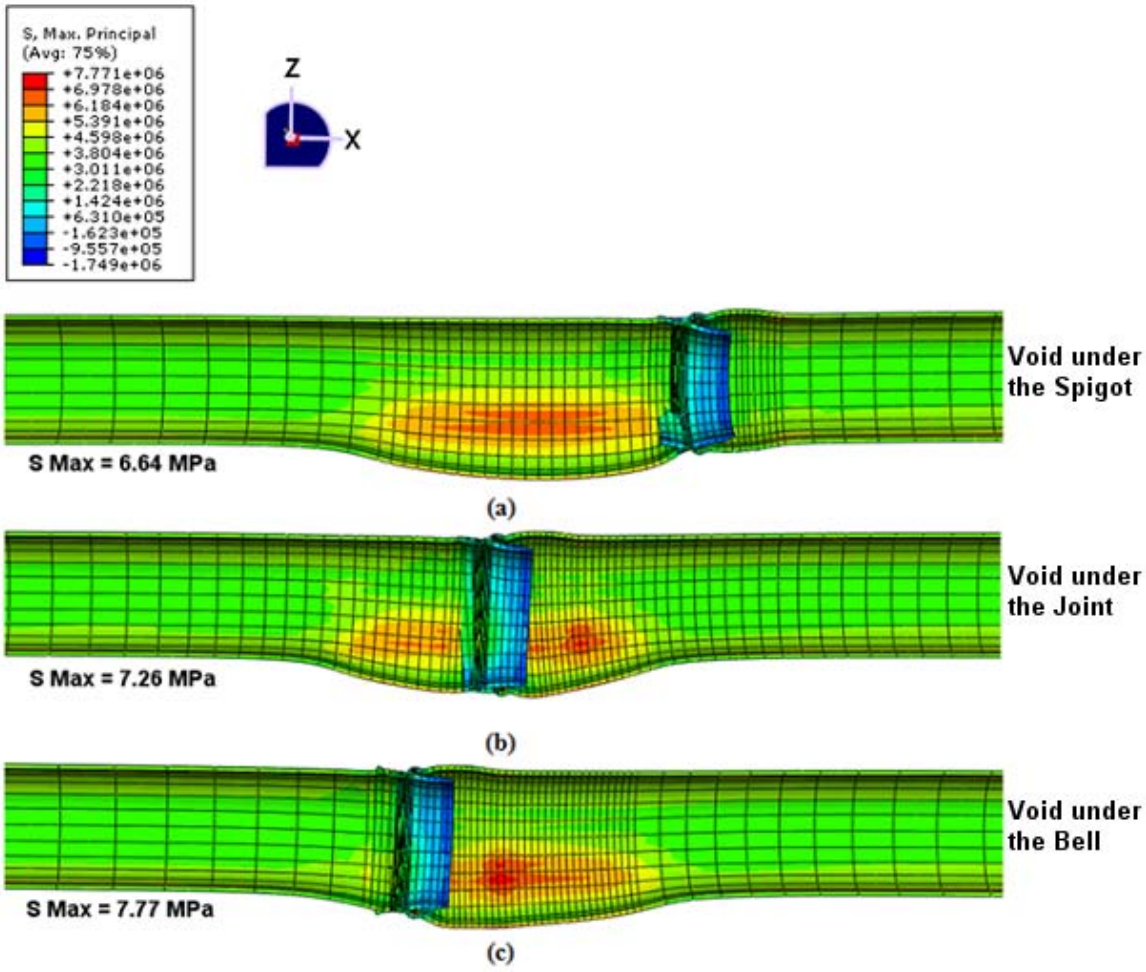

Figure A.17 Comparison of bending along the pipe over the void for void length of 30cm, and void angle under the invert of 60° (a) void under the spigot, (b) void under the joint, (c) void under the bell (deflections are magnified by 100); Balkaya et al., 2012.

A.4.4 Analysis of beams on elastic springs

First-generation analysis of the longitudinal response of buried pipe systems generally employs 'beam-on-elastic-spring' models for the pipe and the soil in which it rests (following the classic text of Hetenyi, 1946). These analyses:

a. model the pipe as a beam with specific value of flexural rigidity (*EI*, dependent on the Young's modulus of the pipe material *E* and the second moment of area of the whole pipe cross-section about a horizontal diameter, *I*)

b. a 'Winkler' (elastic spring) model for the soil where the vertical force applied by the soil to the pipe, per unit length along the pipe axis, is expressed as a function of the spring (Winkler) stiffness of the soil *k* (or sometimes *E'*) times the vertical deformation at that point on the pipeline.

This approach makes no attempt to model the local circumferential stresses around the pipe circumference, but represents all stresses in the form of stress resultants, that is the total vertical shear force acting across the pipe wall, the total longitudinal bending moment, and sometimes the axial force (where the model is also representing axial force and deformation). Examples of these analyses used for Civil pipe infrastructure include the work of Jeyapalan and Abdel-Magid (1987), Rajani et al. (1996) and Rajani and Tesfamariam (2004). The model representation of Jeyapalan and Abdel-Magid (1987) is shown in Figure A.18. Three pipes were modeled, though nonuniform support was focused on the central pipe segment. Joint characteristics were neglected, and the beam was essentially modeled as continuous (full moment transfer without rotation was modeled between pipe segments at the joints). Beam-on-elastic-spring analyses have been extended by the oil and gas pipeline community to include explicit modeling of the pipe structure (as a circular shell), restrained using elastic springs on the outside surface both around the circumference and along the pipe axis. These pipelines are generally very long, continuous pipelines (featuring welded connections), and loading is dominated by high internal pressures rather than the external earth or fluid loads. Existing models in this field have limited relevance to the current study on jointed culvert structures.

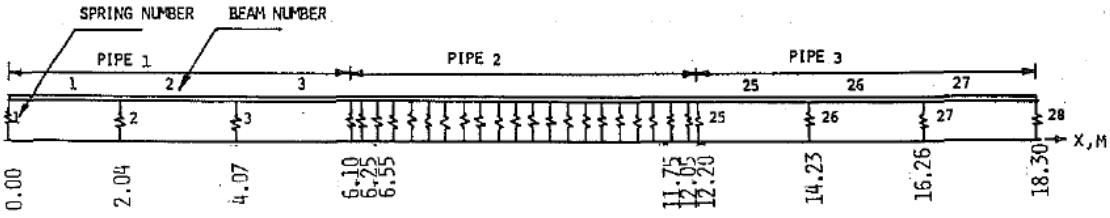

Figure A.18 Spring model of Jeyapalan and Abdel-Magid (1987), showing individual spring numbers referenced in their analysis.

In their study, Jeyapalan and Abdel-Magid (1987) provided a list of spring stiffness values to represent each of the bedding conditions they defined (shown earlier in Figure A.8). These are presented in Table A.5 and Table A.6 below. While the pipe stiffness values are not relevant to the current study, the spring stiffness values may be of value in the beam-on-elastic-spring modeling to determine behavior (stress resultants and deformations) at joints.

Table A.5 Pipe and support properties used by Jeyapalan and Abdel-Migid (1987).

Installation condition (1)	Pipe diameter (m) (2)	Moment of intertia at barrel I_B (m^4) (3)	Moment of inertia at connection I_c (m^4) (4)	Modulus of elasticity E (kN/m^2) (5)	Spring stiffness K (kN/m^2) (6)	UD load intensity (kN/m) (7)	Support settlement at bell (m) (8)
Normal	1.22	0.0086	0.054	13.8×10^3	383.0	52.7	0.0
Overdug Bell Hole	1.22	0.0086	0.054	13.8×10^3	4.30	52.7	0.05
Mounds in Stiff Bedding	1.22	0.0086	0.054	13.8×10^3	3,926.0	62.0	0.05
Mounds in Soft Bedding	1.22	0.0086	0.054	13.8×10^3	3,638.0	57.6	0.05
Underdug Bell Hole	1.22	0.0086	0.054	13.8×10^3	3,352.0	52.7	0.0

Table A.6 Individual spring values used by Jeyapalan and Abdel-Migid (1987).

Installation condition (1)	Spring numbers 1, 2, 3, and 26, 27, 28[a] (kN/m) (2)	Spring numbers 4, 5, 24, 25 (kN/m) (3)	Spring numbers 9 and 20 (kN/m) (4)	Rest of springs (kN/m) (5)
Normal	773.0	58.4	117.0	117.0
Overdug Bell Hole	773.0	0.73	117.0	117.0
Mounds in Stiff Bedding	773.0	58.4	1,197.0	117.0
Mounds in Soft Bedding	773.0	58.4	1,109.0	117.0
Underdug Bell Hole	773.0	511.0	117.0	58.4

The local circumferential stresses are not examined in beam-on-elastic-spring models since the primary focus is on axial stress and strain resulting from longitudinal curvature. There are two other significant limitations of the Winkler approach. First is its characterization of vertical soil support to the pipe (vertical force per unit length transferred from the soil) in terms of the absolute pipe displacement. The second is the difficulty of interpreting how surface load attenuates through the ground and reaches the pipe (since there is no explicit representation of the overlying soil). The model neglects the impact of rigid body movements of the soil mass relative to the pipe, and it also neglects interaction through the soil from location to location. Klar et al (2005) provide a useful explanation of the limitations of spring models, in their discussion of pipes responding to differential ground movements associated with tunneling.

Benmansour et al. (1997) developed a beam-on-elastic-spring model considering two kinds of nonuniformities along the pipeline as discussed in an earlier section. Their model incorporated explicit representation of the pipe joints, where rotational stiffness between pipe segments defined as different from the flexural rigidity of the pipe barrel, Figure A.19. They used this to examine the impact of joint stiffness, and found this to be significant.

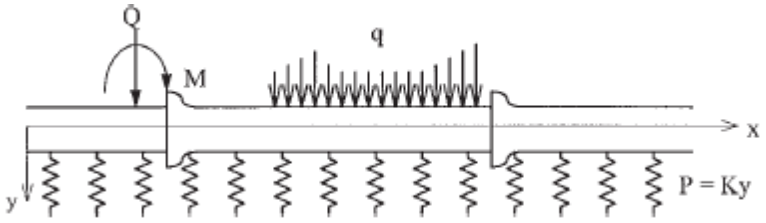

Figure A.19 Computational model of Benmansour et al. (1997)

Examples of other kinds of simplified longitudinal pipe bending models include the work of Poulos (1974) who studied longitudinal pipe bending due to surface load (the problem defined earlier in Figure A.14). His representation of the pipe is essentially the same as the ‘beam on spring’ models, but he used elastic continuum theory to develop a flexibility or stiffness matrix for the soil, rather than springs. This approach has the advantage that it introduces interaction through the soil, and is an improvement on springs while remaining relatively straightforward. It can also be adapted to consider loads on the ground surface.

In the three-dimensional finite element study of Trickey and Moore (2007), the performance of the Poulos approach was examined in comparisons to their three-dimensional elastic finite element solutions, and this shows that the Poulos solution has some shortcomings. Solutions for maximum deflection ρ_{max} and maximum longitudinal bending moment M are presented in Figure A.15 for a pipe with length L equal to 25 times its diameter d, and a range of burial depths c. These illustrate results for a range of pipe flexibility ratios K_r defined by elastic soil modulus E_s and structural properties

$$K_r = \frac{EI}{E_s L^4}$$

They demonstrate that the peak moment and deflection obtained by Poulos were reasonable (his peak moments appear somewhat conservative). However, he calculated these to reach peak values for pipe at some depth below the ground surface (rather than when the pipe is directly at the ground surface as one might expect).

A.5 Summary and conclusions

A.5.1 Design criteria

A.5.1.1 Current practice

Current design is semi-empirical, and is largely the responsibility of product manufacturers (pipe suppliers and joint component suppliers). Design of joint components (e.g. gaskets) is generally conducted by third parties (e.g. gasket suppliers), based on experience.

A.5.1.2 Demand (expected deformations and forces across joints)

There has been almost no study of demand. The exception would be the beam-on-elastic-spring analyses that have attempted to determine behavior at the joint using idealized ground support conditions (different kinds of nonuniform bedding, for example). Therefore, work is needed for a range of different pipe geometries, pipe types, and burial conditions, to:

- assess shear force that will act across the joint
- assess bending force that will act across the joint
- assess axial force that will act across the joint
- assess expected magnitude of rotation of one pipe relative to the other across the joint
- assess expected magnitude of vertical translation of one pipe relative to the other across the joint
- assess the expected magnitude of axial displacement of one pipe relative to the other across the joint

A.5.1.3 Resistance (ability to accommodate expected deformations and forces)

Section 26.4 of the current AASHTO Bridge Specifications provide information on the requirements for:

- capacity of the joint to resist shear force, perhaps expressed as a percentage of the capacity of the pipe barrel to resist shear force

- capacity of the joint to resist moment, perhaps expressed as a percentage of the capacity of the pipe barrel to resist moment
- capacity of the joint to resist axial tension, perhaps expressed as a percentage of the total required axial force capacity of the pipe barrel

There do not appear to be any generic requirements for the joint to tolerate specific amounts of movement across the joint:

- vertical displacement
- rotation (except that joint leakage tests in the laboratory based on ASTM C443-05a, for example, examines leakage after rotation opening the joint by 0.5 in. (13 mm) at one point on the external circumference
- axial extension or compression

A.5.1.4Leakage at joints

To date, there appear to be no clear directives regarding contact pressures required between components of the joint system (the pressures between rubber gasket and bell, and rubber gasket and spigot, for example). Instead, joint performance in laboratory tests and in the field has been examined after product development (using inspection, as well as pressure and vacuum tests). This left manufacturers to adjust their products when they considered that inadequate performance was affecting product sales or profitability.

Proprietary information may exist regarding details of gasket design, or other aspects of interaction across the joint to prevent soil or water movement through the joint. However, if so, this is not published and does not provide a standard framework on which to base a design.

A.5.1.5Construction conditions

A number of nonuniform bedding and loading conditions have been identified by researchers featuring

i. voids under specific parts of the pipe
ii. pipe resting on the bell or hard regions in the bedding
iii. pipe moving from regions featuring one kind of soil materials, to a second region with different kind of soil present
iv. surface loads above the joint, or applied mid-span

There are no explicit statements or requirements for pipe design to resist longitudinal bending as a result of specific construction conditions i.e. surface loads, changes in soil bedding stiffness or complete loss of bedding (say as a result of a void under the pipe).

The large scale laboratory tests undertaken on six different pipe products include components of all these sources of nonuniform bedding and loading conditions. The proposal is to have two tests examining:

i. poor burial, where voids occur under the pipes, or soil is not compacted adequately, followed by surface loading over the joints or some distance from the joints
ii. good burial in accordance with AASHTO practice (where pipes are placed on soft uniform bedding, and where backfill is placed and compacted besides and over the pipe)

A.5.2 Laboratory testing

A.5.2.1 Standard tests for joint leakage (undistorted and distorted)

Tests like ASTM C969. C924, C1103 and C1214 are likely effective measures of joint leakage. However, they do not provide guidance on limiting pressures (those that initiate leakage), and cannot be used to infer the long-term leakage performance of rubber or other time dependent gasket and pipe materials (e.g. time dependent movement of the bell and spigot in HDPE pipes). For internal pressure, it may be possible to develop a test where the internal pressure of water within the pipe is increased steadily, to measure the pressures needed to initiate leakage. This might then be adapted to conduct long-term studies, to see how time to failure of specific systems under sustained pressure is related to the fraction of internal pressure that is applied. Unfortunately, vacuum testing limits application of external pressure to one atmosphere, and ingress of water is likely a more serious issue for culvert structures than for pressure pipes.

The leakage testing defined in ASTM D3212 includes leakage assessment for local pipe deformation to 5%. The leakage testing defined in ASTM C 1628 includes assessment for reinforced concrete pipes where axes are rotated across the joint (rotation angle dependent on pipe diameter; the extent of rotation is fixed by the length of gap change across the joint at one point on the external joint circumference). These tests might be used directly, or adapted to permit a single standard test protocol that is effective for both flexible and rigid culverts. First, however, these test conditions need to be placed in the context of field loading conditions, either through the field survey, the computer analyses, or the laboratory or field test results.

The current project deals with the structural design of culvert joints, rather than the design and performance of joint seals. Leakage testing, therefore, should be the subject of future projects.

A.5.2.2 Standard tests for joint strength and stiffness

The AASHTO Bridge Design specifications feature statements about required capacity of joints in shear and moment as a proportion of barrel strength, and an axial force of a specified magnitude of axial pulling force. However, test methods for measuring moment, shear and axial force capacity in the pipe or across the pipe barrel are not specified. A joint testing frame was therefore developed (as reported in Appendix H) to examine joints in shear and bending (or rotation).

A.6 Reference list

A.6.1 Standards and design manuals

American Association of State Highway and Transportation Officials (AASHTO). 2009. 2nd edition of the AASHTO LRFD Bridge Construction Specification, Section 26.4.2.

American Society of Testing and Materials (ASTM) A760-09 Corrugated Steel Pipe, Metallic-Coated for Sewers and Drains ASTM International, 100 Barr Harbor Drive, PO Box C700, West Conshohocken, PA, 19428-2959 USA

American Society of Testing and Materials (ASTM) A796-06 Structural Design of Corrugated Steel Pipe, Pipe-Arches, and Arches for Storm and Sanitary Sewers and Other Buried Applications, ASTM International, 100 Barr Harbor Drive, PO Box C700, West Conshohocken, PA, 19428-2959 USA

American Society of Testing and Materials (ASTM) A798-07 Practice for Installing Factory-Made Corrugated Steel Pipe for Sewers and Other Applications ASTM International, 100 Barr Harbor Drive, PO Box C700, West Conshohocken, PA, 19428-2959 USA

American Society of Testing and Materials (ASTM) C 76-08 Standard Specification for Reinforced Concrete Culvert, Storm Drain, and Sewer Pipe, ASTM, ASTM International, 100 Barr Harbor Drive, PO Box C700, West Conshohocken, PA, 19428-2959 USA

American Society of Testing and Materials (ASTM) C 443-05a, Joints for Circular Concrete Pipe and Manholes, Using Rubber Gasket, ASTM International, 100 Barr Harbor Drive, PO Box C700, West Conshohocken, PA, 19428-2959 USA

American Society of Testing and Materials (ASTM) C 497-05, Standard Test Methods for Concrete Pipe, Manhole Sections, or Tile, ASTM International, 100 Barr Harbor Drive, PO Box C700, West Conshohocken, PA, 19428-2959 USA

American Society of Testing and Materials (ASTM) C 877-08 , External Sealing Bands for Noncircular Concrete Sewer, Storm Drain and Culvert Pipe, ASTM International, 100 Barr Harbor Drive, PO Box C700, West Conshohocken, PA, 19428-2959 USA

American Society of Testing and Materials (ASTM) C 924-02, Standard Procedure for Testing Concrete Pipe Sewer Lines by Low-Pressure Air Test Method, ASTM International, 100 Barr Harbor Drive, PO Box C700, West Conshohocken, PA, 19428-2959 USA

American Society of Testing and Materials (ASTM) C 969-02, Standard Practice for Infiltration and Exfiltration Acceptance Testing of Installed Precast Concrete Pipe Sewer Lines, ASTM International, 100 Barr Harbor Drive, PO Box C700, West Conshohocken, PA, 19428-2959 USA

American Society of Testing and Materials (ASTM) C 990-09, Joints for precast concrete pipe and box, and other sections using preformed flexible joint sealants for use in storm sewers and culverts, ASTM International, 100 Barr Harbor Drive, PO Box C700, West Conshohocken, PA, 19428-2959 USA

American Society of Testing and Materials (ASTM) C 1103–03, Joint Acceptance Testing of Installed Precast Concrete Pipe Sewer Lines, ASTM International, 100 Barr Harbor Drive, PO Box C700, West Conshohocken, PA, 19428-2959 USA

American Society of Testing and Materials (ASTM) C 1214-02, Test Method for Concrete Pipe Sewerlines by Negative Air Pressure (Vacuum), ASTM International, 100 Barr Harbor Drive, PO Box C700, West Conshohocken, PA, 19428-2959 USA

American Society of Testing and Materials (ASTM) C1628-06, Joints for Concrete Gravity Flow Sewer Pipe, Using Rubber Gaskets, ASTM International, 100 Barr Harbor Drive, PO Box C700, West Conshohocken, PA, 19428-2959 USA

American Society of Testing and Materials (ASTM) D3212–07 Joints for Drain and Sewer Plastic Pipes Using Flexible Elastomeric Seals, ASTM International, 100 Barr Harbor Drive, PO Box C700, West Conshohocken, PA, 19428-2959 USA

American Society of Testing and Materials (ASTM) F477–08 Elastomeric Seals (Gaskets) for Joining Plastic Pipe ASTM International, 100 Barr Harbor Drive, PO Box C700, West Conshohocken, PA, 19428-2959 USA

American Society of Testing and Materials (ASTM) F667–06 Large Diameter Corrugated Polyethylene Pipe and Fittings ASTM International, 100 Barr Harbor Drive, PO Box C700, West Conshohocken, PA, 19428-2959 USA

American Society of Testing and Materials (ASTM) F1417–05 Standard Test Method for Installation Acceptance of Plastic Gravity Sewer Lines Using Low-Pressure Air ASTM International, 100 Barr Harbor Drive, PO Box C700, West Conshohocken, PA, 19428-2959 USA

American Society of Testing and Materials (ASTM) F1668–08 Standard Guide for Construction Procedures for Buried Plastic Pipe ASTM International, 100 Barr Harbor Drive, PO Box C700, West Conshohocken, PA, 19428-2959 USA

American Concrete Pipe Association (ACPA) Concrete Pipe Design Manual (accessed September 2009)

Canadian Standards Association (CSA) A257.3-03 Joints for circular concrete sewer and culvert pipe, manhole sections, and fittings using rubber gaskets, CSA Standards, 5060 Spectrum Way, Suite 100 Mississauga, Ontario L4W 5N6 CANADA

Corrugated Steel Pipe Institute, 2002. Handbook of Steel Drainage and Highway Construction Products, 481 pp.

A.6.2 Articles

Arockiasamy, M. Chaallal, O., and Limpeteeprakarn, T. 2006. Full-Scale Field Tests on Flexible Pipes under Live Load Application, J. Perf. Constr. Fac. 20, 21.

Balkaya, M. and Moore, I.D. 2009. Analysis of a gasketted PVC pipe-joint, Transportation Research Record, Transportation Research Board, Washington D.C. (Paper No. 09-3101), Number 2131, pp. 113-122.

Balkaya, M. Moore, I.D. and Sağlamer, A. 2012. Study of nonuniform bedding due to voids under jointed PVC water distribution pipes, Geotextiles and Geomembranes, article GEGE 1736, posted online Feb 21, 2012.

Benmansour, A., Abdallah, A., Masrouri, F. and Auginet, G. 1997. Analyse fiabiliste du comportement axial des conduites d'assainissement, Canadian Geotechnical Journal, 1997, 34, pp 329-343 (Reliability analyses of axial behavior of sewer pipes).

Brachman, R.W.B., Elshimi, T., Mak, A. and Moore, I.D. 2011. Testing and Analysis of a Deep-corrugated Large-span Box Culvert Prior to Burial, Journal of Bridge Engineering, ASCE, doi:10.1061/(ASCE)BE.1943-5592.0000202.

Buco, J. 2007. Analyse et modélisation du comportement mécanique des conduites enterrées, PhD thesis, Department of Civil Engineering, INSA, Lyon, 286pp.

Buco, J.; Emeriault, J.; Le Gauffre, P. and Kastner, K. 2006. Statistical and 3D numerical identification of pipe and bedding characteristics responsible for longitudinal behavior of buried pipe, Pipelines 2006, ASCE, 10pp.

Buco, J.; Emeriault, J.; and Kastner, K. 2008. Full-Scale Experimental Determination of Concrete Pipe Joint Behavior and Its Modeling, Journal of Infrastructure Systems, ASCE, Vol. 14(3)_230-240.

Dittel, C. and Quasada, G. 2008. Innovation by Evolution Modern Techniques for Integral Pipe Joint design, ASCE Pipelines 2008, Atlanta, GA

Duncan, J.M. 1979. Behavior and Design of Long-Span Metal Culverts, *Journal of the Geotechnical Engineering Division*, Vol. 105, No. 3, March 1979, pp. 399-418

Elachachi, S. M., Breysse, D., Houy, L. 2004. Longitudinal variability of soils and structural response of sewer networks, Computers and Geotechnics, Vol. 31, p 625–641.

Fernando, N. S. M., Small, J. C. and Carter, J. P. 1996. Elastic analysis of buried structures subject to three-dimensional surface loading, Int. J. Numer. Anal. Meth. Geomech., 20, 331-349.

Hetenyi, M. 1946. Beams on Elastic Foundation, University of Michigan Press, Ann Arbor, Mich.

Jeyapalan, J.K. and Abdel-Magid, B. M. 1987. Longitudinal Stresses and Strains in Design of RPM Pipes. J. of Transportation Engineering, ASCE, 113(3), pp. 315-331.

Katona, M.G. 1978. Analysis of long-span culverts by the finite element method. Transportation Research Record 678, TRB, National Research Council, Washington DC pp. 59-66.

Katona, M.G. and Akl, A.Y. 1987. Design of buried culverts with stress-relieving joints. Transportation Research Record 1129, TRB, National Research Council, Washington DC pp. 39-54.

Kienow, K.K., 1998. Pipe Joint Failure Caused by an Inadequately Specified Constructed Environment, Proceedings, Pipelines in the Constructed Environment, ASCE Pipeline Division Conference, San Diego CA, 433-450.

Klar, A., Vorster, T. E. B., Soga, K., and Mair, R. J. (2005). Soil-pipe-tunnel interaction: Comparison between Winkler and elastic continuum solutions. Geotechnique, 55(6), 461-466.

Kurdziel, J.M. 2002. Design of Profile Gaskets, Transportation Research Board Annual Conference, Paper 02-2828 Washington, D.C. January.

Kurdziel, J.M. 2004. Design of Profile Gaskets for Corrugated Polyethylene Pipe, Pipelines 2004 146, 85.

Moore, I.D. and Brachman, R.W., 1994. Three-dimensional analysis of flexible circular culverts. Journal of Geotechnical Engineering, American Society of Civil Engineers, Vol. 120, No. 10, pp. 1829-1844.

Moore, I.D. and B. Taleb, 1999. Metal culvert response to live loading Performance of three-dimensional analysis. Transportation Research Record No. 1656, Underground and Other Structural Design Issues. National Research Council, Washington, pp. 37-44.

Mueller, R.I. 1998. Practical Repair Procedures for Concrete Pressure Pipe, Proceedings, Pipelines in the Constructed Environment, ASCE Pipeline Division Conference, San Diego CA, p. 742-751.

Pearson, F. H. 1977. Beam Behavior of Buried Rigid Pipelines, Journal of the Environmental Engineering Division, ASCE, 103(5), pp. 767-784.

Poulos, H. G. 1974. Analysis of longitudinal behavior of buried pipes. Proc., Conf. on Analysis and Design in Geotechnical Engineering, ASCE, Austin, Tex., 189–223.

Rahman, S. and Watkins, R.K. 2005. Longitudinal mechanics of buried thermoplastic pipes: analysis of PVC pipes of various joint types, Pipelines 2005, ASCE, 1105-1116.

Rajani, B., Zhan, C., and Kuraoka, S. 1996. Pipe-soil interaction analysis of jointed water mains. Can. Geotech. J., 33, 393–404.

Rajani, B. and Tesfamariam, S. 2004, Uncoupled axial, flexural, and circumferential pipe–soil interaction analyses of partially supported jointed water mains Canadian Geotechnical Journal, 41, 997-1010.

Roberts, B.C. 2002. Coupling Systems for Corrugated Steel Pipe, Transportation Research Board Annual Conference, Paper 02-4092 Washington, D.C. January.

Romer, A.E. and Kienow, K.K. 2004. Rubber Gasket Concrete Pipe Joints[ellipsis (horizontal)]Eliminating the Smoke and Mirrors, Pipelines 2004 146, 86

Toliver, T. 2002. Joint Design and Analysis for 36-in. Corrugated High-Density Polyethylene Pipe, Transportation Research Board Annual Conference, Paper 02-4134, Washington, D.C. January.

Trickey, S.A. and Moore, I.D. 2007. Three-dimensional response of buried pipes under circular surface loading, Journal of Geotechnical and Geoenvironmental Engineering, ASCE, Vol. 133(2), pp. 219-223.

Survey of Culvert and Joint Usage and Performance, US DOTs

Contents

B.1 Survey input

The survey of DOTs featured input from the 23 States and one Province, arising from the individuals listed in Table B.1. These States represent 69% of the US population occupying 50% of the land area. The survey form used is shown at the end of the appendix. Thirteen of the states completed the second table in the survey, related to joint performance, while five others provided some input on joint performance. Seven States and one Province provided additional input on specific issues affecting culvert joints and these details are recorded at the end of the Appendix.

A number of states indicated that they do not keep data on culvert or joint usage or performance.

B.2 Culvert usage.

Table B.2 provides a summary of culvert types in use. Of those states where usage rates were indicated

- all states except PA indicated that reinforced concrete (RCP) culverts were common
- most states use corrugated steel pipes (CSP), though usage ranged from ‘most’ in PA, to rare in some Atlantic states (FL, MA, NH; no usage in SC)
- many jurisdictions have some usage of corrugated aluminum pipes (CAP), particularly those in Atlantic states
- use of HDPE and PVC pipes is variable; most States use these to some extent (except MA; HDPE rare and PVC never used in SD; use of HDPE and PVC is rare in TX; AR permits these as side drains only)

Based on this assessment, the strategy to test RCP, CSP and thermoplastic pipes in the laboratory and in the field appears reasonable, since they are all in use. There is no plan to test corrugated aluminum pipes, since in most jurisdictions they are rare, and they are also expected to have characteristics similar to corrugated steel.

B.3 Joints in reinforced concrete pipes

Two joint types were predominant for reinforced concrete pipes:

i. bell and spigot with gasket is common or the dominant joint type used in seven states; only five states indicate no usage of this joint option;

ii. tongue and groove joints (generally featured in larger diameter pipes) is used with mastic in sixteen states; usage of this configuration represents most installations in four states, it is common in four, and it sees some use in eight others; three states indicate use without providing frequency; UT indicates usage is rare and nine states imply no usage of this option.

Four states indicate that tongue in groove joints are commonly used without a seal, though one of these (MN) requires a Geotextile wrap to prevent fines migration. Four others indicate some or rare use of these unsealed joints.

Four states indicate that it is common to use tongue and groove joints with a gasket (AR indicated use without providing frequency, though use is likely common since no other joint options are listed RCP with tongue and groove).

Performance of joints with gaskets (bell and spigot or tongue and groove) was generally rated as good (ten states), though KS rated these as satisfactory and MN as variable (some good, some poor).

Performance of joints with mastic sealant was rated as good (three states), satisfactory (five states), and variable (MN).

Performance of joints without sealant was given different ratings by different states: good (two states), satisfactory (three states), variable (MN), and poor (UT and VA).

B.4 Joints in corrugated steel pipes

Sixteen states indicated use of band joints to connect CSP without gaskets, and ten indicated use of band joints with O rings (MN indicated this was used rarely). Sleeve gaskets were employed in seven states (rarely in DE, sometimes in FL, and unstated frequency in CA, IL and UT). Three states indicated use of CSP with gasketted bell and spigot joint.

Many states rated performance of joints in CSP as satisfactory. However, UT indicated that gasketted bell and spigots were poor (likely due to pull-out), bands with O rings were rated as variable in CT and good in CA, MO, VA and WS, and performance of band joints without gaskets was rated as good in CA and SD, and variable in AZ, CT and some parts of VA.

B.5 Joints in HDPE and PVC pipes

With only some exceptions, thermoplastic pipe usage features gasketted bell and spigot joints. Mastic joints were referenced in AZ and CO, and joints with flexible seal were indicated in IL.

B.6 Choices for buried pipe testing in the laboratory

Two laboratory tests were undertake for reinforced concrete pipes, two for corrugated steel, and one each for HDPE and PVC. These were chosen as follows:

I. 24in. (small) diameter RCP with bell and spigot joint, sealed with a gasket; this is the most common configuration for small diameter (bell and spigot) RC pipes in the field
II. 48in. (medium) diameter RCP with tongue and groove, sealed with mastic; is the most common configuration for larger diameter reinforced concrete pipe (tongue and groove) in the field; however, mastic is almost never used with new structures; instead, gaskets are used if the joint needs to be sealed; otherwise, the joint is left without sealant. Since the 24 inch diameter pipe featured a gasketted joint, the 48 inch diameter pipes were tested without seals.
III. 36 in. CSP with band and without seal; this is the most common configuration for CSP
IV. 36in. CSP with band and two O rings; this is the second most common configuration for CSP
V. 60in. HDPE pipe with gasketted bell and spigot joint
VI. 36in. PVC pipe with gasketted bell and spigot joint

Table B.1 Survey respondents

Jurisdiction	Name	Position	Type	Performance	% area	% pop.
Alabama	Butch Bolling	Materials Engineer	Yes	No	1.5%	1.5%
Arizona	Ken Akoh-Arrey	Chief Drainage Engineer	Yes	Yes	3.2%	2.2%
Arkansas	Michael C. Benson	Materials Engineer	Yes	No	1.5%	1.0%
California	Glenn DeCou	Chief, Drainage Design	Yes	Yes	4.6%	12.1%
Colorado	Scott Rees	Area Engineer	Yes	Yes	2.9%	1.6%
Connecticut	Michael Masayda	Transp. Principal Engineer	Yes	Yes	0.2%	1.2%
Delaware	Jim Pappas	Materials & Research Eng.	Yes	No	0.1%	0.3%
Florida	Rick Renna	State Drainage Engineer	Yes	Yes	1.9%	6.0%
Illinois	Gary Kowalski	Chief, Policies, Stnds, Specs	Yes	No	1.6%	4.2%
Kansas	Jim Richardson	Road Design Leader	Yes	Yes	2.3%	0.9%
Louisiana	L.J. Tulier	Engineering Tech. DCL	Yes	Yes	1.5%	1.4%
Massachusetts	John Grieco	Dir. of Research & Materials	Yes	Some	0.3%	2.1%
Minnesota	Andrea Hendrickson	State Hydraulic Engineer	Yes	Some	2.5%	1.7%
Montana	Mark Goodman	Hydraulic Engineer	Yes	Yes	4.2%	0.3%
New Hampshire	Alan Rawson	Admnstrtr Bureau Mat.&Res.	Yes	Yes	0.3%	0.4%
Ontario (Canada)	Art Groenveld	Sr. Engr, Drainage Design	Yes	No	C(10.8%)	C(34.3%)
Pennsylvania	Beverly Miller	Civil Engineer Consultant	Yes	No	1.3%	4.1%
South Carolina	Henry Cross	Design Standards Engineer	Yes	Some	0.9%	1.5%
South Dakota	Unknown	Unknown	Yes	Yes	2.2%	0.3%
Tennessee	Bill Trolinger	Assistant Materials Engineer	Yes	Yes	1.2%	2.0%
Texas	McClelland / Freeby	Bridge Engineer	Yes	Yes	7.6%	8.2%
Utah	Denis Stuhff	Sr. Hydraulic Engineer	Yes	Yes	2.4%	0.9%
Virginia	John Schuler	State Geotech. Program Mngr	Yes	Yes	1.2%	2.6%
Washington	Matt Witecki	State Hydraulics Engineer	Yes	Some	2.0%	2.1%

Table B.2 Culvert usage: y=yes (extent not indicated), m=most; c=common; s=some; r=rare; n=never

State	AL	AR	AZ	CA	CO	CT	DE	FL	IL	KS	LA	MA	MN	MO	NH	OH	ON	PA	SC	SD	TN	TX	UT	VA	WS
RCP	m	y	y	y	y	y	m	c	y	y	m	c	m	y	y	y	y	s	y	m	c	y	y	c	c
CSP	c	y	y	y	y	y	s	r	y	y	s	r	s	y	r	y	y	m	n	c	c	s	y	c	c
CAP	r	y	n	y	y	y	r	s	y	y	s	r	r	y	y/n		y	r	y	n	r	r	y	c-r[1]	r
HDPE	y	sdo[2]	y	y	y	y	s	s	y	y	s	n	s	y	y	y	y	r	y	r	s	r	y	c-r	c
PVC	y	sdo	y	y	y	y	r	s	y	y	s	n	r	y	y/n	y	y	r	y	n	r	r	y	c-r	r

Table B.3 RCP joints usage: x=used but frequency not indicated; m=most; c=common; s=some; r=rare; n=never
performance: (g)=good; (s)=satisfactory; (v)=variable; (p)=poor

State	AL	AR	AZ	CA	CO	CT	DE	FL	IL	KS	LA	MA	MN	MO	NH	OH	ON	PA	SC	SD	TN	TX	UT	VA	WS
bell & spigot with gasket[3]	y	y		y (g)	m	m (g)	m	c (g)	y	m (s)	m (g)		c (v)	c (g)	c (g)		y		m	r (g)			m (g)	r (g)	m (g)
tongue & groove & gasket		y		y (g)				c (g)					c (v)												
tongue & groove - no gasket			m (s)										c[4] (v)							m (g)	c (g)	r (s)	r (p)	r (p)	s (s)
tongue & groove & mastic	y			y[5] (g)	m (g)	s (s)	s - ell[6]		y			m (s)	c (v)	c (s)			y	c	s	s (g)		m (s)	r (s)	m	
preformed rubber seal									y															s (s/g)[7]	

[1] c-r=common in some parts of VA, rare in others
[2] sdo=side drains only
[3] sometimes called the single off-set joint
[4] must have Geotextile wrap if used without sealant
[5] mastic or at least mortar.
[6] ell= large elliptical pipes
[7] will perform if placed in the right conditions

Table B.4 CSP joints usage: y=used but frequency not indicated; a=all; m=most; c=common; r=rare; n=never
performance: (g)=good; (s)=satisfactory; (v)=variable; (p)=poor

State	AL	AR	AZ	CA	CO	CT	DE	FL	IL	KS	LA	MA	MN	MO	NH	OH	ON	PA	SC	SD	TN	TX	UT	VA	WS
bell & spigot & gasket											y (s)										y		y (p)		
band with sleeve gasket				y (g)	s		r	s	y								y						y (s)		
band with O rings				y (g)	s	y (v)	m				y (s)		r	s (g)			y							c (g)	a (g)
band without gasket	c	y	a (v)	y (g)	s	y (v)				m (s)			m[4] (s)	c (v)	s (s)		y	c		a (g)	y (s)	a (s)		c (s/v)	
welded																	y								
threaded																	y								

Table B.5 HDPE: y=used; m=most; c=common; r=rare; n=never; performance: g=good; s=satisfactory; v=variable; p=poor

State	AL	AR	AZ	CA	CO	CT	DE	FL	IL	KS	LA	MA	MN	MO	NH	OH	ON	PA	SC	SD	TN	TX	UT	VA	WS
bell & spigot & gasket	y			m (g)	m	m (g)	m	c (g)	y	m[8] (s)	x (v)		c					c			g	a (s)	x (g)		a (g)
bell & spigot – no gasket				n									s[4]												
band & sleeve gasket				s (g)			r							s						r				s(g)	
Band - no gasket		y												s	r (s)								x (p)		
mastic			a (g)		m (g)																				
flexible seal									y																

Table B.6 PVC: y=used; a=all; m=most; c=common; r=rare; n=never; performance: g=good; s=satisfactory; v=variable; p=poor

State	AL	AR	AZ	CA	CO	CT	DE	FL	IL	KS	LA	MA	MN	MO	NH	OH	ON	PA	SC	SD	TN	TX	UT	VA	WS
bell & spigot & gasket	x		m (s)	a (g)	m	m	m	m (g)	y	m[8] (s)	x (v)		c								m (g)	a (s)		r (v)	a (g)
bell & spigot – no gasket													s[4]											r (v)	
band & sleeve gasket															r (s)									s (g)	
weld or mastic					m (g)		r																		
flexible seal									y																

[8] Indicated use of mastic not a gasket.

B.7 Other input.

CO

RCP: Joint type: If contractor takes care with applying mastic sealant or o-ring and precautions when fitting together, most joints function properly. Majority of our problems with this pipe type are when the contractor does not apply the mastic on the bottom of the pipe, or if the bell/spigot connection is damaged during installation.

Pipe type: Corrugated Steel and Corrugated Aluminum. Joint type: Most installations are in fairly dry environments and/or for short runs (e.g. driveways) and see water for short periods of time, or a single section of pipe is of sufficient length so as a joint may not be needed. Installations that are in an environment that will not corrode or abrade the pipe invert, joints have functioned successful.

Pipe type: HDPE and PVC. Joint type: It is our experience that the bell and spigot joints of both of these pipe types provide a solid "snap tight" connection. If they are installed within deflection tolerances, it is expected that the joint will function well. I am unaware of any information (positive or negative) regarding the long term quality of these joints at CDOT.

MN:

MN indicated that Corrugated Metal Pipes (with band-type joints) do not have major joint separation issues, except for in flume (high slope) applications.
MN indicated that 10% of RCPs had at least one joint separate, and 2.6% of CSP had at least one joint separate.

MO:

Pipe type: Use a lot of CSP/SSPPC/RCP pipe on projects. Allow hydraulically equivalent pipe options for CSP/RCP/CAP pipe when appropriate and let the contractor select most cost effective. Also have to have equal service life. Use HDPE for approach pipes only in 18" and 24" diameter.
Joints in RCP: Require irrigation class joints for all storm drains, irrigation crossings, or live streams, so this means bell and spigot and o-ring gaskets. All intermittent or dry drainages involve mastic and tongue and groove.
Joints in CSP: Live streams require hugger bands and o-ring gaskets; Otherwise standard bands without gaskets.

ON:

Pipe type: MTO through the introduction of its MTO Gravity Pipe Design Guidelines May 2007 accepts the following pipe types for use on its highways provided that the pipe materials satisfy the following design parameters:

- Serviceability as defined by the Design Service Life (DSL) criteria;
- Durability defined by the Estimated Material Service Life (EMSL) of a pipe material;
- Hydraulic function as defined by the hydrology and hydraulic criteria defined by the MTO Highway Drainage Design Standards February 2008; and
- Structural integrity as defined through the relevant OPSS Height of Fill tables for an accepted pipe material.

Joint type: MTO has defined its pipe joint requirements as follows:

- High pressure restricting the movement of water and soil materials through the joint;
- Low pressure restricting soil movement through the joint but permitting some water movement through the joint; and
- No pressure which does not restrict water and soil movement through the joint.

Performance (give details if possible when performance is poor): MTO has implemented post installation inspections in 2009 for its contracts as warranted. This program will give base installed pipe conditions including joints. Long term inspections through its maintenance contracts is expected to give us a better assessment of the long term reliability and performance of the various joint types that are currently accepted for use on its contracts.

Experience with pipe joints is not well known at this time. Generally, the element of pipe failure seems to be more predominant as a result of pipe materials' inability to provide the long term service needs more so than joint failures. Some years down the road, MTO may have better information available than what we have today.

SC:

SCDOT does not have historical data on pipe joints installed within SCDOT rights-of-way, however, as the pipe specification SC-M-714 was developed, several aspects of joint performance were revealed.

- Mastic joint materials typically compress and will not "rebound" if pipe are repositioned, therefore they are less desirable than rubber gaskets in locations where infiltration and exfiltration are a concern. Mastic joint materials are only allowed on reinforced concrete pipe. SCDOT established a minimum 10 psi pressure rating for all joint types.

- Based on industry recommendations, a rubber gasketted pipe achieving a 13 psi pressure rating under laboratory conditions would be more suitable for locations where infiltration/exfiltration is a concern. AASHTO M 315 joints for RCP correspond to this configuration. SCDOT allowed the HDPE and Aluminum pipe industries to test their rubber gasketted pipe in a similar manner to evaluate the 13 psi pressure rating. Only 13 psi rubber gasketted joints are allowed in SCDOT coastal counties, and in other locations specified by the engineers.

Other joints such as field splices and cast in place concrete collars (not technically a joint) are allowed on a limited basis where required. These joints must be adequately protected to prevent soil migration.
Also, again based on industry recommendations, another major factor in joint performance is differential settlement between pipe segments. SCDOT developed minimum foundation requirements to help minimize poor joint performance due to differential settlement. This procedure is covered in SC-M-714 and the Standard Drawings.
The third major change in our specification that should improve joint performance is post installation inspection. Video camera inspection of installed pipe should help identify pipe that were not properly installed and allow these items to be corrected before projects are completed.
SCDOT implemented SC-M-714 in July 2007. As projects are completed and pipes are inspected, SCDOT should gain a better understanding of pipe performance. This process should also establish a baseline performance for pipe that can later be used for comparison to monitor long term performance of pipe.

TX:

RCP, T&G w/ mastic. The vast majority of pipe culvert installations on TxDOT projects are RCP. The most common joint type is tongue and groove with mastic. There have been some instances of the joints separating with accompanying leakage of water and infiltration of soil, but these instances are rare and generally do not lead to serious problems.

UT:

Band joint on HDPE is now obsolete – and was prone to piping of fines.

VA:

VDOT breaks state up into 9 districts, as well as having a central office in the capital city, Richmond; 3 districts and 1 central office engineer responded to this survey; in Virginia, soils east of I-95 (the natural Fall Line of states Atlantic-draining rivers) are acidic and generally clay or high clay/silt content and deep. In western districts soil mantle is generally shallow. Pipe joint materials are generally accepted on manufacturer's certification and/or in conjunction with an approved list. Most known problems with joints have been from misalignment. Pipe joints are not something typically inspected.

B.8 Survey form used to solicit information

Survey : Usage of specific culvert joints. For NCHRP 15-38. Please return by October 9, 2009 to, Ian Moore, moore@civil.queensu.ca .

2. Your name: 2. DOT:

3. Job title: 4. email:

Table 1. Usage of joints; Place approximate % of culverts and joints in this category, or use a word to indicate how common (e.g. all, most, common, some, rare, never) or tick if it occurs or is permitted but frequency is unknown.

Pipe Type	Usage permitted by DOT Yes/No or %	Bell and spigot & rubber gasket	Tongue and groove		Band-type			Other (please specify)	
			Mastic sealant	No sealant	No gasket	O-ring(s)	Sleeve Gasket		
Reinforced concrete									
Corrugated steel									
Corrugated Aluminum									
HDPE									
PVC									

Table 2. Overall performance of joints (if you do cannot provide this, please return the survey without this information): Use G (good), S (satisfactory), V (variable i.e. some good, some poor), P (many poor)

Pipe Type	Bell and spigot & rubber gasket	Tongue and groove		Band-type			Other (please specify)	
		Mastic sealant	No sealant	No gasket	O-ring(s)	Sleeve Gasket		
Reinforced concrete								
Corrugated steel								
Corrugated Aluminum								
HDPE								
PVC								

Further details of experience with specific joint types (repeat page as needed)

Pipe type

Joint type

Performance (give details if possible when performance is poor).

B.9 Detailed data provided on performance of culvert joints by Florida DOT

B.9.1 Introduction

This appendix describes experience in Florida regarding the performance of culvert joints. The objectives of this work are to

- collect information regarding issues affecting performance of culvert joints,
- document the principal concerns of Florida DOT staff regarding culvert performance, and
- examine performance of joints in reinforced concrete, corrugated steel, and thermoplastic (HDPE and PVC) culverts.

The information was gathered during a two day visit to Florida by Dr Moore in February 2010. Meetings were held with Mr. Rick Renna (State Drainage Engineering) and his colleague Mr. Larry Ritchie. Further information was collected from their colleagues. The information was supplied through verbal communications and records of pipe inspections.

B.9.2 Key concerns

The four top issues associated with culverts reported by Florida DOT are

- gaps at joints
- leaks at joints
- pipe deflections
- cracks in reinforced concrete culverts

The first two of these four are associated with joints. Approximately 80% of problems are associated with two issues: 40% of problems concern cracks in concrete pipes, and 40% concern problems joints.

FDOT policy is to:

1. insist on water tight joints, permitting no leakage (soil tight joints are no longer accepted)
2. inspect pipes early, after cover soil reaches 3ft
3. design joints to withstand external water pressure of up to 20ft head (very rarely more); use of a 5 psi (35 kPa) water pressure design limit covers most installations (this corresponds to 12ft or 3.5m of head); this may be increased if a specific project requires it

4. inspect pipes and pipe joints using laser ring profilers and video micrometer inspection measuring gaps across the joints; many producers do not meet the specification

The DOT is developing joint gap measurement protocols. The goal is to have protocols that are objective and repeatable. This is complicated by the fact that there are no standards for the inspection equipment (though the WRc has a standard, it is not very technical and is not considered adequate). Inspection equipment from three sources is being used. Unfortunately inspection reports are difficult to read, being different from each contractor. Currently work is underway to standardize reporting, and to tighten calibration criteria. One company has developed a test bench – a standard referencing tool for calibration of their equipment. Another company is working to develop an ASTM standard for 3D profilers. These developments are needed so that pipe laying contractors cannot reasonably criticize the reliability of the pipe inspection equipment. Other states (e.g. Utah, Pennsylvania and Michigan) have expressed interest in this work in Florida.

A review of joint performance from images was conducted. Typical problems observed:
- gaskets rolling on the spigot into the deepest part of the bell during assembly, leading to leakage
- rotation of the joints leading to large gaps at the widening part of the joint
- construction damage to the end of joints (bell and spigot in RCP for example)

Inspection reports are expected to indicate when the joint gap is too wide – however the required minima are not generally specified. Therefore, there is a need to determine the range of acceptable joint gaps for each product (or perhaps product class).

B.9.3 Issues affecting joints in reinforced concrete pipes

Florida DOT Standard Specifications for Road and Bridge Construction (2010) specifies minimum requirements for the distance from gasket to the taper on the spigot (0.75 in.). This is intended to ensure the assembled joint permits some flexure in the field. However, none of the five manufacturers of RCP in Florida have products that satisfy that criterion. Indeed, many have zero of negative gap (i.e. the gasket sits on the taper). The history of this dimensional choice is not clear.

There is no known demonstration that any of these joints remain sealed once there is rotation across it e.g. using a laboratory test under pressure with different levels of rotation. DOTs would like to know what the requirements are for the gasket position relative to the taper.

Florida DOT Standard Specifications for Road and Bridge Construction (2010) specifies maximum gap once the pipes are assembled and buried. The gap must not exceed 5/8 in. for pipe diameter from 12 in. to 24 in., 7/8 in. for diameters between 24 and 66 in. and 1 in. for pipes with diameter 72in or larger.

B.9.4 Issues affecting joints in corrugated steel pipes

Flexible (steel and thermoplastic) pipe deformations are limited to 5%.

In the past, there have been difficulties with CSP connections in Florida. The standard steel band with two bolts was fitted with a neoprene gasket (12 inch wide, ¾ inch thick) aimed at producing a semi-water-tight joint. It theoretically seals, however it was found much better to use the hugger band.

Florida DOT has not seen issues with transferring load from one pipe to the next, and it appears that load capacity of band connections is adequate.
Manufacturing used to allow 5% deflection from one pipe to the next. However, if one pipe is ovalled and the other is not, it is very difficult to obtain a seal.

Geometrical limits are needed for joints in corrugated steel pipes. For example, limits on maximum gap size are needed for comparison with gaps measured during post-construction inspection.

B.9.5 Issues affecting joints in thermoplastic pipes

Joint performance in these systems has generally been satisfactory (there are no consistent signs of problems). Flexible pipe deformations (diameter changes) are limited to 5%. However, geometrical limits are needed for joints in HDPE and PVC pipes (so that gap size measured during post-construction inspection can be assessed as adequate or inadequate). The PVC pipe has been found to have a very good connection, since it was designed for use in sanitary sewers.

Laboratory testing of culvert joints

Table of Contents

C.1 Introduction

This appendix describes laboratory testing of the six culvert products examined during the project. The objectives of these tests were to:

- Produce measurements of jointed pipe response under controlled laboratory conditions
- Examine pipe response under live loads as well as earth loads
- Determine three dimensional behavior under simulated vehicle loading at service and ultimate loads levels
- Examine shallow buried pipe response at two different cover depths
- Examine pipe response under different quality (good and poor) burial conditions
- Examine joint behavior prior to burial and after burial, to establish the kinematic (deformation) characteristics of the joint and the manner in which loads are transferred from one pipe to the other
- Provide data that can be interpreted using beam-on-elastic spring analysis to establish both demand (expected loads and deformations) and resistance (load capacity and deformation capacity) of joints; those back-calculated measures of demand are to be used in establishing a procedure for structural design of culvert joints
- Provide data for future calibration of more advanced computer analyses for use in joint design

The following pipes were tested (see **Figure C.1**):

a. 24 inch (610mm) diameter reinforced concrete pipe ‘RCP’ with gasketted bell and spigot joint
b. 36 inch (915mm) diameter corrugated steel pipe ‘CSP’ with unsealed band joint
c. 60 inch (1525 mm) diameter high density polyethylene pipe ‘HDPE’ with gasketted bell and spigot joint
d. 36 inch (915mm) diameter polyvinyl chloride ‘PVC’ pipe with gasketted bell and spigot joint
e. 48 inch (1220mm) diameter reinforced concrete pipe ‘RCP’ with unsealed tongue and groove joint
f. 36 inch (915mm) diameter corrugated steel ‘CSP’ pipe with gasketted band joint

a. 24 inch (610mm) diameter reinforced concrete pipe with gasketted bell and spigot joint

b. 36 inch (914mm) diameter corrugated steel pipe with unsealed band joint

c. 60 inch (1524 mm) diameter high density polyethylene pipe with bell and spigot joint

d. 36 inch (914mm) diameter PVC pipe with gasketted bell and spigot joint

e. 48 inch (1220mm) diameter reinforced concrete pipe with unsealed bell and spigot joint

Figure C.1. Images of the six test pipes examined

C.2 Reinforced concrete pipes

Both 24 in. (610mm) and a 48 in. (1220mm) reinforced concrete pipes were examined when buried, under simulated service loading and full factored vehicle loads (to establish the ultimate limit state). Furthermore, articulation tests were performed on the 24 in. (610mm) diameter pipe while subjected to internal and external pressure (tests to measure rotational characteristics of the joint before burial). The details of these experiments are described below.

C.2.1 Articulation test

A series of tests were performed on the 24 in. (610mm) reinforced concrete pipe to investigate the rotational stiffness characteristics of the gasketted bell and spigot joint. The pipe was assembled and tested under positive pressure and partial vacuum. It is expected that internal and/or external pressures act on the gasket and other components of culvert joints under certain conditions (internal pressure may arise when the pipe is flowing to capacity, and external pressure can occur when the pipe is located below the external groundwater surface). To investigate the stiffness of the joint as it rotates (the relationship between moment and rotation of the joint), and to evaluate the effect of internal or external pressure on the stiffness of the joint, articulation tests were performed on a section of assembled pipe prior to burial.

C.2.1.1 Instrumentation

Reflective prisms were placed on the top part of the pipe to measure three dimensional displacements with the aid of a servo-controlled total station (survey equipment). In addition, string potentiometers were mounted in the main joint and at the mid-span of each barrel to measure the vertical displacement of these points. The location of the elements described can be seen in **Figure C.2**. A pressure gage transducer was employed to measure the levels of pressure/vacuum inside the pipe. This element was mounted in one of the sealing plates.

C.2.1.2 Test configuration

These tests were performed inside the pit of the GeoEngineering laboratory prior to burial. The pipe consisted of two complete pipes and a half-segment of pipe at each end. Each of the three joints in the system was sealed with a gasket. Steel plates were placed at the two ends of the pipe to make the pipe airtight with the aid of rubber sheets and silicon. The end plates were anchored to the side-walls of the test pit so that no net axial force developed along the axis of the pipe as result of the differential pressure across the end plates. Such axial forces would not be expected in a culvert when buried in the field, and the concern was that those forces would adversely influence the rotational characteristics of the joints.

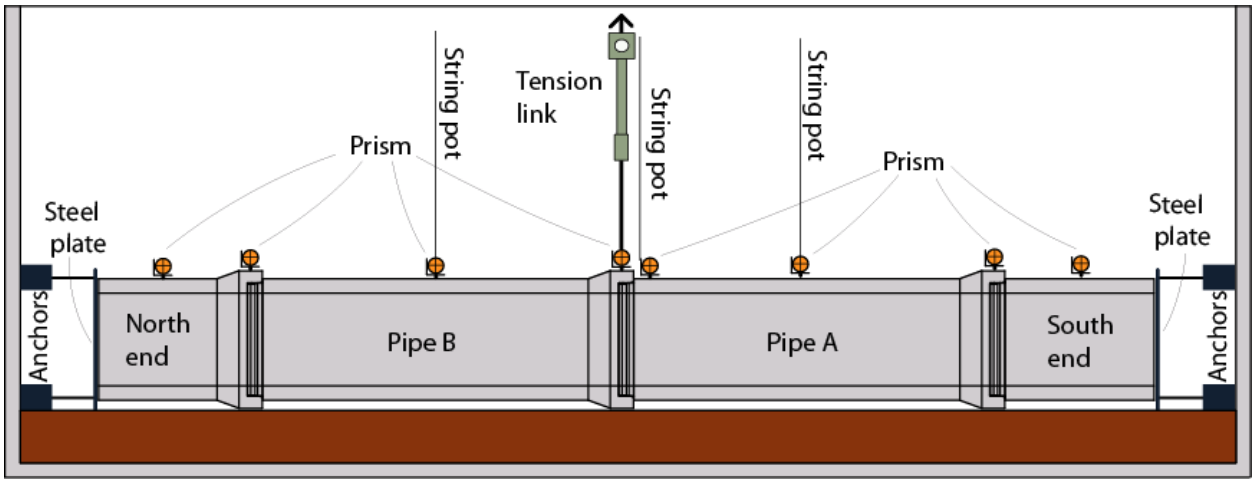

a. View of experimental configuration in the GeoEngineering laboratory.

b. Cross-section showing testing details.

Figure C.2. Configuration of the articulation test on the 24 in (610mm) reinforced concrete pipe.

Once the pipe was assembled and sealed, a steel cable was placed around the bell and used to lift the center of the pipe employing the actuator mounted above the test pit. The actuator and the steel cable were connected through a tension link which was used to measure the force needed to lift the pipe to the desired distance. That distance selected based on the maximum pull of the joint according to the manufacturer and was measured using a string potentiometer attached to the central joint. The articulation tests were performed at atmospheric pressure and with different values of positive pressure and vacuum (see **Table C.1** for the pressures utilized).

Table C.1. Pressures for the articulation test of the 24 in (610mm) reinforced concrete pipe.

Type of pressure	Pressure	Absolute pressure
Atmospheric pressure	0 kPa (0 psi)	101.3 kPa (14.7 psi)
Positive	15 kPa (2.17 psi)	116.3 kPa(16.86 psi)
Positive	30 kPa (4.35 psi)	131.3 kPa(19.04 psi)
Positive	45 kPa (6.52 psi)	146.3 kPa(21.22 psi)
Vacuum	-15 kPa (-2.17 psi)	86.3 kPa(12.51 psi)
Vacuum	-30 kPa (-4.35 psi)	71.3 kPa (10.34 psi)
Vacuum	-60 kPa (-8.7 psi)	41.3 kPa (5.99 psi)
Vacuum	-85 kPa (-12.32 psi)	16.3 kPa (2.36 psi)

C.2.1.3 Results

Figures C.3 and **C.4** show the measured values of vertical load versus deflection at the central joint during the tests with internal pressure and vacuum respectively. These demonstrate that internal and external fluid pressure acting on the gasket does have some measurable effect on the joint rotation characteristics. Whether these stiffness changes make a difference to the joint performance will be examined through calculations using the computer models of the buried jointed pipe system. **Figure C.6** shows the vertical displacement of the pipe during one of the tests.

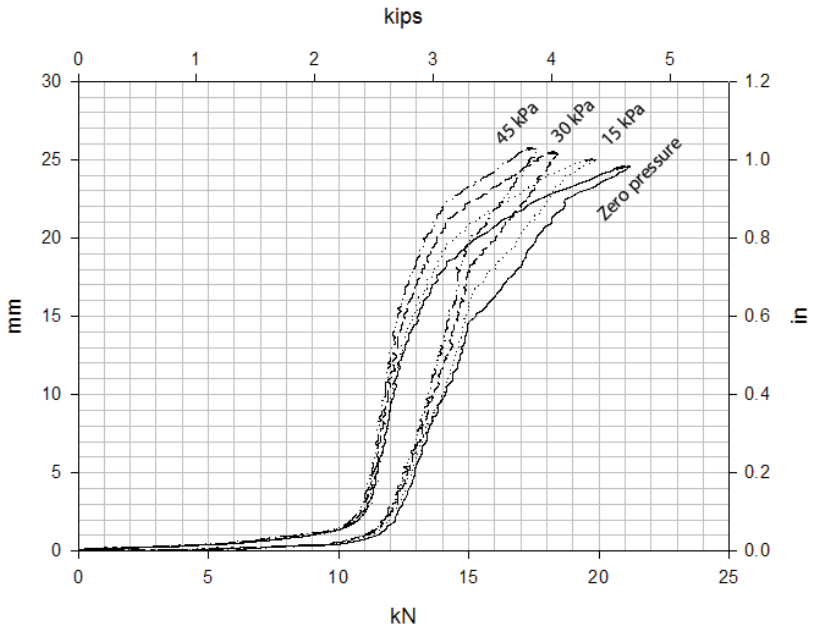

Figure C.3. Load versus deflection measured during articulation testing of the 24 in (610mm) reinforced concrete pipe; positive internal pressure

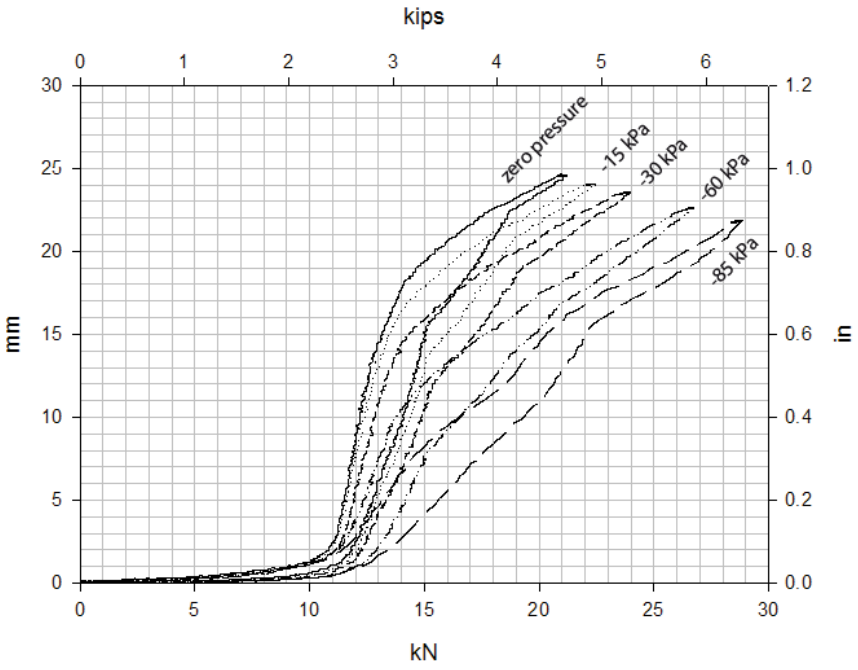

Figure C.4. Load versus deflection measured during articulation testing of the 24 in (610mm) reinforced concrete pipe; negative internal pressure.

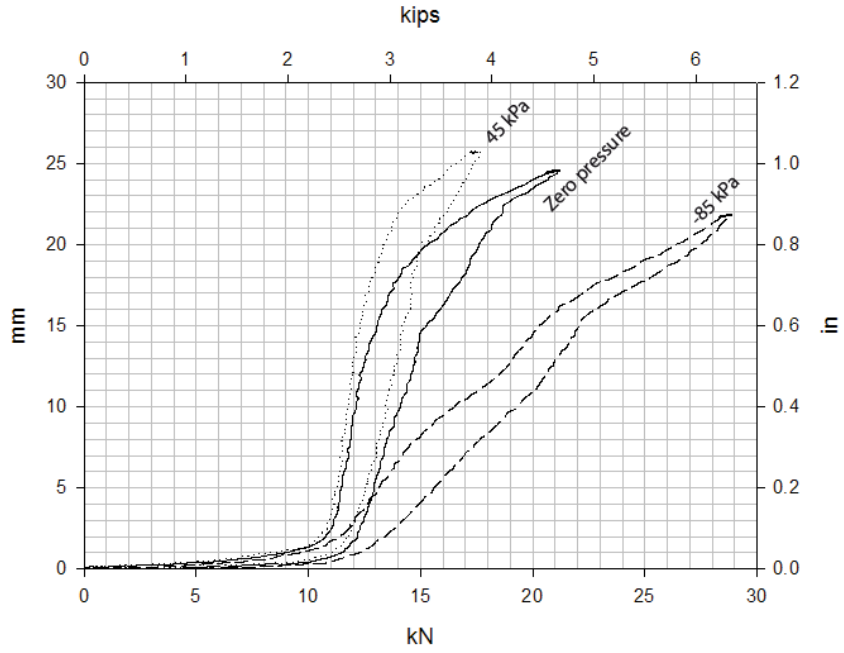

Figure C.5. Load versus deflection measured during articulation test of the 24 in (610mm) reinforced concrete pipe; comparison for minimum and maximum pressures.

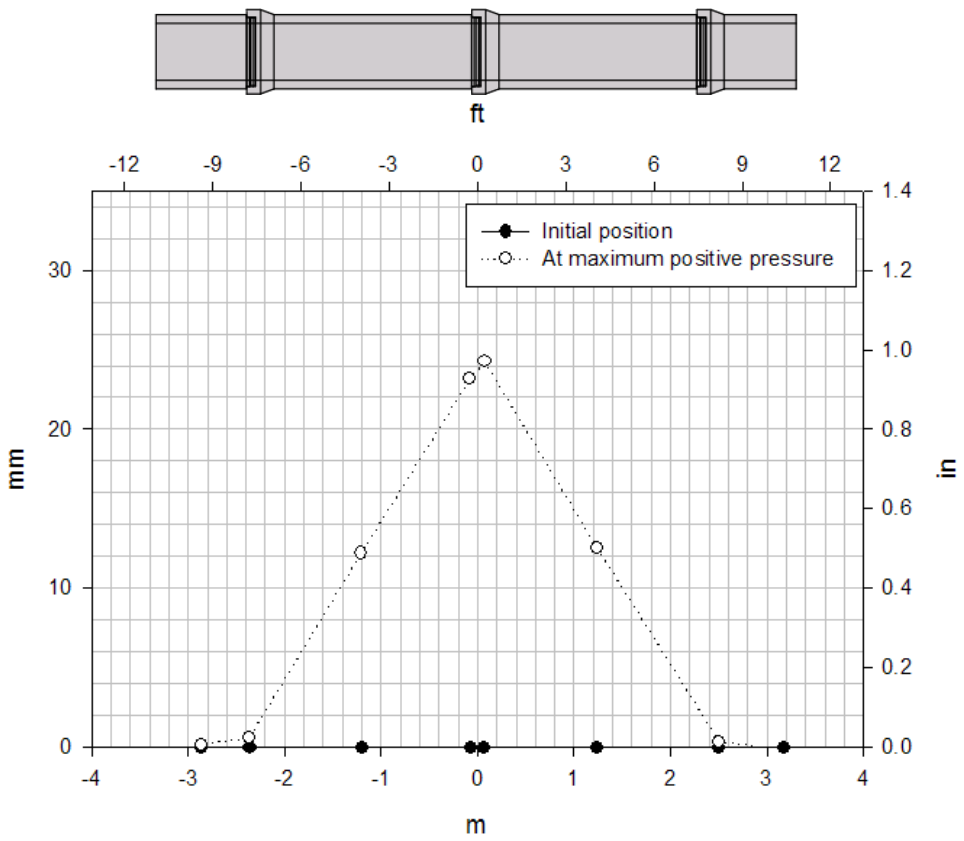

Figure C.6. Maximum pipe deformations during articulation testing of the 24 in (610mm) reinforced concrete pipe at the maximum positive pressure.

C.2.2 Buried pipe tests

Service loading tests under burial conditions were performed on the 24 in. (610mm) and 48 reinforced concrete pipes described above. Different burial depths and surface loading locations were examined for each pipe and variation of the burial quality was inspected for the 24 in (610mm) specimen. The instrumentation employed for each product and the details of the tests are described in the following sections.

C.2.2.1 Instrumentation

Electrical strain gages were attached to the 24 in. (610mm) diameter pipe to monitor circumferential and axial strains, as well as some rosettes to permit shear to be assessed at some locations. **Figure C.7** illustrates the location and orientation of the strain gages. In addition, reflective prism were placed inside the pipe to measure three dimensional displacements with the aid of a servo-controlled total station (survey equipment). The location of these elements can be seen in **Figures C.8** and **C.9**. The 48 in. (1220mm) diameter pipe was instrumented with reflective prisms to measure three dimensional displacements. The location of these components can be seen in **Figures C.10** and **C.11**.

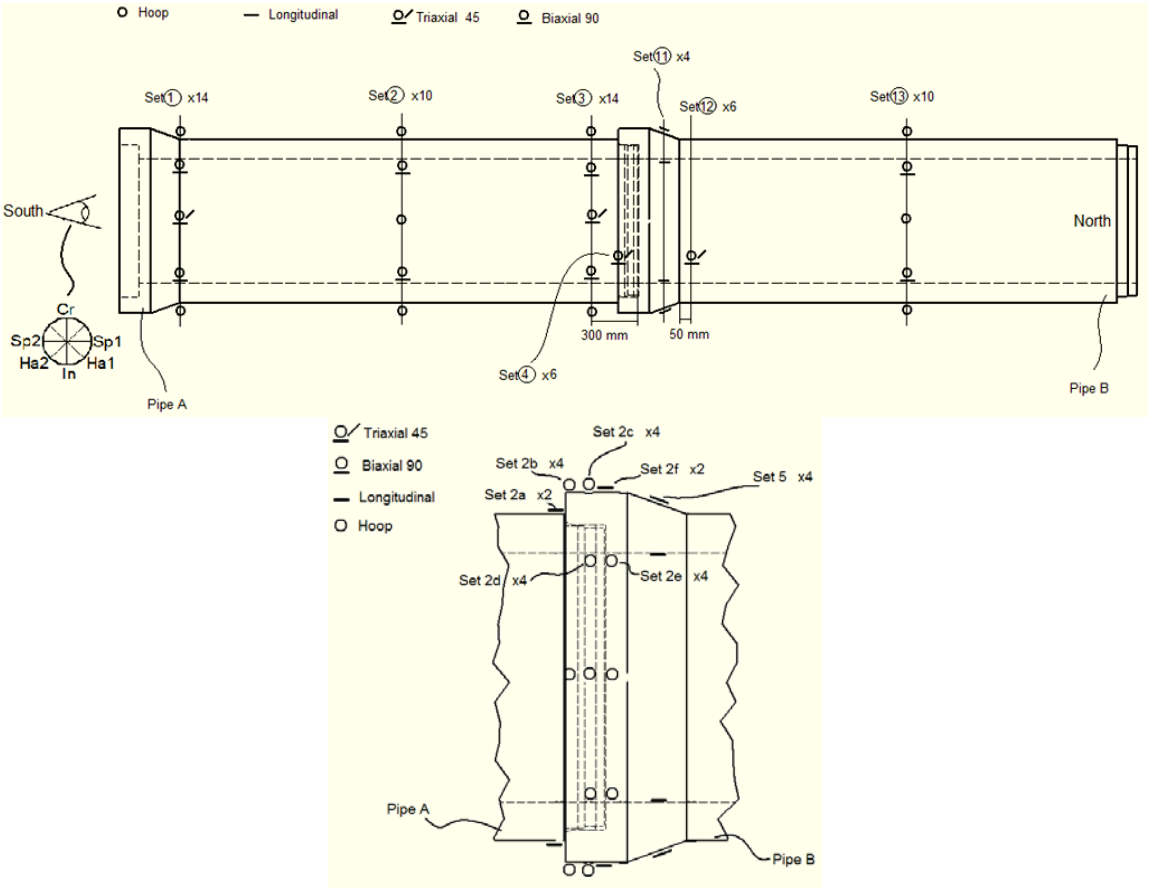

Figure C.7. Strain gage locations in the 24 in (610mm) diameter reinforced concrete pipe.

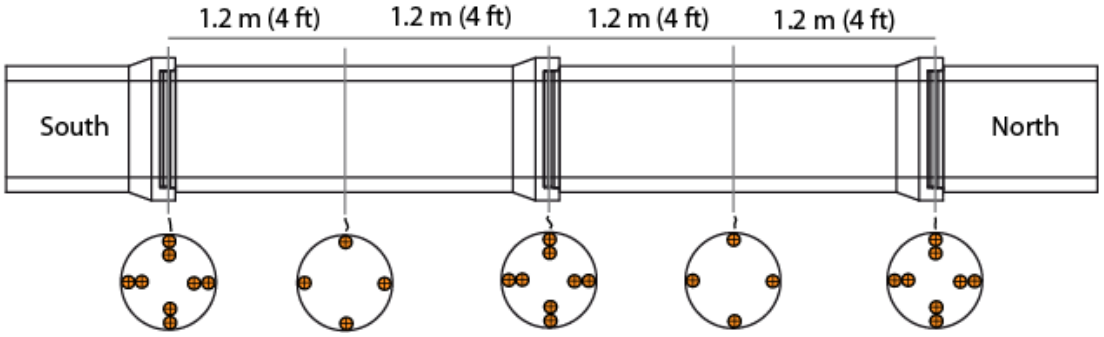

Figure C.8. Location of reflective prisms in the 24 in (610mm) diameter reinforced concrete pipe.

Figure C.9. View of the prisms after placement in the 24 in (610mm) diameter reinforced concrete pipe.

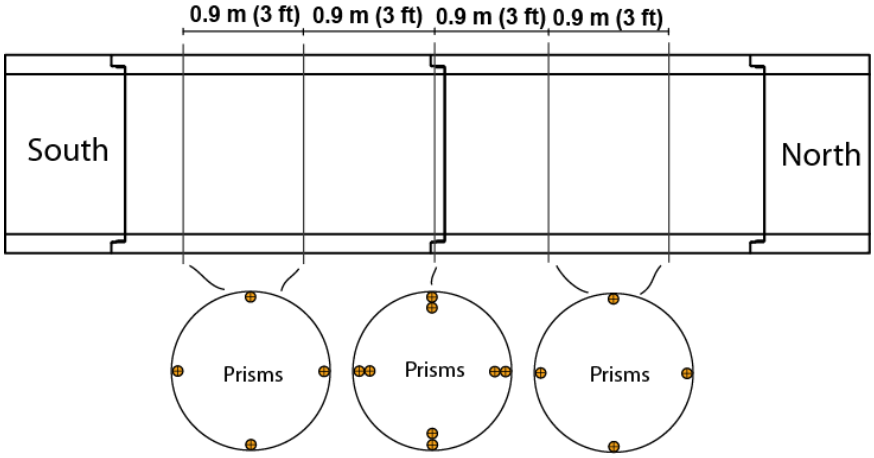

Figure C.10. Location of reflective prisms in the 48 in (1220mm) diameter reinforced concrete pipe.

Figure C.11. View of the prisms after placement in the 48 in (1220mm) diameter reinforced concrete pipe.

C.2.2.2 Test configuration

Two burial qualities were used to examine the 24 in. (610mm) diameter pipe, both employing rubber gaskets in every joint of the system. The first, illustrated in **Figure C.12**, involves poor burial practice where a compacted foundation was first prepared and then the pipe was laid directly on the bells. Since the bells protrude beyond the main pipe barrel (i.e. the bells have larger outside diameter than the barrel), this means that the pipes experience significant longitudinal bending and that the loads are transfer to the bedding through the bells in this configuration. Though this is certainly not recommended practice, the objective was to examine the consequences for pipe and joint response.

The second burial configuration for the 24 in. (610mm) diameter pipe was based on accepted AASHTO practice, as illustrated in **Figure C.13**. All buried pipe testing was conducted with backfill composed of a well graded sand-gravel mixture (Type 1 material constructed to 90-95% of maximum dry density obtained in a standard Proctor test). The same configuration was employed for the 48 in. (1220mm) diameter pipe and is illustrated in **Figure C.14**, however no gasket or sealant was employed in the joints of this pipe. Simulated service loading was performed at 2 ft (610mm) and 4 ft (1220mm) of burial cover for each specimen and burial quality. In every test, the end-walls of the embankment constructed over the test pipes were made of steel grids covered with geosynthetic (see **Figure C.15**). This choice of a flexible end-wall was designed to minimize any stiffening effect of those end treatments on the jointed pipe response.

Loading was applied using a 2000kN (220 US ton) capacity actuator mounted over the test pit, and restrained by a reaction frame anchored into the limestone below. Loading was applied through a steel plate having the design dimensions of the standard AASHTO wheel pair at the end of a design axle, **Figure C.16.** For all tests, the load was applied in three different positions along the test pipe; this involved loading over the central pipe joint, then at 3ft (0.9m) intervals to the North and South of that position. The loading was designed to represent the action of one wheel pair at the end of a single 32000 lbf (143 kN) axle. Half that single axle (the load on one wheel pair) is 16000 lbf. Considering multiple presence factor of 1.2, and impact factors of 1.25 at 2ft of burial, and 1.17 at 4ft of burial, the factored service load becomes 24000 lbf (107 kN) at 2ft of cover, and 22500 lbf (99.9 kN) at 4ft of cover. For reasons of simplification and to facilitate comparisons of joint response at the two different cover depths, all ‘service load’ testing was conducted up to 22.5 kips (100kN). Nonetheless, the loading was stopped at 17.9 kips (80 kN) for the poor burial case of the 24 in. (610mm) diameter pipe to prevent cracking of the reinforced concrete pipe before the ultimate load testing.

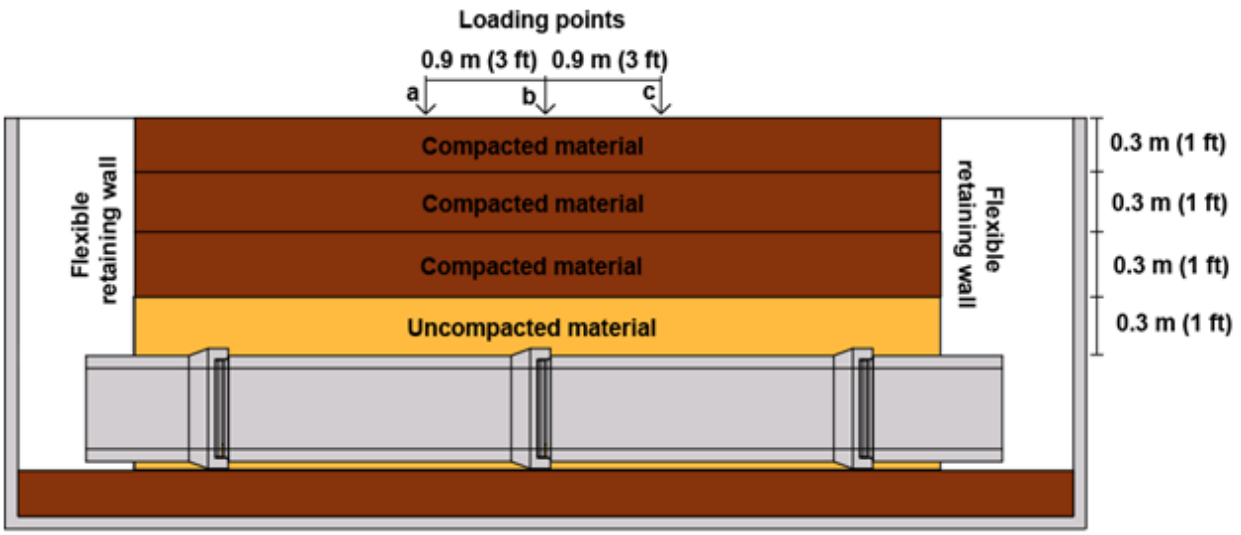

(a) Longitudinal section

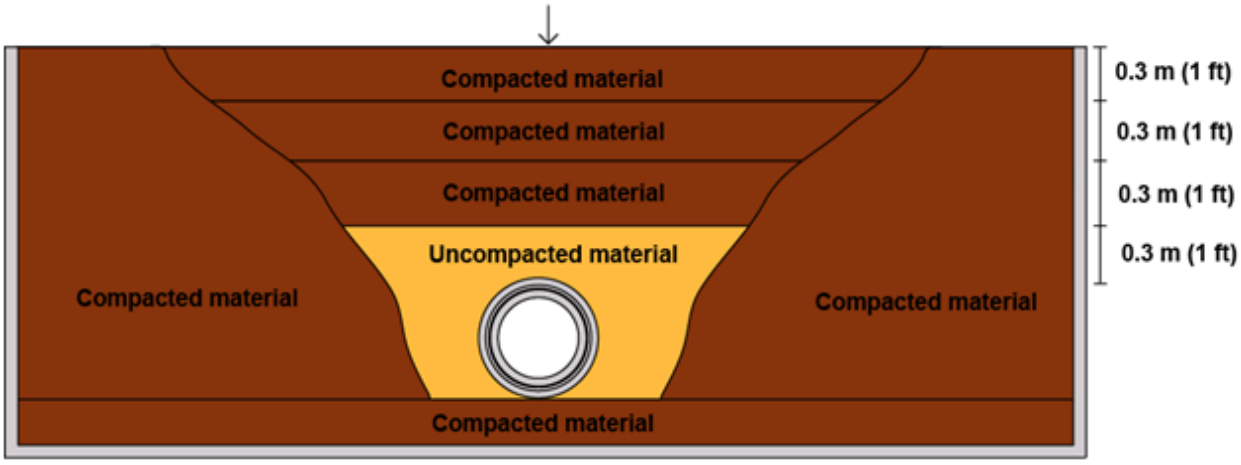

(b) Sectional normal to pipe axis

Figure C.12. Configuration of poor burial condition for the 24 in (610mm) diameter reinforced concrete pipes at 4ft (1220mm) of cover; burial where pipe bells are placed directly on the compacted bedding.

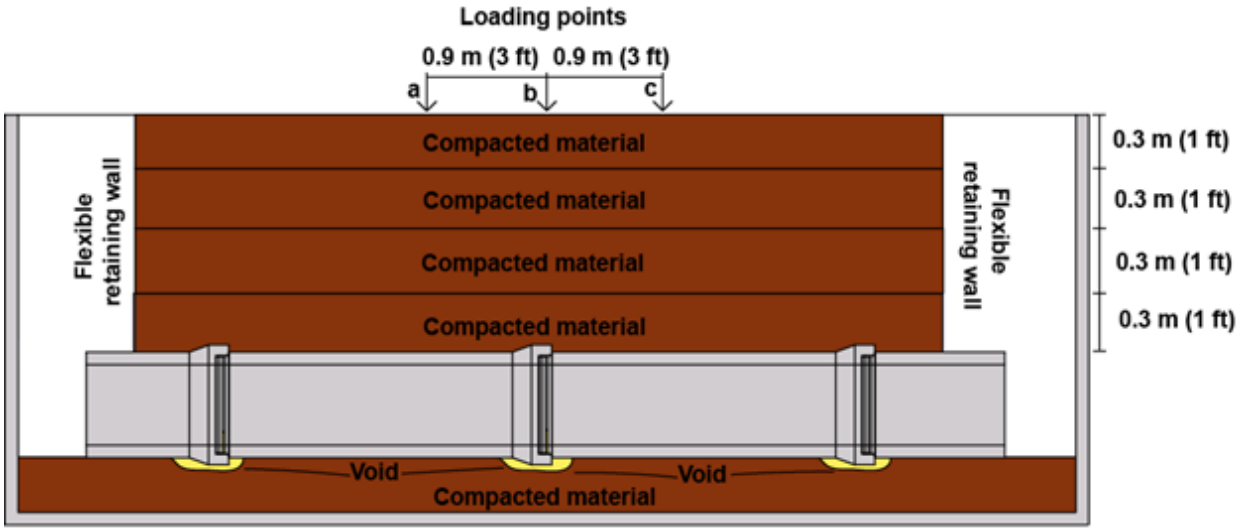

(a) Longitudinal section

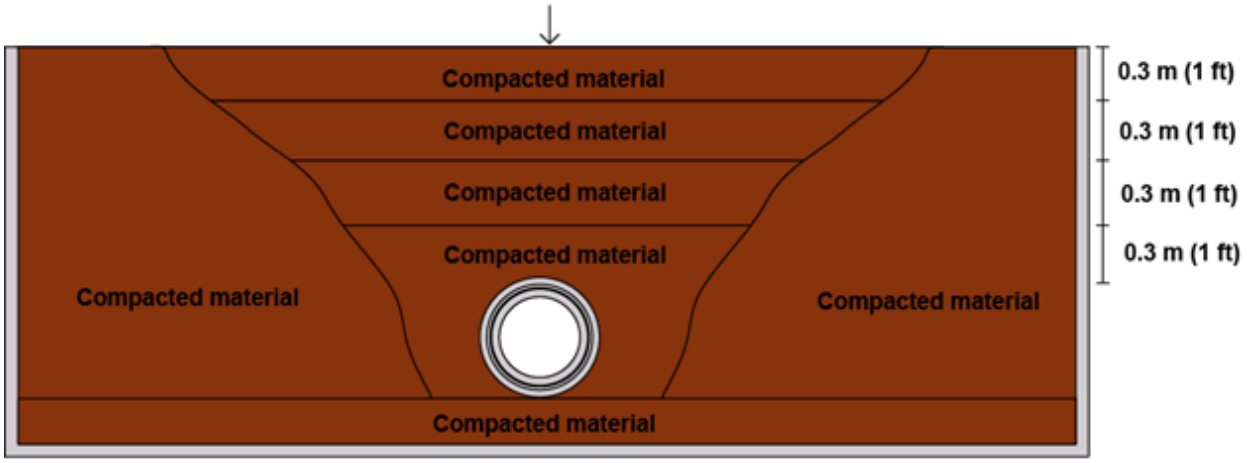

(a) Sectional normal to pipe axis

Figure C.13. Configuration of good burial condition for the 24 in (610mm) diameter reinforced concrete pipes at 4ft (1220mm) of cover; burial in accordance with AASHTO LRFD Bridge Construction Specifications.

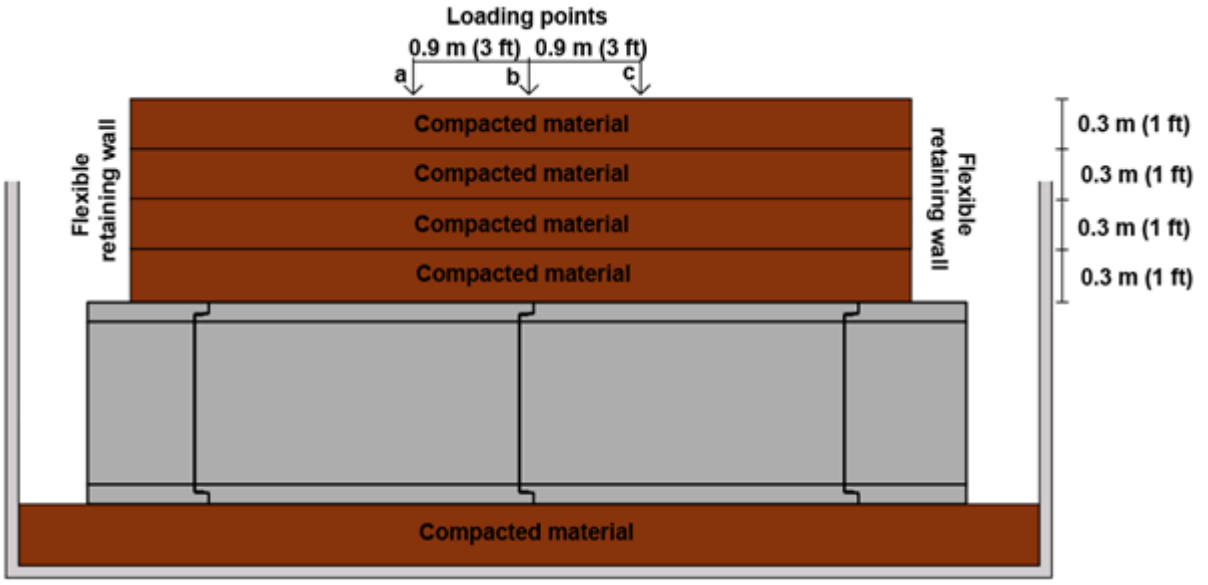

(a) Longitudinal section

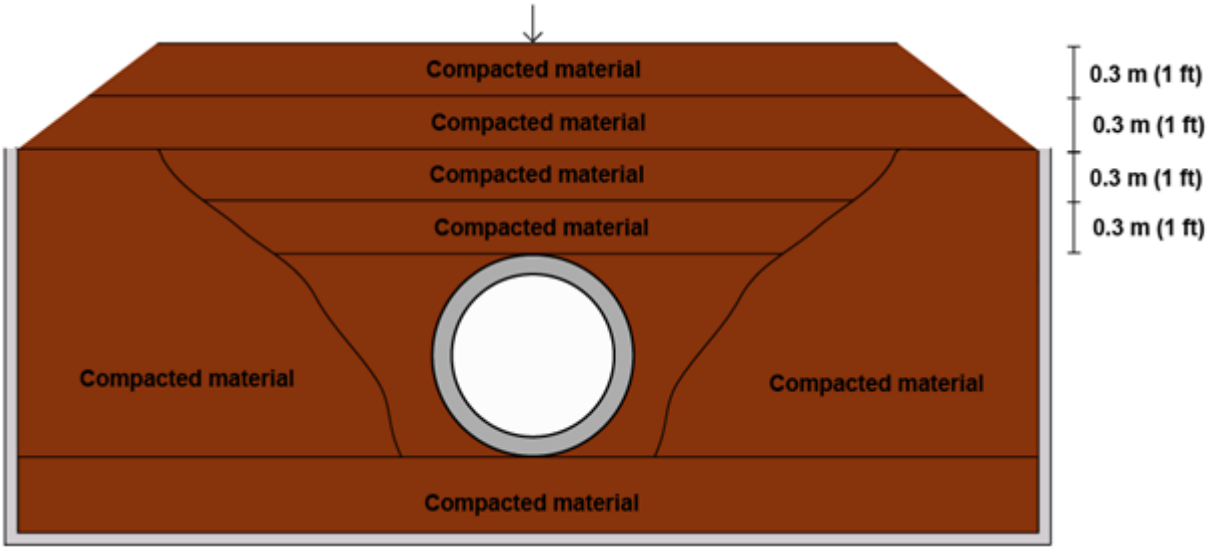

(a) Sectional normal to pipe axis

Figure C.14. Configuration of good burial condition for the 48 in (1220mm) diameter reinforced concrete pipes; burial in accordance with AASHTO LRFD Bridge Construction Specifications.

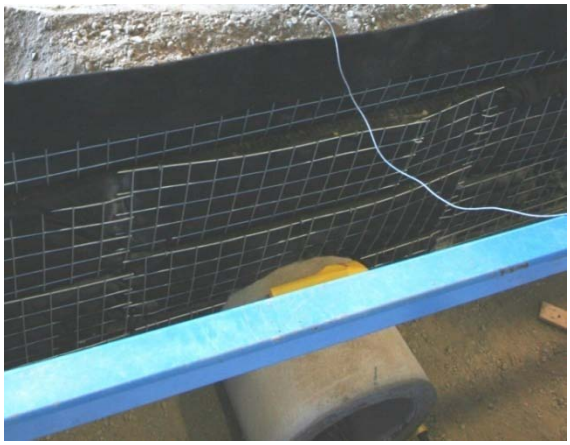

Figure C.15. Grid with Geosynthetic used for the end-wall treatment for all burial testing (shown here with 4ft of cover soil over the 24 in diameter specimen).

Figure C.16. Actuator on the reaction frame, applying load to steel pad on the ground surface over the reinforced concrete test pipes (24 in diameter specimen left hand side and 48 in diameter specimen on the right hand side)

C.2.2.3 Results

Tables C.2 and **C.3** provide the circumferential response of the bell, spigot and barrels for the tests performed on the 24 in. (610mm) diameter pipes. Axial response was in general negligible therefore is not shown here. The largest circumferential strains were registered at the bell. These results clearly show:

- Circumferential strain patterns associated with ovaling deformations in the bell
- Invert and crown behavior in the bell that is essentially identical when the pipe is buried in good backfill, while the invert strains are significantly higher for the poor burial condition (likely because the bell invert rests directly on the stiff foundation)
- The crown strains that are somewhat higher in the spigot than the invert values, for all burial conditions
- Strain pattern that is very symmetric about the vertical diameter; this reflects the uniform quality of the instrumentation, and the burial conditions
- Strains in the bell and spigot that are 2 to 3 times higher at 2ft of cover, compared to 4ft of cover
- Tensile strains in the bell that are 3 to 4 times higher for the poor burial case
- Strains at the barrel mid-spans are very small (all shown here as zero) for the poor burial case (likely because the pipe carries little load to its invert which was initially above the foundation); these strains are small but not zero for the good burial case, and with the surface load placed over the central joint, the strains are essentially equal for each barrel mid-point on either side of the central joint

Figures C.17 to **C.19** show the patterns of absolute crown deformation along the 24 in. (610mm) diameter pipe. These illustrate the influence of burial depth, soil support conditions and the position of the live load relative to the central joint. In particular:

- The much higher vertical deformations for poor burial (three times larger)
- The almost symmetric nature of deformations when load is placed directly over the central joint
- The effect of applying load to one side or the other side of the joint, producing higher deformations in the pipe under the load.

Figures C.20 and **C.21** show the patterns of absolute crown deformation along the 48 in. (1220mm) diameter pipe. These illustrate the influence of burial depth and the position of the live load relative to the central joint.

Table C.2. Circumferential strain in the bell and spigot; recorded at incremental load of 80 kN (17.9 kips); behavior for different burial depths, soil support conditions, and load locations all recorded.

	Location	Poor burial						Good burial					
		At 4 ft (1.2 m) cover			At 2 ft (0.6 m) cover			At 4 ft (1.2 m) cover			At 2 ft (0.6 m) cover		
		-3 ft	0 ft	3 ft	-3 ft	0 ft	3 ft	-3 ft	0 ft	3 ft	-3 ft	0 ft	3 ft
		με	με	με	με	με	με	με	με	με	με	με	με
ε_{00}	**Bell, Invert, Inside**	4	27	25	0	75	41	0	6	4	3	16	7
ε_{00}	**Bell, Crown, Inside**	0	18	25	0	58	41	0	5	5	2	18	7
ε_{00}	**Bell, Springline1, Inside**	1	-20	-24	6	-49	-28	0	-15	-11	0	-39	-16
ε_{00}	**Bell, Springline2, Inside**	0	-17	n/a	0	-43	-28	0	-14	-12	0	-39	-14
ε_{00}	**Spigot, Invert, Inside**	14	7	0	25	18	0	2	5	0	2	14	0
ε_{00}	**Spigot, Crown, Inside**	19	13	0	31	22	0	9	7	0	20	16	0
ε_{00}	**Spigot, Springline1, Inside**	-18	-8	0	-37	-18	0	-7	-5	0	-12	-12	0
ε_{00}	**Spigot, Springline2, Inside**	n/a	n/a	0	n/a	n/a	0	n/a	-5	0	n/a	-11	0

Table C.3. Circumferential strain in the mid-span barrels; at incremental load of 80 kN (17.9 kips); behavior for different burial depths, soil support conditions, and load at 0 ft offset (i.e. directly over the joint).

	Location		Poor burial		Good burial	
			At 4 ft of cover	At 2 ft of cover	At 4 ft of cover	At 2 ft of cover
ε_{00}	**Barrel 1, Invert**	**Inside**	0	0	7	16
		Outside	0	0	-8	-12
ε_{00}	**Barrel 1, Crown**	**Inside**	0	0	4	9
		Outside	0	0	-2	-3
ε_{00}	**Barrel 1, Springline 1**	**Inside**	0	-2	-3	-8
		Outside	0	3	2	6
ε_{00}	**Barrel 1, Springline 2**	**Inside**	0	-1	-3	-8
		Outside	0	3	2	6
ε_{00}	**Barrel 2, Invert**	**Inside**	0	0	7	13
		Outside	0	0	-7	-11
ε_{00}	**Barrel 2, Crown**	**Inside**	0	0	3	5
		Outside	0	0	-2	-4
ε_{00}	**Barrel 2, Springline 1**	**Inside**	0	0	-3	-6
		Outside	0	0	2	5
ε_{00}	**Barrel 2, Springline 2**	**Inside**	0	0	-5	-6
		Outside	0	0	2	5

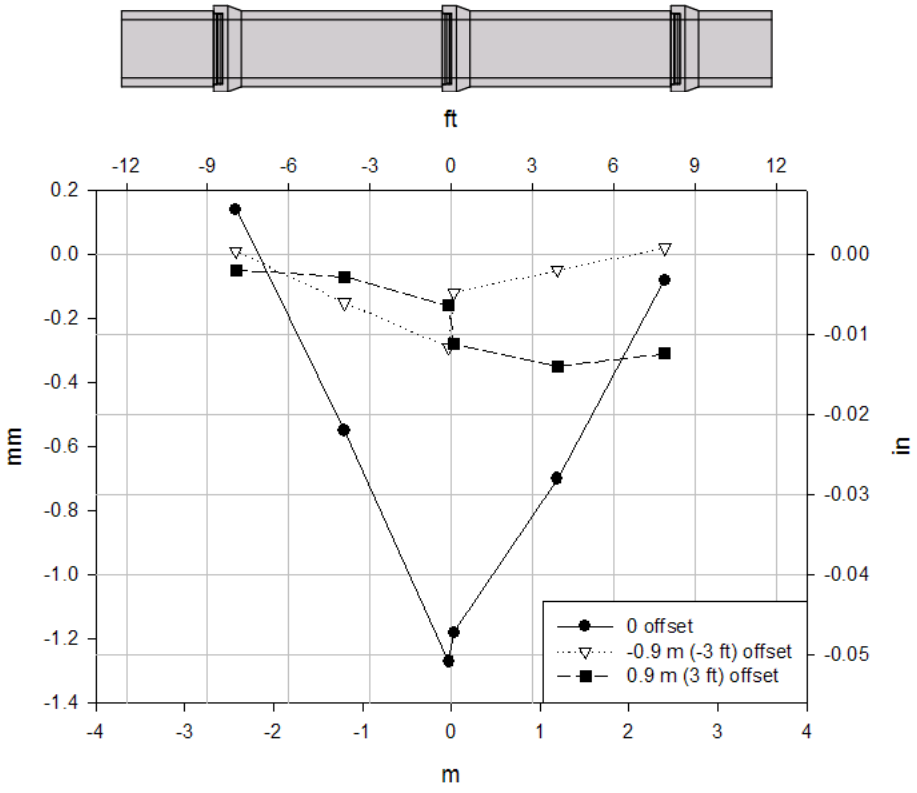

(a) 4 ft (1220mm) burial depth

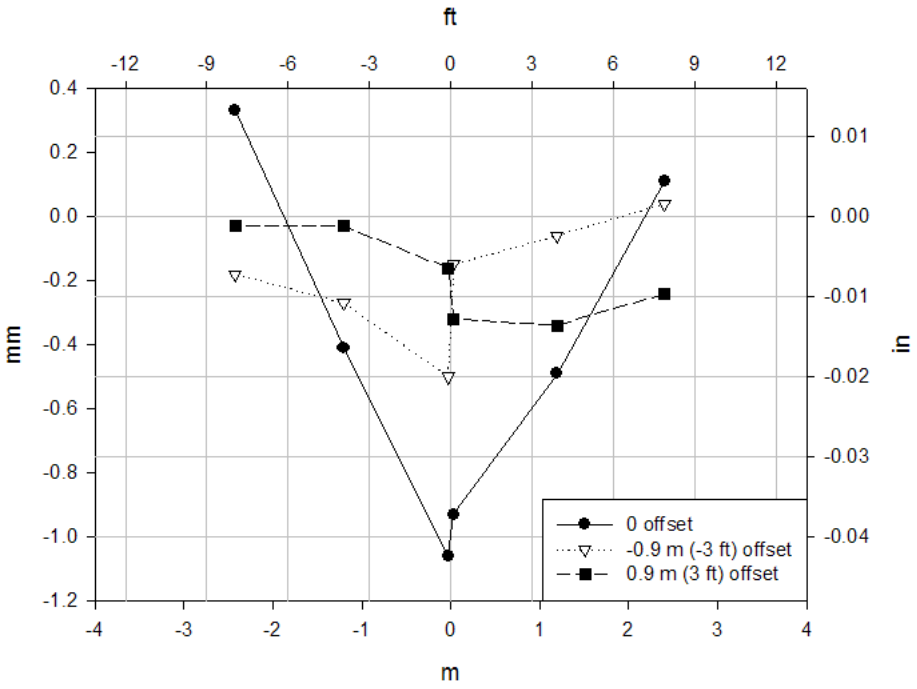

(b) 2 ft (610mm) burial depth

Figure C.17. Vertical crown displacements of the 24 in (610mm) diameter reinforced concrete pipe; effect of load position for poor burial conditions.

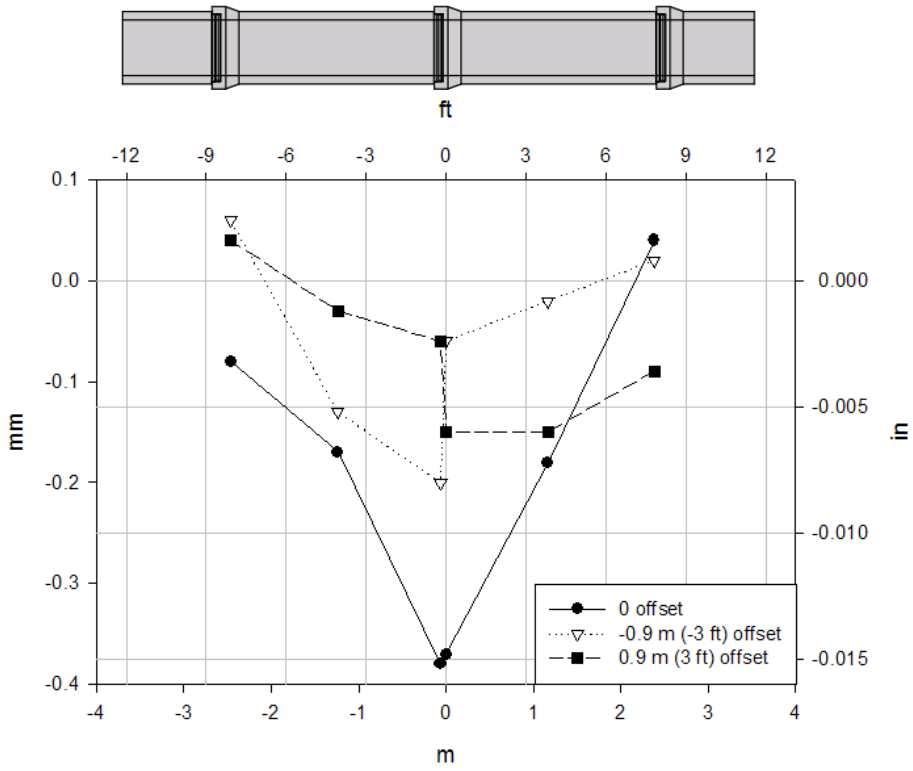

(a) 4 ft (1220mm) burial depth

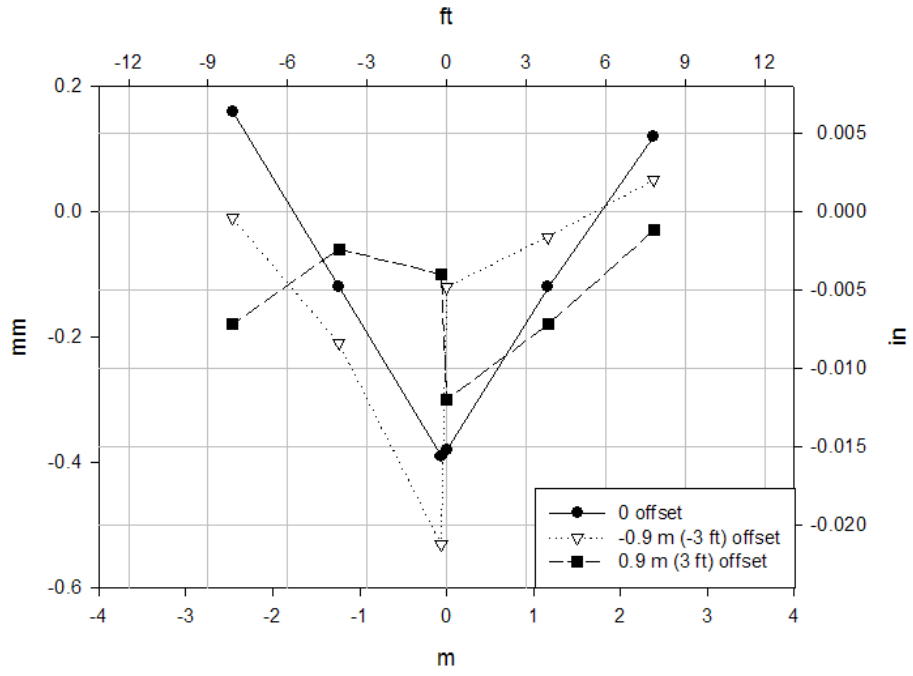

(b) 2 ft (610mm) burial depth

Figure C.18. Vertical crown displacements of the 24 in (610mm) diameter reinforced concrete pipe; effect of load position for good burial conditions.

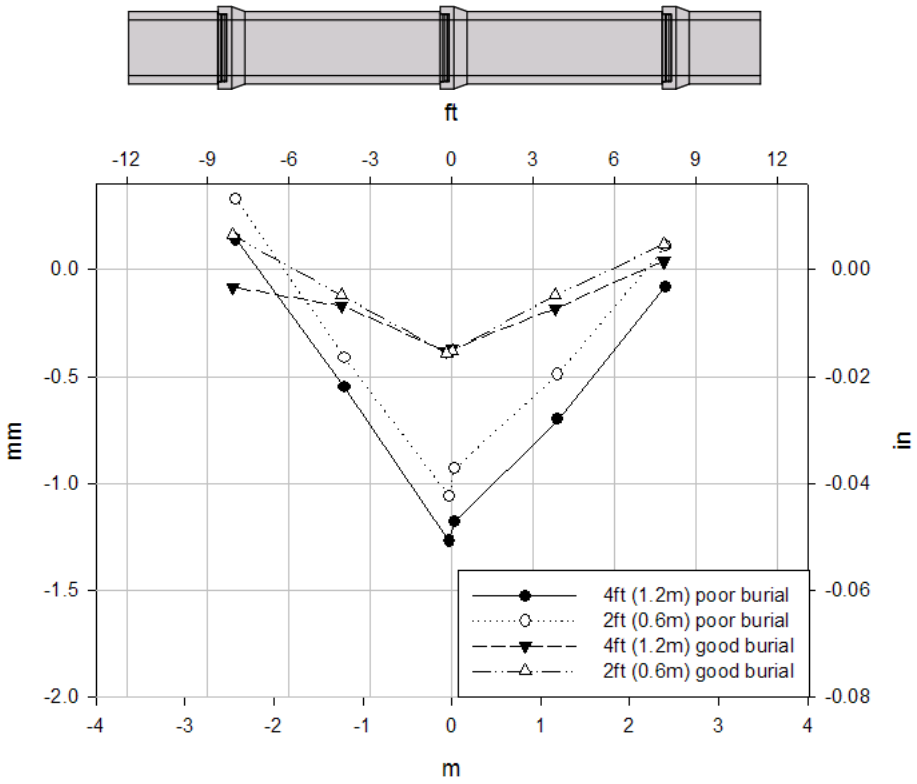

Figure C.19. Vertical crown displacements of the 24 in (610mm) diameter reinforced concrete pipe, load applied directly over the joint; comparison of burial depth and burial condition.

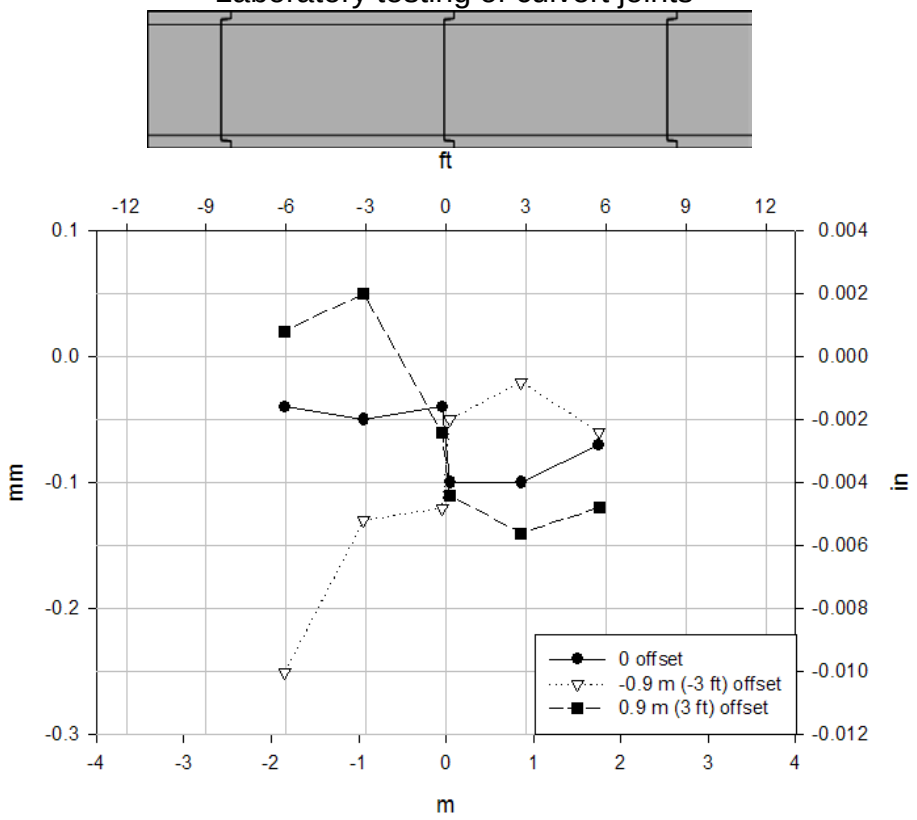

(a) 4 ft (1220mm) burial depth

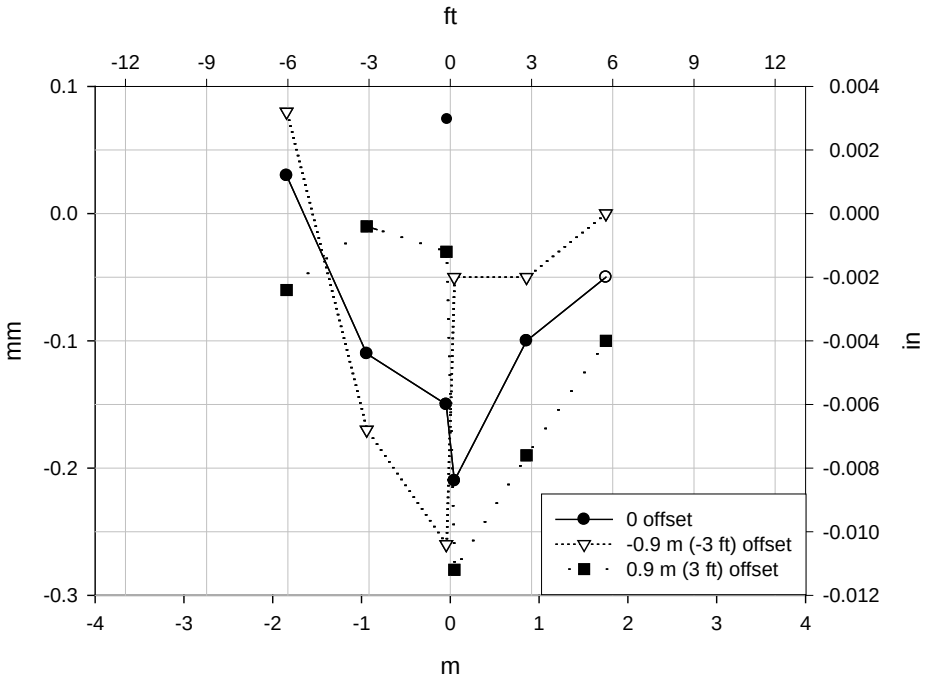

(b) 2 ft (610mm) burial depth

Figure C.20. Vertical crown displacements of the 48 in (1220mm) diameter reinforced concrete pipe; effect of load position for good burial conditions.

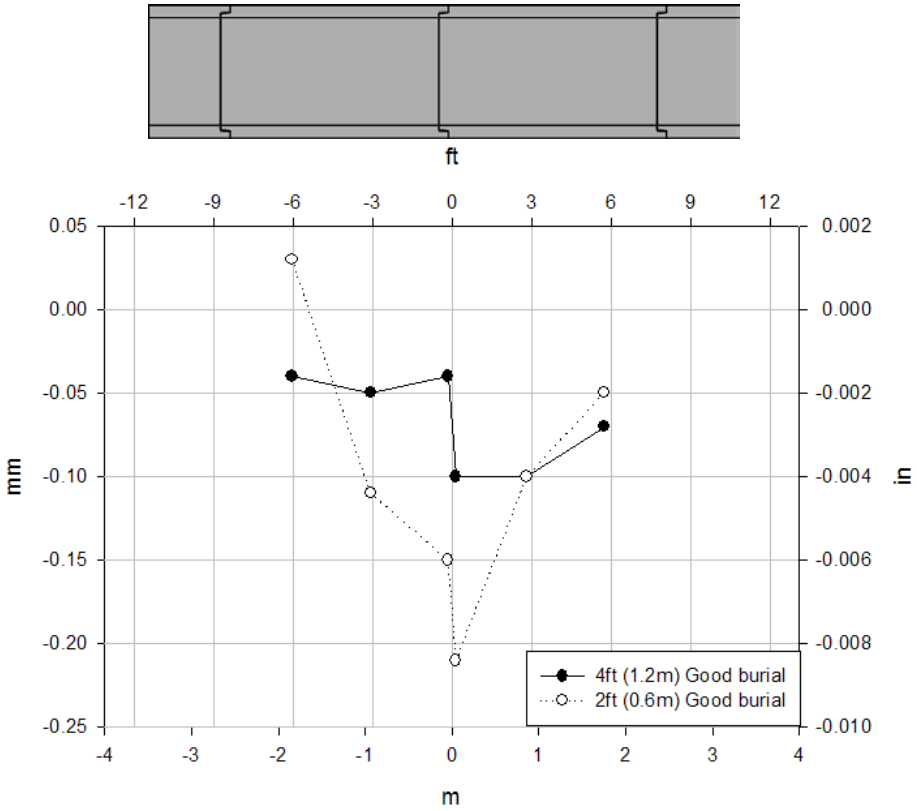

Figure C.21. Vertical crown displacements of the 48 in (1220mm) diameter reinforced concrete pipe, load applied directly over the joint; burial depth comparison.

C.2.3 Ultimate limit state test

This test was performed for the 24 in (610mm) and the 48 in (1220mm) diameter reinforced concrete pipes. The purpose of these tests was to subject the joints of each specimen to live loading until failure of the jointed pipes or some other limit of the loading system; both tests were limited by bearing failure of the soil under the loading pads. Details of these tests are presented below.

C.2.3.1 Instrumentation

The instrumentation employed for these tests was the same as the one employed during the service loading testing described before. Strain gages and reflective prisms were placed in the 24 in. (610mm) diameter pipe (see **Figures C.7** and **C.8**) while only reflective prisms were employed in the 48 in. (1220mm) diameter pipe (see **Figure C.10**).

C.2.3.2 Test configuration

Both reinforced concrete pipe specimens were tested at 2 ft (610mm) of cover, with good burial conditions according to AASHTO guidelines and with the load applied directly over the joint. A larger loading area than the one employed during the service load testing was used to prevent or delay bearing failure of the soil (see **Figure C.22**). The rest of the configuration for this test was the same as the one described for the service loading.

Figure C.22. Increased size of the loading pad employed in the ultimate limit test of the reinforced concrete pipes (to prevent or delay bearing capacity failure under the loading pad).

C.2.3.3 Results

The initial cracking for the 24 in. (610mm) diameter pipe was register by the strain gages on the bell at a load of 52 kips (230kN); the initial cracking at the spigot was registered at 61 kips (270kN). A maximum surface load of 132 kips (587kN) was applied above this specimen. The crack pattern can be seen in **Figures C.23** to **C.25**. It appears that the load on the ground surface over the central joint caused the bell and spigot at the joint to move down (assisted by the fact that the bell was placed into a pre-excavated void filled with uncompacted soil), and this produced hogging in the pipe barrels. The incremental diameter change register by the prism can be seen in **Figure C.28** while the crown displacement of the pipe is illustrated in **Figure C.29**.

The 48 in. (1220mm) diameter pipe was loaded to a maximum of 157 kips (700kN) at the ground surface creating the cracking patterns shown in **Figure C.30**. Essentially only longitudinal cracks at the crown and invert of the joint elements could be seen. **Figure C.31** shows the incremental diameter change of the joint elements while the incremental displacement of the pipe crown can be seen in **Figure C.32**.

(a) Bell

(b) Spigot

Figure C.23. Crack pattern in the invert of the 24 in. (610mm) diameter reinforced concrete pipe

(a) Bell

(b) Spigot

Figure C.24. Crack pattern in the crown of the 24 in. (610mm) diameter reinforced concrete pipe

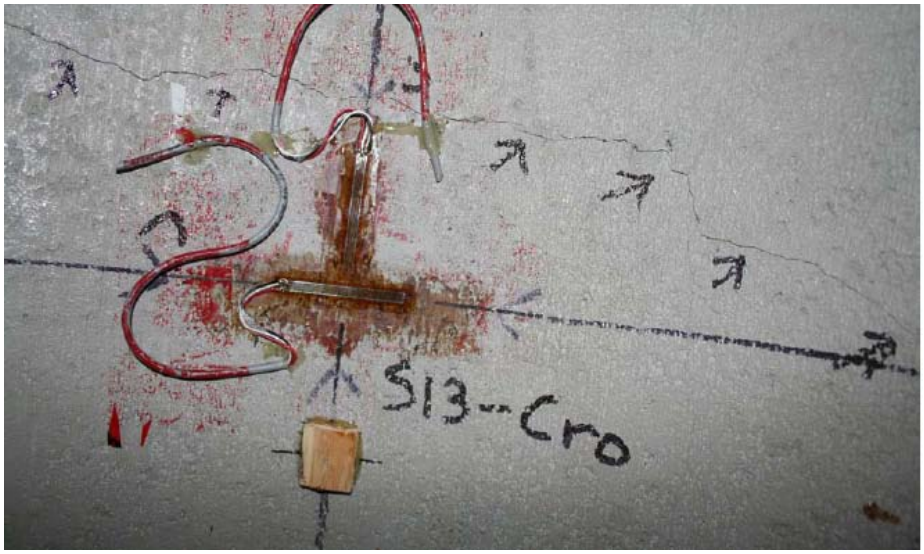

Figure C.25. Circumferential crack about mid-span in one of the 24 in. (610mm) diameter reinforced concrete pipes; the crack ran from about the 7 O'clock position right around the circumference past the crown to the 5 O'clock position; no crack was visible at the invert.

Figure C.26. Close-up of the invert of the 24 in. (610mm) diameter reinforced concrete pipe at the central joint; the joint is open about 1 in (25mm).

Figure C.27. Close-up of the crown of the 24 in. (610mm) diameter reinforced concrete pipe at the central joint; joint open about 0.5 in (12.5mm).

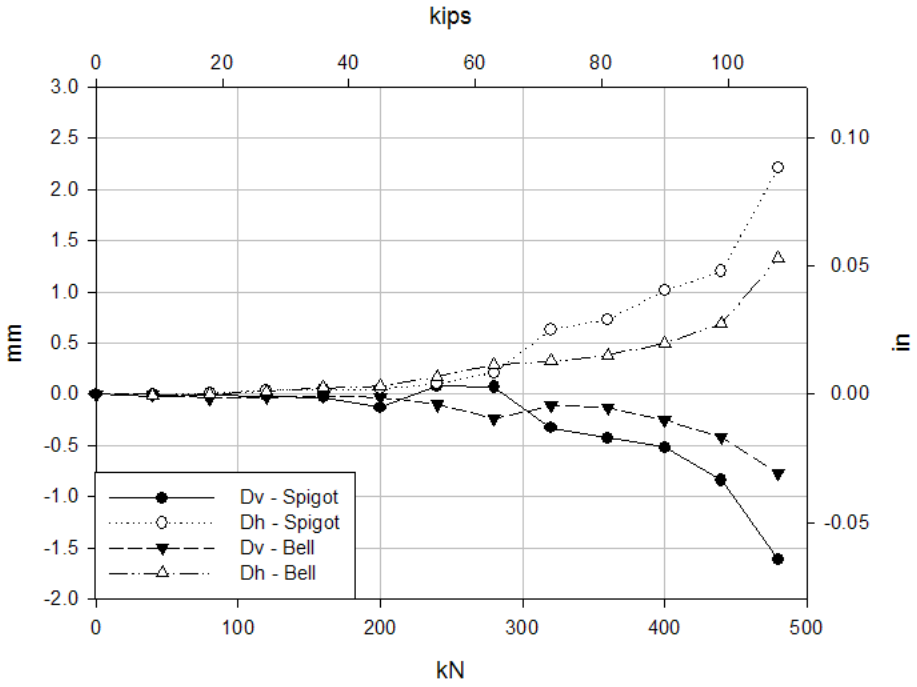

Figure C.28. Incremental diameter change in the joint elements of the 24 in. (610mm) reinforced concrete pipe during the ultimate limit state test.

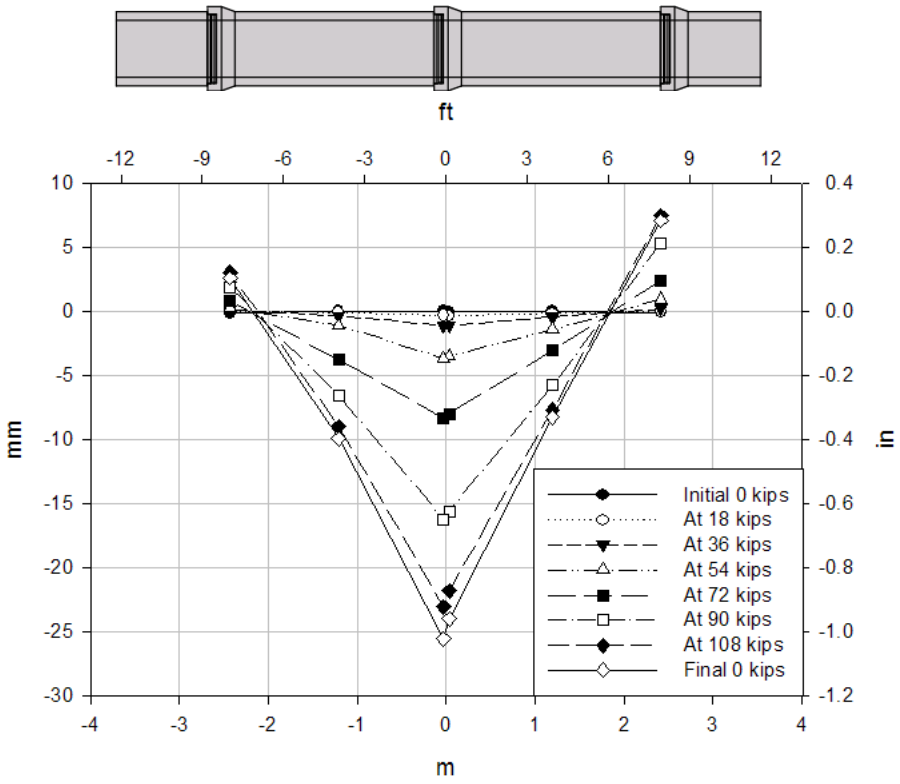

Figure C.29. Incremental crown displacement of the 24 in. (610mm) diameter reinforced concrete pipe during the ultimate limit state test.

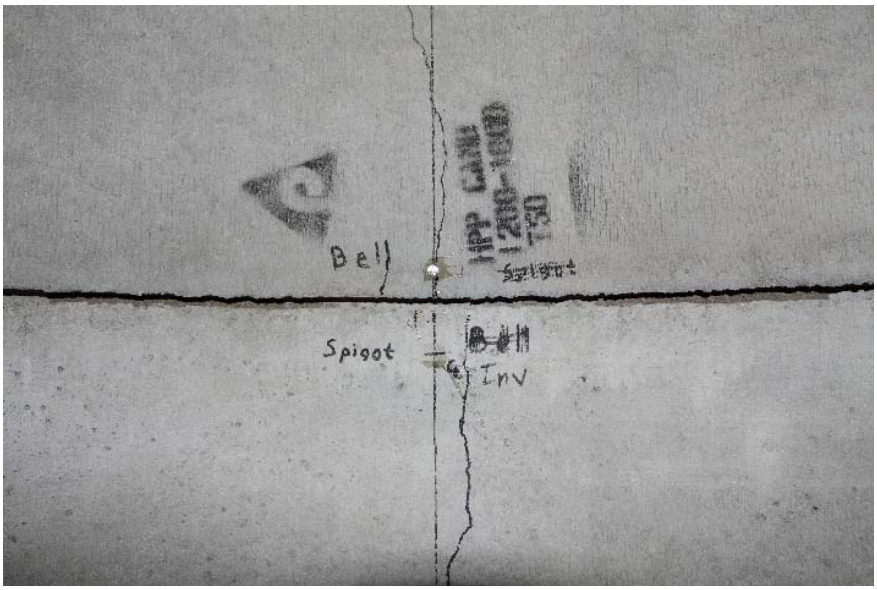

(a) Invert

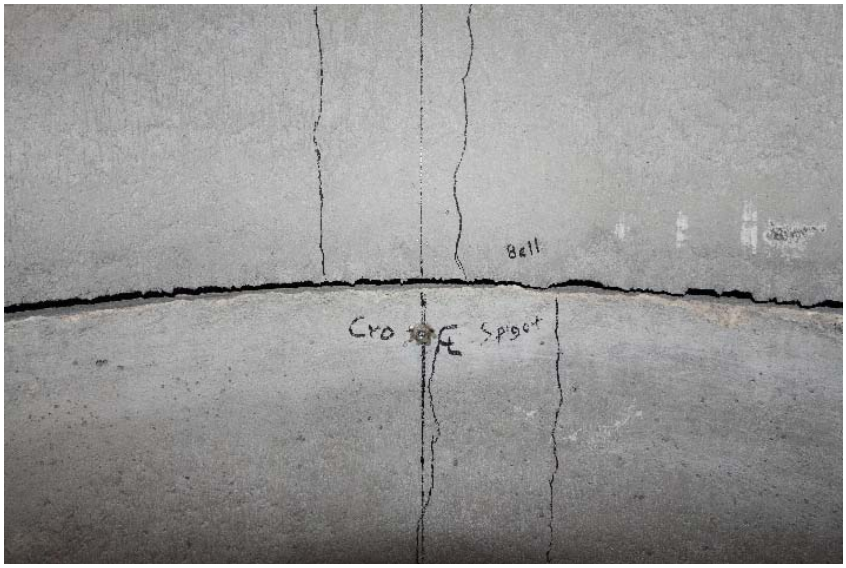

(b) Crown

Figure C.30. Crack pattern of the 48 in. (1220mm) diameter reinforced concrete pipe

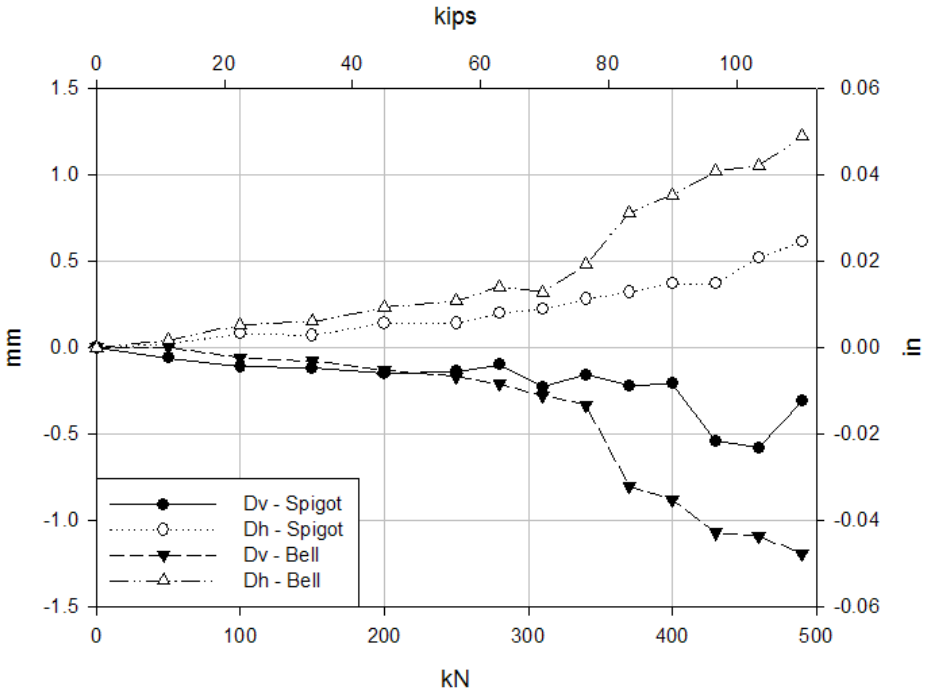

Figure C.31. Incremental diameter changes in the joint elements of the 48 in. (1220mm) diameter reinforced concrete pipe during the ultimate limit state test.

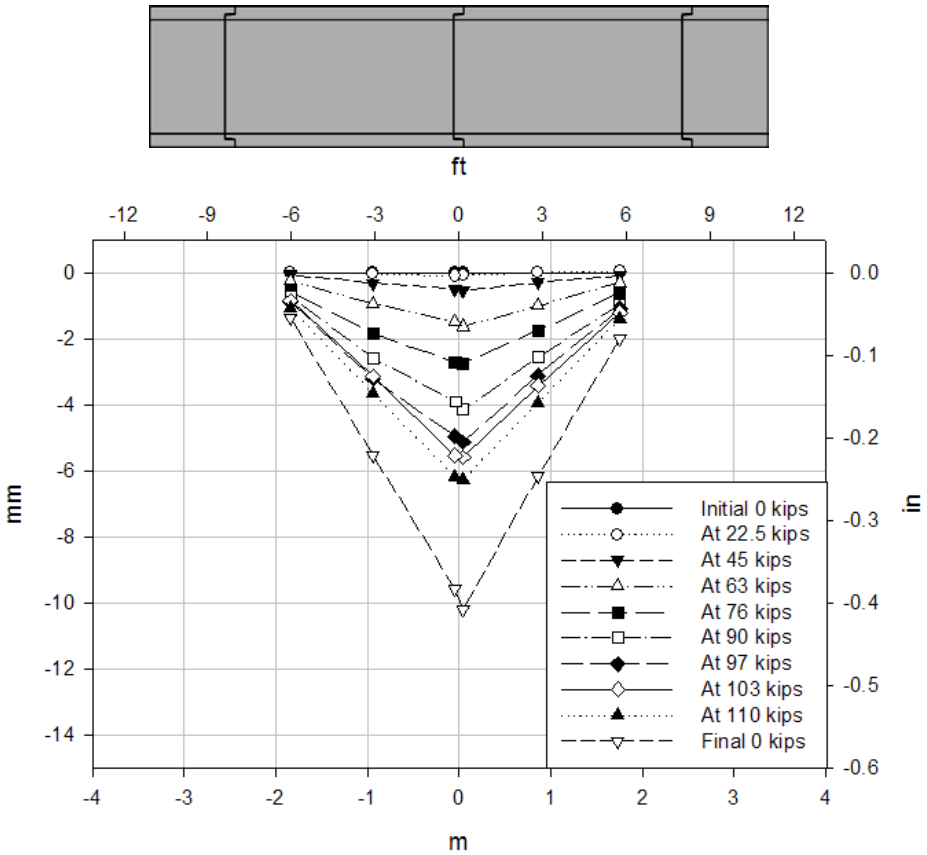

Figure C.32. Incremental crown displacement of the 48 in. (1220mm) diameter reinforced concrete pipe during the ultimate limit state test.

C.3 Corrugated steel pipes

Two 36 in. (915mm) diameter corrugated steel pipes with a hugger band joint were tested, one of them without sealing the joint and the other with O-ring type gaskets. First, bending tests were performed on the pipes to observe the rotation characteristics of each joint. Second, the pipes were buried and tested under service loadings. Two burial depths and different loading locations were examined for each pipe while different burial conditions were defined for the case where the joint was sealed with O-ring type gaskets. Finally, ultimate limit states were performed for each specimen. The details of these tests are presented below.

C.3.1 Bending test

The pipes were subjected to bending in a pure moment arrangement to investigate the response of the hugger band as it transfers moment from one pipe to the other across the joint and the effect of the presence of the O-rings. These tests were performed prior to burial inside the pit of the GeoEngineering laboratory.

C.3.1.1 Instrumentation

Both corrugated steel pipes were instrumented with electrical strain gages placed in the joint elements and in the barrels to measure strains in the circumferential, axial and helical directions (along the direction of the helix). The location of the strain gages can be seen in **Figures C.33** and **C.34** for the case without O-rings and with O-rings respectively. In addition, reflective prisms were placed in the crown, invert and springlines along the pipe of each specimen to measure displacements and changes in diameter. String potentiometers were also used in some locations to measure variations in the diameter and the displacement of the joint. The location of these elements can be seen in **Figures C.35** and **C.36** for the case without O-rings and with O-rings respectively.

Set	Element	Type of gage	Location inside	Location outside	Description
1	Pipe A	Triaxial	Cro, Inv, Sp x2	n/a	Valley, 3 ft (0.9m) from joint
2	Pipe A	Triaxial	Cro, Inv, Sp x2	n/a	Crest, 3 ft (0.9m) from joint
3	Pipe A	Biaxial	Cro, Inv, Sp x2	n/a	First valley after band
4	Pipe A	Biaxial	Cro, Inv, Sp x2	n/a	Second crest after band
5	Band	Biaxial	Cro, Inv	Cro, Inv	
6	Band	Triaxial	Cro, Inv, Sp x1	Cro, Inv, Sp x1	
7	Band	Biaxial	Cro, Inv	Cro, Inv	
8	Pipe B	Biaxial	Cro, Inv, Sp x2	n/a	Second crest after band
9	Pipe B	Biaxial	Cro, Inv, Sp x2	n/a	First valley after band

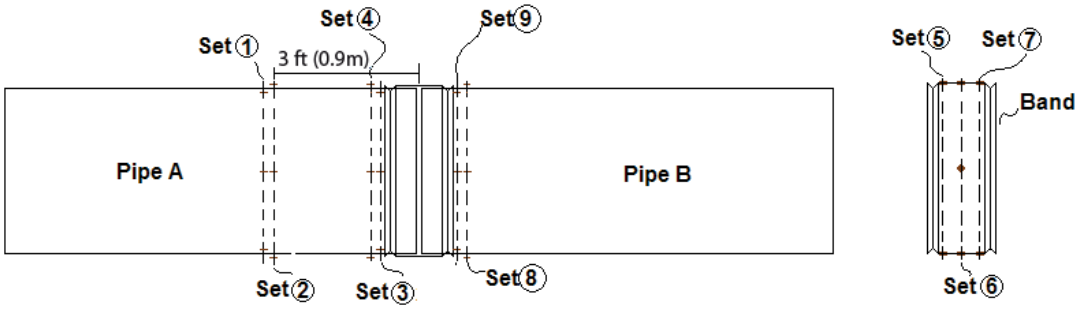

Figure C.33. Strain gage scheme for the 36 in. (915mm) diameter corrugated steel pipe without O-rings.

Set	Element	Type of gage	Location inside	Location outside	Description
1	Pipe A	Triaxial	Cro, Inv, Sp x2	n/a	Valley, 3 ft (0.9m) from joint
2	Pipe A	Triaxial	Cro, Inv, Sp x2	n/a	Crest, 3 ft (0.9m) from joint
3	Pipe A	Biaxial	Cro, Inv, Sp x2	n/a	First valley after band
4	Pipe A	Biaxial	Cro, Inv, Sp x2	n/a	First crest after band
5	Band	Biaxial	n/a	Cro, Inv, Sp x1	
6	Band	Triaxial	Cro, Inv, Sp x1	Cro, Inv, Sp x1	
7	Band	Biaxial	n/a	Cro, Inv, Sp x1	
8	Pipe B	Biaxial	Cro, Inv, Sp x2	n/a	First crest after band
9	Pipe B	Biaxial	Cro, Inv, Sp x2	n/a	First valley after band

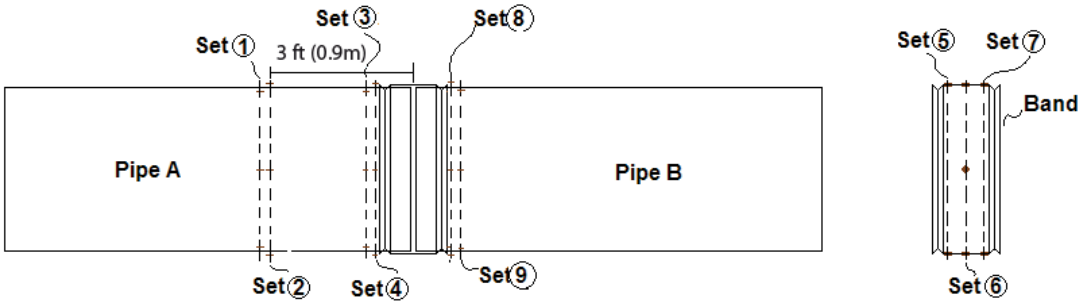

Figure C.34. Strain gage scheme for the 36 in. (915mm) diameter corrugated steel pipe with O-rings.

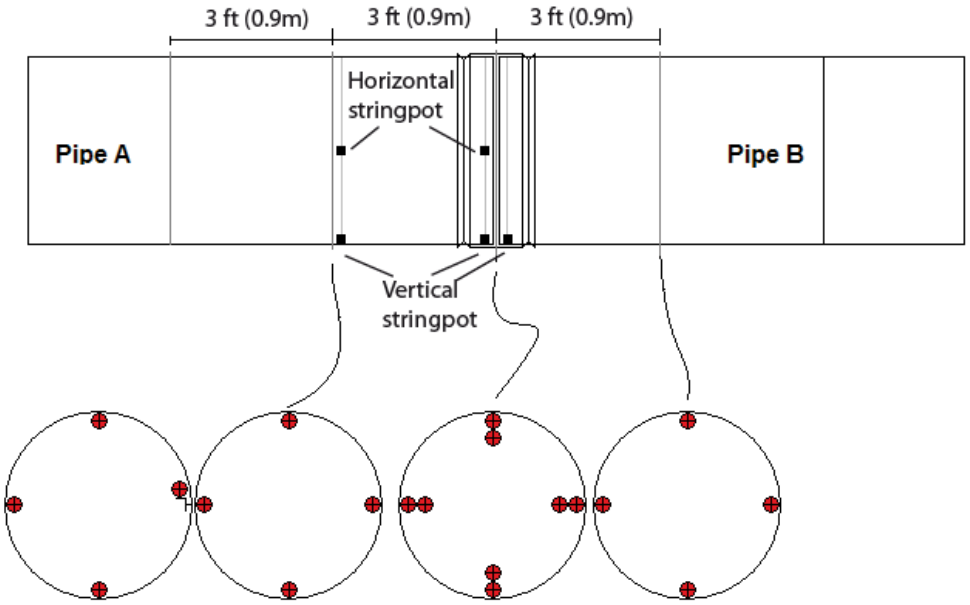

Figure C.35. Reflective prism and string potentiometer scheme for the 36 in. (915mm) diameter corrugated steel pipe without O-rings.

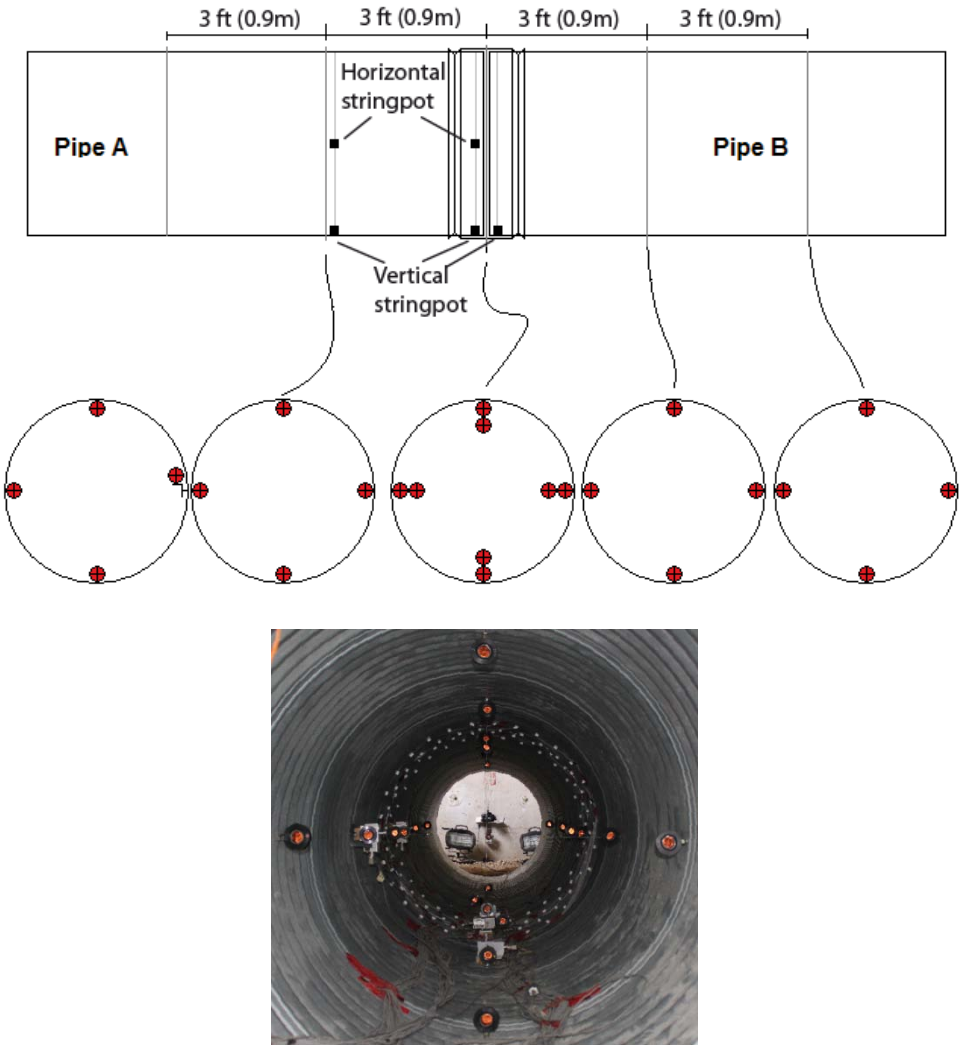

Figure C.36. Reflective prism and string potentiometer scheme for the 36 in. (915mm) diameter corrugated steel pipe with O-rings.

C.3.1.2 Test configuration

A four point bending test was performed to each of the assembled pipe system as shown in **Figure C.37** and **Figure C.38**. No guidelines were used to assemble the pipe with no gasket since is a situation not recommended by the manufacturer. For the case where O-rings were used, the manufacturer guidelines where followed and consisted in:

- Fit and align the band
- Tighten the bolts in the band until it was snug
- Tap around the perimeter of the band with a rubber mallet (releasing tension)
- Repeat procedure until a final torque of 25-50 lbf*ft

In each case the pipe was rested in wooden blocks placed under the barrel while an I-beam was employed to transfer the load next to the joint subjecting it to pure moment. **Figure C.39** shows

details of one of these tests. The load was applied with an actuator placed above the pit mounted on beams while a string potentiometer placed at the top of the joint measured the displacement; set to 1 in (25mm) for both cases.

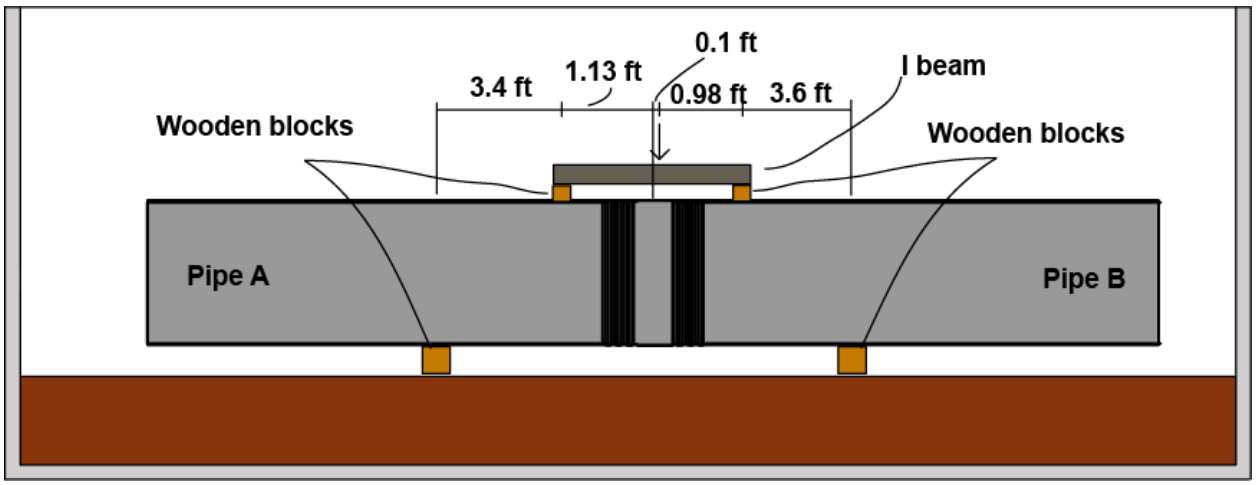

Figure C.37. Bending test configuration of the 36 in. (915mm) corrugated steel pipe without gasket.

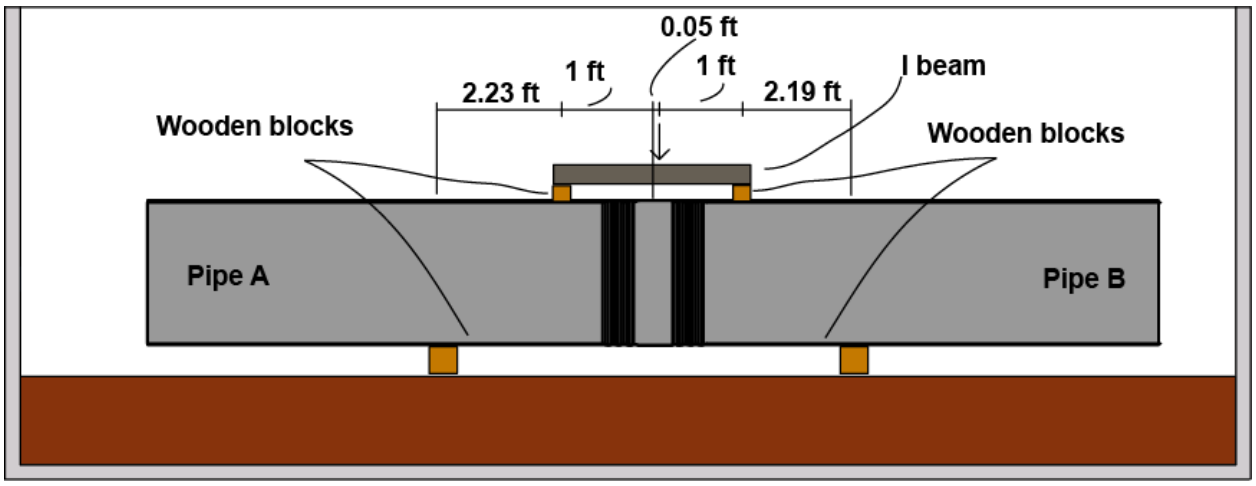

Figure C.38. Bending test configuration of the 36 in. (915mm) corrugated steel pipe with O-rings.

(a) Support condition.

(b) Loading condition.

(c) Overall pipe arrangement - image

Figure C.39. Bending test of one of the 36 in. (915mm) diameter corrugated steel pipe.

C.3.1.3 Results

The goal of these tests was to investigate the response of the hugger band as it transfers moment from one pipe to another across the joint. The response was different when employing O-rings. For the case without O-rings, the response was found to be in two parts as illustrated in **Figure C.40**. It appears that during initial loading, the deformations were composed of two parts – elastic distortion of the pipe and band, and inelastic deformation of the band relative to the pipe (associated with slip at the band-pipe contacts). Then, a series of unload-reload cycles were imposed, which demonstrate a largely elastic incremental behavior (featuring fully recoverable deformation). It is expected that in a buried pipe configuration, the application of soil loads would mobilize any sliding between band and pipe that would be expected. Subsequent response under surface load would be expected to be recoverable (elastic). This type of recoverable deformation was seen in the field tests reported in Appendix D.

Therefore, incremental strain response during cyclic loading is illustrated in **Figure C.41**. Preliminary analysis of these strains indicates that the pattern of incremental circumferential strains implies ovaling in the band during vertical loading (decrease in vertical diameter and increase in horizontal diameter that produces tensile strain on the outside of the band at springlines, and compressive strain at crown and invert).

The response observed in the case where the O-rings were employed was essentially linear elastic during the initial loading and during the loading cycles applied afterwards. This behavior can be observed in **Figure C.42**. The distortion imposed to the joint, i.e. changes in diameter, was fully recovered after the load was removed. In the same way, the displacement imposed to the joint was recovered almost completely. The recorded strains also shown recoverable linear or bilinear behavior and their magnitude were smaller than those measured in the case where no O-rings were used, **Figure C.43**.

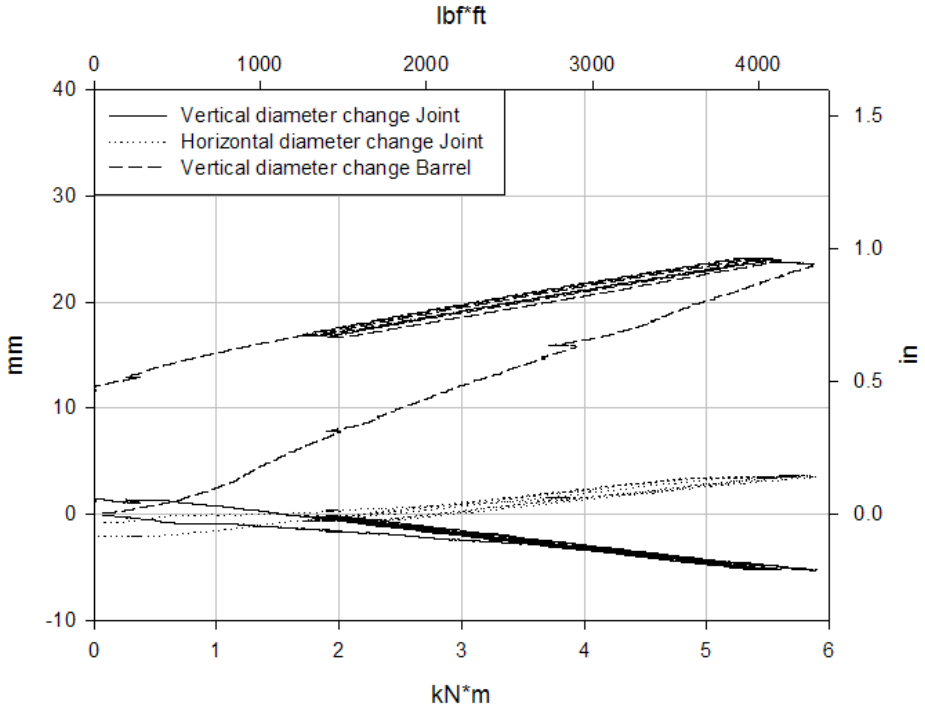

Figure C.40. Record of imposed vertical displacement and record of changes in joint diameter during initial and cycling loading; 36 in. (915mm) diameter corrugated steel pipe without O-rings.

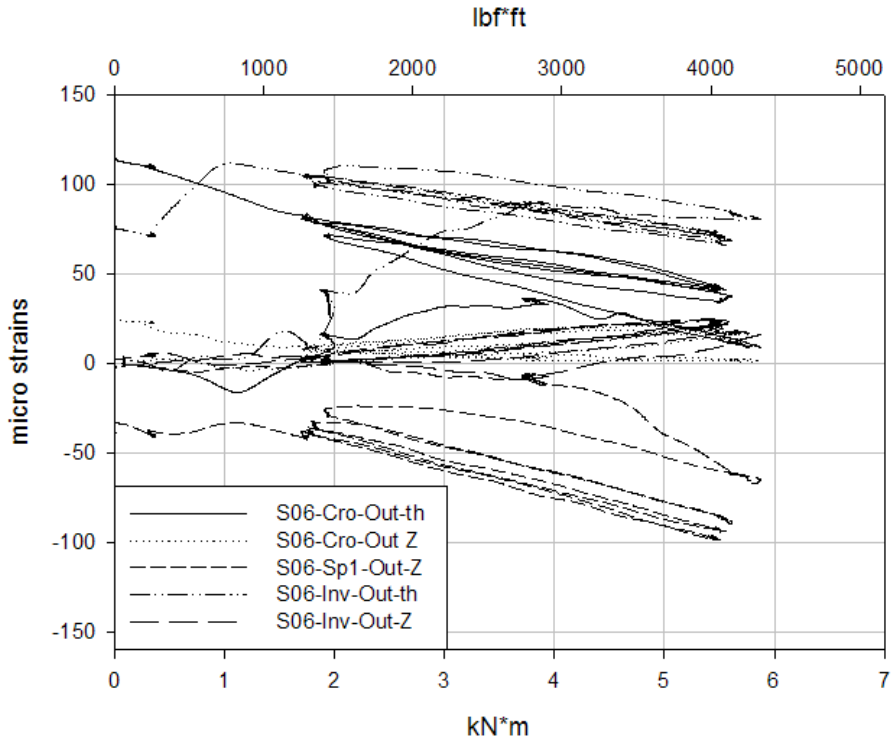

Figure C.41. Measured strains at some locations at the band during bending test; 36 in. (915mm) diameter corrugated steel pipe without O-rings.

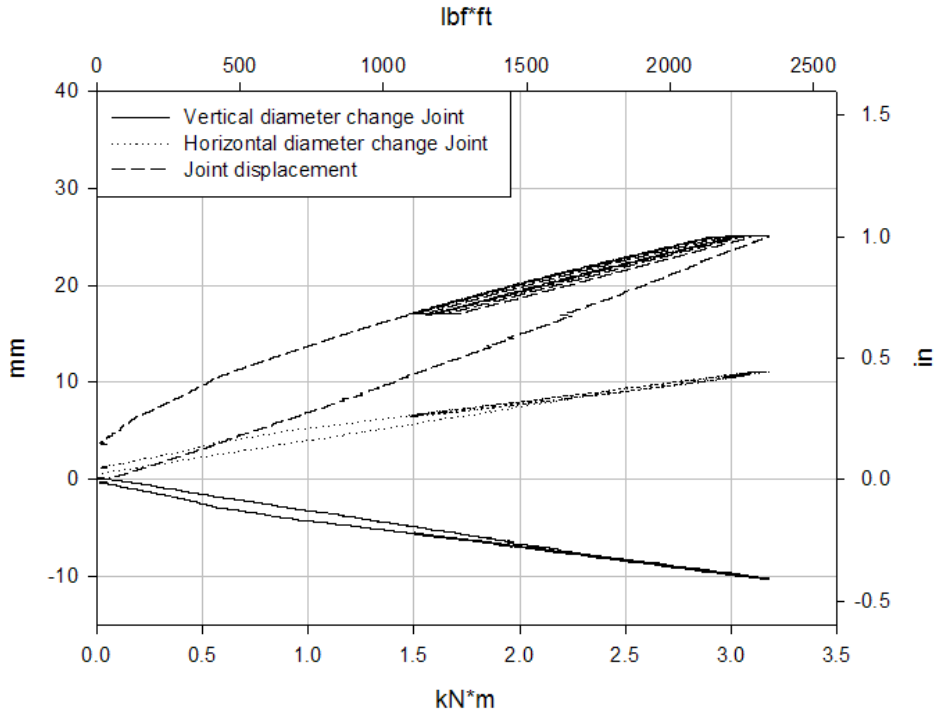

Figure C.42. Record of imposed vertical displacement and record of changes in joint diameter during initial and cycling loading; 36 in. (915mm) diameter corrugated steel pipe with O-rings.

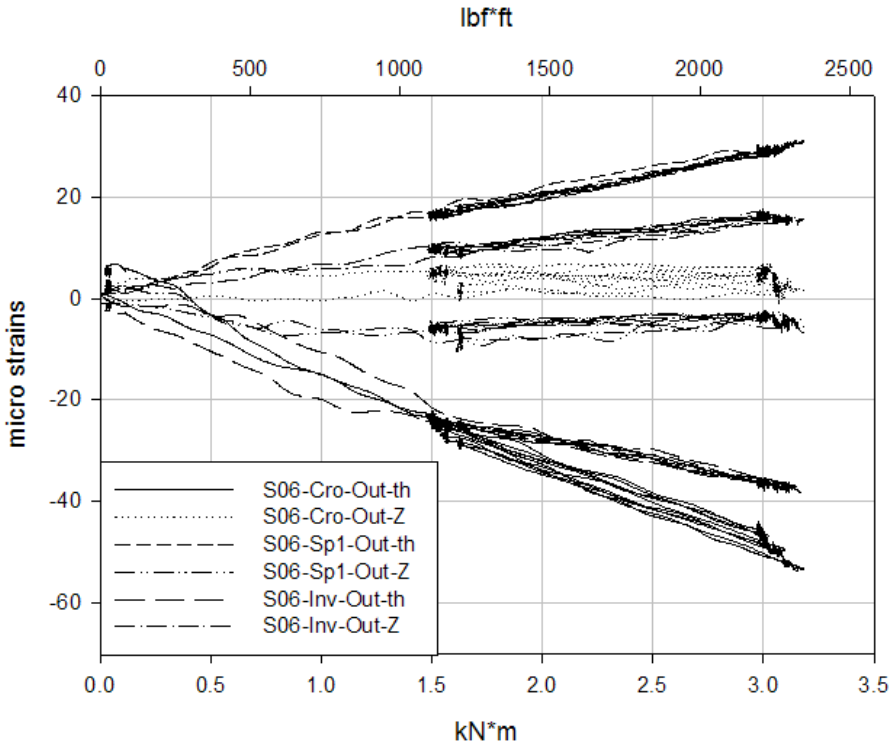

Figure C.43. Measured strains at some locations of the band during bending test; 36 in. (915mm) diameter corrugated steel pipe with O-rings.

C.3.2 Buried pipe tests

The two corrugated steel pipes were tested under burial responding to live loads. The case where no O-rings were employed was tested at adequate AASHTO burial condition, at two burial depths and different locations of the live load relative to the joint. The case where the joint was sealed with O-rings was tested at three burial conditions, including adequate burial conditions. This pipe was also tested at different burial depths and different locations of the live load relative to the joint. The details of each test are described herein.

C.3.2.1 Instrumentation

The instrumentation employed in these tests was the same for each case as the one described in the bending test. Electrical strain gages were attached to the pipes and hugger band to monitor axial, circumferential and helical strains (those along the direction of the helix) while reflective prisms were placed along the pipe to measure displacements and changes in diameter. In addition, string potentiometers were placed at the joint and at the barrel, 3 ft (0.9m) from the joint, to measure vertical and horizontal changes in diameter (see **Figures C.33** to **C.36** for details).

C.3.2.2 Test configuration

The corrugated steel pipe without O-rings was buried in accordance with AASHTO guidelines (Type 1 backfill compacted to 90 to 95 % of maximum standard Proctor dry density) in the configuration show in **Figure C.44**, and then was subjected to surface loads. Only two pipe segments were used connected with a single 'hugger band' joint without sealing elements. Two burial depths were examined: 2 ft (610mm) and 4 ft (1220mm). Three locations of the surface load were tested in each burial depth: directly over the joint and at 3 ft (0.9m) from the joint in each direction over the pipe.

For the corrugated steel pipe with O-rings, three burial conditions were examined. The first burial condition is illustrated in **Figure C.45** and consisted in leaving a void of approximately one diameter length and depth of 1/6 diameter under the joint of the pipe before burial. The remaining of the burial was performed in accordance with AASHTO guidelines. The second burial condition consisted in placing loose material around one of the two pipes of the system (from the invert to the crown) while the rest of the burial was made in accordance with AASHTO guidelines. **Figure C.46** shows this condition. These first two burial conditions were examined at 2 ft (610mm) of cover and at three locations of the surface load; directly over the joint and at 3 ft (0.9m) offset from the joint in each direction over the pipe. The third condition consisted of good burial in accordance with AASHTO guidelines (the same conditions as those for the pipes where no O-rings were employed). Two burial depths were examined: 2 ft (610mm) and 4 ft (1220mm). Three locations of the surface load were tested for each burial depth as described before.

Loading was applied using a 2000kN (220 US ton) capacity actuator mounted over the test pit, and restrained by a reaction frame anchored into the limestone below. Loading was applied through a steel plate having the design dimensions of the standard AASHTO wheel pair at the end of a design axle, **Figure C.47**. The loading was designed to represent the action of one wheel pair at the end of a single 32000 lbf axle (143 kN). Half that single axle (the load on one wheel pair) is 16000 lbf. Considering multiple presence factor of 1.2, and impact factors of 1.25 at 2ft of burial, and 1.17 at 4ft of burial, the factored service load becomes 24000 lbf (107 kN) at 2ft of cover, and 22500 lbf (100 kN) at 4ft of cover. For reasons of simplification and to facilitate comparisons of joint response all 'service load' testing was conducted up to 22.5 kips (100kN). The poor backfill cases were loaded with only half the service load to prevent damage of the specimen.

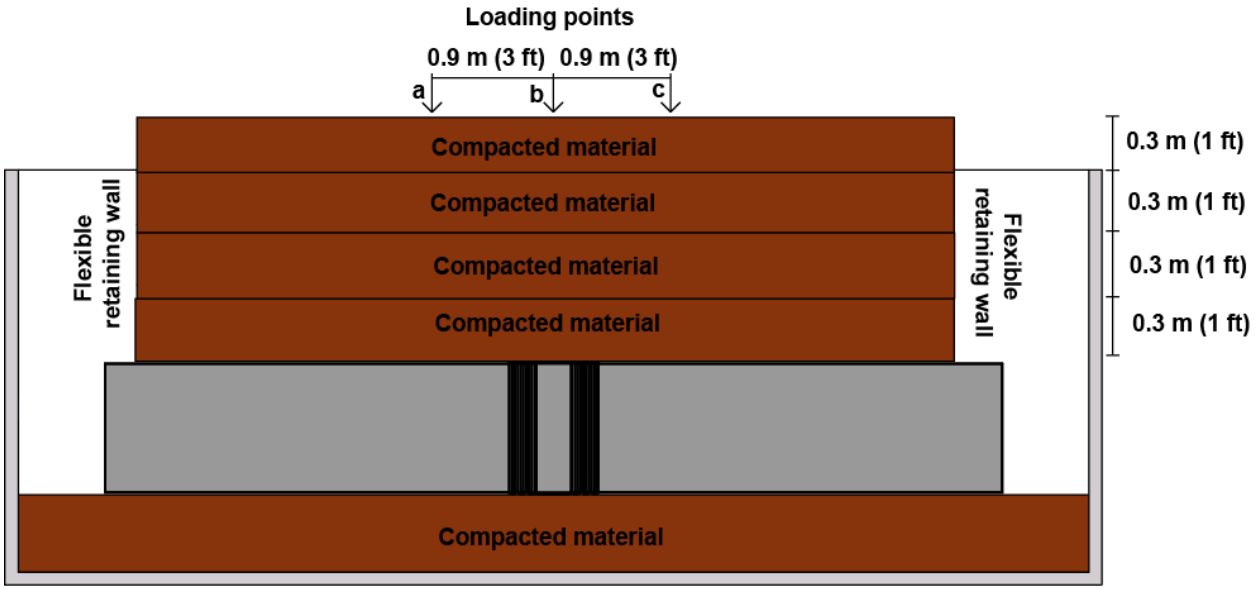

(a) Longitudinal section

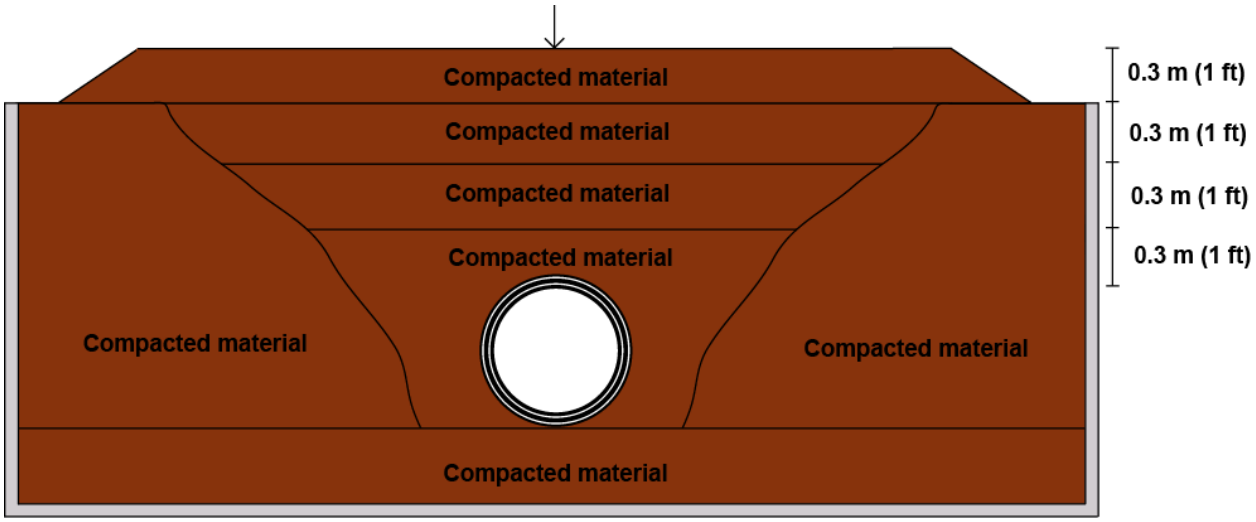

(b) Section normal to pipe axis

Figure C.44. Configuration of good burial condition for the 36 in. (915mm) diameter corrugated steel pipe without O-rings (in accordance with AASHTO LRFD Bridge Construction Specifications).

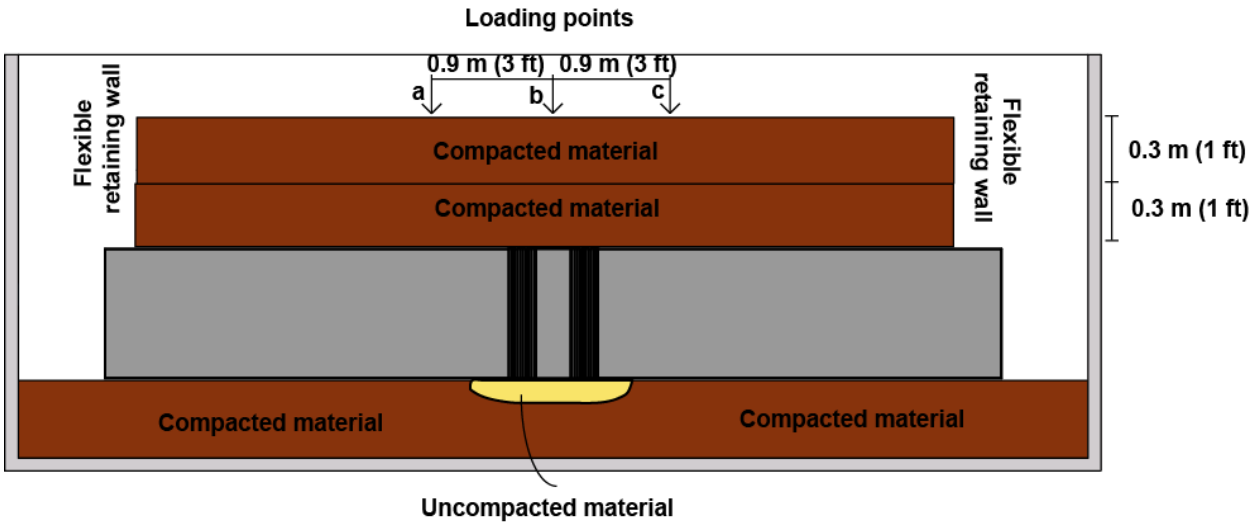

(a) Longitudinal section

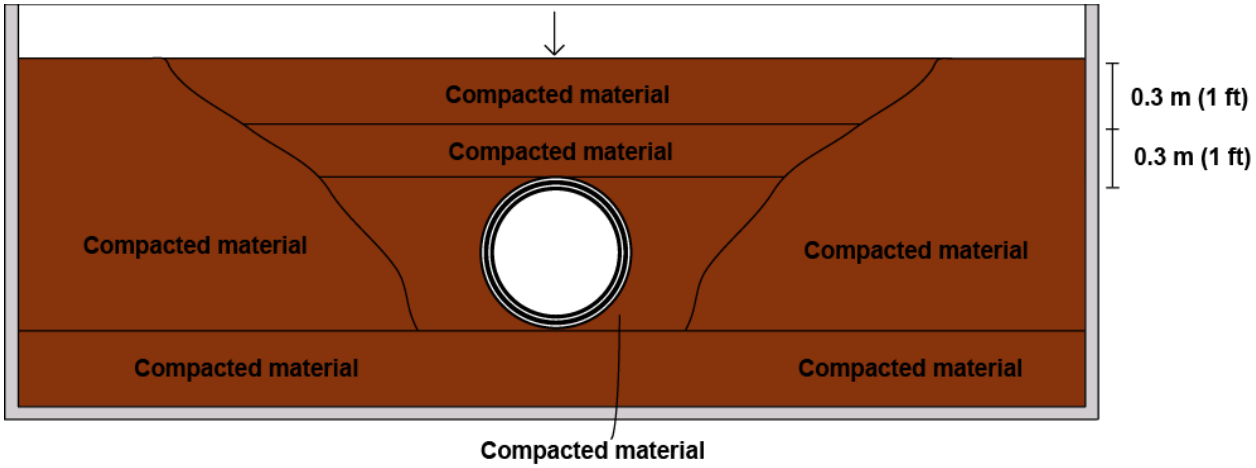

(b) Section normal to pipe axis

(c) Void details

Figure C.45. Configuration of poor burial condition for the 36 in. (915mm) diameter corrugated steel pipe with O-rings; void under the joint.

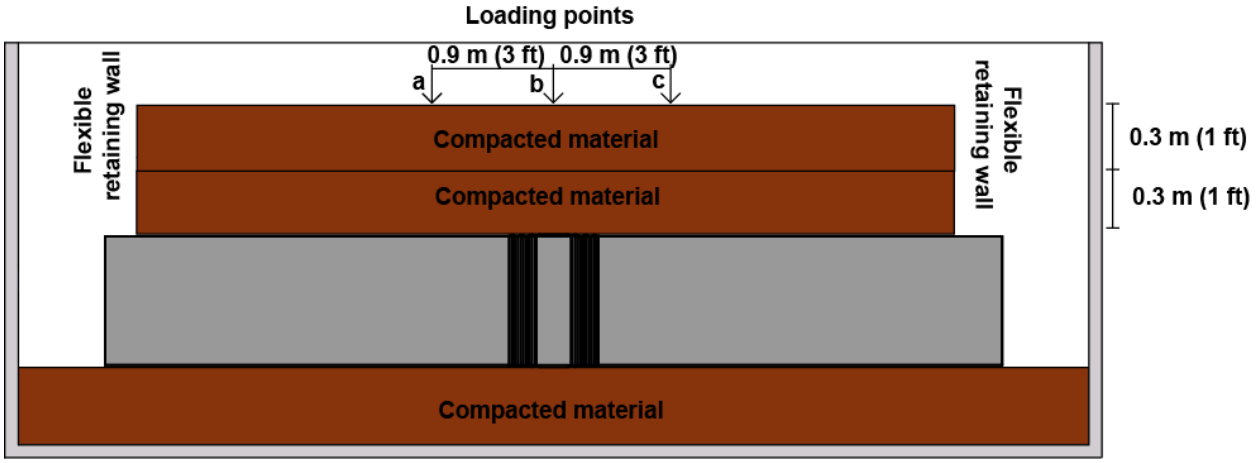

(a) Longitudinal section

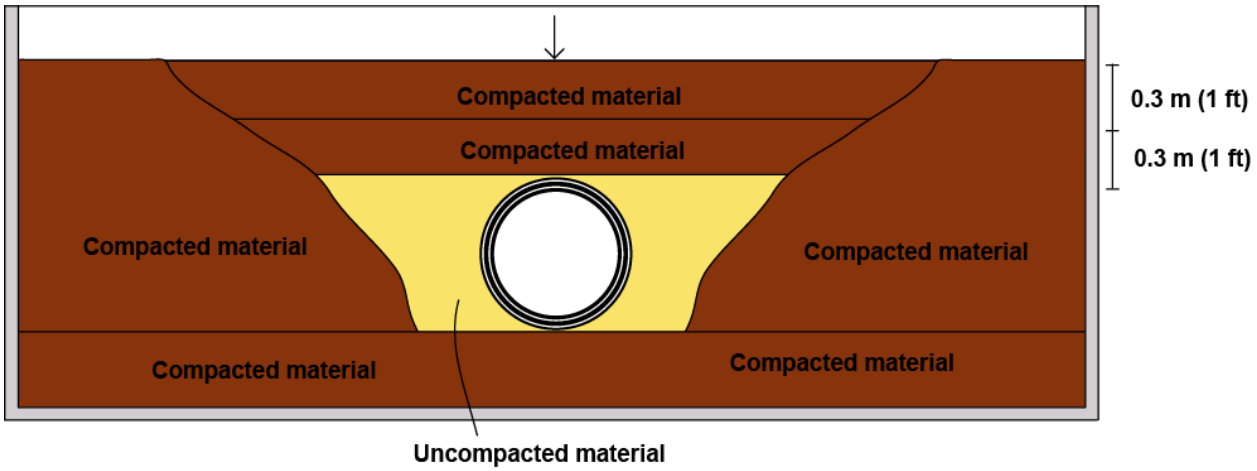

(b) Section normal to pipe axis

(c) Burial details

Figure C.46. Configuration of poor burial condition for the 36 in. (915mm) diameter corrugated steel pipe with O-rings; loose soil supporting one pipe.

(a) 4 ft (1220mm) of cover (b) 2ft (610mm) of cover

Figure C.47. Actuator loading of the 36 in. (915mm) diameter corrugated steel pipe at two burial depths

C.3.2.3 Results

Changes in diameter in the joint and barrels were obtained from the reflective prism data. For the case where no O-rings were employed and the loading was applied directly over the joint, the response in the joint was non-linear as can be seen in **Figures C.48** and **C.49**. The magnitudes of changes in diameter in the barrel were smaller at 3 ft (0.9m) from the joint and close to zero at 6 ft (1.8m); the response in some cases was also non-linear. At 2ft (610mm) of cover higher diameter changes were observed and non-linearity is more pronounced.

Figures C.50 and **C.51** show the changes in vertical and horizontal diameter of the corrugated steel pipe with O-rings buried in poor conditions, loading directly over the joint and at 11.25 kips (50kN) live load (i.e. half the full factored service load). For the case with a void under the joint, the response of the joint and barrels was linear and the effects of the load reduced at 6 ft (1.8m) from the joint. The case where one of the pipes of the system was buried in loose soil showed non-linear joint and barrels responses. The magnitudes of the changes in diameter in the joint were similar to those observed in the case with the void under the joint; however, larger changes in diameter were observed in the pipe that was buried in loose material.

The response observed in the corrugated steel pipe where O-rings were employed and good burial conditions were examined can be seen in **Figures C.52** and **C.53**. The response in the joint was non-linear and the magnitudes of changes in diameter were smaller 3 ft (0.9m) from the joint and close to zero at 6 ft (1.8m); the response of the barrels in some cases was also non-linear. Non-linearity is more pronounced at 2ft (610mm) of cover and higher diameter changes were observed at this burial depth.

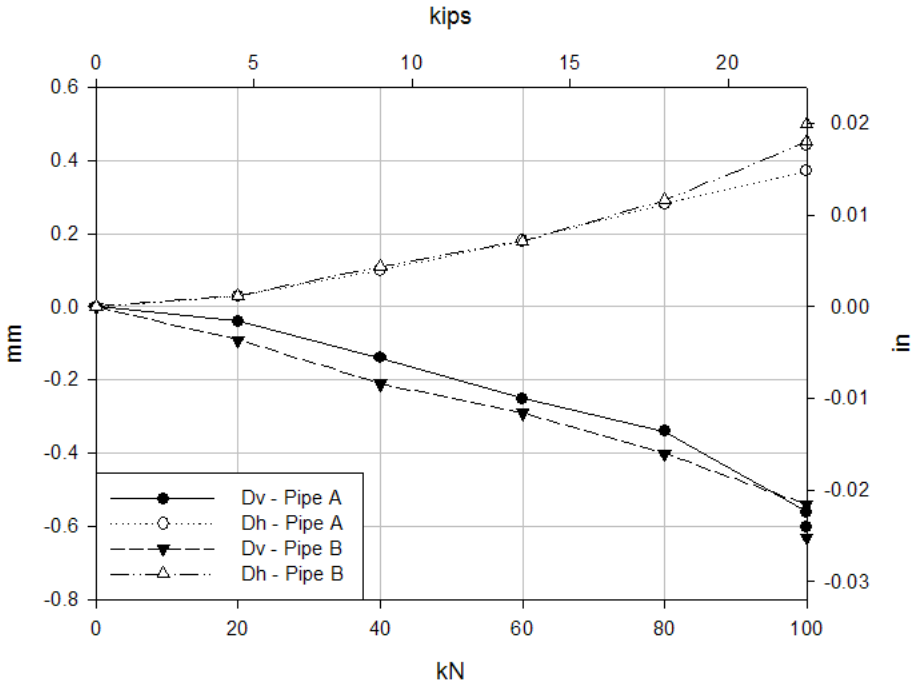

(a) Joint

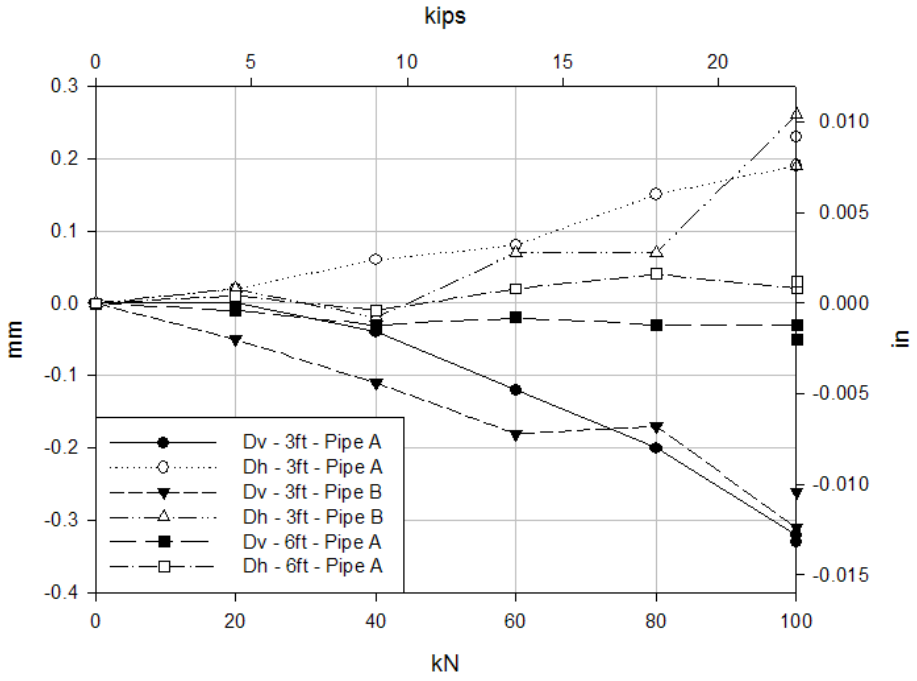

(b) Barrels

Figure C.48. Incremental diameter changes of the 36 in. (915mm) diameter corrugated steel pipe with no gasket; 4 ft (1220mm) of cover, surface load over joint.

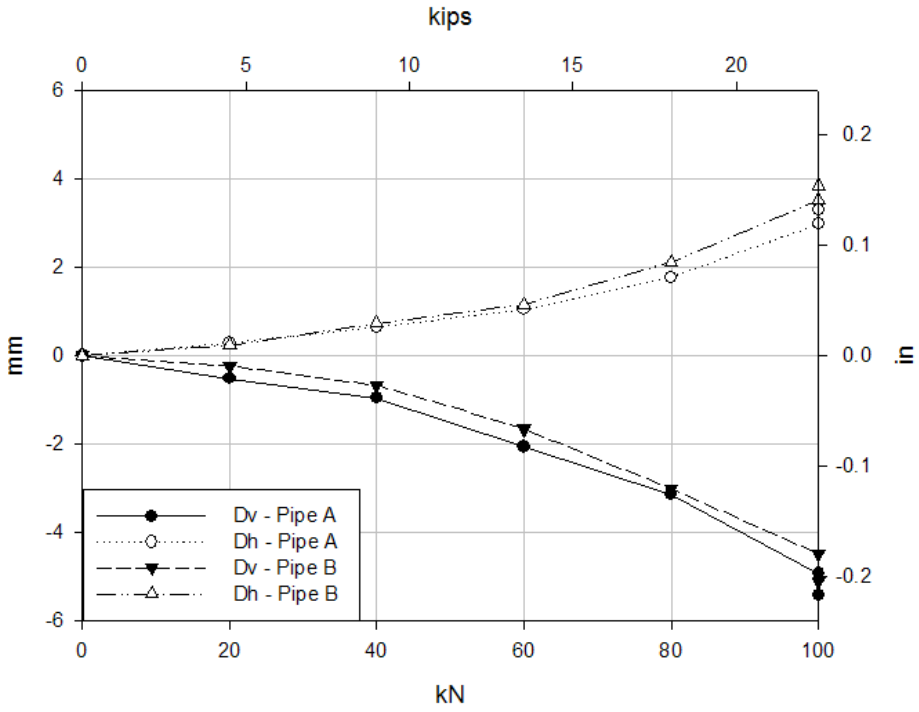

(a) Joint

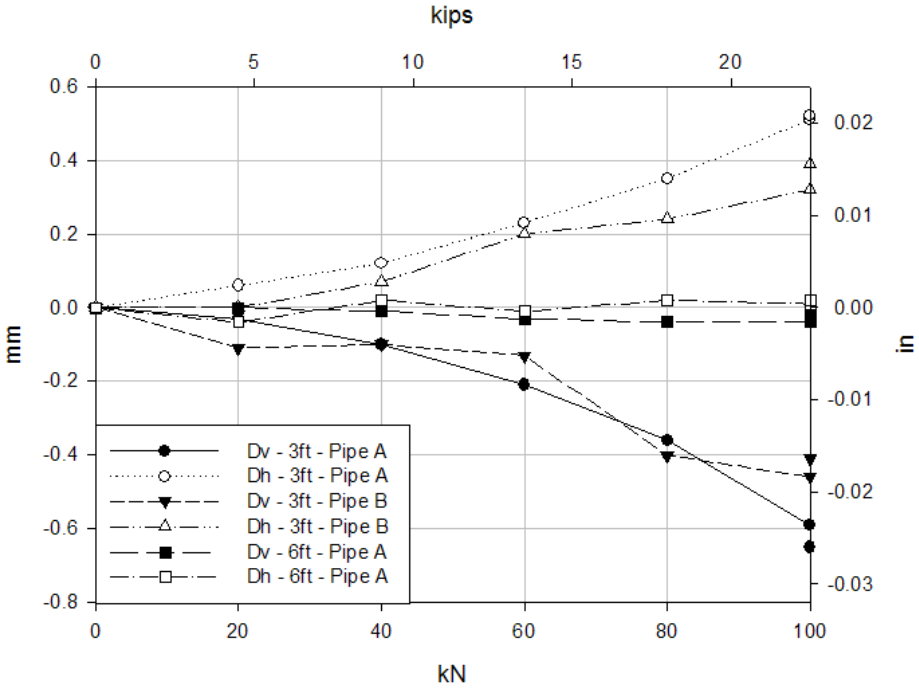

(b) Barrels

Figure C.49. Incremental diameter changes of the 36 in. (915mm) diameter corrugated steel pipe without O-rings; 2 ft (610mm) of cover; surface load over joint.

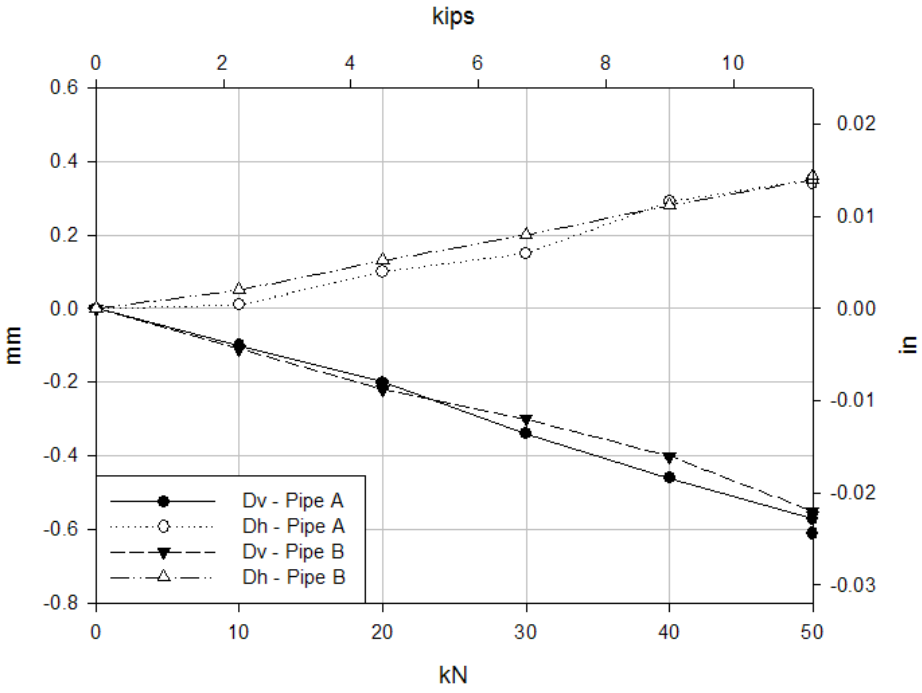

(a) Joint

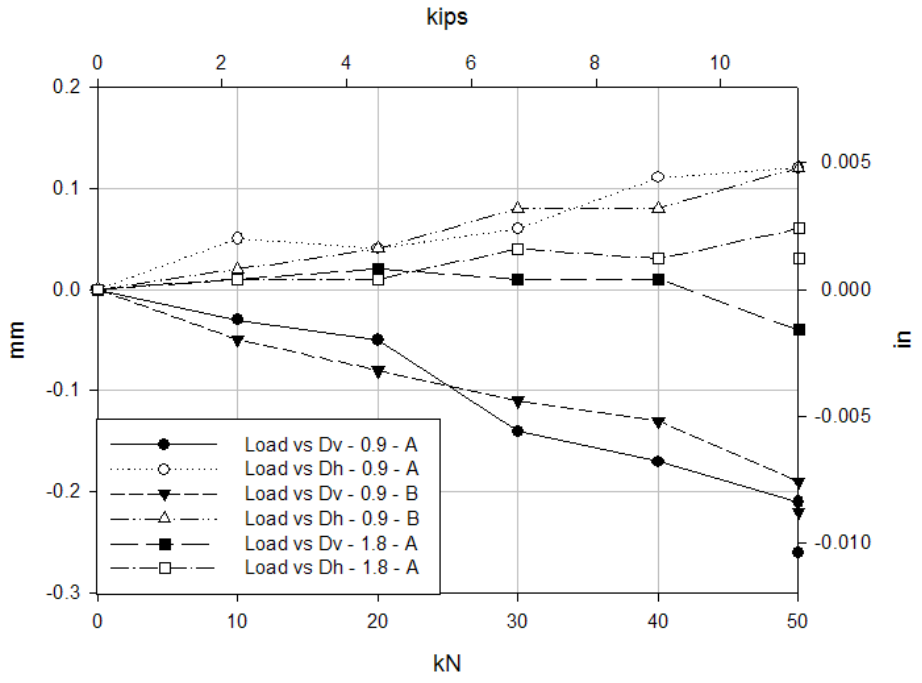

(b) Barrels

Figure C.50. Incremental diameter changes of the 36 in. (915mm) diameter corrugated steel pipe with O-rings; 2 ft (610mm) of cover; surface load over joint; void under joint burial.

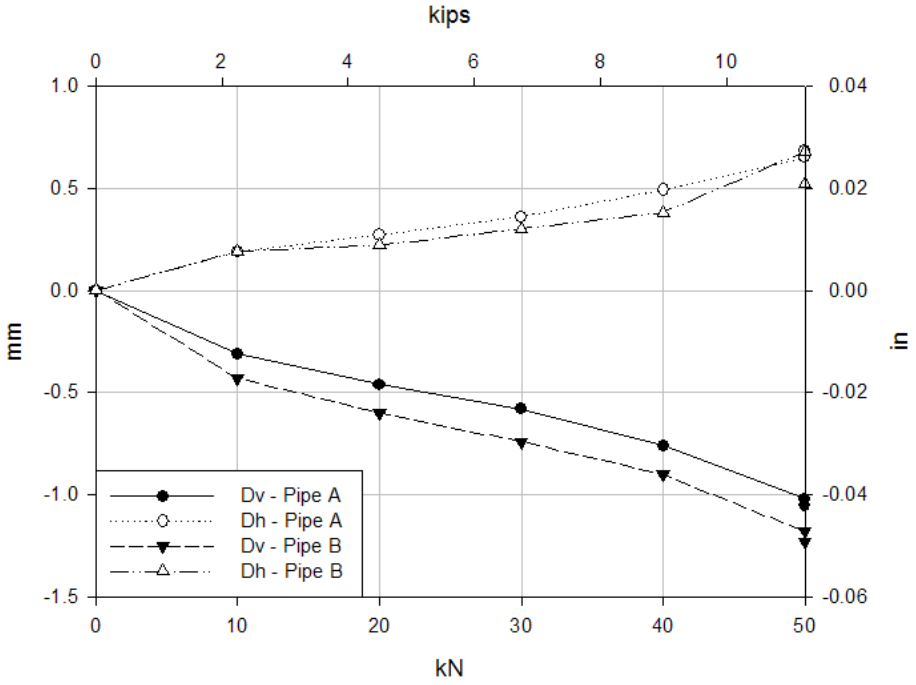

(a) Joint

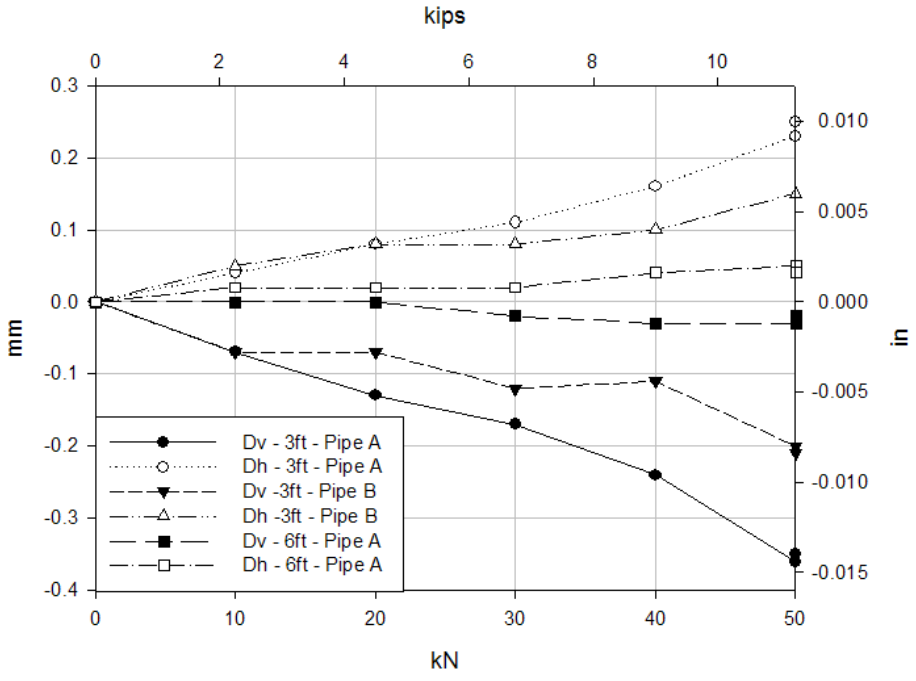

(b) Barrels

Figure C.51. Incremental diameter changes of the 36 in. (915mm) diameter corrugated steel pipe with O-rings; 2 ft (610mm) of cover; surface load over joint; poor backfill around one pipe.

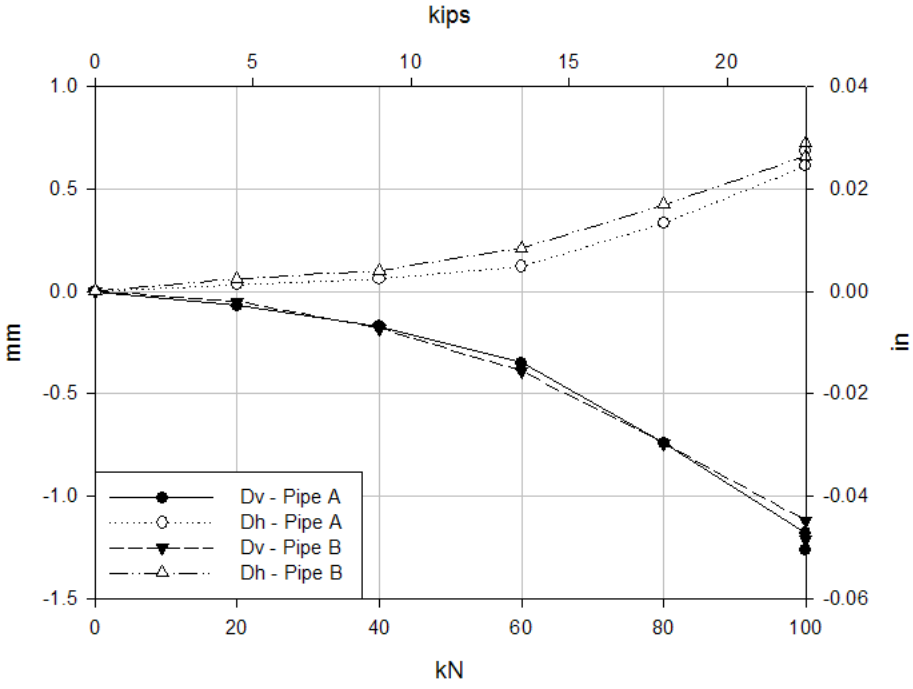

(a) Joint

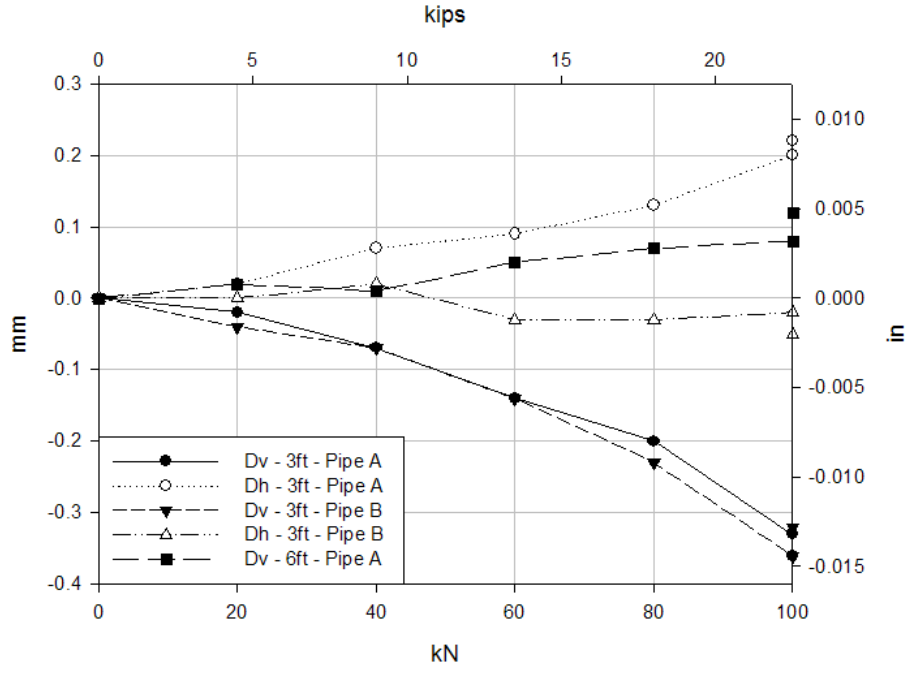

(b) Barrels

Figure C.52. Incremental diameter changes of the 36 in. (915mm) diameter corrugated steel pipe with O-rings; 4 ft (1220mm) of cover; surface load over joint; good burial.

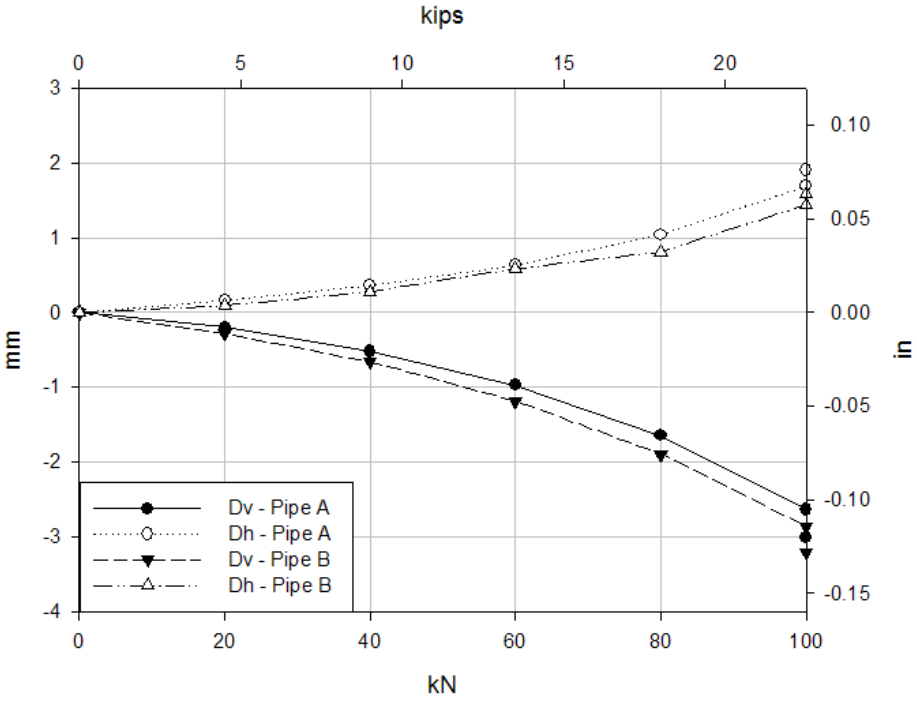

(a) Joint

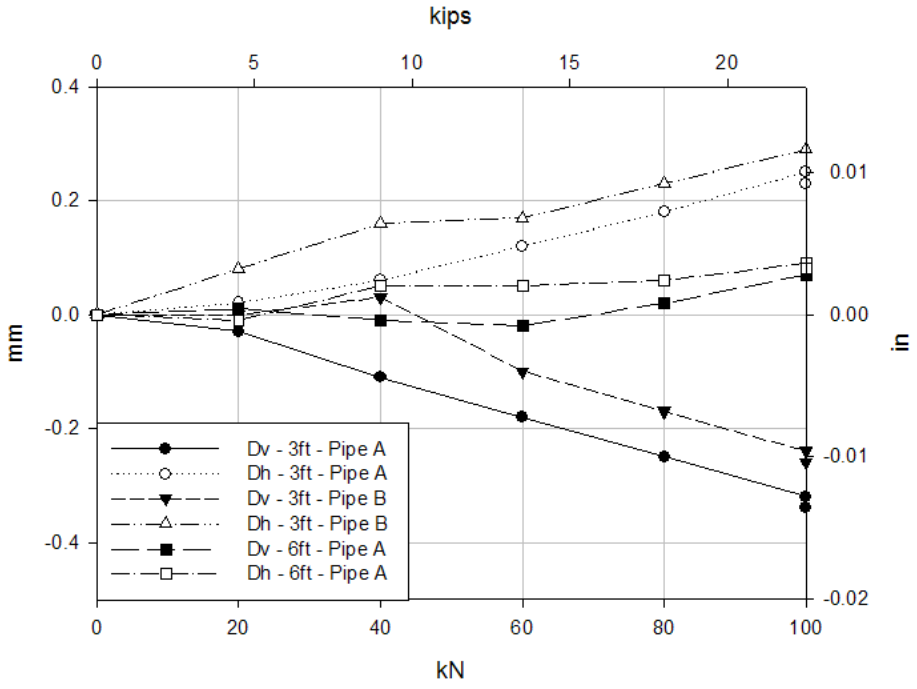

(b) Barrels

Figure C.53. Incremental diameter changes of the 36 in. (915mm) diameter corrugated steel pipe with O-rings; 2 ft (610mm) of cover; surface load over joint; good burial.

The data from the reflective prisms was also employed to plot vertical displacements of the springlines in the pipe while the live load was applied over pipes at different burial depths, burial conditions and load locations. Springline displacements rather than crown displacements were employed since they represent a global response of the pipe while the crown movements include localized responses due to the flexibility of the pipe (vertical diameter change). **Figure C.54** shows the springline displacement of the corrugated steel pipe without O-rings at two burial depths while the service load was applied (i.e. 22.5 kips). A symmetric response was observed at both burial depths when the load was applied with a 3 ft (0.9m) offset from the joint in both directions of the pipe. A larger magnitude of displacement was observed a 2 ft (610mm) of cover. Furthermore these results show that the load effect induced more localized behavior at 2 ft (610mm) of cover since the displacement of the barrels were similar at both burial depths.

Figure C.55 shows the response of the corrugated steel pipe with O-rings under poor burial conditions and loaded at half the service load (i.e. 11.25 kips). The results observed in the case with a void under the joint have small magnitudes but symmetric behavior can be observed when the load was offset on either side of the joint. Alternatively, the case where one of the pipes was buried in loose soil showed a non-symmetric response when the surface load was applied offset from the joint in both directions. As expected, a larger displacement was observed in the springlines of the pipe buried in loose material while the other side had magnitudes similar to the case where a void was constructed under the joint.

When good burial conditions were used for the corrugated steel pipe with O-rings, a symmetric response was observed for the offset loading at 4 ft (1220mm) and 2 ft (610mm) of cover as can be seen in **Figure C.56**. The largest displacements were observed at 2 ft (610mm) of cover and a more localized effect of the load at this burial depth was observed as well. **Figure C.57** shows the comparison of the cases with and without O-rings at the two examined burial depths while loaded directly over the joint. A comparison of the poor burial conditions examined for the corrugated steel pipe with O-rings can also be seen. Under good burial conditions, the largest displacement was observed for the pipe where no O-rings were used. Perhaps the O-rings compressed and took some of the displacement when transmitting forces from the band to the end of the pipes in the joint. No difference was observed when comparing the poor burial conditions.

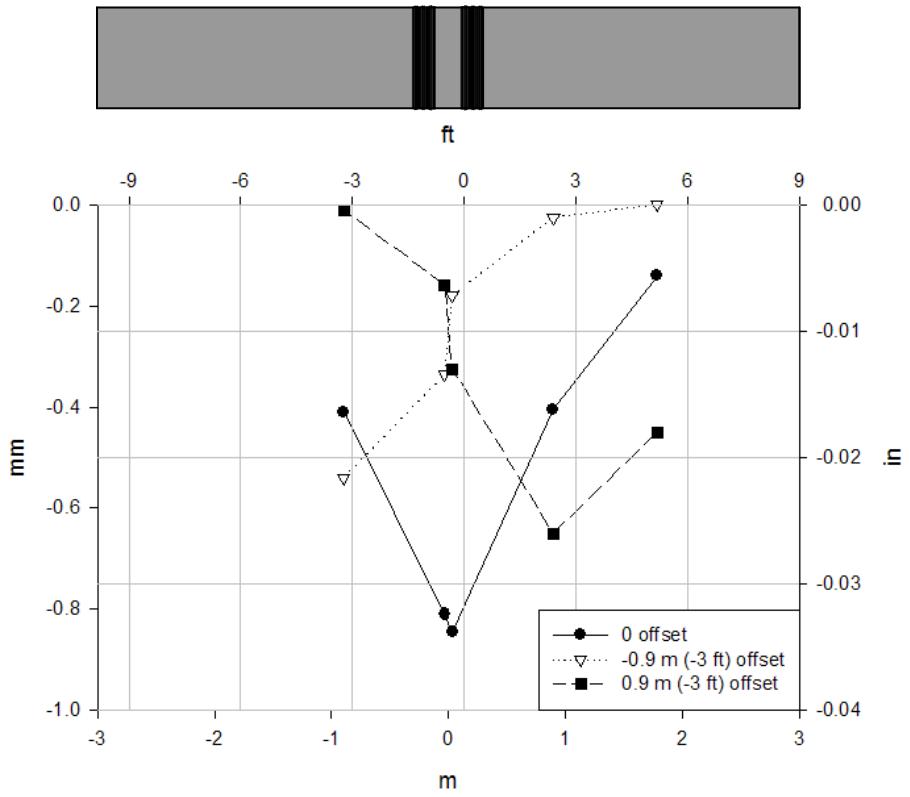

(a) At 4 ft (1220mm) of cover

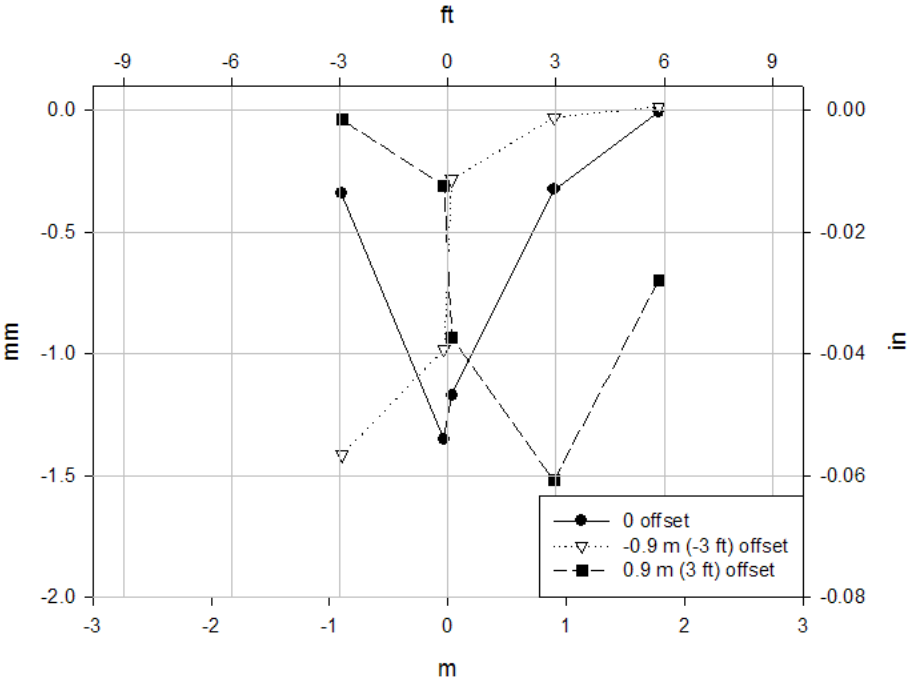

(b) At 2 ft (610mm) of cover

Figure C.54. Vertical springline displacements of the 36 in. (915mm) diameter corrugated steel pipe without O-rings; three loading locations.

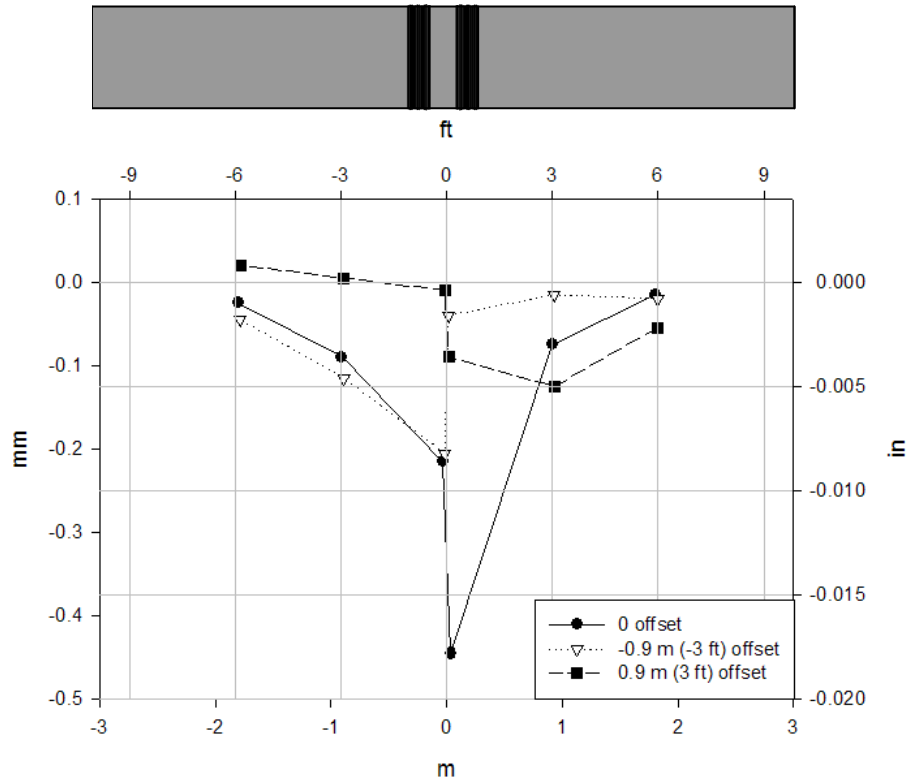

(a) Void under joint

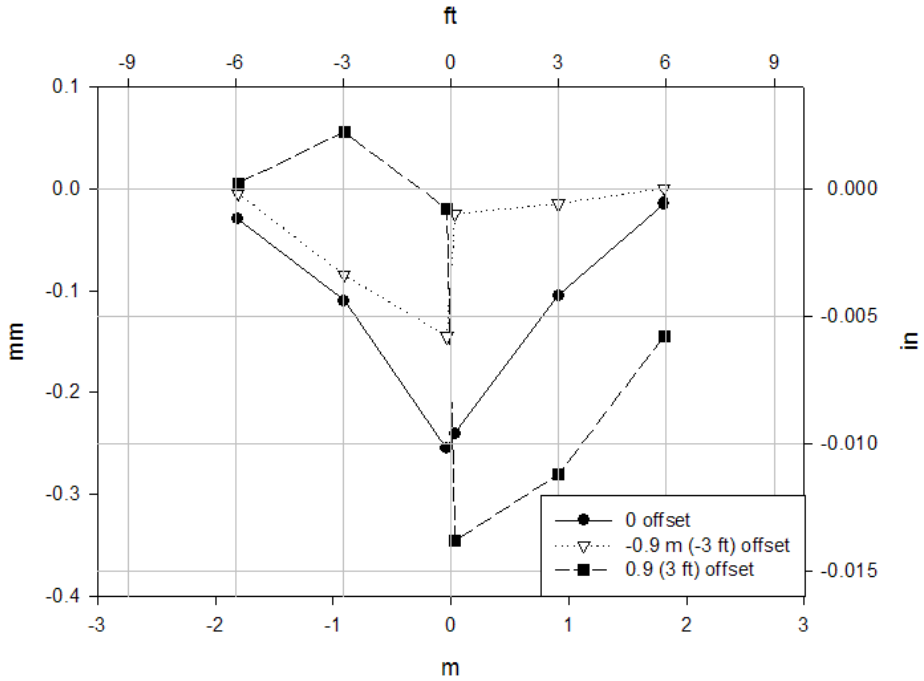

(b) Poor backfill of one of the pipes

Figure C.55. Vertical springline displacements of the 36 in. (915mm) diameter corrugated steel pipe with O-rings; poor burial conditions at 2 ft (610mm) of cover; three loading locations.

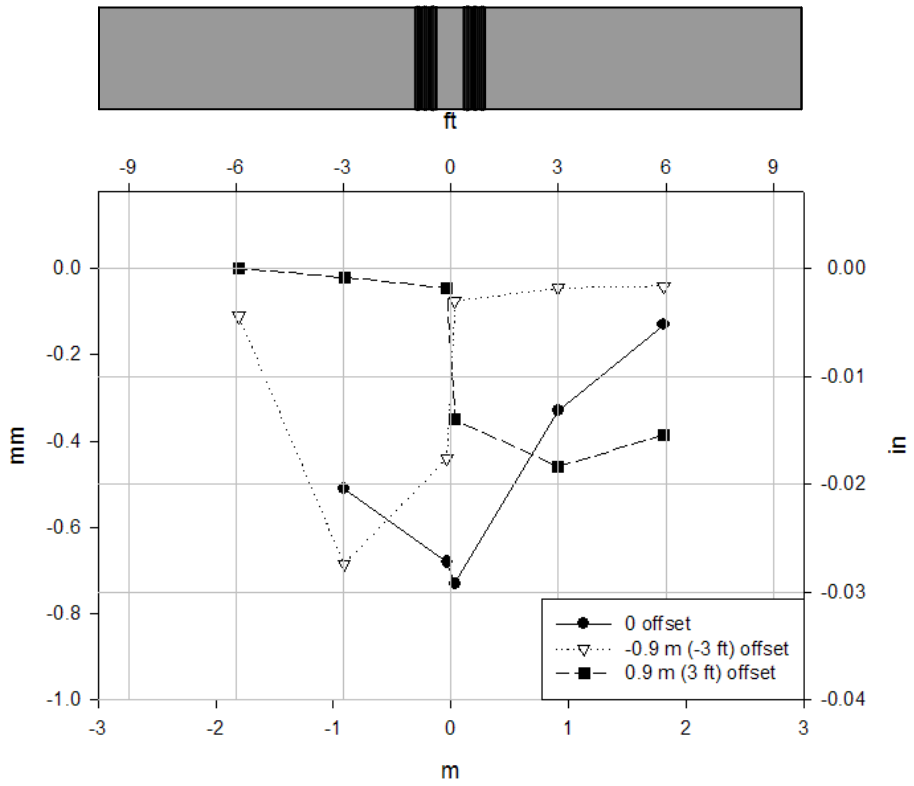

(a) At 4 ft (1220mm) of cover

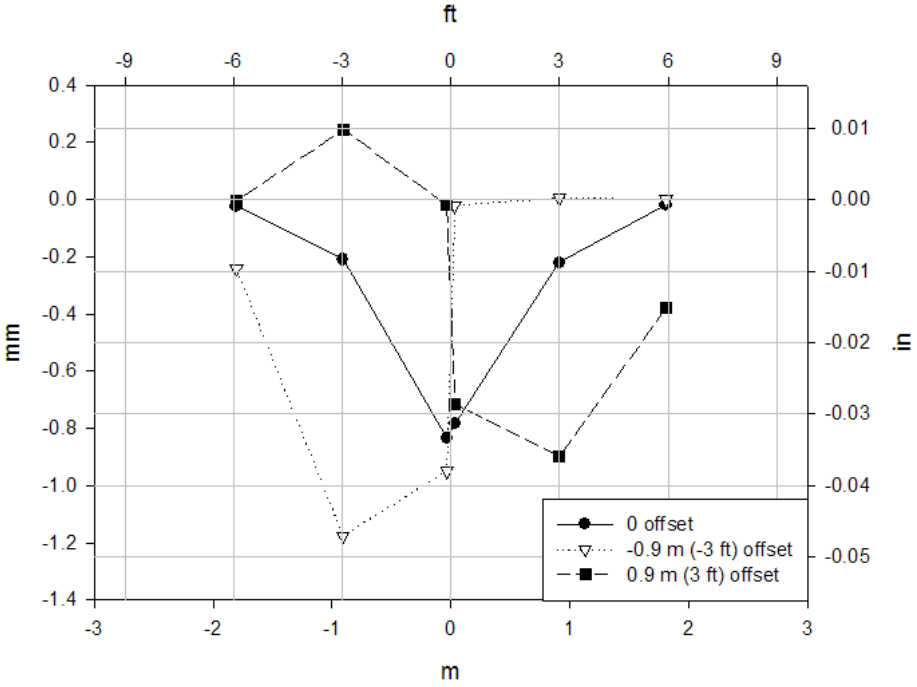

(b) At 2 ft (610mm) of cover

Figure C.56. Vertical springline displacements of the 36 in. (915mm) diameter corrugated steel pipe with O-rings; three loading locations.

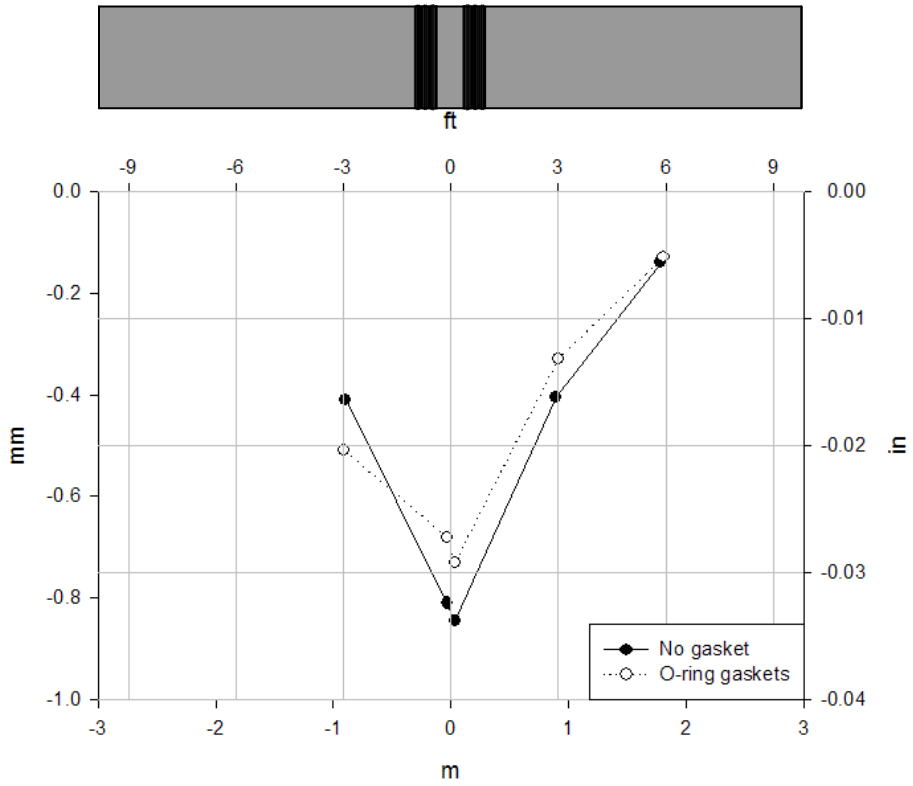

(a) At 4 ft (1220mm) of cover

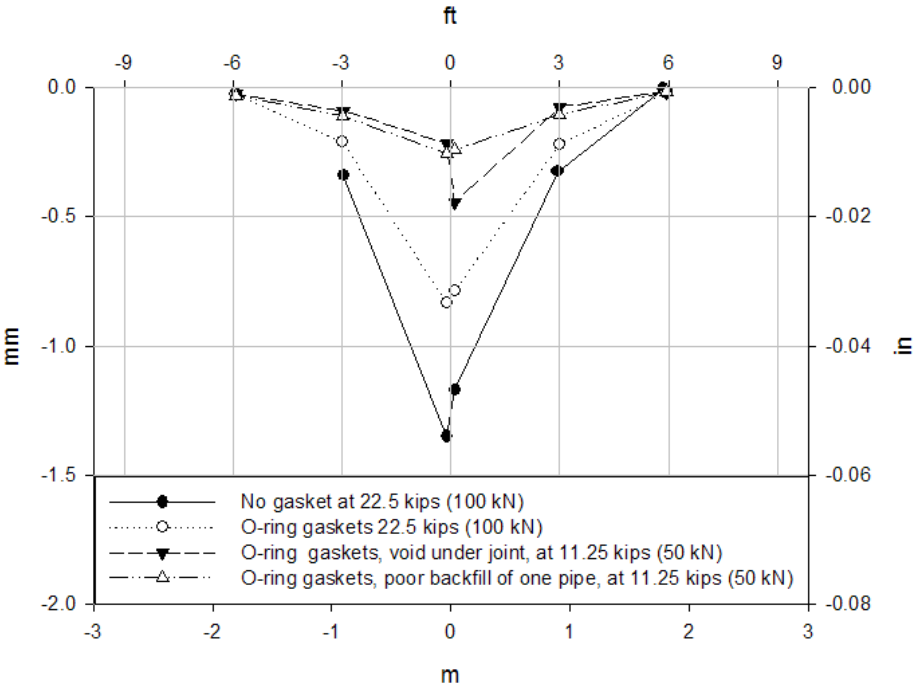

(b) At 2 ft (610mm) of cover

Figure C.57. Comparison of vertical springline displacements for the 36 in. (915mm) diameter corrugated steel pipes; loading directly over joint.

C.3.3 Ultimate limit state test

The 36 in. (915mm) diameter corrugated steel pipes without O-rings and with O-rings described above were tested to their ultimate limit state while buried. The purpose of these tests was to observe the maximum load that could be applied to each case and to observe the failure mode of these specimens when loading directly over the joint. The details of these tests are presented below.

C.3.3.1 Instrumentation

The instrumentation employed for these tests was the same as that employed in the buried tests described above. Electrical strain gages were placed in the barrels and band of the corrugated steel pipe to measure circumferential, helical and axial response. In addition, reflective prisms were attached to regions in the joint and barrels in the crown, invert and springlines locations. These elements measured displacements and changes in diameter along with string potentiometers. Details can be seen in **Figures C.33** to **C.36**.

C.3.3.2 Test configuration

Both corrugated steel pipes were tested at 2 ft (610mm) of cover and with good burial conditions (i.e. in accordance with AASHTO guidelines) and with the load applied directly over the joint. A larger loading area than the one employed during the service loading was utilized to prevent premature bearing failure of the soil (see **Figure C.58**). An important difference between the two tests was the level of compaction achieved. For the case where no O-rings were used, a 90 % average standard Proctor compaction was achieved in the soil supporting and surrounding the pipe and in the soil above. Alternatively, the pipe where O-rings were employed was buried in soil with 90% average standard Proctor compaction and the soil above it had an average of 95% standard Proctor compaction. Both burial conditions are considered good practice according to AASHTO guideless, however this difference affects the strength of the soil-pipe structure.

Figure C.58. Configuration of the ultimate limit state test for the 36 in. (915mm) diameter corrugated steel pipe; size of the loading pad was increased to prevent bearing failure.

C.3.3.3 Results

The largest strains during the ultimate limit state test of the corrugated steel pipe without gasket were registered at the re-rounded end of the pipes. It appears that the strength limit of the barrel rather than the band was reached; see **Figures C.59** and **C.60**. In almost every case the strains accelerate after load passed 40 kips (175kN), and the strain increases accelerate after 45 kips (200kN). The maximum applied load was 50.6 kips (225kN). Strains exceed 2000 με in various locations, i.e. beyond the yield strain for the steel with yield stress of 57 ksi (400MPa).

Figures C.61 and **C.62** show the strains registered during the ultimate limit state test of the specimen where O-rings were used. Similarly to the previous case, the largest strains were recorded at the re-rounded end of the pipes, i.e. the strength limit of the barrel was reached rather than the strength limit of the band. Most of the gages registered strain acceleration after 40 kips (175kN) until failure. The maximum applied load was 67.4 kips (300kN). Strains exceed 2000 με in some locations in the barrels and band.

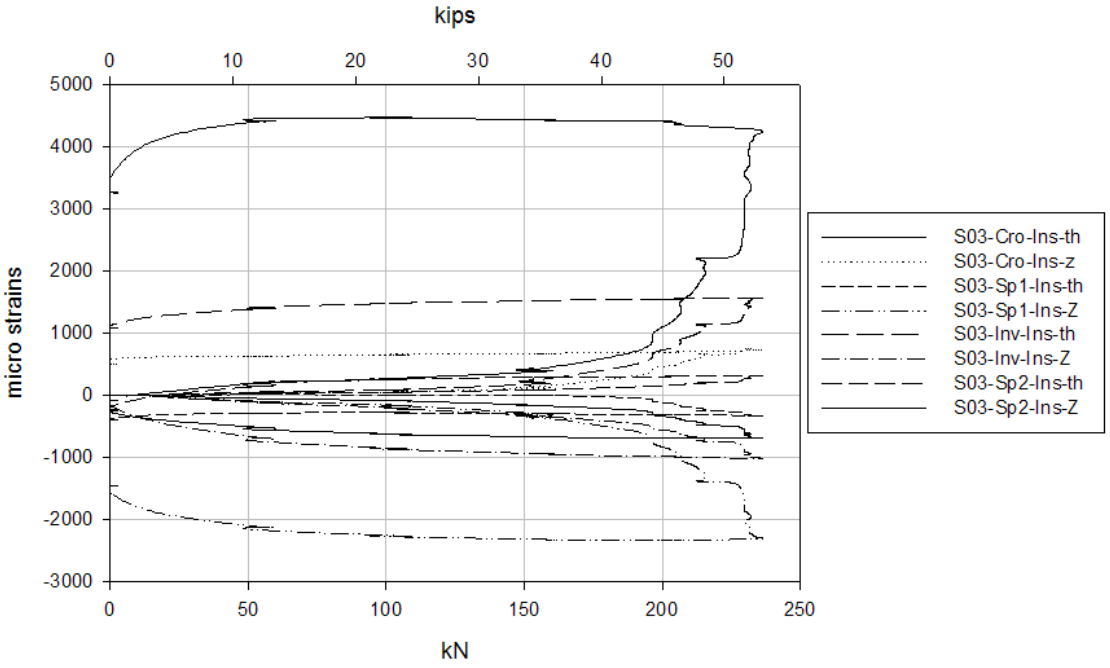

(a) Strains in the corrugated pipe barrel at section S03

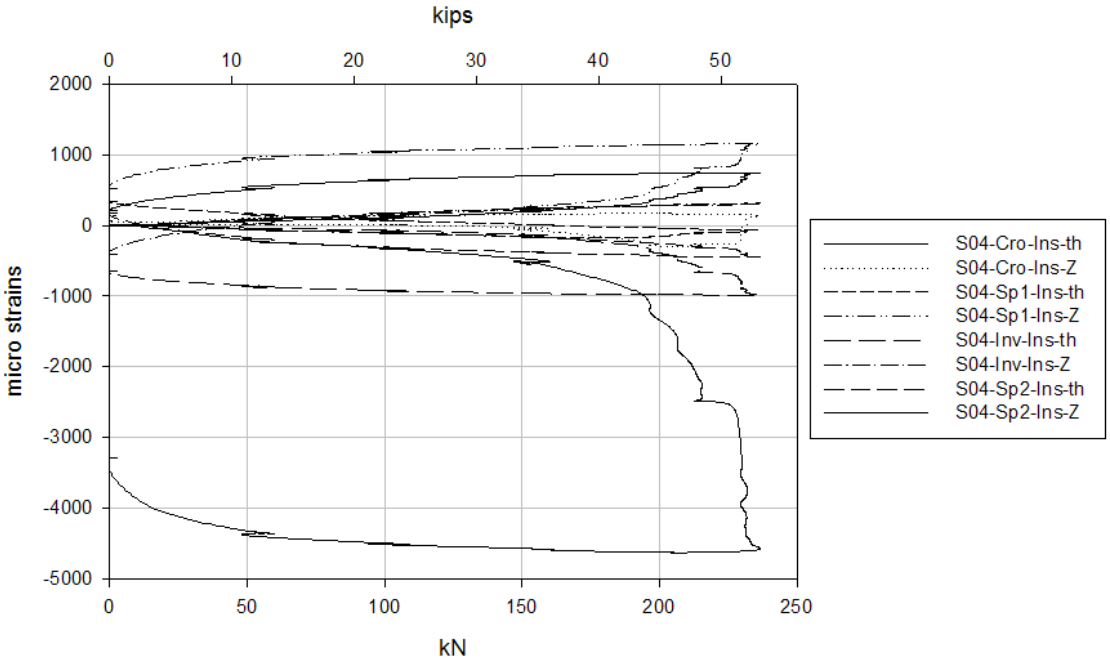

(b) Strains in the corrugated pipe barrel at section S04

Figure C.59. Strains recorded at the barrels during the ultimate limit state test of the 36 in. (915mm) diameter corrugated steel pipe without O-rings.

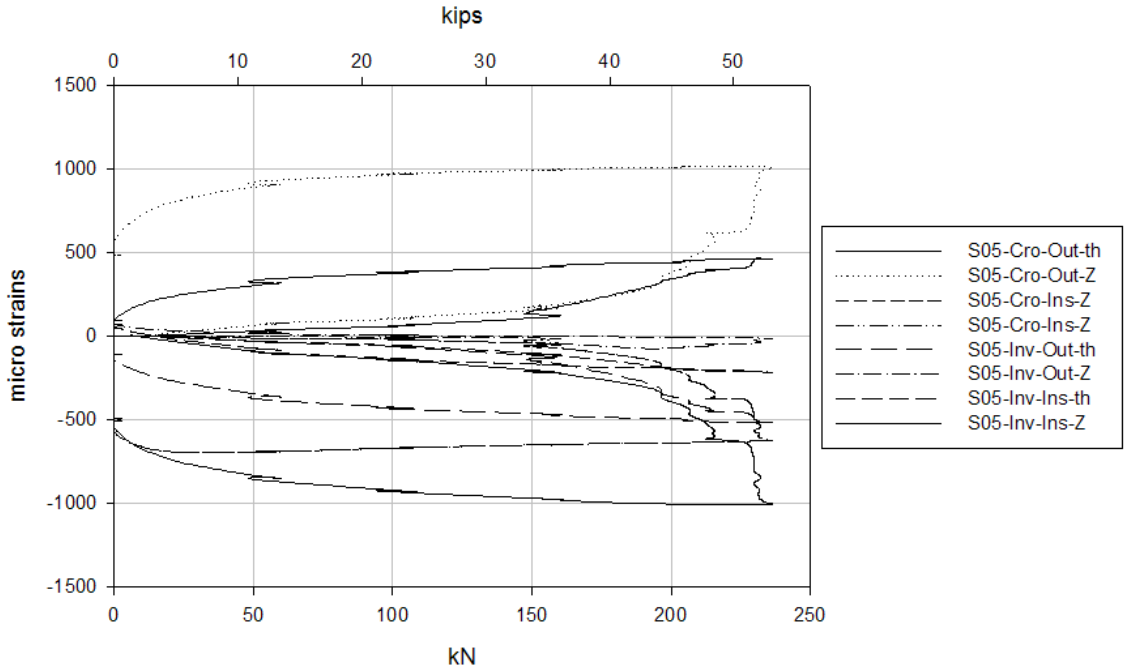

(a) Strains in band at section S05

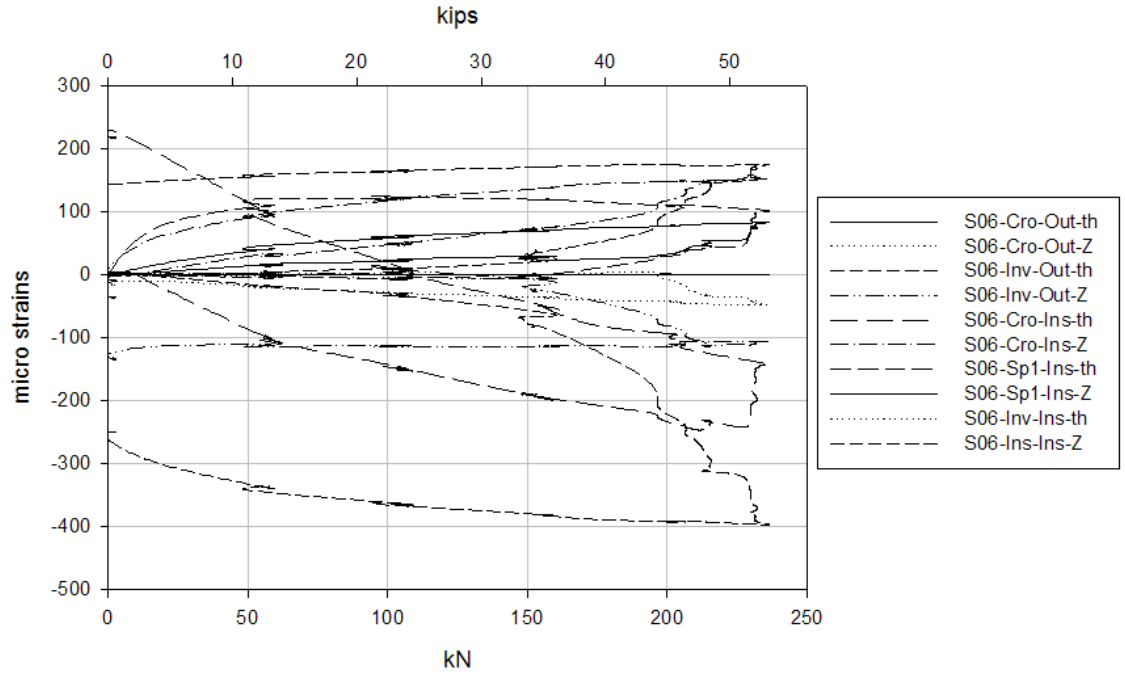

(b) Strains in band at section S06

Figure C.60. Strains recorded at the 'hugger' band during the ultimate limit state test of the 36 in. (915mm) diameter corrugated steel pipe without O-rings.

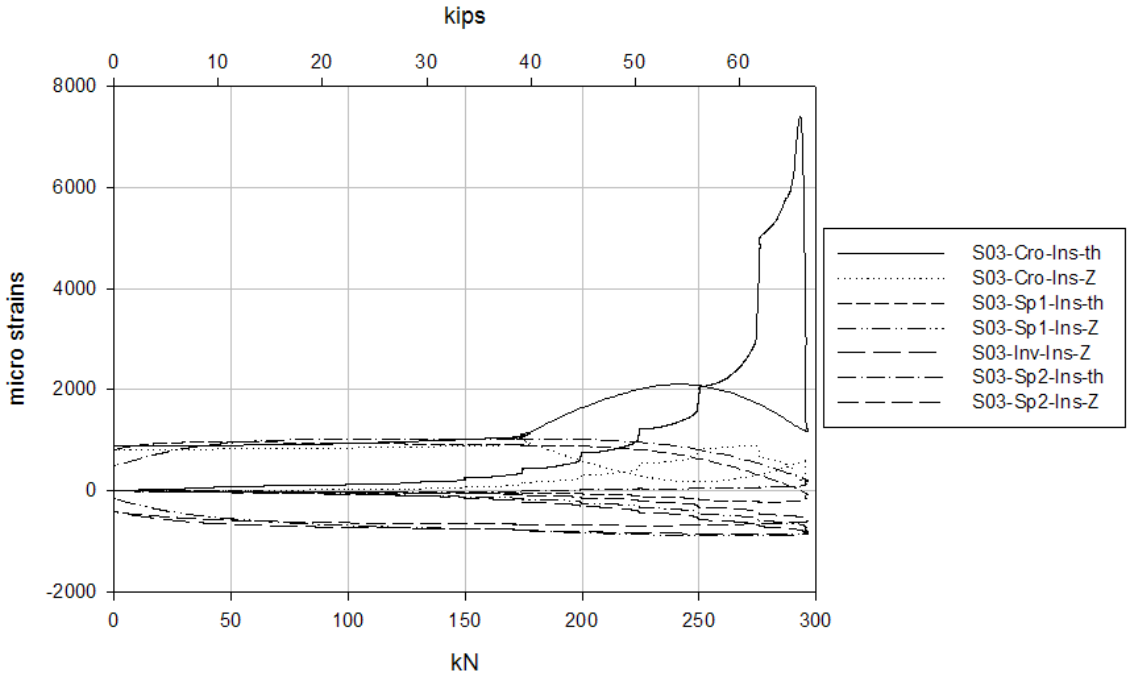

(a) Strains in the corrugated pipe barrel at section S03

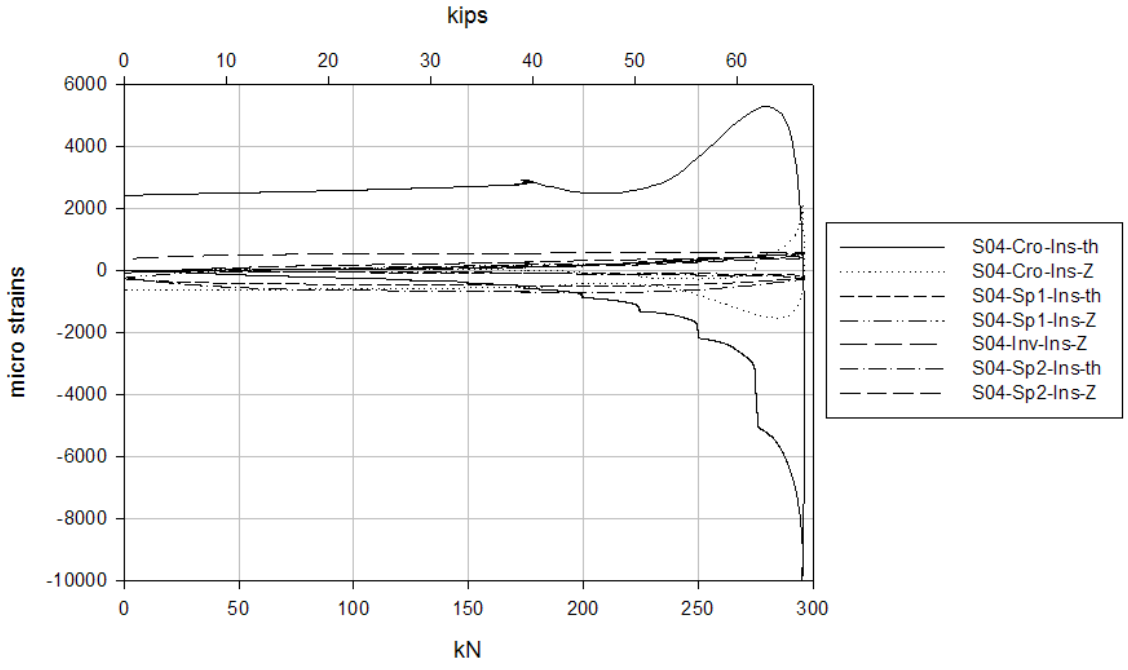

(b) Strains in the corrugated pipe barrel at section S04

Figure C.61. Strains recorded at the barrels during the ultimate limit state test of the 36 in. (915mm) diameter corrugated steel pipe with O-rings.

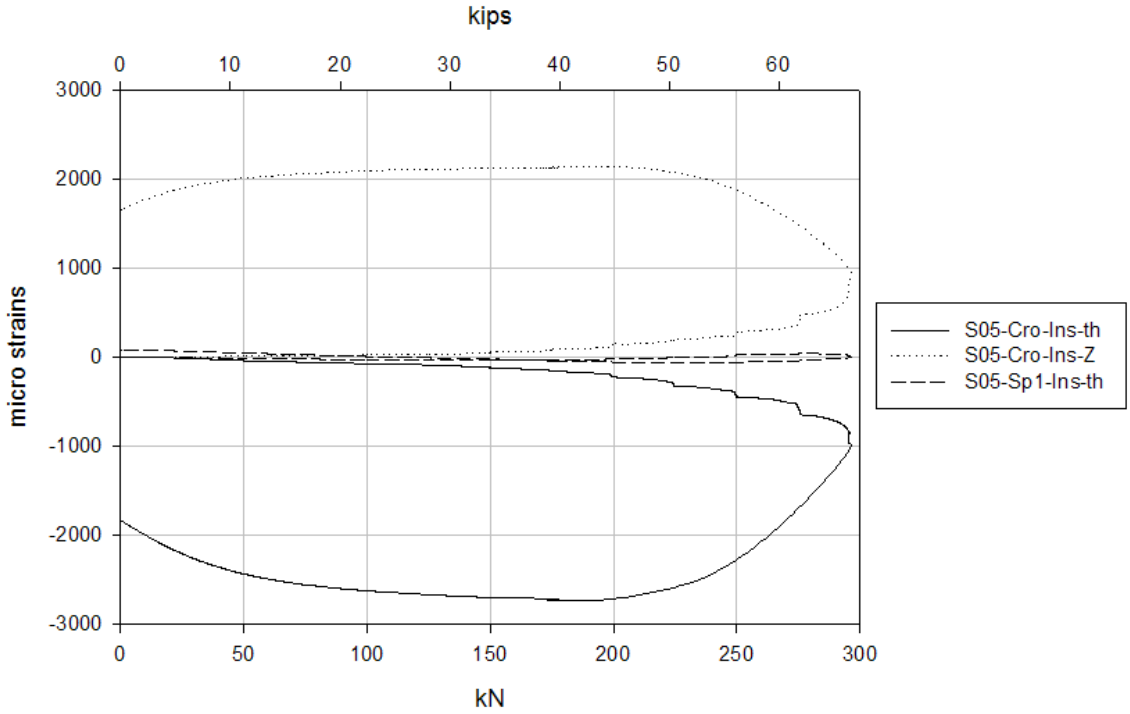

(a) Strains in band at section S05

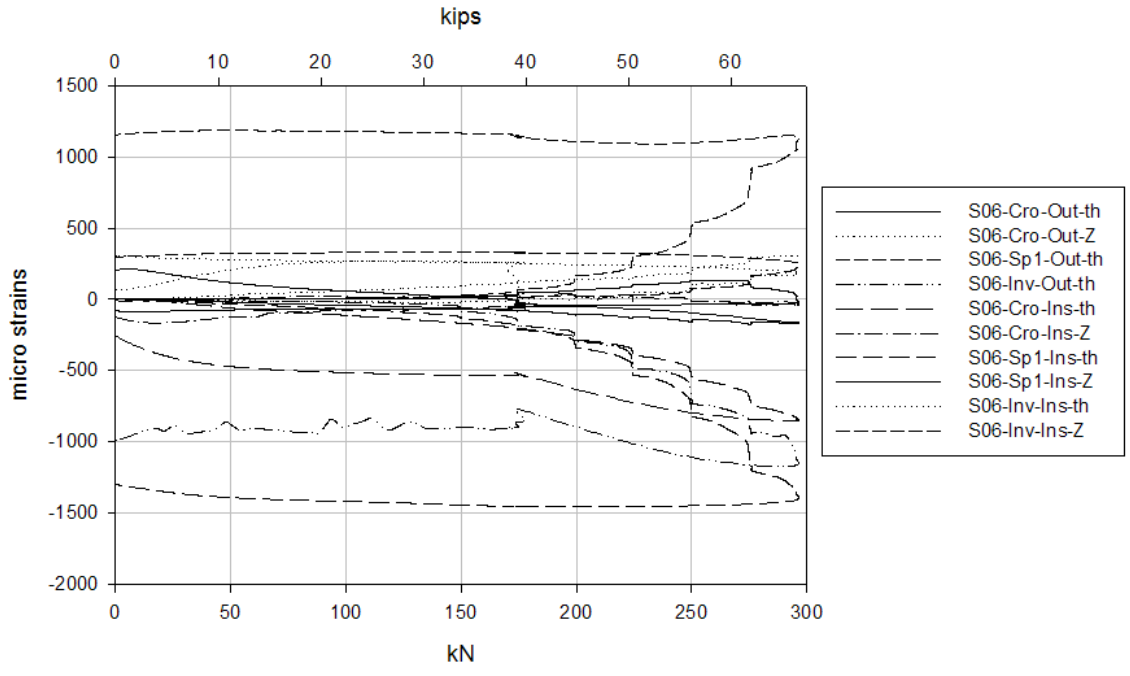

(b) Strains in band at section S06

Figure C.62. Strains recorded at the band during the ultimate limit state test of the 36 in. (915mm) diameter corrugated steel pipe with O-rings.

The diameter changes in the joint registered by the reflective prisms and string potentiometer during the ultimate limit state test of the corrugated steel pipe without O-rings can be seen in **Figure C.63**. Due to excessive distortion, the reflective prisms in the joint could only register changes until 45 kips (200kN). However the string potentiometers show the data for the entire loading-unloading process. A linear behavior was observed until 33.7 kips (150kN) and an acceleration of the distortion was observed until the maximum applied load. These results suggest ovaling of the joint and the response matches with the one observed in the strain gage data.

Figure C.64 shows the measured diameter changes of the joint during the ultimate limit state test of the specimen with O-rings. The reflective prisms could register changes until 61.8 kips (275kN) of load while the string potentiometers captured the complete loading spectrum. A linear behavior was observed until 33.7 kips (150kN) and then the distortion accelerated until 67.4 kips (300kN). This behavior matches the response registered by the strain gages and is similar to the response observed in the specimen with no gasket.

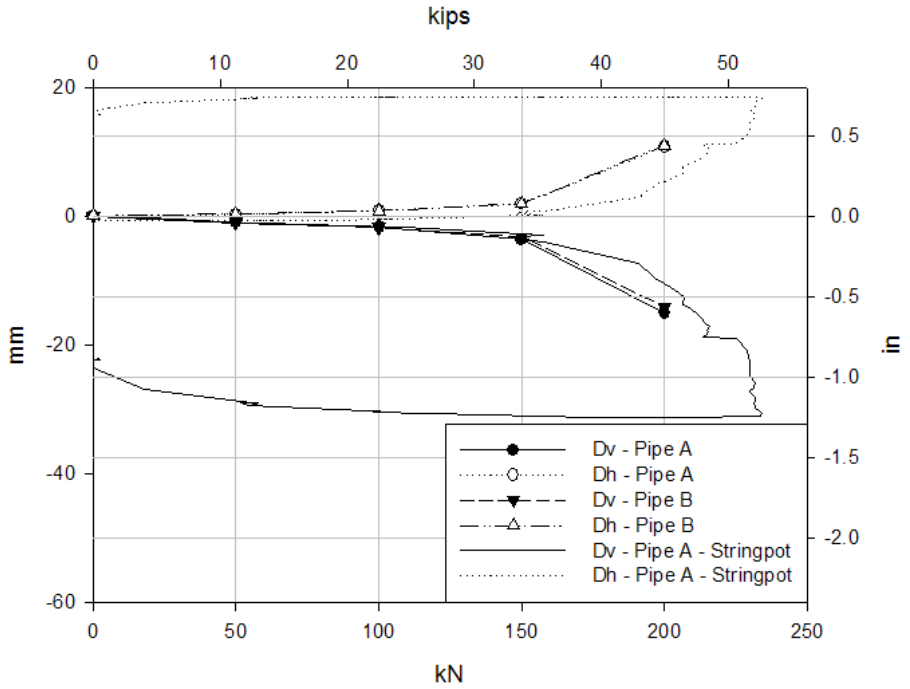

Figure C.63. Incremental diameter changes of the joint during the ultimate limit state test of the 36 in. (915mm) diameter corrugated steel pipe without gasket; reflective prisms and string potentiometers data.

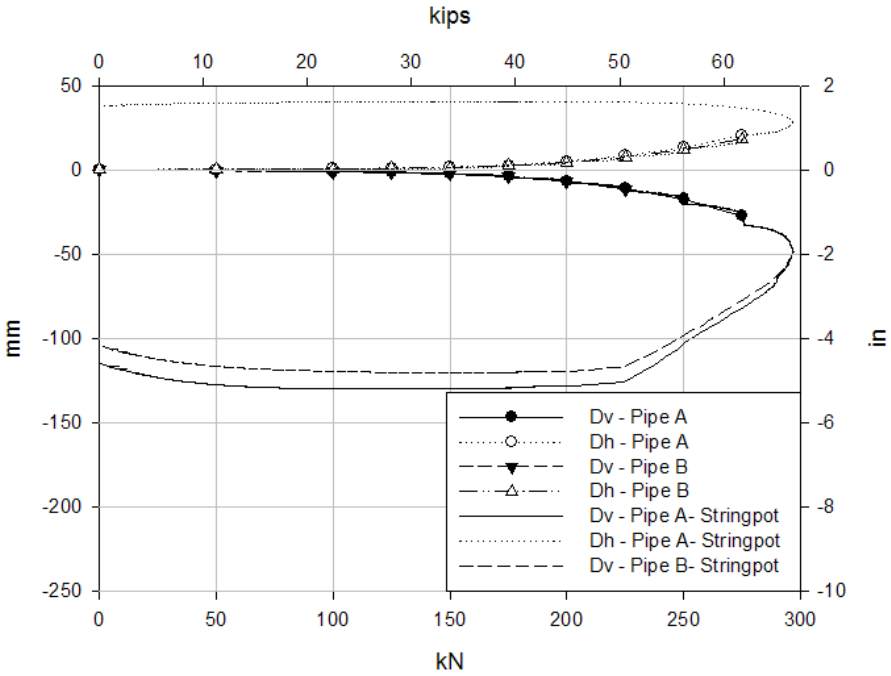

Figure C.64. Incremental diameter changes of the joint during the ultimate limit state test of the 36 in. (915mm) diameter corrugated steel pipe with O-rings; reflective prisms and string potentiometers data.

Given the flexibility of these pipes, springline vertical displacements of the pipe are shown instead of crown displacements. This data represents a global behavior of the pipe rather than localized. **Figure C.65** shows the springline vertical displacement measured during the ultimate limit state test of the corrugated steel pipe without O-rings. The reflective prism could only register displacements until 45 kips (200kN) due to excessive displacements. A large change in vertical displacement occurred after 33.7 kips (150kN); response matching the strain gage and diameter change data are presented above.

Figure C.66 shows the springline vertical displacement registered in the ultimate limit state test of the specimen with O-rings. The data shown was measured until 61.8 (275kN) of load. Larger increments in vertical displacement were observed after 33.7 kips (150kN) until the maximum value registered. This behavior matches the response of the strain gage and diameter change data presented earlier. In addition, the response of the two specimens was similar. **Figures C.67** and **C.68** show the specimens after being tested. The specimen with O-rings distorted more since a larger load was applied.

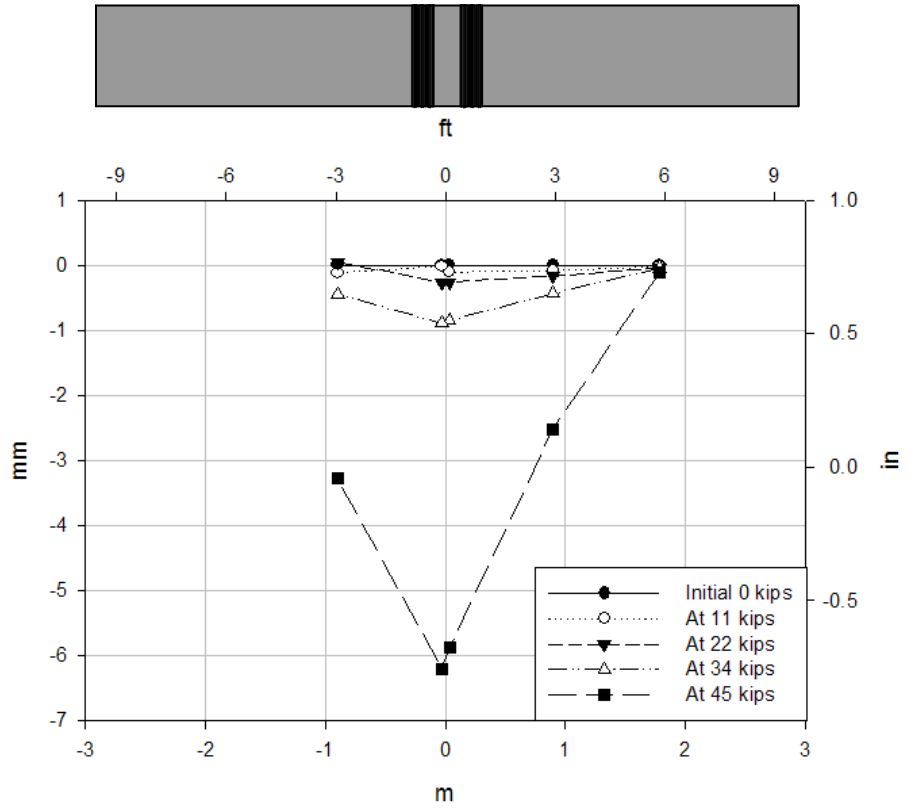

Figure C.65. Incremental springline vertical displacement during the ultimate limit state test of the 36 in. (915mm) diameter corrugated steel pipe without O-rings.

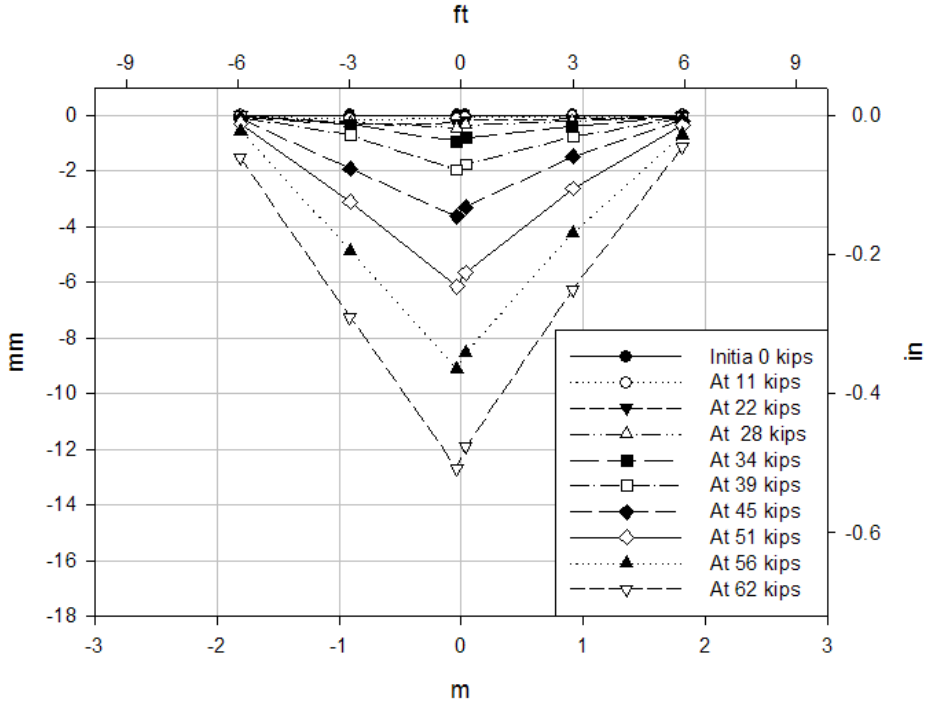

Figure C.66. Incremental springline vertical displacement during the ultimate limit state test of the 36 in. (915mm) diameter corrugated steel pipe with O-rings.

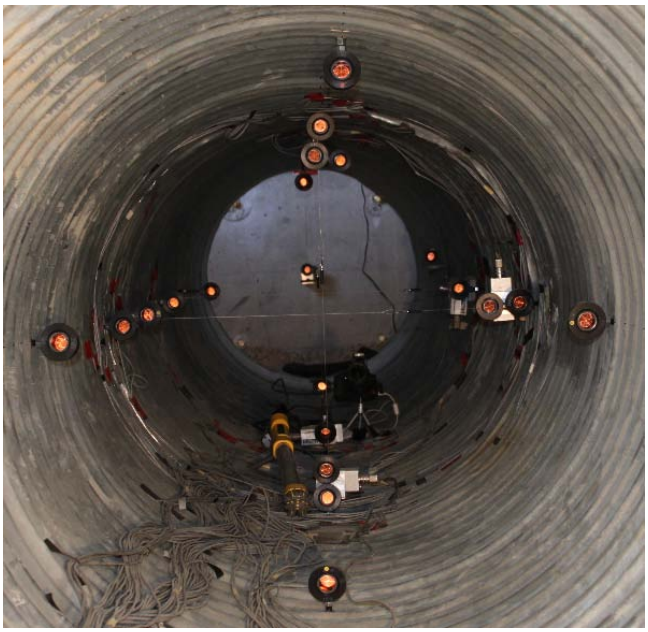

(a) Internal view

(b) External view

Figure C.67. Corrugated steel pipe without O-rings after ultimate limit state test.

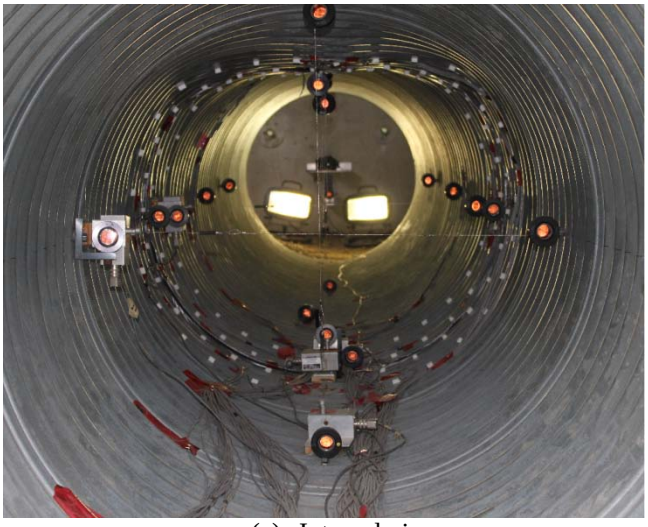

(a) Internal view

(b) External view

Figure C.68. Corrugated steel pipe with O-rings after ultimate limit state test.

C.4 Thermoplastic pipes

Two thermoplastic pipes were examined under burial conditions with fully factored service loads at different burial depths, loading locations and burial qualities in some cases. Bending tests were performed prior to burial for one of the specimens. Finally, ultimate limit state tests were performed for each specimen. The pipes examined were:

- 60 in. (1525m) corrugated High Density Polyethylene (HDPE) with a gasketted bell and spigot joint
- 36 in. (915mm) corrugated Polyvinyl Chloride (PVC) with a gasketted bell and spigot joint

C.4.1 Bending test

The 36 in. (915mm) diameter corrugated PVC specimen was tested in a pure bending arrangement to investigate the rotation characteristics of its gasketted bell and spigot joint. These tests were performed prior to burial inside the pit. The details of these tests are presented below.

C.4.1.1 Instrumentation

The assembled PVC pipe consisting of two pipes and a rubber gasket was instrumented with reflective prisms to measure changes in diameter and displacements. These elements were placed in the crown, invert and springlines in the joint and barrels. In addition, string potentiometers were attached to the joint and barrels to measure changes in diameter. The location of these elements can be seen in **Figure C.69**.

C.4.1.2 Test configuration

This test was performed prior to burial inside the pit of the GeoEngineering laboratory. The pipe was loaded in a four point bending configuration to induce moment without shear force across the joint. Wooden blocks were used as reactions as well as loading points. In addition, an I-beam was used to distribute the load which was applied with an actuator mounted above the pit. A string potentiometer was attached to one of the loading points to control the displacement of the test. **Figure C.70** shows the test configuration.

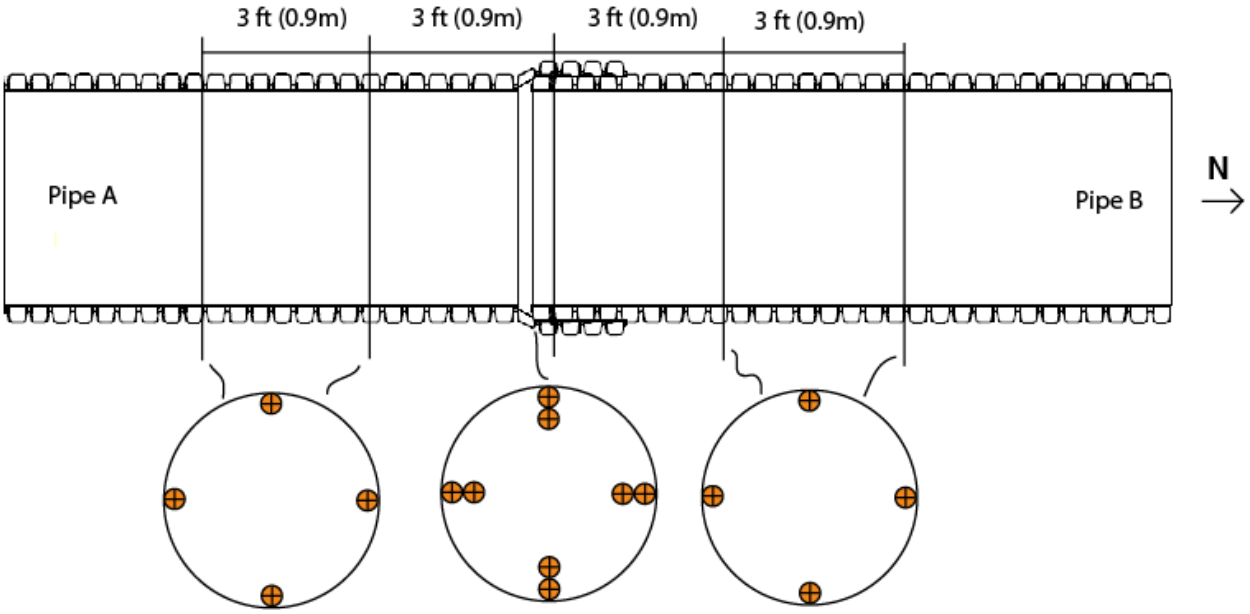

(a) Reflective prisms

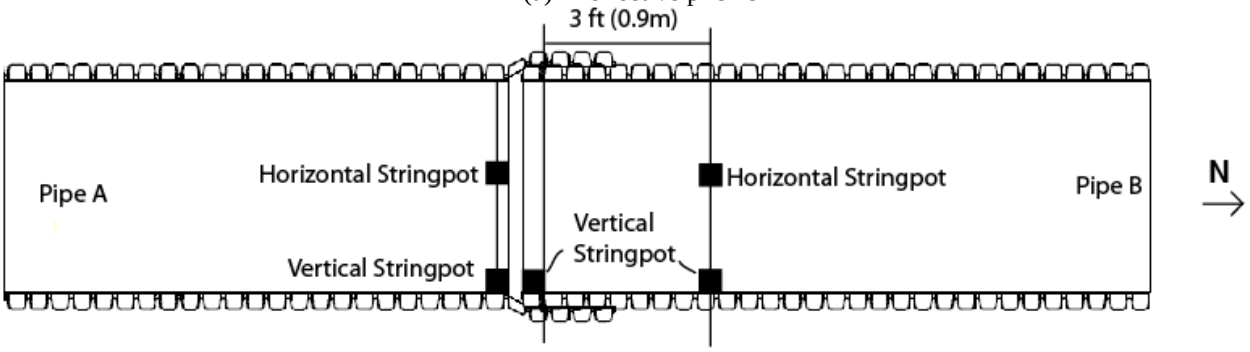

(b) String potentiometers

(c) Instrumented pipe

Figure C.69. Instrumentation of the 36 in. (915mm) diameter PVC pipe for the bending test.

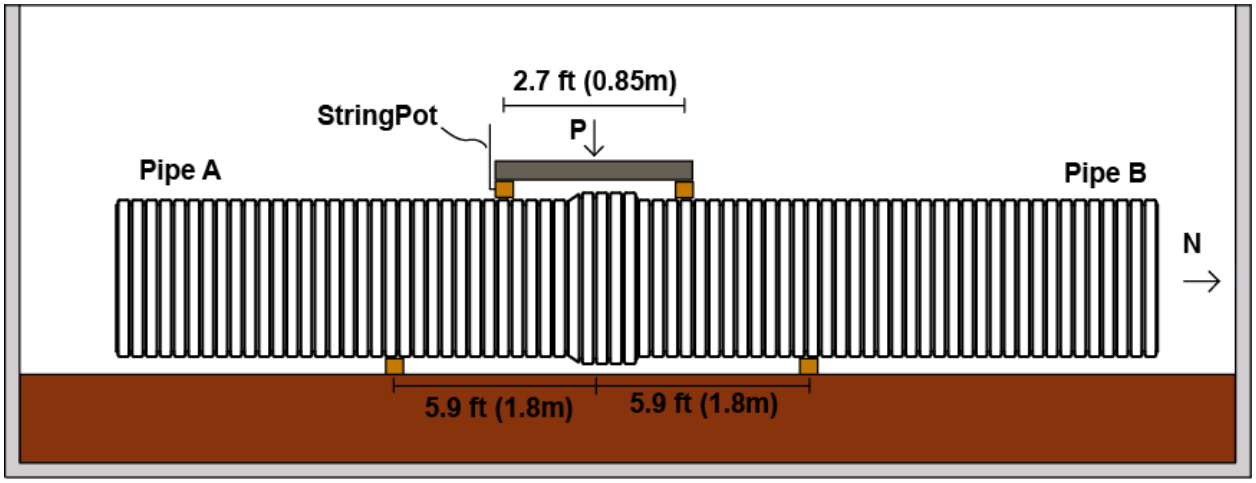

(a) Schematic

(b) Actual test

(c) Loading points

(d) Reaction detail

Figure C.70. Bending test details of the 36 in. (915mm) diameter PVC pipe

C.4.1.3 Results

Figure C.71 shows the response registered by the string potentiometer mounted on one of the loading points. During initial loading, sliding of the joint was observed after 1300 lbf.ft (1.75kN.m) until a maximum displacement of 1.2 in. (31 mm) was applied. Then followed cyclic loading in which the response of the system was linear and repeatable. When the load was removed, part of the displacement observed during the initial loading remained. Small changes in diameter were registered by the string potentiometer placed in the joint, see **Figure C.72**. The distortion caused by the loading was linear during the initial and cyclic loadings. The bell distortion was fully recovered but some distortion registered in the spigot was permanent.

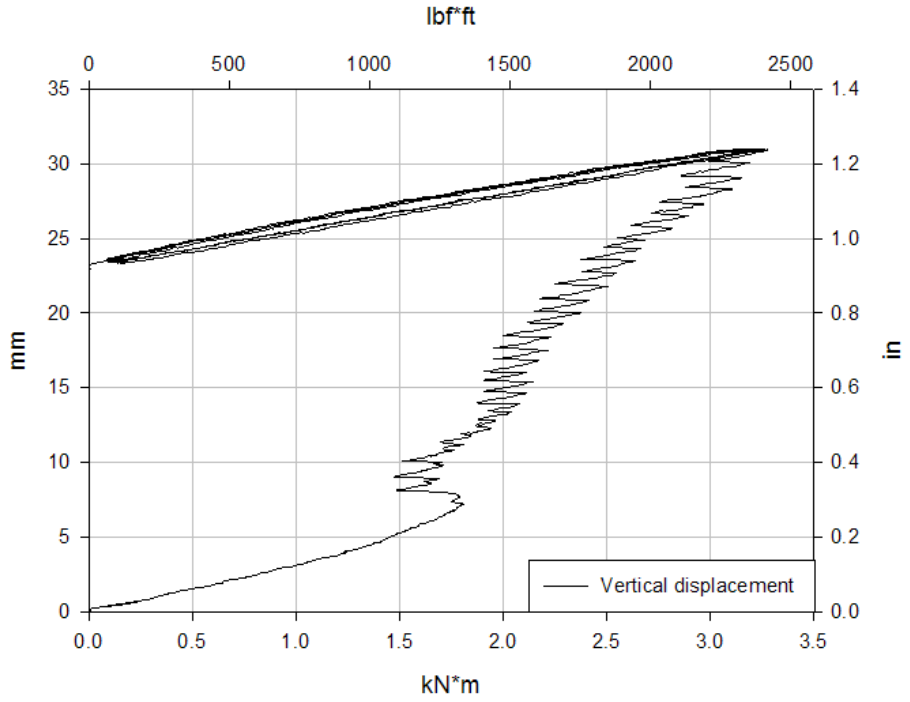

Figure C.71. Displacement of loading point during the bending test of the 36 in. (915mm) PVC pipe

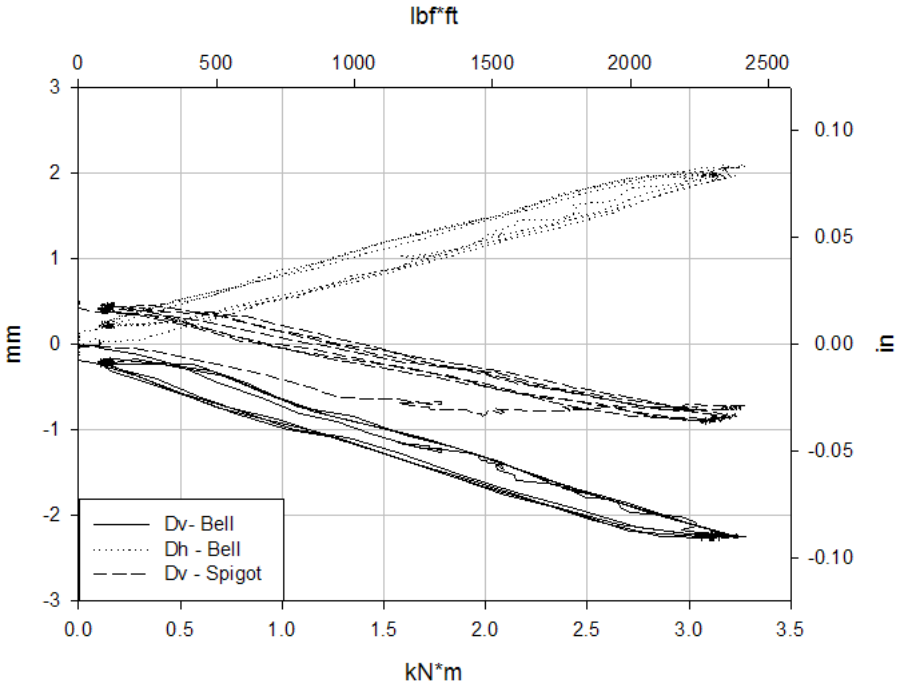

Figure C.72. Diameter change of the joint during the bending test of the 36 in. (915mm) PVC pipe

C.4.2 Buried pipe tests

The PVC pipe and the HDPE pipe were tested under good burial conditions at different burial depths and loading locations to observe the behavior of the joints when subjected to service live loading. In addition, poor burial conditions were defined and examined for the PVC pipe. The specifics of these tests are described below.

C.4.2.1 Instrumentation

The instrumentation in the PVC specimen employed in this test configuration was the same as the one employed during the bending test. Reflective prisms were mounted on the crown, invert and springlines of the joint and barrels to measure vertical displacements and changes in diameter. In addition, string potentiometers were mounted in some locations to register vertical and horizontal changes in diameter, see **Figure C.69**.

The assembled 60 in. (1525mm) diameter HDPE pipe consisting of two pipes and a rubber gasket had similar instrumentation. Reflective prisms were attached to the joint elements and barrels of the pipe to measure changes in diameter and vertical displacements. Also, string potentiometers were mounted to measure vertical and horizontal changes in diameter. **Figure C.73** shows the location of the instrumentation elements of the HDPE pipe.

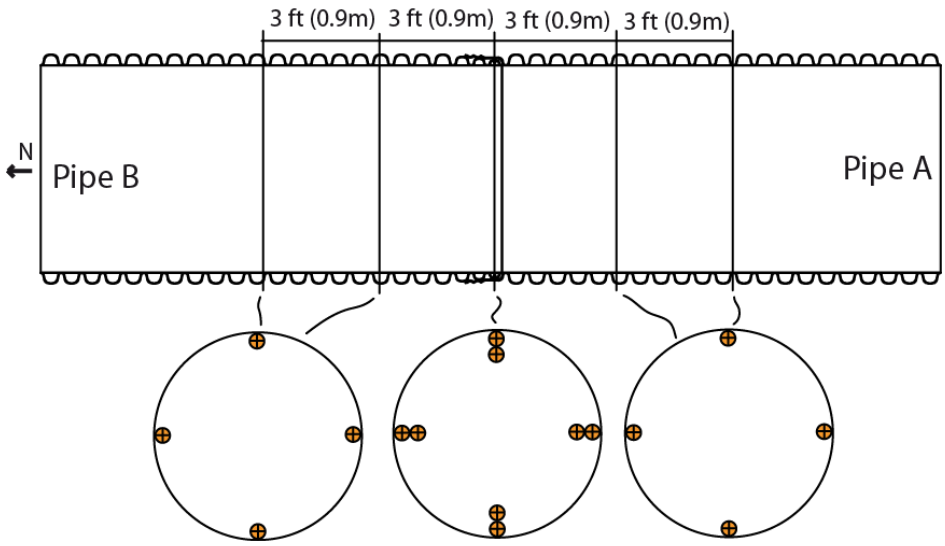

(a) Reflective prisms

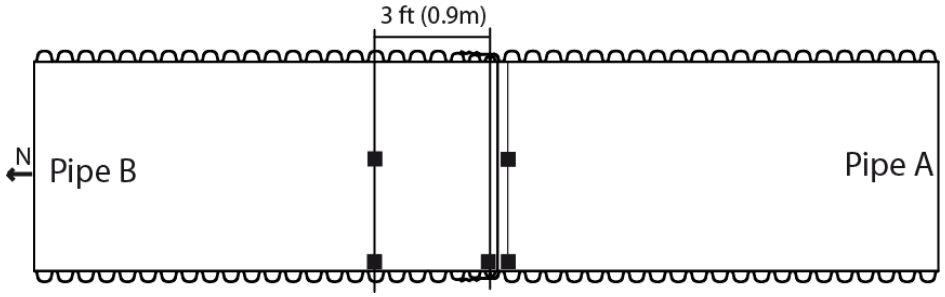

(b) String potentiometers

(c) Instrumented pipe

Figure C.73. Instrumentation of the 60 in. (1525mm) diameter HDPE pipe

C.4.2.2 Test configuration

The 36 in. (915mm) diameter PVC pipe was tested under two different 'poor' burial configurations at 2 ft (610mm) of cover and three loading locations above the pipe. The first condition consisted of placing the pipe over a void extending to both sides of the joint to induce larger rotation of the pipe during live loading. The rest of the burial was made according to AASHTO guidelines (i.e. Type 1 soil, compacted 90 to 95% of maximum standard Proctor dry unit weight). A schematic of this burial condition can be seen in **Figure C.74**. The second burial condition consisted of leaving a void under the spigot of the joint while the bell was well supported. The purpose of this condition was to induce larger shear in the joint. The rest of the burial was performed following AASHTO guidelines, see **Figure C.75**. The 'poor' burial conditions were examined under half the service load, i.e. 11.25 kips (50kN), to prevent damaging the pipe. The third burial condition followed AASHTO guidelines and a schematic can be seen in **Figure C.76**. This configuration was examined at 4 ft (1220mm) and 2 ft (610mm) of burial cover and at three different loading locations.

In a similar manner, the 60 in. (1525mm) diameter HDPE pipe was buried following good installation practice according to AASHTO. Type 1 soil was employed and compacted 90 to 95% of maximum Proctor dry unit weight. The pipe was examined at 2 ft (610mm) and 4 ft (1220mm) of cover and the load was applied in three different locations during each burial depth. A schematic of this configuration can be seen in **Figure C.77**. In all cases, the end-walls of the embankment constructed over the test pipes were made of steel grids covered with geosynthetic. This choice of a flexible end-wall was designed to minimize any stiffening effect of those end treatments on the jointed pipe response.

For both thermoplastic pipes, loading was applied using a 2000kN (220 US ton) capacity actuator mounted over the test pit, and restrained by a reaction frame anchored into the limestone below. Loading was applied through a steel plate having the design dimensions of the standard AASHTO wheel pair at the end of a design axle, **Figure C.78.** For all tests, the load was applied in three different positions along the test pipe; this involved loading over the central pipe joint, then at 3ft (0.9m) intervals to the North and South of that position. The loading was designed to represent the action of one wheel pair at the end of a single 32000 lbf axle (143 kN). Half that single axle (the load on one wheel pair) is 16000 lbf. Considering multiple presence factor of 1.2, and impact factors of 1.25 at 2ft of burial, and 1.17 at 4ft of burial, the factored service load becomes 24000 lbf (107 kN) at 2ft of cover, and 22500 lbf (100 kN) at 4ft of cover. For reasons of simplification and to facilitate comparisons of joint response at the two different cover depths, all 'service load' testing was conducted up to 22.5 kips (100kN).

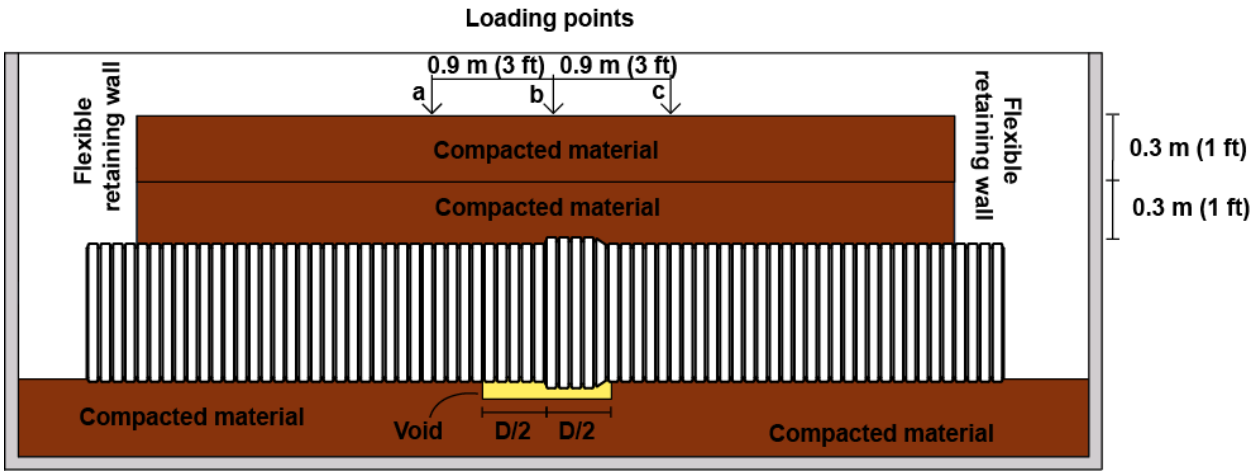

(a) Longitudinal section

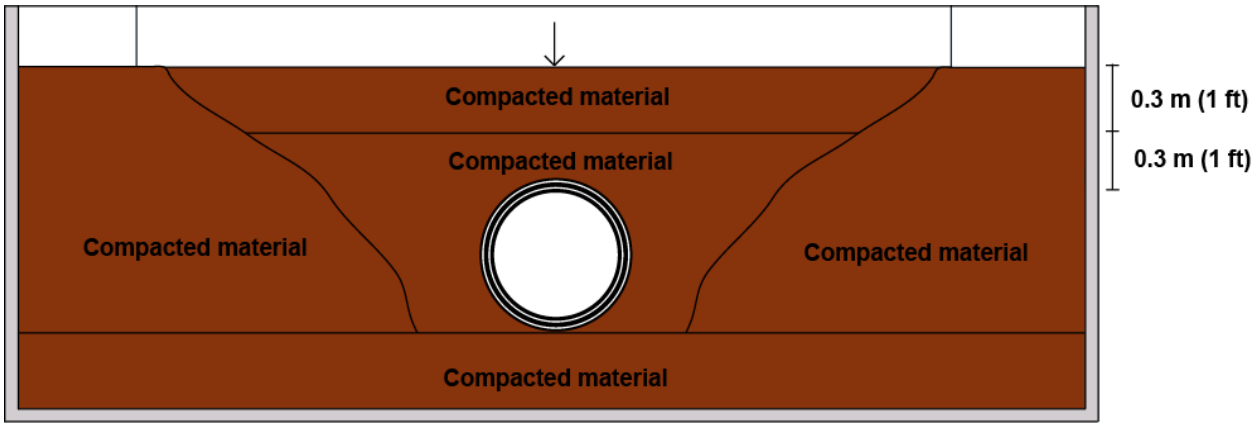

(b) Section normal to the pipe axis

(c) Void details

Figure C.74. Configuration of poor burial condition for the 36 in. (915mm) diameter PVC pipe; void under joint.

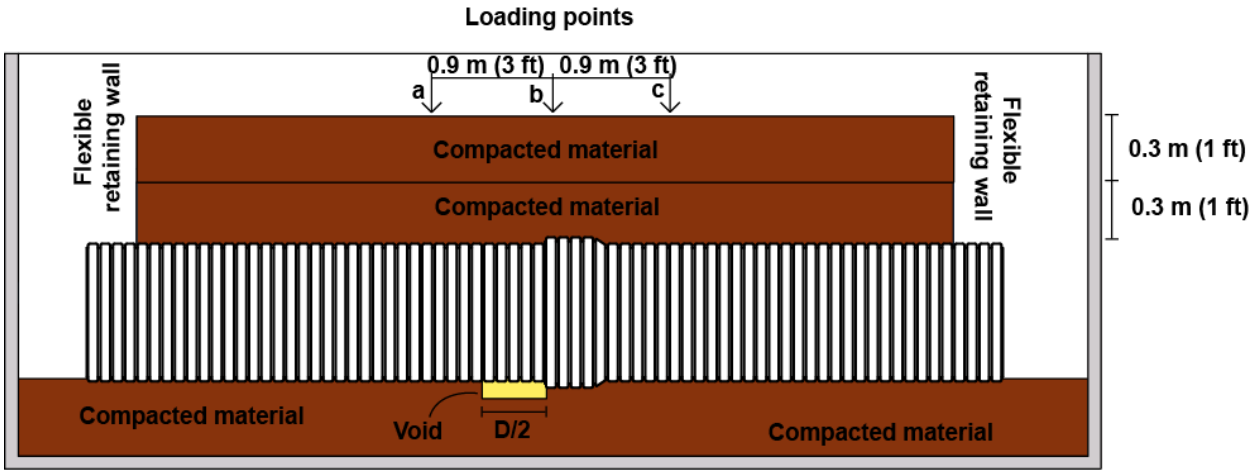

(a) Longitudinal section

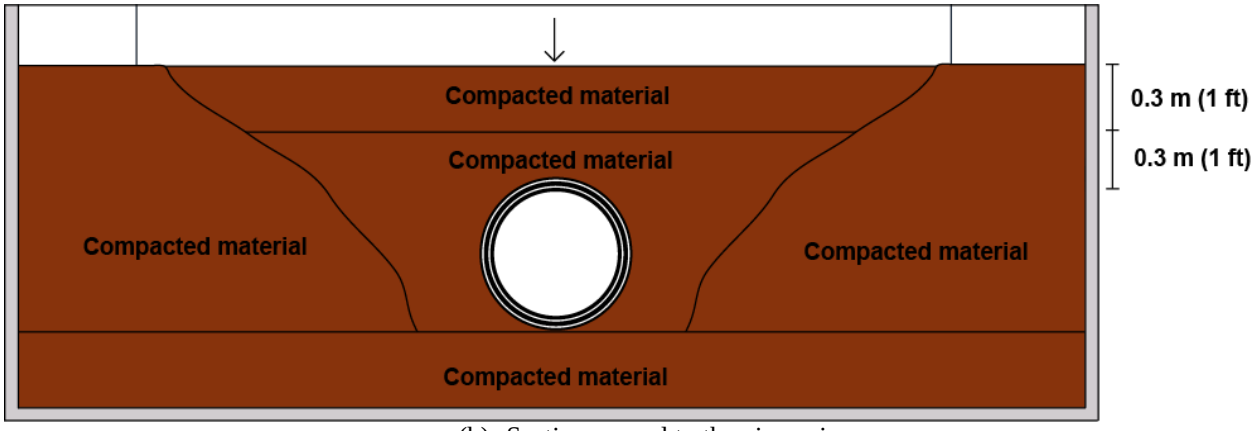

(b) Section normal to the pipe axis

(c) Void details

Figure C.75. Configuration of poor burial condition for the 36 in. (915mm) diameter PVC pipe; void under spigot.

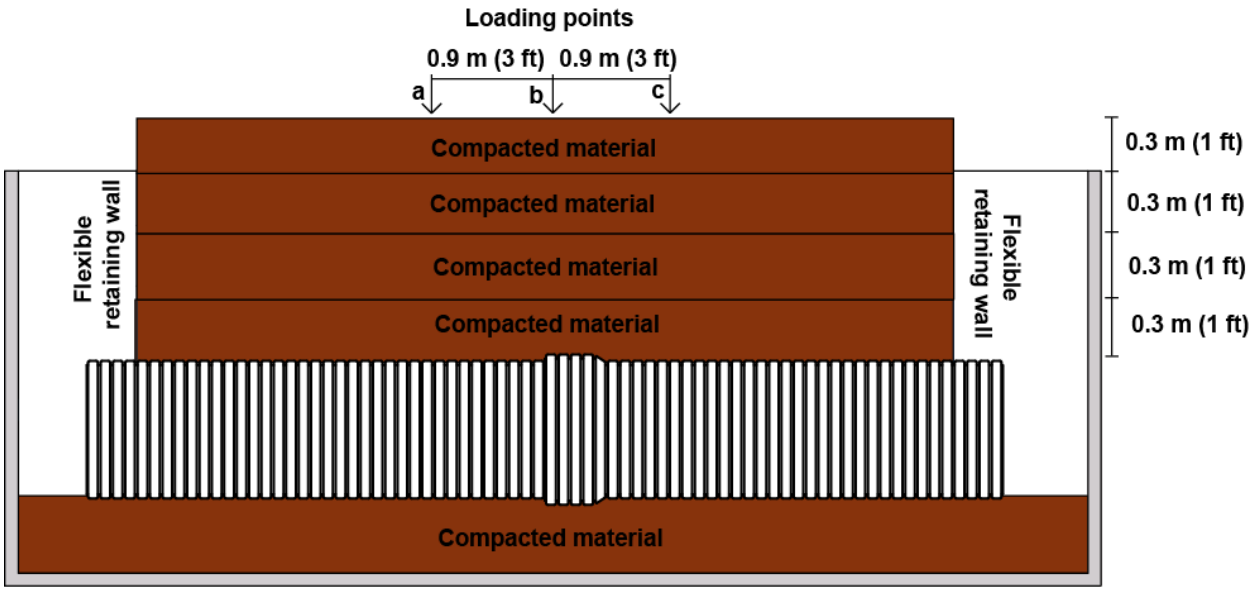

(a) Longitudinal section

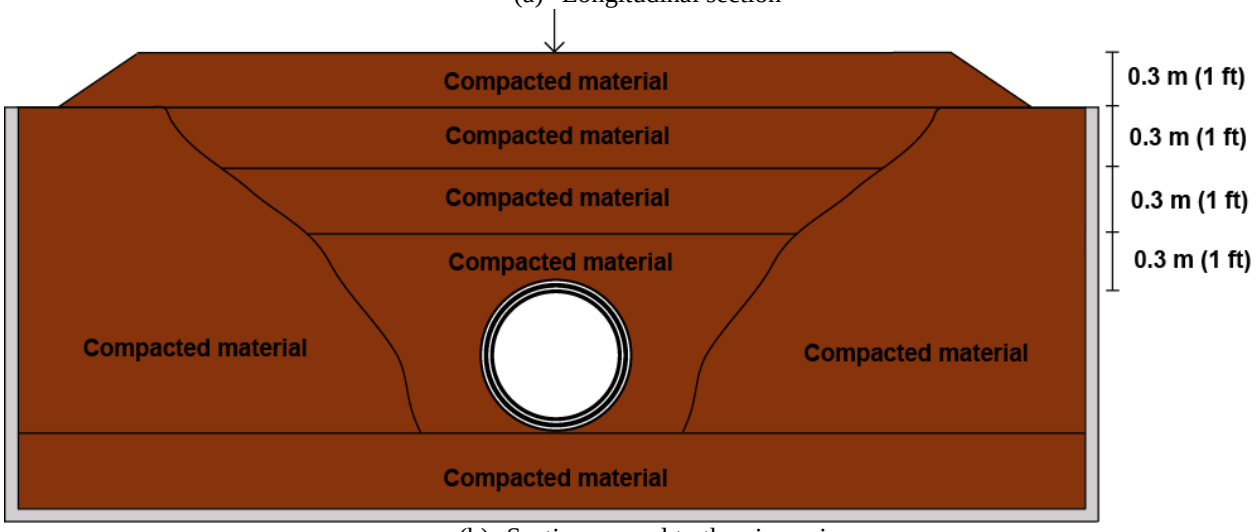

(b) Section normal to the pipe axis

(c) Burial process

Figure C.76. Configuration of the good burial condition for the 36 in. (915mm) diameter PVC pipe.

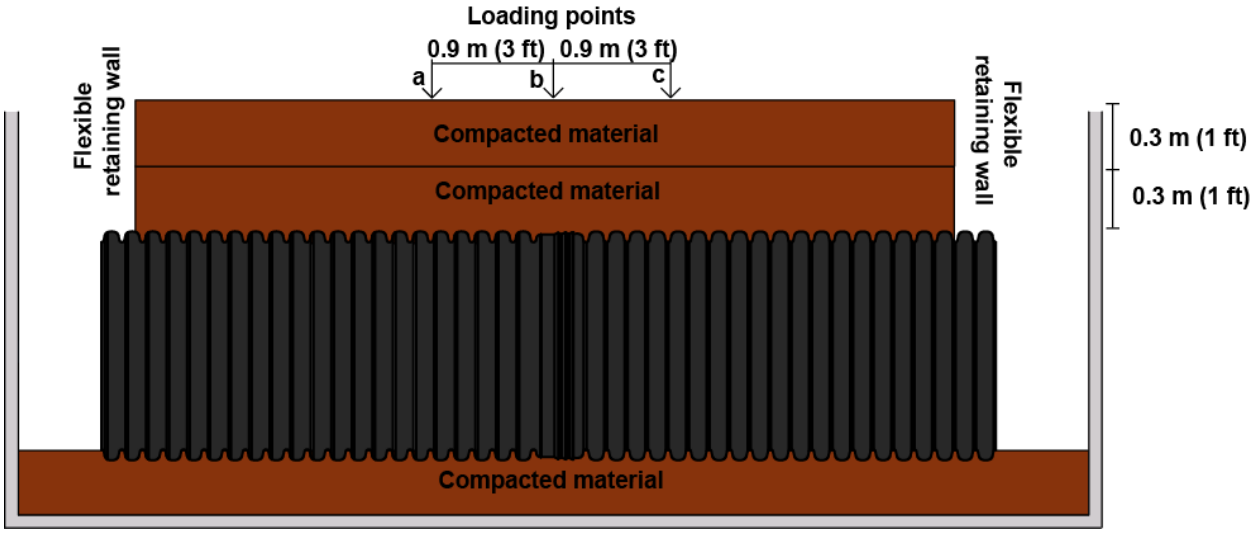

(a) Longitudinal section

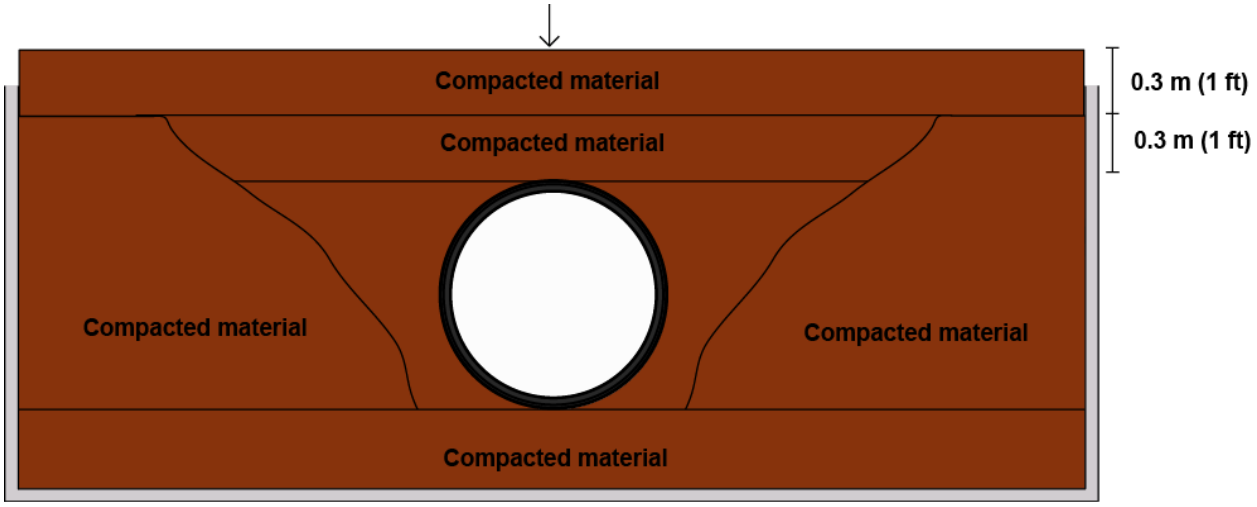

(b) Section normal to the pipe axis

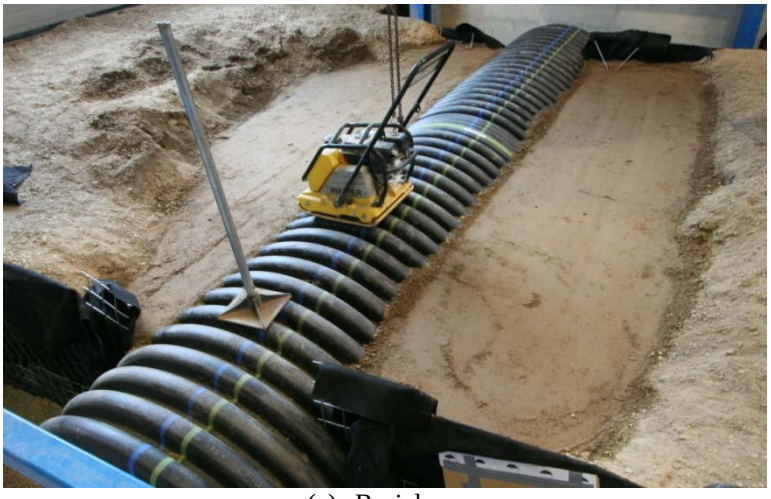

(c) Burial process

Figure C.77. Configuration of the burial condition for the 60 in. (1525mm) diameter HDPE pipe.

Figure C.78. Steel loading plate, loading column and 2000 kN (220US ton) capacity actuator.

C.4.2.3 Results

Diameter changes in the joint and barrels of the 36 in. (915mm) diameter PVC pipe were obtained from the reflective prism data. **Figure C.79** shows the changes registered during the 'void under the joint' burial condition while the system was loaded directly over the joint. A linear response in diameter changes in the joint elements was observed during loading. The diameter changes in the barrels were smaller and seem linear too although their magnitudes were close to the precision limits of the total station. **Figure C.80** shows the changes in diameter observed during the 'void under the spigot' burial condition. The response of the joint was linear while the magnitudes for the barrels were considerably smaller. In all cases, the magnitudes were larger than the ones observed during the 'void under joint' burial condition. This can be attributed to the soil attracting more load during the first case, i.e. positive arching. **Figures C.81** and **C.82** show incremental horizontal and vertical diameter changes registered during the tests for good burial while the system was loaded directly over the joint at burial depths of 4 ft (1220mm) and 2 ft (610mm) respectively; the response in both cases was linear.

The changes in diameter registered by the reflective prisms in the 60 in. (1525mm) diameter HDPE pipe can be seen in **Figures C.83** and **C.84**. The response of the vertical diameter in the joint was non-linear while the horizontal changes are closer to a linear response in both cases. The response of the barrels had a similar behavior but considerably smaller magnitudes for the 4 ft (1220mm) of cover case. This behavior indicates local deformation of the crown or non-uniform distortion, i.e. hoop compression, of the joint which is associated with the large diameter of the pipe and its mechanical/geometrical properties.

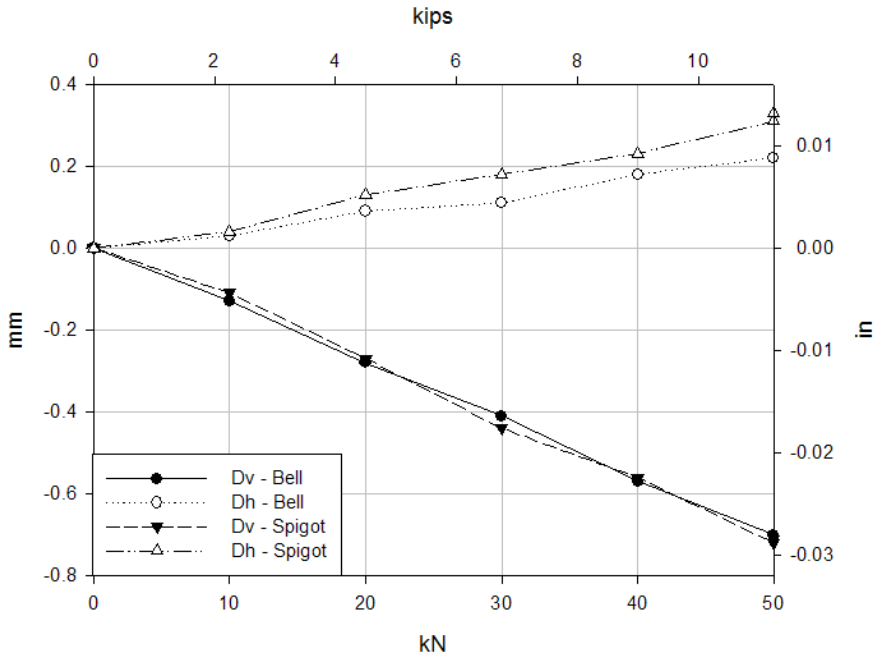

(a) Joint

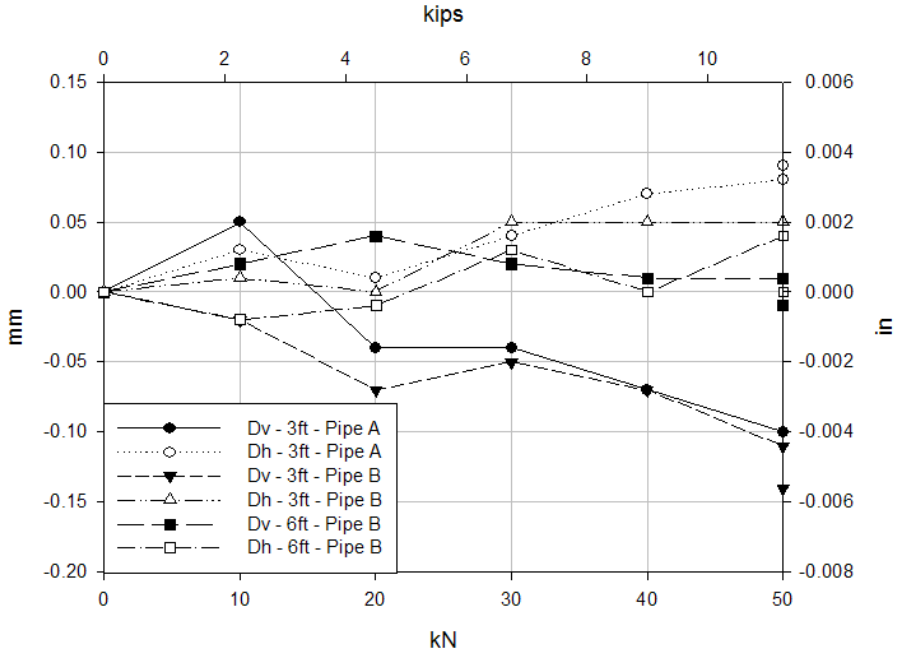

(b) Barrels

Figure C.79. Incremental diameter changes of the 36 in. (915mm) diameter PVC pipe; 2 ft (610mm) of cover, surface load over joint, void under joint burial.

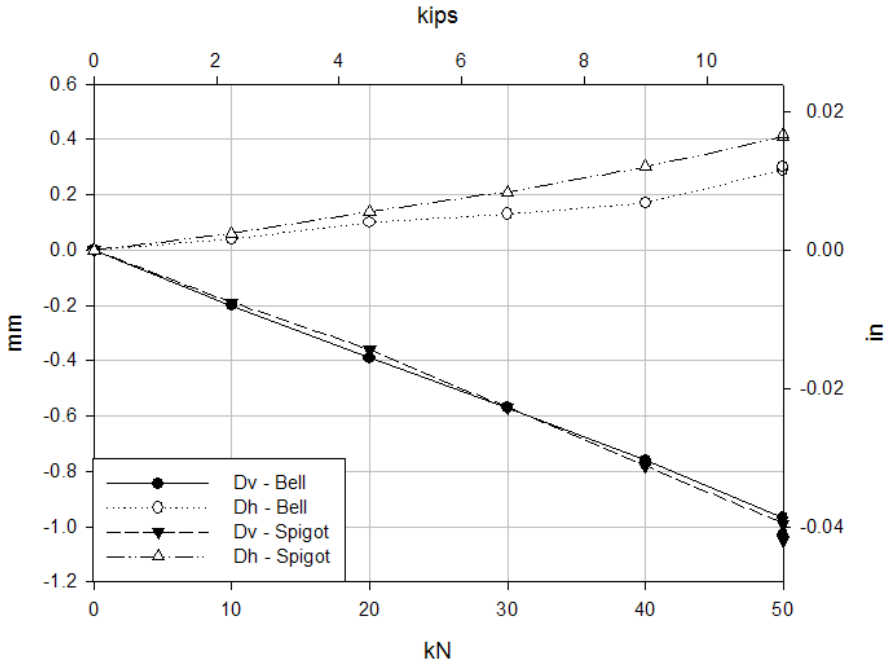

(a) Joint

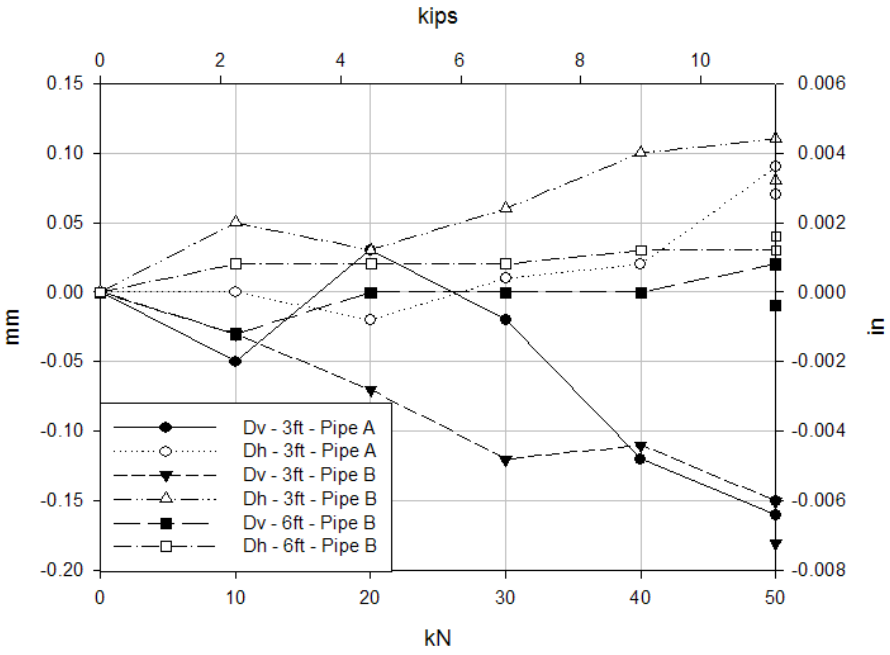

(b) Barrels

Figure C.80. Incremental diameter changes of the 36 in. (915mm) diameter PVC pipe; 2 ft (610mm) of cover, surface load over joint, void under spigot burial.

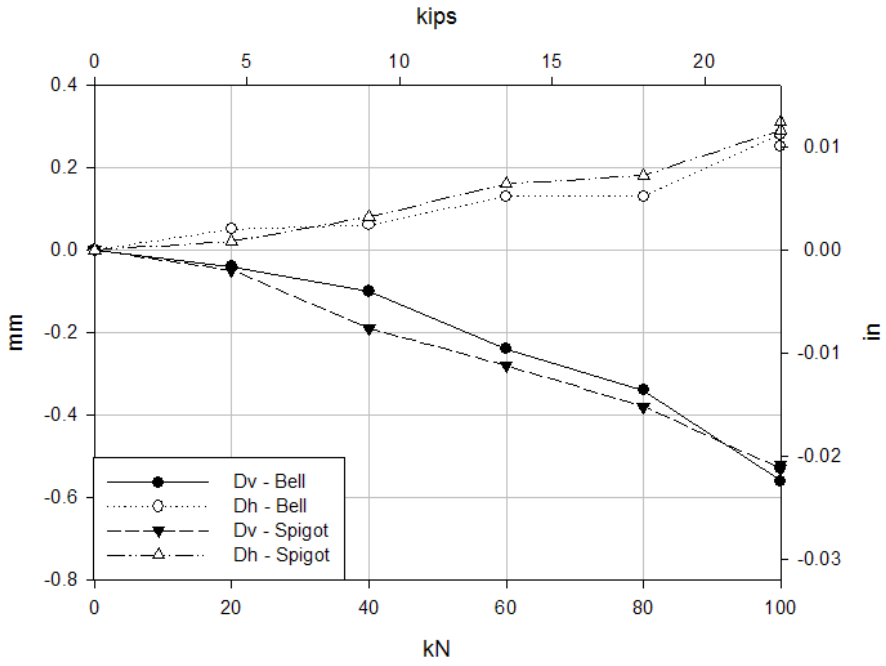

(a) Joint

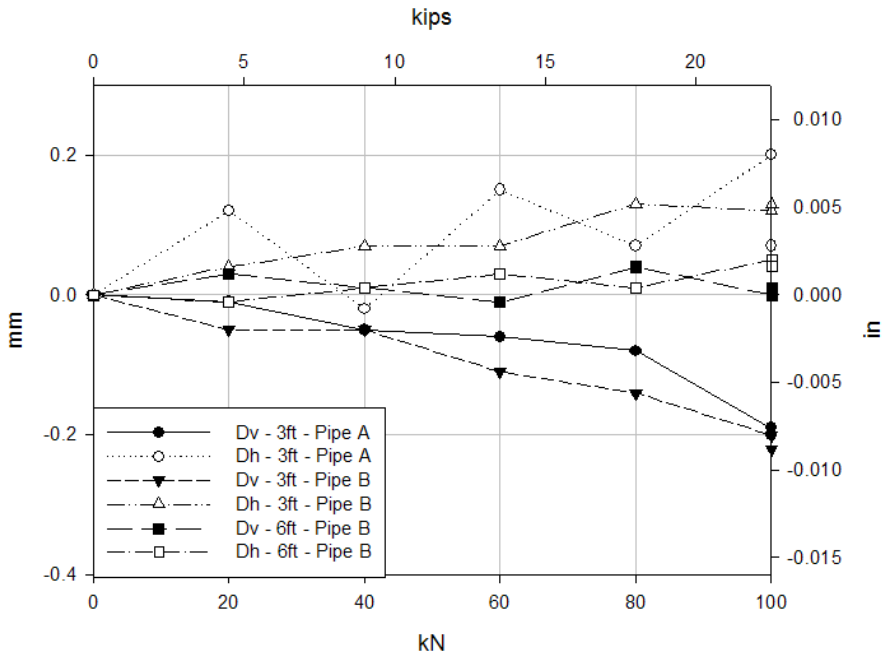

(b) Barrels

Figure C.81. Incremental diameter changes of the 36 in. (915mm) diameter PVC pipe; 4 ft (1220mm) of cover, surface load over joint, good burial.

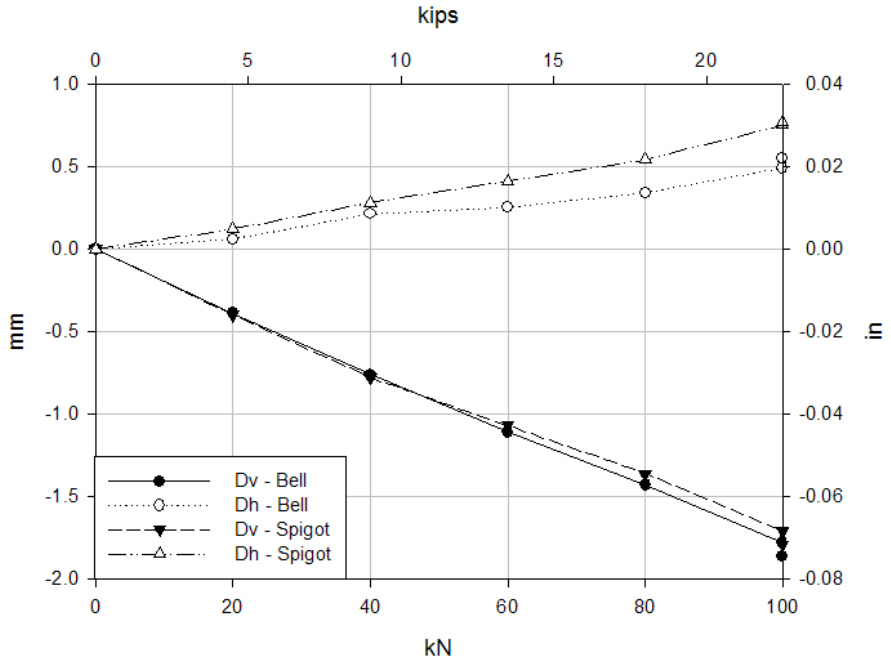

(a) Joint

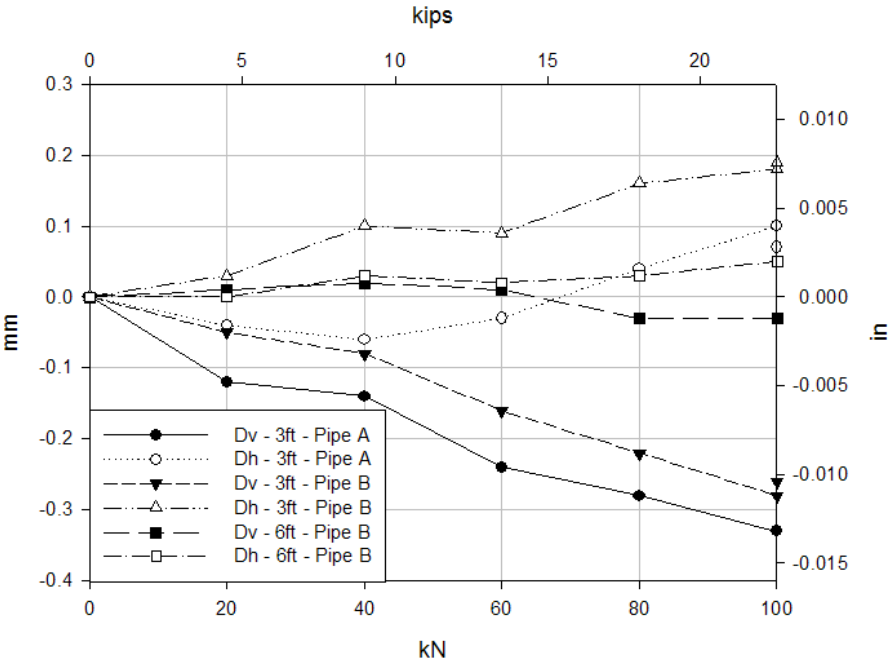

(b) Barrels

Figure C.82. Incremental diameter changes of the 36 in. (915mm) diameter PVC pipe; 2 ft (610mm) of cover, surface load over joint, good burial.

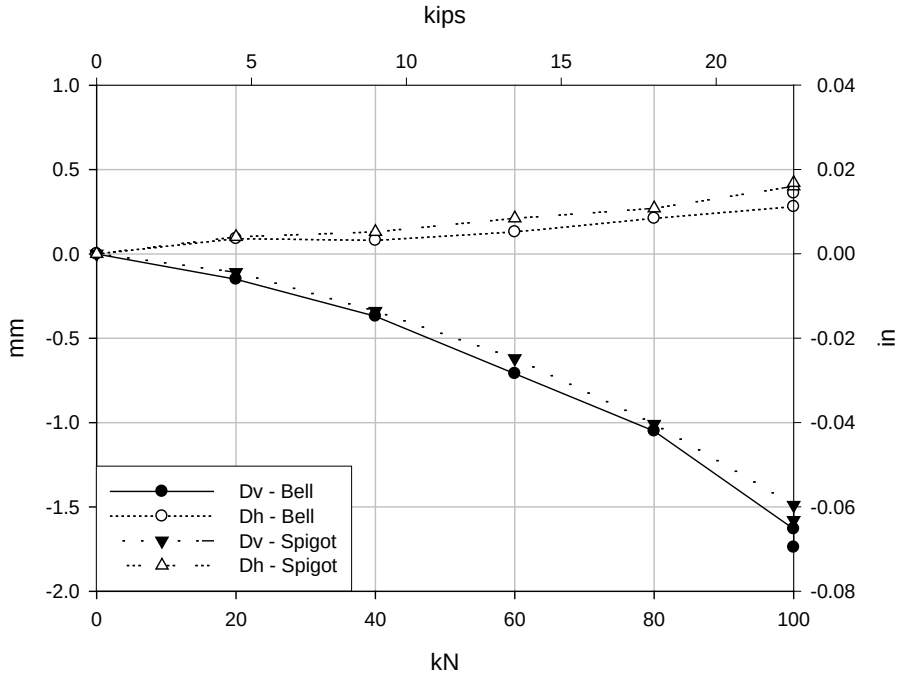

(a) Joint

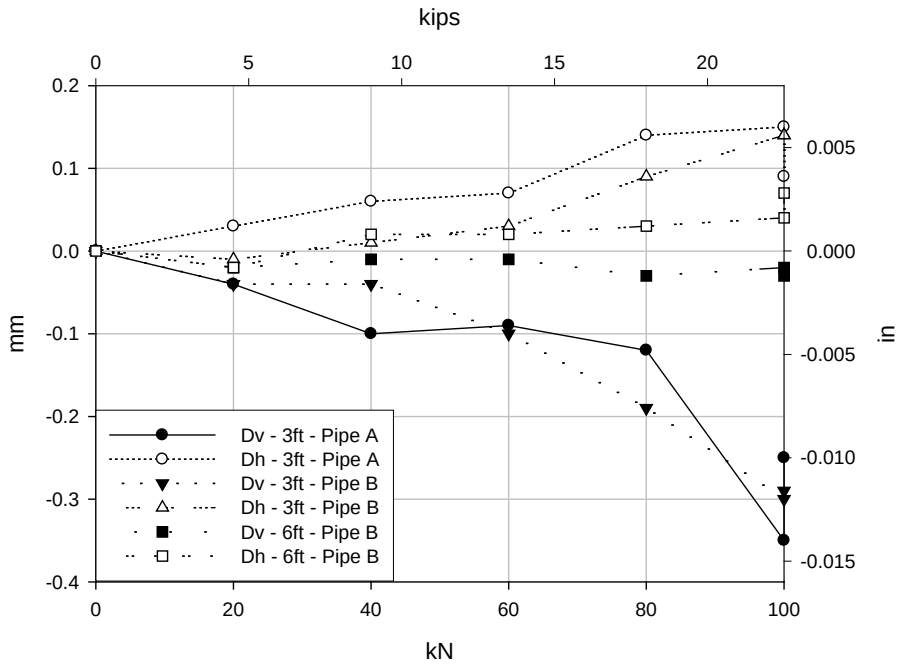

(b) Barrels

Figure C.83. Incremental diameter changes of the 60 in. (1525mm) diameter HDPE pipe; 4 ft (1220mm) of cover, surface load over joint, good burial.

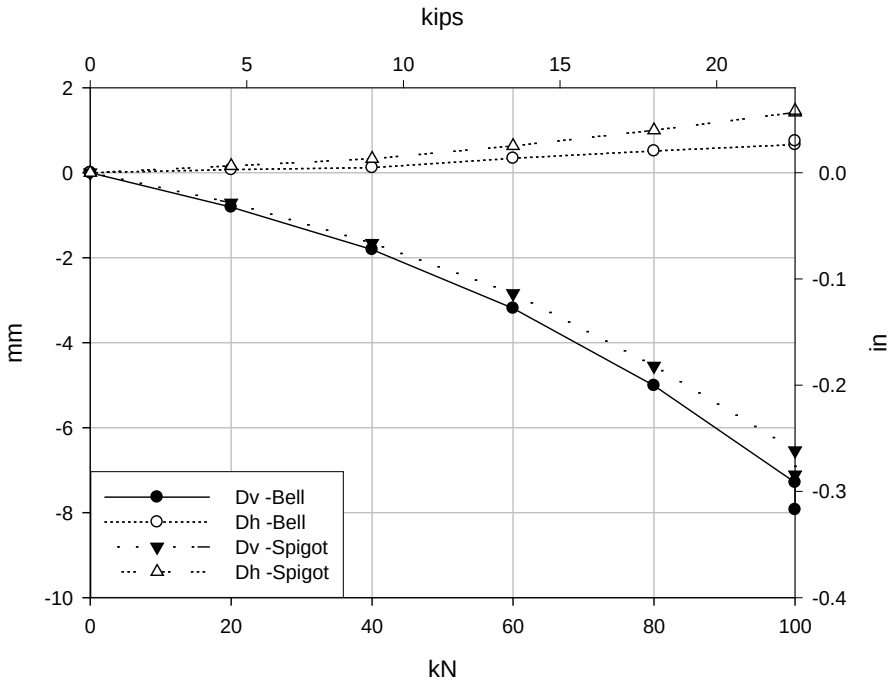

(a) Joint

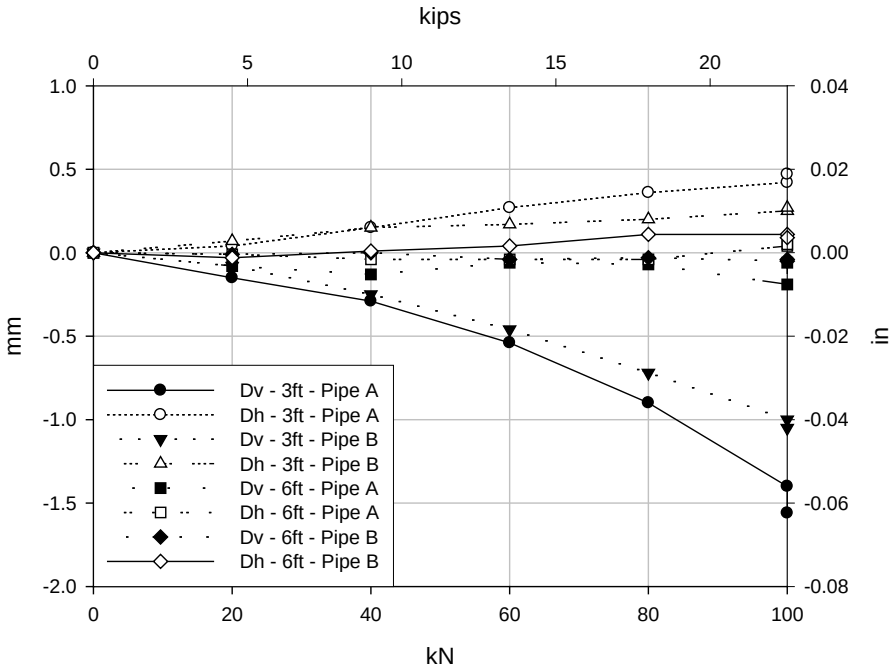

(a) Barrels

Figure C.84. Incremental diameter changes of the 60 in. (1525mm) diameter HDPE pipe; 2 ft (610mm) of cover, surface load over joint, good burial.

Vertical displacements of the springlines while the live load was applied were obtained from the reflective prisms data. Springline displacements rather that crown displacements were used since they represent the global response of the pipe while the crown values represent a local response including ovaling of the flexible thermoplastic pipe. **Figure C.85** shows the springline vertical displacement of the 36 in. (915mm) diameter PVC pipe during live loading. The results are presented for the two 'poor' burial conditions at 2 ft (610mm) of cover with half the service load (i.e. 11.25 kips) applied a three different locations. For the 'void under the joint' burial, a larger displacement was observed when the system was loaded in the offset over the spigot pipe compared to the opposite offset. This is likely due to the gasket compressing more between the joint elements and allowing more movement of the spigot due to the void. A similar effect was observed when the load was applied directly over the joint since a larger displacement in the spigot was registered. The 'void under the spigot' case caused larger shear in the joint as can be seen in these results.

Figure C.86 shows the springline vertical displacements registered during the service loading of the PVC specimen at adequate burial conditions. The figure shows results for two burial depths and three loading locations. A non-symmetric response was observed when the load was offset 3 ft (0.9m) in both directions from the joint. Larger displacements were registered when the load was applied above the spigot pipe. **Figure C.87** shows a comparison of the two 'poor' burial cases and the good burial case at the two burial depths. The results presented are for the system loaded directly over the joint.

The results for the 60 in. (1525mm) diameter HDPE pipe are presented in **Figure C.88**. The response observed in the vertical springline displacements of the pipe was essentially symmetric when the load was offset from the joint location; the service load was 22.5 kips (100kN). This response was observed at 4 ft (1220mm) and 2 ft (610mm) of cover, however, the magnitude of the springline vertical displacements of the joint at 2 ft (610mm) of cover was significantly larger. This also generated larger shear on the joint caused by the compression of the gasket between the joint elements, see **Figure C.89**.

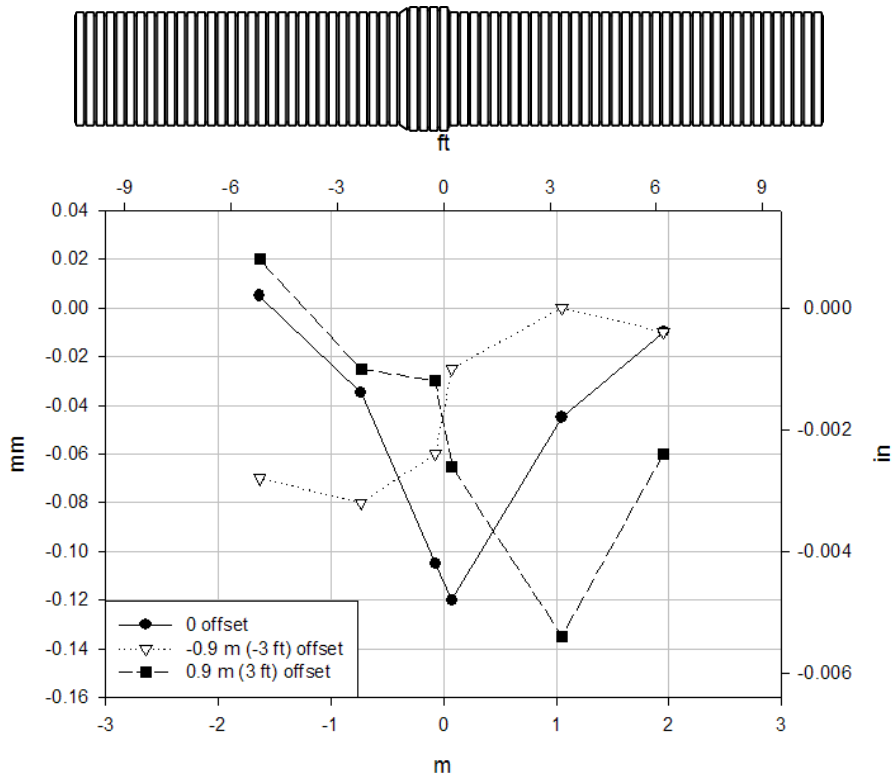

(a) Void under joint

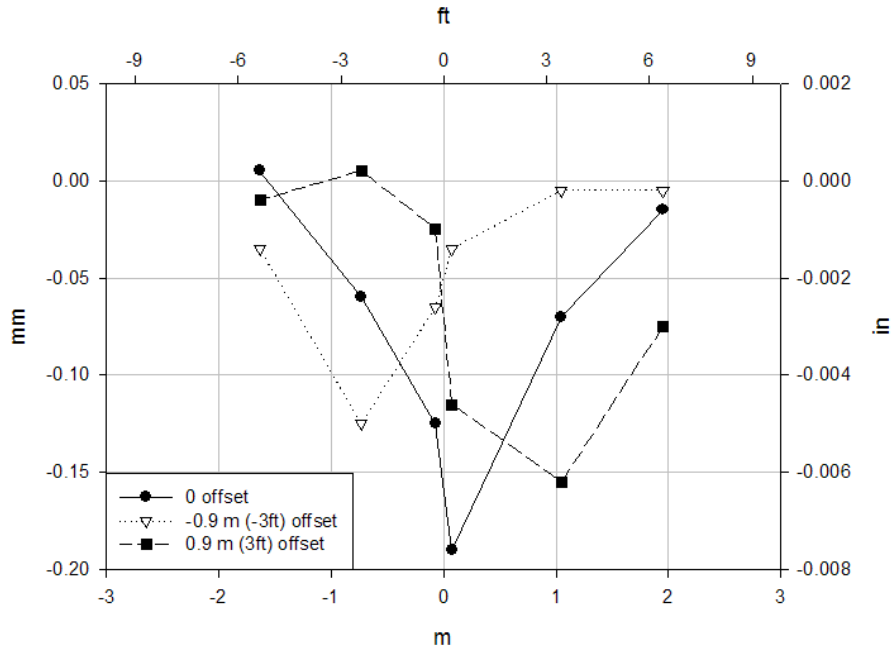

(b) Void under spigot

Figure C.85. Vertical springline displacements of the 36 in. (915mm) diameter PVC pipe; 2 ft (610mm) of cover, three loading locations, 'poor' burial conditions.

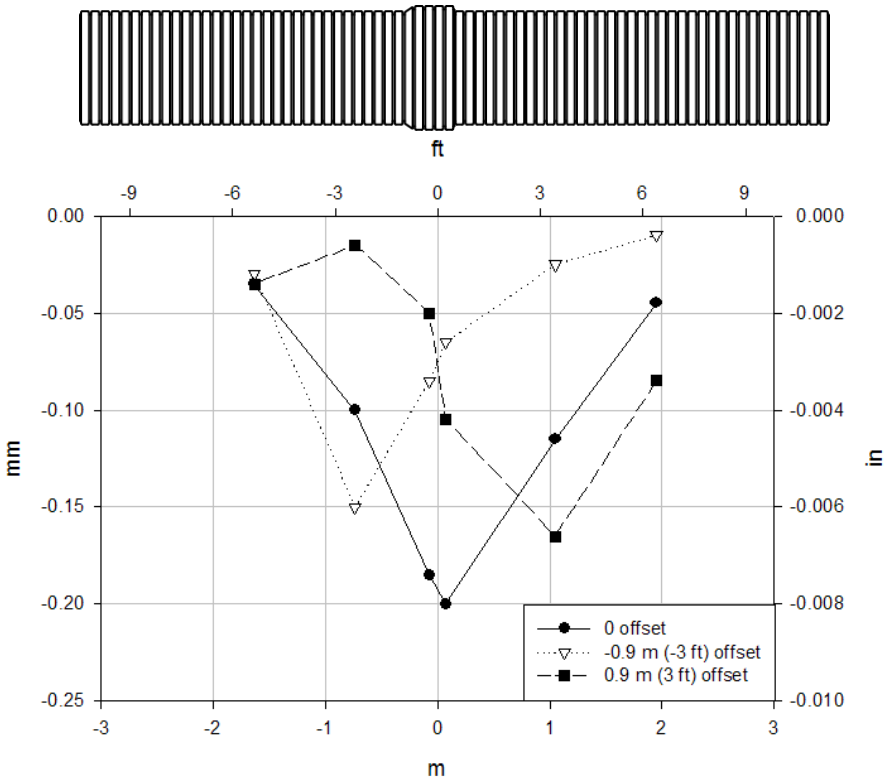

(a) 4 ft (1220mm)

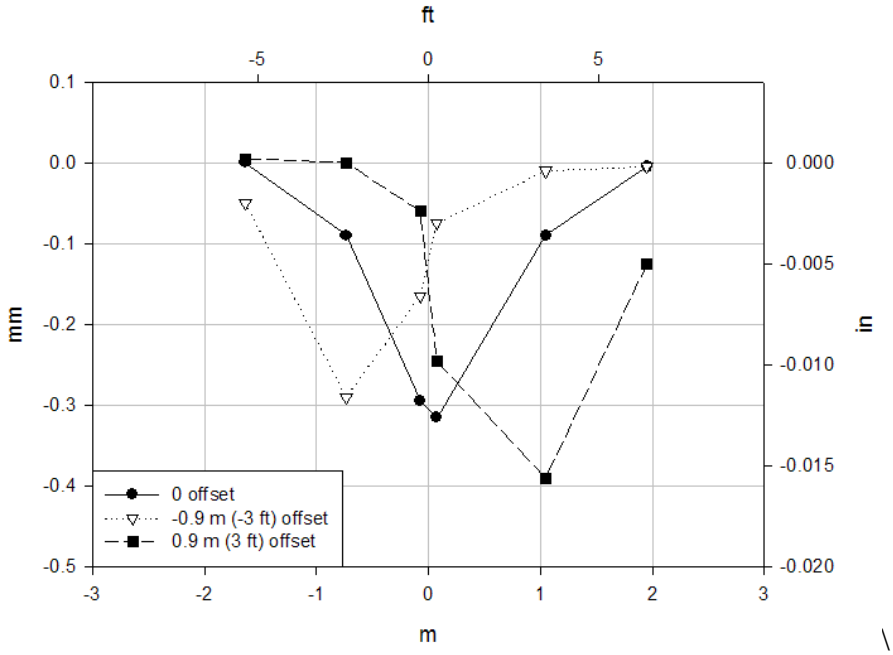

(b) 2 ft (610mm)

Figure C.86. Vertical springline displacements of the 36 in. (915mm) diameter PVC pipe; three loading locations, good burial conditions.

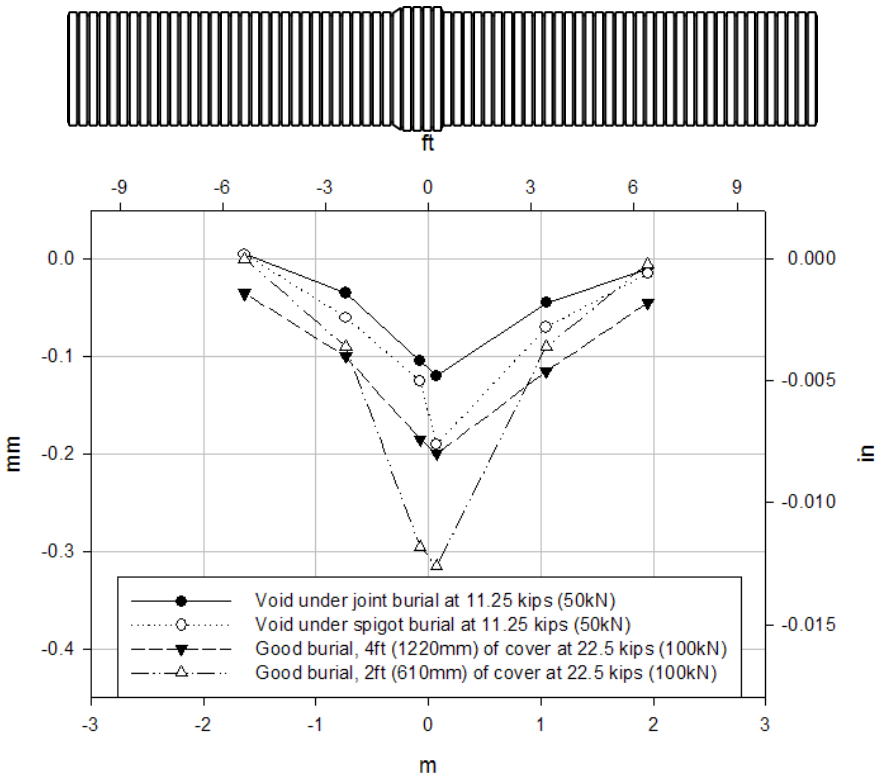

Figure C.86. Vertical springline displacements comparison for the 36 in. (915mm) diameter PVC pipe; loading over the joint.

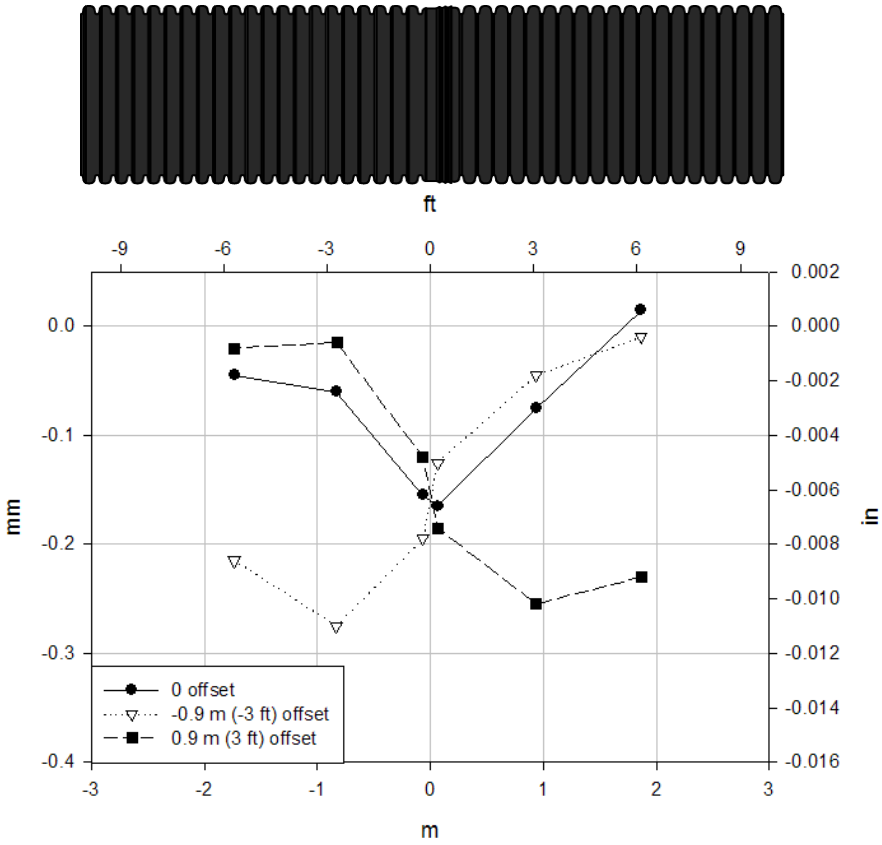

(a) 4 ft (1220mm) of cover

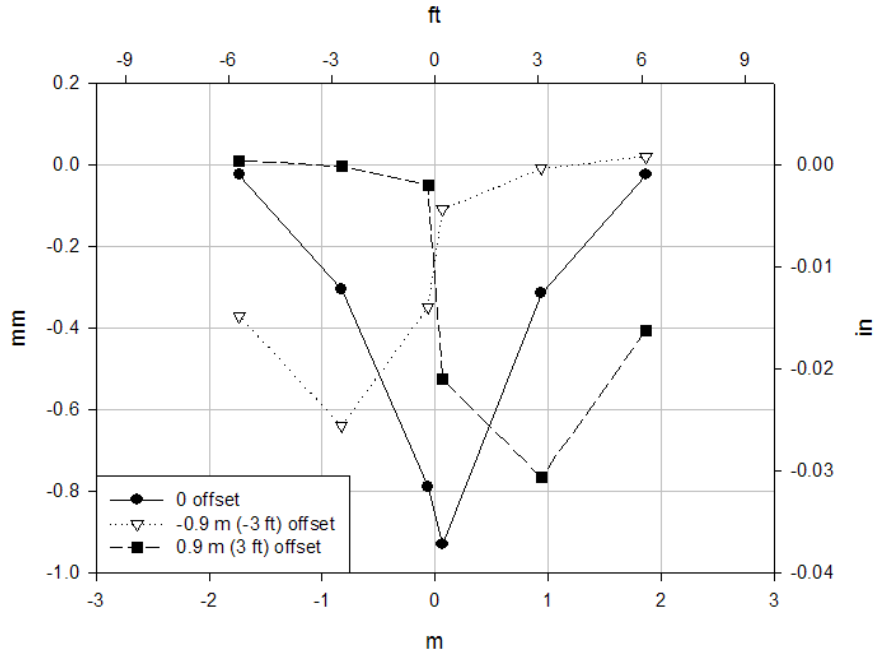

(b) 2 ft (610mm) of cover

Figure C.88. Vertical springline displacements of the 60 in. (1525mm) diameter HDPE pipe; three loading locations, good burial conditions.

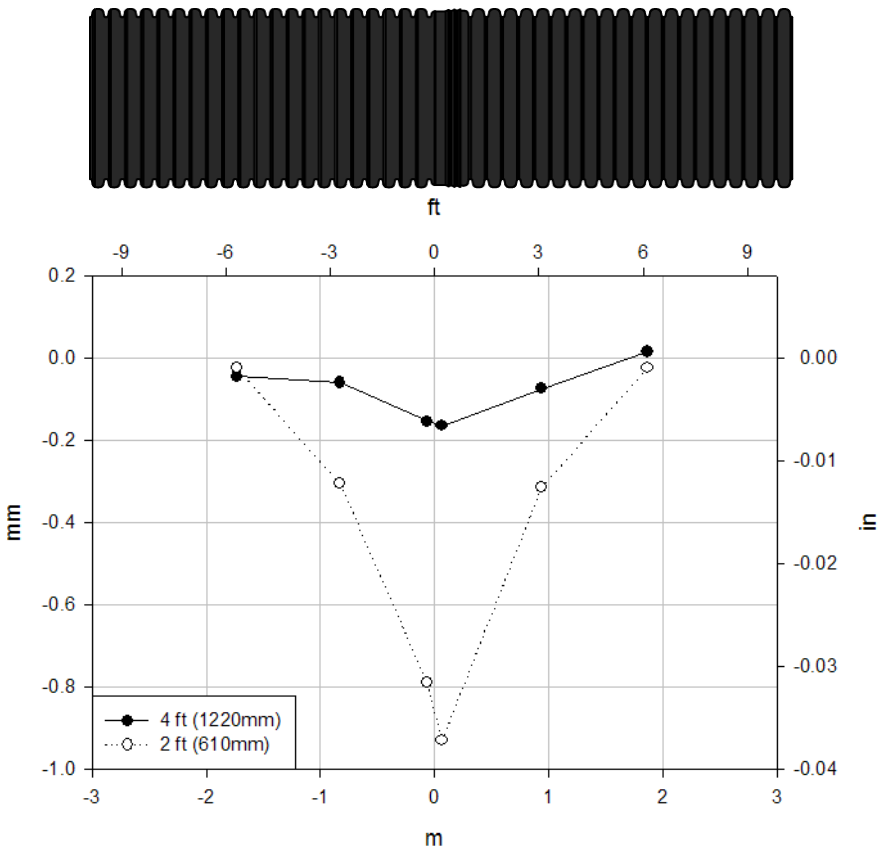

Figure C.89. Vertical springline displacements comparison for the 60 in. (1525mm) diameter HDPE pipe; loading over the joint.

C.4.3 Ultimate limit state tests

The 36 in. (915mm) diameter PVC pipe and the 60 in. (1525mm) diameter HDPE specimens were tested under burial conditions to their ultimate strength. The purpose of these tests was to observe the maximum load that could be applied to each specimen and to observe their failure mode when loading directly over the joint. The details of these tests are presented below.

C.4.3.1 Instrumentation

The instrumentation employed in these tests was the same as the one employed during the service loading tests. Reflective prisms were placed along the pipes of the PVC and the HDPE to measure horizontal and vertical diameter changes. The prisms were also employed to measure vertical displacements of the crown, invert and springlines in locations of the joint and barrels. In addition, string potentiometers were attached to both specimens to measure changes in diameter of the joint elements and barrels. The details of the instrumentation of the PVC and HDPE specimens can be seen in **Figures C.69** and **C.73** respectively.

C.4.3.2 Test configuration

Both thermoplastic pipes were tested at 2 ft (610mm) of cover, with good burial conditions (satisfying AASHTO guidelines) and with the load applied directly over the joint. The area of load applied to the surface was increased to prevent premature bearing failure of the soil. The test configuration for the 36 in. (915mm) diameter PVC pipe and for the 60 in. (1525mm) diameter HDPE pipe can be seen in **Figures C.90** and **C.91** respectively.

Figure C.90. Ultimate limit state test configuration of the 36 in. (915mm) diameter PVC pipe.

Figure C.91. Ultimate limit state test configuration of the 60 in. (1525mm) diameter HDPE pipe.

C.4.3.3 Results

Diameter changes were register by the reflective prisms and by the string potentiometers during the ultimate limit state tests. **Figure C.92** shows the vertical and horizontal diameter changes recorded for the joint elements of the 36 in. (915mm) diameter PVC pipe. The reflective prisms were able to measure changes until 67.5 kips (300kN) while the string potentiometer measured the entire loading-unloading history. The maximum load sustained by the system was 112.5 kips (500kN). Acceleration of the diameter changes was observed after 45 kips (200 kN) until the system could not sustain more load. The magnitudes of the horizontal diameter changes registered at higher loads were about half the vertical diameter changes. This indicates ovaling of the joint elements in addition to hoop compression (circumference decrease).

The vertical and horizontal diameter changes of the joint elements registered during the ultimate limit state test of the 60 in. (1525mm) diameter HDPE pipe can be seen in **Figure C.93**. These results were measured by the reflective prisms and by the string potentiometers during the entire loading range until a maximum load of 65.7 kips (292kN). The behavior was non-linear as registered in the service load testing and kept increasing until the maximum load. The ratio between the vertical and horizontal diameter changes indicate substantial 'hoop compression' (circumferential shortening) in addition to ovaling.

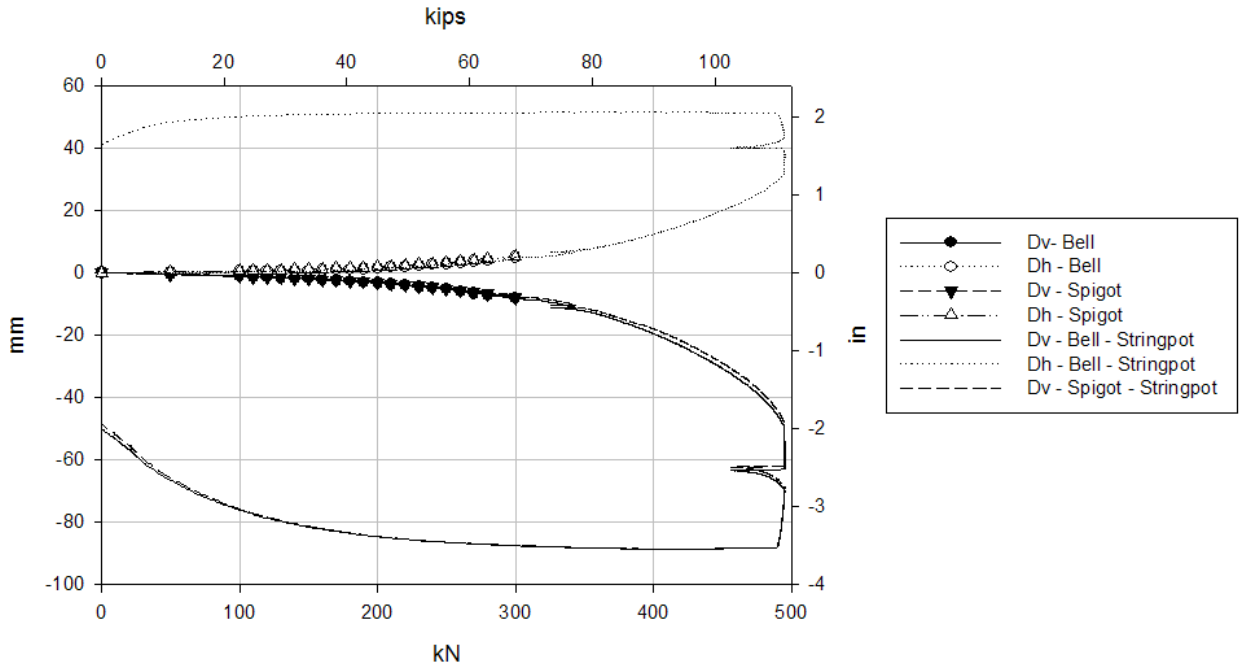

Figure C.92. Incremental diameter changes of the joint during the ultimate limit state test of the 36 in. (915mm) diameter PVC pipe; Reflective prisms and string potentiometers data.

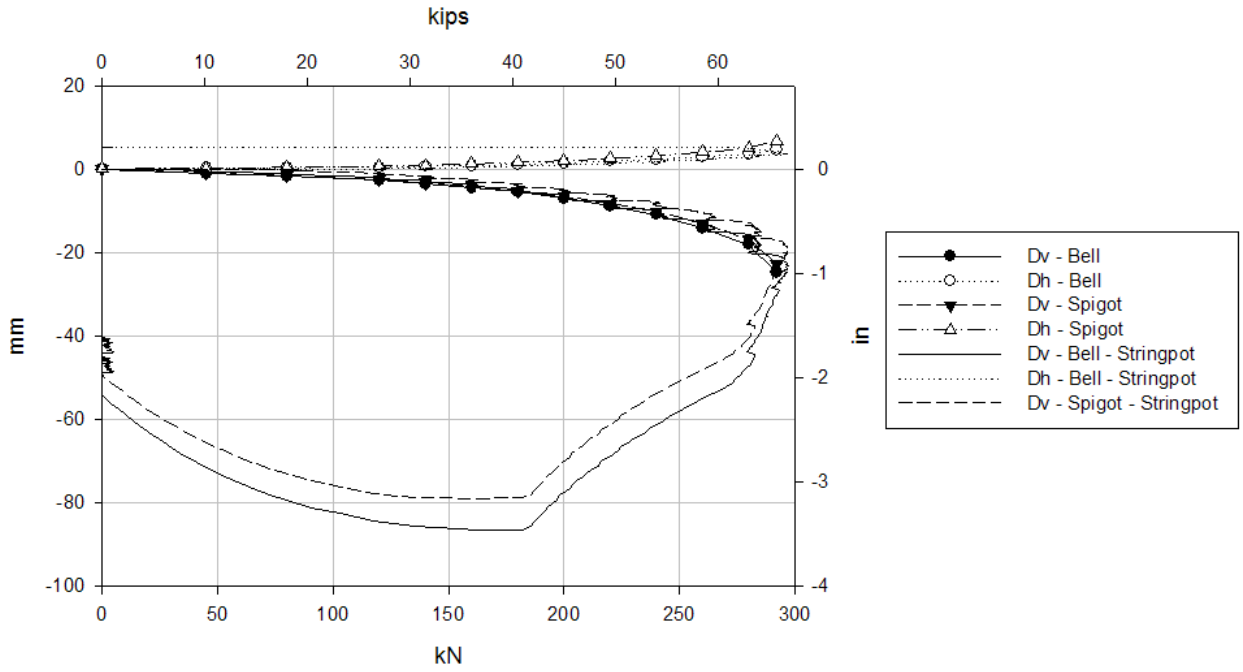

Figure C.93. Incremental diameter changes of the joint during the ultimate limit state test of the 60 in. (1525mm) diameter HDPE pipe; Reflective prisms and string potentiometers data.

The reflective prism data was also employed to measure vertical displacements of the pipes. With the purpose of showing global behavior rather than localized, the vertical displacements of the springlines are presented. **Figure C.94** shows the incremental vertical springline displacements for the 36 in. (915mm) diameter PVC pipe during the ultimate limit state test. The vertical displacement response accelerates while equal increments of load were applied. The results presented for the PVC pipe could only be measured until a load of 67.5 kips (300kN) due to excessive distortion of the pipe. These results also show a localized response of the pipe since the prisms placed 6 ft (1.8m) from the joint in both directions register small movements during these range of loading.

The results for the vertical springline displacement measured with the reflective prisms in the 60 in. (1525mm) diameter HDPE pipe can be seen in **Figure C.95**. These results were measured for the complete ultimate limit state test. The vertical displacement response accelerates while equal increments of load were applied. Similar to the PVC pipe, the vertical springline displacements show the localized behavior of the HDPE pipe since the magnitude of the displacement of prisms placed at 6 ft (1.8m) of the joint in both directions barely moved during the ultimate limit state test.

Figures C.96 and **C.97** show the PVC and HDPE pipes after the ultimate limit state tests. The PVC pipe exhibited a ductile failure and its deflection was governed by ovaling, although the effect of hoop compression could also be seen in the response. Neither cracks nor local buckling was observed after the test. The HDPE pipe also showed a ductile failure and its deflection was governed by hoop compression. Local buckling was observed close to the shoulders in the bell and spigot of the joint but no cracks were observed.

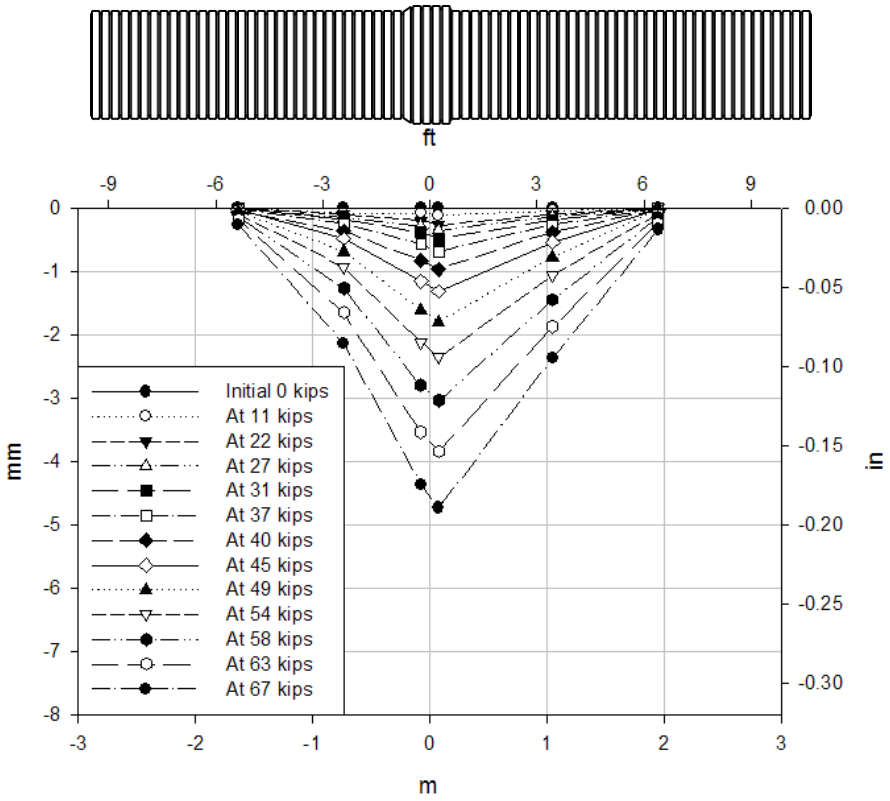

Figure C.94. Incremental springline vertical displacement during the ultimate limit state test of the 36 in. (915mm) diameter PVC pipe.

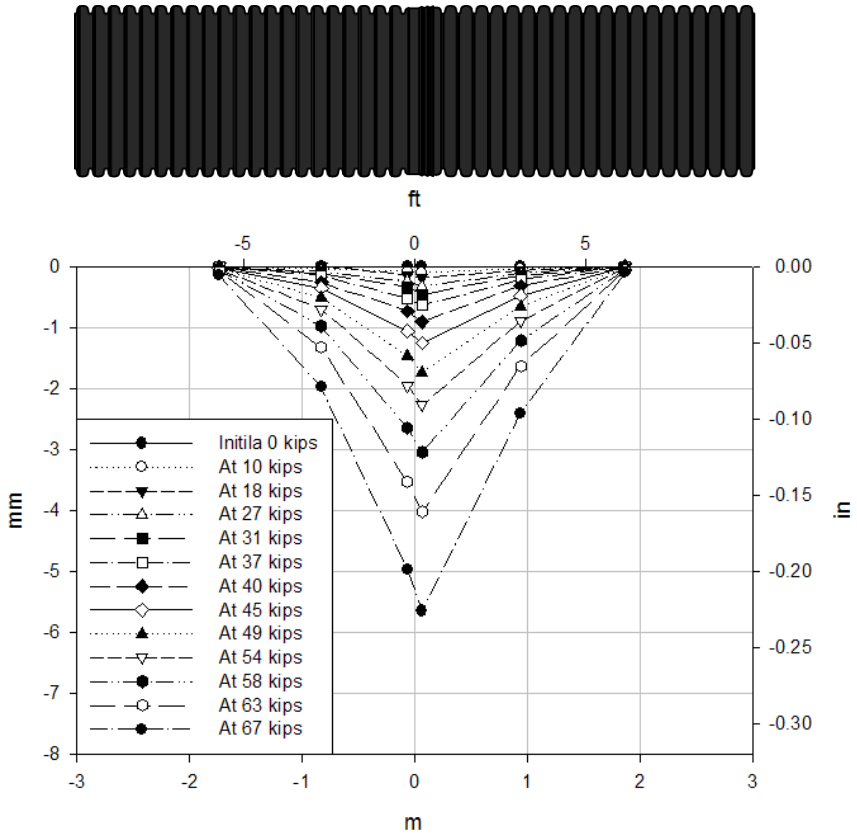

Figure C.95. Incremental springline vertical displacement during the ultimate limit state test of the 60 in. (1525mm) diameter HDPE pipe.

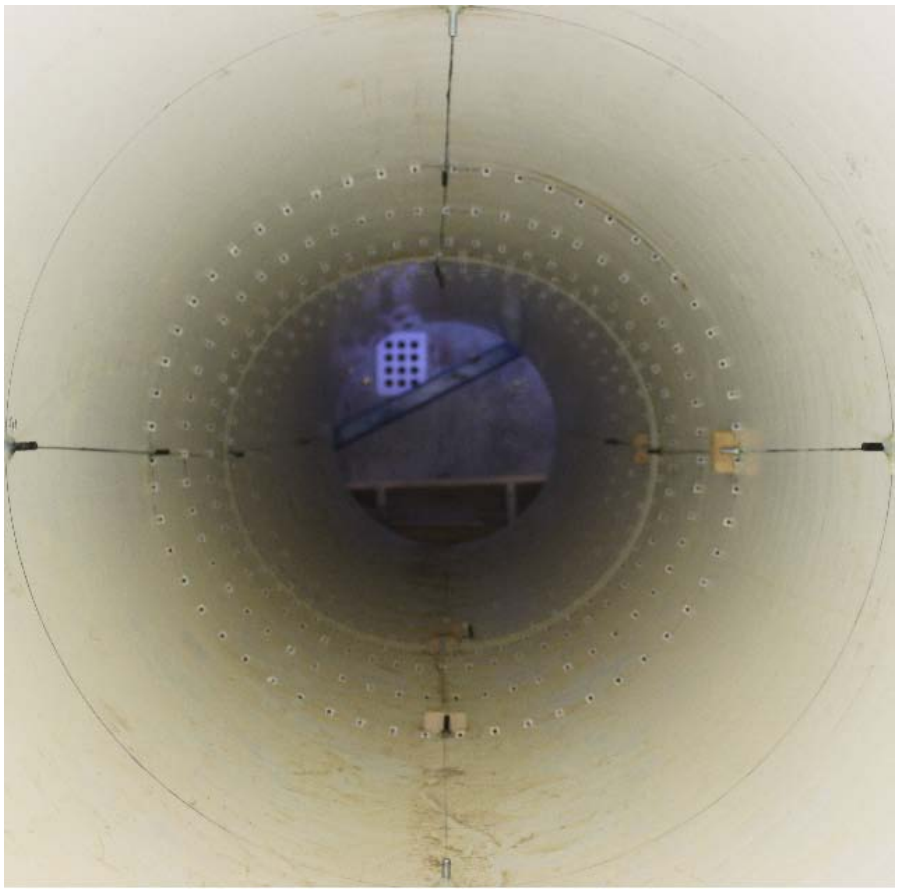

Figure C.96. PVC pipe after ultimate limit state test.

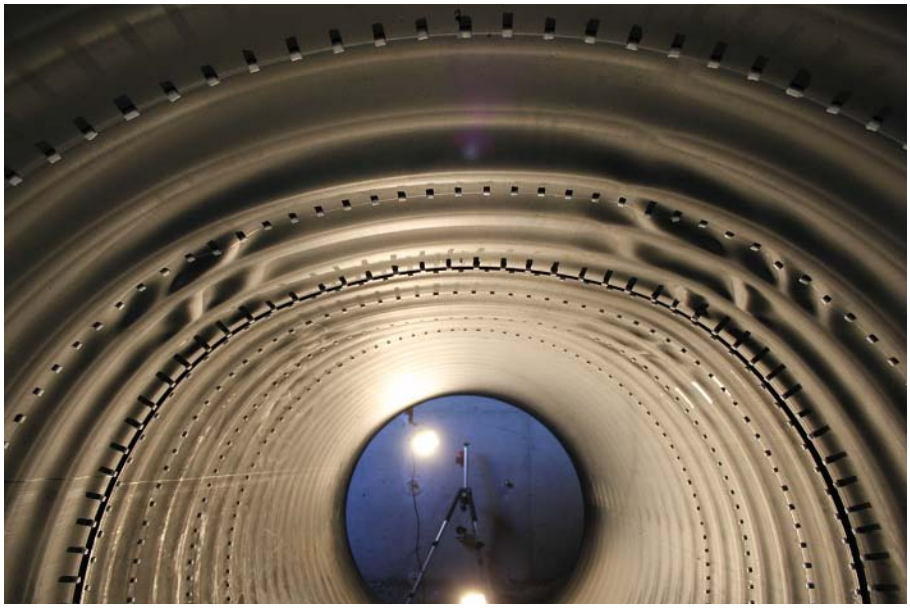

Figure C.97. HDPE pipe after ultimate limit state test.

Field testing

Contents

Introduction

To better understand the joint behavior of existing culverts, six culverts were tested in the field in Ohio. A heavily loaded truck was stopped or driven over the culverts to measure the static and dynamic response of the culverts and their joints. The testing trucks contained loads that were near to or exceeding the legal hauling limits of the roadway. Two in-service corrugated metal pipe (CMP), two reinforced concrete (RC) and one high-density polyethylene (HDPE) pipe culverts were tested. Another HDPE culvert was tested during the installation of the culvert.

This following section describes test culverts, instrumentation and the field testing setup. A portable measurement system and a laptop computer were used to measure and store data from displacement sensors and strain gauges attached to the test culverts. The last sections present the measurements.

Description of Field Test Culverts

The name of each culvert consists of the culvert type followed by the diameter followed by the backfill depth. A culvert named CMP-D4-F1.5 implies a corrugated metal pipe with a 4 ft (1.2 m) diameter and 1.5 ft (0.45) backfill depth. Table D.1 lists important culvert information.

Table D.1 Properties of Test Culverts (1 in. = 2.54 cm, 1 ft = 0.30 m)

Culvert Name	Inner Diameter (ft)	Backfill Height (ft)	Joint	Wall Thickness (in.)	Typical Segment Length (ft)
CMP-D4-F1.8	4.0	1.8	Band	3/32	12 or 20
CMP-D3-F2.5	3.0	2.8	Band	1/8	20
RC-D7-F4.7	7.0	4.7	Tongue & Groove	8	5

RC-D4.5-F2	4.5	2.0	Tongue & Groove	6	6
HDPE-D3-F4.7	3.0	4.7	Bell-Spigot	-	19.5
HDPE-D3.5-F3.5	3.5	3.5	Bell-Spigot	-	20

Description of Test Culvert CMP-D4-F1.8

This is a circular corrugated metal culvert located in Pike County in Southern Ohio on County Road 76 with straight-line-mileage (SLM) of 2.80. SLM is measured from the southernmost or westernmost point in Ohio along the route. The culvert consists of two spirally corrugated longitudinal sections connected by a band type joint. The longer section has a length of 20 ft (6.1 m). The shorter 12 ft (3.66 m) segment is installed on the upstream end of the culvert. The pitch of the corrugation, i.e., centerline distance between consecutive corrugations, is 2.675 in. (6.8 cm), and the depth of the corrugation is 7/16 in. (1.11 cm). The culvert is orientated perpendicular to the roadway. Culvert damage consists of ovaling, some joint leakage and rusting along the invert. This culvert was tested on November 17th, 2009. The instrumented test culvert is shown in Figure D.1

.

a) Loading on the culvert b) Strain gauges and displacement sensors installed on the culvert

Figure D.1 Load application and instrumentation of CMP-D4-F1.8

Description of Test Culvert CMP-D3-F2.5

This is a corrugated metal culvert located in Pike County in Southern Ohio on County Road 76 with SLM of 1.60. This culvert with a diameter of 3 ft (0.9 m) and backfill height of 2.5 ft (0.76) was smaller and deeper than the first test culvert (CMP-D4-F1.8). The culvert consists of two 20 ft (9.1 m) sections. The pitch of the corrugation is 2.675 in. (6.8 cm), and the depth of the corrugation is 0.5 in. (12.7 cm). The culvert has a skew angle of 35 degrees. Culvert damage consists of some joint leakage and rusting along the invert. This culvert was tested on November 17th, 2009. The testing of this culvert is shown in Figure D.2.

Figure D.2 Testing of CMP-D3-F2.5 under static truck loading

Description of Test Culvert RC-D7-F4.7

This reinforced concrete culvert is located in central Ohio in Logan County on State Route 274 with SLM of 15.00. This relatively large culvert consists of concrete sections 5 ft (1.52 m) in length. The type of the culvert joints is tongue and groove with mastic seal. Culvert damage consists of slight separation in the mastic seal in some joint locations. Overall, the joint was in decent condition. The culvert has a skew angle of 8 degrees with respect to transverse direction of the roadway No significant damage was observed near the instrumented joint locations, where the testing was conducted. This culvert was tested on December 17th, 2009. Photographs of this culvert are shown in Figure D.3.

a) Instrumentation setup inside the culvert b) Testing

Figure D.3 Instrumentation and testing of RC-D7-F4.7

Description of Test Culvert RC-D4.5-F2

This reinforced concrete culvert is located in central Ohio in Franklin County on County Road 148 with SLM of 0.82. This culvert consists of 6 ft (1.83 m) long sections joined together with a bell and spigot joint. Significant joint deterioration is observed in this culvert including concrete cracking very near to several of the joints and damage to the seal. This culvert with a diameter of 4 ft (1.2 m) was smaller than the other RC culvert described above. It was also much closer to the road surface. The culvert is perpendicular to the longitudinal direction of the roadway and thus has no skew angle. This culvert was tested on December 18th, 2009. Figure D.4 shows the culvert instrumentation and front wheel of the test truck placed over the culvert.

a) Close-up view of instrumentation b) Testing

Figure D.4 Instrumentation and testing of RC-D4.5-F2

Description of Test Culvert HDPE-D3-F4.7

This corrugated, double-walled HDPE culvert is located in central Ohio in Franklin County on County Road 12 with SLM of 8.53. The pitch of the corrugation is 4.5 in. (11.43 cm), and the depth of the corrugation is 2 in. (5.1 cm). This culvert with no skew angle had no visible damage. The culvert was tested on December 18th, 2009. The instrumentation installed inside the culvert near the tested joint is shown in Figure D.5.

a) Instrumentation b) Testing

Figure D.5 Close-up view of instrumentation and testing of HDPE-D3-F4.7

Installation of Test Culvert HDPE-D3.5-F3.5

This corrugated HDPE pipe was installed in Hilliard, OH at the intersection of Scioto Darby Rd, and Heywood Dr. The pipe consists of 20 ft (6.09 m) sections joined together with a gasket seal. The pitch of the corrugation is 6.25 in. (15.88 cm) and the corrugation depth is 3.25 in. (8.26 cm). This culvert was tested during and immediately after its installation on August 17th, 2010. Measurements were taken during the placement and compaction of the backfill, and during surface loading from a front end loader. Displacement sensors installed inside the HDPE pipe and static load applied on the pipe are shown in Figure D.6.

a) Instrumentation b) Testing

Figure D.6 Instrumentation near test joint and load application on HDPE-D3.5-F3.5

Loading Schemes

Static Loading

Culverts were tested using a truck with a weight near to or exceeding the legal hauling limit. As part of static loading, front or rear axle of the truck was placed over the crown or edges of the test culvert and displacements and strains were measured for approximately one to two minutes to make sure stable and constant displacements were measured under the sustained static load. A total of 15 static load cases were selected for each experiment.

Loading presented in Figure D. consists of the following static load cases: front axle over the first culvert edge (F1), front axle over crown (F2), front wheel over the second culvert edge (F3), center or first rear axle over the first culvert edge (R1), rear wheel over the crown (R2), and rear axle over the second culvert edge (R3). Depending on the distance between the front and rear axles and culvert diameter, the front wheel load may still apply load on the culvert during load case R1 (or R2 and R3). Loading is also classified according to the position of wheels over the tested joint. Figure D.8 consists of the following load cases: the truck centered on joint (C), the two side wheels centered on the joint (SC), and the truck located immediately to the right of the joint (S). The load cases used in static testing are a combination of the load application points

described in Figure D. and the wheel locations shown in Figure D.. A typical sample load combination would be load combination SC-F3. This combines load case SC from Figure D. with load case F3 from Figure D.; when the front axle of the truck is over the edge of the culvert while two side wheel right over the culvert joint. The only combination that was not tested was load case SC from Figure D. combined with load cases F1, F2 and F3 from Figure D..

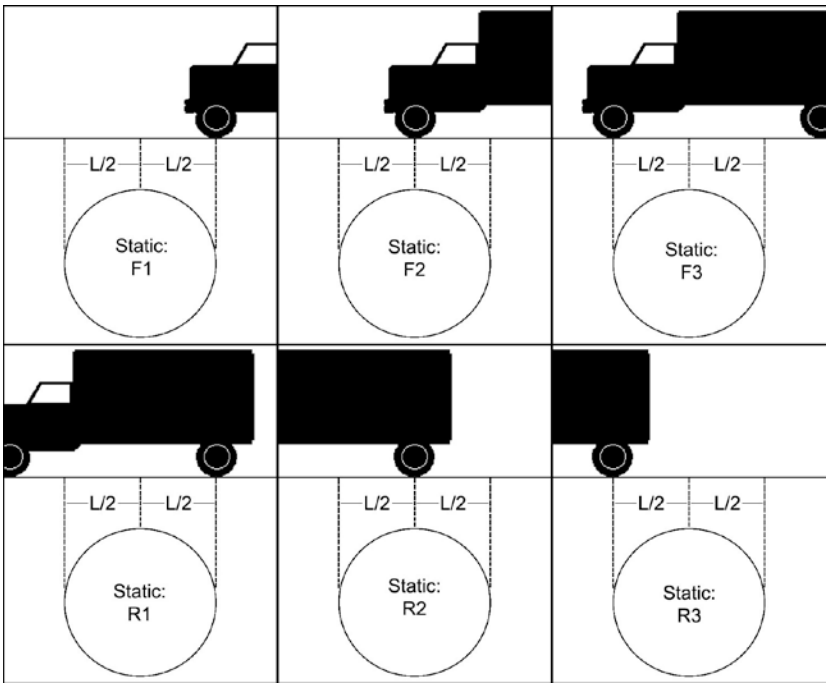

Figure D.7 Static load cases F1, F2, F3, and R1, R2, R3 (upstream side view)

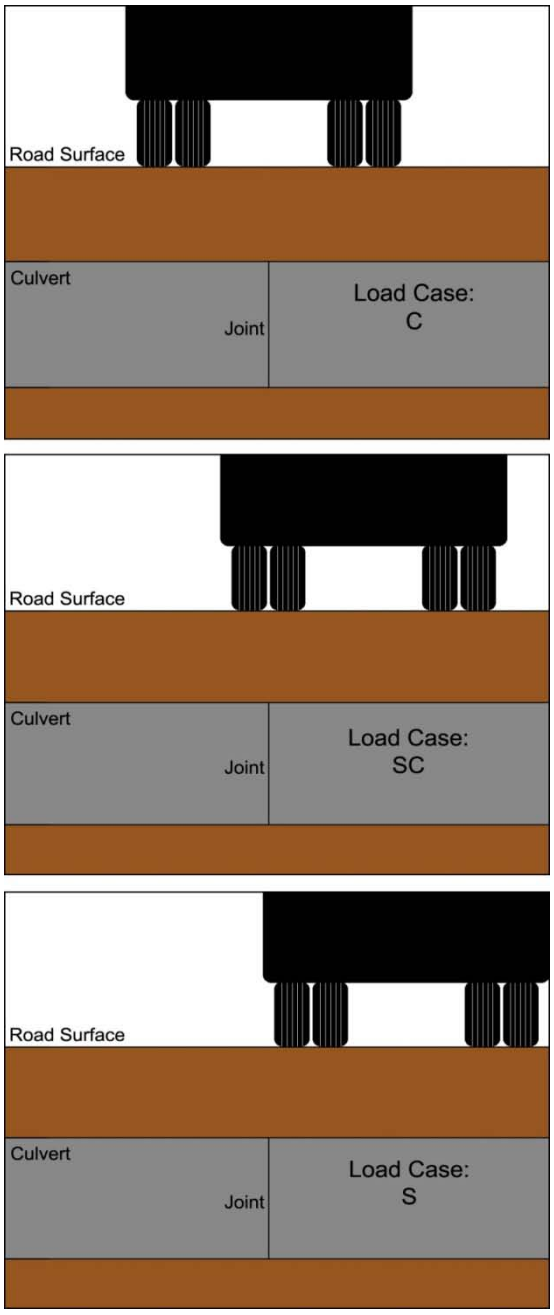

Figure D.8 Static and live load cases (rear end view)

Dynamic Loading

Loaded trucks were driven over the culvert at a series of speeds. This dynamic truck loading represents typical loading on the culvert. The trucks were driven at 5, 10, 20 and 30 mph (8, 16, 32, and 48 km/h). In some cases, the road conditions limited the speed at which the trucks could

be driven. This series of speeds was repeated for load cases C and S from Figure D.. Eight dynamic load tests were performed on each culvert except for culvert HDPE-D3-F4.7 where guard rails prevented testing of load case C. No dynamic loading was conducted on HDPE-D3.5-F3.5 because the culvert was freshly installed, and the loading equipment and construction site were not suitable for such testing

Magnitude of Applied Loading

Two separate trucks and one front end loader were used for the testing. Each truck had two wheels on the front steering axle and four wheels on the rear axle. Although the second truck had three axles, the middle axle of Truck #2 was raised during all experiments. The front end loader, which was used during the last test, had two wheels on each axle. Specific truck information is provided in

Table D.1. The trucks and front end loader are shown in Figure D..

Table D.1 Testing truck information (1 kip = 4.4 kN, 1 ft = 0.3 m)

Truck #No.	Test Culverts	Truck Weight (kips)		Axle Spacing (ft)	Distance Between Rear Wheel Pairs (ft)
		Steering Axle	Rear Axle		
1	CMP-D4-F1.8 and CMP-D3-F2.5	13.3	29.8	14	4.67
2	RC-D7-F4.7, RC-D4.5-F2, and HDPE-D3-F4.7	17.1	28.6	14	4.67
3	HDPE-D3.5-F3.5	24	8.5	9.5	4.3

a) Truck #1 b) Truck #2 c) Truck #3: Front End Loader

Figure D.9 Trucks used for loading the culverts

Instrumentation Schemes

Instrumentation consisted of linear displacement sensors and strain gauges. Seven of the eight linear displacement sensors had a precision of 0.001 in. (25 μm) while one of the sensors had a precision of 0.0002 in. (5 μm). The uni-axial strain gauges had a sensitivity of 5 micro-strain. Table D.1 displays the type and number of strain gauges and linear displacement sensors used in each test.

Table D.1 List of linear sensors and strain gauges used during tests

Culvert	Number of Sensors	
	Linear Displacement Sensors	Strain Gauges
CMP-D4-F1.8	6	12
CMP-D3-F2.5	6	12
RC-D7-F4.7	7	0
RC-D4.5-F2	8	0
HDPE-D3-F4.7	8	0
HDPE-D3.5-F3.5	8	0

Concrete and Plastic Culvert Instrumentation

Figure D.10 shows the arrangement of sensors in the testing of culvert RC-D7-F4.7. The same instrumentation scheme was used in culverts RC-D4.5-F2 and HDPE-D3-F4.7. Position A shown in Figure D.10 is at the crown of the culvert while positions B and D are at the springline. Position C varied in each culvert depending on the water level and positioning of the sensor frame. Position C is between 30 and 45 degrees below the springline in all culverts.

Two linear displacement sensors were mounted to each arm of the frame to measure the movement of the inner surface of the culvert. One sensor was placed on each side of the joint. The two-sensor combination allows for measurement of movement in the transverse direction and separation at the joint. The two-sensor setup can be seen in Figure D.11 at sensor location B, and in Figure D.12 at location A, where the horizontal distances from each sensor to the centerline of joint are equal, 3.5 in. (8.9 cm), i.e., total distance between the sensors is 7 inches (18 cm). Linear displacement sensors were placed longitudinally at positions A and C. These sensors measure longitudinal movement across the joint. The longitudinal sensor at position A is not pictured in Figure D.1 because it could not be properly secured during the test of culvert RC-D7-F4.7. In all

other culverts, the longitudinal sensor was offset by up to 15 degrees from the crown in the direction of B to facilitate placement of the instrumentation frame structure.

The instrumentation frame structure was secured to the culvert segment opposite of the truck loading in load case S shown in Figure D.. The instrumentation frame is considered to be on the upstream side of the joint as depicted in Figure D.13.

Reflective prisms were installed by researchers from Queens University who work on the greater NCHRP project that this paper is a part of. Prisms can be seen in photos showing the testing of both RC pipe culverts, and the HDPE-D3-F4.7 test culvert. This instrumentation is not described here because it is not used in this report.

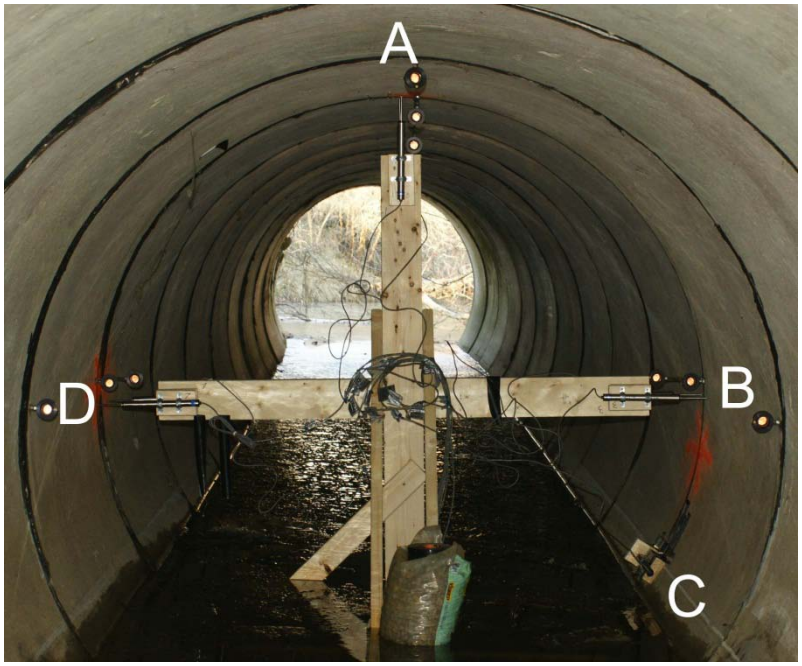

Figure D.10 Upstream side view of sensor placement (RC-D7-F4.7)

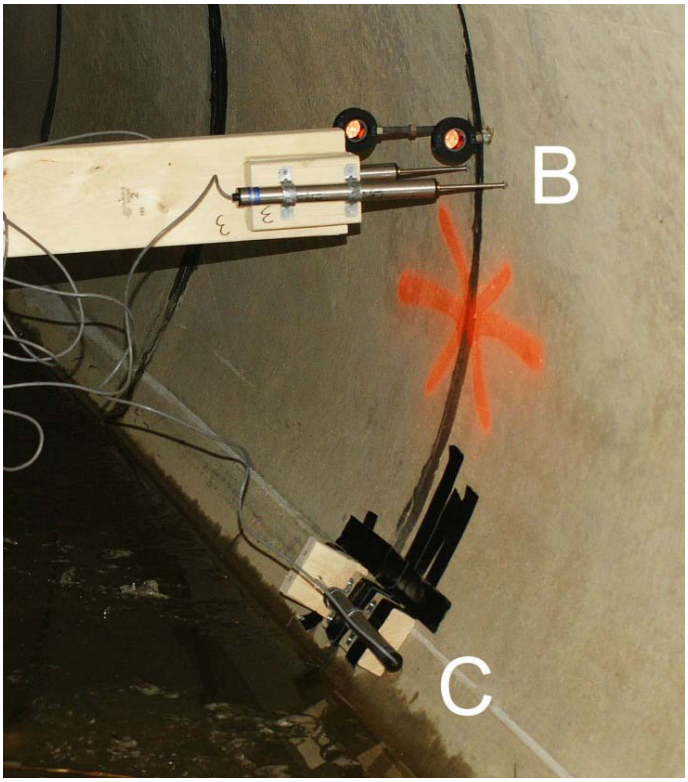

Figure D.11 Close-up of upstream side view of sensor placement (RC-D7-F4.7)

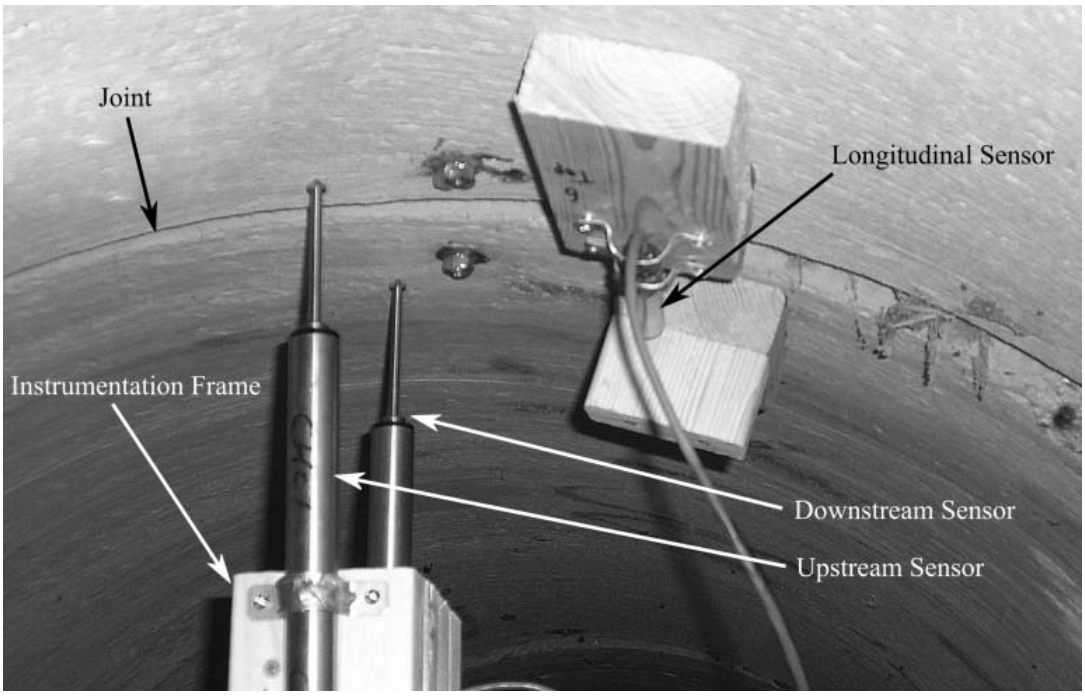

Figure D.12 Upstream side view of location A (RC-D4.5-F2)

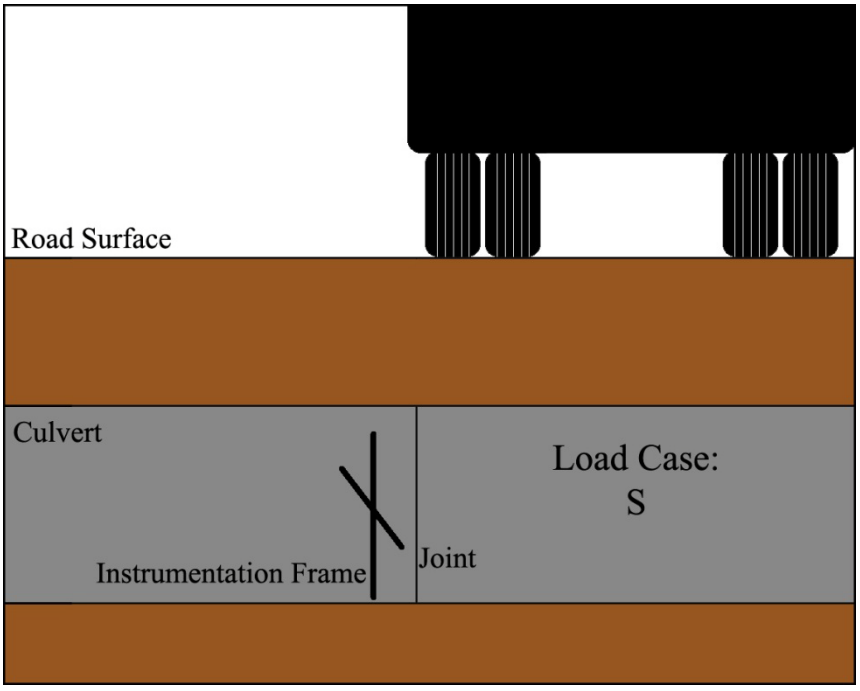

Figure D.13 Position of instrumentation frame relative to truck loading scheme

CMP Culvert Instrumentation Scheme

Testing of the metal culverts CMP-D4-F1.8 and CMP-D3-F1.5 consists of a slightly different setup than the one above. Six linear displacement sensors were used on the metal culverts. Position D was ignored for CMP tests. Strain gauges were placed at positions A and C. Figure D.1414 shows the instrumentation from the right side of the joint in culvert CMP-D4-F1.8.

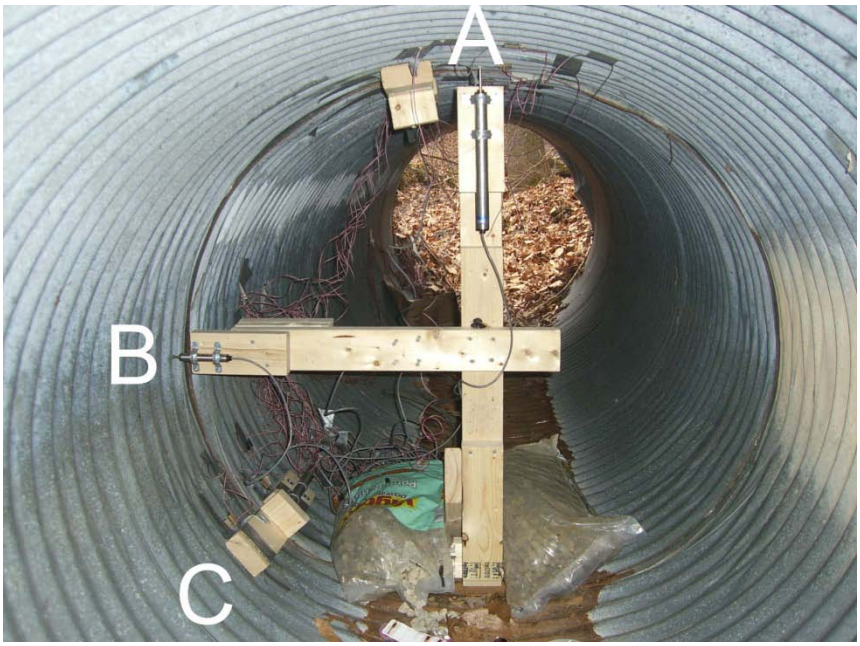

Figure D.14 Upstream side view of test setup for CMP-D4-F1.8

The CMP strain gauge arrangement is depicted in Figure D.15. Strain gauges #7 through #14 are placed at position ‘A’ at the crown of the culvert. Actual positioning is offset by up to 15 degrees to allow spacing for other sensors. Gauges #15 through #18 are placed at position ‘C’ as shown in Figure D.1414. Gauges depicted as a dot measure the strain around the circumference of the culvert (in the transverse direction of the culvert). Gauges depicted as a line measure the strain along the length of the culvert (in the longitudinal direction of the culvert).

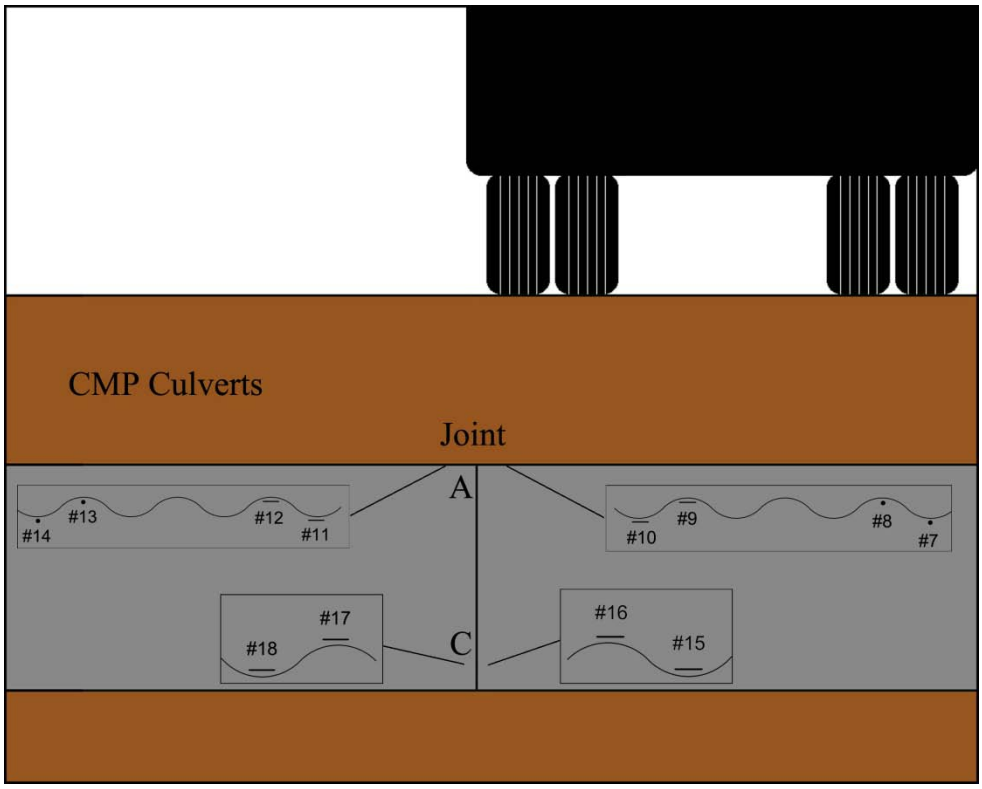

Figure D.15 Arrangement of strain gauges in the CMP culverts

Experimental Test Results

Introduction

This section presents data gathered from tests of five in-service culverts and one pipe installation. The in-service culverts include two CMP (corrugated metal pipe), two RC (reinforced concrete), and one HDPE (high-density polyethylene) culvert. The last experiment was conducted during the installation of a HDPE pipe. The in-service culverts were subjected to both static and dynamic truck loading. The pipe installation was subjected to the placement and compaction of backfill and static truck loading.

Dynamic loading consisted of trucks travelling between 5 mph (8 km/h) and 30 mph (48 km/h) over the culverts. Due to the terrain, the 30 mph (48 km/h) speed was not always reached. Static loading of the in-service culverts was applied by a truck at multiple locations above each culvert as depicted in Figure D.7 and Figure D.8. Static loading of the pipe installation was applied using construction equipment rather than a loaded truck. Deflection measurements were taken vertically at the crown and horizontally at the springline on the upstream and downstream sides of the joint. Longitudinal movement across the joint was also measured using longitudinally placed displacement sensors. This longitudinal movement is used to determine a rotation as described in this appendix. Strains were measured at twelve different locations on the two CMP culverts. Experimental data is presented from the CMP-D4-F1.8 culvert test to represent the in-service culvert tests. This culvert generally had the largest deflections of the in-service culverts due to its shallow backfill depth and flexibility. The final test pipe is referred to as HDPE-D3.5-F3.5. Data is presented here from the installation of HDPE-D3.5-F3.5.

Horizontal and Vertical Deformations at the Joint

Deflection measurements were taken at the crown of the culvert and at the springline. Two crown sensors were placed to measure vertical deflections on the upstream and downstream sides of the joint. Crown sensors give a measurement of the change in vertical diameter of the culvert. Two springline sensors were placed to measure horizontal deflections on upstream and downstream sides of the joint. Springline sensors take measurements on only one side of the culvert. Therefore, they give a measurement of the change in horizontal radius of one side of the culvert. The springline sensors take measurements on the side of the culvert that the truck approaches as it drives over the culvert. Measurements are presented for culvert CMP-D4-F1.8.

In each of the measured dynamic displacement time histories, there are two peaks (Figure D.17 through Figure D.20). The first peak corresponds to the load applied by the drive axle. The second peak corresponds to the load of the rear axle. In all cases, the rear axle applied a heavier load than the drive axle (see Table D.1). In all load cases, the vertical diameter decreased and the horizontal diameter increased, as illustrated in Figure D.1.

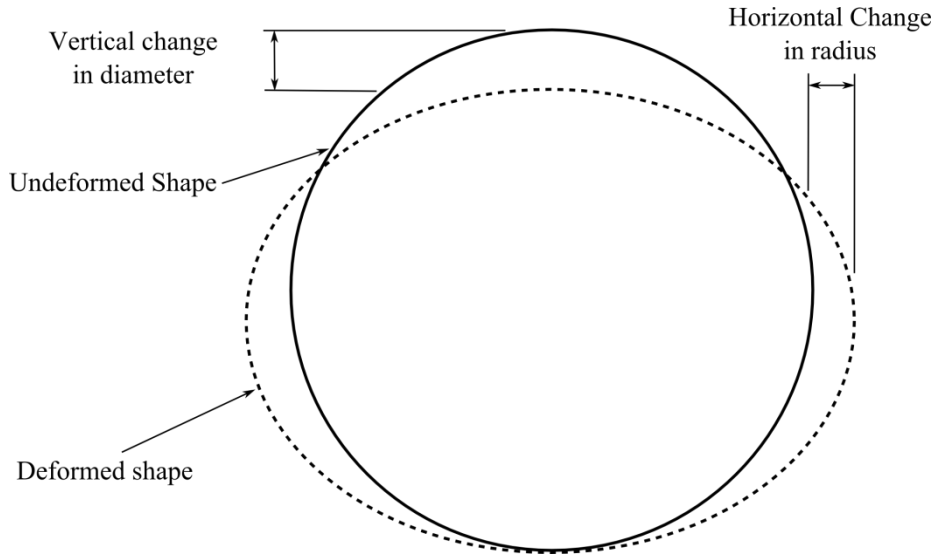

Figure D.16 Deformed shape of a pipe culvert under loading.

Horizontal and Vertical Deflection of CMP-D4-F1.8

The vertical and horizontal response of CMP-D4-F1.8 under dynamic loading is shown in Figure D.17 through Figure D.20. The response to static loading is shown in Figure D.21, Figure D.22, and Figure D.23. Deflections were measured under load cases C and S at truck speeds of 5, 10, 20, and 30 mph (8, 16, 32, and 48 km/h). In load case C, the truck is centered on the joint as it drives over the culvert. In load case S, the truck is on the downstream side of the joint with the edge of the truck directly over the joint (Figure D.8). The difference of the deformation measurements is the measurement from the downstream sensor subtracted from the measurement of the upstream sensor. It gives a measurement of how the two culvert segments, connected at the joint being tested, deflect relative to each other in the vertical or horizontal direction in the plane (cross section) of the joint. It will be referenced as the “measurement difference” in the rest of this appendix.

Dynamic Response of CMP-D4-F1.8

The physical meaning of measured deformations is shown in Figure D.16. The increase in truck speed seemed to have little effect on the vertical change in diameter and the measurement difference during the S load cases (Figure D.17). During the C load cases, the increase in speed also had little effect on the vertical change in diameter (Figure D.18). However, the increase in truck speed caused the measurement difference to become increasingly large. An increase in truck speed reduced the time in which the culvert is supporting loading. For example, loading time was approximately 1.5 seconds at 5 mph (8 km/h) and 0.3 seconds at 30 mph (48 km/h) in Figure D.17 when each axle was passing over the culvert.

Under S loading, the increase in truck speed had no discernible effect on the change in horizontal radius (Figure D.19). Under C loading, the increase in truck speed tended to increase both the horizontal change in radius of each sensor and the measurement difference (Figure D.20). The measurement difference was quite large under C loading. The horizontal measurement difference was often greater than the measurement from the downstream sensor during C loading. This implies a significant amount of pulling apart at the springline. This can be seen in Figure D.20.

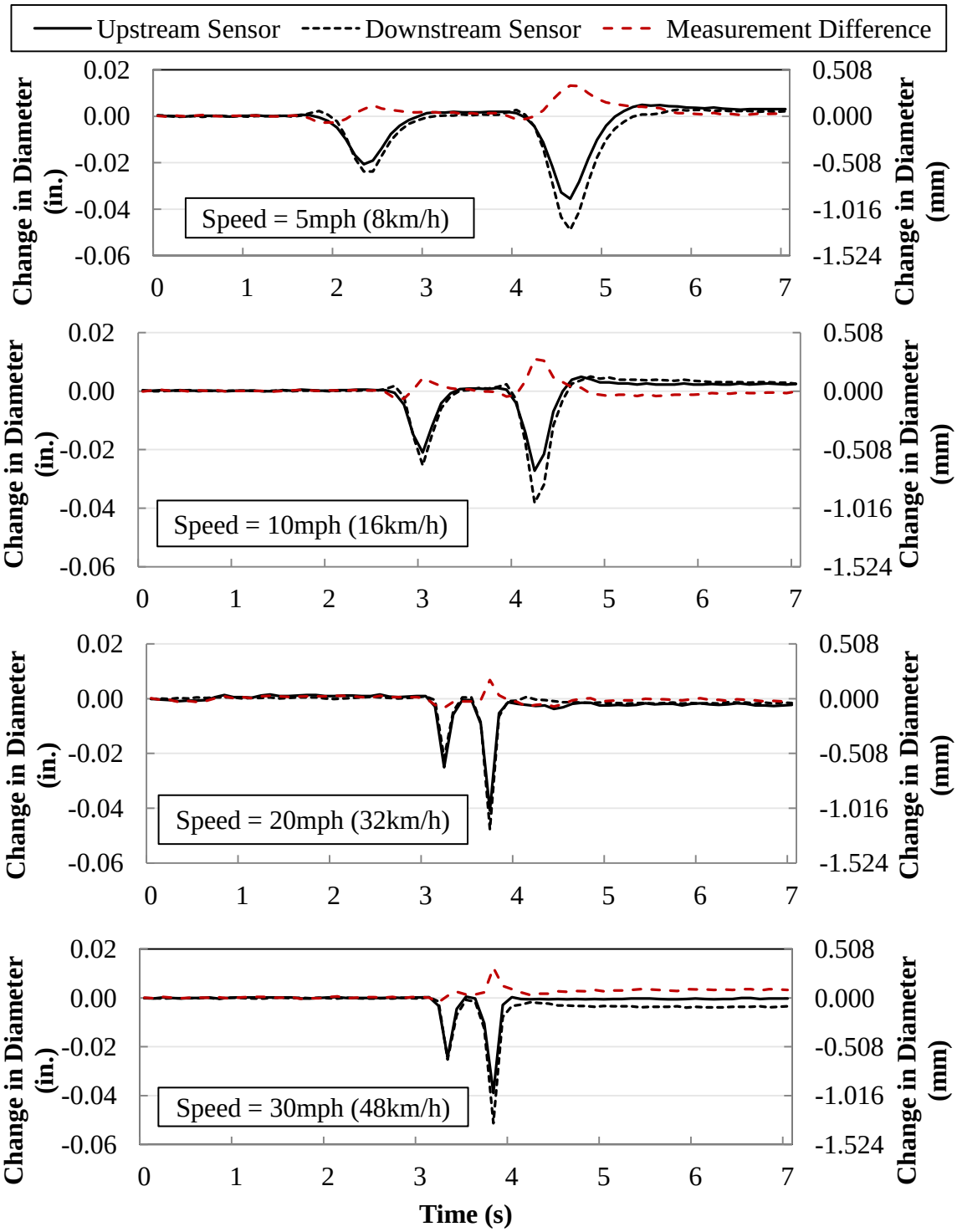

Figure D.17 Vertical change in diameter of CMP-D4-F1.8 under dynamic loading case S, measured at the upstream and downstream sensors

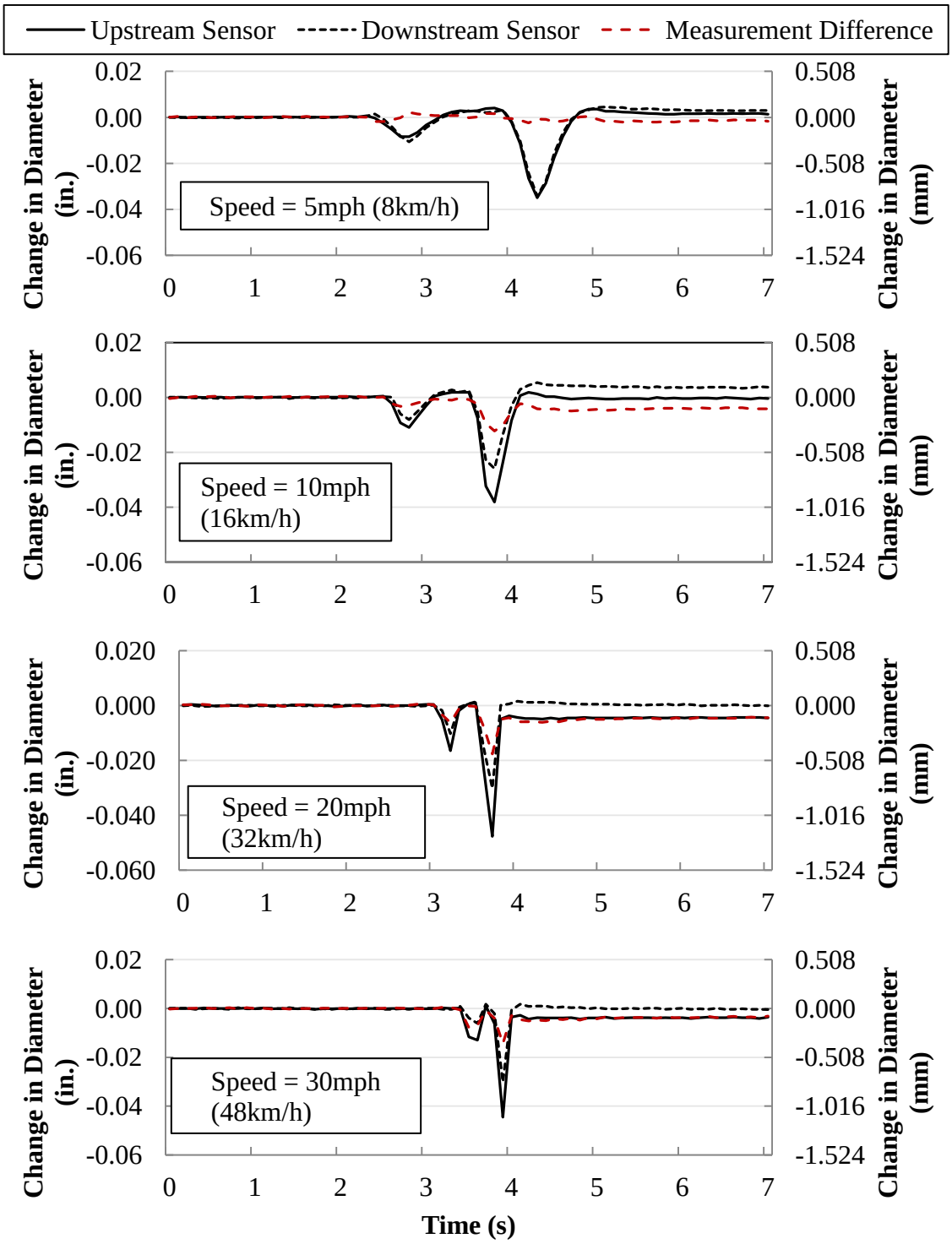

Figure D.18 Vertical change in diameter of CMP-D4-F1.8 under dynamic loading case C, measured at the upstream and downstream sensors

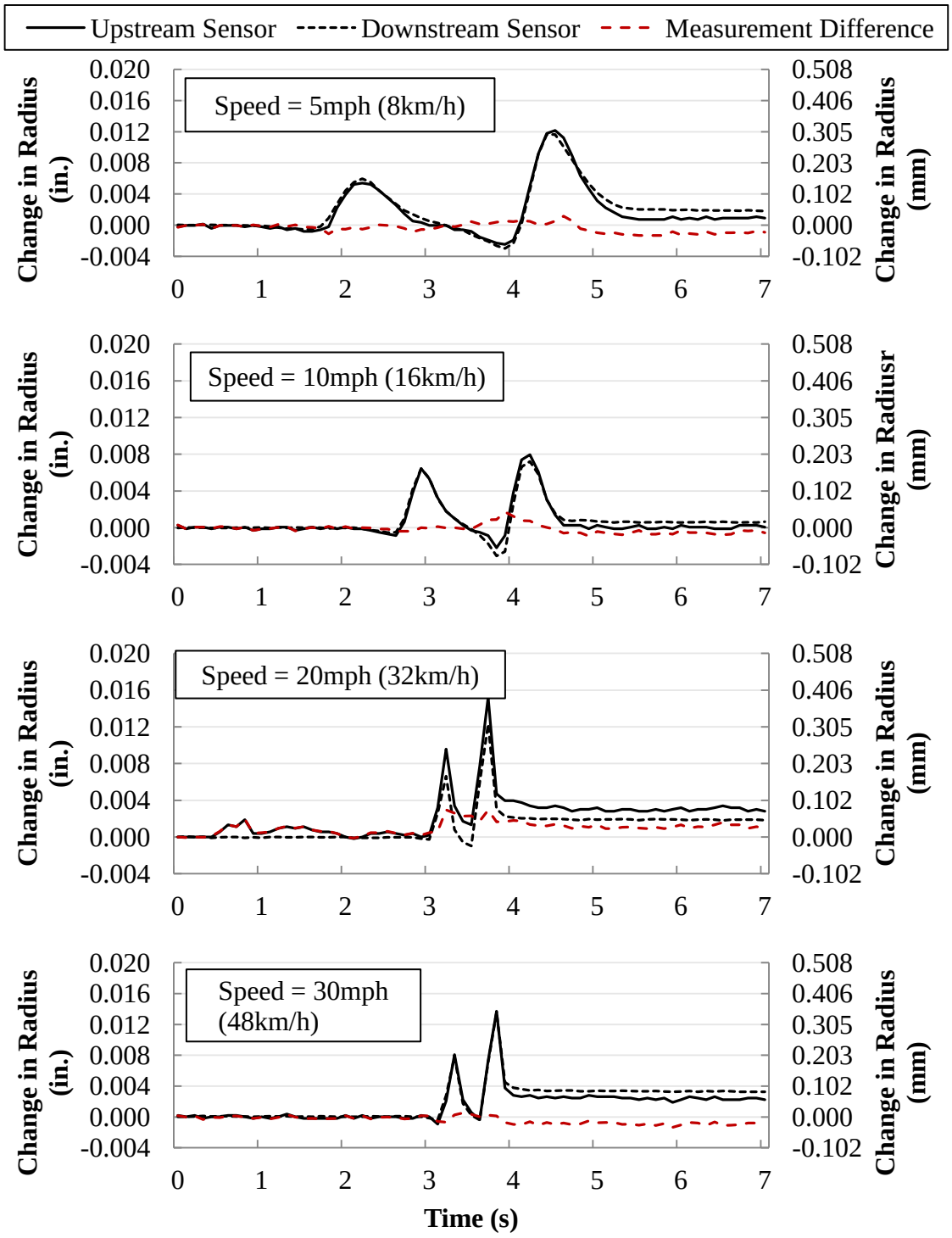

Figure D.19 Horizontal change in radius of CMP-D4-F1.8 under dynamic loading case S, measured at the upstream and downstream sensors

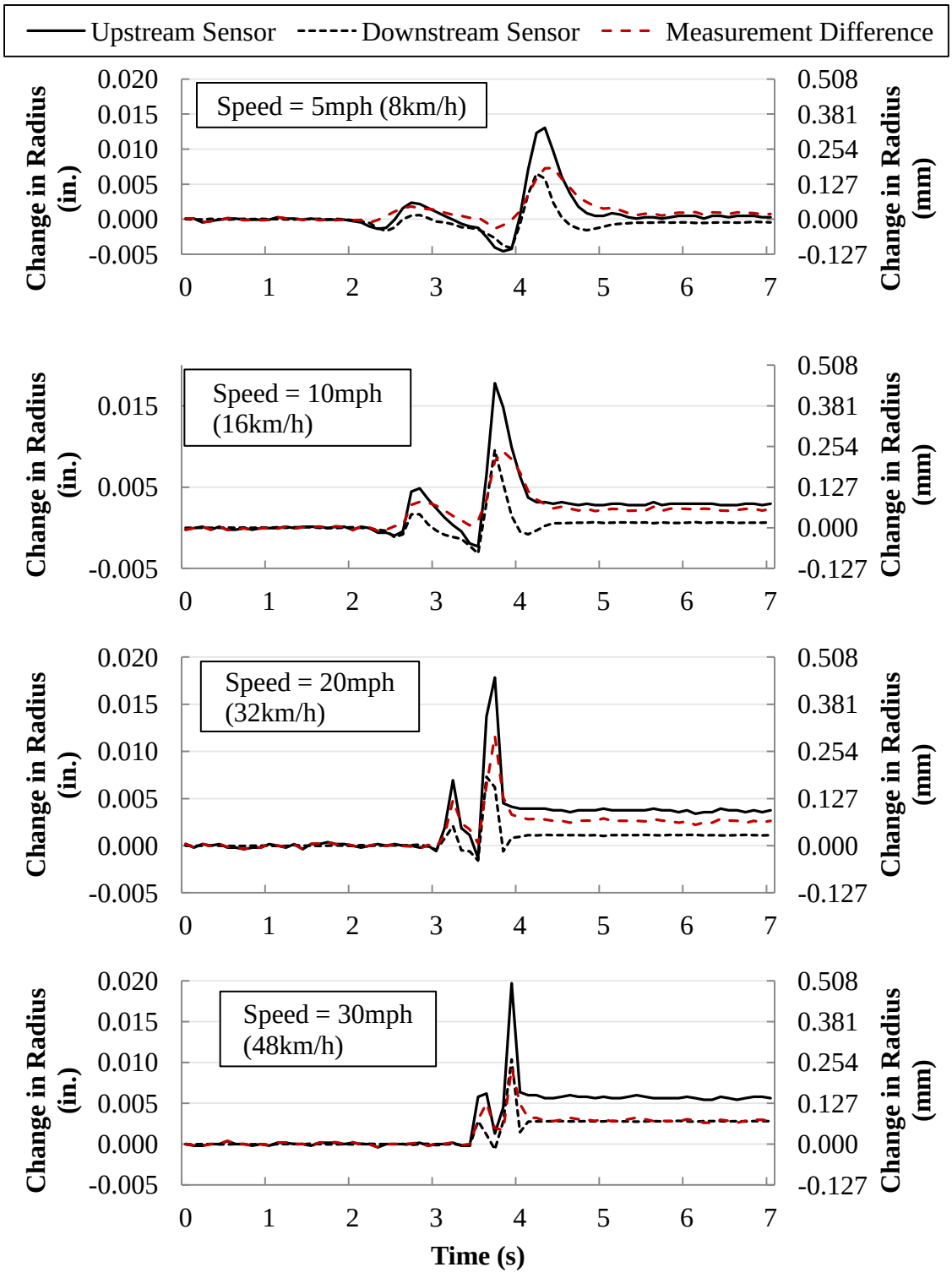

Figure D.20 Horizontal change in radius of CMP-D4-F1.8 under dynamic loading case C, measured at the upstream and downstream sensors.

Static Response of CMP-D4-F1.8

The measured static response of CMP-D4-F1.8 is shown in Figure D.21 and Figure D.23. A close-up of the static response is shown in Figure D.22 to help the reader better understand the results. Total static loading experiment took approximately 1900 seconds. The S-R2, C-R2, and SC-R2 load cases were expected to produce the largest deflections because loading from the rear axle (the heaviest) was directly above the crown of the culvert (Figure D.7). All load cases were described earlier. The maximum vertical change in diameter was measured during the SC-R2 load case. The maximum measurements during SC-R2 are changes in diameter of -0.069 in. from the upstream sensor and -0.073 in. from the downstream sensor. The following comments pertain to load cases S-R2, C-R2, and SC-R2. The S-R2 produced the smallest changes in vertical diameter though they were only marginally smaller than changes in vertical diameter under the C-R2 load case. The sensor difference of SC-R2 was significantly smaller than that of C-R2 or S-R2.

Measurements from the springline sensors are shown in Figure D.23. Interestingly, the largest changes in radius were measured during the SC-R1 load case. This was unexpected because axle was not directly above the crown. The largest measurements were expected to be during the S-R2, C-R2, and SC-R2 load cases because in these cases, the load is directly above the crown. Of the three load cases expected to produce largest deformations (S-R2, C-R2, and SC-R2), the S-R2 load case produced the smallest horizontal change in radius. This is consistent with vertical change in diameter measurements where the S-R2 also resulted in the smallest measurement of the three. As the static loading progressed, residual permanent deformations were observed probably due to settlement of the soil. The residual deformations were generally small.

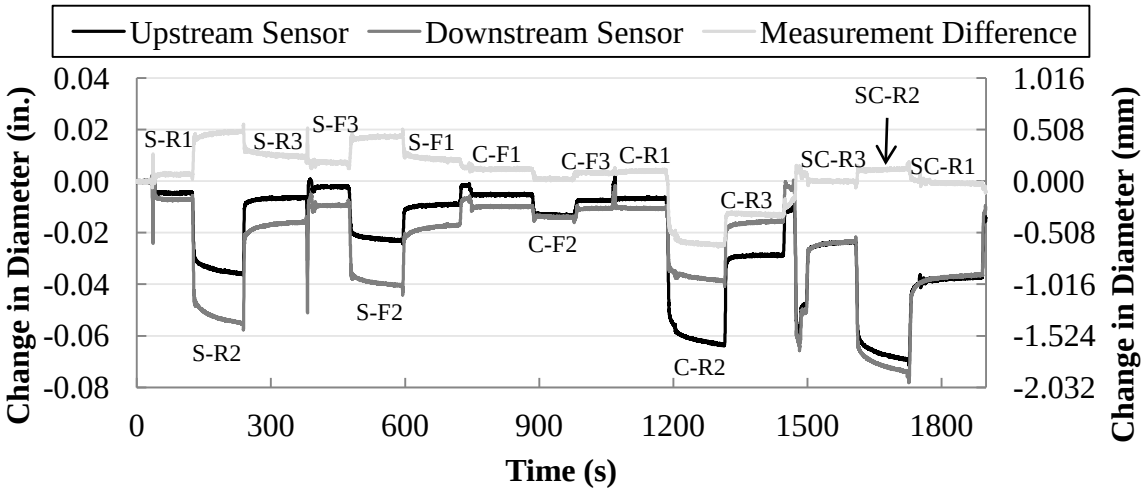

Figure D.21 Vertical Change in diameter of CMP-D4-F1.8 under static loading measured at the upstream and downstream sensors.

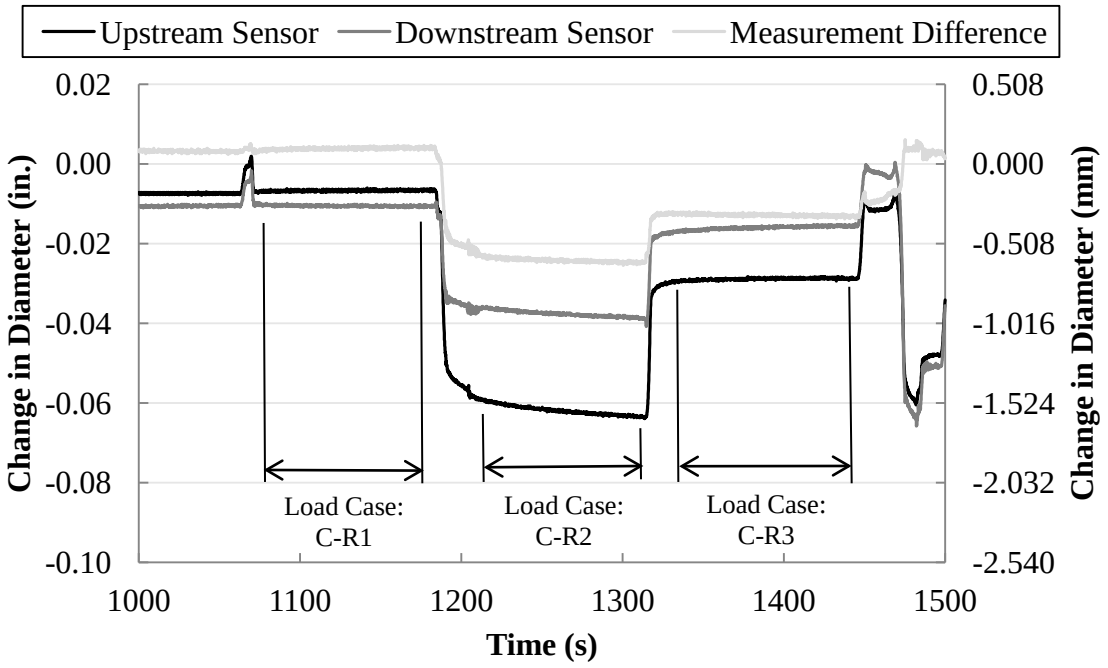

Figure D.22 Close-up of the measured static displacement history shown in Figure D.21

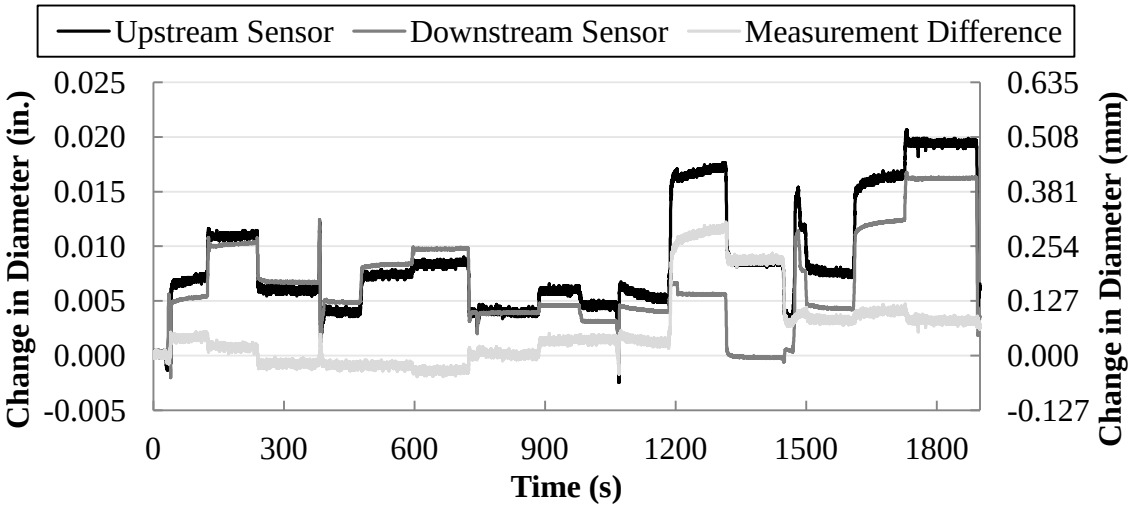

Figure D.23 Horizontal change in radius of CMP-D4-F1.8 measured at the upstream and downstream sensors.

Horizontal and Vertical Deflections of the Other Four In-Service Culverts

All of the tested culverts exhibited a decrease in vertical diameter and increase in horizontal diameter as a result of loading. The smallest deflections were measured during the test of RC-D7-F4.7. This is due to the rigid concrete structure and the large depth of fill above the culvert. The test of HDPE-D3-F4.7 also exhibited small deflections even though the culvert is made of a flexible material. The measured deflections of HDPE-D3-F4.7 were generally smaller than that of RC-D4.5-F2 under the same load cases. The HDPE culvert is under 4.7 ft (1.4 m) of fill and the RC culvert is under 2 ft (0.6 m) of fill. This shows that increased burial depth can have a significant impact in reducing the deflections in culvert pipes.

Horizontal and Vertical Deflections Measured During Installation of Pipe HDPE-D3.5-F3.5

Measurements of the vertical change in diameter of pipe HDPE-D3.5-F3.5 are shown in Figure D.24 and Figure D.25. Measurements of the horizontal change in radius are shown in Figure D.26 and Figure D.27. In each series of two, the first figure corresponds to the placement and compaction of backfill. The second figure shows the response during construction equipment loading. The greatest diameter change was measured, during the placement and compaction of the backfill. Measurements from the construction equipment loading are quite small in comparison. The vertical diameter change caused by placement and compaction is roughly ten times larger than the change caused by equipment loading. Horizontal radius change was roughly 20 times larger during placement and compaction of backfill than equipment loading. Equipment loading is described earlier.

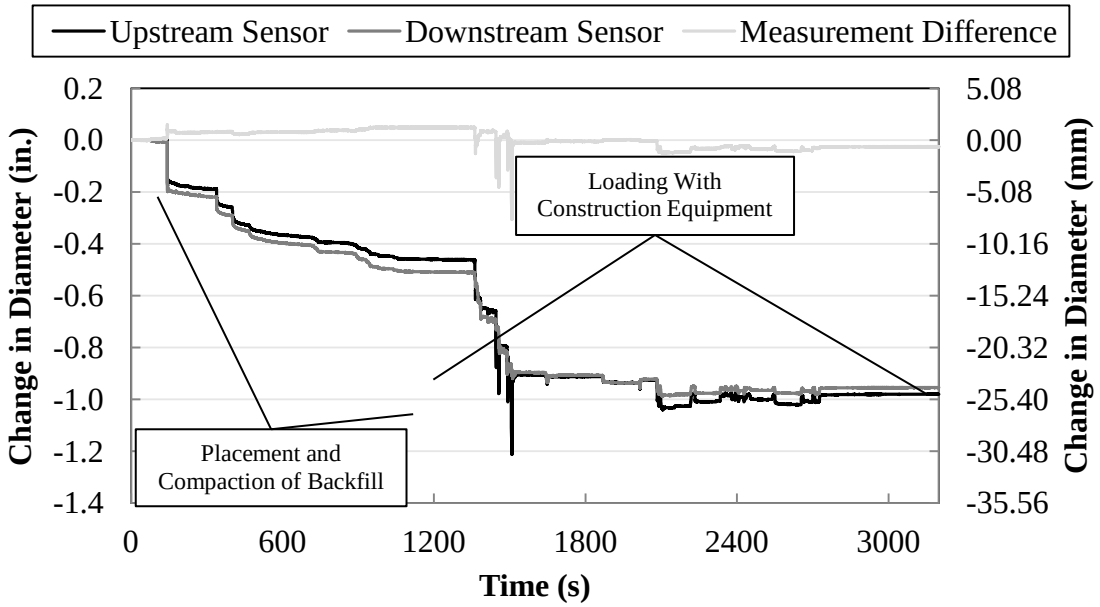

Figure D.24 Vertical change in diameter during the complete testing of HDPE-D3.5-F3.5

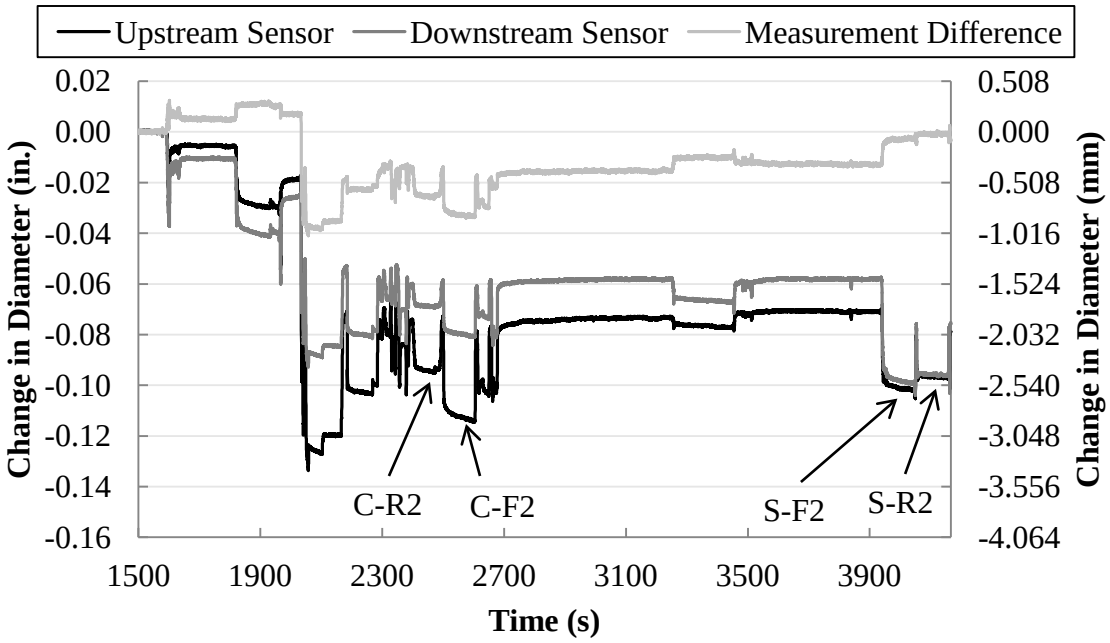

Figure D.25 Vertical change in diameter during construction equipment loading of HDPE-D3.5-F3.5

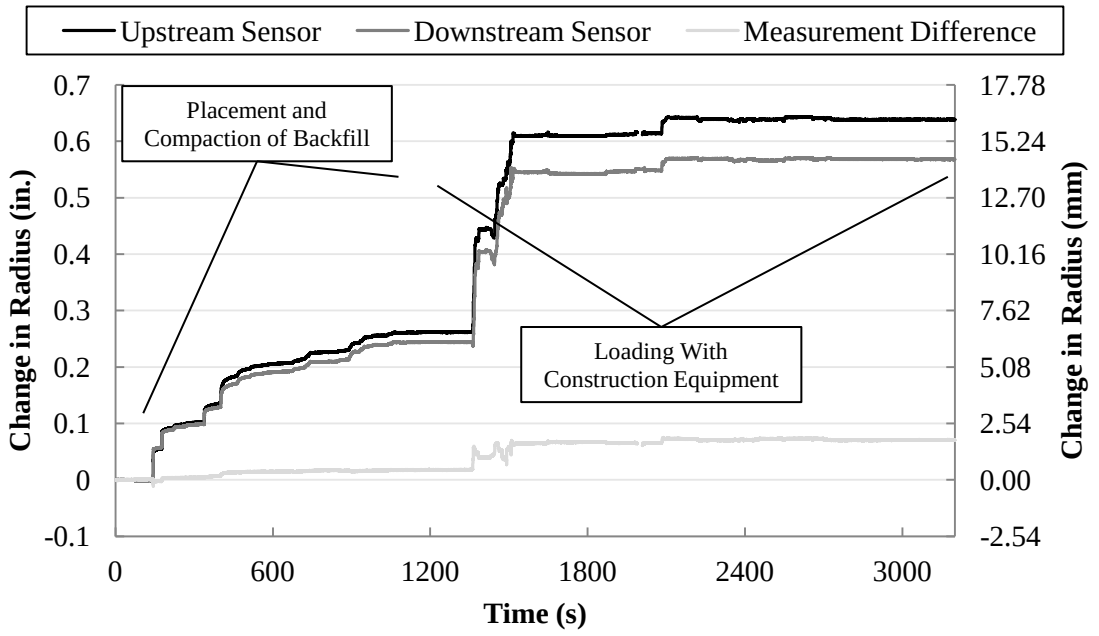

Figure D.26 Horizontal change in radius during the complete testing of HDPE-D3.5-F3.5

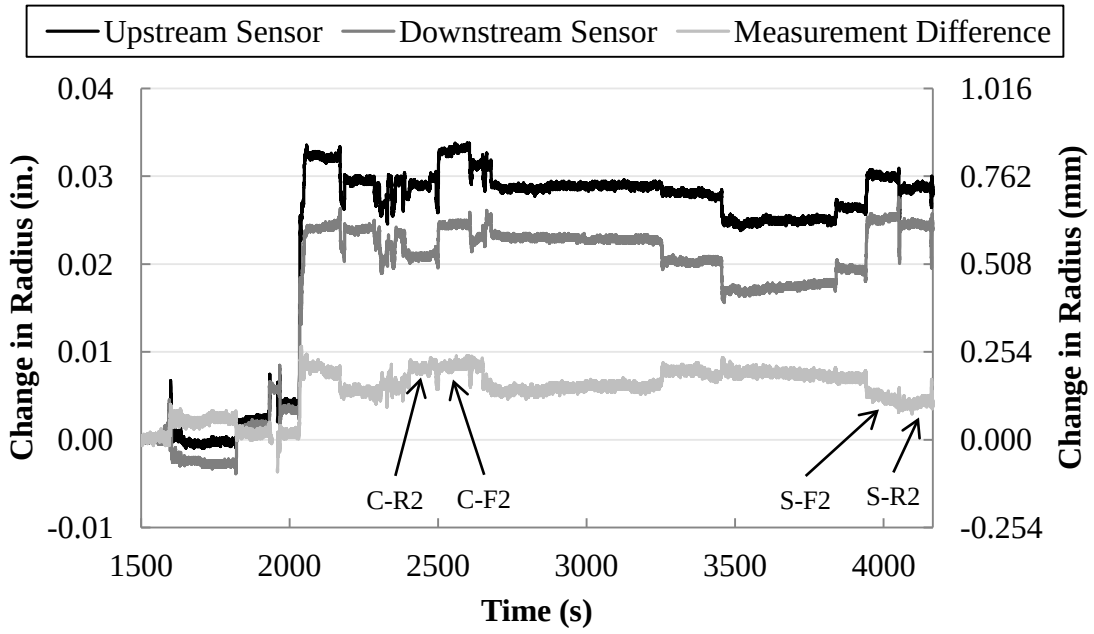

Figure D.27 Horizontal change in radius during construction equipment loading of HDPE-D3.5-F3.5

Strain Measurements

Strain measurements were taken during the test of the two CMP culverts. Strain histories measured at eleven locations on culvert CMP-D4-F1.8 during static loading are shown in Figure D.28. Strain measurements in the same culvert during dynamic loading are shown in Figure D.29. The dynamic loading charts show spikes that are not indicated by specific load cases. These are from the loading truck backing up over the culvert to reset for another dynamic load test. Strain gauges were positioned in the longitudinal and transverse direction on the upstream and downstream sides of the joint. Gauges 7 through 14 were located at the crown of the culvert. Gauges 15 through 18 were located approximately 45 degrees upward from the invert of the culvert as shown in Figure D.13. These gauges will be referenced as “near the invert”. Half of the crown gauges (7, 8, 13, and 14) are oriented parallel to the corrugation and measure hoop strains. Half of the crown gauges (9, 10, 11, and 12) are oriented transverse to the corrugation and measure longitudinal strains. All of the gauges near the invert are oriented transverse to the corrugation (Figure D.).

Longitudinal strain indicates the presence of longitudinal forces pulling apart or pushing together the jointed pipes. The maximum longitudinal strains (gauges #9 through #12 and #15 through #18) were similar at the crown and near the invert in both metal culverts. This indicates that longitudinal forces are not significantly reduced at locations other than the crown even though measured deflections at locations other than the crown were reduced, as indicated in previous sections.

The largest measured strain in CMP-D4-F1.8 is 280×10^{-6}. This measurement is taken from gauge #14 during static load C-R2. Gauge #14 measures hoop strain at the crest of the corrugation at the crown. The largest measured strain in CMP-D3-F2.5 is 130×10^{-6}. It is taken from gauge #11 during static load case S-R1. Gauge #11 measures longitudinal strain at the crest of the corrugation at the crown. This indicates that both longitudinal and hoop forces affect the performance of the joint. Both strains are well below the theoretical yield strain of $1{,}241 \times 10^{-6}$ for 36 ksi steel.

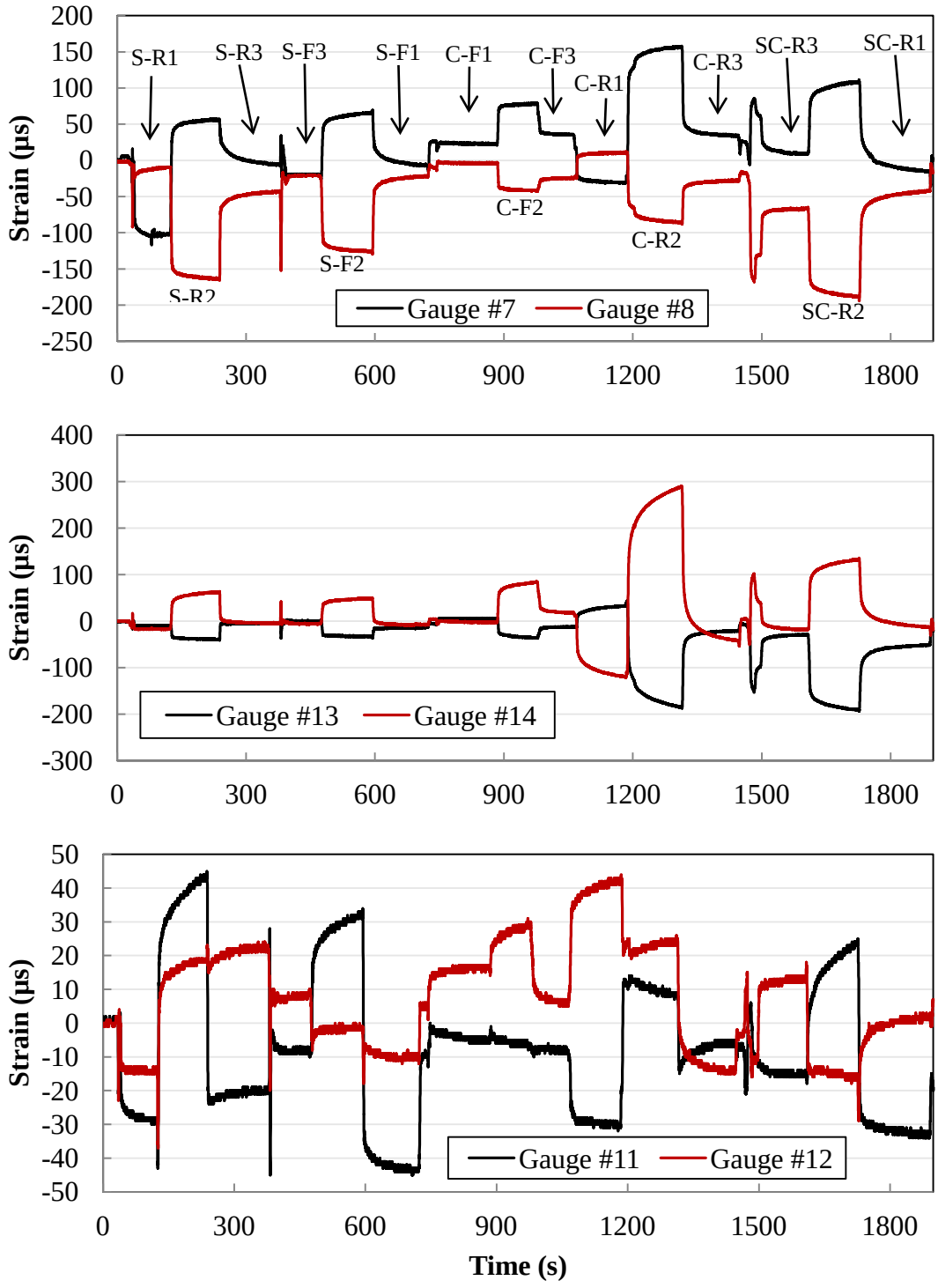

Figure D.28 Strain measurements during static loading of CMP-D4-F1.8

Figure D.28 Continued

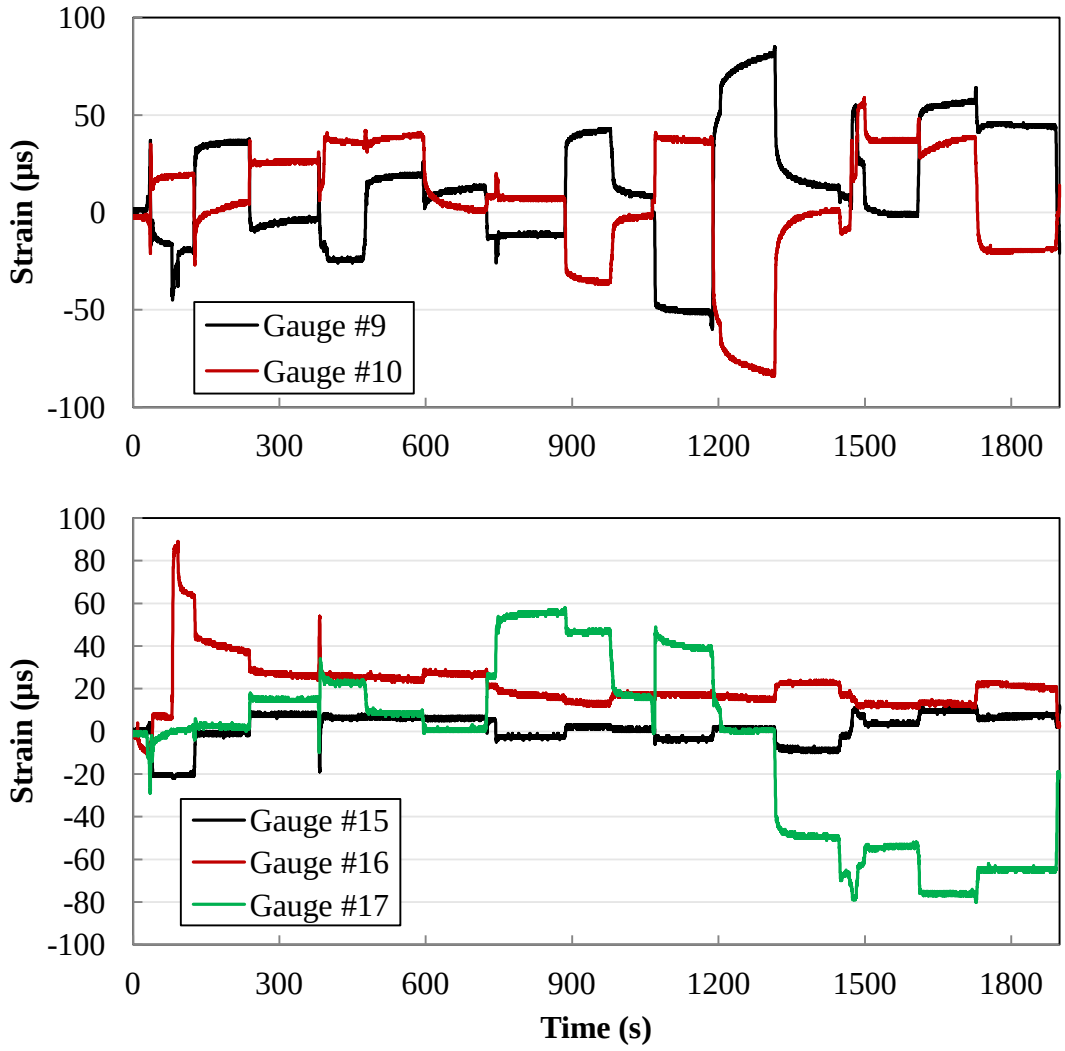

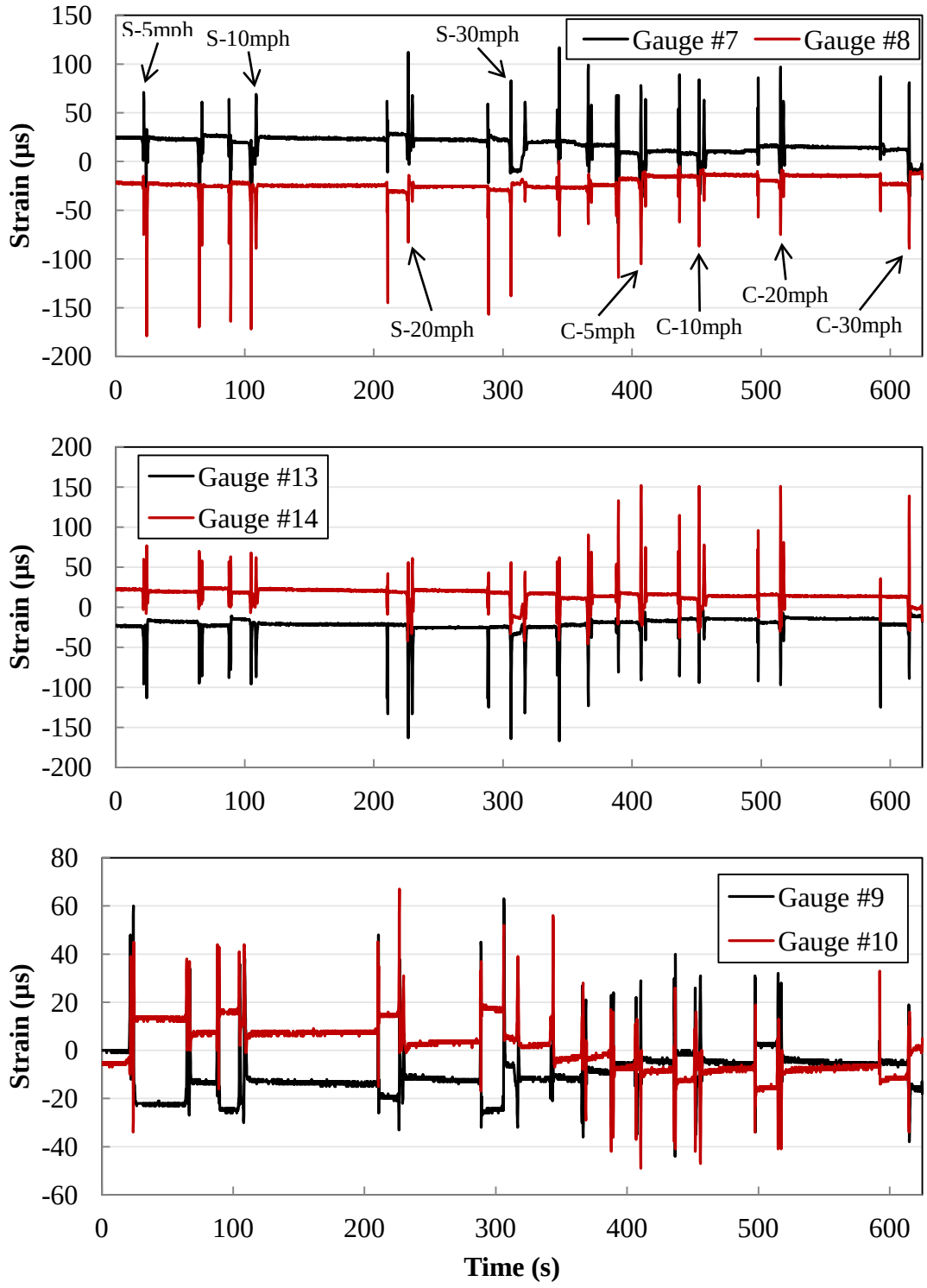

Figure D.29 Strain measurements during dynamic loading of CMP-D4-F1.8

Figure D.29 Continued

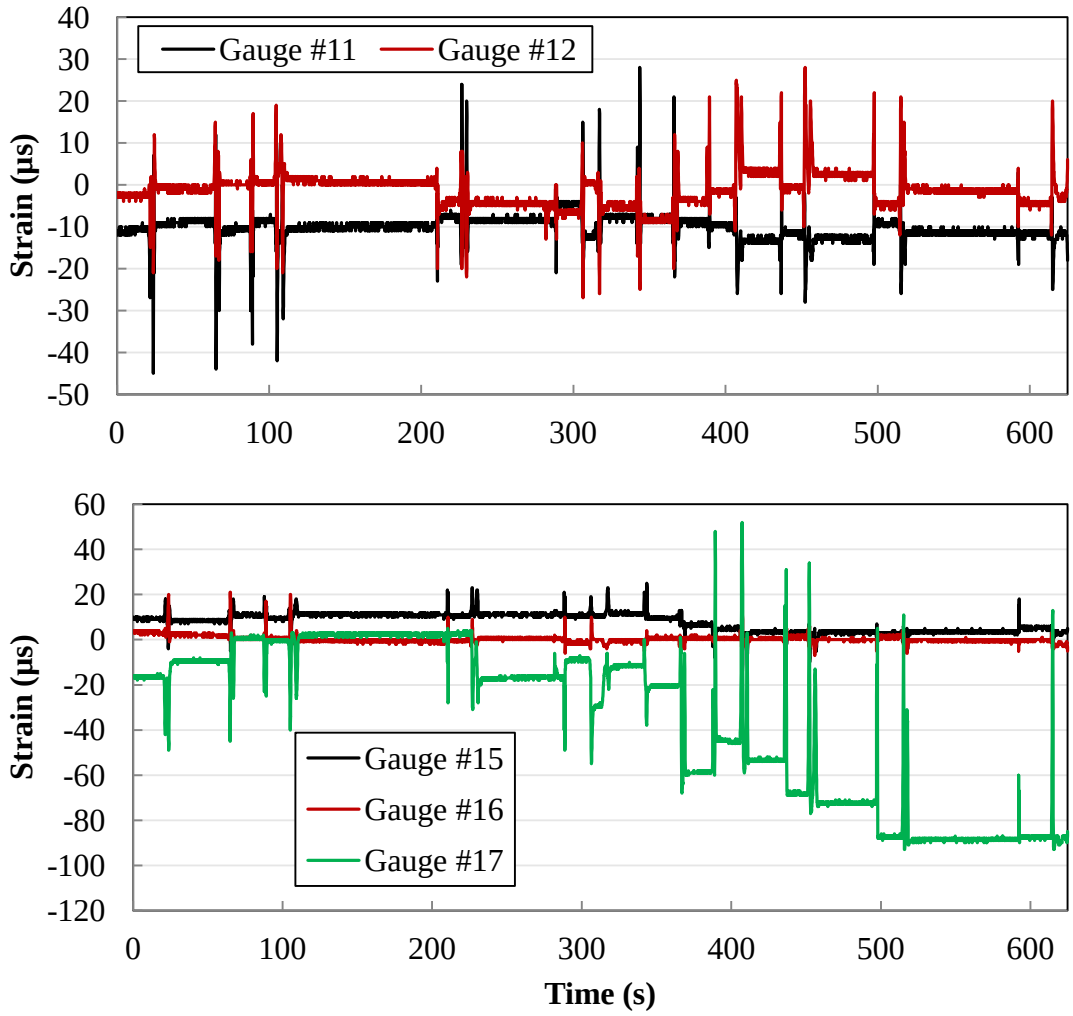

Culvert Rotation About the Springline

When loaded, the culverts tend to be pushed downward beneath the loading. Away from the load location, the culverts can have little or no downward movement. The combination of the loaded segment of the culvert segment moving downward and unloaded segments of the culvert remaining in their original position can cause the culvert to appear to rotate about the springline. Two connected culvert segments can rotate independently of each other. When this happens, the relative rotation can become apparent at the joint location.

The relative rotation of two test culvert segments is measured using the longitudinally placed sensors near the crown and near the invert of the culvert. Positioning of the sensors was described earlier. These two sensors measure longitudinal movement of the two culvert segments relative to each other. If the connected culvert segments are pulling apart at the crown of the joint and being pushed together at the invert of the joint, then the culvert tends to be rotating upward about the springline. This upward rotation will be considered positive as shown in Figure D.30.

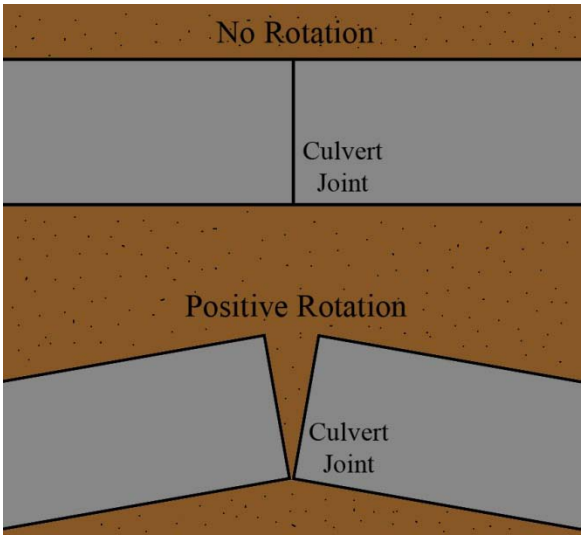

Figure D.30 Illustration of rotation of culvert segments

Culvert rotation is calculated using the measurements from the longitudinal sensor near the crown (“Top Sensor”) and the longitudinal sensor near the invert (“Bottom Sensor”). The crown measurement is subtracted from the measurement near the invert to get the difference of the two measurements. The difference of the two measurements and the vertical distance between the sensors allows the culvert rotation to be calculated. This method works when the loading is directly above the crown of the culvert as in load cases R2, and F2 as depicted in Figure D.. When the load is not directly above the crown of the culvert, as in load cases F1, F3, R1, and R3, the culvert will not rotate precisely about the springline, making this method is less accurate.

Joint Rotations of CMP-D4-F1.8

The joint rotations of culvert CMP-D4-F1.8 under dynamic loading cases S and C are shown in Figure D.32 and Figure D.34, respectively. The original measurements from the longitudinal sensors near crown and the invert are shown in Figure D.31 and Figure D.33. Joint rotations under static loading are shown in Figure D.35. In the dynamic rotation plots, the first peak represents the drive axle passing over the culvert. The second peak represents the rear axle passing over the culvert. The loading from the S loading cases caused a negative rotation at the joint. Under the S load cases, the truck load was located on the downstream side of the joint. This caused the downstream culvert segment to be pushed downward. The joint was thus pushed downward and a negative rotation was produced. The loading from the C load cases produced a positive rotation at the joint. Here, the wheel loads were positioned 3 ft (0.9 m) from the joint on the upstream and downstream sides (Figure D.8). The culvert segments were pushed downward at the location of the wheel loads. The joint, being between the two loads, was then forced to rotate upward (as in Figure D.30).

The rotations caused by static loading were larger than the rotations caused by dynamic loading. For the ‘C’ rotations, the largest dynamic loading measurement is 0.015 degrees while the largest static loading measurement is 0.02 degrees. For the ‘S’ rotations, the largest dynamic loading measurement is 0.005 degrees while the largest static loading measurement is 0.01 degrees. The magnitude of the ‘C’ rotations is much larger than the magnitude of the ‘S’ rotations. This was noticed in both dynamic and static loading. The static ‘C’ rotations were the largest measured rotations. The maximum and minimum observed rotations are 0.02 degrees and -0.01 degrees under load cases C-R2 and S-R2 respectively.

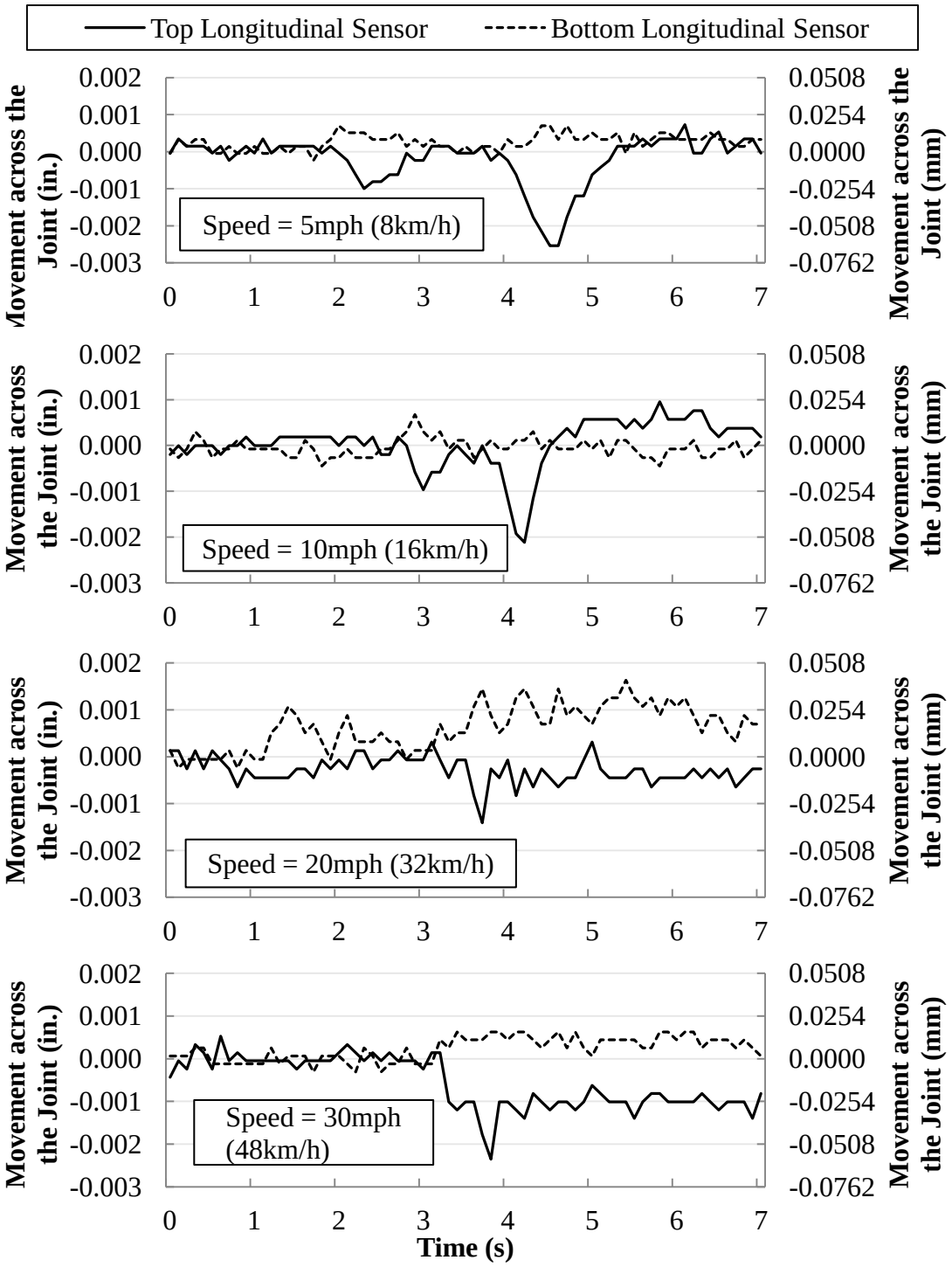

Figure D.31 Longitudinal movement across the joint of CMP-D4-F1.8 under dynamic load case S, measured at the 'top' and 'bottom' locations

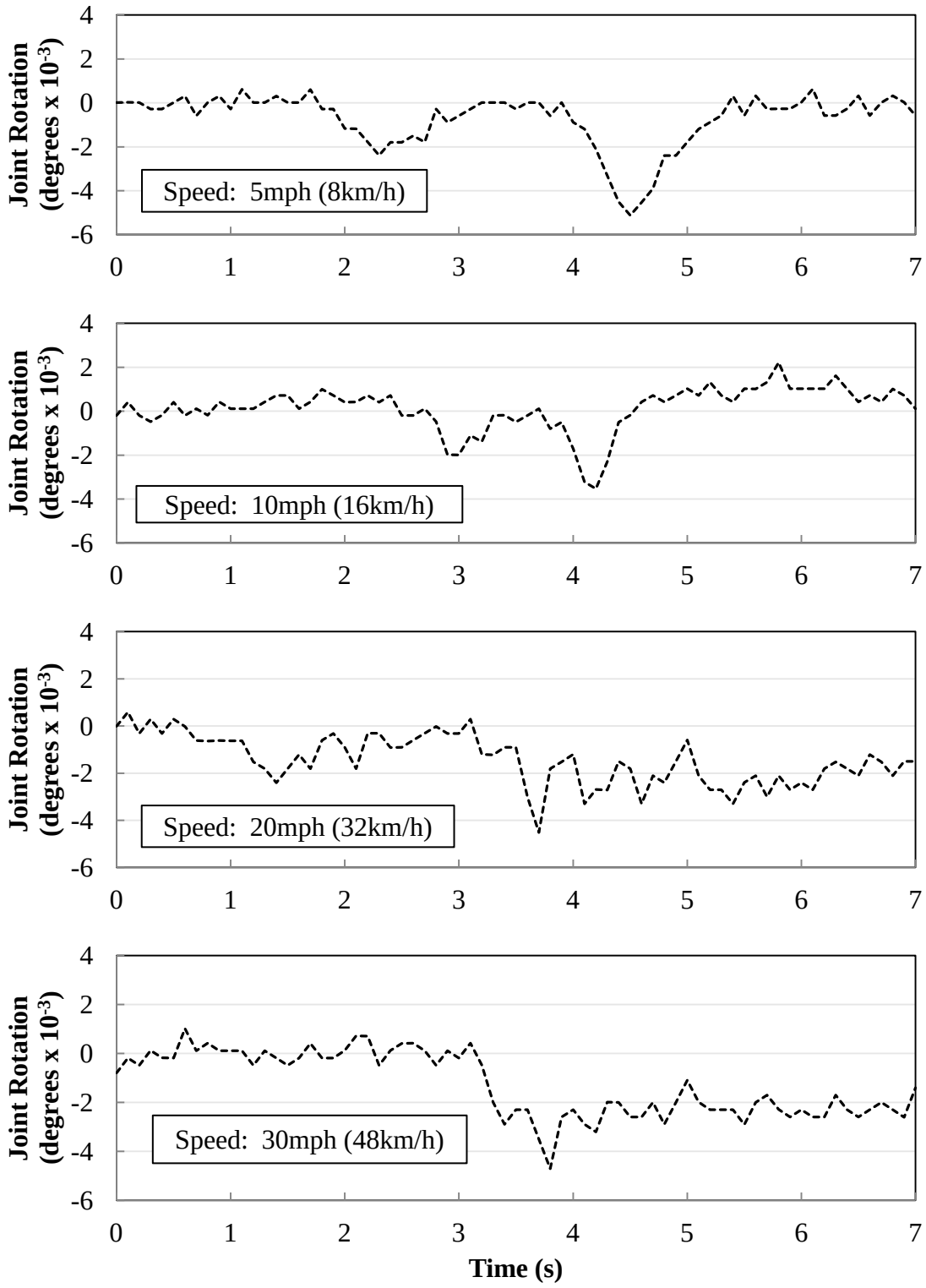

Figure D.32 Joint rotation of CMP-D4-F1.8 under dynamic loading case S.

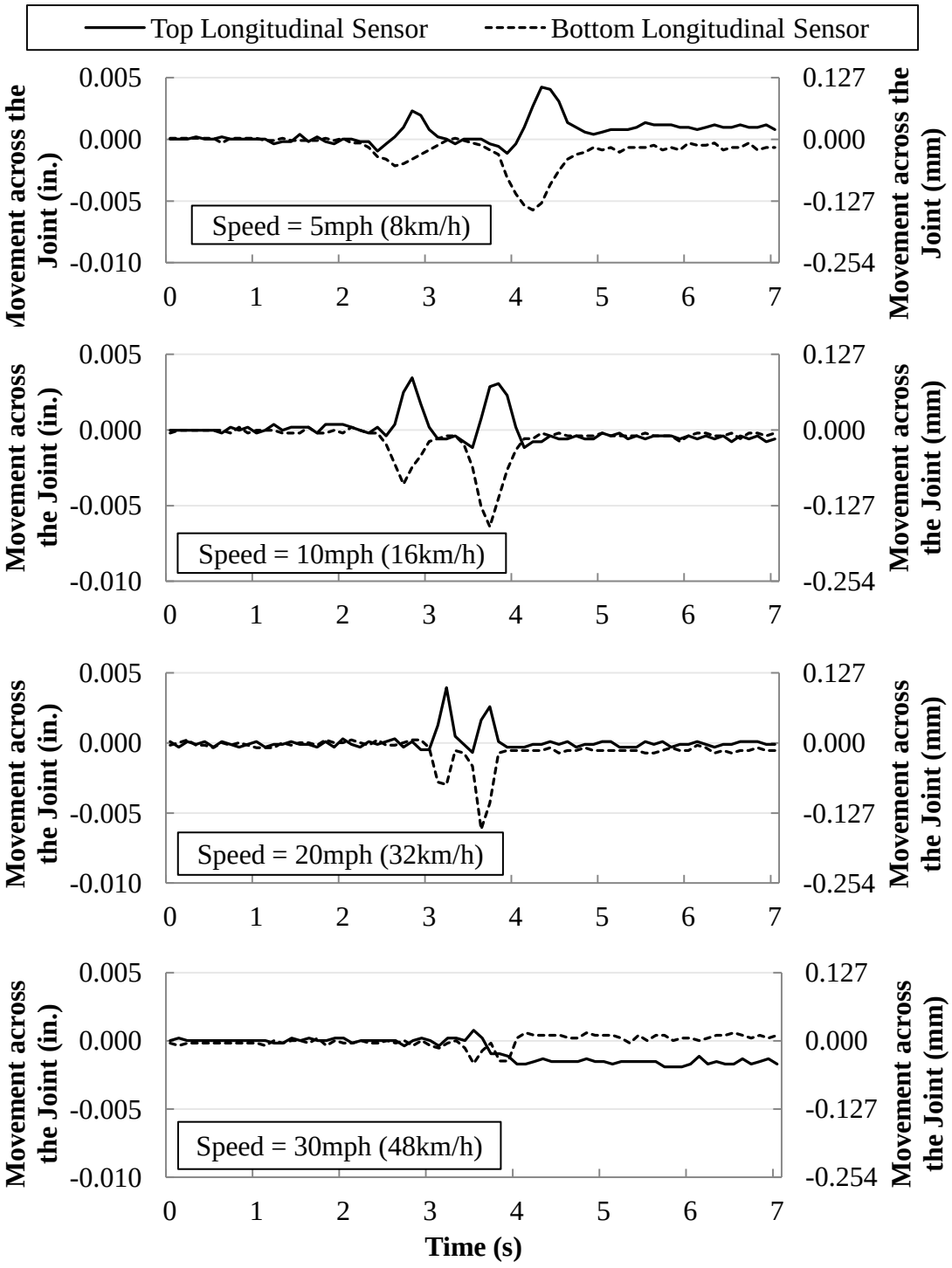

Figure D.23 Longitudinal movement across the joint of CMP-D4-F1.8 under dynamic load case C, measured at the ‘top’ and ‘bottom’ locations

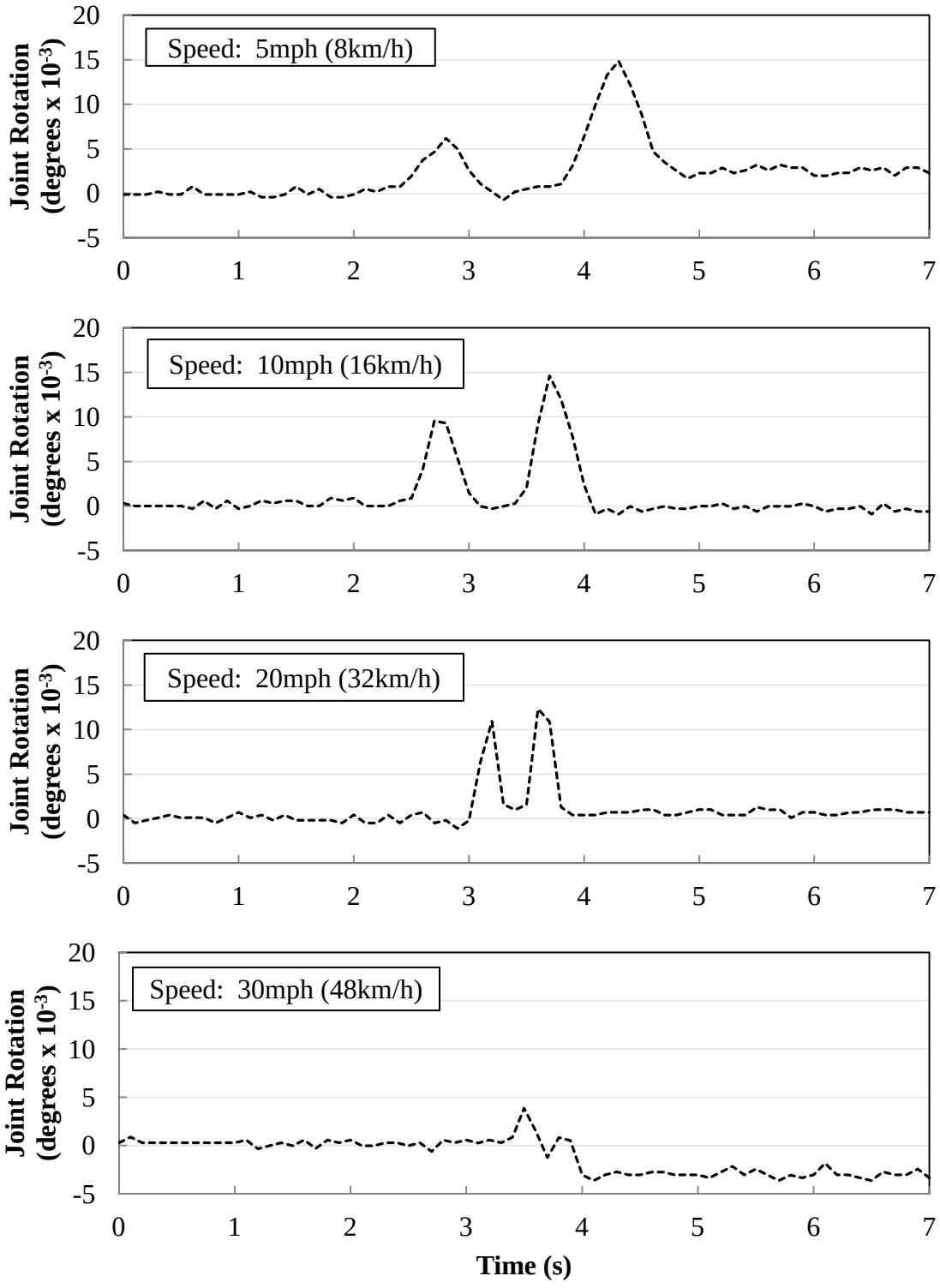

Figure D.34 Joint rotation of CMP-D4-F1.8 under dynamic loading case C.

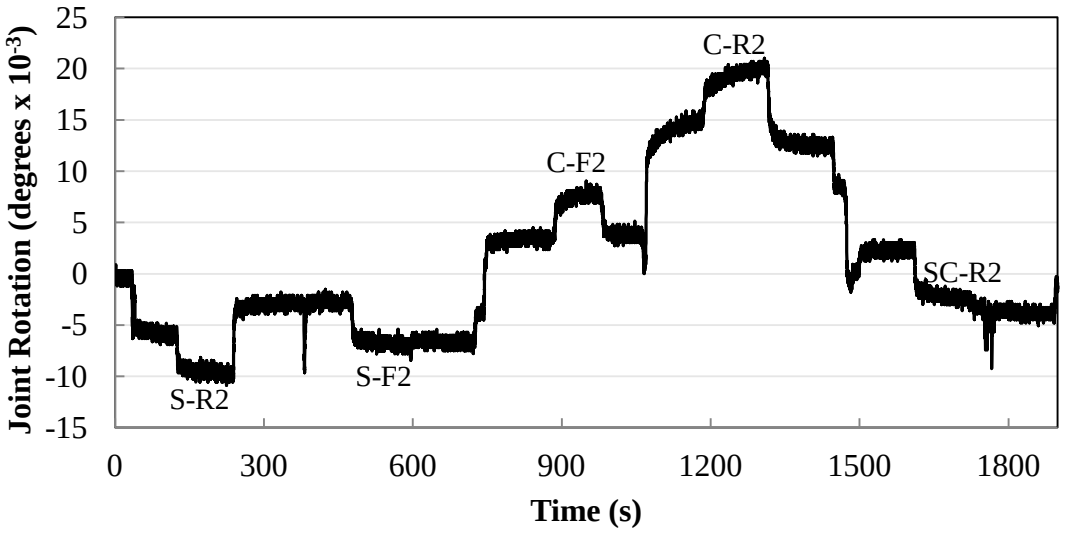

Figure D.35 Joint rotation of CMP-D4-F1.8 under static loading.

Joint Rotation of Pipe HDPE-D3.5-F3.5 During Its Installation

The joint rotation was measured during three distinct portions of the test. The joint rotation during the complete testing is shown in Figure D.36. The joint rotation during the placement of backfill all along the pipe is shown in Figure D.37. In general, the placement of the backfill directly onto the joint accounts for all of the negative rotation. The continuously increasing rotation that starts at around 300 seconds is a result of placement of the backfill downstream from the joint. The sharp negative change in rotation at roughly 140 sec occurred due to backfill being dropped directly on the joint (Figure D.37).

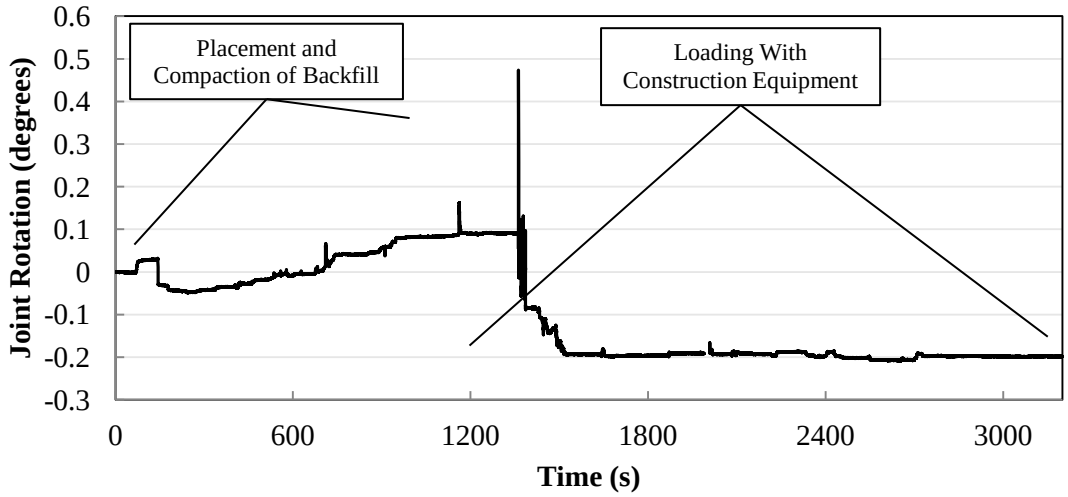

Figure D.36 Joint rotation during the complete testing of HDPE-D3.5-F3.5

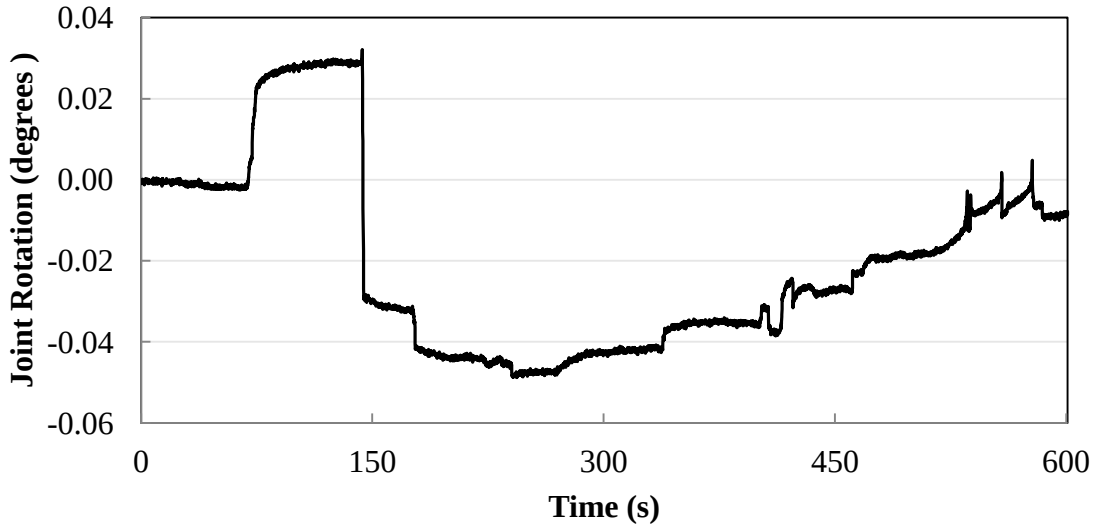

Figure D.37 Joint Rotation of HDPE-D3.5-F3.5 during the placement of backfill.

The joint rotation during the compaction of the backfill is shown in Figure D.38. The compactor being used vibrated in order to properly compact the soil. Initially, the compactor began working downstream from the joint. Compaction directly above the joint begins at approximately 750 seconds. The data in Figure D.38 starts where Figure D.37 stops. The compaction of the backfill

directly above the joint was the greatest cause of rotation during the test and resulted in a total of -0.29 degrees of rotation. The placement of the backfill resulted in large rotations. Once backfill was completely placed, the rotation returned nearly to zero degrees.

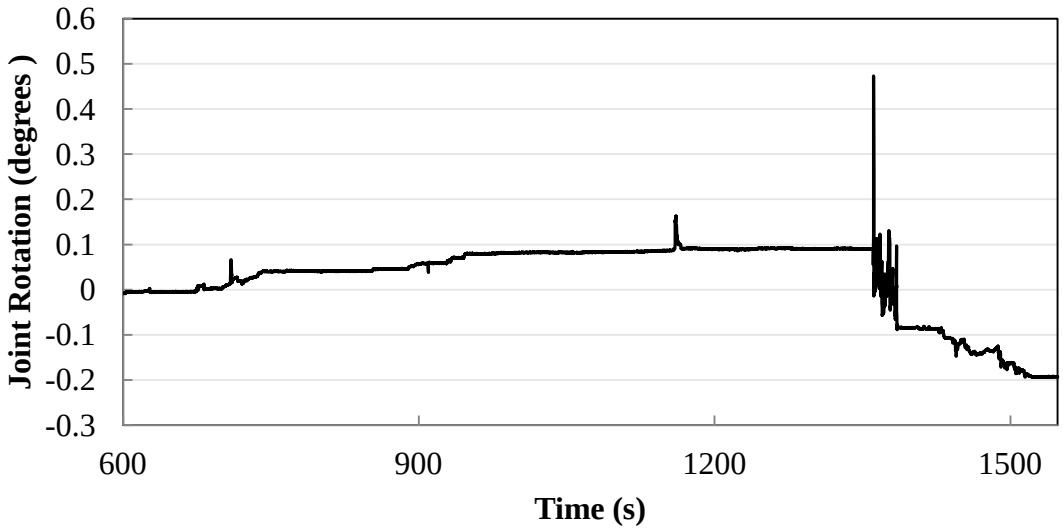

Figure D.38 Joint Rotation of HDPE-D3.5-F3.5 during compaction of backfill.

The joint rotation during the construction equipment loading is shown in Figure D.39. The data in the figure has been zeroed (from -0.2 degrees in Figure D.38) to better observe the effect of equipment loading. In this test, the ‘S’ loading accounted for a positive rotation at the joint while ‘C’ loading accounted for a negative rotation. This is completely opposite the results of CMP-D4-F1.8 where ‘C’ loading caused positive rotation and ‘S’ loading caused negative rotation. This is likely the result of the greater load spreading caused by the increased burial depth.

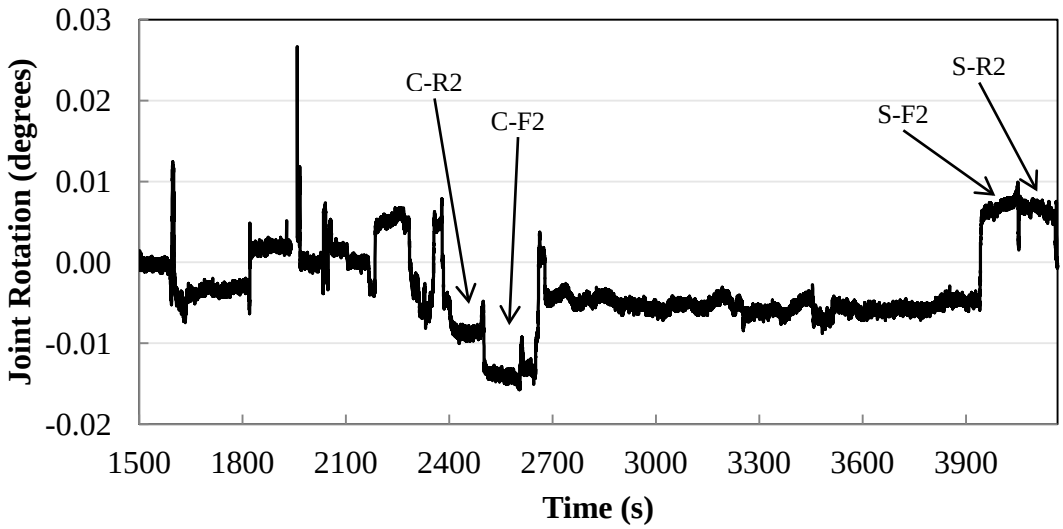

Figure D.39 Joint Rotation of HDPE-D3.5-F3.5 during the construction equipment loading.

The Effect of Dynamic Loading

It is necessary to investigate whether dynamic loading or static loading produces larger deflections in the buried pipe culverts. The maximum movement under dynamic loading is shown as a percentage of static movement in Figure D.40. Two culvert tests are omitted from Figure D.40c because joint rotation was not able to be calculated in test culverts RC-D7-F4.7 and HDPE-D3-F4.7 due to sensor error and sensor noise respectively. In all but one case, the dynamic loading caused movements that are smaller than the movements caused by static loading. It is not always clear whether maximum deflections increase or decrease as the truck speed increases. On average, the pipe movements under dynamic loading are 73% of that under static loading. Using static loading for analysis will yield the most conservative results.

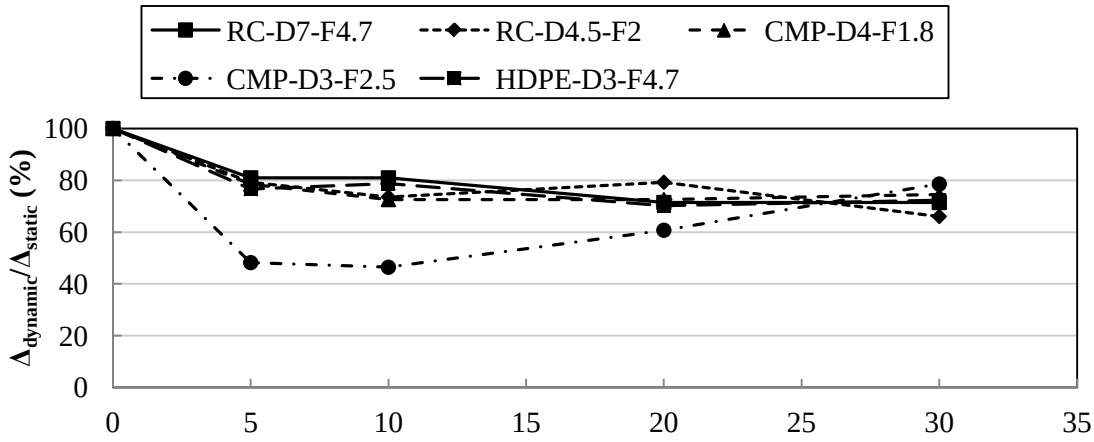

a) Vertical Deflection

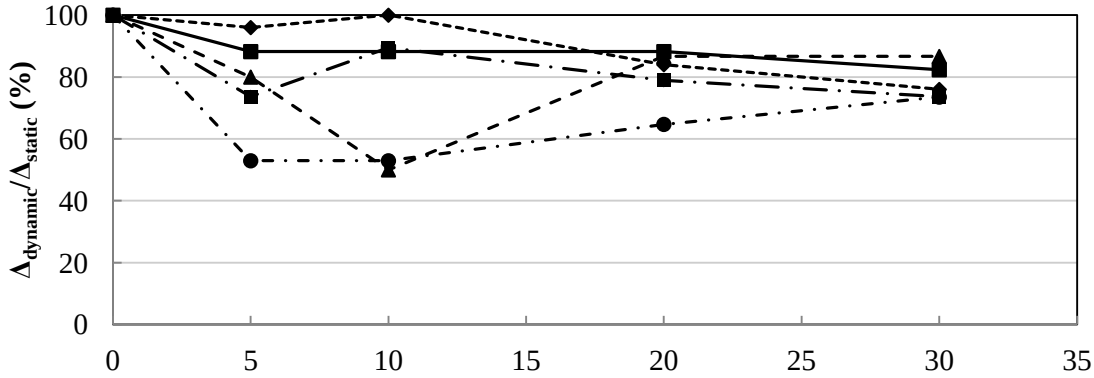

b) Horizontal Deflection

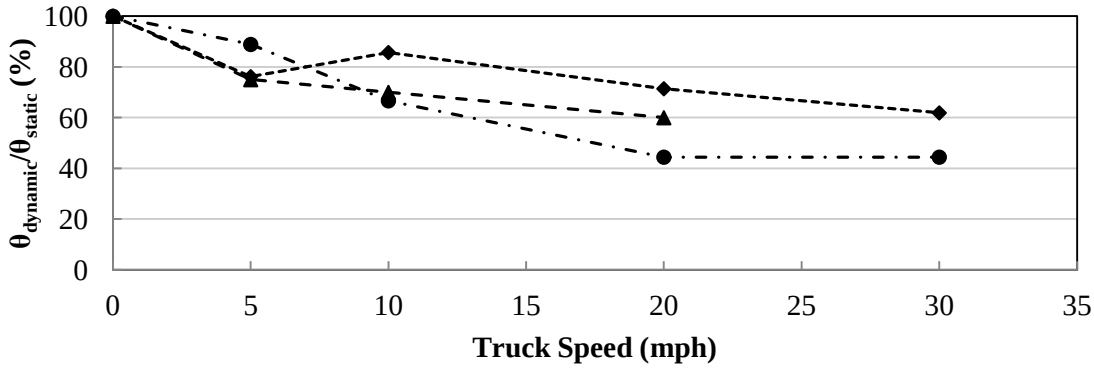

c) Joint Rotation

Figure D.40 Measured dynamic movements as a percentage of static movement. Load cases producing the largest movement are used. (1 mph = 1.6 km/h)

Conclusions

Results are presented for the testing of five in-service culverts and one culvert installation. Movements measured during the culvert installation are significantly larger than movements measured during any of the surface loading tests. Installation plays an important role in creating permanent deformations in pipes and in causing potential problems such as leakage at the joints. In all cases, movement measured during dynamic loading is less than or equal to movement measured during static loading. Static loading measurements can be conservatively used in beam-on-springs modeling and analysis of culverts.

Appendix E. Explanation of simplified design approach and design examples

Contents

Introduction

The simplified design methods for rigid and flexible pipes are described here and used to produce example calculations.

First, design for circumferential response is discussed. Next, the proposals for simplified design of rigid pipes are introduced, solutions based on an approximation of the buried concrete pipe system as two rigid beams on elastic springs, interacting at a moment release joint, and this is introduced in the next section. Following that, the design approach for buried flexible pipes is introduced – equations based on analysis of two very long flexible pipes connected across a joint (since the deformations in flexible pipes attenuate rapidly so behavior across one joint is independent of what happens at the joints on the other ends of those two pipe segments). Simplified solutions are described both for moment transfer joints and moment release joints.

The empirical choice of soil stiffness for use in that design model is discussed in the fifth section of this appendix. Sections six and seven discuss the approach being proposed for design under earth and surface loads, respectively. A brief discussion is then included of the material that has

been drafted to consider for inclusion in the AASHTO LRFD Bridge Design Specifications. The last section of this appendix presents example calculations for:

i. 24 inch diameter reinforced concrete pipe with moment release joint at 2ft, 4ft, 8ft, and 20 ft burial depths

ii. 48 inch diameter reinforced concrete pipe with moment release joint at 2ft, 4ft, 8ft, and 20 ft burial depths

iii. 36 inch diameter corrugated steel pipe with moment transfer joint at 2ft, 4ft, 8ft, and 20 ft burial depths

iv. 36 inch diameter corrugated steel pipe with moment release joint at 2ft, 4ft, 8ft, and 20 ft burial depths

v. 36 inch diameter PVC pipe with moment release joint at 2ft, 4ft, 8ft, and 20 ft burial depths

vi. 60 inch diameter HDPE pipe with moment release joint at 2ft, 4ft, 8ft, and 20 ft burial depths

Performance of 2D analysis models for circumferential design of pipe ends

In addition to developing design to account for longitudinal effects in jointed pipes (shear and bending across joints), measurements taken during the project permit assessment of the circumferential behavior of the pipe ends. Pipe ends include bells for pipes with bell and spigot connections (concrete and thermoplastic pipes), and the re-rounded ends of the helically wound corrugated steel test pipes joined using hugger bands. This section examines how existing provisions in the AASHTO LRFD Bridge Design Specifications and some other well-known design equations perform relative to measurements made on the reinforced concrete, corrugated steel, HDPE and PVC test pipes.

Specific aspects of the response of the pipe ends that have been examined are as follows:

I. Circumferential moments in the bells of reinforced concrete pipes

II. Changes in pipe diameter in the ends of corrugated steel pipes, and in the bells of the HDPE and PVC test pipes

Both of these issues is examined in turn. The equations being examined are outlined, and then comparisons are made between calculated and measured behavior. In each case, the performance of the equations for the barrel of the pipe (away from the pipe ends) is also examined. This establishes the performance of the circumferential (2D) design models for those sections of the pipe they were initially developed for (the barrels), and so puts the performance of the equations for design of the pipe ends in perspective relative to design equation performance for the barrels.

Moments in reinforced concrete pipe

The pressures at the top of the barrels and joint of a buried 24 in. (0.6m) reinforced concrete pipeline were calculated employing AASHTO guidelines. The pressures were calculated for each element (i.e. barrel and bell) when subjected to a 100 kN surface load at 1.2m (4ft) and then 0.6m (2ft) of cover. Subsequently, the moments at the springlines, crown and invert were calculated employing the following closed-form solutions:

$$M_{cro} = M_{inv} = \frac{WR}{\pi} \qquad [E.1]$$

$$M_{sp} = WR\left(\frac{1}{\pi} - \frac{1}{2}\right) \qquad [E.2]$$

where

M_{cro} = *Moment at crown*

M_{inv} = *Moment at invert*

M_{sp} = *Moment at springline*

W = *Load*

R = *Mean diameter*

Furthermore, the radius of curvature was obtained employing the calculated moments, the wall geometry, and the representative modulus of elasticity estimated from three edge bearing tests performed on sections of a 24 in. reinforced concrete pipe:

$$M = \frac{E \cdot I}{\rho} \quad \therefore \quad \rho = \frac{E \cdot I}{M} \qquad [E.3]$$

where

$$I = \frac{t^3}{12} = second\ momet\ of\ area$$

E = Representative modulus of elasticity

M = Moment at a given location

ρ = Radius of curvature at a given location

t = pipe wall thickness

The differences between internal and external strains are then calculated employing eq. E.4:

$$\frac{1}{\rho} = \frac{\varepsilon_1 - \varepsilon_2}{t} \quad \therefore \quad \varepsilon_1 - \varepsilon_2 = \frac{t}{\rho} \qquad [E.4]$$

where

1/ρ = curvature

ε_1 = inner surface strain

ε_2 = outer surface strain

t = pipe wall thickness

These strain difference results are presented in Table E.1 for the barrels and in Table E.2 for the bells. These tables also show the data measured in the experiments for the same conditions, as well as results obtained using the three dimensional finite element analysis described in the Interim report. The strain difference is proportional to changes in curvature, and also proportion to circumferential bending moment when pipe response is elastic.

These tables indicate that:

- Readings at the two locations in the barrels were very similar, suggesting that the experimental data is consistent and reproducible.
- The simple design models provide estimates of change in curvature in the barrels (i.e. bending moment) that are generally close to those that were observed, or in some cases conservative (values about 50% higher than the measurements).
- In accordance with established understanding, the strain differences (i.e. curvatures and bending moments) at the invert were higher than those elsewhere.
- In general, the finite element calculations for strain difference in the barrel are closer to the measurements than are the simplified design calculations. Therefore, the differences

between observations and the simplified design calculations based on [E.1 to E.4] are due to the soil-pipe interaction captured in the finite element solutions, but more approximately represented in the design equations.

- Measurements in the bell featured similar patterns of behavior, but strain differences (therefore curvature changes and moments) at the springlines that were higher than those obtained using the simplified design equations. The three dimensional finite element results at the springline were much closer to the measurements.
- Measurements at the crown and invert were smaller than the calculations. This was likely because the bell was placed within a void in the bedding (so that the pipe did not rest directly on the bell). Since the base of the bell might actually rest on the bedding, it is not desirable to reduce design values for moment at these locations based on ideal burial.

Vertical diameter change calculations in CS, PVC and HDPE pipes

Vertical changes in diameter of three types of pipe were calculated when subjected to a surface load of 100 kN at 4ft (1.2m) and 2 ft (0.6m) of cover. Eq. E.5 was employed to calculate the changes in diameter. The geometrical and mechanical properties of the pipes employed in the calculations were obtained from AASHTO standards. However, section properties for the HDPE data were extrapolated since data was not available for the 60in pipe. The products examined were:

- 36 in. (0.9m) corrugated steel pipe
- 36 in. (0.9m) corrugated PVC pipe
- 60 in. (1.5m) corrugated HDPE pipe

$$\Delta Dv = \left[\frac{q_v}{\frac{E_p A_p}{R} + 0.57\, M_s} + \frac{D_L K_B q_v}{\frac{E_p I_p}{R^3} + 0.061 M_s} \right] D \qquad [E.5]$$

where

ΔD_v= *Vertical diameter change*

q_v = *Pressure at crown*

E_p = *Elastic modulus of pipe*

A_p = *Area of pipe wall*

I_p = *Second moment of area of pipe wall*

R =*Mean radius*

D = *Mean diameter*

M_s = *Tangent constrained modulus of soil*

D_L = *Deflection lag factor (1)*

K_B = *Bedding coefficient (0.1)*

The results are presented in Tables E.3 to E.5 along with the values measured during the tests for the barrels and joints. The experimental data was obtained employing reflective prisms and a total station while the pipeline was loaded directly over each element (i.e. the barrels or the joint). The soil modulus was selected using the Selig (1990) nonlinear elastic model parameters for SW90 backfill. Expected tangent modulus was selected for stress levels at the springline of the pipe.

From these comparisons, it is concluded that:

- All calculations are conservative relative to the measurements.
- Deflections observed in the barrels of the corrugated steel pipe are generally of similar magnitude to those observed at the pipe ends under the hugger band; this is likely because the hugger band adds little to the stiffness of the system; separate design estimates of deflection in the pipe ends under the hugger band are not likely needed.
- There was greater variation in deflections observed in the barrels and bell of the PVC pipe. However, it again appears that the design calculations are consistently conservative relative to the measurements.
- The deflections in the bell and spigot of the HDPE pipe were generally smaller than those in the barrels. Again, there does not appear to be any need to conduct additional deflection calculations to check performance of the bell.

Simplified design model for rigid pipes based on the two-pipe approximation

Experimental and computational work has been undertaken to develop simplified design equations based on approximations for 'imperfect' bedding that involved a length of void under the pipe invert. Laboratory experiments introducing voids under corrugated steel and PVC pipes did not lead to strong support for design based on a specified length of invert without adequate support. Therefore, different approaches have been sought. Two approaches have been developed – one for rigid pipes and another for flexible pipes.

Measurements of buried reinforced concrete pipe response to surface load indicate that the high stiffness pipe segments act almost like rigid links, with their vertical movement and rotation dependent on the magnitude of the applied loads, the eccentricity of the applied loads from the pipe centerline, and the stiffness of soil support. The two pipes interact across the moment release joint that connects them, and a shear force develops across that joint sufficient to ensure

that the vertical deformations of the two pipes at the joint are the same. Appendix F presents the formulation of the solutions for shear force and pipe deformations (including rotation across the joint). Since there are only two pipes involved, exact algebraic solutions are derived. The principal reason that the two-pipe approximation is conservative is because it considers just one pipe on either side of the joint being considered, and it neglects the resistance provided by all the other pipe segments beyond those two adjacent pipes. Appendix F includes additional discussion of the conservative nature of the 'two beam'-on-elastic-spring approximation compared to finite element solutions for beam on elastic-springs involving more pipe segments. Joint designers could still undertake the more-detailed finite element analyses modeling many pipes if they wished to reduce the conservatism of the design. All work on rigid pipes assumes use of moment release (e.g. gasketted bell and spigot) joints.

Simplified design model for flexible pipes based on the Heténi solutions

Laboratory experiments conducted on corrugated steel, PVC and HDPE pipes have demonstrated that deformations in flexible pipes resulting, say, from surface live loads, attenuate rapidly away from the location of load application. As a result, while surface loads in the vicinity of a joint connecting two shallow buried pipe segments influence that joint, the deformations become negligible at the other ends of the two pipe segments. Therefore, solutions for shear, moment and rotation have been developed assuming that the two pipes are very long, and that the response is not affected by either the location or characteristics of those other joints. Appendix F presents the formulation of the simplified design equations for flexible pipes, for both moment transfer (e.g. band) joints, and moment release (e.g. gasketted bell and spigot) joints. The design equations are developed using various closed-form solutions for beams on elastic foundations developed by Heténi (1948).

Choice of soil stiffness

Soil stiffness k_{soil} has been back-calculated using the test data presented in Appendix C using two procedures.

First, the design equations developed in Appendix F were used to back-calculate soil stiffness that produced the observed pipe deformations (joint rotations in pipes tested featuring moment release joints, and vertical pipe movements in pipes tested with moment transfer joints). Figure

E.1 presents those values in units of force per unit displacement per unit of horizontal area (pipe length and pipe width). The values range from 26 to 190 MN/m^3 (165 to 1210 kips/ft^3). This figure indicates that

- there is considerable variation in values for the same pipe loaded at different locations; stiffness changes by a factor of 2 or more between the lowest and highest values back-calculated by for a specific pipe and burial depth
- there is no clear correlation of spring stiffness with burial depth; while the expectation is that the deeper cases would correspond to higher values of k_{soil}, there is no clear trend of that kind in the data
- there is no clear trend whereby k_{soil} is a function of pipe stiffness; values for the rigid pipes (reinforced concrete) do not appear to be a different population than those for flexible pipes; therefore, a single value of k_{soil} is proposed for use with all the pipe products.

A design value of k_{soil}=30 MN/m^3 (191 kips/ft^3) is proposed, and is used later in this appendix to undertake example calculations. This value is shown in Figure E.1, and is between those suggested by Terzaghi for surface footings on loose to medium density soil.

An alternative strategy is to interpret the buried pipe test results using finite element analyses of the beam on elastic spring approximation. This permits curve fitting that captures more than just rotation and vertical movement at the joint. Finite element analysis permits the whole pattern of response along the pipe to be assessed, and data sets obtained for offset surface load as well as data for load on the ground surface centered directly over the culvert joint. Analyses of this kind were undertaken for three of the pipe products, and Figure E.2 presents the resulting values of soil stiffness expressed in units of force per unit displacement per unit of horizontal area (pipe length and pipe width). The values shown in Figure E.1 are included in Figure E.2 for comparison. This shows that this alternative approach to determining soil stiffness produces data with a similar range of values, and again without clear correlation with regard to burial depth or pipe stiffness. For each of these three culvert types where load was centered over the joint, both approaches to back-calculating soil stiffness were employed. This revealed that soil stiffness was almost always about 30% higher when back-calculated using finite element analysis.

Design for earth load

It was recognized at the commencement of this project that no rotation or shear force occurs across a joint connecting pipes subjected to uniform earth loads, if they are constructed to have uniform soil support (under these circumstances, both pipes settle downward equal amounts, so no load transfer or rotation occurs across the joint). Tests were undertaken on both corrugated steel and PVC pipes where construction was undertaken leaving short lengths of pipe invert without bedding support, either adjacent to or straddling the joint (a gap was left under the pipe invert). However, the data collected from those tests did not show clear evidence of the impact of this region of poor soil support. Furthermore, the choice of void length being considered was some arbitrary– based on local bending effects under surface loading and 'judgement' regarding what size of "imperfection" (improper soil support) to be considered in design. Given these difficulties, this type of imperfection was discarded as a potential imperfection for use in design.

Perhaps the most likely cause of shear force and rotation across a joint connecting two deeply buried pipes is that associated with differences in degree of compaction and therefore the soil stiffness for the pipes on either side. This might result from precipitation during construction (since moisture content in the soil has a significant effect on the density and stiffness of the compacted soil), a change in the backfill soil being supplied to the site, or a change in personnel and therefore effort undertaken compacting the soil. For this reason, the 'two-pipe' analyses developed in Appendix F were formulated considering the soil support to the pipe on one side of the joint (say, to the 'left', k_L) as being distinct from the soil support to the other pipe (that on the 'right', k_R). Solutions were then developed considering different ratios of right hand support to left hand support, k_R/k_L. Simplified design equations for shear and rotation are then proposed in Appendix F where $k_R = 2k_L$ (i.e. using soil stiffness of k_{soil} on one side and 2 k_{soil} on the other). This is illustrated in Figures F.4a and F.6. For this magnitude of change in soil support across a joint, the two-pipe solution indicates that shear force transferred across a moment release joint connecting two rigid pipes is equal to $1/12^{th}$ (i.e. 8.3%) of the total vertical earth load acting on each rigid pipe segment. For the extreme case where the soil support on one side is rigid (e.g. very poor practice involving placement of one pipe directly on a rock foundation), the solution indicates that shear force transferred is 25% of the total vertical earth load acting on each rigid pipe segment. The value of 8.3% is proposed for use in the simplified design method since change in soil support by a factor of 2 is considered to be a reasonable design case (for example,

an increase in soil density from 90% to 95% of the maximum value from a standard Proctor test approximately doubles soil modulus).

For flexible pipes, the shear force transferred is influenced by a characteristic longitudinal bending parameter $\lambda = \sqrt[4]{\frac{k_{soil} OD}{4\ EI}}$ which has units of 1/length (where EI is the flexural rigidity of the whole pipe bending in the axial direction). Maximum shear for moment release joints is $0.157/\lambda$ times the earth load per unit length along the pipe, while for moment transfer joints the maximum shear force is $0.154/\lambda$ times the earth load per unit length along the pipe. Maximum moment is $0.058/\lambda^2$ times the earth load per unit length along the pipe.

Design for vehicle load

Influence diagrams for load on a single 10 inch (0.25 m) by 20 inch (0.5 m) wheel pad and a single axle (featuring two such wheel pads) were presented in the June 2011 Quarterly report. These demonstrated that shear force and angle of rotation are always more severe considering just a single wheel pad, rather than a pair (i.e. an axle). Since situations can occur where just one end of the axle is over the jointed pipeline (e.g. the culvert might not be at 90^o to the centerline of the highway so the vehicle passes across the jointed culvert at another angle), design should be based on a single wheel.

The attenuation of surface load effects with depth is captured in the AASHTO LRFD Design Specifications using a rectangular loading area that increases with depth (Section 3.6.1.2.6). A tandem axle will feature two wheel pads 4 ft (1.2 m) apart, and this spreading distance between the two axles reduces vertical design pressures at the crown of the culvert by considerably more than the additional load from the extra pair of wheels increases them. Therefore, the single axle design truck produces higher design pressures. For this reason, joint design for surface load should be based on 16000 lbf (71.3 kN) on a 10 inch (0.25 m) by 20 inch (0.5 m) load pad (i.e. the configuration used in the buried pipe experiments reported in Appendix C).

Surface load positions leading to peak rotation and peak shear force across joints connecting rigid pipes are different. Peak rotation results when the center of the load pad is directly over the joint. Peak shear results when the edge of the loaded rectangle over which the load has spread at depth H just touches the joint. These loading conditions are illustrated in Figures F.4b and F.4c.

Surface load positions leading to peak shear force and peak rotation or moment across joints connecting flexible pipes are also different. Just as it did for rigid pipes, peak shear force across a joint connecting flexible pipes also results when the edge of the loaded rectangle over which the load has spread at depth H just touches the joint. Peak moment in moment transfer joints occurs when the surface load is centered over the joint, and peak rotation in moment release joints also occurs when the surface load is centered over the joint.

Draft changes to the AASHTO LRFD Bridge Design Specifications

Appendix G presents edits proposed to the following sections of the AASHTO LRFD Bridge Design Specifications:

- Section 12.5.2 defining the strength limit states – minor changes needed to include the joint design limit states.
- Section 12.5.5 to define resistance factors for use with these new limit states.
- Section 12.6.2 defining the service limit states – minor edits needed to include calculations of differential settlements along the pipe needed for joint design.

Section 12.15 is a new section proposed to cover the structural design of culvert joints. It includes material defining the two kinds of joints (moment release and moment transfer), to discuss design for circumferential effects, then requirements to support shear force and moment or rotation values transferred across the joint. It concludes with a section describing procedures for use of the finite element method to undertake beam on elastic spring analysis of a jointed pipe system.

Example calculations

Figure 3 presents example calculations for a 24 inch (0.6 m) diameter reinforced concrete pipe at burial depth of 2 ft (0.6 m).

Figure 4 presents example calculations for a 48 inch (1.2 m) diameter reinforced concrete pipe at burial depth of 20 ft (6.1 m).

Figure 5 presents example calculations for a 36 inch (0.9 m) diameter corrugated steel pipe with moment transfer joint at burial depth of 4 ft (1.2 m).

Figure 6 presents example calculations for a 36 inch (0.9 m) diameter corrugated steel pipe with moment release joint at burial depth of 4 ft (1.2 m).

Figure 7 presents example calculations for a 36 inch (0.9 m) diameter PVC pipe with moment release joint at burial depth of 2 ft (0.6 m).

Figure 8 presents example calculations for a 60 inch (1.5 m) diameter HDPE pipe with moment release joint at burial depth of 20 ft (6.1 m).

In each case, details are provided in the right hand column describing the sources of each equation and input value, defined by:

- The pipe geometry and section properties (procedures for estimating the flexural rigidity EI for the pipe in longitudinal bending like a beam are outlined in Appendix I)
- The burial condition
- The AASHTO LRFD Bridge Design Specifications
- Equations developed in Appendix F
- The back-calculated soil support stiffness (as discussed in an earlier section)

These example pipes have then been examined at a variety of burial depths, and the results summarized in Tables E.1, E.2 and E.3 below. These indicate that:

- Rotations are all small; this is consistent with what has been seen during the loading tests conducted during Project 15-38 both in the laboratory and in the field;
- Shear forces and rotations are largest at minimum soil cover, they decrease substantially, then increase again at the highest cover depths;
- The magnitude of the shear forces is substantial; for example, values for concrete pipe exceeding 8 kips (36 kN) for the shallowest and deepest cases;

The design calculations for thermoplastic pipes have been undertaken using the short term modulus values specified in the AASHTO LRFD Bridge Design Specifications. This short term value produces higher value of vertical arching factor, and therefore short term loads that are longer than long term loads. Design calculations of demand (expected shear force, bending moment or rotation) are then compared to short term measurements of resistance (strength).

Table E.1. Strains ε_1- ε_2 in pipe barrels (units of μ strain)

		Pipe 1	Pipe 2	Simplified Calculations	linear elastic FEA
Barrel 1.2 m of cover	**Springline 1**	-25	-28	-24.3	-27
	Springline 2	-30	-30	-24.3	-27
	Crown	34	29	42.6	30
	Invert	47	43	42.6	23
Barrel 0.6 m of cover	**Springline 1**	-43	-48	-66.5	-55
	Springline 2	-51	-47	-66.5	-55
	Crown	58	55	116.5	70
	Invert	76	66	116.5	47

Note. ε1 and ε2 are inside and outside strains respectively

Table E.2. Strains ε_1- ε_2 in the bell (units of μ strain)

		Pipe 2	Simplified Calculations	linear elastic FEA
Bell 1.1575 m of cover	**Springline 1**	-28	-13	-28.3
	Springline 2	-28	-13	-28.3
	Crown	16.2*	24	31
	Invert	16.2*	24	26
Bell 0.5475 m of cover	**Springline 1**	-66	-39	-65
	Springline 2	-66	-39	-65
	Crown	37.8*	68.5	57
	Invert	41.4*	68.5	89

Notes.

1. ε1 and ε2 are inside and outside strains respectively

2. Pipe 2 contributed the Bell to the joint that was instrumented, so no results are included for Pipe 1

3. *Inferred data (data was not measured on both the inner and outer surfaces, so change in curvature was estimated using one set of measurements)

Table E.3. Calculated versus measured changes in diameter in mm (1 inch = 25.4mm); 36 in. CSP

		Calculation	Test data			
Case	**Burial depth**	**Barrel**	**North barrel**	**Joint**	**Joint**	**South barrel**
36 in. CSP with no gasket	**4 ft (1.2m)**	-1.7	-1.32	-0.71	-0.81	-1.15
	2 ft (0.6m)	-5.8	-3.5	-4.93	-4.49	-4.81
36 in. CSP with gasket	**4 ft (1.2m)**	-1.7	-0.92	-1.18	-1.12	-0.98
	2 ft (0.6m)	-5.8	-3.07	-2.63	-2.86	-2.66

Table E.4. Calculated versus measured changes in diameter in mm (1 inch = 25.4mm); 36 in. PVC

		Calculation	Test data			
Case	**Burial depth**	**Barrel**	**North barrel**	**Spigot**	**Bell**	**South barrel**
36 in. PVC	**4 ft (1.2m)**	-2.4	-0.91	-0.83	-0.86	-0.66
	2 ft (0.6m)	-7.7	-3.58	-2.28	-2.48	-2.29

Table E.5. Calculated versus measured changes in diameter in mm (1 inch = 25.4mm); 60 in. HDPE

		Calculation	Test data			
Case	**Burial depth**	**Barrel**	**North barrel**	**Spigot**	**Bell**	**South barrel**
60 in. HDPE	**4 ft (1.2m)**	-4.8	-2.26	-1.49	-1.63	2.28
	2 ft (0.6m)	-15	-8.92	-6.54	-7.29	-7.92

Table E.6 Summary of simplified design requirements (shear force and rotation angle) for two reinforced concrete pipes at four burial depths.

		Burial depth							
		2 ft	0.61 m	4 ft	1.22 m	8 ft	2.44 m	20 ft	6.1 m
ID 24 inch	V_{j-d}	6407 lbf	28.5 kN	4001 lbf	17.8 kN	3795 lbf	16.9 kN	8686 lbf	38.7 kN
	θ_{j-d}	0.18 degrees		0.098 degrees		0.044 degrees		0.055 degrees	
ID 48 inch	V_{j-d}	8895 lbf	39.6 kN	6488 lbf	28.9 kN	8067 lbf	35.9 kN	17305 lbf	77.1 kN
	θ_{j-d}	0.12 degrees		0.074 degrees		0.037 degrees		0.058 degrees	

Table E,7 Summary of simplified design requirements (shear force and moment) for a corrugated steel pipe with moment transfer joint at four burial depths.

	Burial depth							
	2 ft	0.61 m	4 ft	1.22 m	8 ft	2.44 m	20 ft	6.1 m
V_{j-d}	3029 lbf	13.5 kN	2208 lbf	9.8 kN	2564 lbf	11.4 kN	5149 lbf	22.9 kN
M_{j-d}	2493 ft lb	3.39 kN.m	1352 ft lb	1.84 kN.m	1561 ft lb	2.12 kN.m	3534 ft lb	4.8 kN.m

Table E.8 Summary of simplified design requirements (shear force and rotation) for three flexible pipes with moment release joints at four burial depths.

Burial depth								
CSP-36in	2 ft	0.61 m	4 ft	1.22 m	8 ft	2.44 m	20 ft	6.1 m
V_{j-d}	3045 lbf	13.6 kN	2231 lbf	9.9 kN	2605 lbf	11.6 kN	5241 lbf	23.4 kN
θ_{j-d}	0.25 degrees		0.08 degrees		0.04 degrees		0.09 degrees	
PVC-36in	2 ft	0.61 m	4 ft	1.22 m	8 ft	2.44 m	20 ft	6.1 m
V_{j-d}	2919 lbf	13.0 kN	2168 lbf	9.7 kN	2534 lbf	11.3 kN	5059 lbf	22.5 kN
θ_{j-d}	0.25 degrees		0.07 degrees		0.04 degrees		0.09 degrees	
HDPE-60in	2 ft	0.61 m	4 ft	1.22 m	8 ft	2.44 m	20 ft	6.1 m
V_{j-d}	5131 lbf	22.9 kN	4582 lbf	20.4 kN	5707 lbf	25.4 kN	10986 lbf	49.0 kN
θ_{j-d}	0.13 degrees		0.06 degrees		0.04 degrees		0.07 degrees	

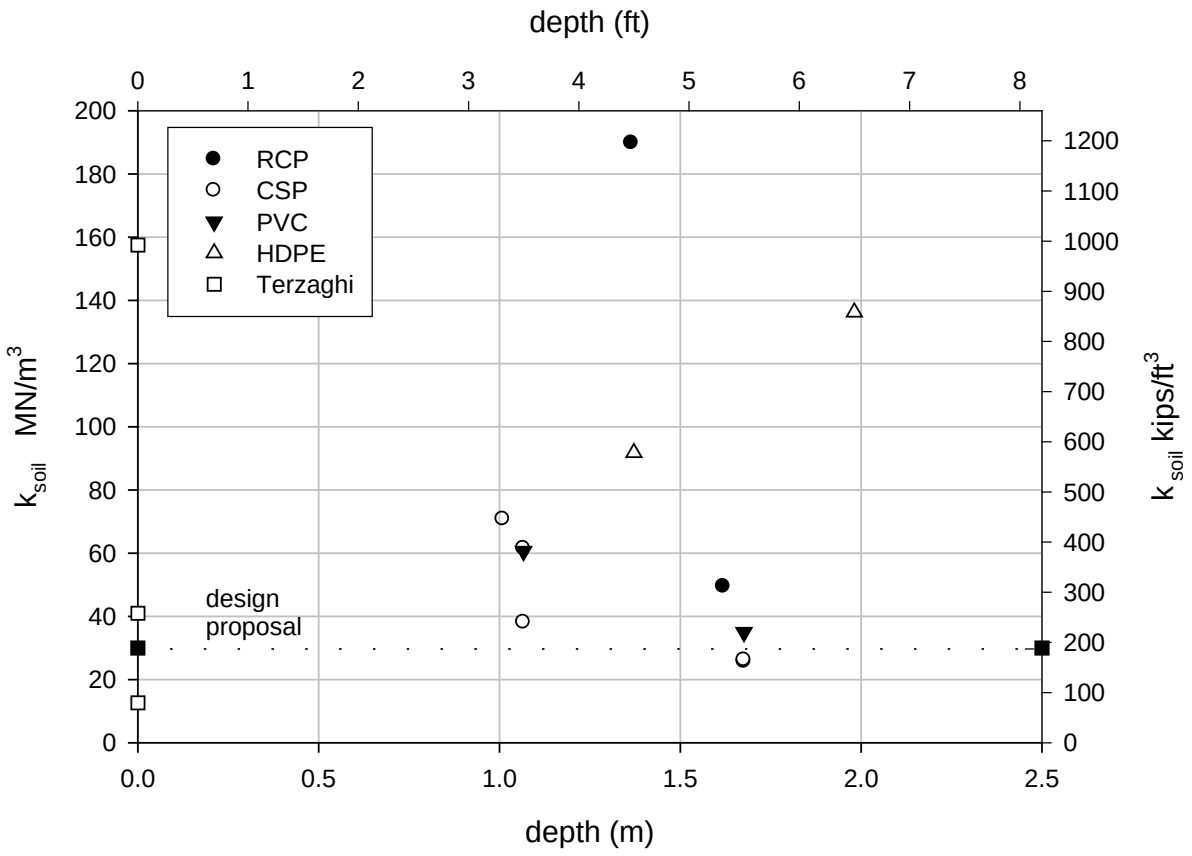

Figure E.1. Values of back-calculated soil stiffness k_{soil} in MN/m^3 for the all six sets of buried pipe experiments obtained using the simplified design equations; Terzaghi values and design recommendation are also shown.

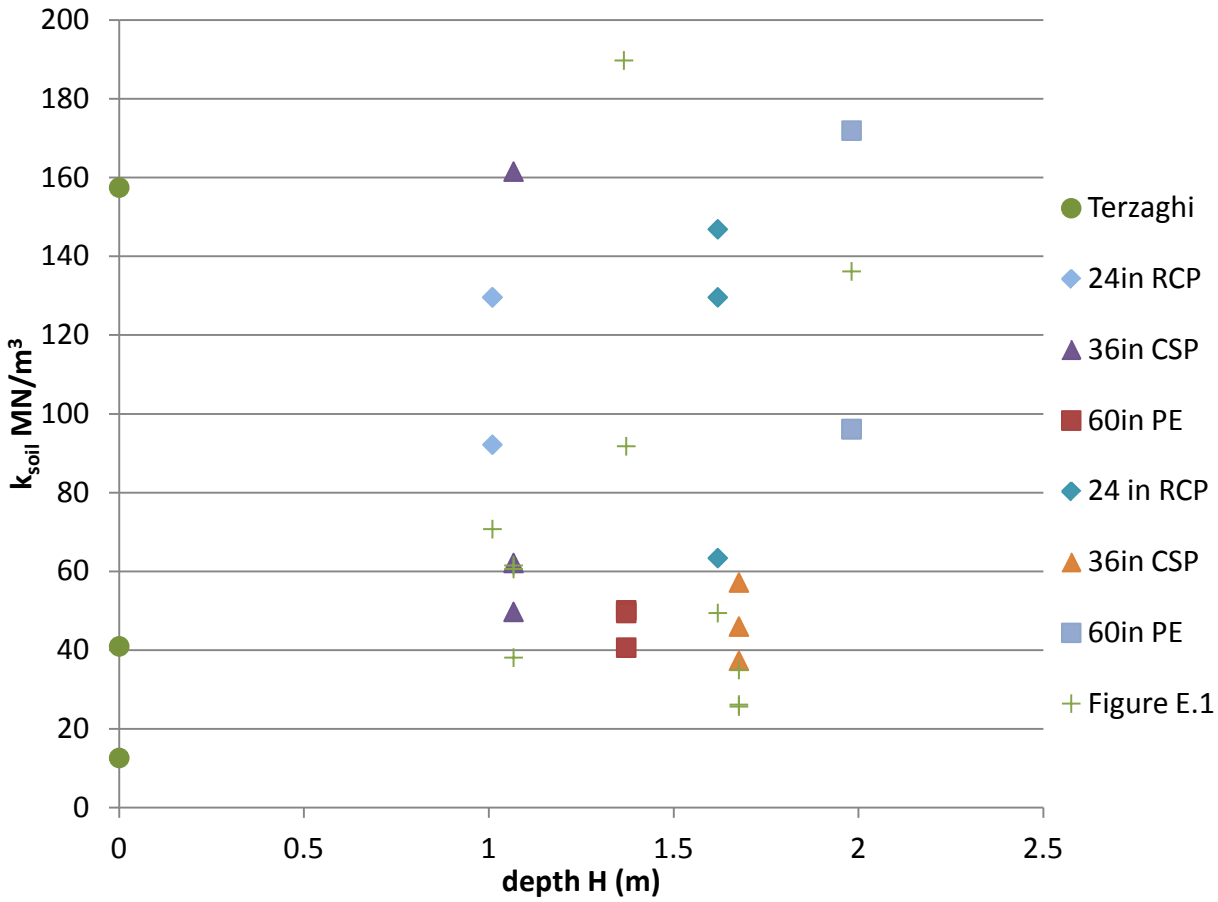

Figure E.2. Values of back-calculated soil stiffness k_{soil} in MN/m^3 obtained using finite element analysis of the first three sets of buried pipe experiments and use of closed for equations for all six pipes ($1MN/m^3$ = 6.3 $kips/ft^3$; 1m=40 in.) .

		US customary		SI		
Internal diameter	ID	2	ft	0.61	m	Pipe geometry
Outside diameter	OD	2.625	ft	0.80	m	Pipe geometry
Depth to pipe crown	h	2	ft	0.61	m	Burial condition
Depth to pipe springline	H	3.3125	ft	1.01	m	Burial condition
Soil unit weight	γS	140	pcf	22	kN/m3	Burial condition
Vertical arching factor	VAF	1.4		1.4		AASHTO LFRD Table 12.10.2.1-3 Section 12
Earth load factor	γE	1.3		1.3		AASHTO LFRD Table 3.4.1-2 Section 3
Earth load per unit length	W_E	2213	lb/ft	32.3	kN/m	[F.41] Appendix F
Live load distribution factor	LLDF	1.15		1.15		AASHTO LFRD Section 3.6.1.2.6
Width of standard wheel pair	W_0	1.67	ft	0.51	m	AASHTO LFRD Section 3.6.1.2.5
Distribution width at depth H	W_0+LLDF*H	5.48	ft	1.67	m	
Length of standard wheel load	L_0	0.83	ft	0.25	m	AASHTO LFRD Section 3.6.1.2.5
Distribution length at depth H	L_0+LLDF*H	4.64	ft	1.42	m	
Proportion of wheel load on the pipe	w	48%		48%		[F.26] Appendix F
Stiffness of soil support	k_{soil}	190706	pcf	30000	kN/m3	Proposed design value back-calculated from tests.
Pipe length (joint center to center)	L_p	7.35	ft	2.24	m	Pipe geometry
Live load factor	γL	1.75		1.75		AASHTO LFRD Table 3.4.1-1 Section 3
Wheel loads		16000	lbf	71.3	kN	Use half of a single axle
Multiple presence factor	m	1.2		1.2		AASHTO LFRD Table 3.6.1.1.2-1 Section 3
Dynamic load allowance	IM	19.3		19.3		AASHTO LFRD Section 3.6.2.2
Total factored surface force	P_L	40098	lbf	178.6	kN	Consider live load factor, multiple presence, dynamic load allowance
Earth load contribution to shear	0.083 W_E L_p	1350	lbf	6.01	kN	[F.49] Appendix F
Surface load contribution to shear	wP_LV	5057	lbf	22.53	kN	[F.39] Appendix F
Shear force across the joint	V_{j-d}	6407	lbf	28.54	kN	Add earth and surface load effects
Earth load contribution to rotation	0.25 W_E/L_P OD k	0.0001504	radians	0.0001504	radians	[F.50] Appendix F
Surface load contribution to rotation	6wP_Lr/$k_{soil}$$L_P^3$OD	0.0029	radians	0.0029	radians	[F.38] Appendix F
Rotation across the joint	θ_{j-d}	0.18	degrees	0.18	degrees	Add earth and surface load effects and convert to degrees.

Figure E.3. Design calculations for 24 in. (0.6m) diameter reinforced concrete pipe at 2 ft (0.6m) burial depth to crown.

		US customary		SI		
Internal diameter	ID	4	ft	1.22	m	Pipe geometry
Outside diameter	OD	5.0	ft	1.51	m	Pipe geometry
Depth to pipe crown	h	20	ft	6.10	m	Burial condition
Depth to pipe springline	H	22.5	ft	6.85	m	Burial condition
Soil unit weight	γS	139.9	pcf	22	kN/m3	Burial condition
Vertical arching factor	VAF	1.4		1.4		AASHTO LFRD Table 12.10.2.1-3 Section 12
Earth load factor	γE	1.3		1.3		AASHTO LFRD Table 3.4.1-2 Section 3
Earth load per unit length	W_E	28369.7	lb/ft	414.6	kN/m	[F.41] Appendix F
Live load distribution factor	LLDF	1.15		1.15		AASHTO LFRD Section 3.6.1.2.6
Width of standard wheel pair	W_0	1.67	ft	0.51	m	AASHTO LFRD Section 3.6.1.2.5
Distribution width at depth H	W_0+LLDF*H	27.52	ft	8.39	m	
Length of standard wheel load	L_0	0.83	ft	0.25	m	AASHTO LFRD Section 3.6.1.2.5
Distribution length at depth H	L_0+LLDF*H	26.68	ft	8.13	m	
Proportion of wheel load on the pipe	w	0.180187		0.180187		[F.26] Appendix F
Stiffness of soil support	k_{soil}	190706	pcf	30000	kN/m3	Proposed design value back-calculated using FEA of QU Tests 1 to 3.
Gasket stiffness	k_G	285103	lbf/in	50	kN/mm	Estimate to be updated when measurements are available
Pipe length (joint center to center)	L_p	7.35	ft	2.24	m	Pipe geometry
Live load factor	γL	1.75		1.75		AASHTO LFRD Table 3.4.1-1 Section 3
Wheel loads		16000	lbf	71.3	kN	Use half of a single axle
Multiple presence factor	m	1.2		1.2		AASHTO LFRD Table 3.6.1.1.2-1 Section 3
Dynamic load allowance	IM	0.0		0.0		AASHTO LFRD Section 3.6.2.2
Total factored surface force	P_L	33600	lbf	149.7	kN	Consider live load factor, multiple presence, dynamic load allowance
Earth load contribution to shear	0.083 W_E L_p	17305	lbf	77.08	kN	[F.49] Appendix F
Surface load contribution to shear	wP_LV	0	lbf	0.00	kN	[F.39] Appendix F
Shear force across the joint	V_{j-d}	17305	lbf	77.08	kN	Add earth and surface load effects
Earth load contribution to rotation	0.25 W_E/L_P OD k	0.0010206	radians	0.0010206	radians	[F.50] Appendix F
Surface load contribution to rotation	$6wP_Lr/k_{soil}L_P^3$OD	0.00	radians	0.00	radians	[F.38] Appendix F
Rotation across the joint	θ_{j-d}	0.06	degrees	0.06	degrees	Add earth and surface load effects and convert to degrees.

Figure E.4 Design calculations for 48 in. (1.2m) diameter reinforced concrete pipe at 20 ft (6.1m) burial depth to crown

		US customary		SI		
Internal diameter	ID	3.00	ft	0.91	m	Pipe geometry
Diameter in contact with soil	OD	3.04	ft	0.93	m	Pipe geometry
Modulus of pipe material	E	4166921622	psf	200000000	kPa	Pipe property
Second moment of area in axial direction	I	0.000405513	ft^4	0.0000035	m4	Pipe geometry
Flexural rigidity of whole pipe along axis	EI	1689741	lbf.ft^2	700	kN.m2	
Vertical arching factor	VAF	1.00		1.00		Implicit in AASHTO LFRD Section 12.7.2.2
Depth to pipe crown	h	4	ft	1.22	m	Burial condition
Depth to pipe springline	H	5.5	ft	1.68	m	Burial condition
Soil unit weight	γ_S	140	pcf	22.00	kN/m3	Burial condition
Earth load factor	γ_E	1.95		1.95		AASHTO LFRD Table 3.4.1-2 Section 3
Earth load per unit length	W_E	4579.50	lb/ft	66.93	kN/m	[F.74] Appendix F
Live load distribution factor	LLDF	1.15		1.15		AASHTO LFRD Section 3.6.1.2.6
Width of standard wheel pair	W_0	1.67	ft	0.51	m	AASHTO LFRD Section 3.6.1.2.5
Distribution width at depth H	W_0+LLDF*H	8.02	ft	2.44	m	
Length of standard wheel load	L_0	0.83	ft	0.25	m	AASHTO LFRD Section 3.6.1.2.5
Distribution length at depth H	L_0+LLDF*H	7.18	ft	2.19	m	
Proportion of wheel load on the pipe	w	38%		38%		[F.52] Appendix F
Stiffness of soil support	k_{soil}	190706	pcf	30000	kN/m3	Proposed design value back-calculated using FEA of QU Tests.
Characteristic length (beam on elastic fdtn)	λ	0.54	1/ft	1.78	1/m	[F.54] Appendix F
Live load factor	γ_L	1.75		1.75		AASHTO LFRD Table 3.4.1-1 Section 3
Wheel loads		16000	lbf	71.3	kN	Use half of a single axle
Multiple presence factor	m	1.2		1.2		AASHTO LFRD Table 3.6.1.1.2-1 Section 3
Dynamic load allowance	IM	10.2		10.2		AASHTO LFRD Section 3.6.2.2
Total factored surface force per unit length	$wP_L/(L_0$+LLDF*H)	1956.9	lbf/ft	28.6	kN/m	Live load factor, multiple presence, dynamic load allowance
Earth load contribution to shear	0.154 W_E / λ	1302.98	lbf	5.81	kN	[F.94] Appendix F
Surface load contribution to shear	wP_Lv	904.89	lbf	4.03	kN	[F.63] Appendix F
Shear force across the joint	V_{j-d}	2207.88	lbf	9.84	kN	Add earth and surface load effects
Earth load contribution to moment	0.058 W_E / λ^2	906.67	lbf ft	1.23	kN.m	[F.101] Appendix F
Surface load contribution to moment	wP_Lm	445.31	lbf ft	0.61	kN.m	[F.60] Appendix F
Moment across the joint	M_{j-d}	1351.98	lbf ft	1.84	kN.m	Add earth and surface load effects

Figure E.5 Design calculations for 36 in. (0.9m) diameter corrugated steel pipe with moment transfer joint at 4 ft (1.2m) burial depth

		US customary		SI		
Internal diameter	ID	3.00	ft	0.91	m	Pipe geometry
Diameter in contact with soil	OD	3.04	ft	0.93	m	Pipe geometry
Modulus of pipe material	E	4.167E+09	psf	200000000	kPa	Pipe property
Second moment of area in axial direction	I	0.0004055	ft^4	0.0000035	m4	Pipe geometry
Flexural rigidity of whole pipe along axis	EI	1689741	$lbf.ft^2$	700	$kN.m^2$	
Vertical arching factor	VAF	1.00		1.00		Implicit in AASHTO LFRD Section 12.7.2.2
Depth to pipe crown	h	4.00	ft	1.22	m	Burial condition
Depth to pipe springline	H	5.52	ft	1.68	m	Burial condition
Soil unit weight	γ_S	139.85	pcf	22.00	kN/m^3	Burial condition
Earth load factor	γ_E	1.95		1.95		AASHTO LFRD Table 3.4.1-2 Section 3
Earth load per unit length	W_E	4579.50	lb/ft	66.93	kN/m	[24] Appendix C
Live load distribution factor	LLDF	1.15		1.15		AASHTO LFRD Section 3.6.1.2.6
Width of standard wheel pair	W_0	1.67	ft	0.51	m	AASHTO LFRD Section 3.6.1.2.5
Distribution width at depth H	W_0+LLDF*H	8.02	ft	2.44	m	
Length of standard wheel load	L_0	0.83	ft	0.25	m	AASHTO LFRD Section 3.6.1.2.5
Distribution length at depth H	L_0+LLDF*H	7.18	ft	2.19	m	
Proportion of wheel load on the pipe	w	38%		38%		[F.52] Appendix F
Stiffness of soil support	k_{soil}	190706	pcf	30000	kN/m^3	Proposed design value back-calculated from laboratory tests.
Characteristic length (beam on elastic fdtn)	λ	0.54	1/ft	1.78	1/m	[F.54] Appendix F
Live load factor	γ_L	1.75		1.75		AASHTO LFRD Table 3.4.1-1 Section 3
Wheel loads		16000	lbf	71.3	kN	Use half of a single axle
Multiple presence factor	m	1.2		1.2		AASHTO LFRD Table 3.6.1.1.2-1 Section 3
Dynamic load allowance	IM	10.2		10.2		AASHTO LFRD Section 3.6.2.2
Total factored surface force per unit length	$wP_L/(L_0$+LLDF*H)	1956.9	lbf/ft	28.6	kN/m	Consider live load factor, multiple presence, dynamic load allowance
Earth load contribution to shear	$0.157\ W_E / \lambda$	1328.37	lbf	5.92	kN	[F.84] Appendix F
Surface load contribution to shear	wP_LV	904.89	lbf	4.03	kN	[F.73] Appendix F
Shear force across the joint	V_{j-d}	2233.26	lbf	9.95	kN	Add earth and surface load effects
Earth load contribution to rotation	$0.0918\ W_E\lambda/(OD\ k_{soil})$	0.00039	radians	0.00039	radians	[F.83] Appendix F
Surface load contribution to rotation	$rwP_L/(L_0$+LLDF*H)	0.00097	radians	0.00097	radians	[F.70] Appendix F
Rotation across the joint	θ_{j-d}	0.08	degrees	0.08	degrees	Add earth and surface load effects and convert to degrees.

Figure E.6 Design calculations for 36 in. (0.9m) diameter corrugated steel pipe with moment release joint at 4 ft (1.2m) burial depth

		US customary		SI		
Internal diameter	ID	3.00	ft	0.91	m	Pipe geometry
Diameter in contact with soil	OD	3.09	ft	0.94	m	Pipe geometry
Modulus of pipe material	E	57503518	psf	2760000	kPa	AASHTO LFRD Table 12.12.3.3-1
Flexural rigidity of whole pipe along axis	EI	1448349	$lbf.ft^2$	600	$kN.m^2$	
Area in hoop direction per unit length	A	0.0144357	ft^2/ft	0.0044	m^2/m	Pipe geometry
Hoop stiffness per unit length	EA	830102	lbf/ft	12144	kN/m	
Constrained modulus of the soil	M_S	66302	lbf/ft^2	3200	kPa	AASHTO LFRD Table 12.12.3.4-1
Normalized hoop stiffness	S_H	0		0		AASHTO LFRD Equation 12.12.3.4-4
Vertical arching factor	VAF	1.00		1.00		AASHTO LFRD Equation 12.12.3.4-3
Depth to pipe crown	h	2.00	ft	0.61	m	Burial condition
Depth to pipe springline	H	3.54	ft	1.08	m	Burial condition
Soil unit weight	γ_S	139.85	pcf	22.00	kN/m^3	Burial condition
Earth load factor	γ_E	1.95		1.95		AASHTO LFRD Table 3.4.1-2 Section 3
Earth load per unit length	W_E	2998.24	lb/ft	43.81	kN/m	[F.74] Appendix F
Live load distribution factor	LLDF	1.15		1.15		AASHTO LFRD Section 3.6.1.2.6
Width of standard wheel pair	W_0	1.67	ft	0.51	m	AASHTO LFRD Section 3.6.1.2.5
Distribution width at depth H	W_0+LLDF*H	5.74	ft	1.75	m	
Length of standard wheel load	L_0	0.83	ft	0.25	m	AASHTO LFRD Section 3.6.1.2.5
Distribution length at depth H	L_0+LLDF*H	4.91	ft	1.50	m	
Proportion of wheel load on the pipe	w	54%		54%		[F.52] Appendix F
Stiffness of soil support	k_{soil}	190706	pcf	30000	kN/m^3	Proposed design value back-calculated from laboratory tests.
Characteristic length (beam on elastic fdtn)	λ	0.56	1/ft	1.85	1/m	[F.54] Appendix F
Live load factor	γ_L	1.75		1.75		AASHTO LFRD Table 3.4.1-1 Section 3
Wheel loads		16000	lbf	71.3	kN	Use half of a single axle
Multiple presence factor	m	1.2		1.2		AASHTO LFRD Table 3.6.1.1.2-1 Section 3
Dynamic load allowance	IM	18.4		18.4		AASHTO LFRD Section 3.6.2.2
Total factored surface force per unit length	$wP_L/(L_0$+LLDF*H)	4357.9	lbf/ft	63.7	kN/m	Consider live load factor, multiple presence, dynamic load allowance
Earth load contribution to shear	$0.157\ W_E / \lambda$	833.60	lbf	3.71	kN	[F.84] Appendix F
Surface load contribution to shear	wP_Lv	2085.36	lbf	9.29	kN	[F.73] Appendix F
Shear force across the joint	V_{j-d}	2918.95	lbf	13.01	kN	Add earth and surface load effects

Earth load contribution to rotation	$0.0918\ W_E\lambda/(OD\ k_{soil})$	0.00026	radians	0.00026	radians	[F.83] Appendix F
Surface load contribution to rotation	r	0.00411	radians	0.00411	radians	[F.70] Appendix F
Rotation across the joint	$\theta_{j\text{-}d}$	0.25	degrees	0.25	degrees	Add earth and surface load effects and convert to degrees.

Figure E.7 Design calculations for 36 in. (0.9m) diameter PVC pipe with moment release joint at 2 ft (0.6m) cover depth

		US customary		SI		
Internal diameter	ID	5	ft	1.52	m	Pipe geometry
Diameter in contact with soil	OD	5.26	ft	1.60	m	Pipe geometry
Modulus of pipe material	E	15792633	psf	758000	kPa	AASHTO LFRD Table 12.12.3.3-1
Flexural rigidity of whole pipe along axis	EI	6396875	$lbf.ft^2$	2650	$kN.m^2$	
Area in hoop direction per unit length	A	0.0480833	ft^2/ft	0.0146558	m^2/m	Pipe geometry
Hoop stiffness per unit length	EA	759362	lbf/ft	11109	kN/m	
Constrained modulus of the soil	M_S	93237	lbf/ft^2	4500	kPa	AASHTO LFRD Table 12.12.3.4-1
Normalized hoop stiffness	S_H	0		0		AASHTO LFRD Equation 12.12.3.4-4
Vertical arching factor	VAF	0.95		0.94		AASHTO LFRD Equation 12.12.3.4-3
Depth to pipe crown	h	20.00	ft	6.10	m	Burial condition
Depth to pipe springline	H	22.63	ft	6.90	m	Burial condition
Soil unit weight	γ_S	139.85	pcf	22.00	kN/m^3	Burial condition
Earth load factor	γ_E	1.95		1.95		AASHTO LFRD Table 3.4.1-2 Section 3
Earth load per unit length	W_E	30706.11	lb/ft	448.52	kN/m	[F.74] Appendix F
Live load distribution factor	LLDF	1.15		1.15		AASHTO LFRD Section 3.6.1.2.6
Width of standard wheel pair	W_0	1.67	ft	0.51	m	AASHTO LFRD Section 3.6.1.2.5
Distribution width at depth H	W_0+LLDF*H	27.69	ft	8.44	m	
Length of standard wheel load	L_0	0.83	ft	0.25	m	AASHTO LFRD Section 3.6.1.2.5
Distribution length at depth H	L_0+LLDF*H	26.86	ft	8.19	m	
Proportion of wheel load on the pipe	w	19%		19%		[F.52] Appendix F
Stiffness of soil support	k_{soil}	190706	pcf	30000	kN/m^3	Proposed design value back-calculated from laboratory tests.
Characteristic length (beam on elastic fdtn)	λ	0.45	1/ft	1.46	1/m	[F.54] Appendix F
Live load factor	γ_L	1.75		1.75		AASHTO LFRD Table 3.4.1-1 Section 3
Wheel loads		16000	lbf	71.3	kN	Use half of a single axle
Multiple presence factor	m	1.2		1.2		AASHTO LFRD Table 3.6.1.1.2-1 Section 3
Dynamic load allowance	IM	0.0		0.0		AASHTO LFRD Section 3.6.2.2
Total factored surface force per unit length	$wP_L/(L_0$+LLDF*H)	237.7	lbf/ft	3.5	kN/m	Live load factor, multiple presence, dynamic load allowance
Earth load contribution to shear	$0.157\ W_E / \lambda$	10832.83	lbf	48.24	kN	[F.84] Appendix F
Surface load contribution to shear	wP_Lv	133.54	lbf	0.60	kN	[F.73] Appendix F
Shear force across the joint	V_{j-d}	10966.38	lbf	48.84	kN	Add earth and surface load effects

Earth load contribution to rotation	$0.0918\ W_E\lambda/(OD\ k_{soil})$	0.00125	radians	0.00125	radians	[F.83] Appendix F
Surface load contribution to rotation		0.00000	radians	0.00000	radians	[F.70] Appendix F
Rotation across the joint	$\theta_{j\text{-}d}$	0.07	degrees	0.07	degrees	Add earth and surface load effects and convert to degrees.

Figure E.8 Design calculations for 60 in. (0.9m) diameter HDPE pipe with moment release joint at 4 ft (1.2m) cover depth

Appendix F. Analytical solutions for response of joints.

CONTENTS

OBJECTIVES

The structural design of joints firstly requires evaluation of demand:

- the expected vertical shear force acting across the joint as a result of earth and live loads
- the expected rotation across moment release joints as a result of earth and live loads
- the expected bending moment across moment transfer joints as a result of earth and live loads

Once demand is established, the second part of the load and resistance factor design process involves measurement of the ability of the joint to resist those loads. Finally, joint adequacy is determined by evaluating whether factored demand is less than factored resistance.

While it is understood that joints connecting buried gravity flow pipes respond in a complex three dimensional manner, it is not considered feasible to determine expected values of force,

moment or rotation using three dimensional finite element analysis. Instead, the use of beam-on-elastic-spring modeling is adopted. The objective of this appendix is to develop exact solutions for expected shear force, longitudinal bending moment and rotation using the beam-on-elastic-spring approximation. First, solutions are developed for two rigid (concrete) pipes connected by a moment release joint. Then, solutions are developed for two flexible (corrugated metal or profiled thermoplastic) pipes connected by either a moment release or moment transfer joint.

MOMENT RELEASE JOINTS CONNECTING RIGID PIPES

Approximations

Measurements of buried reinforced concrete pipe response to surface load indicate that the high stiffness pipe segments act almost like rigid links, with their vertical movement and rotation dependent on the applied loads and the stiffness of the surrounding soil. Therefore, analyses are developed here to capture that behavior using beam-on-elastic-spring modeling without the need for finite element analysis. The objective of this appendix is to present the solution developed to

a. model two concrete pipes interacting across a moment release joint
b. provide the magnitude of the shear force acting between them, for both earth and live loads
c. provide the angle of joint rotation that develops
d. consider the possibility that the gasket used in the joint permits vertical displacement as shear force is transmitted from one pipe to the other
e. provide simplified expressions suitable for the AASHTO LFRD Bridge Design Specifications for maximum joint rotation and maximum shear force resulting from wheel loading at the ground surface
f. provide a rational approach for determining shear force and joint rotation for deep burial, and simplified expressions suitable for the AASHTO LFRD Bridge Design Specifications

General formulation

Consider the two pipes shown in Figure F.1a. The pipe on the left is supported by elastic springs of stiffness k_L having units of vertical stress per unit of spring deformation. That pipe has length L_L and is subjected to vertical force F_L at eccentricity e_L. The characteristics of the pipe on the right are similar.

The vertical deflection at the center of the left hand pipe v_L and at the center of the right hand pipe v_R, Figure F.1b, are given by

$$v_L = \frac{F_L}{OD\ L_L\ k_L} \qquad [F.1]$$

$$v_R = \frac{F_R}{OD\ L_R\ k_R} \qquad [F.2]$$

where the spring stiffness for the soil under the left and right hand pipes, in units of force per unit deflection, are $OD\ L_L\ k_L$ and $OD\ L_R\ k_R$ respectively.

Rotations also result, Figure F.1b. To calculate these rotations, consider pure rotation of a beam, Figure F.2, which produces linear distributions of spring deflection, and therefore linear distribution of soil reactions from the springs. Calculating the moment resultant associated with that $k_{soil}\ OD\ L^3\ \theta/12$, and setting this equal to the moment of applied forces ($F_L\ e_L$ and $F_R\ e_R$ on the left and right beams respectively), expressions are obtained for the rotations

$$\theta_L = \frac{12\ F_L\ e_L}{k_L OD\ {L_L}^3} \qquad [F.3]$$

$$\theta_R = \frac{12\ F_R\ e_R}{k_R OD\ {L_R}^3} \qquad [F.4]$$

Now, if the response of the two beams is independent, then the relative vertical movement across the joint is

$$v_J = \left(v_L + \frac{\theta_L\ L_L}{2}\right) - \left(v_R - \frac{\theta_R\ L_R}{2}\right) \qquad [F.5]$$

i.e.

$$v_J = \frac{F_L}{OD\ L_L\ k_L}\left(1 + \frac{6e_L}{L_L}\right) - \frac{F_R}{OD\ L_R\ k_R}\left(1 - \frac{6e_R}{L_R}\right) \qquad [F.6]$$

Now, a shear force actually develops across the joint, V_J, Figure F.1c, and the magnitude of this force will be such that vertical deflections across the joint are compatible. The incremental beam deformations that result from the shear can be calculated from the earlier equations, where $F_L = -V_J$, $e_L = \frac{L_L}{2}$, $F_R = V_J$ and $e_R = -\frac{L_R}{2}$.

$$\Delta v_L = \frac{-V_J}{OD\ L_L\ k_L} \qquad [F.7]$$

$$\Delta v_R = \frac{+V_J}{OD\ L_R\ k_R} \qquad [F.8]$$

$$\Delta\theta_L = \frac{-6\ V_J}{k_L OD\ {L_L}^2} \qquad [F.9]$$

$$\Delta\theta_R = \frac{-6\,V_J}{k_R OD\,{L_R}^2} \qquad [F.10]$$

which produces relative vertical displacement across the joint

$$\Delta v_J = \left(\Delta v_L + \frac{\Delta\theta_L\,L_L}{2}\right) - \left(\Delta v_R - \frac{\Delta\theta_R\,L_R}{2}\right) \qquad [F.11]$$

and
therefore

$$\Delta v_J = \frac{-4V_J}{OD\,L_L\,k_L} + \frac{-4V_J}{OD\,L_R\,k_R} \qquad [F.12]$$

Now, the action of the shear forces is to eliminate most of the net shear displacement across the joint (enforcing vertical compatibility) so

$$v_J + \Delta v_J = v_G \qquad [F.13]$$

where the term v_G represents the shear displacement associated with deformation of a gasket with stiffness k_G

$$k_G v_G = V_J \qquad [F.14]$$

Gasket stiffness k_G has units of force per unit length. Gasket stiffness could be measured using laboratory testing where shear force is applied across the joint.

Therefore the shear force can be evaluated from:

$$V_J = 0.25(v_J - \frac{V_J}{k_G})\,\frac{OD}{\frac{1}{L_L\,k_L} + \frac{1}{L_R\,k_R}} \qquad [F.15]$$

i.e.

$$V_J = 0.25 v_J R_G\,\frac{OD}{\frac{1}{L_L\,k_L} + \frac{1}{L_R\,k_R}} \qquad [F.16]$$

where

$${R_G}^{-1} = 1 + \frac{0.25\,OD}{k_G\left(\frac{1}{L_L\,k_L} + \frac{1}{L_R\,k_R}\right)} \qquad [F.17]$$

is a multiplier representing how gasket stiffness influences shear force across the joint. For a rigid gasket,

$$R_G = 1 \qquad [F.18]$$

while for two pipes of uniform length L on soil with uniform stiffness k_{soil}

$$R_G{}^{-1} = 1 + \frac{0.125\ OD\ L\ k_{soil}}{k_G} \quad [F.19]$$

Calculations for shear force across the joint will always be conservative when the gasket is assumed rigid and so most of the remaining discussion in this appendix is based on that assumption (i.e. $R_G = 1$) .

Now, introducing the magnitude of v_J into the expression for V_J gives

$$V_J = 0.25\ R_G \frac{\left[\frac{F_L}{L_L\ k_L}\left(1 + \frac{6e_L}{L_L}\right) - \frac{F_R}{L_R\ k_R}\left(1 - \frac{6e_R}{L_R}\right)\right]}{\frac{1}{L_L\ k_L} + \frac{1}{L_R\ k_R}} \quad [F.20]$$

The net rotation across the joint θ_J then becomes

$$\begin{aligned}\theta_J &= \theta_L - \theta_R + \Delta\theta_L - \Delta\theta_R \\ &= \frac{12}{OD}\left(\frac{F_L\ e_L}{k_L\ L_L{}^3} - \frac{F_R\ e_R}{k_R\ L_R{}^3}\right) - \frac{6\ V_J}{OD}\left(\frac{1}{k_L L_L{}^2} - \frac{1}{k_R L_R{}^2}\right)\end{aligned} \quad [F.21]$$

For the case of uniform pipe segment lengths L and uniform soil stiffness k

$$V_J = 0.125\ R_G\ OD\ L\ k_{soil}\ v_J \quad [F.22]$$

or when the expression for v_J is introduced

$$V_J = 0.125\ R_G\left[F_L\left(1 + \frac{6e_L}{L}\right) - F_R\left(1 - \frac{6e_R}{L}\right)\right] \quad [F.23]$$

Response to live load

The loading system is now divided into live (surface vehicle) loading and earth loading and these cases are treated separately. Since the equations are all linear and elastic, the total response can be obtained using superposition (summing the shear force components calculated for live and earth loading, and then the rotation components). In this section, expressions are derived for F_L, e_L, F_R, and e_R which can be used to calculate V_J and θ_J using the equations developed in the previous section.

Consider a force on the ground surface with magnitude of P_L (wheel loading increased by multiple presence factor, dynamic load allowance, and live load factor) distributed over an area featuring length L_0 parallel to the pipe axes, and width W_0 perpendicular to the pipe axes, Figure F.3. Approximating load spreading with depth using the load prism with sides at slope LLDF, pressure at depth H is

$$\frac{P_L}{(L_0 + LLDF.\ H)(W_0 + LLDF.\ H)} \quad [F.24]$$

Now, only the pressures that fall within the external pipe diameter OD act across the pipe, so the force per unit length along the pipe at depth H, is

$$F_H = \frac{w\, P_L}{L_0 + LLDF\,.\,H} \qquad [F.25]$$

where w is given by

$$w = \frac{\min\{OD, W_0 + LLDF.\,H\}}{(W_0 + LLDF.\,h)} \qquad [F.26]$$

The position of the centerline of the surface load is defined as distance x left of the pipe joint, Figure F.3. The lengths the load acts on the left and right pipelines are defined as x_L and x_R respectively, where the sum of these two values is equal to the total length over which the load acts along the pipeline,

$$x_L + x_R = L_0 + LLDF\,.\,H \qquad [F.27]$$

Now, consider the geometry of the load system, Figure F.3, where a choice is made to simplify the conditions to cases where the load is centered on or to the left of the joint (response for loads to the right can be found from these same equations with the frame of reference reversed). The length the load acts along the left hand pipe is therefore

$$x_L = \min\{\frac{L_0 + LLDF\,.\,H}{2} + x, L_0 + LLDF\,.\,H\} \qquad [F.28]$$

and this provides the total force and eccentricity of that force on the left hand pipe

$$F_L = \frac{w\, P_L}{L_0 + LLDF\,.\,H}\, x_L \qquad [F.29]$$

$$e_L = \frac{L_L}{2} - \max\{\frac{x_L}{2}, x\} \qquad [F.30]$$

Again, consideration of the loading geometry gives the length the load acts along the right hand pipe

$$x_R = \max\{\frac{L_0 + LLDF\,.\,H}{2} - x, 0\} \qquad [F.31]$$

so that

$$F_R = F_h\, x_R \qquad [F.32]$$

$$e_R = -\frac{L_R}{2} + \frac{x_R}{2} \qquad [F.33]$$

The value of e_R is immaterial when $x_R = 0$ so there is no need to adjust the expression for e_R when right force is zero.

Now, consider a surface load placed directly over the joint, the load position expected to produce maximum joint rotation, Figure F.4b. If

$$L_L = L_R = L > (L_0 + LLDF\,.\,H)/2 \quad [F.34]$$

then

$$e_L = -e_R = \frac{L}{2} - \frac{L_0 + LLDF\,.\,H}{4} \quad [F.35]$$

and

$$F_L = F_R = 0.5wP_L \quad [F.36]$$

Given that this symmetric loading produces $V_J = 0$, then

$$\theta_J = \frac{12}{OD}\left(\frac{F_L\{L - (L_0 + LLDF\,.\,H)/2\}}{k_{soil}\,L^3}\right) \quad [F.37]$$

which expressed in terms of the total surface force P_L is

$$\theta_J = \frac{6\,w\,P_L}{k_{soil}\,L^3\,OD}\{L - (L_0 + LLDF\,.\,H)/2\} \quad [F.38]$$

Now, the maximum shear force across the joint will develop when x is just large enough to bring all of the load onto the left hand pipe, Figure F.4c, i.e. $x=0.5(L_0 + LLDF\,.\,H)$. This is because placement of the load any further left will move the load closer to its left end and so reduce shear transfer to the pipe to the right, and any placement further right will reduce the load on the left pipe and increase it on the right, again reducing the magnitude of shear force transfer. This then gives

$$V_J = w\,P_L\ \{0.5 - \frac{3(L_0 + LLDF\,.\,H)}{8L}\} \quad [F.39]$$

This equation should not be used when depth is sufficient to produce $(L_0 + LLDF\,.\,H) > L$, since for that case part of the load will fall to the left of the left hand pipe.

Response to earth load

The values of force and eccentricity for pipe under soil with unit weight γ_S, load factor γ_E, and vertical arching factor VAF are

$$F_L = W_E L_L, \qquad F_R = W_E L_R \quad [F.40]$$

where

$$W_E = \gamma_E VAF\,H\,\gamma_S\,OD \quad [F.41]$$

and $$e_L = e_R = 0 \quad [F.42]$$

Substitution of these into the expressions for shear force and rotation across the joint yields

$$V_J = 0.25\, R_G\, W_E \frac{[\frac{1}{k_L} - \frac{1}{k_R}]}{\frac{1}{L_L\, k_L} + \frac{1}{L_R\, k_R}} \quad [F.43]$$

and $$\theta_J = -\frac{6\, V_J}{OD}\left(\frac{1}{k_L {L_L}^2} - \frac{1}{k_R {L_R}^2}\right) \quad [F.44]$$

For uniform lengths and soil stiffness these become

$$V_J = 0 \quad [F.45]$$

and $$\theta_J = 0 \quad [F.46]$$

which are the expected values for perfectly uniform loading.

However, consider the likely situation in the field where pipe construction practice produces stiffer soil support for one pipe compared to the other (e.g. soil support for the right hand pipe k_R is greater than for the left hand pipe k_L). For uniform pipe lengths L,

$$V_J = 0.25\, R_G\, W_E\, L \frac{\frac{k_R}{k_L} - 1}{\frac{k_R}{k_L} + 1} \quad [F.47]$$

and $$\theta_J = -\frac{1.5\, R_G\, W_E \frac{\frac{k_R}{k_L} - 1}{\frac{k_R}{k_L} + 1}}{L\ k_L OD}\left(1 - \frac{k_L}{k_R}\right) \quad [F.48]$$

When soil stiffness on the right is twice the value on the left, Figure F.4a, $\frac{k_R}{k_L} = 2$ the shear force becomes

$$V_J = R_G\, W_E\, L\, /12 \quad [F.49]$$

and the joint rotation becomes (for k_L=k_{soil})

$$\theta_J = -\frac{R_G\, W_E}{4\, L\, k_{soil}\, OD} \quad [F.50]$$

A range of results are shown in Table F.1 for other values of $\frac{k_R}{k_L}$. These indicate that even for the right hand side pipe sitting on rigid bedding, maximum shear is limited to one quarter of the total overburden load applied to the pipe.

Table F.1 Shear force across the joint and joint rotation for different bedding stiffness values.

$\frac{k_R}{k_L}$	1	2	3	5	k_R rigid
$\frac{V_J}{R_G W_E L}$	0	1/12	1/8	1/6	1/4
$\frac{\theta_J L k_L OD}{R_G W_E}$	0	-1/4	-1/2	-4/5	-3/2

Simplified design equations for Reinforced Concrete pipe

Simplified design equations have been obtained from the two-beam analysis for concrete pipe.

1. Earth loads

Equations [F.49] and [F.50] provide the shear force and rotation across the joint for the case where the stiffness of the soil on the right is twice that on the left.

2. Vehicle loads

Equations [F.38] and [F.39] provide the rotation and shear force across the joint for wheel load at the ground surface. For shallow buried pipes, this would be calculated using the fully factored wheel loading (at one end of the single axle load configuration). For deep buried pipes, it might be calculated considering construction loads of at some minimum cover height.

To back-calculate soil stiffness from laboratory or field measurements of pipe response to surface load, the rotation can be measured under central load, and then [F.38] can be used to back-calculate a soil stiffness that corresponds to observed pipe response.

Conservative nature of the 'two-beam' approximation

Figure F.5 shows the central joint being considered with three pipe segments on either side. Figure F.5a shows these in the undeformed position, and Figure F.5b shows them under the influence of a surface load. There are a number of approximations implicit in calculations based on just two pipes that act to reduce the stiffness of the system.

1. Zero moment transfer: the two-beam model assumes that moments transferred between the two beams are zero; a gasketted bell and spigot joint will feature small but not zero flexural

stiffness, and so small moments will be transferred across the joint that reduce rotations and therefore the shear force being transferred; however, the effect of the ‘zero moment approximation’ is likely small.

2. Zero restraint at the other end of the pipes: the two-beam model neglects any shear force or moment applied to the left hand end of the left pipe, and the right hand end of the right pipe; these result from restraint provided by the adjacent pipes; this additional restraint reduces the rotations so they are less than those for the two-beam approximation, and therefore the magnitude of the shear force being transferred across the central joint is overestimated by the two-beam model. This approximation likely has a larger effect on the calculations than approximation 1.

3. Infinite shear stiffness of the gasket: the two-beam model incorporates gasket compression under shear (the term R_G); if the decision is made to neglect this compliance (modeling the gasket as having infinite stiffness), conservative estimates of shear force and rotation result. Laboratory measurements for gasket stiffness k_G can be used to quantify the effect of this approximation employing equation [F.19].

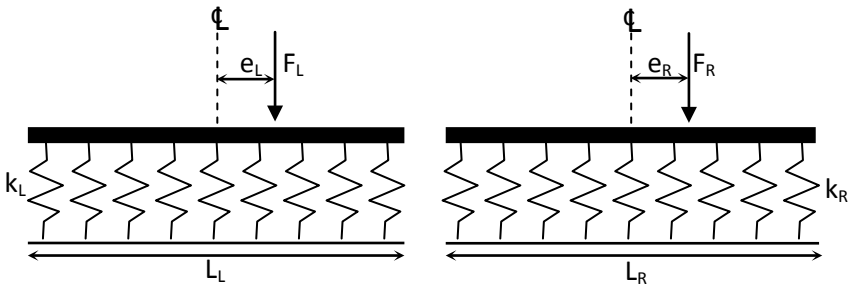

a. geometry and loading conditions

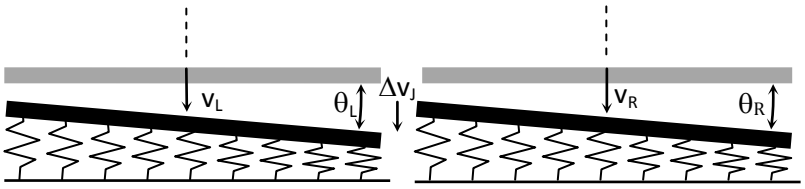

b. response if not connected at the joint

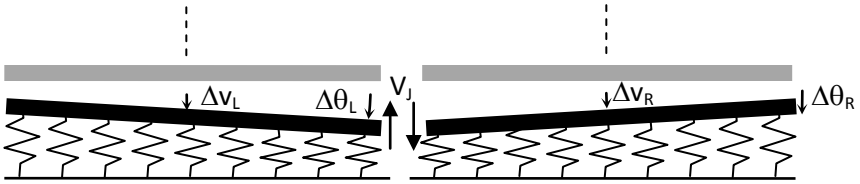

c. action of the shear force across the joint V_J making vertical deflections compatible (incremental deformations shown here with positive sign, not the sense producing compatibility across the joint)

Figure F.1 Load, deformations and shear force for two rigid pipes connected at a moment release joint.

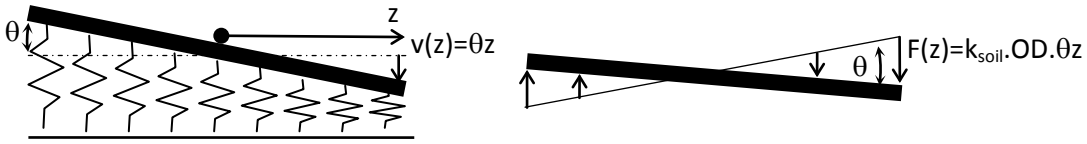

a. Linear distribution of deflections **b. Linear distribution of spring forces**

Figure F.2 Linear distributions of deflections and forces resulting from beam rotation θ.

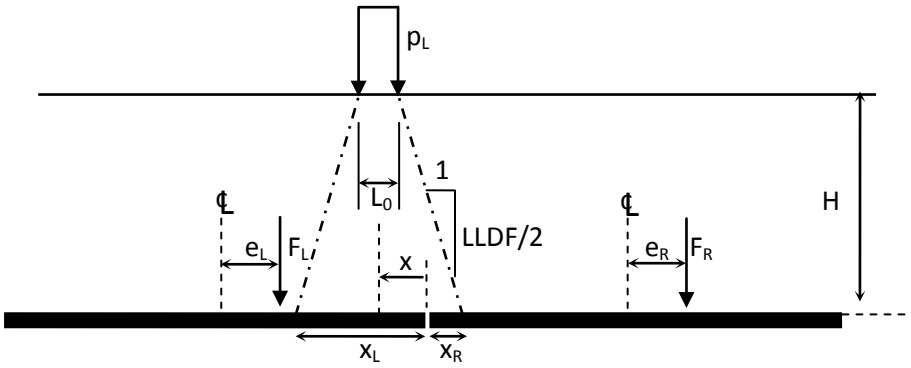

Figure F.3 Surface load reacting two rigid pipes connected at a joint.

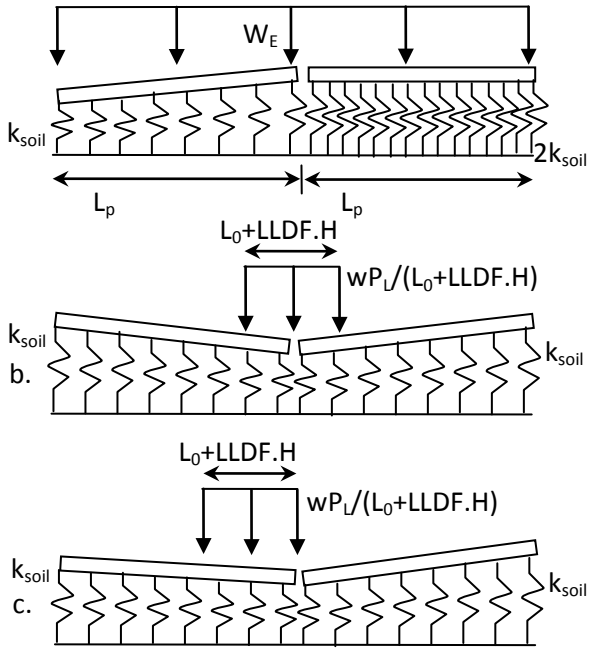

a. Earth load response

b. Surface loading for peak joint rotation

c. Surface loading for peak shear force

Figure F.4 Load cases for calculating shear force and rotation of rigid pipes with moment release joint

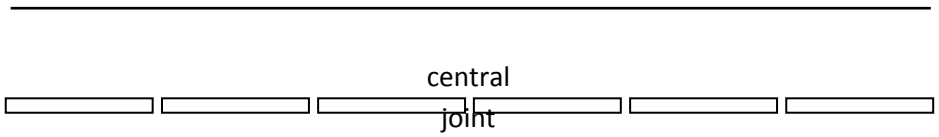

a. undeformed position, showing three pipe segments on either side of the central joint

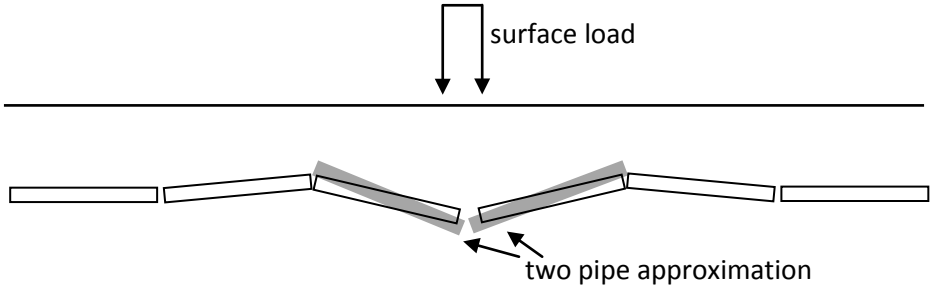

b. deformed position, showing response of six pipe system and the two pipe approximation (grey)

Figure F.5 The multiple pipe system illustrating the conservative nature of the two pipe approximation.

RESPONSE OF TWO FLEXIBLE PIPES CONNECTED BY A JOINT.

Introduction

Measurements of buried corrugated metal and thermoplastic pipe responses to surface load indicate that the very flexible pipe segments have local behavior in the vicinity of the region of surface load and the joint, but that moments, shears, and rotations quickly decay so the other ends of the pipes are not important (the length of the pipe segments has negligible impact on what happens across the joint). Therefore, analyses are developed here to capture that behavior using beam-on-elastic-spring modeling for very long ("semi-infinite") pipes without the need for finite element analysis. The solutions of Hetényi (1948)[1] are employed to achieve the following objectives:

a. model two flexible pipes interacting across either moment release or moment transfer joints
b. provide the magnitude of the shear force acting between them, for both earth and live loads
c. provide the angle of joint rotation that develops in moment release joints

[1] Hetényi, M. (1948) Beams on elastic foundation: theory with applications in the fields of Civil and Mechanical engineering, University of Michigan Press, Ann Arbor, MI, 255pp.

d. provide simplified expressions suitable for the AASHTO LFRD Bridge Design Specifications for maximum shear force and maximum rotation or moment transferred across the joint resulting from wheel loading acting at the ground surface
e. provide simplified expressions suitable for the AASHTO LFRD Bridge Design Specifications for maximum shear force and maximum rotation or moment transferred across the joint resulting from earth loads.

Response to surface loads of a moment transfer joint

Consider the pipes responding to surface load as shown in Figure F.6a. It will be conservative to assume that the longitudinal bending stiffness of a moment transfer joint is the same as the rest of the pipes, and under those circumstances, the response can be assessed as it if was a single pipe subjected to surface load. Approximating load spreading with depth using the load prism with sides at slope LLDF, the pressures that fall within the external pipe diameter OD act across the pipe and the force per unit length along the pipe at depth H, is

$$F_H = \frac{w\, P_L}{L_0 + LLDF\,.\,H} \qquad [F.51]$$

where w is given by

$$w = \frac{\min\{OD, W_0 + LLDF.\,H\}}{(W_0 + LLDF.\,h)} \qquad [F.52]$$

Now, the moment and shear can be obtained using the exact solution developed by Hetényi (1948)[2] for an infinitely long pipe subject to uniformly distributed loading F_H over the region a<c<b, Figure F.6, where moment and shear at x=c are given by

$$M_c = \frac{F_H}{4\lambda^2}(B_{\lambda a} + B_{\lambda b}) \qquad [F.53]$$

where

$$\lambda = \sqrt[4]{\frac{k_s}{4\,EI}} = \sqrt[4]{\frac{k_{soil} OD}{4\,EI}} \qquad [F.54]$$

$$B_{\lambda x} = e^{-\lambda x}\sin\lambda x \qquad [F.55]$$

and

$$V_c = \frac{F_H}{4\lambda}(C_{\lambda a} - C_{\lambda b}) \qquad [F.56]$$

where

$$C_{\lambda x} = e^{-\lambda x}(\cos\lambda x - \sin\lambda x) \qquad [F.57]$$

$$k_s = k_{soil}\, OD \qquad [F.58]$$

Now, the peak shear force and longitudinal bending moment values need to be assessed, and the moment transfer joint designed to accommodate these. To obtain peak moment, the local maximum is calculated at the turning point where gradient of M is zero, so that

[2] Hetényi (1948) p15.

$$\frac{\mathrm{dM}}{\mathrm{dc}} = \mathrm{V} = 0 \qquad [F.59]$$

This occurs at the central position where a=b, and so

$$\mathrm{M_J} = \frac{\mathrm{F_H} e^{-(\frac{\lambda L_H}{2})} \sin(\frac{\lambda L_H}{2})}{2\lambda^2} \qquad [F.60]$$

and

$$\mathrm{L_H} = \mathrm{L_0} + \mathrm{LLDF}\,.\,\mathrm{H} = 2\mathrm{a} = 2\mathrm{b} \qquad [F.61]$$

The maximum shear, however, occurs at the ends of the loaded region, where

$$\mathrm{a} = L_H,\ \mathrm{b} = 0 \qquad [F.62]$$

so that

$$\mathrm{V_J} = \frac{\mathrm{F_H}}{4\lambda}[e^{-\lambda L_H}(\cos\lambda L_H - \sin\lambda L_H) - 1] \qquad [F.63]$$

Response to surface load across a moment release joint

Now, consider the case of surface loading for pipes connected through a moment release joint, Figure F.6b. This case can be evaluated by considering the solution for two semi-infinite beams connected by the joint, where loading of width *a* acts on the pipe to the left of the joint, and width *b* on the pipe to the right of the joint. Hetényi (1948)[3] gives the deflections of a beam with loading over a length *l* adjacent to the pipe end (the joint) as

$$y = \frac{\mathrm{F_H}}{2\mathrm{k_S}}[(1 + \mathrm{B}_{\lambda l} - \mathrm{C}_{\lambda l})\mathrm{A}_{\lambda x} - (1 + 2\mathrm{B}_{\lambda l} - \mathrm{C}_{\lambda l})\mathrm{B}_{\lambda x} + (2 - \mathrm{D}_{\lambda x} - \mathrm{D}_{\lambda(l-x)})] \qquad [F.64]$$

for locations where $x \le l$. This expression can be differentiated with respect *x* to obtain rotation

$$\theta = \frac{dy}{dx} = \frac{\mathrm{F_H}}{2\mathrm{k_S}}[-2\lambda(1 + \mathrm{B}_{\lambda l} - \mathrm{C}_{\lambda l})\mathrm{B}_{\lambda x} - \lambda(1 + 2\mathrm{B}_{\lambda l} - \mathrm{C}_{\lambda l})\mathrm{C}_{\lambda x} + (\lambda\mathrm{A}_{\lambda x} - \lambda\mathrm{A}_{\lambda(l-x)})] \qquad [F.65]$$

moment

$$\frac{M(x)}{EI} = \frac{d^2y}{dx^2} = \frac{\mathrm{F_H}}{2\mathrm{k_S}}[-2\lambda^2(1 + \mathrm{B}_{\lambda l} - \mathrm{C}_{\lambda l})\mathrm{C}_{\lambda x} + 2\lambda^2(1 + 2\mathrm{B}_{\lambda l} - \mathrm{C}_{\lambda l})\mathrm{D}_{\lambda x} - (2\lambda^2\mathrm{B}_{\lambda x} + 2\lambda^2\mathrm{B}_{\lambda(\mathrm{x}-l)})] \qquad [F.66]$$

[3] Hetényi (1948) p27.

and shear

$$\frac{V(x)}{EI} = \frac{d^3y}{dx^3} = \frac{\mathrm{F_H}}{2\mathrm{k_S}}[4\lambda^3(1 + \mathrm{B}_{\lambda l} - \mathrm{C}_{\lambda l})\mathrm{D}_{\lambda x} - 2\lambda^3(1 + 2\mathrm{B}_{\lambda l} - \mathrm{C}_{\lambda l})\mathrm{A}_{\lambda x} - \left(2\lambda^3\mathrm{C}_{\lambda x} - 2\lambda^3\mathrm{C}_{\lambda(\mathrm{x}-l)}\right)] \quad [F.67]$$

where

$$\mathrm{A}_{\lambda x} = \mathrm{e}^{-\lambda x}(\cos\lambda x + \sin\lambda x) \quad [F.68]$$

and

$$\mathrm{D}_{\lambda x} = \mathrm{e}^{-\lambda x}\cos\lambda x. \quad [F.69]$$

Peak rotation occurs when half the load is on each side of the joint, $l=\frac{L_H}{2}$, the ends of each pipe deflect downwards equally, rotations are equal and opposite, and the total rotation across the joint θ_J is twice the end value for one pipe given by equation [F.64]

$$\theta_J = \frac{\mathrm{F_H}\lambda}{\mathrm{k_S}}[-2\mathrm{B}_{\lambda\frac{L_H}{2}} + \mathrm{C}_{\lambda\frac{L_H}{2}} - \mathrm{A}_{\lambda\frac{L_H}{2}}] = -\frac{4\mathrm{F_H}\lambda}{\mathrm{k_S OD}}\mathrm{e}^{-0.5\lambda L_H}\sin 0.5\lambda L_H \quad [F.70]$$

Peak shear occurs when all surface load reaches one pipe only. The maximum end deflection develops when the surface load acts right to the end, a deflection that can be obtained from [F.63] with $l=L_H$

$$y_{L_H} = \frac{\mathrm{F_H}}{2\mathrm{k_S}}\left[2 + \mathrm{B}_{\lambda L_H} - \mathrm{C}_{\lambda L_H} - \mathrm{D}_{\lambda L_H}\right] = \frac{\mathrm{F_H}}{\mathrm{k_S}}(1 + \mathrm{e}^{-\lambda L_H}(\sin\lambda L_H - \cos\lambda L_H)) \quad [F.71]$$

Now, Hetényi (1948)[4] provides the solution for the end deflection of a semi-infinite beam with a vertical force P_1 at the end, where for the current problem, the vertical force of interest is the shear force $\mathrm{V_J}$ passed across the moment release joint where the equal and opposite end shears each contribute to an end deflection equal to half of y_{L_H}

$$y_{P_1} = \frac{2\mathrm{P_1}\lambda}{\mathrm{k_S}} = \frac{2\mathrm{V_J}\lambda}{\mathrm{k_S}} = \frac{y_{L_H}}{2} \quad [F.72]$$

Solution of the second half of equation [F.72] provides the required value of the maximum shear force induced across the moment release joint

$$\mathrm{V_J} = \frac{\mathrm{F_H}}{4\lambda}[1 + \mathrm{e}^{-\lambda L_H}(\sin\lambda L_H - \cos\lambda L_H)] \quad [F.73]$$

This is the same magnitude as that for peak shear force across a moment transfer joint [F.63].

[4] Hetényi (1948) p24.

Response to earth loads

The loading per unit length W_E along a flexible pipe of external diameter OD at depth H in soil of unit weight γ_S, given load factor γ_E and vertical arching factor VAF, is

$$W_E = \gamma_E \text{VAF } H \gamma_S \text{ OD} \quad [F.74]$$

Consider two pipes with different levels of ground support, Figure F.7a. The pipe on the left has soil support characterised by k_L and the pipe on the right has soil support characterised by higher stiffness k_R. If the two pipes are not connected at the joint, Figure F.7b, a difference in vertical deflection develops, Δv_J equal to

$$\Delta v_J = W_E \left[\frac{1}{k_L} - \frac{1}{k_R}\right] \quad [F.75]$$

When the pipes are connected at the joint, the difference in displacement is eliminated by the action of moment and shear forces transferred across the joint, M_J and V_J respectively, Figure F.7b,

$$\Delta v_J = v_L + v_R \quad [F.76]$$

For a moment release joint the end moments are zero

$$M_J = 0 \quad [F.77]$$

For a moment release joint, the deformations on the left hand and right hand pipes resulting from the end shear must produce a total vertical movement of Δv_J. Reuse of the left part of [F.72] provides

$$\Delta v_J = \frac{2V_J\lambda_L}{k_L} + \frac{2V_J\lambda_R}{k_R} = W_E \left[\frac{1}{k_L} - \frac{1}{k_R}\right] \quad [F.78]$$

so

$$V_J = -\frac{W_E}{2} \frac{\frac{1}{k_L} - \frac{1}{k_R}}{\frac{\lambda_L}{k_L} + \frac{\lambda_R}{k_R}} \quad [F.79]$$

Hetényi (1948)[4] also provides the solution for rotation caused by end force P_1

$$\theta = -\frac{2P_1\lambda^2}{k_s} \quad [F.80]$$

so considering contributions from each pipe, the total rotation across the moment release joint is

$$\theta_J = W_E \frac{\frac{1}{k_L} - \frac{1}{k_R}}{\frac{\lambda_L}{k_L} + \frac{\lambda_R}{k_R}} \left(\frac{\lambda_L^2}{k_L} - \frac{\lambda_R^2}{k_R}\right) \quad [F.81]$$

For the specific case of

$$\frac{k_R}{k_L} = 2 \quad [F.82]$$

then

$$\theta_J = \frac{W_E \lambda_L}{k_L} \frac{1 - 2^{-0.5}}{2 + 2^{0.25}} \approx 0.0918 \frac{W_E \lambda_L}{k_L} \quad [F.83]$$

and

$$V_J = \frac{W_E}{\lambda_L (4 + 2^{1.25})} \approx 0.157 \frac{W_E}{\lambda_L} \quad [F.84]$$

For moment transfer joint, the deformation equality [F.76] still holds, and rotations at the ends of each pipe are identical (assuming that the coupling has longitudinal bending stiffness equal to the pipes themselves)

$$\theta_L = \theta_R \quad [F.85]$$

Now, consider the moment M_J and shear V_J producing rotation and deflection at the point where the soil stiffness changes. Hetényi (1948)[5] provides solutions for the impact of force P_1 and moment M_1:

$$y_{P_1} = \frac{2P_1\lambda}{k_s} \quad [F.86]$$

$$\theta_{P_1} = -\frac{2P_1\lambda^2}{k_s} \quad [F.87]$$

$$y_{M_1} = -\frac{2M_1\lambda^2}{k_s} \quad [F.88]$$

$$\theta_{M_1} = \frac{4M_1\lambda^3}{k_s} \quad [F.89]$$

The total magnitude of deflections must equal the difference that develops due to the change in soil stiffness,

[5] Hetényi (1948) p24-25.

$$\frac{2V_J\lambda_L}{k_L}+\frac{2V_J\lambda_R}{k_R}-\frac{2M_1\lambda_L^2}{k_L}-\frac{2M_1\lambda_R^2}{k_R}=W_E\ [\frac{1}{k_L}-\frac{1}{k_R}] \qquad [F.90]$$

and these actions also produce rotations of equal magnitude

$$-\frac{2V_J\lambda_L^2}{k_L}-\frac{4M_1\lambda_L^3}{k_L}=-\frac{2V_J\lambda_R^2}{k_R}+\frac{4M_1\lambda_R^3}{k_R} \qquad [F.91]$$

Equation [F.91] can be used to determine the relationship between shear force and moment:

$$M_1=0.5\ V_J\frac{\frac{\lambda_R^2}{k_R}-\frac{\lambda_L^2}{k_L}}{\frac{\lambda_R^3}{k_R}+\frac{\lambda_L^3}{k_L}} \qquad [F.92]$$

And substitution of this into [F.90] produces

$$V_J=W_E\frac{\frac{1}{k_L}-\frac{1}{k_R}}{2\left(\frac{\lambda_L}{k_L}+\frac{\lambda_R}{k_R}\right)+\frac{(\frac{\lambda_R^2}{k_R}-\frac{\lambda_L^2}{k_L})^2}{\frac{\lambda_R^3}{k_R}+\frac{\lambda_L^3}{k_L}}}$$

and

$$M_1=0.5\ W_E\frac{\left(\frac{1}{k_L}-\frac{1}{k_R}\right)(\frac{\lambda_R^2}{k_R}-\frac{\lambda_L^2}{k_L})}{2\left(\frac{\lambda_L}{k_L}+\frac{\lambda_R}{k_R}\right)(\frac{\lambda_R^3}{k_R}+a\frac{\lambda_L^3}{k_L})+\ (\frac{\lambda_R^2}{k_R}-\frac{\lambda_L^2}{k_L})^2}$$

For the specific case of

$$\frac{k_R}{k_L}=2 \qquad [F.93]$$

then

$$V_J=\frac{W_E}{\lambda_L}\frac{0.5}{2\ (1+2^{-0.75})+\frac{(2^{-0.5}-1)^2}{2^{-0.25}+1}}\approx 0.154\frac{W_E}{\lambda_L} \qquad [F.94]$$

and

$$M_1=0.5\frac{V_J}{\lambda_L}\frac{2^{0.5}-2}{2^{0.75}+2}\approx -0.0123\frac{W_E}{\lambda_L^2} \qquad [F.95]$$

However, while maximum shear occurs at the point where soil stiffness changes, this is not the location of maximum moment. That occurs some distance away from the stiffness transition (over the lower stiffness soil). To obtain the maximum moment, the expressions for moment and

shear force in the beam over the lower stiffness soil are assembled from Hetényi's expressions for these stress resultants due to the shear force P_1 and moment M_1 at that transition point

$$V = -P_1 C_{\lambda x} - 2\,\lambda_L M_1 B_{\lambda x} \qquad [F.96]$$

and

$$M = -\frac{P_1}{\lambda_L} B_{\lambda x} + M_1 A_{\lambda x} \qquad [F.97]$$

The point of maximum moment is located at the turning point, that is where the gradient of moment (the shear force) is zero. Solving [F.96] for V=0 gives

$$P_1(\cos\lambda x - \sin\lambda x) = -2\lambda_L M_1 \sin\lambda x \qquad [F.98]$$

so

$$\tan\lambda x = \frac{P_1}{P_1 - 2\lambda_L M_1} \qquad [F.99]$$

and for $\frac{k_R}{k_L} = 2$ this yields

$$\tan\lambda x \approx \frac{0.154}{0.154+2 \text{ x } 0.0123} \text{ and therefore } \lambda x \approx 0.712 \qquad [F.100]$$

Substitution into [F.97] then provides the maximum moment

$$M_J = -\frac{P_1}{\lambda_L} e^{-\lambda x} \sin\lambda x + M_1 e^{-\lambda x}(\cos\lambda x + \sin\lambda x) \approx 0.0580 \frac{W_E}{\lambda_L^2} \qquad [F.101]$$

Back-calculation of soil stiffness from laboratory and field observations

The solutions which have been presented permit shear force, moment, and rotation to be estimated provided pipe geometry, loading conditions, and soil stiffness are known. However, one limitation of beam-on-elastic-spring modeling is that the soil stiffness is not an independent soil parameter. Rather, it is a model dependent parameter that is a function of the soil, structural and geometrical conditions of the problem. The best approach to estimating this parameter is to back-calculate it from laboratory and field measurements of pipe response under surface load. However, it is either very difficult or impossible to measure moment and shear force in test pipes without changing the pipe characteristics and therefore the readings. A better approach is to use back-calculated soil stiffness from observations of the pipe deformations. For moment release joints, this can involve surface loading centered over the pipe joint, and use of [F.90] and measurement of the rotation that develops across the joint. However for moment transfer joints, the rotation across the joint is close to zero. Therefore, a beam-on-elastic-spring solution is needed for vertical deformation under surface load so that observations of vertical movement

under the center of the loaded region of length L_H can be employed. Hetényi (1948)[2] provides the deformations for the general case

$$y = \frac{F_H}{2k_S}(2 - D_{\lambda a} - D_{\lambda b}) \quad [F.102]$$

Deflection at the central position where a=b=L_H/2 are then

$$y = \frac{F_H(1 - e^{-(\frac{\lambda L_H}{2})}\cos(\frac{\lambda L_H}{2}))}{k_S} \quad [F.103]$$

Numerical calculations to check the solutions

Finite element analyses have been performed to check each of these solutions. The results are presented in Table F.2. These calculations were performed using consistent SI units and US Customary equivalents are not provided.

Two pipes three metres long have been used in the calculations with elements of length 0.1m. The corrugated steel pipe being considered has external pipe diameter OD of 0.94m, flexural rigidity EI of 700 kN.m^2 and axial stiffness EA of 700000 kN. The value of spring stiffness of the soil used was k_{soil} = 25,000 kN/m^3. Multiplying k_{soil} by OD, a soil stiffness per unit length k_L of 235 kN/m^2 is obtained, and since finite elements of length 0.1 m are used, the stiffness of the soil spring under each node is given by 23.5 kN/m. For live load calculations, the soil stiffness under the right hand pipe is set to the same amount. For earth load calculations, the soil stiffness per unit length under the right hand side is doubled.

The live load example features burial of the springline at 0.61 m. Loading on a standard wheel pair of 71 kN is considered acting on the ground surface over an area 0.25 m by 0.51 m (the standard geometry of a wheel pair). Using a live load distribution factor LLDF of 1.15 (the value for granular backfill), live load factor of 1.75, impact factor of 24.8, and multiple presence factor of 1.2, the total force per unit length along the pipe is 152 kN/m. The vertical shear force acting across the joint, the bending moment acting across a moment transfer joint, and the rotation across a moment release joint are calculated using equations [F.60], [F.63], [F.70] and [F.73], and the results are shown in Table F.2.

The earth load example features burial to 6.1m depth in soil with unit weight of 22 kN/m^3. Considering an earth load factor of 1.3 and a vertical arching factor for corrugated steel pipe of 1.1 (while this value is appropriate for a corrugated steel pipe, the AASHTO value of 1.0 is proposed for use in design and has been employed in the examples presented in Appendix E). These produce load per unit length of 180.3 kN/m. The vertical shear force acting across the joint, the bending moment acting across a moment transfer joint, and the rotation across a

moment release joint are calculated using equations [F.83], [F.84], [F.94] and [F.101], and the results are also given in Table F.1.

Most results from the simplified equations and the finite element analyses are close (within 10%). However, finite element analyses for joint rotations are more sensitive to the discretisation (number and size of the finite element), so the numerical errors are higher.

Table F.2 Design values of shear force, bending moment and rotation across moment release and moment transfer joints, as calculated using design equations and finite element analyses; equation numbers are shown in square brackets []; percent difference of finite element values compared to design equations are also given.

	Shear force kN		**Bending Moment** kN.m		**Rotation** degrees	
Case	FEA	Equation	FEA	Equation	FEA	Equation
Live load – Release	26.7 -1.1%	27.0 [F.73]	Not applicable	Not applicable	0.76 -6.1%	0.81 [F.70]
Live load – Transfer	26.8 -0.6%	27.0 [F.63]	8.41 -1.1%	8.50 [F.60]	Not applicable	Not applicable
Earth load – Release	16.5 -0.5%	16.6 [F.84]	Not applicable	Not applicable	0.057 -17%	0.069 [F.83]
Earth load – Transfer	16.9 3.0%	16.4 [F.94]	3.22 (0.79[6]) -11% (4%)	3.61 (0.76) [F.101] ([F.95])	Not applicable	Not applicable

[6] Values in parentheses are the moment calculated at the joint when the change in soil stiffness occurs at the joint.

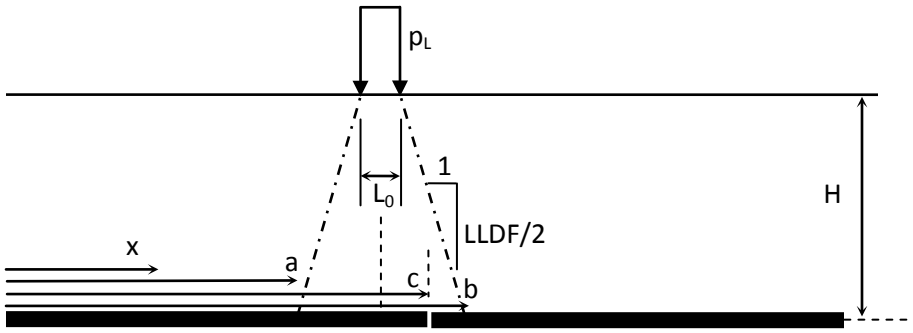

a. surface load on two buried pipes

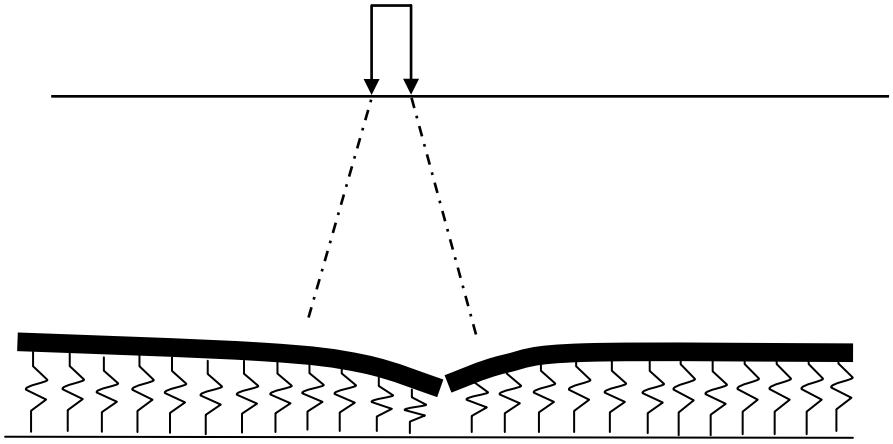

b. deformations for two pipes with moment release joint

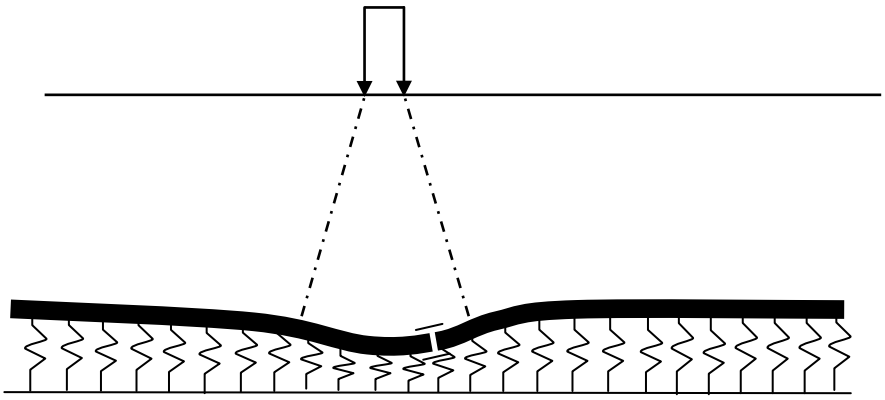

c. deformations for two pipes with moment transfer joint

Figure F.6 Surface load and deformations for two flexible pipes connected at moment release or moment transfer joints

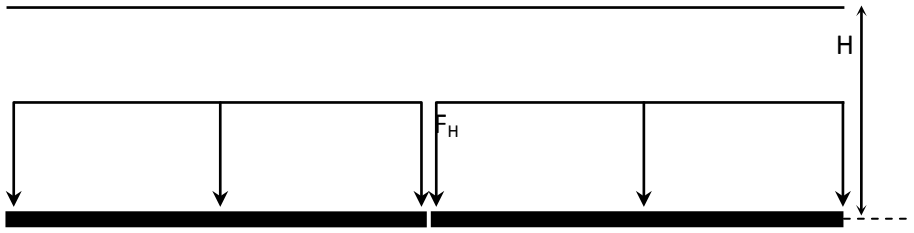

a. earth loads

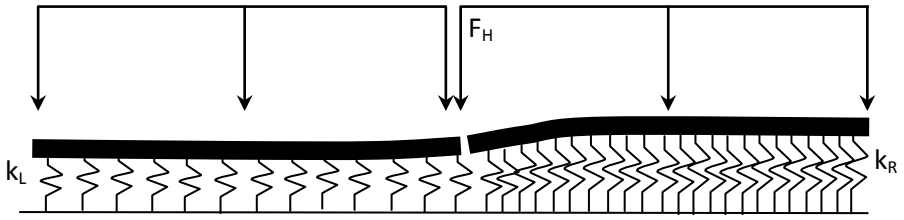

b. deformations for two pipes with changing soil support and moment release joint

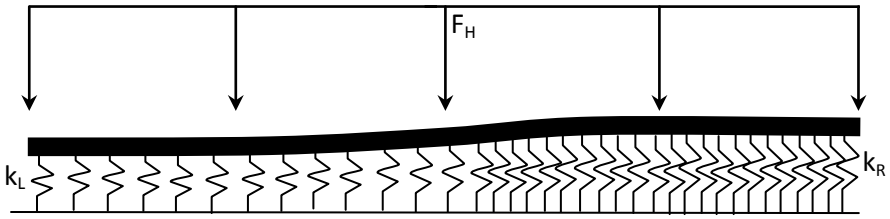

c. deformations for two pipes with changing soil support and moment transfer joint

Figure F.7 Earth loads acting on two flexible pipes supported by two different bedding stiffnesses.

12.5.3 STRENGTH LIMIT STATE

Buried structures and tunnel liners shall be investigated for construction loads and at Strength Load Combinations I and II, as specified in Table 3.4.1-1, as follows:

For metal structures:

… add

- joint failure

For concrete structures:

… add

- joint failure of pipes only

For thermoplastic pipe:

… add

- joint failure

12.5.5 Resistance Factors

…

Table 12.5.5-1 Resistance factors for buried structures

Structure Type	Resistance Factor
Metal Pipe, Arch, and Pipe Arch Structures	
Helical pipe with lock seam or fully welded seam: … • Minimum pipe joint strength – simplified design model • Minimum pipe joint strength – design using beam on spring model	 0.67[1] 0.67
Reinforced Concrete Pipe	
Direct Design Method … • Minimum pipe joint strength – simplified design model • Minimum pipe joint strength – design using beam on spring model	 0.67 0.67
Thermoplastic Pipe	
PE and PVC pipe … • Minimum pipe joint strength – simplified design model • Minimum pipe joint strength – design using beam on spring model	 0.67 0.67

[1] Value is that already used for longitudinal seam strength.

12.6.2 Service Limit State

C12.6.2

… add

12.6.2.2 Settlement

12.6.2.2.1 General

The effect of longitudinal differential settlement on structural requirements of joints shall be determined as specified in Article 12.6.2.2.2. Other effects of differential settlement shall be determined as specified in Article 10.6.2:

- Differential settlement between the pipe and the backfill, and
- Settlement of footings and unbalanced loading of skewed structures extending through embankment slopes.

12.6.2.2.2 Longitudinal Effects on joints

The effect on joints of differential settlement along the length of buried pipes shall be determined as specified in Article 12.15. Longitudinal differential settlement for other structures shall be determined in accordance with Article 10.6.2.4. Pipes and culverts shall be fitted with joints to resist shear force and bending moments meeting the requirements of Section 12.15.

C12.6.2.2.2

Specific calculation procedures are available for longitudinal differential settlements across joints in concrete, corrugated steel and thermoplastic pipes.

…

12.15 DESIGN OF PIPE JOINTS

12.15.1 Moment release and moment transfer joints

Structural design of culvert joints must consider the stress resultants and deformations that can develop across the joint, and ensure these do not exceed the capacity of the joint. Structural design will consider two classes of joints:

I. Moment release joints (joints that permit rotation but do not transfer moment):

II. Moment transfer joints (joints that transfer moment but do not permit rotation):

C12.15.1

Examples of moment release joints include bell and spigot joints with or without gasket or flexible sealant.

Examples of moment transfer joints include band joints with and without sealing systems.

12.15.2 Circumferential performance

Culvert joints should be designed to withstand hoop thrust, circumferential bending moment, and ovaling deflection. This shall be undertaken using procedures outlined in Sections 12.7, 12.10, and 12.12.

C12.15.2

Components requiring assessment for circumferential performance under external earth and vehicle loads include the bells in bell and spigot joints, and the pipe ends to be covered with band connections.

12.15.3 Capacity of joint to transfer force and moment

All joints shall be designed to carry vertical shear force $V_{j\text{-}d}$ (lbf, kN), the vertical shear force acting across the joint. Moment-transfer joints must also be able to carry the longitudinal moment across the joint $M_{j\text{-}d}$ (lbf.ft, kN.m).

These stress resultants ($V_{j\text{-}d}$ and $M_{j\text{-}d}$) shall be calculated using one of two different procedures, either

- simplified equations based on interaction between two segments, or
- beam-on-spring modeling for multiple segments and joint systems.

C12.15.3

The expectation is that the simplified procedure which considers two pipe segments interacting at a joint (with other segments neglected), will produce higher values of shear force and moment, since it neglects the restraint to those two segments coming from the other segments they are connected to. Beam-on-spring modeling can account for factors such as :

- more than two segments, and therefore the restraint provided to each end of the segments considered on either of the joint being designed
- the non-zero rotational stiffness and finite (not infinite) shear stiffness for moment release joints
- the finite (not infinite) flexural and shear stiffness of moment-transfer joints.

12.15.4 Capacity to accommodate shear and rotation

The joint shall accommodate deformations associated with longitudinal differential settlement. This includes shear rotation $\theta_{j\text{-}d}$ (degrees) and displacement $\delta_{j\text{-}d}$ (in., mm).

These deformations ($\theta_{j\text{-}d}$ and $\delta_{j\text{-}d}$) shall be calculated using two different procedures, either

a. simplified equations based on interaction between two segments, or
b. beam-on-elastic-spring modeling.

C12.15.4

The expectation is that the simplified procedure will produce higher values of shear displacement and rotation, since it neglects the effects described in C12.15.3.

12.15.5 Vehicle loads and earth loads

Factored vertical earth pressures at the crown resulting from earth loads shall be calculated using the procedures for concrete, corrugated steel and thermoplastic pipes:

W_E = γ_E VAF γ_s OD H (lbf/ft, kN/m), for

γ_E = load factor for earth load

VAF = vertical arching factor

γ_s = unit weight of soil (pcf, kN/m^3)

OD = outside diameter (ft, m)

H = height of fill over pipe springline (ft, m)

Factored surface load P_L shall be calculated using the procedures in Section 3, where

P_L = total factored surface load for a wheel pair at the axle end (lbf, kN)

The portion of that surface load that reaches the pipe and its distribution will be calculated considering live load spreading in Section 3.6.1.2.6. The proportion w that acts across the pipe is a function of the outside diameter of the pipe relative to the spreading width at the depth of the pipe springline H:

For _____

w = _____

or else

w =

C12.15.5

The same loadings used to examine circumferential limit states are employed for joint calculations. Live loads are based on calculations in Section 3.6.1.2.6. Earth loads are based on vertical arching factors VAF

- in Section 12.10.2.1 for reinforced concrete pipes
- in Section 12.12.3.4 for thermoplastic pipes
- a value of 1.0 for corrugated steel pipes

For pipes featuring external surface of cylindrical shape (e.g. reinforced concrete, profiled thermoplastic pipes featuring a external surface parallel to the pipe axis), then OD is simply the external diameter of the pipe.

For pipes featuring corrugated external surface, then OD is the average diameter of that external surface.

P_L includes consideration of live load factor, dynamic load allowance, and multiple presence factor.

Since the pipe is being modeled as a beam-on-elastic springs, the elevation of the pipe springline is equivalent to the neutral axis of the equivalent beam, and live loads and earth loads are calculated relative to that elevation.

for

W_0 = width of load transverse to pipe axis (ft, m)

LLDF = live load distribution factor

12.15.6 Simplified design models

12.15.6.1 Rigid (reinforced concrete) pipes

The simplified design model considers the two rigid pipe segments illustrated in Figure 12.15.6.1. These feature:

L_p = length of the pipe segments from joint centerline to joint centerline (ft, m)

k_{soil} = soil stiffness = 30000 kN/m^3 = 191000 pcf

k_G = shear stiffness of the gasket (lbf/in, kN/mm)

L_0 = length of surface load (ft, m)

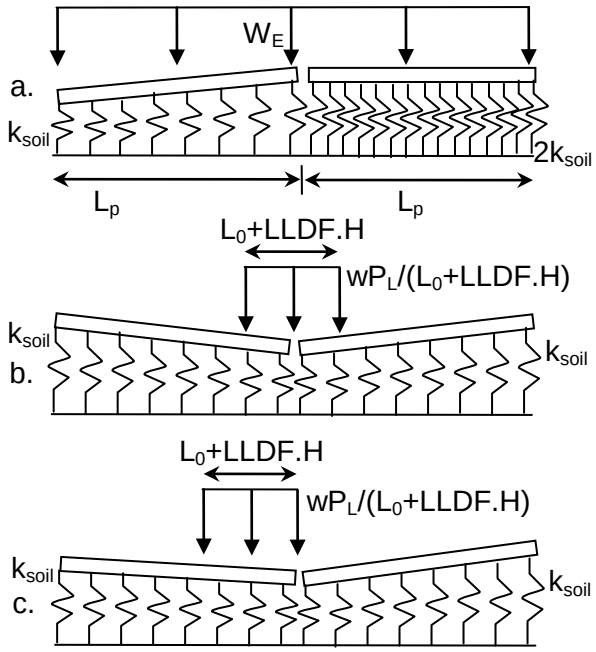

a. Earth load response
b. Vehicle loading for peak joint rotation
c. Vehicle loading for peak shear force

Figure 12.15.6.1 Load cases for calculating shear force and rotation across moment release joints in rigid pipes.

Design value of shear force across the joint is:

$V_{j\text{-}d}$ = 0.083 W_E L_p + w P_L v (lbf, kN)

where

C12.15.6

C12.15.6.1

Buried pipe experiments and analyses (Moore et al., 2012[2]) have been performed to investigate the nature of shear and moment transfer across joints in rigid and flexible pipe. These experiments have been used to develop both the simplified and the beam-on-elastic-spring procedures. The k_{soil} value here (expressed as force per unit length per unit area under the pipe) is a lower bound value back-calculated from the experiments.

For simplified design, rigid pipes are designed considering the behavior of one pipe on either side of the moment release joint. It is assumed that the joint has zero rotational stiffness (no moment is transferred across the joint).

For earth loading shown in Figure 12.15.6.1a, shear force across the joint and rotation only develop if the system is imperfect. The simplified design model considers the case where the soil stiffness supporting the pipe on one side of the joint is double that on the other side of the joint (as a result of changes in construction practice). Other stiffness changes have been examined by Moore et al. (2012[2]).

For vehicle loads, the maximum rotation is calculated considering a wheel pair centered over the joint, Figure 12.15.6.1b, since this produces the largest joint rotation. The maximum shear force occurs when the wheel load just falls onto one of two pipes, Figure 12.15.6.2b.

[2] This reference will likely be the final project report for NCHRP 15-38.

$v = \left|0.5 - \frac{3(L_0+LLDF.H)}{8L_P}\right|$

Design value of rotation across the joint is

$\theta_{j\text{-}d} = \frac{180}{\pi}\{0.25\frac{W_E}{k_{soil}\, L_P\, OD} + \frac{6\, w\, P_L\, r}{k_{soil}\, L_P^3\, OD}\}$ (degrees)

for

$r = L_P - (L_0 + LLDF.H)/2 \prec 0$ (ft, m)

Design value of shear displacement across the joint is

$\delta_{j\text{-}d} = \frac{V_{j-d}}{k_G}$ (in., mm)

The shear force transferred across the joint and rotation are calculated neglecting any compression of the gasket under shear. That value of shear force can then be used to estimate shear displacement if the finite shear stiffness of the gasket is known.

12.15.6.2 Flexible pipes

The simplified design models consider the two flexible segments illustrated in Figure 12.15.6.2. These feature:

EI = longitudinal bending stiffness of whole pipe responding as a beam (lbf.ft^2, kN.m^2)

k_{soil} = soil stiffness = 30000 kN/m^3 = 191000 pcf

$\lambda = \sqrt[4]{\frac{k_{soil}\, OD}{4\, EI}}$ (1/ft, 1/m)

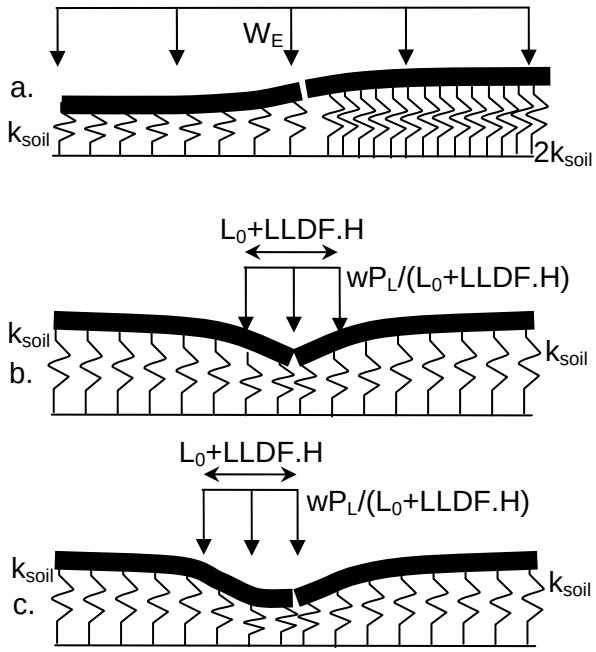

a. Earth load response

b. Vehicle loading for peak rotation (or moment)

c. Vehicle loading for peak shear force

Figure 12.15.6.2 Load cases for calculating shear force and moment or rotation across joints in flexible pipes

C12.15.6.2

Laboratory experiments conducted on corrugated steel, PVC and HDPE pipes demonstrate that deformations in flexible pipes resulting from surface live loads attenuate rapidly away from the location of load application. As a result, while surface loads in the vicinity of a joint connecting two shallow buried pipe segments influence that joint, the deformations become negligible at the other ends of the two pipe segments. Simplified design solutions for shear, moment and rotation have therefore been developed assuming the two pipe segments to be very long, and joint response unaffected by either the location or characteristics of other joints along the pipeline. The design equations were developed by Moore et al. (2012) from solutions for beams on elastic foundations from Hetényi (1948).[3]

Both moment release and moment transfer joints were considered. Equations for moment transfer joints were developed considering the joint as having the same longitudinal bending characteristics as the pipe barrels. This should produce conservative estimates of moment and shear force for joints with lower stiffness. Equations for moment release joints were developed considering the joint as

[3] Hetényi (1948) Beams on elastic foundation: theory with applications in the fields of Civil and Mechanical engineering, University of Michigan Press, Ann Arbor, MI, 255pp.

Design values for shear force and bending moment across a moment transfer joint are:

$$V_{j\text{-}d} = 0.154\frac{W_E}{\lambda} + \frac{w\ P_{L\ v}}{L_0 + LLDF\ H}\ \text{(lbf, kN)}$$

where

$$v = \left|\frac{1+e^{-\lambda L_H}(\sin\lambda L_H - \cos\lambda L_H)}{4\lambda}\right|$$

$$M_{j\text{-}d} = 0.058\frac{W_E}{\lambda^2} + \frac{w\ P_{L\ m}}{L_0 + LLDF\ H}\ \text{(lbf.ft, kN.m)}$$

where

$$m = \left|\frac{e^{-\frac{\lambda L_H}{2}}\sin\frac{\lambda L_H}{2}}{2\lambda^2}\right|$$

Design values for shear force and rotation across a moment release joint are:

$$V_{j\text{-}d} = 0.157\frac{W_E}{\lambda} + \frac{w\ P_{L\ v}}{L_0 + LLDF\ H}\ \text{(lbf, kN)}$$

$$\theta_{j\text{-}d} = \frac{180}{\pi}\left\{0.0918\frac{W_E\lambda}{k_S OD} + \frac{w\ P_{L\ r}}{L_0 + LLDF\ H}\right\}\ \text{(degrees)}$$

where

$$r = \left|\frac{4\lambda}{k_S OD}e^{-\frac{\lambda L_H}{2}}\sin\frac{\lambda L_H}{2}\right|$$

having zero rotational stiffness and zero gasket compression under shear.

C15.7.2 includes discussion on how to determine EI for the pipe.

The parameter λ is the inverse of a characteristic length that controls the attenuation of deformations along a buried flexible pipe, and the extent to which the loads produce shear and bending or rotation across a joint.

For earth loading shown in Figure 12.15.6.2a, shear force across the joint and moment or rotation only develop if the system is imperfect. The simplified design model considers the case where there is a sudden transition of soil stiffness from the normal design value, to one twice as large (as a result of changes in construction practice). Other stiffness changes have been examined by Moore et al. (2012). Maximum shear force and maximum rotation occurs when the joint is at the point immediately above the transition in soil stiffness. However, maximum moment in moment transfer joints occurs when the joint is a distance $0.712/\lambda$ before the transition in to higher soil stiffness.

For vehicle loads, the maximum rotation in moment release joints or maximum moment in moment transfer joints is calculated considering a wheel pair centered over the joint, Figure 12.15.6.2b. The maximum shear force occurs when the wheel load just falls onto one of two pipe segments, Figure 12.15.6.2c.

12.15.7 Beam-on-Elastic-Spring Analysis

12.15.7.1 Geometry

Finite element analysis is performed using any conventional structural analysis program, with the buried pipes and their joints represented by a series of beam elements, Figure 12.15.7.1. The analysis features consideration of two or more complete pipe segments and the joints between them and at their ends.

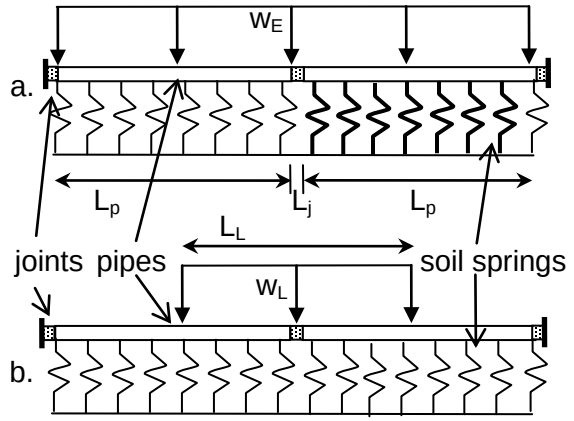

a. Earth load analysis
b. Vehicle load analysis (centered load example)

Figure 12.15.7.1 Geometry used in beam-on-elastic-spring analysis of two jointed pipe segments

The joint length should be selected, either the gap between the two pipe ends or some nominal value associated with the length of the band connector or the pipe bell. Then the elements for the remainder of the pipe should be set, which

12.15.7.2 Stiffness of the beam elements

The longitudinal bending stiffness of the beam elements representing the pipe is used to capture the longitudinal bending characteristics of the pipe barrel, EI_{pipe}, considering it as acting like a beam. The longitudinal bending stiffness of the beam elements representing the joints is used to capture the resistance of the joint to rotation.

C12.15.7

C12.15.7.1

The analysis features two complete pipe segments and the joints between them and on each end. Since springs are being used to represent the ground, there is no load transfer by shear or foundation settlement through the soil associated with other more distant pipe segments. That means only the outer joints are available to impose the effects of load from any pipe segments beyond the two centered on the joint being examined.

This assumption is reasonable for both rigid and flexible pipes. Figure C12.15.7.1a shows how for rigid pipes, the high flexural stiffness ensures the pipe segments deform like rigid beams. The response beyond the ends of the two segments on either side of the joint is small and can be neglected. The low flexural stiffness of corrugated steel and thermoplastic pipes means that the deformations localize near the joint, and the other ends of those pipe segments have little or no impact on the response, Figure C12.15.7.1b.

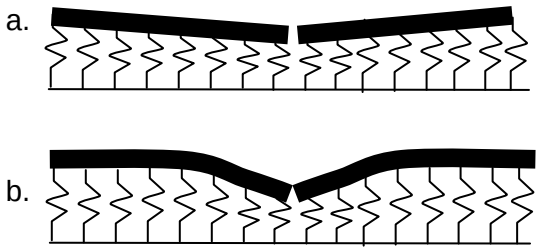

a. Rigid pipe segments rotate like rigid bodies
b. Flexible pipe segments experience localized deformation

Figure C12.15.7.1 Deformation patterns at pipe joints

C12.15.7.2

Flexural rigidity EI_{pipe} can be calculated for plain pipe as:

$EI_{pipe} = E_{pipe} \pi (OD^4-ID^4)/64$ (lb.in^2, N.mm^2)

where:

For moment release joints, the flexural rigidity of the joint can be set equal to 1/20th of the flexural rigidity of the pipe, or the value of stiffness back-calculated from a pipe joint rotation test. A value of 1/20th of the flexural rigidity of the pipe is sufficiently small to ensure that the pipe deformations on either side of the joint are not influenced by joint stiffness (any further reduction in stiffness is not likely to influence the deformations).

For moment transfer joints, the flexural rigidity of the joint can be set as equal to the flexural rigidity of the pipe or the value back-calculated from pipe joint tests. If the flexural rigidity is higher than that of the real connection, it should produce conservative calculations of the moment being passed across the joint.

12.15.7.3 Stiffness of the soil springs

Unless site specific data is available, the soil stiffness is set equal to

k_{soil} = vertical earth pressure per unit deformation

= 191000 pcf = 30000 kN/m^3

The springs representing the soil support provided to each node along the structure need to be calculated, with units of force per unit deformation:

$k_{spring} = k_{soil}$ OD L_{elem} (lb/ft, kN/m)

where:

OD = mean diameter of the soil-pipe boundary defined in Section 12.5.5 (ft, m)

L_{elem} = average length of the two beam elements on either side of the node being considered (ft, m)

E_{pipe} = modulus of the pipe material (psf, kPa)

ID = internal pipe diameter (ft, m)

Pipe bending tests can be performed by loading a corrugated or profiled pipe in four-point bending, and the EI_{pipe} back-calculated from the measured deformation. Alternatively, some calculation procedures have been developed considering the corrugated or other wall geometry (e.g. Moore et al., 2012).

C12.15.7.3

Moore et al. (2012) report on tests of concrete, corrugated steel, HDPE and PVC pipes buried in sandy gravel to depths over the crown of 2ft (0.6m) and 4ft (1.2m). Pipe response at the joint was measured under a simulated wheel pair (one end of an axle) applied at the ground surface over the joints, and then two additional tests where the wheels were positioned 3 ft (0.9m) on one side of the joint, and then 3 ft (0.9m) on the other side. Each of these tests was then examined using beam-on-elastic-spring analysis, and the spring stiffness back-calculated for each test, to reproduce the measured response. A range of k_{soil} values was obtained (falling between 26 and 190 MN/m^3). The value recommended here for use in design calculations is a reasonable conservative value for that soil stiffness. For comparison, Terzaghi (1943) provides values of 13, 41 and 157 MN/m^3 for surface loads acting on loose, medium dense and dense sand deposits, respectively.

Spring stiffness used under each node in the finite element analysis has units of force per unit deformation. This is calculated by considering the horizontal area under the pipe represented by the node. Stiffnesses of the soil springs will vary along the pipe. For example, stiffness adjacent to the joints will be lower if the joint element is shorter.

For earth load calculations, the stiffness of springs are doubled to represent the zone where soil stiffness is doubled. Greater stiffness increases can be assessed if higher stiffness changes need to be considered.

12.15.7.4 Boundary conditions

The outside ends of the left hand and right hand joint elements are restrained against vertical movements and rotation. The base of each soil spring is restrained against vertical movement and rotation.

C12.15.7.4

The analysis will also need to feature one node fixed against horizontal movement. This can be any node in the mesh.

12.15.7.5 Analysis of earth loads

Earth load analysis is performed by considering the soil-supported pipe system where changes in soil stiffness occur during construction. A stiffness change of at least two should be considered to produce shear, moment and rotation under earth loads.

C12.15.7.5

The earth load analysis case should be considered separately from the live load case, since it involves increasing the soil stiffness at or near the joint which would not lead to conservative estimates of live load response. Changes in soil stiffness are discussed further in C12.15.6.2.

12.15.7.6 Analysis of vehicle loads

The location of the vehicle load should be considered in at least the two positions shown in Figures 12.15.6.1 and 12.15.6.2 so as to obtain the maximum shear and rotation or moment.

C12.15.7.6

The vehicle load analysis case will consider uniform soil stiffness.

Appendix H. Joint testing frame for measuring the structural capacity of joints.

Contents

H.1 Introduction

Project 15-38 to develop structural design requirements for culvert joints has primarily focused on determining demand (expected shear force, rotation or bending moment) acting across moment release and moment transfer joints between rigid and flexible pipes, considering the effect of both live loads and earth loads. However, to complete the structural design assessment of joints, measurements are needed of the capacity (the strength or resistance) of the joint to accommodate the demands (the second key step in the design process). This appendix outlines the testing frame developed to undertake those assessments. First, the objectives of the test frame design and the approximations employed are outlined. Next, the schematics of the frame are provided. Finally, tests on three representative pipes are presented – a 24 inch (0.6 m) diameter reinforced concrete pipe with gasketted bell and spigot joint, a 36 inch diameter corrugated steel pipe (CSP) with hugger band joint, and a 36 inch diameter PVC pipe with gasketted bell and spigot joint. To complete the process, the load limits obtained during the joint tests are compared with the maximum demands obtained from the example calculations presented in Appendix E, for culverts at the two limits considered here: 2 ft (0.6 m) of cover under an AASHTO design vehicle, and for a culvert at 20 ft (6.1 m) cover under earth loads.

H.2 Objectives of the Pipe Joint Test and the Approximations

The process of determining expected shear force, longitudinal bending moment or rotation across the joint requires consideration of the longitudinal response of the soil-pipe system, and consideration of the impact of pipe stiffness, soil stiffness, and the joint characteristics. Whether the designer employs the simplified design equations developed for rigid and flexible pipes in Appendix F, or finite element analysis representing the pipe as a series of beam elements and the soil as a series of elastic springs, the estimates of demand require consideration of the longitudinal pipe-soil interaction. Therefore, the estimates of shear force, bending moment or rotation include considerations of the stiffness of the soil and pipe components of the system. The primary simplification of the joint testing apparatus is the inclusion of the structural components (the two pipes and the components connecting them), but not the soil. Therefore, any contributions of the soil to the strength of the joint (its ability to resist shear force and moment) are neglected. This should provide conservative measures of joint capacity.

To examine whether the conservative measurements of joint strength resulting from “structure-only” testing are also reasonable (i.e. not excessively conservative), consider the approaches used to design pipe barrels for circumferential response. Circumferential strength of both rigid and flexible pipes is significantly influenced by the soil surrounding it. For rigid pipes, this results in bedding factors greater

than unity (reductions in circumferential bending moment relative to those generated in a D-load test at a specific value of vertical applied force). For flexible pipes, it results in behavior dominated by hoop thrust, and the strength under parallel plate loading is understood to be a small fraction of the strength of the pipe-soil composite. To assess joints parallel to the pipe axis tying, say, multi-plate structures together and subjected to hoop forces and circumferential moments, the plates to be tested are joined together and tested in universal test machines to determine axial force and moment capacity. These tests are generally not undertaken with soil present. Instead, the two plates connected by the seam being tested are placed in the loading frame and subjected to the hoop force or moment that is expected to develop (force and moment values that were calculated considering the soil-structure interaction). So, this is analogous to what is being proposed with the current project – calculations of expected shear force, longitudinal bending moment or rotation considering soil-structure interaction, but tests of the structural components only.

The load frame was designed with the following objectives:

1. ability to test shear capacity, with only small values of moment being developed;

2. ability to test moment capacity (or rotation), with only small values of shear force developed;

3. ability to accommodate rigid and flexible pipes;

4. ability to accommodate pipes with diameters from 12 inch (0.3 m) to 60 inch (1.5 m);

5. ability to accommodate the axial forces that develop when the ends of pipes are sealed and they are tested under internal pressure or vacuum (forces resulting from differential pressures on the end) so that there is no axial force transfer through the joint.

This fifth requirement is to accommodate future research with the test frame to study sewers and other pipes subjected to internal or external fluid pressures (external fluid pressure will be represented using vacuum). The current project focuses on culverts under gravity flow without any external groundwater pressure, and internal and external pressures are not considered further in this appendix.

H.3 Description of the Pipe Joint Testing Frame

Figures H.1 to H.3 show the fabrication drawings for one half of the test frame. Figures H.4 to H.8 show different photographs of the frame set up for shear strength testing of the corrugated steel pipe. The two halves of the frame are identical, except that one half is designed to be stationary (it rests on steel supports that are anchored to laboratory floor), and the other half is fabricated to be mobile (without steel floor supports). After the pipes are strapped into place with the joint spanning between the two halves of the test frame, the mobile half of the frame is held in position differently depending on whether the joint is being tested in shear or moment:

a. For shear testing, the mobile half is supported at one end by the joint between the two pipes, Figure H.7 (there is no pin connecting the two halves), and the other end is supported by a removable timber support, Figure H.8. As axial force is applied by the loading column onto the curved loading plate, Figure H.9, shear force develops across the joint. Downward movement of the joint relative to the other

ends of the two halves of the test frame (which both rest on the laboratory floor), produces some rotation and moment in addition to the shear force which is applied.

b. For moment testing, the mobile half is supported at one end by a pin connecting the two halves of the test frame, located directly under the joint, Figure H.11. The other end of the frame is suspended and a load cell used to measure the vertical force required to hold it in place, Figures H.12 and H.13. The end is then lowered, and changes in the force needed and the distance of that force from the pin are used to calculate the moment being applied through the joint. Joint rotation can be measured using linear displacement transducers inside the pipe (measuring the opening or closing of the joint at the crown and invert). Rotation can also be determined from a measurement of the vertical movement of the end of the frame being lowered. A small shear force will also develop, equal to the incremental force used to hold the free end of the frame.

To accommodate pipes of different sizes, and to reduce the possibility that the pipe in the stationary half of the frame experiences a line load along its invert (undesirable for a flexible pipe), the stationary half of the frame is fitted with a steel tray that holds bedding sand. This distributes the reaction across the base of the pipe between the haunches.

H.4 Example Results

Tables H.1 to H.3 summarize the results of the limit states testing of the pipes evaluated in the loading frame. In each case the maximum applied load (shear, moment) or rotation are provided. These are then factored by the recommended resistance factor of 0.67. Finally, these are compared to the factored demands for these products calculated in Appendix E.

Calculation of moment acting through the joint is undertaken using the load measured through a load cell holding the end of the rotating section of the rotating frame, and the measured distance of that loading point to the fulcrum (the hinge used to connect the two parts of the frame together). Some of the moments have been corrected by those recorded using a test where the frame was rotated without pipes being present (denoted ‘corrected moments’). Since the peak corrected moment applied during the test of the corrugated steel pipe was only 2700 ft.lb (3.6 kN.m), the moments applied during the earlier testing reported in Appendix C are also included in Table H.2 (that test applied moments of 4400 ft.lb, 6 kN.m).

Calculation of shear force through the joint is based on an assumption that all of the vertical force applied to the crown of the pipe contributing the spigot to the joint is transferred through the joint to the bell. Consideration of the distances of the load point to the gasket, and to the other end of the frame indicates that more than 95% of the load would be transferred through the pipe joint.

In all tests, the resistance equalled or exceeded the factored demand, and in most cases the factored resistance exceeded the factored demand. In no case did the joint being tested reach a state of failure (i.e. ultimate limit state) at the maximum load achieved (this is signified in the tables using the “>” sign before all these results). This indicates that all the products tested satisfied the structural design requirements for the burial conditions that were considered, and testing to higher loads would likely indicate that the joints are capable of supporting more demanding burial conditions.

Figures H.14 to H.18 provide details of the measured responses during the tests. These indicate that:

- The moment versus rotation characteristics of the gasketted bell and spigot joint in the PVC pipe shown in Figure H.14 are rather complex, with various changes in stiffness; this is interpreted as being associated with stick-slip characteristics of the gasket distorting, then sliding inside the bell, in repeated cycles (stiffness is higher when the gasket is distorting, and it is reduced during a period of sliding).
- Measurements were made of relative axial movements between the two pipe ends across the joint connecting the two corrugated steel pipes, both at the crown and invert, Figure H.15, with the pipe ends becoming closer at the invert, and further apart at the crown (as might be expected); these were used to calculate rotation at the joint (using the distance between these measurements, namely the internal pipe diameter); these end rotations are compared to the rotation of the test frame in Figure H.16; more than 80% of the frame rotation is induced as a relative rotation of the two pipe ends, so it appears that the band connection is accommodating substantial rotations (it is not at all acting as rigid link transferring moments between the two ends of the steel pipes); for the tests reported in Appendix C, the rotations between pipe ends were small; therefore it appears that by strapping the two corrugated steel pipe segments to the steel frame, the test induces rotations across the hugger band connector that do not occur in buried pipes; further refinement of the simplified models presented in Appendix F might be undertaken to consider partial moment transfer, to assess the level of conservatism of the design procedure based on zero rotation and full moment transfer
- Since the ends of the two corrugated steel pipe segments permitted rotation, the corrugated steel pipe is also included in Table H.3 where rotational capacity is examined; like the pipes with bell and spigot joints, the rotation accommodated by the hugger band is considerably higher than expected rotation conservatively calculated assuming the pipe segments are connected by a moment release joint;
- Figure H.17 shows the changes in diameter that resulted as rotation was imposed across the band connecting the two corrugated steel pipes (the so-called ‘brazier’ effect where longitudinal bending of a pipe leads to diameter change); at the maximum level of shear force applied, the increase in horizontal diameter of the moving pipe (the one strapped to the frame that was rotating downwards) was about 1%, and about 0.5% for the pipe it was connected to; decreases in vertical diameter were somewhat smaller.
- The shear experiments on the PVC, corrugated steel and concrete pipes, Figure H.18 all resulted in some residual deformation; that deformation may be associated with movement of the pipe resting on sand into that bedding material.

Table H.1 Comparison of factored shear resistance to factored demand (resistance factor 0.67)

	Max. shear		Factored resistance		Factored demand	
Product	lbf	kN	lbf	kN	lbf	kN
36 in. PVC	>6700	>30	>4500	>20	5100	22.5
36 in. CSP	>5200	>23.4	>3500	>15.7	5100	22.9
24 in. RCP	>22000	>100	>15000	>67	8700	38.7

Table H.2 Comparison of factored moment resistance to factored demand (resistance factor 0.67)

	Max. Moment		Factored resistance		Factored demand	
Product	ft.lb	kN.m	ft.lb	kN.m	ft.lb	kN.m
36 in. CSP	>2700 >4400[C]	>3.6 >6[C]	>1800 >3000[C]	>2.4 >4[C]	3500	4.8

[C]: maximum moment applied during testing reported in Appendix C.

Table H.3 Comparison of factored rotation to expected rotation (resistance factor 0.67)

Product	Max. rotation	Factored resistance	Factored demand
36 in. PVC	>4^{o}	>2.7^{o}	0.25^{o}
36 in. CSP	>4^{o}	>2.7^{o}	0.25^{o}
24 in. RCP	>3.8^{o}	>2.5^{o}	0.18^{o}

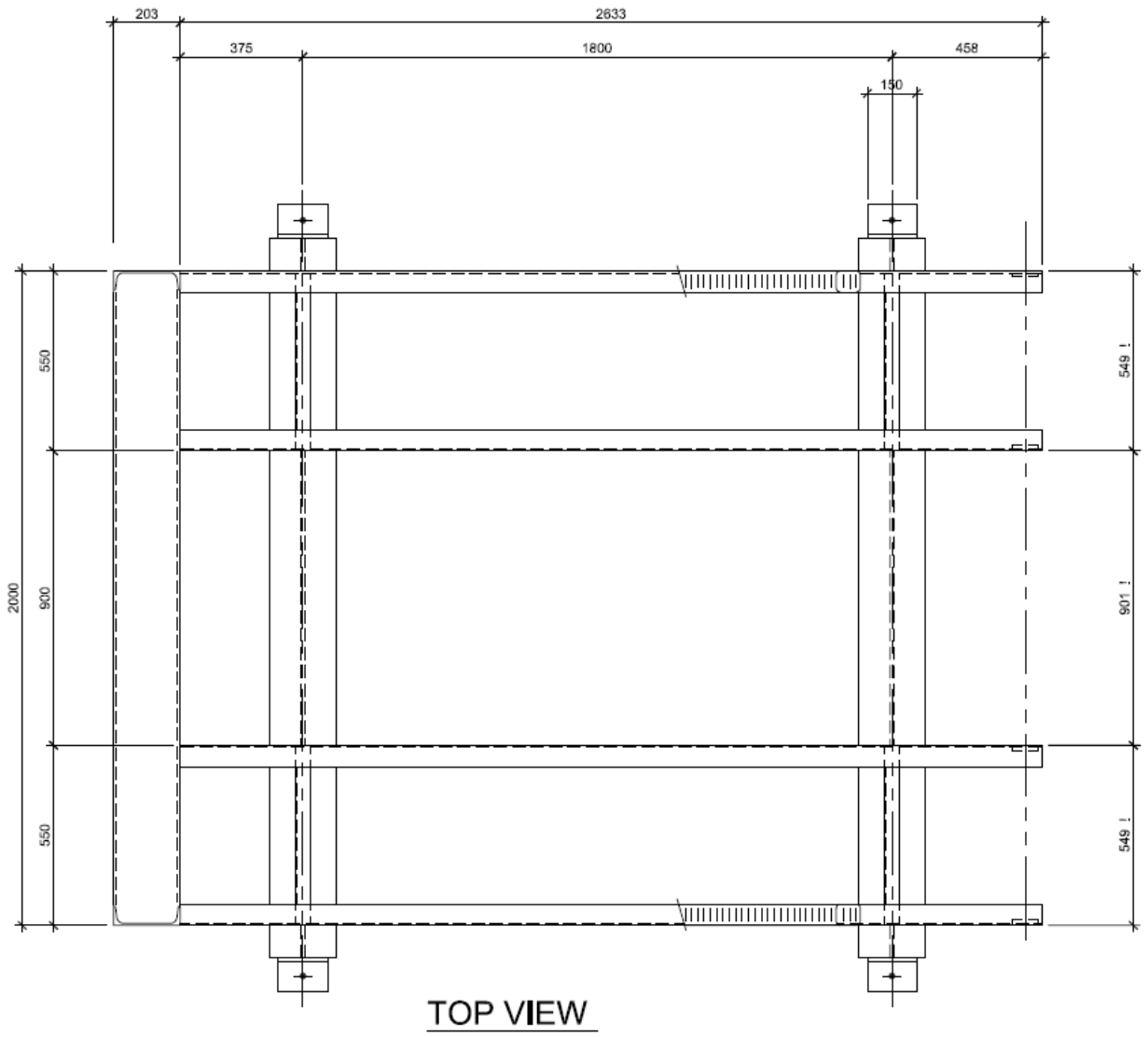

Figure H.1 Plan view of the half of the loading frame anchored to the test floor; the other half is similar, but without steel supports anchoring the frame to the floor.

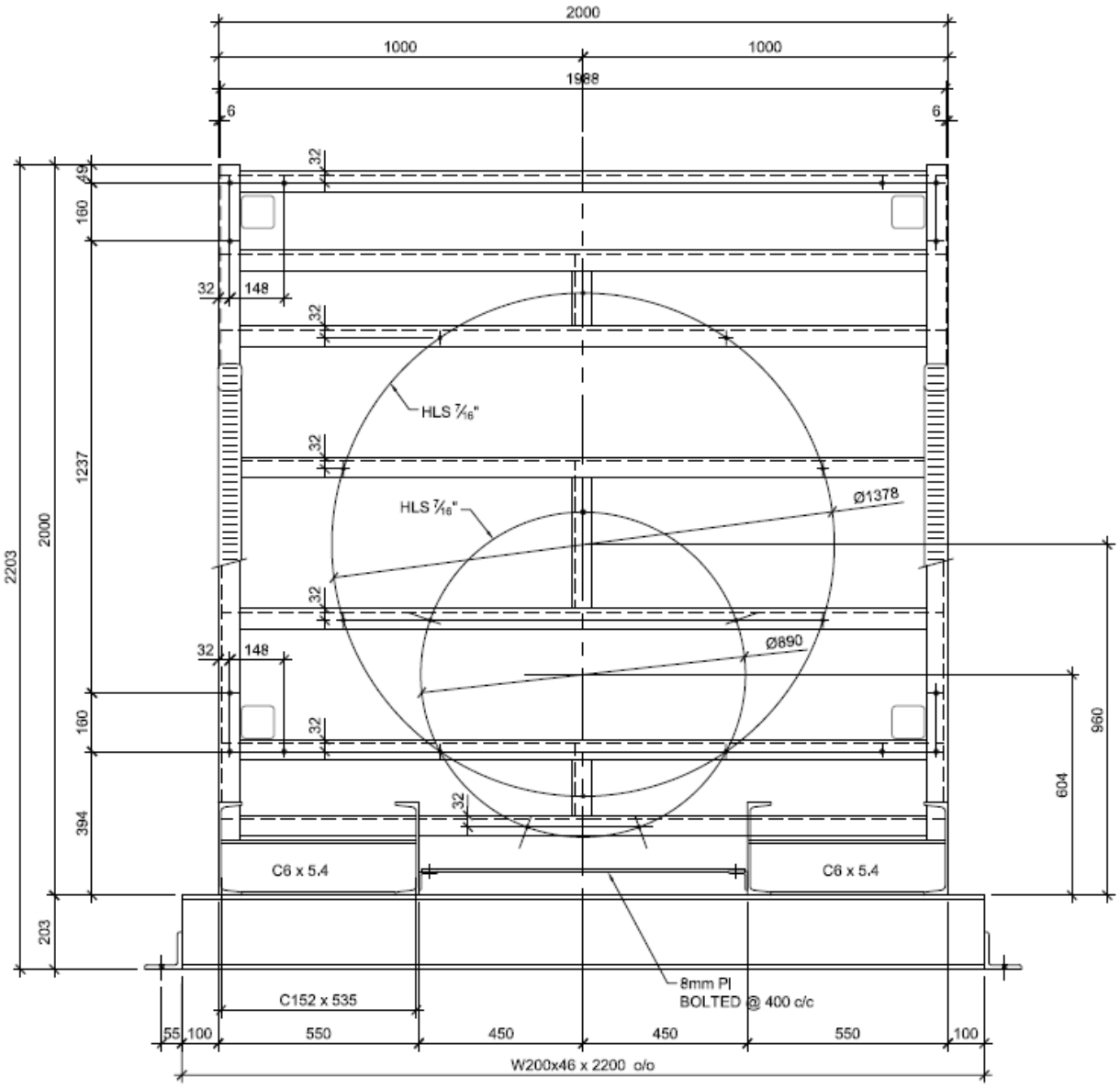

SECTION A - A
SYMMETRIC ABT C/L

Figure H.2 Elevation view looking at one end of the loading frame; frame designed for pipes 24 inch to 60 inch internal diameter.

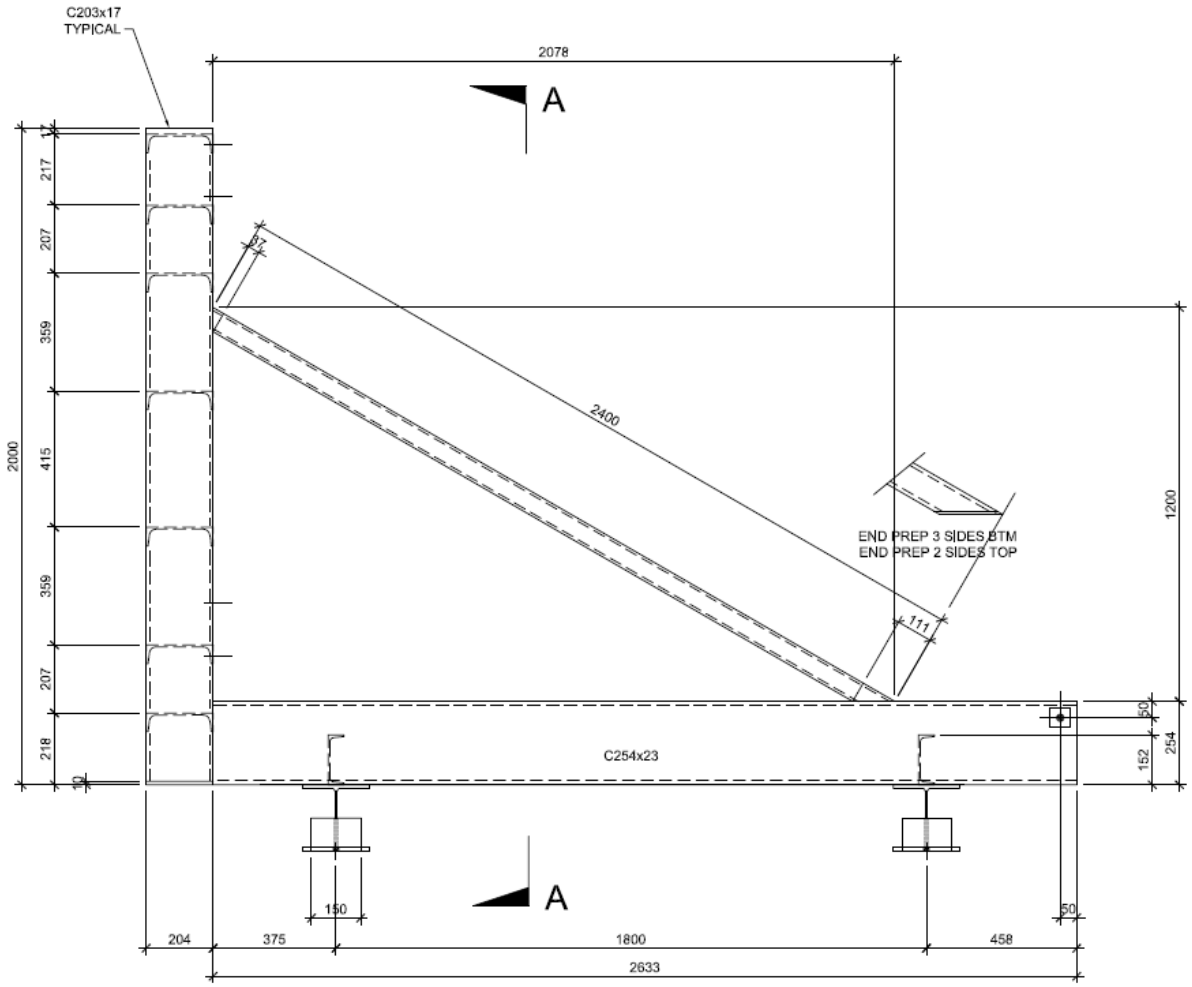

Figure H.3 Side view of the half of the frame anchored to the floor.

Figure H.4 Test frame in position for shear force testing; this arrangement shows additional longitudinal ties connecting the top corners of the end frames; these ties carry end reactions when sealing plates cover the pipe ends, these are tied to the end frames, and pipe has internal pressure or vacuum (future project).

Figure H.5 Test frame (top view); this image shows the frame without the additional longitudinal ties; this configuration is used when testing joints without internal fluid pressure or vacuum.

Figure H.6 Loading system used to apply shear force (2000 kN actuator restrained by reaction frame anchored to the rock below; actuator fitted with 200 kN load cell).

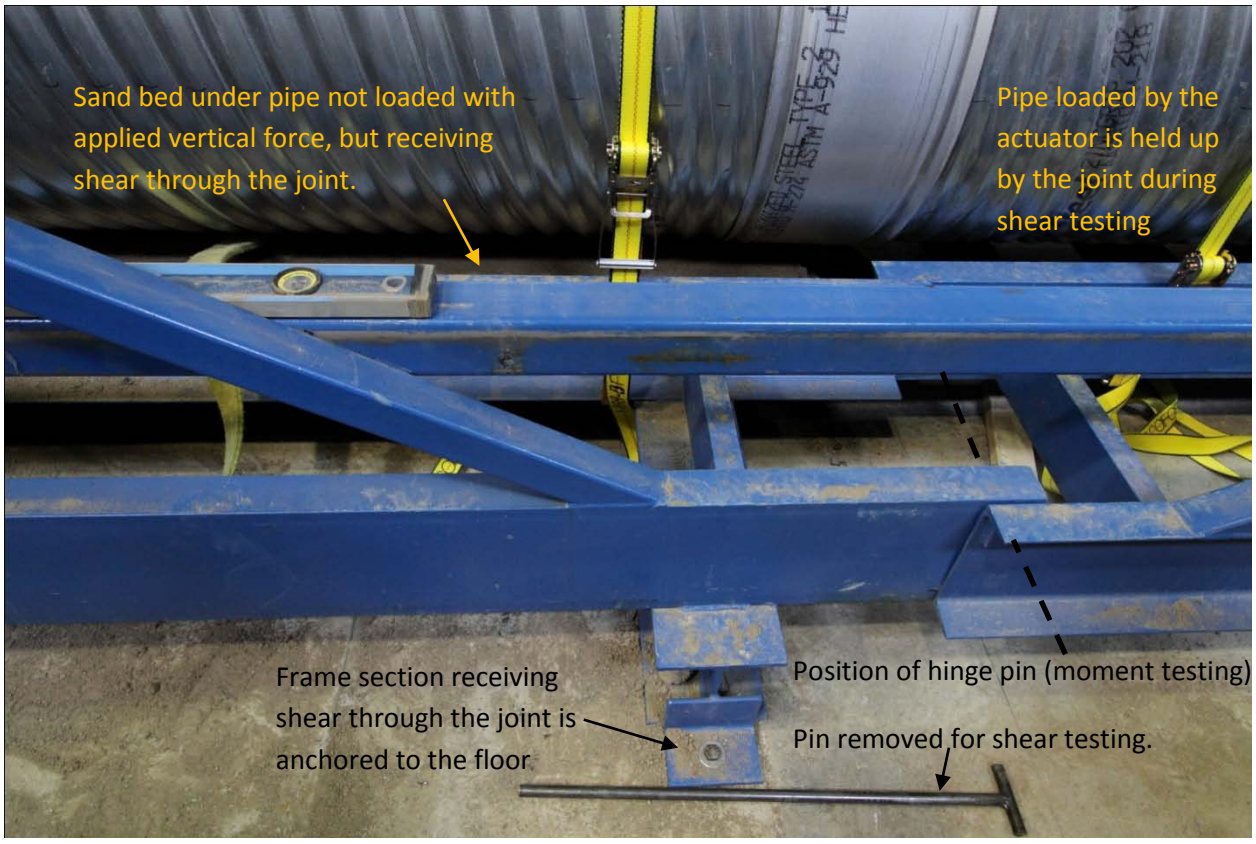

Figure H.7 Detail of connection between the two frames; the left hand frame is anchored to the floor of the laboratory; for moment (or rotation) testing, the two parts are connected by a hinge pin at the centre, and the actuator is used to hold the other end of the right hand frame; for shear testing, the hinge pin is removed, and the other end of the right hand frame is supported on a removable timber block.

Figure H.8 End of loading frame on timber support. Figure H.9 Curved load plate and column.

Figure H.10 Instrumentation used during shear testing of the corrugated metal pipe.

Figure H.11 Pin inserted for moment and rotation testing of the PVC pipe.

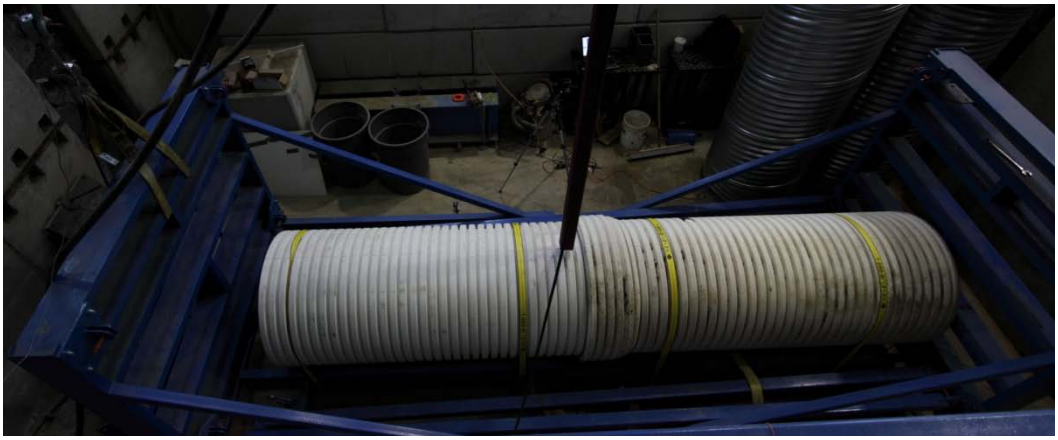

Figure H.12 The left hand end of the frame is held level then lowered for rotation testing of the PVC pipe.

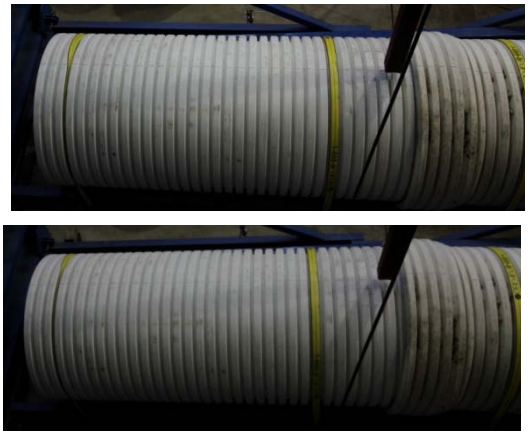

Figure H.13 Images of PVC pipe at commencement and end of rotation testing.

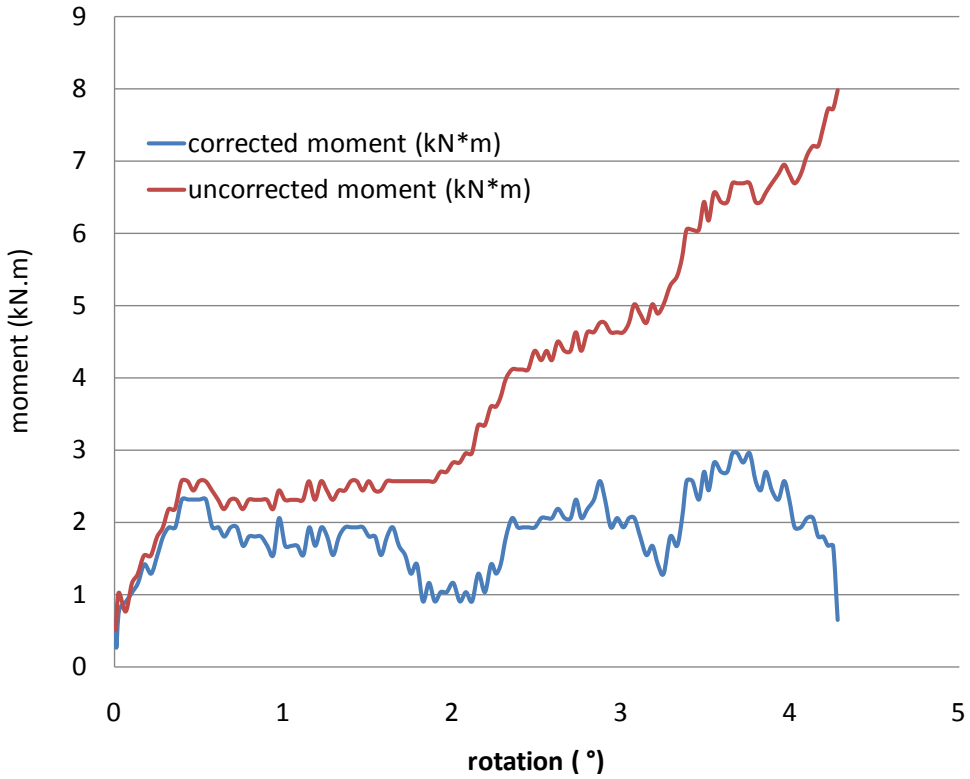

Figure H.14 Moment versus frame rotation for PVC pipe (1 kN.m = 737 ft.lb).

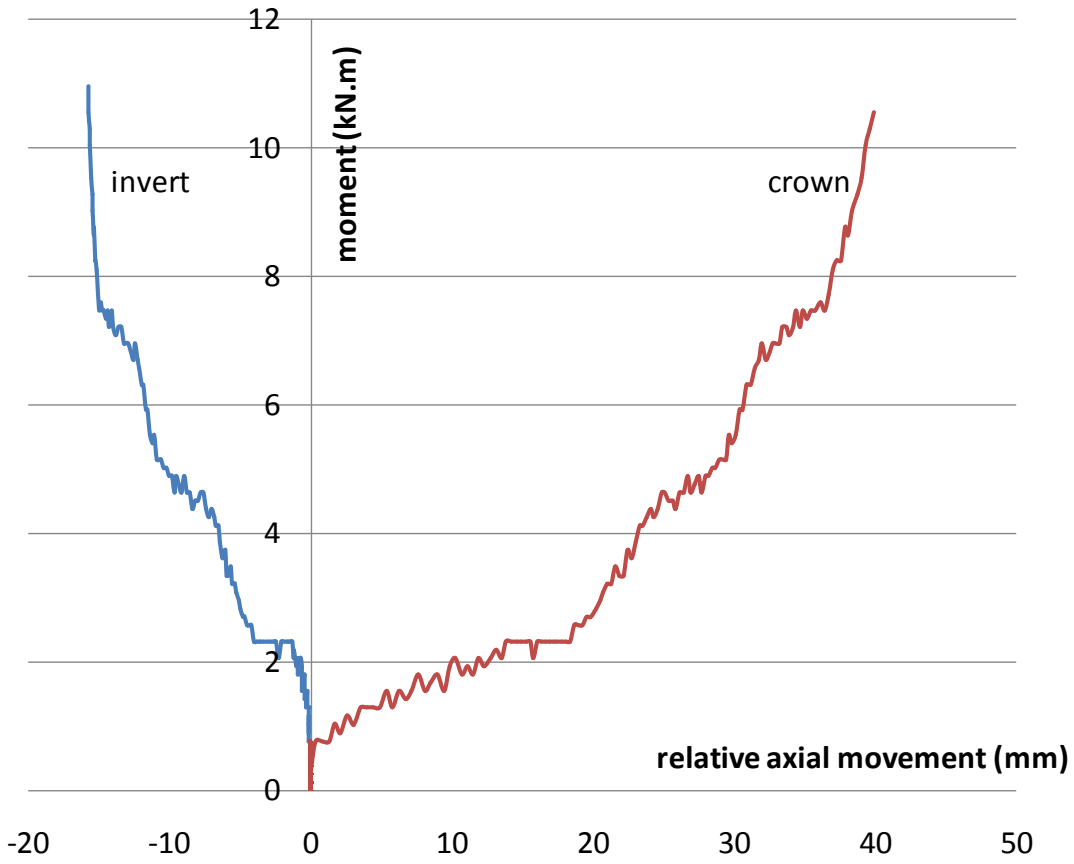

Figure H.15 Axial movements between the crowns and inverts of the two pipe ends for the corrugated steel pipe during articulation testing; shown versus uncorrected moment (1 mm = 0.04 in.; 1 kN.m = 737 ft.lb).

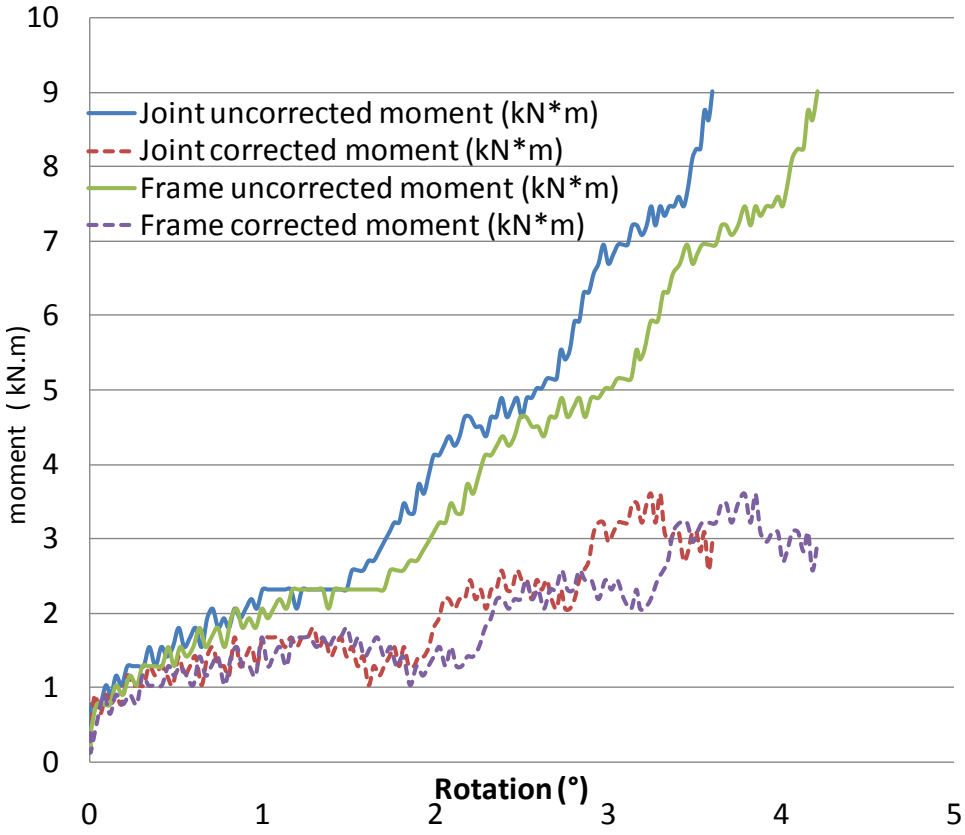

Figure H.16 Moment versus rotation for corrugated steel pipe; rotation based on frame movement and rotation between the pipe ends at the joint (measurements shown on Figure H.15); 1 kN.m = 737 ft.lb.

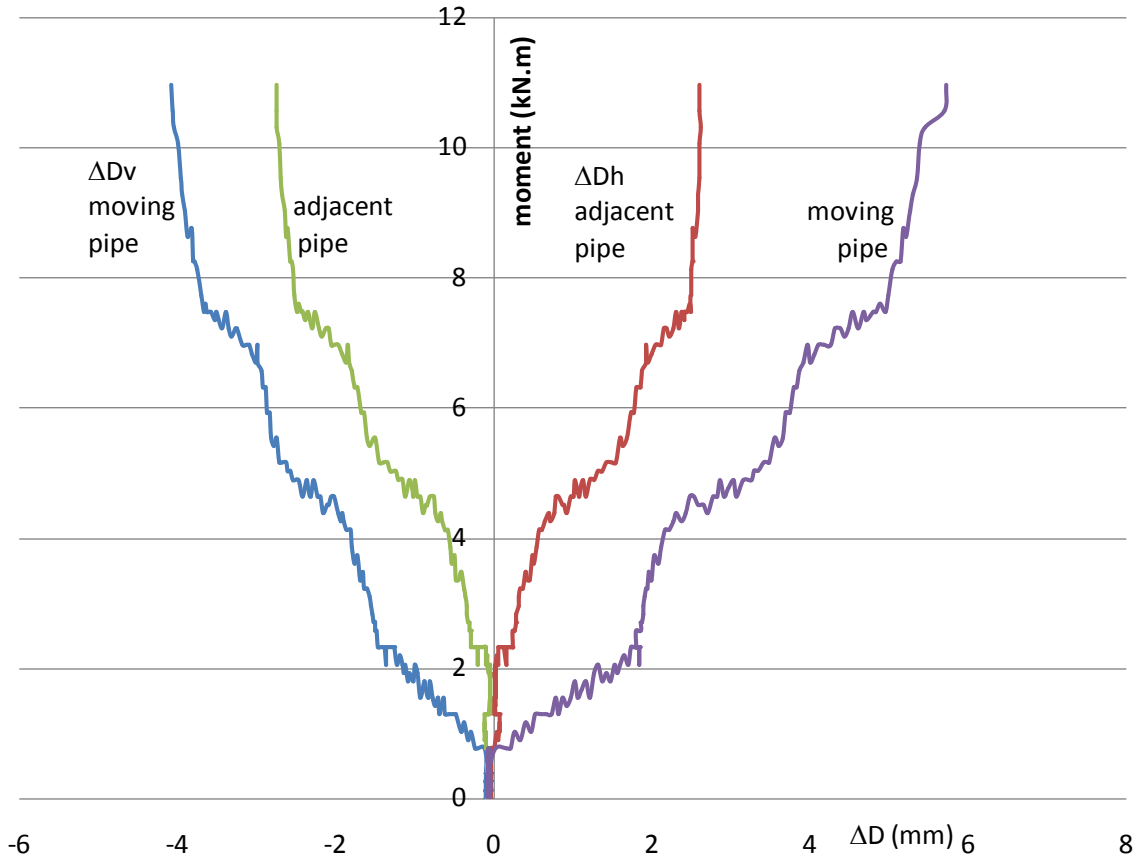

Figure H.17 Uncorrected moment versus change in diameter for corrugated steel pipe (1 kN.m = 737 ft.lb).

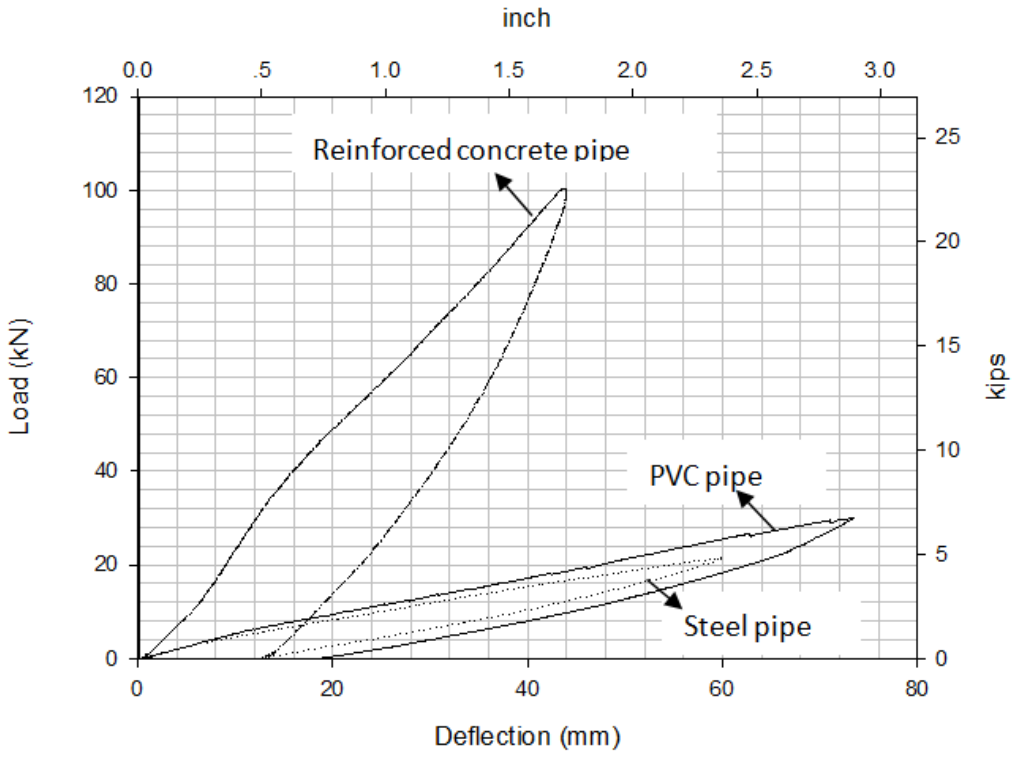

Figure H.18 Shear force versus stroke for PVC, corrugated steel and reinforced concrete pipes.

Appendix I Flexural Rigidity of Flexible Pipes

Contents

INTRODUCTION

It is necessary to determine the flexural rigidity *EI* of the pipes that will be analyzed with the beam-on-springs model. Flexural rigidity of the pipe greatly affects the movements predicted by modeling. Determining *EI* of a RC pipe is relatively straightforward due to its simple geometry. Determining *EI* for the flexible corrugated steel (CS) pipes and HDPE pipes is much more complicated due to the complex geometry of the corrugations. This Appendix presents methods for determining the stiffness of both HDPE and corrugated steel pipes based on the assumption that the corrugations can be modeled as equivalent straight sections with an effective thickness (Figure I.1b).

FLEXURAL RIGIDITY OF CORRUGATED STEEL PIPE

Determining the flexural rigidity, *EI*, of corrugated steel pipe is somewhat complicated because the corrugation reduces the longitudinal stiffness of the pipe. Longitudinal stiffness is further affected by the seams that are formed every one to three feet along the length of the pipe. Seams are caused by strips of corrugated steel being wrapped helically or annularly to form the pipe shape and then welded together. Longitudinal stiffness of corrugated metal pipes is addressed in Havens (1993) and Havens (1995). The equations presented in Havens' research rely on knowledge of the ratio of the hoop strain to longitudinal strain in the pipe. This ratio is experimentally measured, and is only provided for one of the common corrugation profiles. Therefore it is necessary to present a method of determining flexural rigidity that can be easily applied without acquiring experimental measurements. Its accuracy is also verified from testing. Without an accurate calculation of *EI*, a beam-on-springs model is useless.

This section approximates the stiffness reduction caused by the corrugation, and ignores the stiffness reduction caused by the seams. Then the calculated stiffness is compared with the measured stiffness of several corrugated metal pipes in order to validate the approximations. In order to determine an

effective *I* value for any pipe, the corrugation profile (Figure I.1a) is modeled as a straight section with an effective thickness, t_{eff} (Figure I.1b).

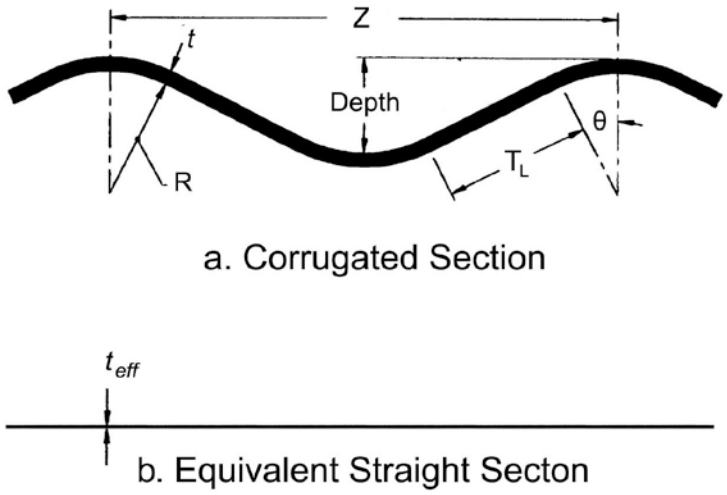

Figure I.1 Typical corrugation profile and an equivalent section used to represent the corrugation.

Standard dimensions for the corrugation sections are usually given by the manufacturers in handbooks such as the Handbook of Steel Drainage & Highway Construction Products (AISI, 1994). The following is the derivation of the t_{eff} for a general corrugation profile.

A small force, *F* is applied to the corrugation (Figure I.2a). A small force is used because any force causes the depth of the corrugation to increase due to the geometry of the system. This decreases the stiffness of the section. In practice, the depth of the corrugation increases only a small amount under normal loading, and therefore the stiffness of the corrugation is reduced only very slightly. A small force ensures the depth of the corrugation is only very slightly reduced. Under the applied small force, the axial deflection is calculated for one fourth of the pitch length as shown in Figure I.2a. The deflection is used to calculate the effective thickness, t_{eff}, of an equivalent straight section is determined so that the corrugation and the equivalent straight section displace the same amount. One fourth of the pitch length is used for calculation because the model can be simplified as fixed at one end with the axial force applied at the other end. The curved section of the corrugation is discretized into *n* equal segments which lie tangent to the curve (Figure I.2b). A mathematical model of the discretized elements is shown in Figure I.3.

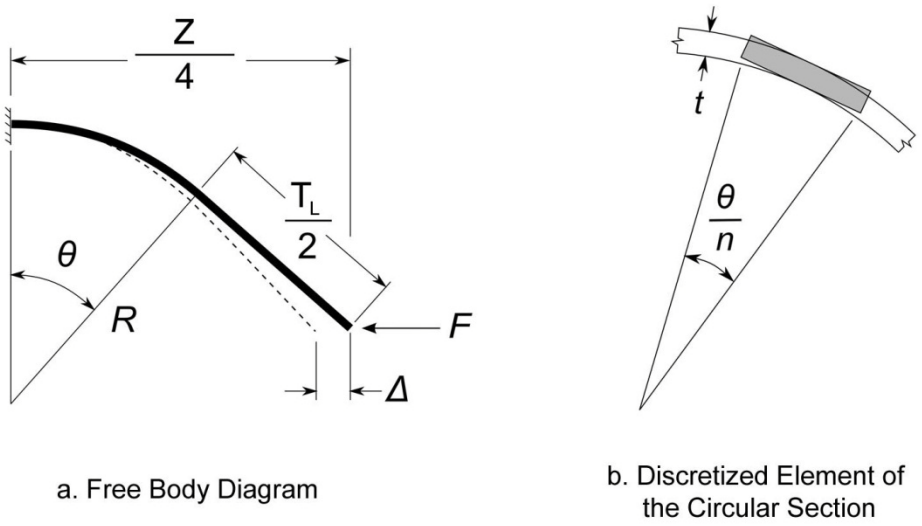

Figure I.2 Mathematical models of the corrugated section

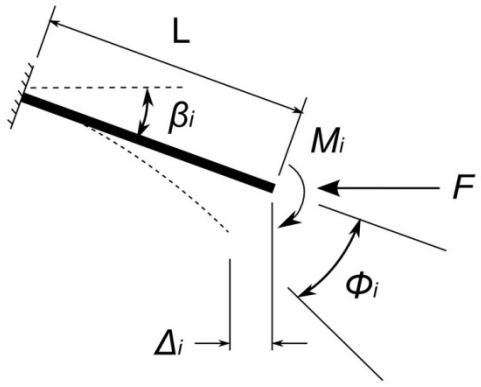

Figure I.3 Mathematical model of discretized element *i*.

The following variables are used in the derivation of an effective thickness.

A = Area of the corrugation per unit length into the page (length^2/length into page)

A_{eff} = Area of the equivalent straight section per unit length into the page (length^2/length into page)

= Orientation angle of discretized element *i* (radians)

Δ = Axial displacement of 1/4 of the pitch length under loading F (length)

Δ_i = Axial displacement of element *i* caused by loading (length)

Δ_{TL} = Axial displacement of the TL/2 segment in Figure I.1a under loading P (length)

d_a = Pipe diameter measured from the centerline of the corrugation (length)

d_c = Depth of the corrugation (length)

F = Small force per unit length into the page applied axially to the corrugation. (force/length)

I = Area moment of inertia of corrugation per length into the page (length^4/length into page)

K_G = Geometric parameter for each corrugation geometry from Havens (1993).

= 0.09215 in.^{3} for 3 × 1 corrugation geometries

= 0.01928 in.^{3} for 2⅔ × ½ corrugation geometries

K_σ = Ratio of hoop stress to longitudinal stress from Havens (1993)

K_λ = Constant based upon the corrugation geometry from Havens (1993)

= 0.3828 in. (0.97 cm) for 3 × 1 corrugation geometries

= 0.2174 in. (0.55 cm) for 2⅔ × ½ corrugation geometries

n = Number of discretized elements used in the analysis

$\emptyset_i$ = Rotation of element i caused by loading Figure I.3

R = Radius of the curved section of the corrugation, defined from the center of the circle to the neutral axis of the steel (length)

r = Pipe radius measured from the centerline of the corrugation (length)

θ = Angle of the curved section of the corrugation (radians)t = Thickness of the corrugation (length)

t_{eff} = Thickness of the equivalent straight section

T_L = Tangent length (length) Z = Distance between two peaks of the corrugation (length)

The length of each discretized element is given by:

$$L = 2R \tan\frac{\theta}{2n} \qquad \text{(I.1)}$$

The orientation angle of any element i is given by Equation I.2. It assumes that the corrugation is divided into n discrete elements which lie tangent to the curve at their midpoints.

$$\beta_i = \frac{\theta}{n}\left[i - \frac{1}{2}\right] \qquad \text{(I.2)}$$

The moment applied to each element i is given by Equation I.3. It consists of the force F multiplied by the vertical distance between the point where the force is applied to the corrugated section (Figure I.2), and the point where the moment is applied to element i

$$M_i = F\left[\frac{T_L}{2}\sin\theta + R\left(-\cos\theta + \cos\beta_i - \tan\frac{\theta}{2n}\right)\right] \qquad \text{(I.3)}$$

The rotation of element i is caused by the moment M_i, and the force F acting on the element. Equation I.4 combines the rotation caused the force and moment, and uses equations of the rotation of a simple beam.

$$\emptyset_i = \frac{M_i L}{EI} + \frac{F\,L^2 \sin\beta_n}{2EI} \tag{I.4}$$

The horizontal deflection of element *i* is caused four kinds of movement. The axial deflection caused by force *F* is $\frac{FL\cos^2\beta_i}{EA}$. The beam deflection cause by force *F* is $\frac{FL^3\sin^2\beta_i}{3EI}$. The beam deflection cause by moment M_i is $\frac{M_i L^2 \sin\beta_i}{2EI}$. The deflection caused by the rotation of all previous elements is $L\left[\cos\beta_i - \cos\left(\beta_i + \sum_{k=1}^{i-1}\emptyset_k\right)\right]$.

Combining the four expressions of deflection just presented yields the horizontal deflection of element *i* under loading which is given in Equation I.9.

$$\Delta_i = \frac{FL\cos^2\beta_i}{EA} + \frac{FL^3\sin^2\beta_i}{3EI} + \frac{M_i L^2 \sin\beta_i}{2EI} + L\left[\cos\beta_i - \cos\left(\beta_i + \sum_{k=1}^{i-1}\emptyset_k\right)\right] \tag{I.5}$$

The deflection of one a segment equal to one half of the tangent length is given in Equation I.10. It is formed by combining the axial deflection caused by force *F*, $\frac{F(T_L/2)\cos^2\theta}{EA}$, the beam deflection caused by force *F*, $\frac{F(T_L/2)^3\sin^2\theta}{3EI}$, and the deflection caused by the rotation of all previous elements, $\frac{T_L}{2}[\cos\theta - \cos(\theta + \sum_{i=1}^{n}\emptyset_i)]$.

$$\Delta_{TL} = \frac{F(T_L/2)\cos^2\theta}{EA} + \frac{F(T_L/2)^3\sin^2\theta}{3EI} + \frac{T_L}{2}\left[\cos\theta - \cos\left(\theta + \sum_{i=1}^{n}\emptyset_i\right)\right] \tag{I.6}$$

The total axial deflection under loading *F* for one fourth of the pitch length can be calculated from Equation I.11. It consists of the deflection of one half of the tangent length plus the sum of the deflection in each of the discretized elements.

$$\Delta = \Delta_{TL} + \sum_{i=1}^{n}\Delta_i \tag{I.7}$$

Equation I.12 gives the total deflection of the equivalent straight section.

$$\Delta = \frac{F\,(Z/4)}{EA_{eff}} \tag{I.8}$$

Rearranging yields Equation I.13,

$$A_{eff} = \frac{FZ}{4E\Delta} \tag{I.9}$$

A, *I*, and *F* are defined per unit length into the page. Assuming the corrugation extends 1 unit length into the page, $A = t$ and $I = t^3/12$. Therefore, t_{eff} is defined by Equation I.14,

$$t_{eff} = \frac{FZ}{4E\Delta} \tag{I.10}$$

This equation can be used to determine the effective thickness of an equivalent straight section that has the same amount of axial displacement as the original corrugation when subjected to axial load *F*. For small forces, *F* cancels out of the equations when combined. This effective thickness can be used to calculate the flexural rigidity *EI* of a corrugated metal pipe. To simplify the process, Table I.1 provides effective thickness values for common corrugation profiles. The values were calculated using $F \approx 0$, and $n = 10000$ discrete elements. As *F* increases, the effective thickness decreases. Axial compression of the corrugation increases the depth of the corrugation thereby increasing the effect of the force on the corrugation. However, the pipe typically yields before any decrease in effective thickness is noticeable. Equation I.15 gives the flexural rigidity of the corrugated metal pipes:

$$EI = \frac{\pi E}{64}\left[\left(d_a + 2t_{eff}\right)^4 - {d_a}^4\right] \tag{I.11}$$

Table I.1 Calculated effective thickness of common corrugation profiles listed in the Handbook of Steel Drainage & Highway Construction (1994) (1 in. = 25.4 mm)

	Corrugation Geometry					
	1½ × ¼	2 × ½	2⅔ × ½	3 × 1	5 × 1	6 × 2
t (in.)	t_{eff} (in.)	t_{eff} (in.)	t_{eff} (in.)	t_{eff} (in.)	t_{eff} (in.)	t_{eff} (in.)
0.0359	0.00055	0.00012	0.00012	0.00003	-	-
0.0478	0.00127	0.00028	0.00029	0.00006	-	-
0.0598	0.00245	0.00055	0.00056	0.00012	0.00012	-
0.0747	0.00464	0.00113	0.00109	0.00024	0.00024	-
0.1046	0.01196	0.00286	0.00294	0.00065	0.00064	0.00017
0.1345	0.02354	0.00591	0.00610	0.00136	0.00136	0.00035
0.1644	0.03944	0.01050	0.01084	0.00246	0.00247	0.00064
0.1838	-	-	-	-	-	0.00088
0.2145	-	-	-	-	-	0.00140
0.2451	-	-	-	-	-	0.00207
0.2758	-	-	-	-	-	0.00293
0.3125	-	-	-	-	-	0.00425
0.3750	-	-	-	-	-	0.00722

Comparison against a measured flexural rigidity is necessary to validate the presented model. Flexural rigidity measurements are known for three separate corrugated steel pipes. The flexural rigidities of three pipes were measured in Havens (1993), and the flexural rigidity of the laboratory test pipe (Lab

Pipe) used in this project was measured, as described in Appendix C. Correct theoretical values for the Lab Pipe are not available using Havens' method because the ratio of hoop stress to longitudinal stress was not measured for that corrugation geometry. Havens uses Equation I.16 to calculate flexural rigidity *EI*.

$$EI = \frac{EP\pi rt}{4K_G}\left[\frac{3}{1+3K_\sigma^2}\right]\left[\frac{rt}{6} + K_\sigma\left(\frac{T_L^3 \sin\theta\cos\theta}{12d_c} + K_\lambda R\right)\right]^2 \qquad \text{(I.12)}$$

Table I.2 Comparison of theoretical and experimentally measured values (1 in. = 25.4 mm; 1 ksi = 6.91 MPa; 1 lbf-in^2 = 2.87x10^{-9} MN-m^2)

Pipe Designation	Havens #1	Havens #2	Havens #3	Lab Pipe
Corrugation Geometry	3 × 1	3 × 1	3 × 1	2⅔ × ½
Inner Diameter (in.)	48	72	96	36
Nominal Thickness (in.)	0.1046	0.0747	0.0747	0.0551
Theoretical effective thickness (in.)	0.00065	0.00024	0.00024	0.00044
Young's modulus *E* (ksi)	29,000	29,000	29,000	29,000
Experimental *EI* (lbf-in^2)	9.11x10^8	1.20x10^9	3.44x10^9	3.85x10^8 [b]
Theoretical *EI* predicted by Havens (lbf-in^2)	8.63x10^8	1.03x10^8	2.13x10^9	[a]
Difference from experimental value (%)	-5.2	-14	-38	[a]
Theoretical *EI* predicted above (lbf-in^2)	8.71x10^8	1.06x10^9	2.49x10^9	2.54x10^8
Difference from experimental value (%)	-4.4	-11	-27	-34

a) No values available because Havens (1993) did not provided hoop strain to longitudinal strain ratio for the 2⅔ × ½ corrugation geometry

b) Average of six measured values

Many pipes consist of helically wrapped corrugation. Helix angles can vary from 6 degrees to 33 degrees for small diameter pipes (Havens 1993). Both the method presented above and Havens' method assume an annularly wrapped corrugation. For small helix angles, less than 8 degrees, the pipes should behave similarly to an annularly corrugated pipe (Havens, 1993). For larger helix angles, the helical wrapping strengthens the pipe. In that case, the method presented above and the method presented by Havens gives conservative estimations of *EI*. Further and more complicated analysis would be necessary to determine how conservative the estimations are. Typically, as pipe diameter decreases, helix angle increases. The smallest diameter pipe that is experimentally measured has an inner diameter of 36 in. (0.91 m) and a helix angle of approximately 14 degrees (Lab Pipe). Using theoretical methods presented above, the error for that pipe is -34%. As expected, the measured flexural rigidity is greater than the calculated flexural rigidity.

The model presented is effective at estimating the flexural rigidity of all four corrugated steel pipes with maximum error of -34% and minimum error of -4.4%. The model presented above is slightly more accurate than Havens' model at predicting the flexural rigidity of all three of his test pipes. However, the new model is more useful because it does not require measurement of the hoop stress to longitudinal stress ratio.

FLEXURAL RIGIDITY OF HDPE PIPES

Determining flexural rigidity of HDPE pipes is challenging because of the complex corrugation profile. Also, almost no detailed information is provided by the manufacturers about the corrugation profile. Often, the only useful information given is the mass of the pipe in lb/ft or kg/m along the length of the pipe. This section presents a rough approximation of the flexural rigidity *EI* of HDPE pipes with an arched corrugation. It is based on the detailed measurements of a corrugation profile in McGrath et al. (2009). It is assumed that the dimensions of an arched corrugation profile scale similarly to the dimensions provided in McGrath et al. (2009). The goal is to provide a method of estimating the flexural rigidity of an HDPE pipe using only the distributed weight of the pipe provided by the manufacturer in lb/ft or kg/m and the diameter of the pipe. This is accomplished the same way as in the previous section by modeling the corrugation as an equivalent straight section with an effective thickness, t_{eff} (Figure I.1b). This method should only be used for double-walled arched corrugations. Detailed measurements of each corrugation profile are necessary to more accurately determine the true *EI* value of HDPE pipes.

The following are used in the derivation of t_{eff} and *EI*.

A = Cross-sectional area of the corrugation (length^2)

A_1 = Area of section 1 in Figure I.2b, per unit width into the page (length^2 / length into the page)

A_2 = Area of section 2 in Figure I.2b, per unit width into the page (length^2 / length into the page)

A_{eff} = Area of the equivalent straight section per unit length into the page (length^2/length into page)

d_i = Inner diameter of the pipe (length)

E = Modulus of elasticity for HDPE. Typically 110,000 psi (758 MPa)

I = Area moment of inertial of an HDPE pipe with an arched corrugation (length^4)

L_1, L_2 = Length of section 1 and 2 (length)

ρ = Density of HDPE plastic = 59.3 lb/ft^3 (0.95 g/cm^3)

t_{eff} = Thickness of the equivalent straight section (length) (Figure I.1b)

t_1, t_2 = Thickness of section 1 and 2 (length) (Figure I.1)

V = Volume of material in a hoop the width of the pitch (length^3)

w = Distributed weight of the pipe (mass / length)

W_h = Weight of material in a hoop the width of the pitch (mass)

Z = Pitch length of the corrugation (length)

The derivation considers the distributed weight and pitch length of the pipe. The distributed weight is multiplied by the pitch length. This gives the weight of a hoop as wide as one pitch length in Equation I.17.

$$W_h = wZ \tag{I.13}$$

The total volume of the material in the hoop is equal to the circumference of the hoop times the cross-sectional area of the hoop, Equation I.18. The circumference is equal to πd.

$$V = A * \pi d_i \tag{I.14}$$

The volume is multiplied by the density, ρ to find the weight of the pipe expressed in terms of the cross-sectional area. The typical density of HDPE pipe is taken to be $\rho = 59.3 \frac{lb}{ft^3}$ $(0.95 \frac{g}{cm^3})$ as provided in JMM (2011). This yields the weight of the hoop in terms of the diameter and cross-sectional area,

$$W_h = A * \rho \pi d_i \tag{I.15}$$

by equating the two hoop weights ($w * pitch = A * \rho \pi d_i$), and solving for A yields,

$$A = \frac{wZ}{\rho \pi d_i} \tag{I.16}$$

A detailed drawing of a corrugation profile with a 6 inch pitch is provided in Figure I.1. Analysis of this profile shows that the main arch of the corrugation provides very little stiffness to a force applied

longitudinally to the pipe (<1%). So, the main arch is removed from the corrugation to provide a reduced section (Figure I.2).

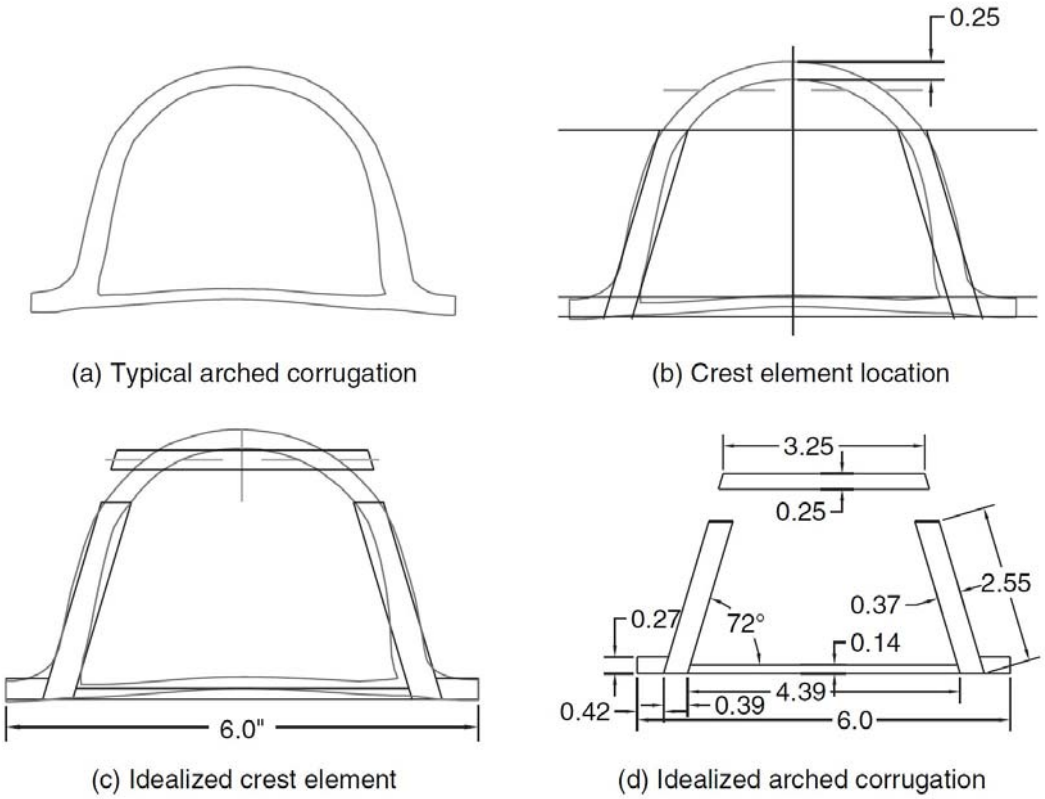

Figure I.1 Detailed measurements and idealization of an HDPE corrugation profile provided by McGrath et al. (2009).

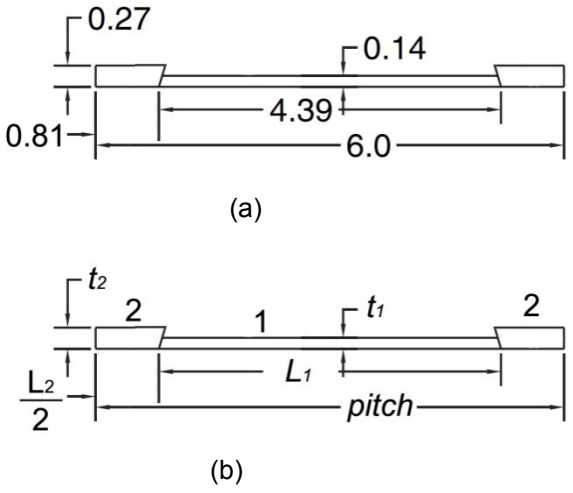

Figure I.2 a) Reduced cross-section of the corrugation (in inches), and b) generalized reduced cross-section of the corrugation.

The relationship in Equation I.21 exists between the reduced cross-section in Figure I.2b and the cross-section with an effective thickness t_{eff}. Note that A_{eff} , A_1 and A_2 are the areas of section 1 and 2 into the length of the page.

$$\frac{L_1}{A_1} + \frac{L_2}{A_2} = \frac{Z}{A_{eff}} \tag{I.17}$$

Since A_{eff} , A_1 and A_2 are area per length into the page, the can be substituted with t_{eff}, t_1, and t_2. This yields Equation I.22.

$$\frac{L_1}{t_1} + \frac{L_2}{t_2} = \frac{Z}{t_{eff}} \tag{I.18}$$

The drawings of the corrugation profile provide the following information. Section 1 of the reduced cross-section accounts for 17.4% of the total cross-sectional area of the corrugation and 73.2% of the total corrugation length. Section 2 of the reduced section accounts for 12.4% of the total cross-sectional area of the corrugation and 26.8% of the total corrugation length. So the Equation I.22 becomes,

$$\frac{0.7317\,Z}{\frac{0.1736\,A}{0.7317\,Z}} + \frac{0.2683\,Z}{\frac{0.1235\,A}{0.2683\,Z}} = \frac{Z}{t_{eff}} \tag{I.19}$$

Solving for t_{eff}, and substituting A from earlier yields,

$$t_{eff} = 0.2727\frac{A}{Z} \tag{I.20}$$

Further substitution yields,

$$t_{eff} = 0.2727\frac{w}{\rho\pi d_i} \tag{I.21}$$

The flexural rigidity EI can be calculated from Equation I.26 for a circular pipe section with an inner diameter d and thickness t_{eff}.

$$EI = \frac{\pi E}{64}\left[\left(d_i + 2t_{eff}\right)^4 - {d_i}^4\right] \tag{I.22}$$

No direct measurements of the flexural rigidity of HDPE pipes were available for comparison. The derivation of the flexural rigidity of the HDPE pipes assumes small loads and elastic material properties. Forces are assumed to be small enough to prevent buckling of the corrugation. For very large forces, slenderness of the pipe walls and buckling need to be considered when assessing the validity of these calculations.

CONCLUSIONS

Methods are presented for determining the flexural rigidity of standard corrugated sections of corrugated steel pipes and HDPE pipes. The corrugated steel pipe method can be used with many of the currently manufactured corrugated steel pipe culverts. The maximum error is 34% for the four test pipes used for the validation of the method presented in this Appendix. The method presented in this Appendix allows the flexural rigidity to be calculated without knowing the ratio of hoop strain to longitudinal strain. Measurement of that ratio is a requirement in calculating *EI* using the method presented in Havens (2003). It is slightly more accurate than Havens' method at predicting the flexural rigidity of the three test pipes available for comparison. Both methods provide conservative estimates of flexural rigidity for small diameter pipes using a corrugation helix angle greater than 8 degrees. The HDPE method is a very rough approximation that should only be used with pipes that have a double-walled arched corrugation as shown in Figure I.1a. Both methods presented in this Appendix assume the material remains elastic and that no buckling occurs.

Finite element analyses

CONTENTS

DEVELOPMENT OF BEAM-ON-SPRINGS MODEL USING EXPERIMENTAL DATA

Buried pipe culverts are modeled here as a beam resting on a series of springs. This appendix investigates finite element (FE) based beam-on-springs modeling for analyzing the pattern of movements observed in the pipes tested in the laboratory (Appendix C) and in the field (Appendix D). The process of data analysis follows several steps. First, the data from the laboratory testing is analyzed. It is best to begin with this data because detailed measurements of vertical, horizontal, and longitudinal movement were taken at six locations along the length of the pipe at the crown, the springline and the invert. In addition, the burial conditions and loading conditions are carefully controlled which should eliminate as much error as possible. If a beam-on-springs model cannot match the results of a carefully controlled laboratory experiment, then it raises doubts as to whether or not it can be used to model existing, or planned pipe culverts. After analysis of the laboratory test results, the field tests data is analyzed to see the effects of real-world burial conditions, years of deterioration caused by weather and tens of thousands, if not hundreds of thousands of repeated loadings.

Development of FE Based Beam-on-Springs Model Using the Laboratory Test Data

A beam-on-springs model of each test culvert is created using finite element, FE, analysis software. Some sort of FE modeling is necessary to solve any beam-on-springs problem. The FE model used here is quite simple and significantly less complex than the full 3D FE modeling that this study is attempting to avoid.

The FE model used to analyze the RC laboratory test pipe described in Appendix C is shown in Figure J.1. The RC test pipe is used for model development because it is the only test pipe where flexural stiffness of the joint is known. The following elements are used in the figure: uniformly distributed vertical stick elements (colored red) represent springs, the inclined discontinuous element is a beam element representing the pipe (in purple), and short linear elements connecting the individual pipes (in teal) are beam elements used to represent the joints, and the vertical arrows represent the distributed loading. The models are created using a spring spacing of 3 in. (7.6 cm). This is small enough to ensure an accurate beam-on-springs model. The middle two pipe elements are 8 ft (2.4 m) long and the outer two pipe elements are 4 ft (1.2 m) long.

This is representative of the test setup. An 18 kip (80 kN) load is applied based on the spreading characteristics of a 2 ft (0.6 m) burial depth.

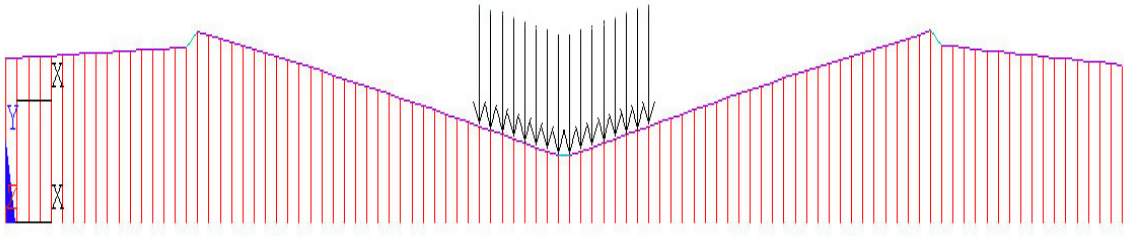

a) Loading centered above the middle joint

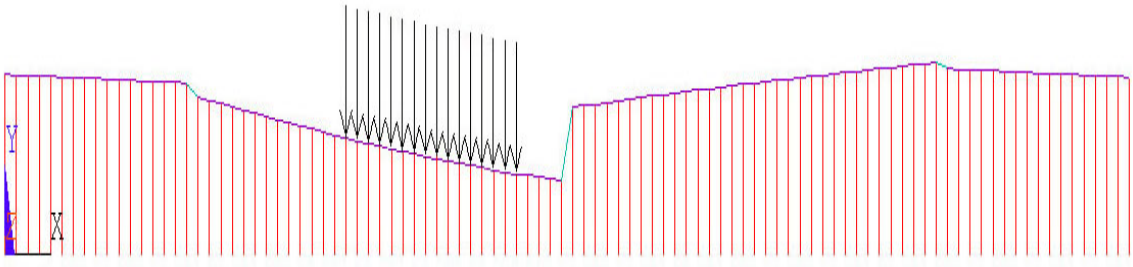

b) Loading centered 3 ft (0.9 m) to the left of the middle joint

Figure J.1 Deflected shape of the beam-on-springs FE model for the RC pipe tested in the laboratory.

In the beam-on-springs model, the only known variables are the flexural and axial stiffness of the pipes, *EI* and *EA*, the Poisson's ratio of the pipe material, ν, and the flexural stiffness of the RC pipe joints, *EI*. The flexural stiffness of each test pipe is calculated using the information presented in Appendix C. The measurements of flexural stiffness, *EI*, of the RC pipe joints are also discussed in Appendix C. The specific values are presented later in this appendix after full discussion of the beam-on-springs model.

Determining the Vertical Movement of Flexible Pipes

It is necessary to determine the vertical displacement of flexible pipes for use in beam-on-springs modeling. Bending of the pipe deforms it from its original circular shape and makes it difficult to determine the vertical movement of the pipe. Measurements of vertical displacement were taken at the crown, the springline, and the invert. If culvert pipes were rigid, measurements of vertical displacement at all three locations would produce the same values.

However, the flexibility of the HDPE and CMP culvert pipes causes vertical displacements to be different at each measurement location. This is problematic because a simple beam-on-springs model assumes that there is only one measurement of vertical displacement at any location along the beam elements. It is important to determine set of measurement data best predicts the overall vertical movement of the pipe. Typically, a flexible pipe deforms into an oval shape. The vertical displacements are largest at the crown and smallest at the invert. In the HDPE pipe, the measured vertical displacement is as large as twelve times the vertical displacement at the springline. This is due to bending of the top half of the pipe beyond normal pipe ovaling. If the pipe deformed as a perfect oval, the crown displacements would be less than two times the springline displacements. The large displacement at the crown seems unsuitable as a predictor of overall pipe movement. The vertical movements measured at the crown, invert, and springline are shown in Figure J.2 for the laboratory test of the CMP pipe under 2 ft (0.6 m) burial and loading offset 3 ft (0.9 m) south. This example illustrates issues discussed in this section.

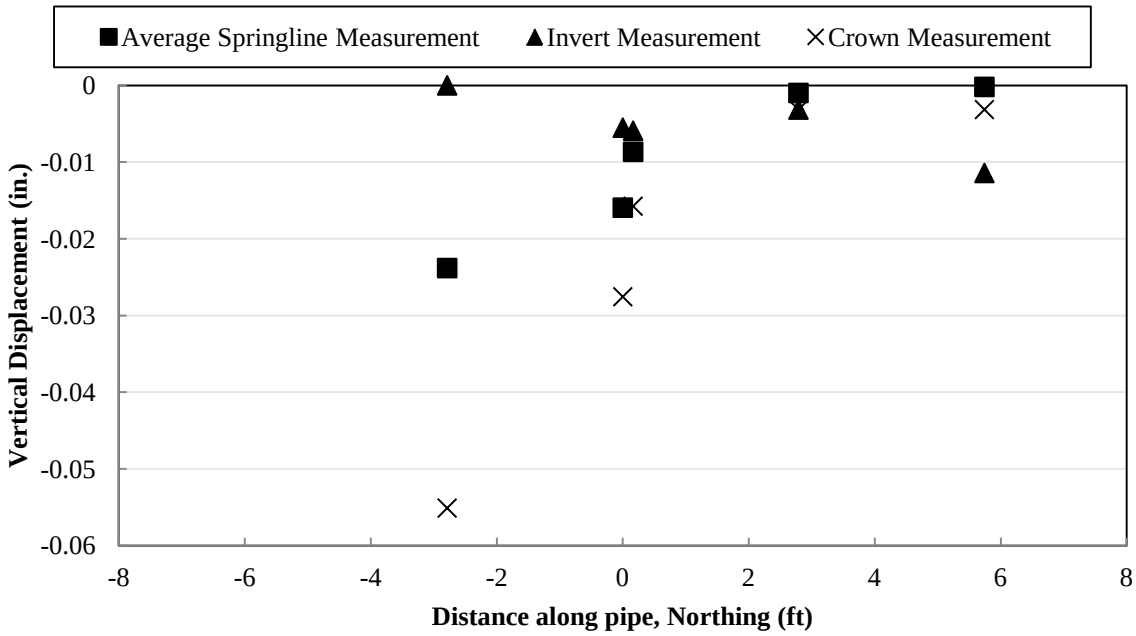

Figure J.2 Vertical displacement measured in the CMP laboratory test with loading positioned 3 ft south, and a 2 ft burial depth (1 ft = 0.3 m; 1 in = 2.54 cm)

The largest vertical displacement is expected to occur directly beneath the loading. This occurred in both the crown and springline measurements. However, largest vertical displacement at the invert was measured at a location other than directly beneath the loading. An example of this is shown in Figure J.2. This is likely due to local bending that cannot be

predicted by a simple beam-on-springs model. Attempts were made to use beam-on-springs modeling to match the invert data, but modeling always predicted the maximum vertical displacement directly beneath the loading. Laboratory tests results showed that vertical displacements at the springline give the best prediction the overall vertical movement of the pipe and will be used with beam-on-springs modeling.

Transfer of Surface Loading to the Pipe

Loading applied at the ground surface spreads out as it is transferred through the soil. Further away from the point directly beneath the surface load, the stress is reduced according to the work of Boussinesq as presented by Watkins and Anderson (1999). This kind of nonlinear behavior is relatively difficult to use with a beam-on-springs model. The simplest method of calculating loading on the pipe is to assume the loading spreads out linearly from the point of surface loading. The linear spreading is characterized by a live load distribution factor, LLDF. This method is used in AASHTO LRFD bridge design specifications for predicting the loading on buried structures.

In order to determine the best LLDF, multiple values were tested against the measured data. Recently, the AASHTO LRFD specifications reduced the LLDF design value from. AASHTO (2002) uses an LLDF of 1.75 and AASHTO (2006) uses an LLDF of 1.15. The smaller value leads to larger pressure over the culvert and results in a more conservative design approach. In order to test the effect of the LLDF value, beam-on-springs models are analyzed using four different LLDF values and the results are compared with the measured vertical displacements to see which distribution factor best matches the pattern of measured vertical displacements. At this point, the spring stiffness is unknown. So, the spring stiffness in each case is selected so that vertical displacement at the central joint is identical to the measured vertical displacement. The results are displayed in Figure J.3. All of the pipe information necessary for modeling is provided in Table J.1. The RC pipe is used for this analysis because the flexural stiffness of the joint is known. Varying the LLDF seems to have a relatively small effect on the overall deflected shape. However, it does seem to have an effect on the spring constant. A smaller LLDF requires a larger spring constant to give the same maximum vertical displacement. An LLDF of 0.75 requires a spring constant 80% larger than the spring constant required by an LLDF of 2 to give the same vertical displacement at the joint. There is not enough evidence here to support the use of any particular LLDF. The more modern approach in AASHTO LRFD is to use an LLDF of 1.15. This will give more conservative results than the older 2002 approach of using an LLDF of 1.75. Further beam-on-springs model development in the following sections uses an LLDF of 1.15.

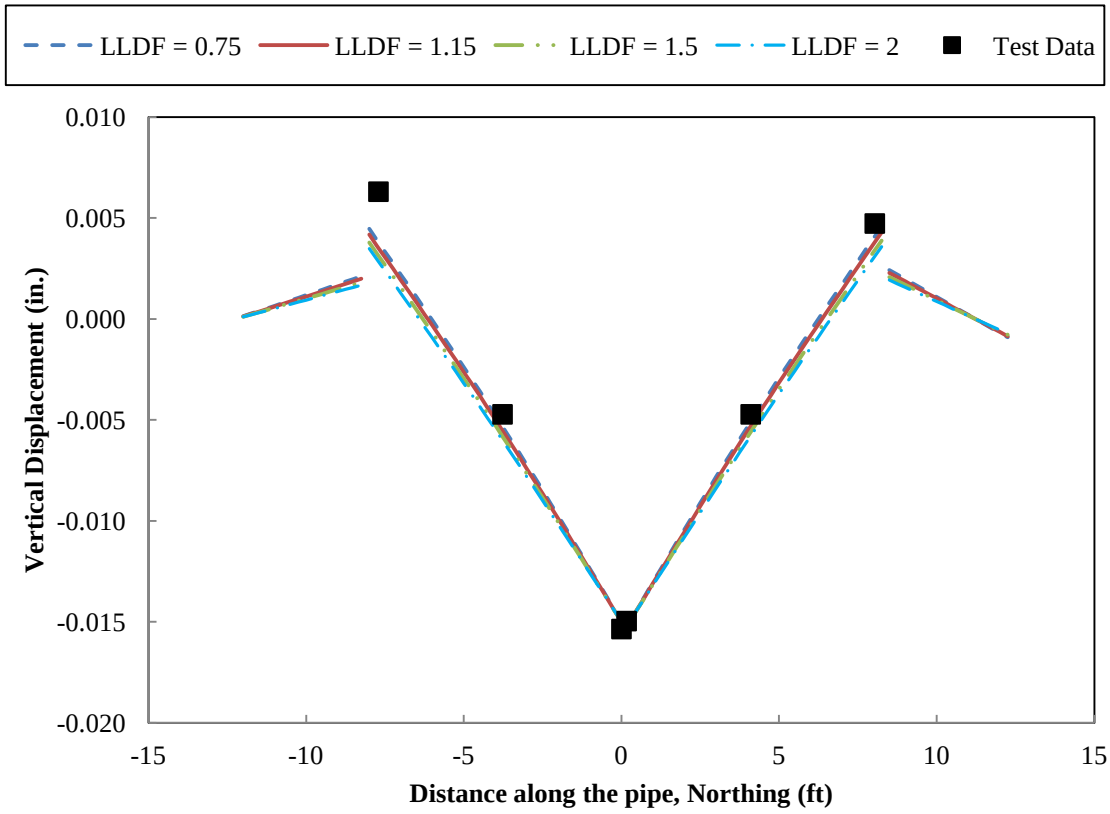

Figure J.3 The effect of LLDF on the calculated vertical displacements for the RC laboratory test pipe with loading centered on the joint (1 in. = 2.54 cm; 1 ft = 0.30 m)

Table J.1 Modeling data for the laboratory test pipes. (1 in. = 0.0254 m; 1 ksi = 6.9 MPa; 1 lbf-in^2 = 2.87x10^{-9} MN-m^2; 1 lbf = 4.4 N; 1 in^4 = 4.2x10^{-7} m^4; 1 in^2 = 6.5x10^{-4} m^2)

	RC	CMP	HDPE
Inner Diameter (in.)	24	36	60
Outer Diameter (in.)	30	37	67
Wall Thickness (in.)	3	0.055	-
Corrugation Geometry	-	2⅔ × ½	Arched Corrugation
Young's Modulus *E* (ksi)	4300	29000	110
Poisson's Ratio	0.2	0.3	0.4
Calculated *EI* (lbf-in^2)	1.01x10^{11}	2.43x10^8	9.2x10^8
Calculated *EA* (lbf)	1.09x10^9	1.59x10^8	1.6x10^7
Joint Length (in.)	3	9	3
I_{pipe} (in^4)	23472	8.38	8384
A_{pipe} (in^2)	254	5.48	141
I_{joint} (in^4)	0.823	5	200
A_{joint} (in^2)	0.445	0.0548	4
I_{pipe}/I_{joint}	28000	1.7	42
A_{pipe}/A_{joint}	570	100	35
Surface Load (lbf)	18000	22000	22000
Loading Plate Dimensions, L×W (in.)	20×10	20×10	20×10

Spring Stiffness

The most important part of a beam-on-springs model is the determination of spring stiffness. It can have a significant effect on the calculated displacements and the calculated internal stresses. Various factors make the determination of spring stiffness of the soil beneath a buried pipe an incredibly challenging endeavor. One problem is in the geometry of the system. The width of the beam affects the spring stiffness of the soil. Most beam-on-springs models are developed for a flat beam resting on the ground surface, not for circular pipes resting on the

ground. The circular shape of the pipe culverts may affect how the soil vertically supports the culvert. Typically, pipe culverts are installed by digging a trench, placing and compacting bedding at the bottom of the trench, placing the pipes at the bottom of the trench and refilling the trench with compacted fill. Spring stiffness of the soil is affected by normal and shear stresses applied to the bottom half of the culvert by both the bedding and backfill material and the original soil material at the bottom of the trench. Soil cohesion also has an effect on the spring stiffness. However, most models ignore soil cohesion because it is very challenging to define its effect. Bedding and backfill material serves the purpose of creating a stiff soil envelope around the culvert. Material properties of the soil envelope are used in determining the spring stiffness.

There are three available models proposed by Biot (1937), Terzaghi (1955), and Vesic (1961) that might be suitable for predicting spring stiffness beneath beams. All three models predict the modulus of subgrade reaction, k_s, for a flat beam resting on the ground surface. The modulus of subgrade reaction is a spring stiffness for pressure applied to the soil surface and has units of force/length^3. Each model predicts the modulus of subgrade reaction using known or expected soil stiffness parameters. The Biot and Vesic models use the soil modulus E_s and Poisson's ratio ν_s to predict the spring stiffness of the soil. The Terzaghi model uses the modulus of subgrade reaction of the soil for a 1 ft (0.3 m) wide beam k_{s1} to predict the spring stiffness of the soil.

It is nearly impossible to know the precise values of E_s and k_{s1} during any of the tests because the soil stiffness is affected by the compaction of the soil. Compaction of the soil changes between each test due to the repeated loading of the soil. It is impossible to predict the precise spring stiffness of the soil beneath each culvert using the three models without precise E_s and k_{s1} values. It is only possible know what the approximate or expected E_s and k_{s1} values are because these values change from test to test. The researchers at Queens University who performed the tests have suggested that the expected soil stiffness parameters are E_s = 5800 psi (40 MPa) and k_{s1} = 365 pci (99.3 MN/m^3) based on the soil compaction and testing of the soil. The Poisson's ratio of the soil is taken to be 0.3. The actual spring stiffness values will be determined using the beam-on-springs modeling. Then the soil stiffness parameters E_s and k_{s1} will be back-calculated from the spring stiffness values and compared to the expected soil stiffness parameters.

In order to determine the actual spring stiffness of the soil beneath each of the three laboratory test pipes during each of the eighteen tests, an iterative process of changing the spring stiffness in each model is used until the maximum calculated displacements equal the maximum measured displacements. These back-calculated spring stiffnesses are shown in Table J.2. The values in this table are the spring stiffness (kip/in.) per unit length of the pipe (in.) yielding units

of ksi. It should be noted that values in this table cannot be compared between the different pipes because the effect of the pipe diameter is not accounted for.

Table J.2 Spring stiffness values for all laboratory tests determined using the beam-on-springs model (1 ksi = 6.9 MPa; 1 ft = 0.30 m)

	RC		CMP		HDPE	
Burial Depth (ft)	2	4	2	4	2	4
Spring stiffness for loading centered on joint (ksi)	13	6.5	8.3	5.0	12	42*
Spring stiffness for loading 3 ft south of joint (ksi)	9.5	13	6.7	7.7	12	24
Spring stiffness for loading 3 ft north of joint (ksi)	13	15	22*	6.2	10	24

*Values considered to be outliers

There is no clear indication that the burial depth has any effect on the spring stiffness of the soil. A wide range of spring stiffness values are observed. In the case of the CMP pipe at 2 ft (0.6 m) burial, the maximum spring stiffness value is 3.3 times as large as the minimum value. There appear to be outliers in the CMP 2 ft (0.6 m) burial tests and the HDPE 4 ft (0.6 m) burial tests. In cases where there are no apparent outliers, the largest range of spring stiffnesses is observed in the RC pipe at 4 ft (1.2 m) burial where the maximum value is 2.3 times as large as the minimum value.

The Biot, Vesic, and Terzaghi models predict the modulus of subgrade reaction for a beam resting on the ground surface. It is postulated that modulus of subgrade reaction of soil beneath and around a circular culvert is twice as large as at the surface (Teng, 1969) because soil tends to be stiffer at depth. The modulus of subgrade reaction predicted in each model is doubled to account for this. The flexible culverts add an additional amount of flexibility to the system and reduce the apparent spring stiffness of the soil. To account for this, it is proposed that the modulus of subgrade reaction predicted by each model be reduced by a factor of 0.7 for the flexible CMP and HDPE pipes. Values from Table J.2 are used to back-calculate the soil stiffness parameters E_s and k_{s1} using each of the three models combined with the doubling factor used by Teng (1969). The beam width used in back-calculation is taken to be the outer diameter of the test pipes. The back-calculated parameters are then averaged for each test culvert and method. They are presented in Table J.3 both with and without the 0.7 reduction factor proposed above. The goal is to show that back-calculated soil stiffness parameters are similar for each test pipe because the same soil was used in each test. For each method, the three average back-

calculated parameters show better agreement with each other when then 0.7 reduction factor is used for the flexible pipes.

Table J.3 Comparison of back-calculated soil stiffness parameters (E_s and k_{s1}) with and without the 0.7 factor proposed for flexible pipes. Outliers identified in

Table J.2 are ignored. (1 psi = 6.9 kPa; 1 pci = 0.27 MN/m^3)

	Average of back-calculated soil stiffness parameters					
	With 0.7 reduction factor			Without 0.7 reduction factor		
Method	RC	CMP	HDPE	RC	CMP	HDPE
Biot E_s (psi)	7567	3330	6453	7567	2414	4677
Vesic E_s (psi)	10180	5104	10363	10180	3672	7456
Terzaghi k_{s1} (pci)	402	298	502	402	209	351

Accounting for 0.7 reduction factor and the doubling factor suggested by Teng, the modulus of subgrade reaction predicted by each model for rigid RC pipes is taken to be:

$$k_{s,rigid} = 2k_{s,model} \quad \text{(J.1)}$$

and for flexible CMP and HDPE pipes:

$$k_{s,flexible} = 1.4k_{s,model} \quad \text{(J.2)}$$

Using each of the models combined with Equations J.1 and J.2, the soil stiffness parameters (k_{s1} and E_s) are back-calculated from values presented in Table J.2 and compared to expected soil stiffness parameters. The back-calculated soil stiffness parameters are tabulated in Table J.4 for each of the three methods and eighteen tests, and compared with expected soil stiffness parameters in Figure J.4.

Table J.4 Back-calculated soil stiffness parameters (E_s and k_{s1}) for all laboratory tests using the Biot, Vesic, and Terzaghi methods (1 ksi = 6.9 MPa; 1 pci = 0.27 MN/m^3; 1 ft = 0.30 m)

Method	Load position	RC		CMP		HDPE	
		2 ft burial	4 ft burial	2 ft burial	4 ft burial	2 ft burial	4 ft burial
Biot E_s (ksi)	Loading centered on joint	8.5	4.4	4.0	2.5	5.0	15.3*
	Loading 3 ft south of joint	6.2	8.5	3.3	3.7	5.0	9.1
	Loading 3 ft north of joint	8.5	9.4	9.5*	3.1	4.2	9.1
Vesic E_s (ksi)	Loading centered on joint	11.4	5.9	6.2	4.0	8.0	25.7*
	Loading 3 ft south of joint	8.3	11.4	5.2	5.9	8.1	15.0
	Loading 3 ft north of joint	11.4	12.7	15.4*	4.8	6.8	15.0
Terzaghi k_{s1} (pci)	Loading centered on joint	454	221	367	220	378	1298*
	Loading 3 ft south of joint	323	454	294	338	373	726
	Loading 3 ft north of joint	454	510	954*	272	307	726

*****Values considered to be outliers

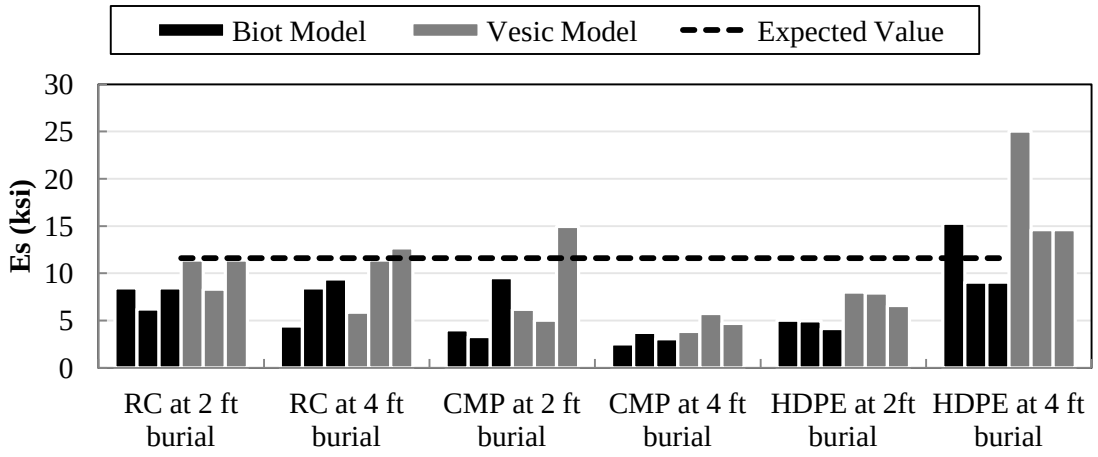

a) Back-calculated E_s values from the Biot and Vesic models

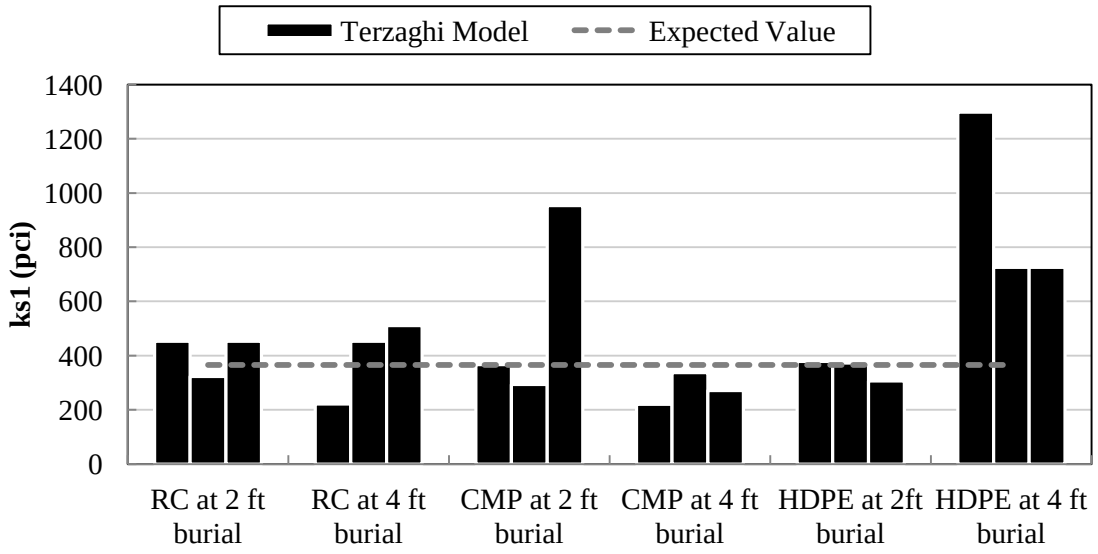

b) Back-calculated k_{s1} values from the Terzaghi model

Figure J.4 Comparison of back-calculated soil stiffness parameters with expected soil stiffness parameters for all 18 tests. (1 ksi = 6.9 MPa; 1 pci = 0.27 MN/m^3)

The accuracy of the back-calculated soil stiffness values is presented in Table J.5. Two of the 18 test values are considered to be outliers and are ignored. Outliers are identified in Table J.4. The

average of the back-calculated values from the Vesic and Terzaghi methods show the best agreement with the expected value. The Terzaghi method is the most accurate and yields back-calculated values that have the smallest range. The "range of values" in Table J.5 is the maximum back-calculated value divided by the minimum back-calculated value. It is a measure of the maximum spread of the data.

Table J.5 Comparison of the accuracy of each model. Outliers are excluded when calculating these values. Values used for calculation and outliers are identified in Table J.4. (1 ksi = 6.9 MPa; 1 pci = 0.27 MN/m^3)

Method	Average Back-Calculated Value	Expected Value	Deviation from Expected Value (%)	Standard Deviation as % of Average Value	Range of Values
Biot E_s (ksi)	5.9	11.6	-49%	41%	4.1
Vesic E_s (ksi)	8.7	11.6	-25%	30%	3.8
Terzaghi k_{s1} (pci)	402	365	+10%	36%	3.3

It is remarkable that the Terzaghi model, which is the most simple of the models, gives the best accuracies, and yield's the narrowest spread of back-calculated values. It is proposed that the Terzaghi model be used for analysis in conjunction with Equations J.1 and J.2 to determine the modulus of subgrade reaction.

Joint Stiffness

Determination of joint stiffness is an extremely complicated matter and depends on the on the geometry and strength of the bell, the spigot, and the interface material. Manufacturers do not provide enough information for independent researchers to accurately predict the shear and moment resistance at the joint. These parameters must be measured or back-calculated. The goal of this study is to give manufacturers a beam-on-springs model so that they can study their new joint designs to see if they are suitable for resisting the forces and displacements that they may be subjected to during their lifetime. Joint stiffness is something that naturally depends on the new joint design. The goal of this section is to investigate how well a beam-on-springs model can capture joint behavior with a single back-calculated joint stiffness used for all six tests on each culvert pipe, Appendix C.

Stiffness of the joint is defined by four parameters: Young's modulus E, moment of inertia I_p, cross-sectional area A_p, and the Poisson's ratio v. The flexural stiffness is dependent on E and I_p.

The shear stiffness is dependent upon E, A_p, and v. The only measured joint stiffness parameter is the flexural stiffness of the concrete pipe joint. In order to determine the other joint stiffnesses, the beam-on-springs model is used to back-calculate values for joint stiffness that matches the data the best. The stiffness of the joint element in the beam-on-springs model is affected by the length of the joint element being used. A long element with a large EI, and a short element with a small EI can have the same resistance to the applied bending moments. The joint length in the CMP pipes is quite close to 9 inches, and the joint length in the HDPE and RC pipes is close to 3 inches. Those values are used in the beam-on-springs modeling. The stiffness of the joint is presented as a ratio of the pipe stiffness to joint stiffness. Beam elements used to model the joint use the same E and v parameters as the pipe. This gives insight into how weak the joint is relative to the pipe. The parameters used in the modeling the joint stiffness were presented in Table J.1.

Model Verification

A final analysis of the accuracy of the model is performed. All beams are analyzed using the values presented in Tables J.1 and J.2. The east and west vertical displacements measured at the springline are averaged to determine the vertical displacement at each measurement location along the length of the pipe. Calculated shear displacements across the joint and joint rotations were presented in Table J.6 and Table J.7, respectively. Methods for calculating shear displacement and joint rotation are presented in Appendix D. Figures J.5 to J.22 present detailed comparisons of the measured and calculated vertical displacements. The spring stiffnesses used in those analyses are presented in Table J.2. The charts give the best understanding of how well the beam-on-springs model matches the measurements.

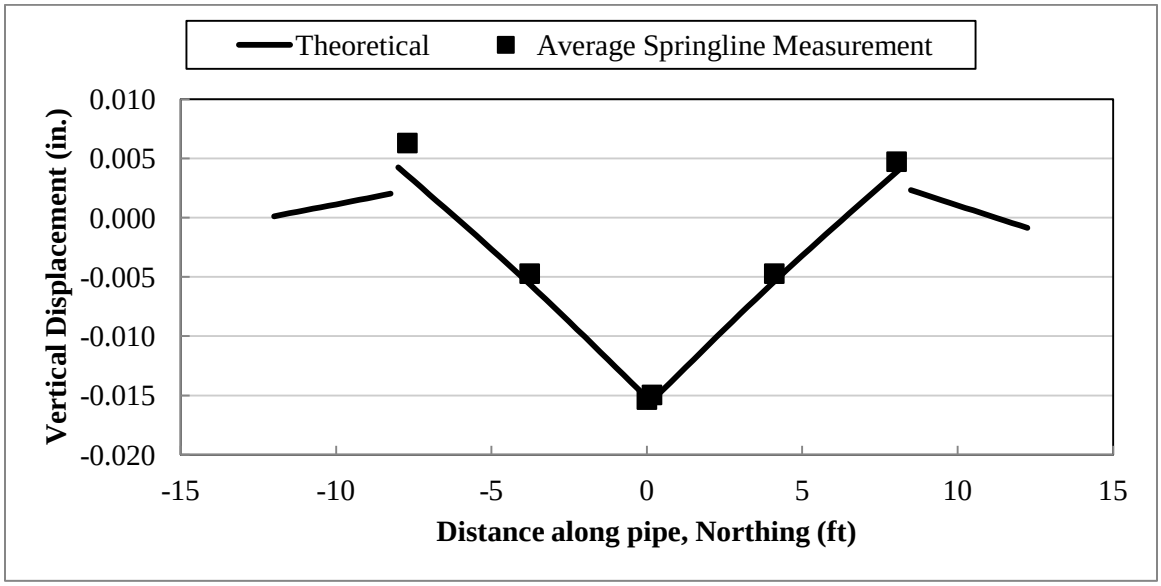

Figure J.5 Theoretical versus measured vertical movement of the RC laboratory test pipe at 2 ft burial and load directly above the joint (1 ft = 0.3 m)

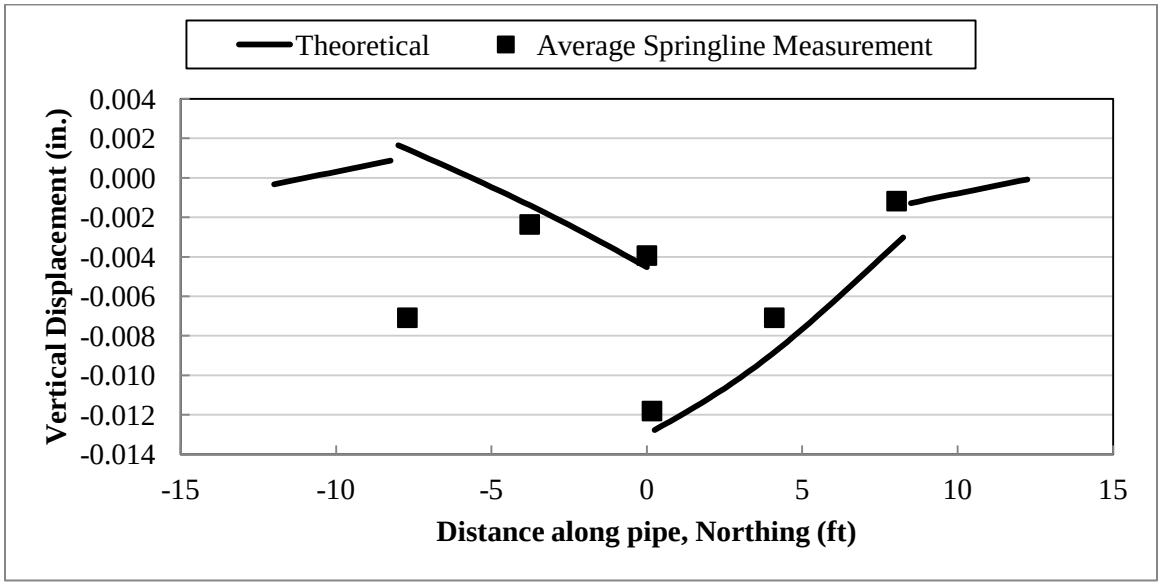

Figure J.6 Theoretical versus measured vertical movement of the RC laboratory test pipe at 2 ft burial and load offset 3 ft north of joint (1 ft = 0.3 m)

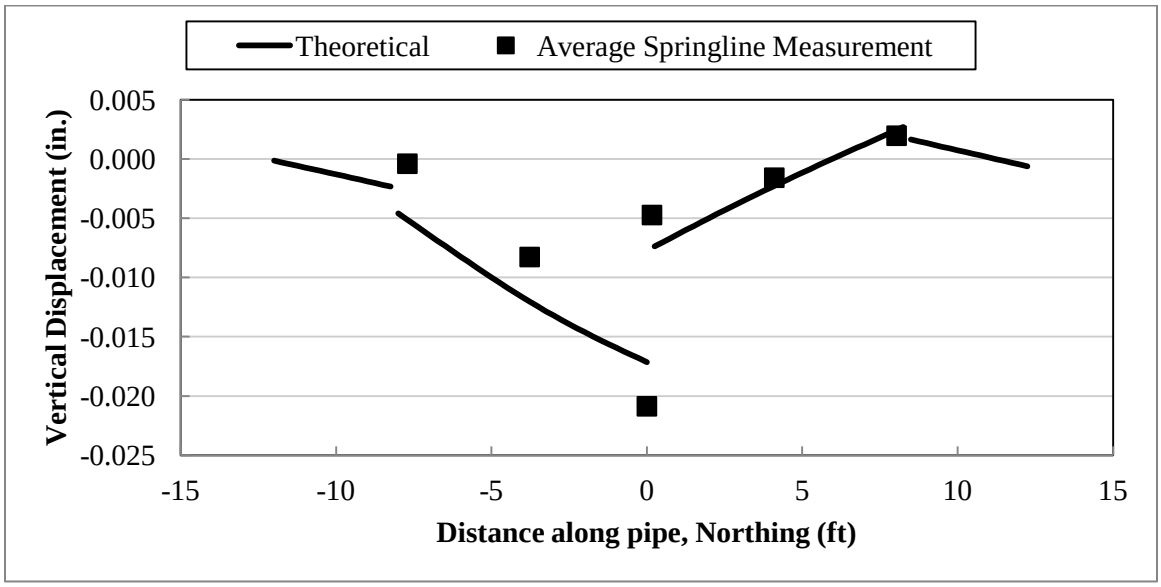

Figure J.7 Theoretical versus measured vertical movement of the RC laboratory test pipe at 2 ft burial and load offset 3 ft south of joint (1 ft = 0.3 m)

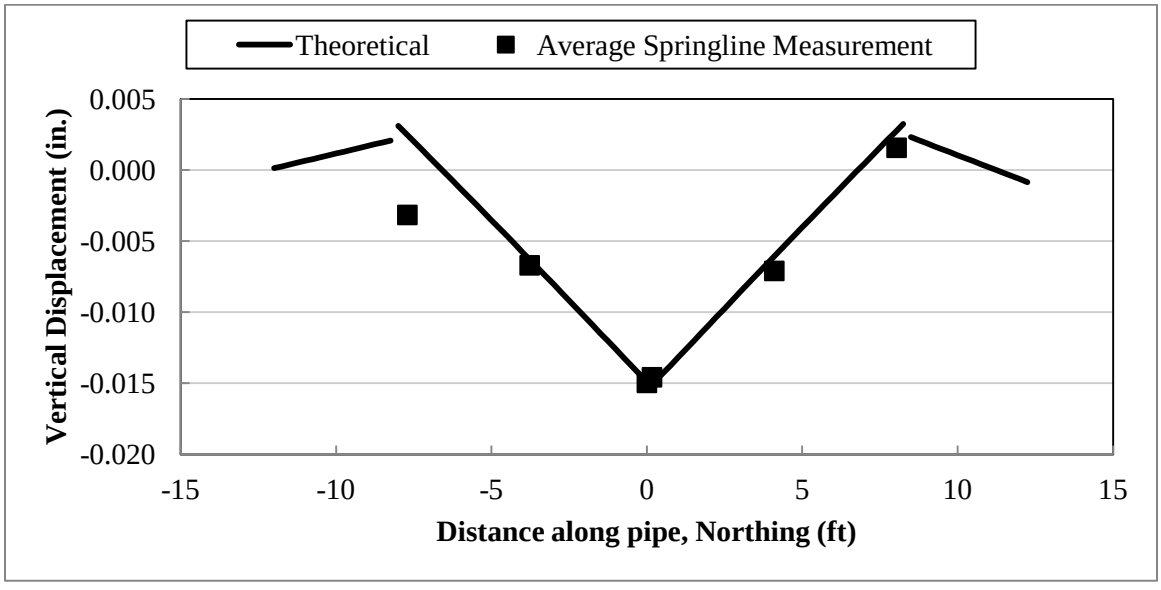

Figure J.8 Theoretical versus measured vertical movement of the RC laboratory test pipe at 4 ft burial and load directly above the joint (1 ft = 0.3 m)

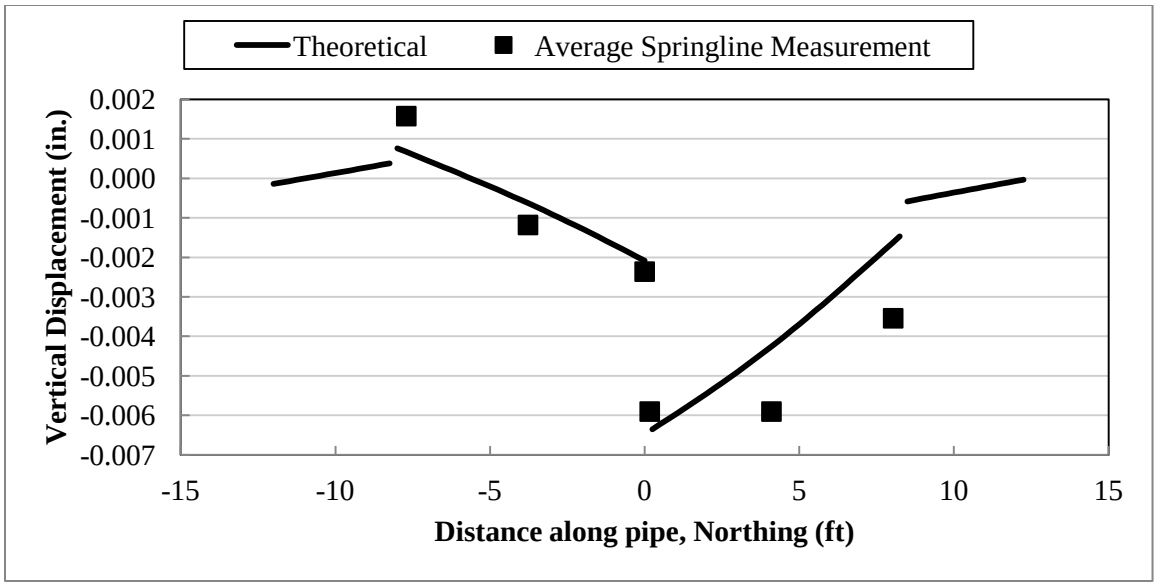

Figure J.9 Theoretical versus measured vertical movement of the RC laboratory test pipe at 4 ft burial and load offset 3 ft north of joint (1 ft = 0.3 m)

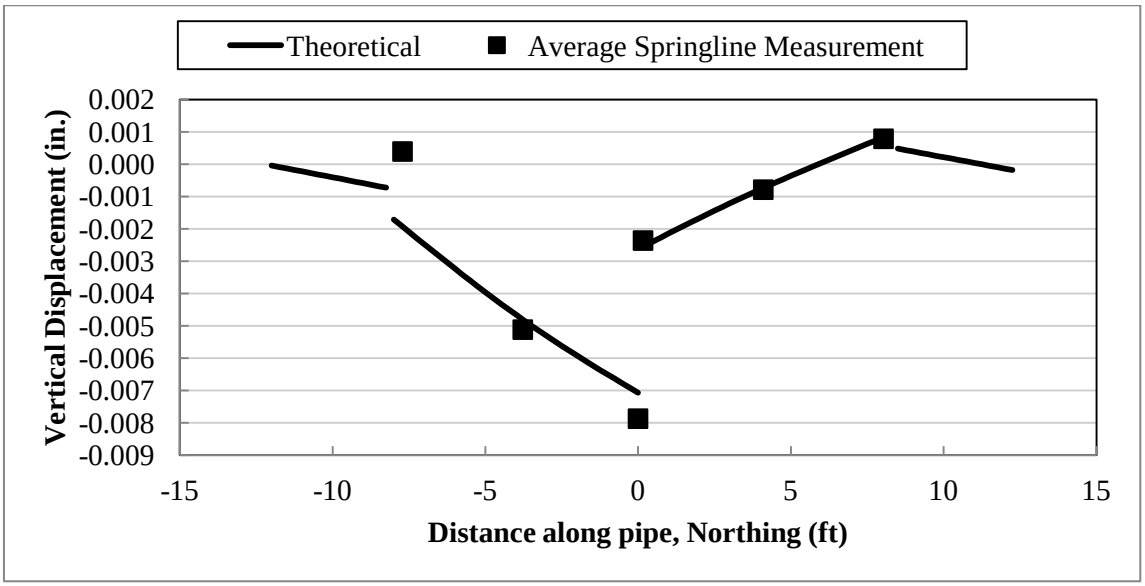

Figure J.10 Theoretical versus measured vertical movement of the RC laboratory test pipe at 4 ft burial and load offset 3 ft south of joint (1 ft = 0.3 m)

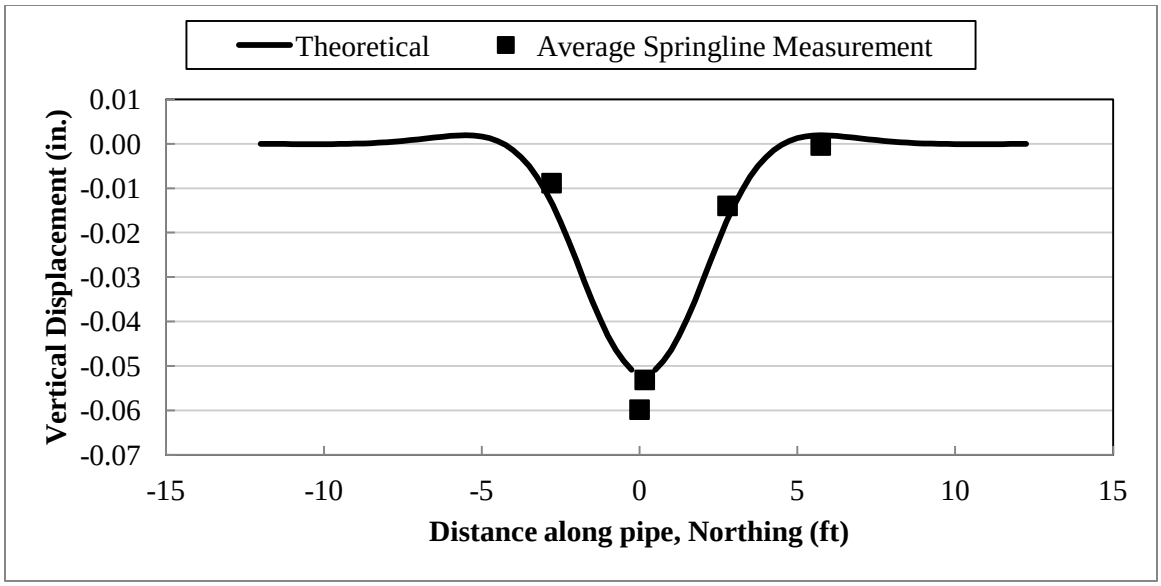

Figure J.11 Theoretical versus measured vertical movement of the CMP laboratory test pipe at 2 ft burial and load directly above the joint (1 ft = 0.3 m)

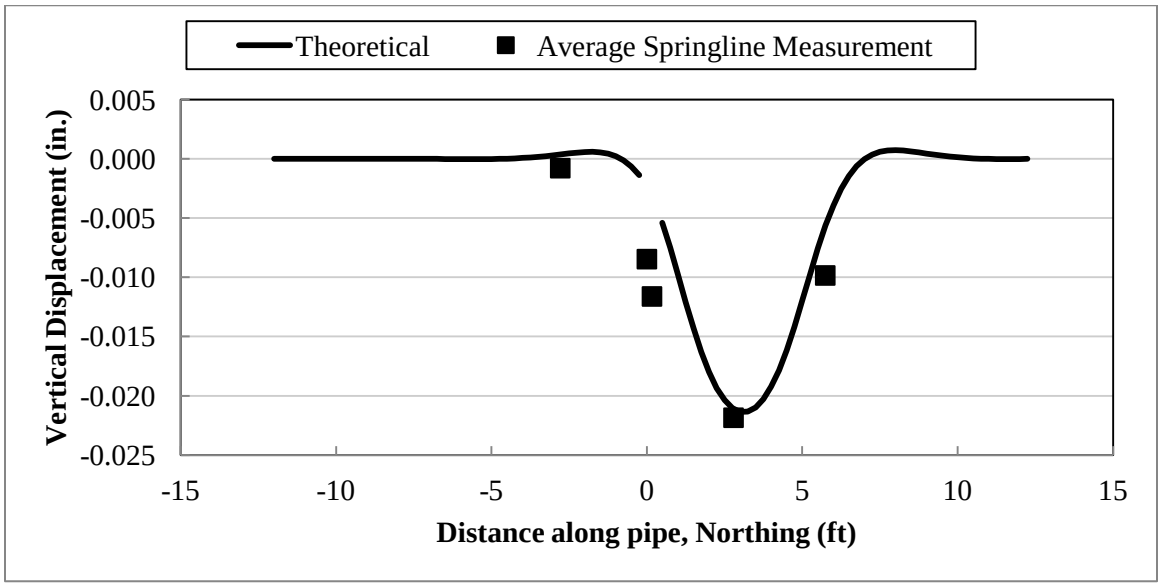

Figure J.12 Theoretical versus measured vertical movement of the CMP laboratory test pipe at 2 ft burial and load offset 3 north ft of joint (1 ft = 0.3 m)

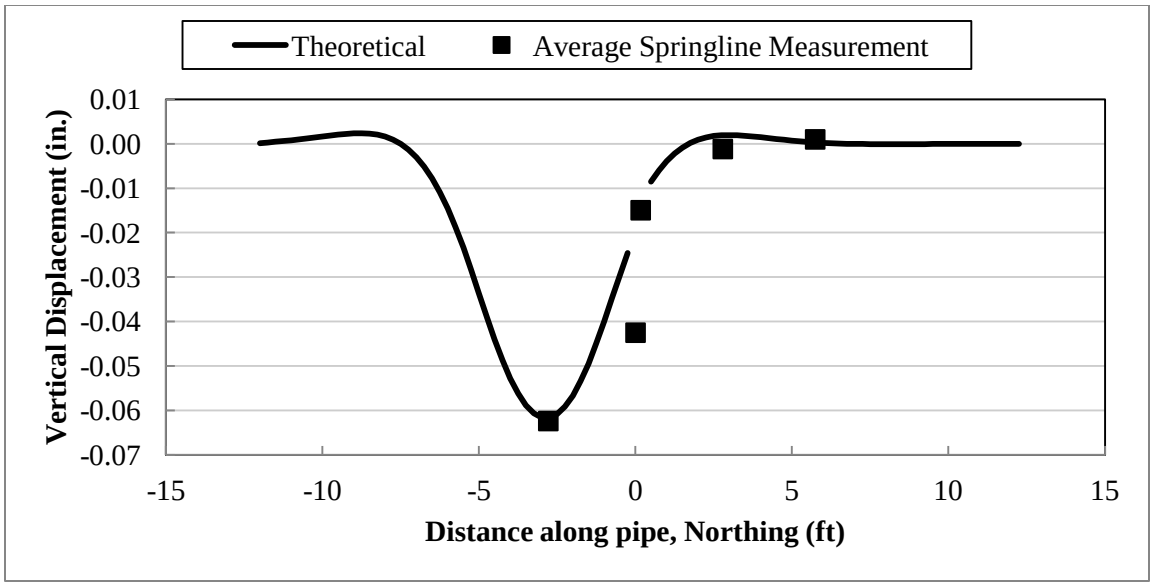

Figure J.13 Theoretical versus measured vertical movement of the CMP laboratory test pipe at 2 ft burial and load offset 3 ft south of joint (1 ft = 0.3 m)

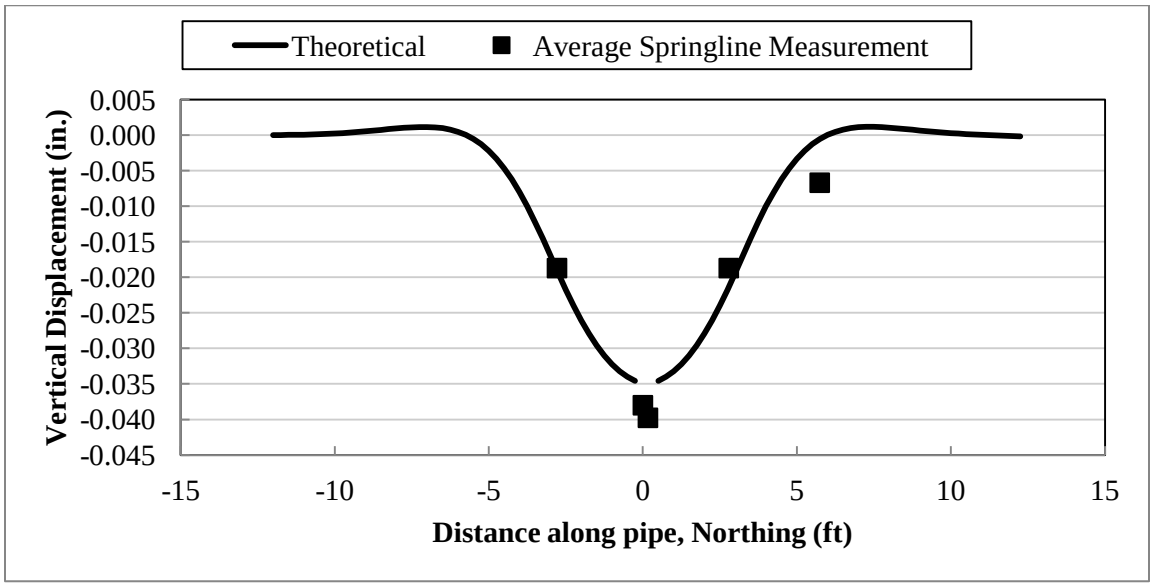

Figure J.14 Theoretical versus measured vertical movement of the CMP laboratory test pipe at 4 ft burial and load directly above the joint (1 ft = 0.3 m)

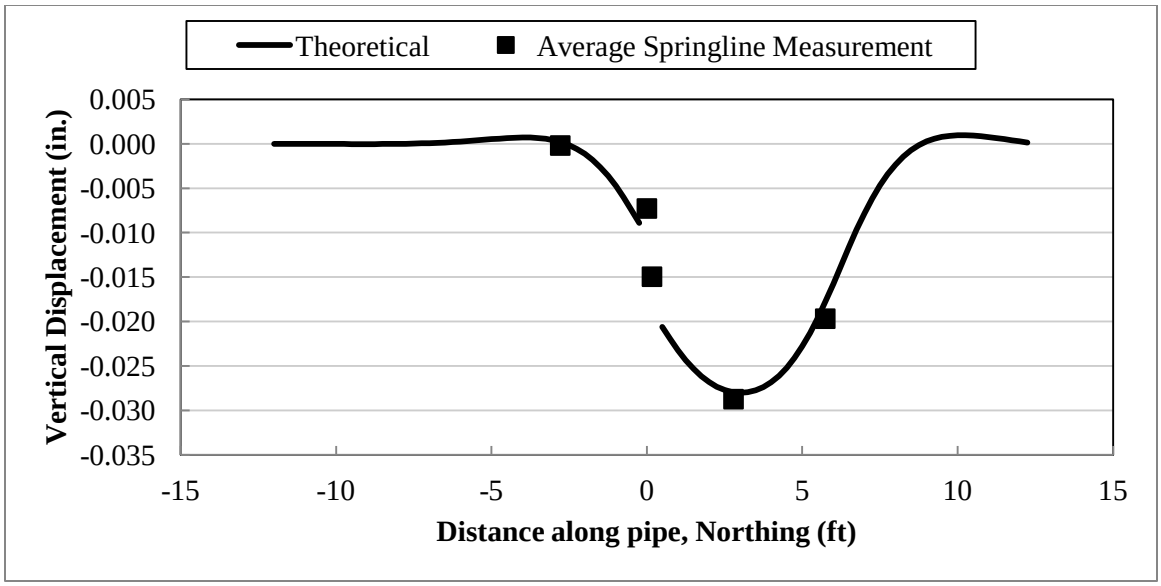

Figure J.15 Theoretical versus measured vertical movement of the CMP laboratory test pipe at 4 ft burial and load offset 3 ft north of joint (1 ft = 0.3 m)

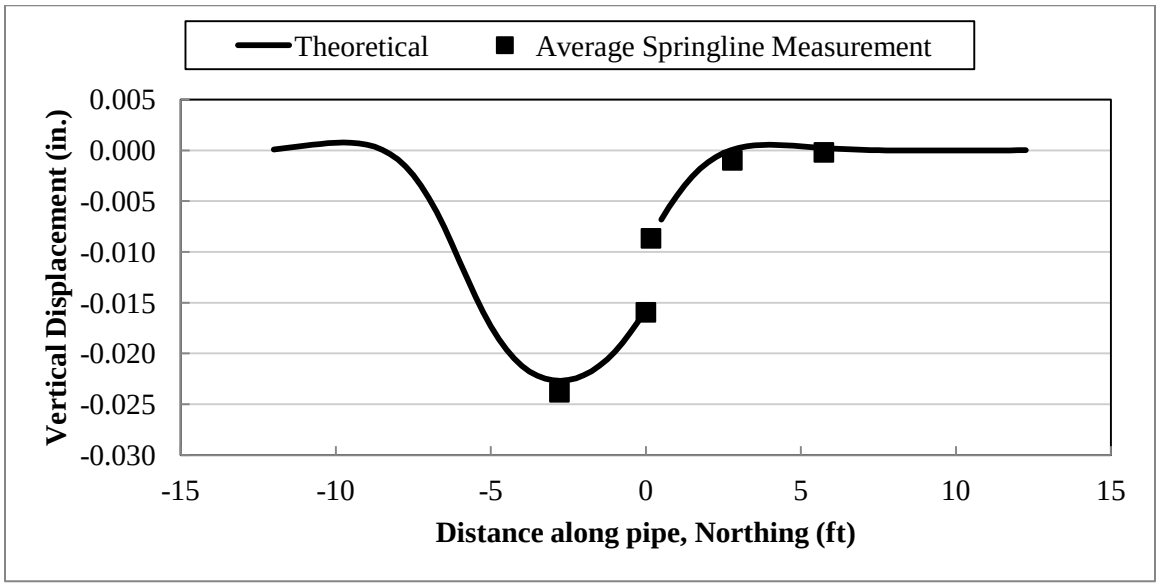

Figure J.16 Theoretical versus measured vertical movement of the CMP laboratory test pipe at 4 ft burial and load offset 3 ft south of joint (1 ft = 0.3 m)

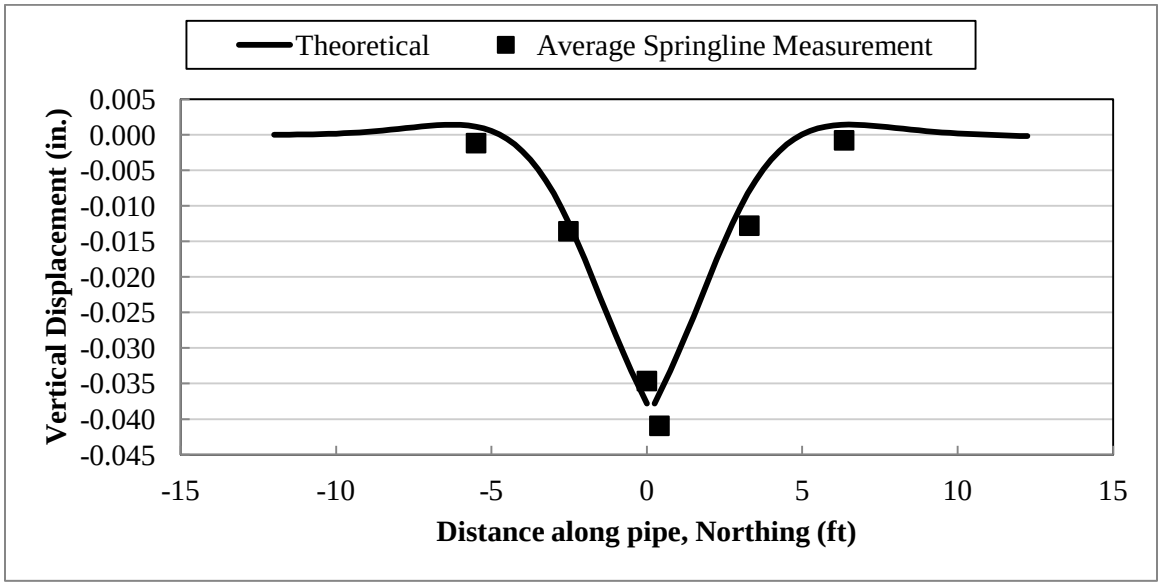

Figure J.17 Theoretical versus measured vertical movement of the HDPE laboratory test pipe at 2 ft burial and load directly above the joint (1 ft = 0.3 m)

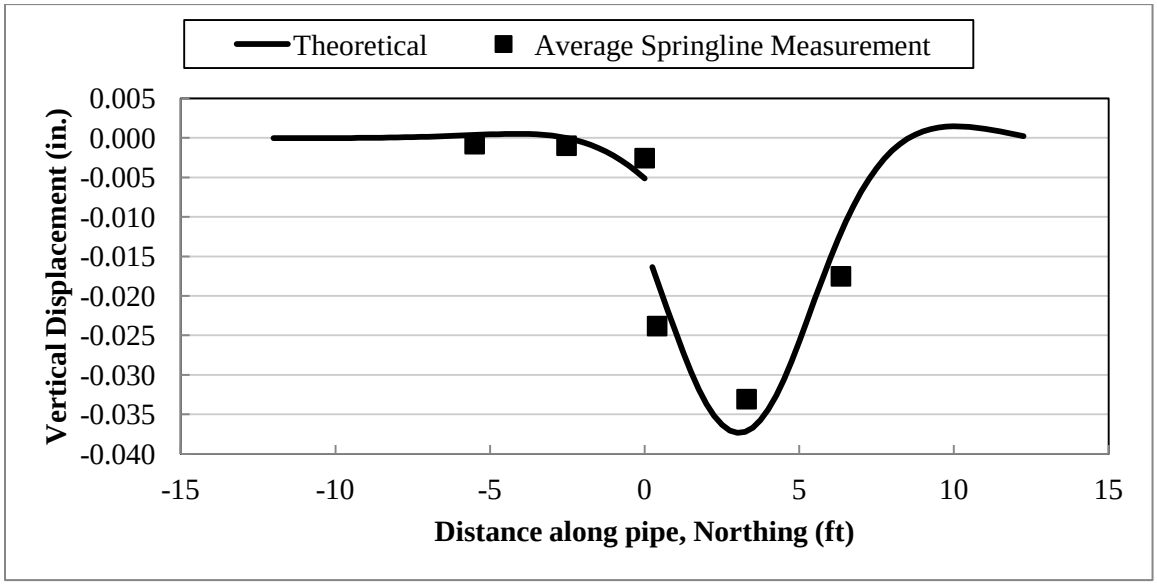

Figure J.18 Theoretical versus measured vertical movement of the HDPE laboratory test pipe at 2 ft burial and load offset 3 ft north of joint (1 ft = 0.3 m)

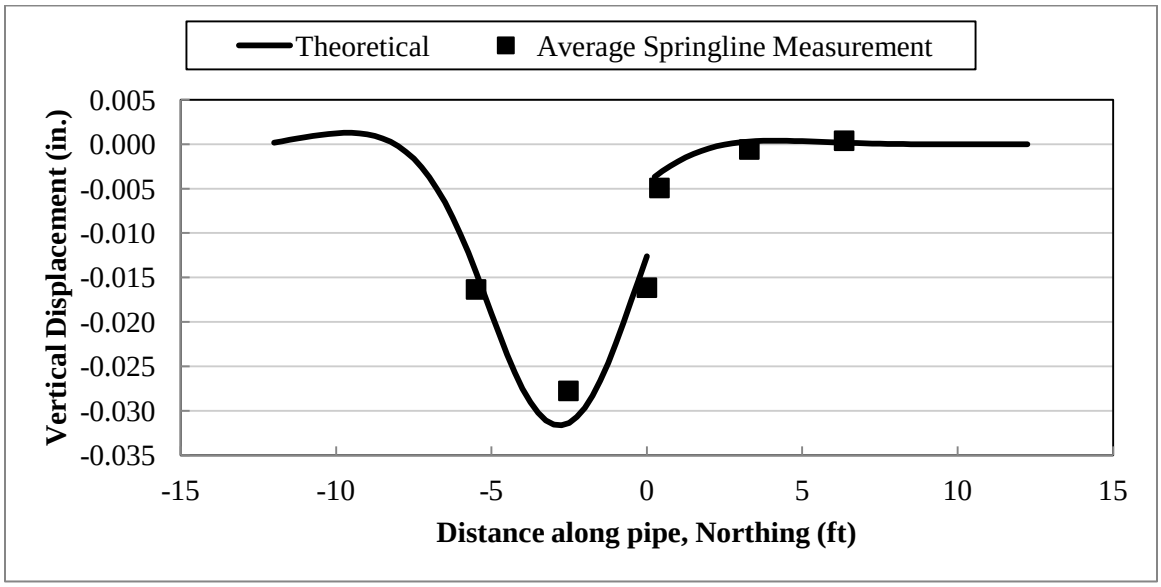

Figure J.19 Theoretical versus measured vertical movement of the HDPE laboratory test pipe at 2 ft burial and load offset 3 ft south of joint (1 ft = 0.3 m)

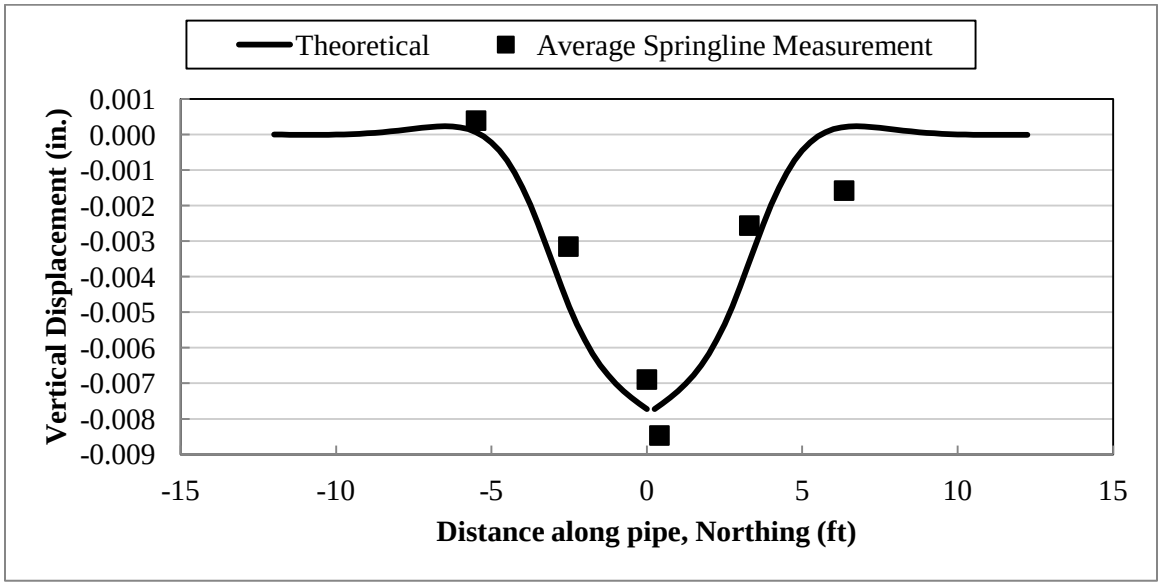

Figure J.20 Theoretical versus measured vertical movement of the HDPE laboratory test pipe at 4 ft burial and load directly above the joint (1 ft = 0.3 m)

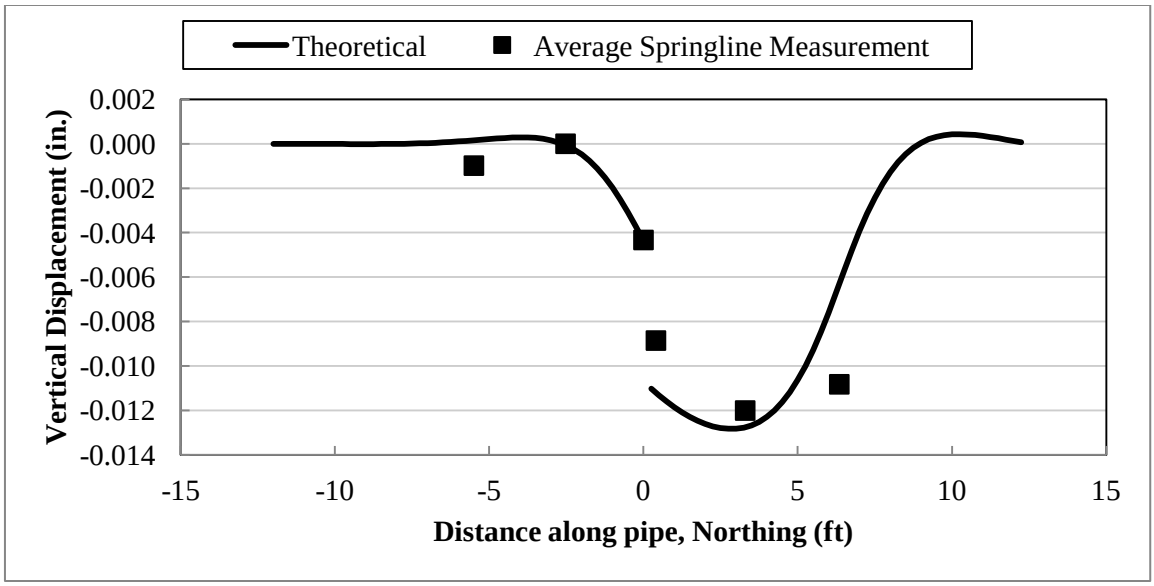

Figure J.21 Theoretical versus measured vertical movement of the HDPE laboratory test pipe at 4 ft burial and load offset 3 ft north of joint (1 ft = 0.3 m)

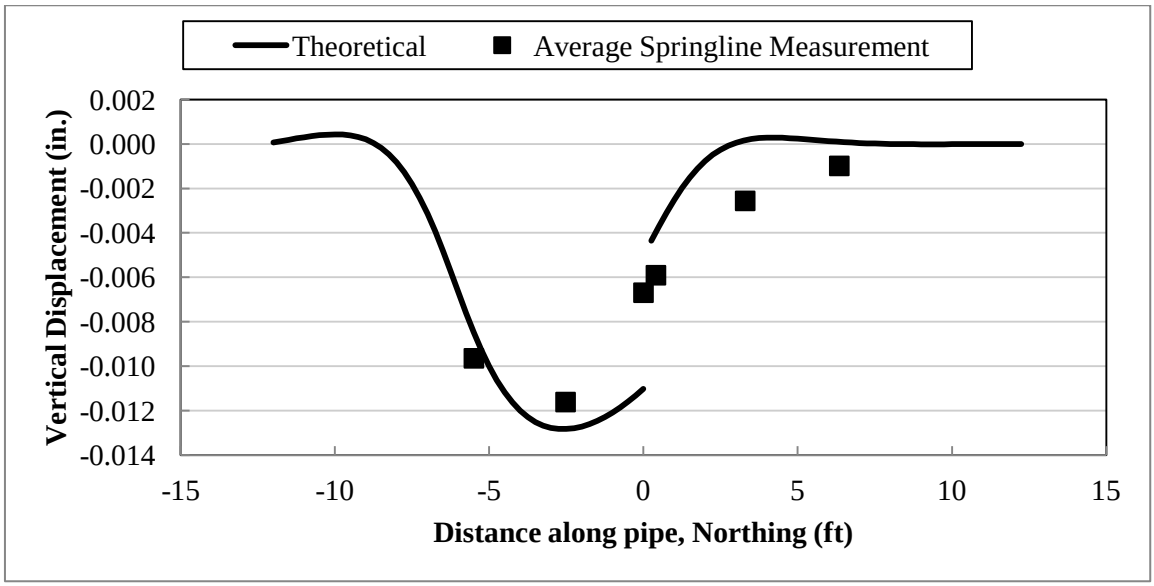

Figure J.22 Theoretical versus measured vertical movement of the HDPE laboratory test pipe at 4 ft burial and load offset 3 ft south of joint (1 ft = 0.3 m)

Table J.6 Measured versus theoretical shear displacements for all 18 laboratory tests (1 in = 2.54 cm; 1 ft = 0.3 m)

		Shear displacement across the pipe joint					
		2 ft burial depth			4 ft burial depth		
		No loading offset	Loading offset 3 ft North	Loading offset 3 ft South	No loading offset	Loading offset 3 ft North	Loading offset 3 ft South
RC	Measured (in.)	-0.0004	0.0079	-0.0161	-0.0004	0.0035	-0.0055
	Theoretical (in.)	0	0.0082	-0.0098	0	0.0043	-0.0046
	Difference from Measured Value (%)	-	5	-40	-	20	-17
CMP	Measured (in.)	-0.0067	0.0031	-0.0276	0.0018	0.0077	-0.0073
	Theoretical (in.)	0	0.0040	-0.0160	0	0.0117	-0.0100
	Difference from Measured Value (%)	-	28	-42	-	52	38
HDPE	Measured (in.)	0.0063	0.0213	-0.0112	0.0016	0.0045	-0.0008
	Theoretical (in.)	0	0.0112	-0.0089	0	0.0067	-0.0067
	Difference from Measured Value (%)	-	-47	-20	-	47	748*

*The shear resistance of the joint appeared unusually stiff

Overall, the model does a decent job of matching the shear displacement across the joint, given the complexities of the buried culvert structures. One weakness is that no shear displacement across the joint can be predicted when the loading is centered on the joint due to the symmetry of the model. However, this is unimportant because the major goal of this model is to predict the maximum displacements for design, and the shear displacements are never largest when the loading is centered on the joint.

Table J.7 Measured versus theoretical joint rotations for all 18 laboratory tests (1 ft = 0.3 m)

		Relative rotation of connected pipes					
		2 ft burial depth			4 ft burial depth		
		No Loading Offset	Loading Offset 3 ft North	Loading Offset 3 ft South	No Loading Offset	Loading Offset 3 ft North	Loading Offset 3 ft South
RC	Measured (deg)	-0.0259	-0.0077	-0.0198	-0.0195	-0.0015	-0.0054
	Theoretical (deg)	-0.0243	-0.0089	-0.0128	-0.0219	-0.0045	-0.0051
	Difference From Measured Value (%)	-6	15	-35	12	198[a]	-6
CMP	Measured (deg)	-0.1586	0.0055	0.0090	-0.0714	0.0129	-0.0005
	Theoretical (deg)	-0.1418	0.0272	0.0507	-0.0580	-0.0032	-0.0023
	Difference From Measured Value (%)	-11	396	465	-19	-125	384
HDPE	Measured (deg)	-0.0863	0.0123	0.0148	-0.0168	-0.0030	0.0038
	Theoretical (deg)	-0.0953	0.0235	0.0295	-0.0119	-0.0054	-0.0037
	Difference From Measured Value (%)	10	91	99	-29	80	[b]

a. Unusual pipe bending is measured in RC pipe, possible measurement error

b. HDPE pipe affected by unusual shear stiffness

The largest percentage error in predicting joint rotation is for the flexible pipes when loading is offset 3 ft (0.9 m) from the joint. This error is generally acceptable because the rotation is relatively small under these load cases. When the measured rotation is small, a small measurable error will produce a large percentage error, as is the case with those loading conditions. The goal of the model is to predict the maximum rotation across the joint for design purposes. Maximum rotation seems to occur when the load is centered on the joint. When loading centered on the joint, the joint rotation error is less than 30%. The theoretical rotations show good agreement with the measured rotations for all pipe types, and especially for the RC pipe for all load cases.

Evaluation of the Model using Field Test Data

The most interesting challenge in getting the beam-on-springs model to match the field test data is the large number of unknowns including soil condition, pipe and joint deterioration, and the effect of the road surface. There are two sets of data that are relied on when performing the beam-on-springs analysis. The vertical displacement data measured at the crown is used to determine shear displacement across the joint, and the longitudinal measurements are used to determine the rotation across the joint.

In Table J.1, joint stiffness is defined relative to the overall pipe stiffness using the terms I_{pipe}/I_{joint} and A_{pipe}/A_{joint}. Those relative values are used to calculate joint stiffness of the field test pipes. It is nearly impossible to know the effects of joint deterioration which is observed in the field test pipes. Significant deterioration is observed in some of the test pipes. In order to determine the spring stiffness of the soil beneath the field test pipes, the spring stiffness in the beam-on-springs model is varied until deflection and rotation values are nearest to the measured values. The determined k_{s1} values from all six field test culverts are equal to or larger than the k_{s1} values from the laboratory test pipes. This includes the freshly installed HDPE-D3.5-F3.5 test pipe. Modeling information for the field test pipes is presented in Table J.8. The measured shear displacements and joint rotations are compared with the predicted values in Table J.9 and Table J.10.

Table J.8 Modeling data for the field test pipes (1 in. = 0.0254 m; 1 ksi = 6.9 MPa; 1 lbf-in^2 = 2.87x10^{-9} MN-m^2; 1 lbf = 4.4 N; 1 in^4 = 4.2x10^{-7} m^4; 1 in^2 = 6.5x10^{-4} m^2; 1 pci = 0.27 MN/m^2)

	RC-D4.5-F2	RC-D7-F4.7	CMP-D4-F1.8	CMP-D3-F2.8	HDPE-D3-F4.7	HDPE-D3.5-F3.5
Inner diameter (in.)	54	84	48	36	36	42
Outer diameter (in.)	66	100	48	36	40	48
Wall thickness (in.)	6	8	0.09375	0.125	-	-
Corrugation geometry	-	-	2⅔ × ½	2⅔ × ½	Arched Corrugation	Arched Corrugation
Young's modulus *E* (ksi)	4300	4300	29000	29000	110	110
Poisson's ratio	0.2	0.2	0.3	0.3	0.4	0.4
Calculated *EI* (lbf-in^2)	2.21E+12	1.06E+13	1.97E+09	2.74E+09	2.48E+08	4.36E+08
Calculated *EA* (lbf)	4.86E+09	9.93E+09	3.42E+08	4.15E+08	5.57E+06	7.15E+06
Joint length (in.)	3	3	9	9	3	3
I_{pipe} (in^4)	514027	2464818	68.1	94.6	2258	3965
A_{pipe} (in^2)	1130	2310	11.8	14.3	50.6	65
I_{joint} (in^4)	18.02	86	40.5	56	53.8	94
A_{joint} (in^2)	2	4.1	0.118	0.146	1.5	1.9

k_{s1} (pci)	1033	224	635	1488	3085	483

Some information learned from the laboratory tests sheds light on the accuracy of the shear displacements. Laboratory tests showed that the vertical displacement at the crown and invert in flexible pipes is too affected by local bending to effectively match the results from a beam-on-springs model. Vertical displacements measured at the crown are often four times as large as the vertical displacements measured at the springline in the CMP laboratory test pipe. For the HDPE laboratory test pipe, crown vertical displacement is as high as 13 times the springline vertical displacement. The shear displacement in the field tests is obtained from the data measured at the crown. This may cause the beam-on-springs model to underestimate the measured shear displacement in those pipes by a significant margin.

Table J.9 Shear displacement across the joint for all in-service culvert tests loaded with the truck's rear wheels.

		Shear Displacement Across the Joint (in.)		
Culvert	Load Case	Measured Movement	Predicted Movement	% of Measured
CMP-D4-F1.8	C-R2	-2.4E-02	0	-
	S-R2	1.8E-02	4.0E-03	22
CMP-D3-F2.5	C-R2	-8.1E-03	0	-
	S-R2	-4.2E-03	-8.3E-04	20
HDPE-D3-F4.7	C-R2	-1.1E-03	0	-
	S-R2	-4.0E-04	-1.5E-04	39
HDPE-D3.5-F3.5	C-R2	-3.3E-02	0	-
	S-R2	-2.0E-03	-1.4E-03	69
RC-D4.5-F2	C-R2	1.0E-03	0	-
	S-R2	4.2E-03	4.5E-04	11
RC-D7-F4.7	C-R2	-3.0E-04	0	-
	S-R2	4.0E-04	3.3E-04	83

The model cannot predict any shear displacement when loading is centered on the joint due to the symmetry of the system. However, magnitude of the shear displacement measured when the loading is centered on the joint (load case C-R2) is often larger than the magnitude of the shear displacement measured when the loading is downstream from the joint (load case S-R2). This is likely due to factors such as unknown burial conditions, soil conditions, and pipe deterioration. The shear displacements measured in the CMP and HDPE field test pipes

seem to be greatly affected by the additional bending at the crown that is observed in the flexible laboratory test pipes. This is expected, and is shown by the fact that the predicted shear displacements are smaller than the measured shear displacements for all of the flexible test pipes. The predicted shear displacement in RC-D4.5-F2 is much smaller than the measured shear displacement likely due to the deterioration of the joint. This pipe had significantly more joint deterioration than any other test pipe.

It is learned from the laboratory tests that it is challenging to use longitudinal measurements to predict the rotation across the joint. In the laboratory, longitudinal measurements are taken at the crown, the springline, and the invert. The tangent of the rotation angle is the difference of the longitudinal displacement at two of the three locations (a, b, or c) divided by the vertical distance between the measurement locations. This gives three separate measurements of rotation for each laboratory test. Depending on which two measurements are used for the calculation, the calculated rotation can vary significantly. In about 50% of the laboratory tests, the calculated joint rotation could either be positive or negative depending on which two longitudinal displacements are used in the calculation. This was thoroughly discussed in Appendix D. This can mean one of two things, either the sensors are inaccurate in the longitudinal direction (which is unlikely), or the longitudinal movement across the joint exhibits slippage or other nonlinear behavior. If it is the latter, then it is understandable that the beam-on-springs model is not successfully matching the joint rotations measured in the field because longitudinal measurements are used to calculate the joint rotation in the field test pipes.

Analysis of the field test data indicates that the field tests have similar problems to the laboratory tests in predicting joint rotation using longitudinal measurements. Some of the predicted rotations are opposite the measured rotations (Table J.11). On average, the magnitude of the predicted rotations is 156% of the magnitude of the measured rotations, and none are less than 55%. Using a reasonable factor of safety should give conservative predictions of the magnitude of the joint rotation. It should also be noted that the displacements measured in the field are very small, in some cases close to zero. Therefore, the calculated percent errors are very sensitive and can increase significantly with very small changes in input model parameters.

Table J.10 Relative rotation of connected pipes for all in-service culvert tests, loaded with the truck's rear wheels.

		Relative Rotation of Connected Pipes (radians)		
Culvert	Load Case	Measured Rotation	Predicted Rotation	% of Measured
CMP-D4-F1.8	C-R2	3.5E-04	1.9E-04	55
	S-R2	-1.6E-04	-2.0E-04	127
CMP-D3-F2.5	C-R2	-4.0E-05	4.0E-05	-100
	S-R2	-6.1E-05	-9.0E-05	147
HDPE-D3-F4.7	C-R2	-1.4E-05	-6.7E-05	475
	S-R2	1.2E-05	-1.6E-05	-127
HDPE-D3.5-F3.5	C-R2	-2.4E-04	1.3E-04	-55
	S-R2	1.3E-04	-1.6E-04	-127
RC-D4.5-F2	C-R2	-3.5E-05	-3.2E-05	93
	S-R2	-3.1E-05	-8.1E-05	257
RC-D7-F4.7	C-R2	*	-1.5E-04	-
	S-R2	*	-1.4E-04	-

*No data due to sensor error

Parametric Study of Pipe Length and Spring Spacing

In developing a beam-on-springs model, it is useful to investigate how factors such as spring spacing and pipe length affect the movement at the joint calculated by the model. In design, it would not be practical for an engineer to fully model a buried pipe out to 200 ft (61 m) from the joint location because loading that far from the joint would have no effect on the joint movement. It is the goal of this section to investigate these factors and make recommendations that will aid in simplifying design.

Effect of Pipe Length

In the model, the pipes must extend far enough to either side of the joint that any loading at the extreme ends will have negligible effect on the movement at the joint. Point loads are placed on the flexible and rigid beam-on-springs models at varying distances from the joint being analyzed. The goal is to see how far away the load needed to be in order to produce negligible movement in the joint. Loading far greater than any loading recommended by AASHTO (2006) is applied to the flexible HDPE pipe culvert model and to a rigid RC pipe culvert

model. In the RC pipe model, pipe segments are 5 ft (1.5 m) long. The vertical movement of flexible and rigid modeled pipes under a point loading of 5000 lbf (22 kN) placed at various distances from the joint are shown in Figure J.23 and Figure J.24. These figures show that loading placed 10 ft (3 m) from the joint for flexible culverts, and 15 ft (4.6 m) from the joint for rigid culverts will have a negligible effect on the joint movement. It is proposed that a beam-on-springs model of flexible HDPE and CMP culverts extend 10 ft (3 m) from the joint. It is also proposed that a beam-on-springs model of rigid RC culverts extend to the larger of either 15 ft (4.6 m) from the joint, or three full pipe segment lengths from the joint.

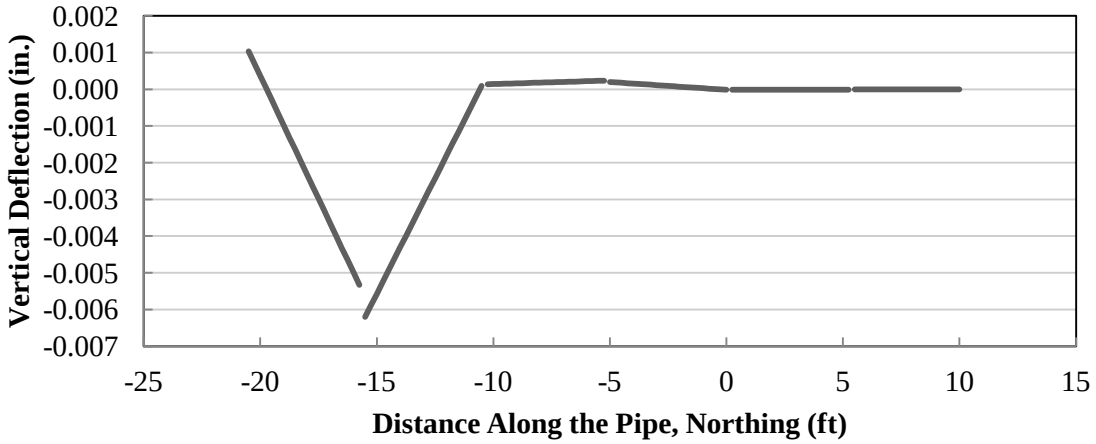

a. Load placed 15 ft from the joint

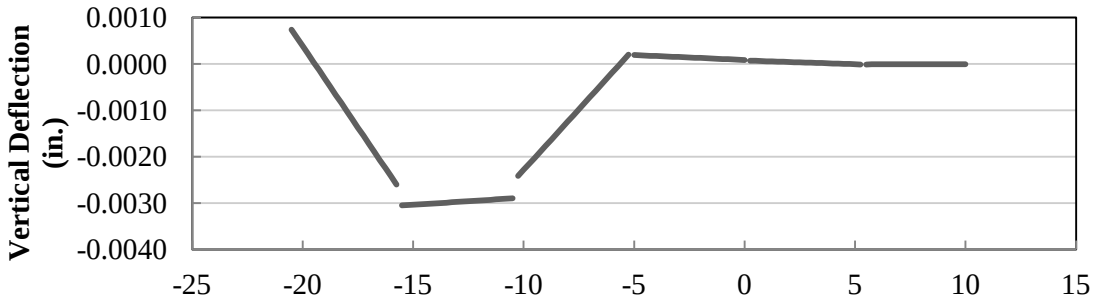

b. Load placed 12.5 ft from the joint

Figure J.23 Effect of 5000 lbf (22 kN) load placed away from the joint of the RC-D7-F4.5 test culvert model. The joint being investigated is located at 0 ft (1 ft = 0.3 m; 1 in = 2.54 cm)

Figure J.23 Continued

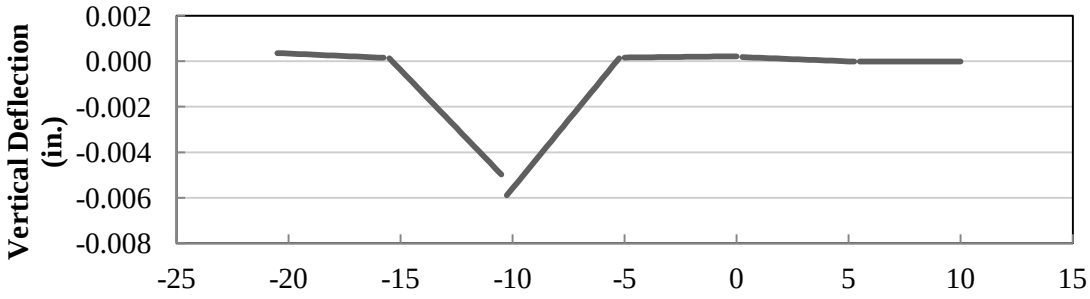

c. Load placed 10 ft from the joint

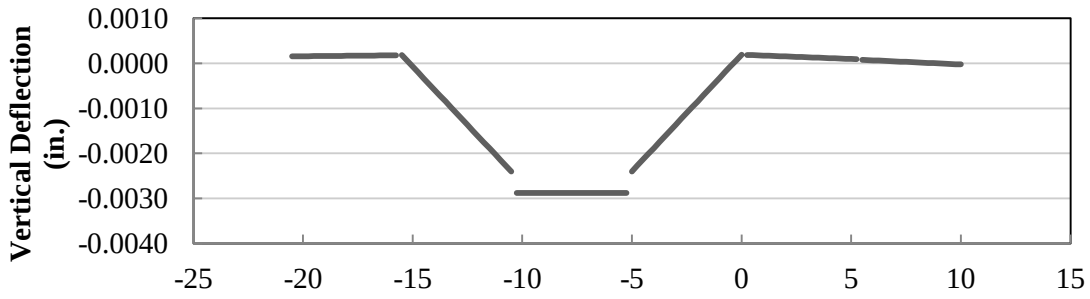

d. Load placed 7.5 ft from the joint

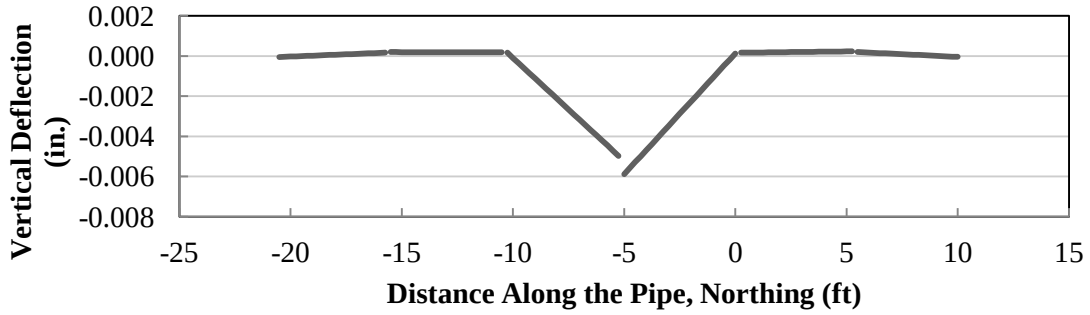

e. Load placed 5 ft from the joint

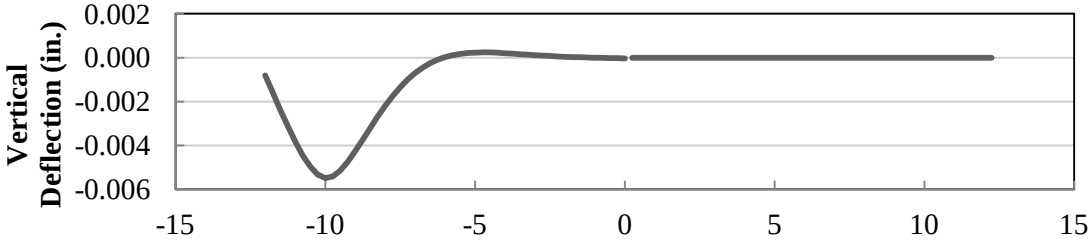

a. Load placed 10 ft from joint

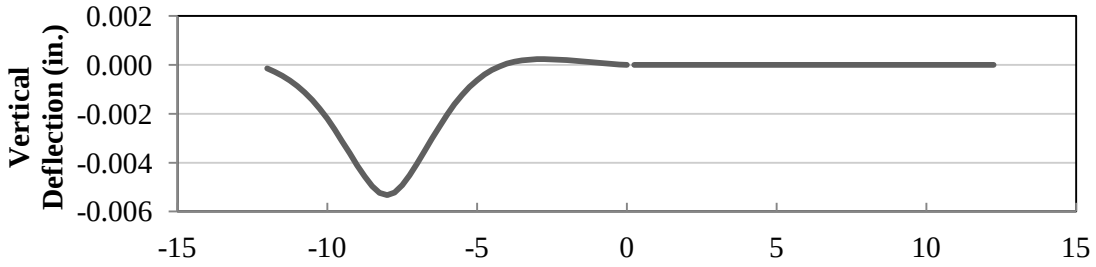

b. Load placed 8 ft from joint

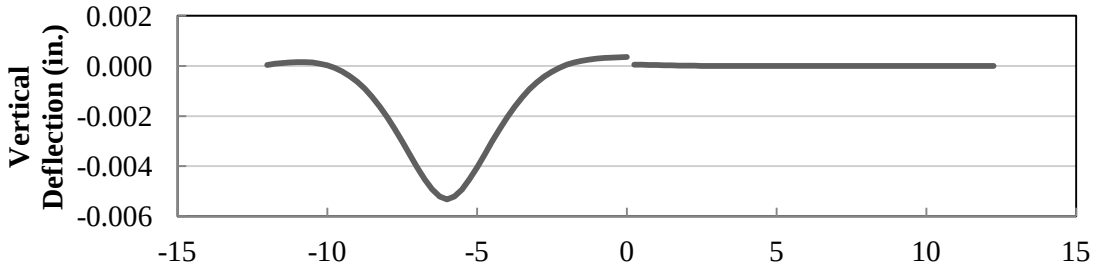

c. Load placed 6 ft from joint

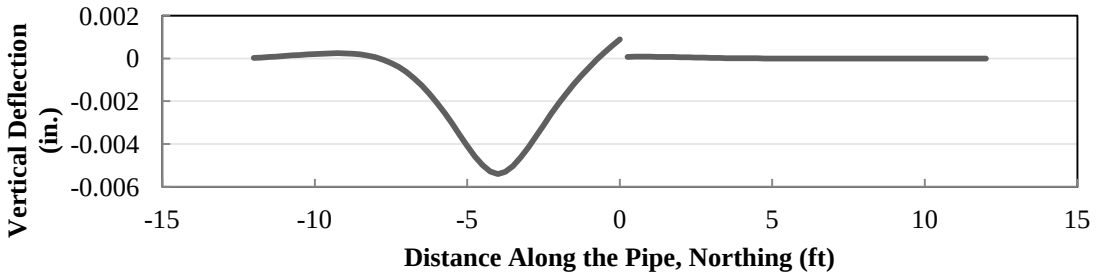

d. Load placed 4 ft from joint

Figure J.24 Effect of 5000 lbf (22 kN) load placed away from the joint of the HDPE laboratory test culvert model. The joint being investigated is located at 0 ft (1 ft = 0.3 m; 1 in = 2.54 cm)

Effect of Spring Spacing

The spacing of the springs beneath the beams plays an important role in the accuracy of any beam-on-springs model. Any increase in spring spacing results in a decrease in accuracy when modeling continuous media such as soil. Spring spacing, *s*, is shown in Figure J.25.

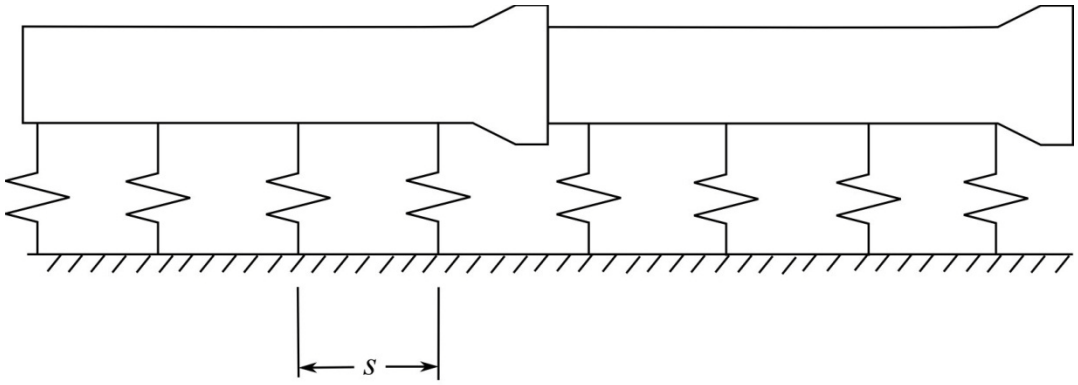

Figure J.25 Springs beneath a buried RC pipe culvert system

The calibration of the beam-on-springs model is performed using a spring spacing of 3 in. (7.6 cm). Given that typical pipe culvert segments are not shorter than 5 ft (1.5 m), it would seem likely that using any spring spacing less than 3 in. (7.6 cm) would have a negligible effect on the final output. A sensitivity analysis is performed for the spring spacing. A spring spacing of 3 in. (7.6 cm) was used as a baseline for determining accuracy. Data gathered from the use of larger spring spacings is compared to the data gathered from using a 3 in. (7.6 cm) spring spacing in order to determine the relative error. Joint rotation and shear displacement across the joint are and compared for spring spacings of 3, 9, 15, 21, 27, and 33 in. (7.6, 23, 38, 53, 39, and 84 cm). Percent error is calculated based on the difference between data from the 3 in. (7.6 cm) baseline spring spacing and the data from the larger spring spacing being analyzed.

Initially, the effect of spring spacing is compared for the rigid RC pipe and the flexible HDPE pipe to determine whether rigid or flexible pipes are more sensitive to an increase in spring spacing. When loading is centered on the joint, and spring spacing is 33 in. (84 cm), the RC pipe model showed a 12% error and the HDPE pipe model showed a 37% error in joint rotation when compared to a 3 in. (7.6 cm) spring spacing. Plots of the calculated vertical displacement with loading centered on the joint are presented in Figure 7.26. The differences in the vertical displacements calculated using multiple spring spacings appear small. However, calculation of joint rotation and shear displacement is amplified by any small change in the calculated vertical displacements. When loading is positioned 3 ft (0.9 m) from the joint, the RC pipe error is 1.3% for shear displacement, and 15% for joint rotation, while HDPE pipe error is 12% for shear displacement and 24% for joint rotation. Comparing the model of the RC lab test with the model of the HDPE lab test shows that flexible pipes are much more sensitive to an increase in spring spacing. Further sensitivity analysis is carried out using the flexible HDPE pipe model.

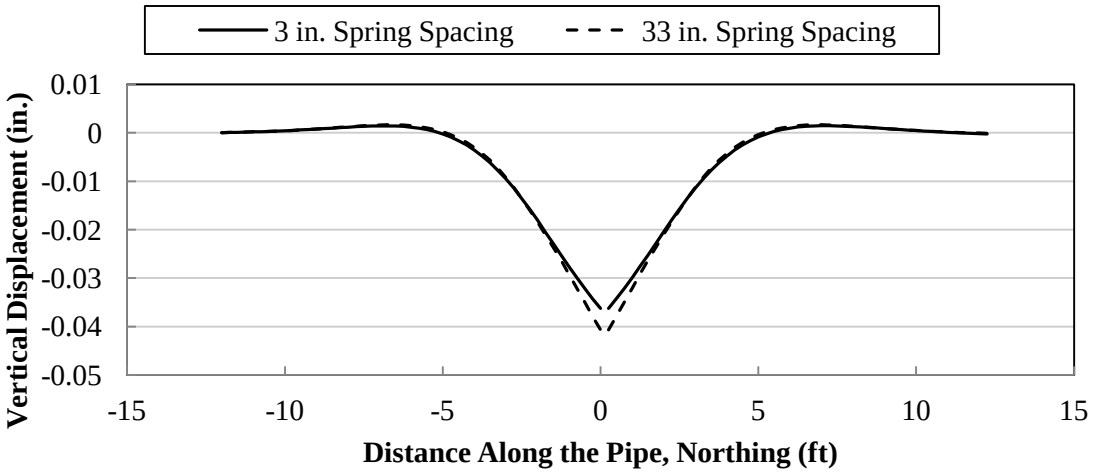

a. Effect of spring spacing on the flexible HDPE model

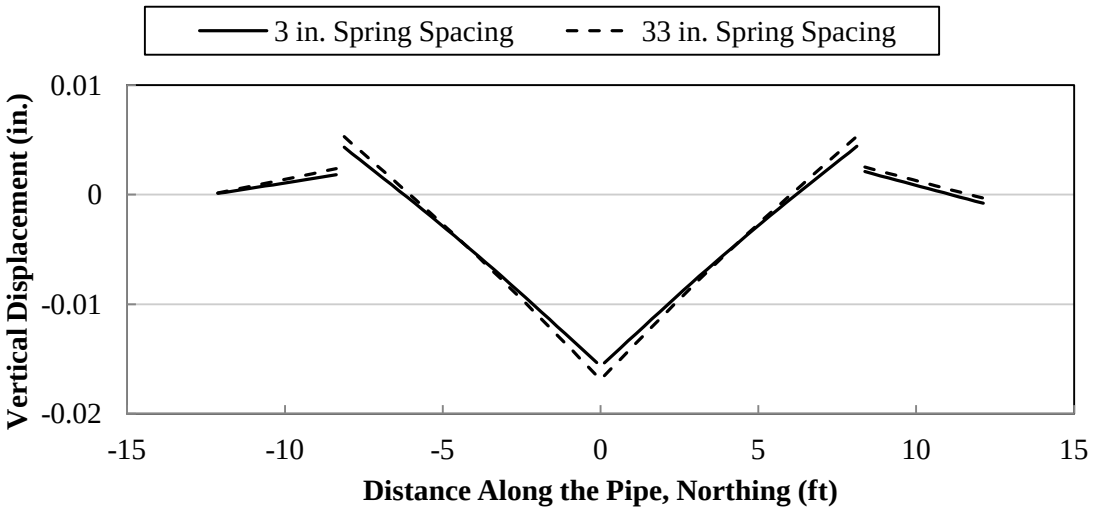

b. Effect of spring spacing on the rigid RC model

Figure J.26 Calculated vertical displacements with loading centered on the joint and a spring stiffness of 7667 psi (1 ft = 0.3 m; 1 in = 2.54 cm; 1 psi = kPa)

The model of the HDPE lab test is analyzed for the above spring spacings, loading offset 3 ft (0.9 m) from the joint, and for the following spring stiffnesses: 100, 333, 1667, 7667, and 23333 lb/in^2 (0.69, 2.3, 11, 53, and 161 MPa). Individual spring stiffness, *k*, is calculated by multiplying the above values (pressure) with spring spacing,

s. These spring stiffness values cover most pipe diameters up to 5 ft (1.5 m) and most k_{s1} values for these models. The calculated errors discussed in this section are tabulated in Tables J.11 and J.12.

Table J.11 Error in shear deflection measurements caused by increased spring spacing for the HDPE laboratory test model (1 in = 2.54 cm; 1 psi = kPa)

	% error of shear deflection					
k (psi)	3 in. spacing	9 in. spacing	15 in. spacing	21 in. spacing	27 in. spacing	33 in. spacing
100	0	0.2	-0.2	-0.5	0.6	0.5
333	0	0.1	-0.3	-0.7	-0.3	-0.6
1667	0	-0.2	-0.6	-1.3	-2.2	-3.4
7667	0	-0.7	-2.2	-4.3	-7.6	-11.6
23333	0	-2.9	-8.9	-19.2	-36.7	-61.3

Table J.12 Error in joint rotation measurements caused by increased spring spacing for the HDPE laboratory test model (1 in = 2.54 cm; 1 psi = kPa)

	% error of joint rotation					
k (psi)	3 in. spacing	9 in. spacing	15 in. spacing	21 in. spacing	27 in. spacing	33 in. spacing
100	0	-1.1	1.0	3.3	0.1	0.8
333	0	0.8	3.2	7.1	9.7	14.9
1667	0	-1.3	-4.5	-9.4	-15.8	-24.4
7667	*	*	*	*	*	*
23333	0	0.0	-0.4	-0.3	1.3	4.5

*Values neglected because rotation is nearly zero, and errors are significantly amplified

For all spring stiffnesses tested, the maximum percent error in for both shear displacement and joint rotation is plotted in Figure J.27. A spring spacing of 12 in. (30 cm) is recommended to be used in a beam-on-spring model. It seems to be a reasonable compromise between accuracy and ease of creating the model in software. For all tested spring stiffness, a spring spacing of 15 in. (38 cm) gave an error in measurements at the joint that was not

more than 9% when compared to the 3 in. (7.6 cm) spring spacing baseline. It is recommended to use a spring spacing equal to or smaller than 15 in. (38 cm) to maintain a high level of accuracy.

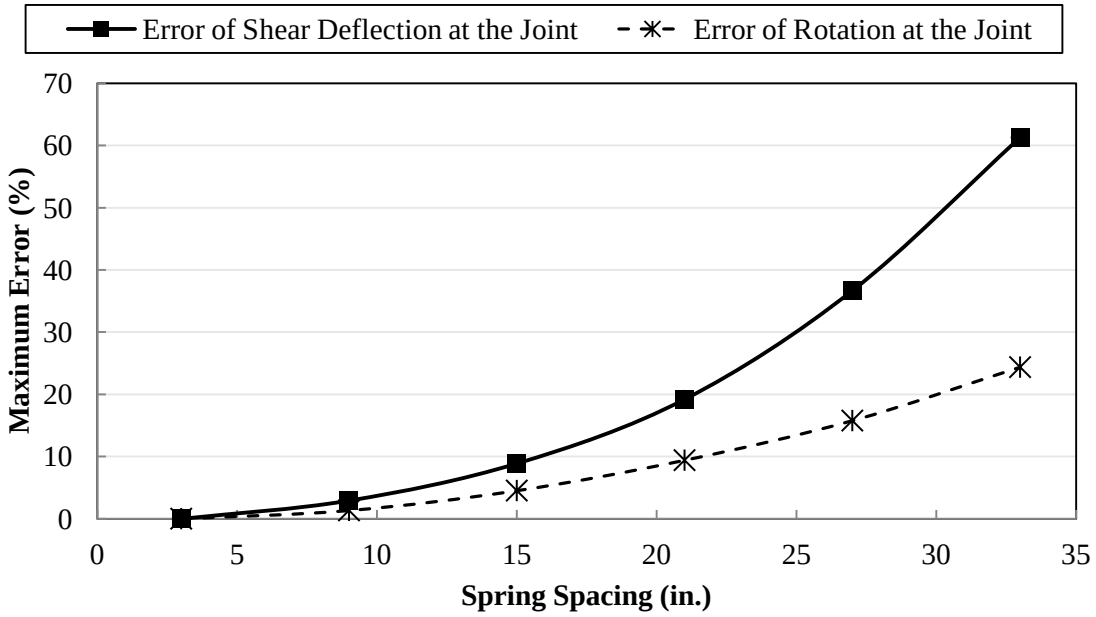

Figure J.27 Effect of spring spacing on model accuracy, the worst cases plotted from Tables J.11 and J.12 (1 in. = 2.54 cm)

The springs should be placed symmetrically about the joint. Springs places asymmetrically about the joint are tested on the HDPE model using a 6 in. (15 cm) spring spacing. Results indicated that using a 6 in. (15 cm) asymmetric spring spacing produced error as high as using a 27 in. (69 cm) symmetric spring spacing. If springs are not placed symmetrically about the joint being investigated, a significant loss in accuracy occurs.

Conclusions

Beam-on-springs modeling is found to be suitable for representing the behavior of buried culvert systems. Multiple beam-on-springs models are tested, and a modified form of the Terzaghi model for soil spring stiffness is found to give the most accurate results, and is recommended for use. A modified form of the Biot model also works reasonably well, but not quite as well as the Terzaghi model. The modified form of the Vesic model produced errors that were too high for use. For the laboratory test pipes, rotational and shear movement across the joint are captured with a reasonable degree of accuracy. The modified Terzaghi model had more trouble precisely predicting the movement measured in the field due to unknown soil conditions, years of deterioration, tens of thousands of repeated loadings, and large amounts of bending at the crown. In all cases, the soil stiffness beneath the field test pipes is equal to or larger than the soil stiffness beneath the laboratory test pipes. This

indicates that soil stiffness values obtained from the laboratory tests can yield conservative results when used in design.

The way in which surface loading spreads as it attenuates through the soil was investigated. It is assumed that the load spreads linearly outward from the point of loading. It suggested that the load application length increases 1.15 units for every 1 unit of depth. This is the same load spreading pattern used in AASHTO (2006).

The effect of the pipe length was tested. It is recommended that the pipes extend 10 ft on both sides of the joint in flexible culvert modeling and the larger of 15 ft, or three full pipe lengths from the joint in rigid culvert modeling. Loads placed further from the joint than these distances will have little effect on the joint movement. The effect of increasing spring spacing was tested. It recommended to use a spring spacing less than or equal to 15 in. (38 cm) in modeling in order to facilitate easy model creation while maintain a high level of accuracy.

Step-by-Step Explanation of Beam-on-Elastic-Springs Modeling

Buried pipe culverts can be represented as a series of beams resting on elastic springs. The springs represent the stiffness of the soil beneath the culvert and beams represent both the culvert pipes and the joints connecting the culvert pipes. The purpose of this section is to summarize and present a method for modeling a buried pipe culvert as a beam resting on a series of springs. The presented model was developed earlier in the appendix using the data presented in other Appendices. The goal of such a model is to predict the rotations and shear displacements at the joint. Beam-on-springs models are investigated for RC, CMP, and HDPE pipes. Individual models are calibrated to take into account the characteristics of each of the three pipe materials. The goal of this section is to present a method of simply predicting the movements at the pipe joint under live surface loading with reasonable accuracy. The solution to a beam-on-springs model presented here can be carried out using any structural analysis or finite element analysis software, such as ANSYS, that can model beams and springs. The following variables are used in the beam-on-springs model. A step-by-step procedure for creating a beam-on-springs model follows the variable list.

A_p = Cross-sectional area of the pipe (length^2)

A_j = Cross-sectional area of the joint (length^2)

d_a = Pipe diameter measured from the centerline of the corrugation (length)

d_i = Inside diameter of the pipe (length)

d_o = Outside diameter of the pipe (length)

E = Modulus of elasticity of the material (force/length^2)

H = Burial depth to the crown (length) (Figure J.28)

I_p = Moment of inertia of the pipe (length^4)

I_j = Moment of inertia of the joint (length^4)

k = Individual spring stiffness beneath the modeled beam (force/length)

k_s = Modulus of subgrade reaction of the soil (force/length^3)

k_{s1} = Modulus of subgrade reaction of the soil for a 1 ft by 1 ft (0.3 by 0.3 m) square plate (force/length^3)

L_0 = Length of contact under wheel pair – parallel to pipe diameter (length) (Figure J.28)

L_L = Live load (force)

P_L = Live load pressure at depth H (force/length^2) (Figure J.28)

s = Spring spacing (length) (Figure J.)

t = Wall thickness of steel pipe (length)

W_0 = Width of contact under wheel pair – parallel to pipe axis (length) (Figure J.28)

w_L = Distributed live load along the pipe (force/length)

v = Poisson's ratio

Step #1: Transfer the Surface Loading to the Culvert

The first step is to determine how the surface loading attenuates through the soil to the surface of the pipe. Typically surface loading will include wheel pairs from trucks or other large vehicles. Equations J.3 and J.4 describe how surface loading is transferred through the soil to the pipe culvert. Figure J.28 illustrates the load spreading with depth defined by

$$P_L = \frac{L_L}{(L_0 + 1.15H)\,(W_0 + 1.15H)} \tag{J.3}$$

$$\begin{aligned} w_L &= P_L d_o \qquad for\ L_L \geq d_o \\ w_L &= P_L L_L \qquad for\ L_L < d_o \end{aligned} \tag{J.4}$$

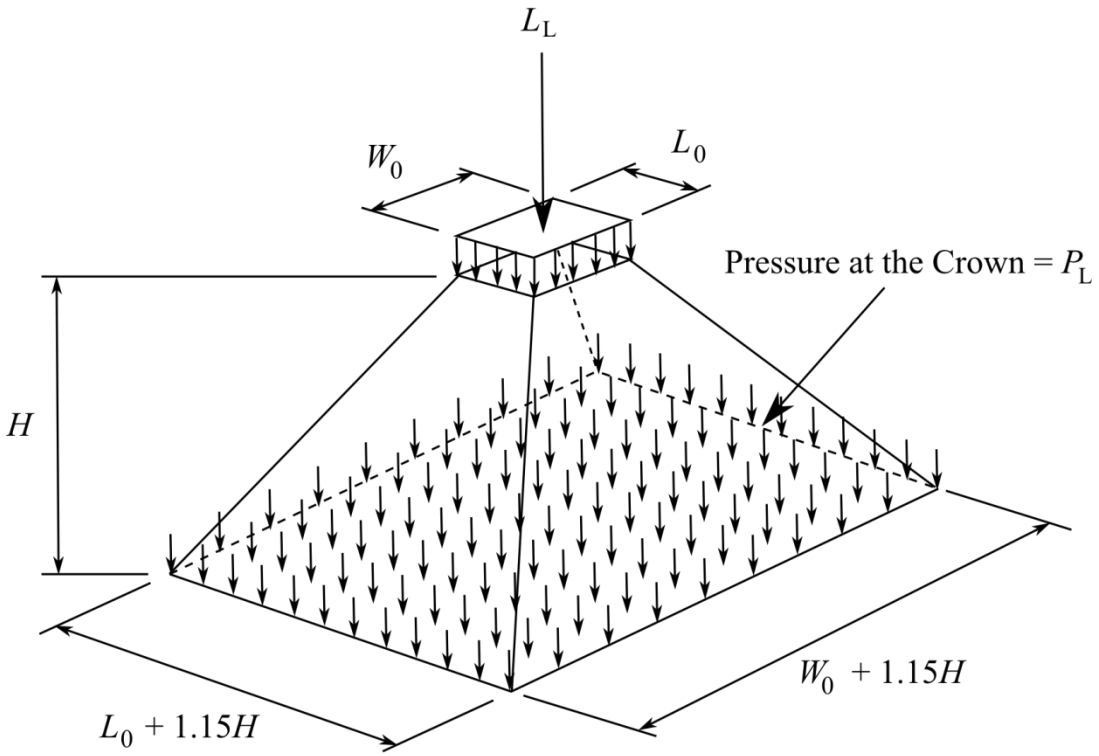

Figure J.28 Illustration of load spreading represented by Equation J.3

Step #2: Determine Pipe Lengths in the Model

The purpose of this model is to determine and examine movement at a particular joint. This section provides guidance as to how far the pipes should extend on either side of the joint. Loading beyond the recommended pipe lengths has limited effect on the joint. Development of these lengths was discussed earlier.

1) For flexible HDPE and CMP pipes, the pipe should extend at least 10 ft (3 m) from the joint.

2) For rigid RC pipes, the pipes should extend at least 15 ft (4.6 m) from the joint, and they should extend to the nearest full pipe length. For example, a culvert with 6 ft (1.8 m) long pipe segments should be modeled up to 18 ft (5.5 m) from the joint.

Step #3: Determine Spacing of Springs Beneath the Culvert

The following are recommendations for spacing the springs beneath the culvert. The recommendations are developed in an earlier section.

1. The springs should be evenly spaced.

2. Spring spacing should not be greater than 15 inches (0.38 m).

3. Springs should be placed symmetrically about the joint being investigated.

Step #4: Determine Stiffness of Springs Beneath the Culvert

Spring stiffness of the soil highly depends on the moisture content, compaction, and type of soil. Spring stiffness can be determined from a modified version of the method recommended by Terzaghi (1955) following the steps below. Determination of spring stiffness was developed in an earlier section.

1) Determine the consistency of the soil and then select k_{s1} from

Table J.3.

Table J.13 Values of k_{s1} in lbf/in.^{3} for beams 1 ft (0.3 m) wide, resting on sand (1 lbf/in.^{3} = 0.27 MN/m^3) (Terzaghi, 1955)

Relative Density of Sand	Loose	Medium	Dense
Dry or moist sand, limiting values for k_{s1}	23-70 46	70-350	350-1150
Dry or moist sand, proposed values	29	150 93	580 350
Submerged sand, proposed values			

2) Determine k_s for rigid RC pipes using Equation J.5, and for flexible HDPE and CMP pipes using Equation J.6 where d_o is in feet units.

$$k_s = 2k_{s1}\left(\frac{d_o + 1}{2d_o}\right)^2 \quad \text{(J.5)}$$

$$k_s = 1.4k_{s1}\left(\frac{d_o + 1}{2d_o}\right)^2 \quad \text{(J.6)}$$

3) Determine the individual spring stiffness k, where s is the spring spacing.

$$k = k_s s d_o \quad \text{(J.7)}$$

Step #5: Determine Flexural and Shear Stiffness of Culvert Pipes

Pipe stiffness is determined by the geometry of the pipe and the material properties. It depends on cross-sectional area of the pipe A_p, moment of inertia of the pipe I_p, young's modulus of the pipe material E, and Poisson's ratio for the pipe material, ν. Cross-sectional area and moment of inertia of reinforced concrete pipe sections can be determined from the Equations J.8 and J.9 and need no special consideration due to their simple geometry of a hollow circular section. Due to the corrugation of the CMP and HDPE pipes, calculation of I_p and

A_p values is much more complex. Appendix I provides guidelines for calculating I_p values for CMP and HDPE pipes. Calculation of A_p for HDPE pipes is also presented in Appendix I. Calculation of A_p for CMP pipes is presented in Equation J.10.

$$A_{p,concrete} = \frac{\pi}{4}\left({d_o}^2 - {d_i}^2\right) \quad \text{(J.8)}$$

$$I_{p,concrete} = \frac{\pi}{64}\left({d_o}^4 - {d_i}^4\right) \quad \text{(J.9)}$$

$$A_{p,metal} = \frac{\pi}{4}\left((d_a + 2t)^2 - {d_a}^2\right) \quad \text{(J.10)}$$

Step #6: Determine the Stiffness of Culvert Joints

Joint stiffness is something that naturally will depend on the new joint design being tested. For the three culvert types and joint designs tested in the laboratory, the joint stiffnesses in Equations J.11 through J.16 were found to work. The values are discussed in an earlier section and originally presented in Table J.1. In most cases, the joint itself has no real definable length when attempting to model it as a beam. There is also no effective way to calculate stiffness of the joint. The following stiffness and joint lengths are empirically determined earlier in the appendix. Young's modulus, *E*, and Poisson's ratio, *v*, are the same as the material the pipe is made of.

1) Reinforced Concrete Pipes with gasketed joints with a joint length of 3 in. (7.62 cm):

$$I_j = \frac{I_p}{28000} \quad \text{(J.11)}$$

$$A_j = \frac{A_p}{570} \quad \text{(J.12)}$$

2) Corrugated HDPE pipes with gasketed joints with a joint length of 3 in. (7.62 cm)

$$I_j = \frac{I_p}{42} \quad \text{(J.13)}$$

$$A_j = \frac{A_p}{35} \quad \text{(J.14)}$$

3) Corrugate Steel Pipes with a hugger-band joint with a joint length of 9 in. (23 cm)

$$I_j = \frac{I_p}{1.7} \quad \text{(J.15)}$$

$$A_j = \frac{A_p}{100} \quad \text{(J.16)}$$

Step #7: Create a Beam-on-Springs Model in Finite Element Software

The final step is to take all of the parameters determined in the earlier steps and create a beam-on-springs modes using finite element software. The pipes and joints are to be modeled using simple 2D beam elements using the appropriate stiffness parameters. The springs are to be modeled using simple spring elements. After

the beams and springs are modeled, the loading should be applied to the model. Then let the software analyze the model and calculate joint rotations and shear displacement at the joint.

THREE DIMENSIONAL FINITE ELEMENT ANALYSIS

Introduction

Finite element procedures have been developed to characterize the response of culvert joints under surface live load. Four Finite Element Analyses (FEA) are reported, examining reinforced concrete pipes under two different burial conditions (i.e. poor burial practice, then good burial conditions in accordance with AASHTO LRFD Construction specifications), and at two different depths (two feet and four feet of cover as tested). Testing was performed in AASHTO Class 1 (GW i.e. graded coarse-grained material), so this is the material that was modeled in the analysis. The work featured:

- development of the three dimensional geometry of the pipes
- explicit representation of the three dimensional geometry of the surface load
- representation of the zones of high stiffness and low stiffness soil associated with the two different burial conditions
- development of a simplified gasketed pipe approximation to represent the rotational stiffness of the joint

Comparisons of strain measured in the reinforced concrete pipes indicate that:

- results for the 'poor burial condition' obtain from the simulations at both burial depths effectively describe the behavior observed in the laboratory experiments; the patterns and magnitudes of the strains were in general similar for all six points being compared
- some discrepancy in calculated strain magnitude for the poor burial case was observed in the bell at the invert location; this may be due to the influence of the steel reinforcement (the reinforcement was not modeled in the FEA), or to the soil models used in the calculations
- results for the 'good' burial condition show the same pattern of behavior as the experiments, though the magnitudes differ more than the results from the 'poor burial condition' analysis; this might be due to the shape of the 'void' under the joint used in the simulation (geometry which was idealized), or it might be due to limitations in the soil model

Comparisons of deflection measured along the crown of the reinforced concrete pipes indicate that:

- measured deflections for the case or poor burial were much higher than those calculated; further work is needed to change the modeling procedures if response under poor burial is to be captured satisfactorily; for example, it may be that shear failure occurs under the invert of the bell, and that elastic-plastic soil modeling is needed for this case
- measured deflections for the case of good burial are about double those calculated using expected soil moduli; if design moduli were employed then the calculations would have been reasonable approximations of the measurements.

Elastic soil modeling has been used in these calculations of pipe response under factored service load. Additional work will be performed in Phase 2 of the project to

- examine the choice of soil parameters, and to determine whether elasto-plastic soil response needs to be modeled to improve calculations
- examine jointed pipe response to earth loads
- model the band connector on the corrugated steel pipes and examine performance of the analysis in calculations of measured deformation and strain
- examine the response of the lined-corrugated HDPE test pipe
- examine the pipes to be tested in Phase 2 of the project

Problem description

Given the geometry of the bell and spigot joint employed in the reinforced concrete test pipes, and the nature of jointed pipe response to surface loading, three dimensional analysis has been developed. This is because longitudinal as well as circumferential responses need to be evaluated.

Two buried conditions were considered for these simulations: 'poor' and 'good' burial conditions. A schematic of the 'poor' burial condition featuring voids under the barrels is shown in Figure J.29, where the bells sit on the compacted foundation and uncompacted material is assumed to be under the barrels of the pipeline. Uncompacted backfill soil is also modeled adjacent to the structure for the first burial layer. Figure J.30 shows the 'good' burial condition where the pipe is modeled as resting on the foundation along the length of the barrel. Localized voids in the foundation were excavated at the location of the bells, and uncompacted soil was placed in and around the joints.

Two burial depths were modeled in these simulations, 2 feet and 4 feet. Figures J.29 and J.30 show the geometry modeled for burial at 4 ft of cover, and also illustrates the location of the surface load. The same arrangement for pipe burial and load location was employed for the case of 2ft of cover. Soil self weight was not considered here, and calculations focussed on the incremental response of the jointed pipe to surface load.

The soil and pipe materials were modeled as linear and elastic, since the experimental data showed response that was linear elastic under the service load.

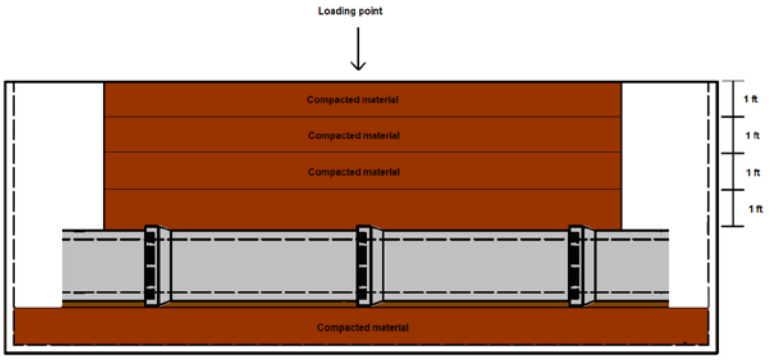

(a) Lateral view

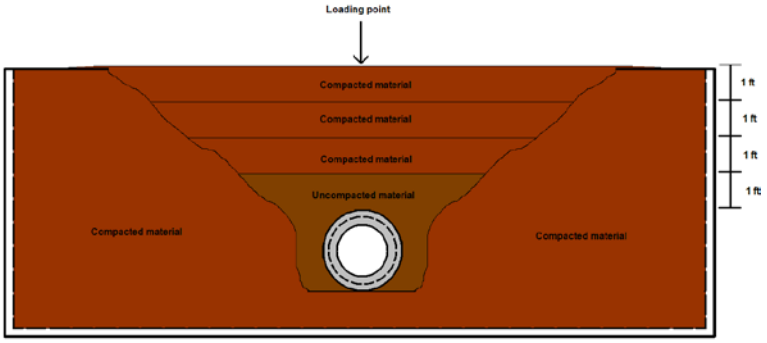

(b) Frontal view

Figure J.29 Schematic of the poor burial condition

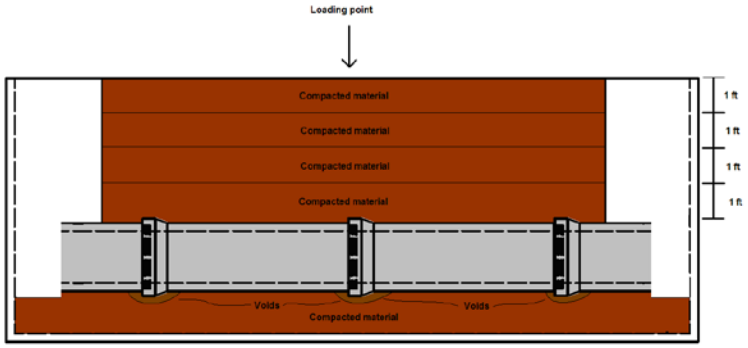

(a) Lateral view

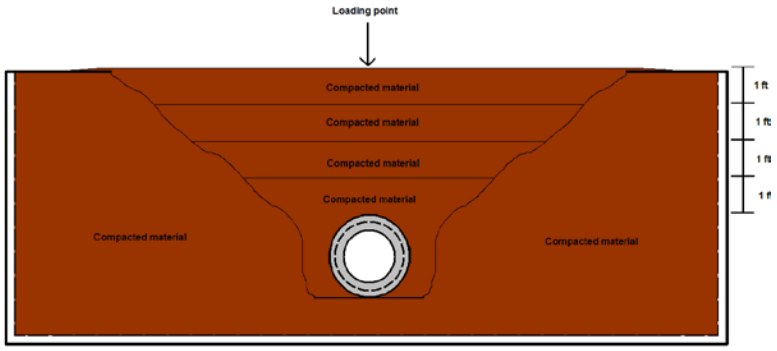

(b) Frontal view

Figure J.30 Schematic of the good burial condition

Modeling

Program used

The general purpose Finite Element code ABAQUS version 6.7 was used to perform the numerical analyses. The geometries, mechanical properties, and details of the models are described in the following subsections.

Geometries

The geometries of the models were based on the arrangement of the experiments. Given the symmetry of the problem, only half of the geometry had to be defined since ABAQUS version 6.7 accommodates symmetric analysis. Figures J.31 and J.32 show the geometries of the pipe and gasket respectively. It's important to mention that the geometry of the gasket was not explicitly defined since its purpose on the model was to transfer loads between pipes; therefore a simple shape was acceptable. However a region of the gasket was defined with different properties and is shown in red in Figure J.32. Figure J.33 shows the geometry of the pipes-gasket assembly (the gasket in red). The previous geometries were the same for all of the simulations.

Figure J.34 illustrates the geometry employed for the 'poor burial condition' at 4 ft of cover. This figure also shows partitions that represent the different burial layers which were used to define different material properties, particularly the geometry defined for the uncompacted material shown in red. In a similar manner Figure J.35 gives details of the 'good burial condition' at 2 ft of cover showing the void under the joint in red. Since the geometries for the soil employed in the remaining simulations are similar they will not be shown herein. As can be seen in Figures J.34 and J.35, the distance between the pipeline and the side was greater than 1.5 times the external diameter of the pipeline in order to reduce the effect of such boundaries. Figure J.36 shows the assembly for the 'poor burial condition' at 4 ft of cover (similar for the other three models). The interaction between the pipes and the soil and between the gasket and the pipes was defined as tied which means that the displacement in the surfaces that are in contact will be the same.

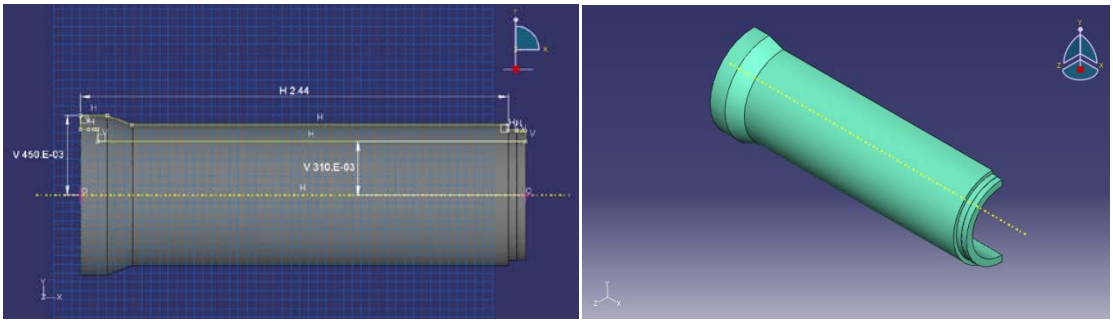

Figure J.30 Geometry of the pipe

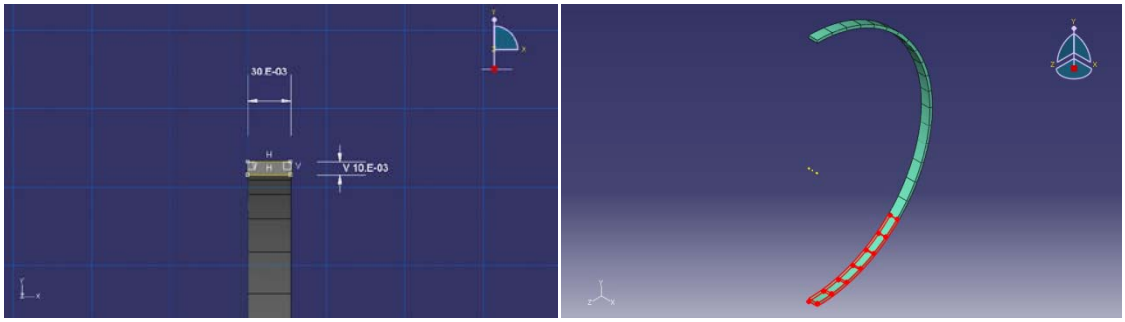

Figure J.32 Geometry of the gasket

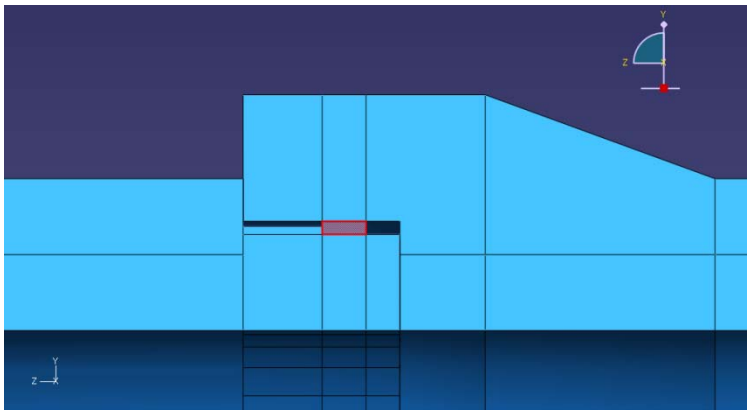

Figure J.33 Geometry of the bell-gasket-spigot assembly

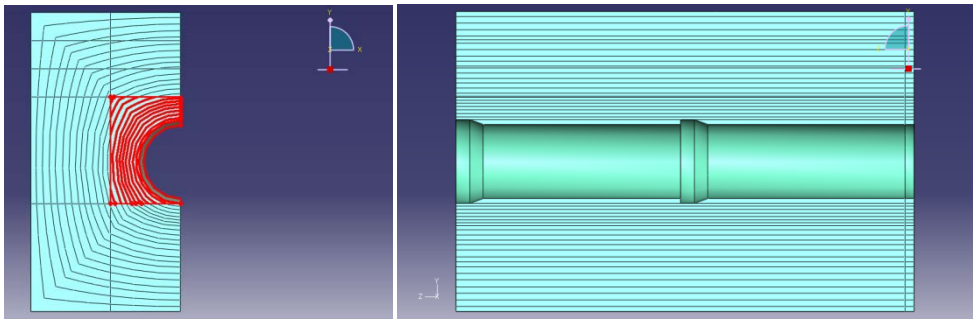

Figure J.34 Geometry of the soil for the poor burial condition at 4 ft of cover

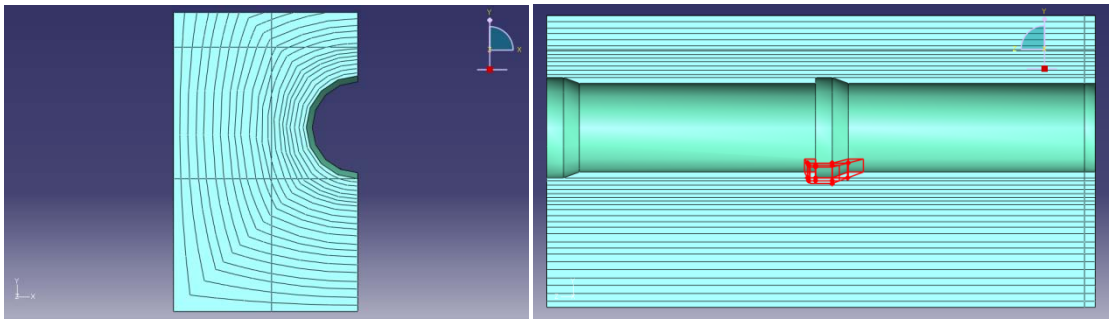

Figure J.35 Geometry of the soil for the good burial condition

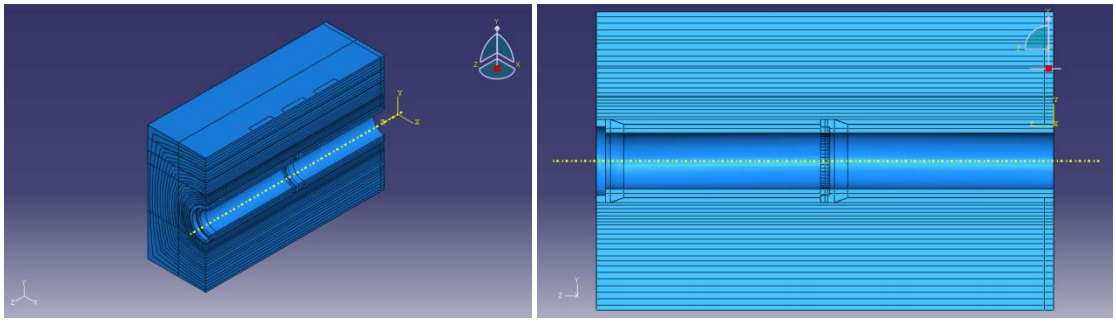

Figure J.36 Assembly for the poor burial condition at 4 ft of cover

Material properties

As mentioned before, the material properties for the elements employed in the simulations were defined as linear elastic, characterized by Elastic Modulus and Poisson's Ratio. Five materials were defined as presented and described in Table J.14. Two sets of soil properties are used here. The first represents "expected" modulus values for the test soil. The second represents "design" modulus values for the test soil (based on the design parameters of McGrath et al. 2002). The first are approximately twice the values of the second.

The model of the gasket was not designed to provide a detailed representation of the local contact stresses between the gasket and the pipe wall. Instead, the objective was to provide a model of the global joint stiffness against rotation. A higher modulus was provided at the bottom region of the gasket so that more of the spigot - bell interaction (load transfer) takes place at the invert rather than at the crown. Additional analyses were performed with 1/3 and 3 times these modulus values, as discussed subsequently.

Table J.14 Material properties and descriptions

Material	Elastic modulus E in MPa (psi)	Poisson's Ratio ν	Description
Soil 1 a. expected b. design	40 (5750) 20 (2880)	0.30	Employed for the regions where compacted material was considered
Soil 2 a. expected b. design	10 (1440) 4 (570)	0.35	Employed for the regions where uncompacted material was considered
Concrete	30000 (4320000)	0.20	Employed for the pipes
Gasket Material 1	1 (144)	0.45	Employed for the upper region of the gasket
Gasket Material 2	10 (1440)	0.45	Employed for the bottom region of the gasket

Boundary conditions

Figure J.37 shows the boundary conditions employed for analysis of the good burial condition at 2 ft of cover. The kinematic boundary conditions were defined as follows:

- symmetry was defined for the model in the 'x' direction of the models due to the nature of the problem
- the remaining lateral faces of the model were restricted against horizontal displacement (i.e. 'x' and 'z' respectively) while the bottom part of the model was restricted in the vertical direction (i.e. 'y')
- the surface load was defined as a pressure applied over an area located directly over the joint, as illustrated in Figure J.37; a pressure was chosen to simulate a force of 50 kN (11,200 lbf) over an area of 0.15 m^2 (232.5 in^2), i.e. 333 kPa (48 psi) since that is the area of the pad used to apply the loads in the

experiments. While maximum surface load of 100 kN (22,400 lbf) was used in the tests, the observed response was linear and a smaller value of force was used for all the simulations and comparisons. The same boundary conditions were applied in all of the models not illustrated here.

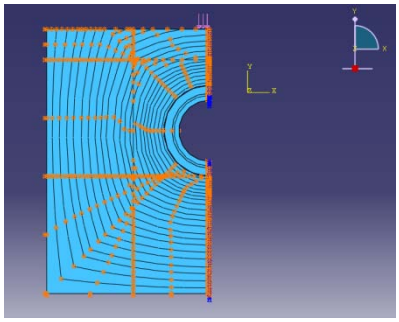

a. end view

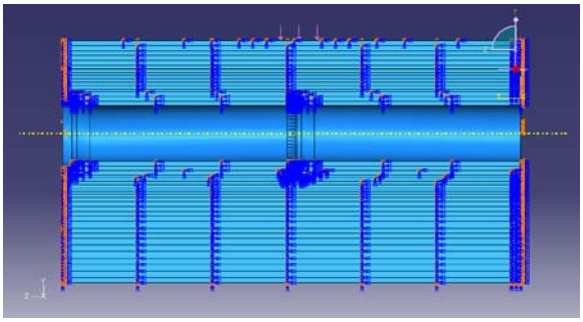

b. side view

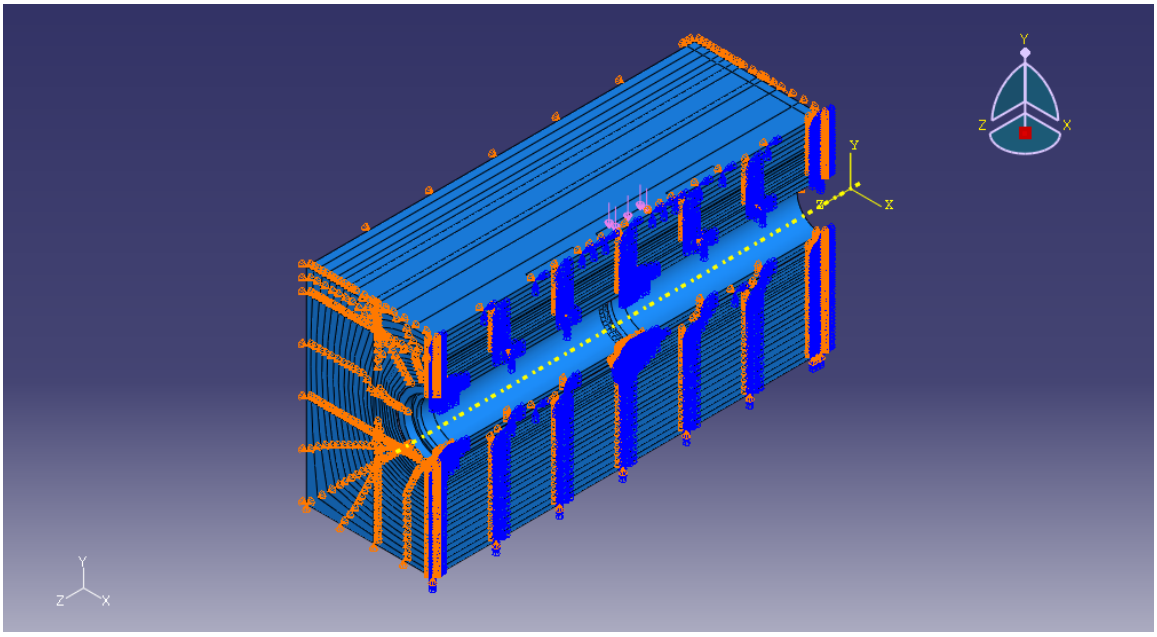

c. perspective view

Figure J.37 Boundary conditions used in the simulation of good burial conditions at 2 ft of cover

Mesh design

Due to the complexity of the geometry, tetrahedral elements were employed to discretize the model. These elements feature quadratic displacements to provide approximations better than those of the four node tetrahedral element (where displacement would be linear). These ten node elements are denoted the '*C3D10M: A 10-node modified quadratic tetrahedron*' in the ABAQUS library. As can be seen in the figures where the geometries were described, partitions were used in the models to induce a mesh pattern that provided finer results in the regions closer to the structure. Figure J.38 shows the discretization (mesh) for the good burial condition at 4 ft (1.2 m) of cover. The meshes employed for the remaining models were similar.

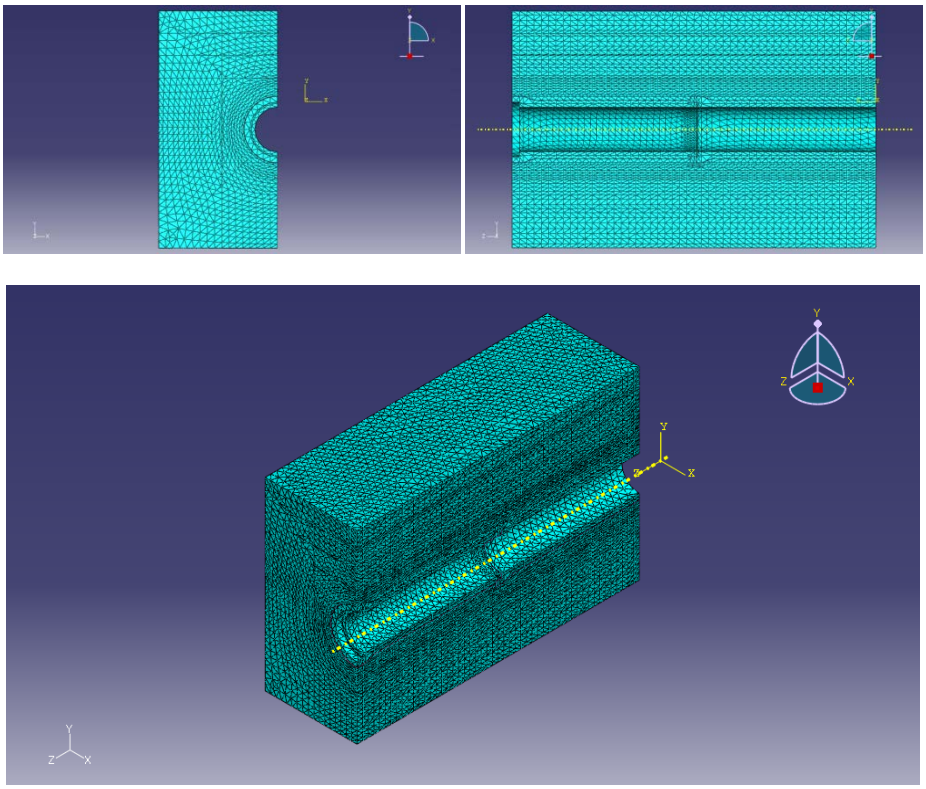

Figure J.38 Mesh used to simulate the good burial condition at 4 ft (1.2 m) of cover

Contours of stress and displacement

Figures J.39 through J.50 show contour plots for vertical displacement (in the *y* direction) and two normal stresses (σ_{xx} and σ_{yy}) in the pipeline for the four simulations performed. The units shown are *meters* for the displacements (1m = 39.4 in.) and *Pascals* for the stresses (1000 Pa = 0.14 psi). Strain results at particular locations are compared with experimental measurements in tables in the following subsection.

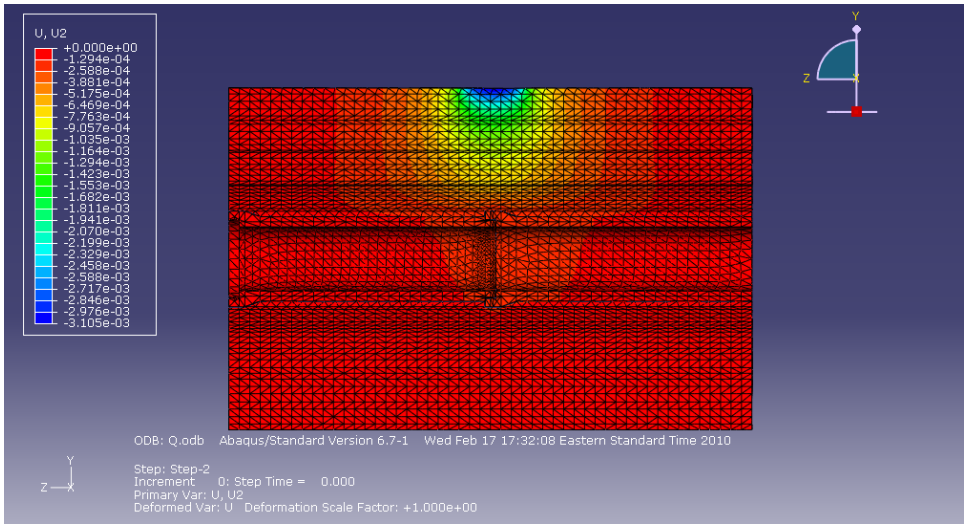

Figure J.39 Vertical displacement for the poor burial condition at 4 ft of cover (1m = 39.4 in.)

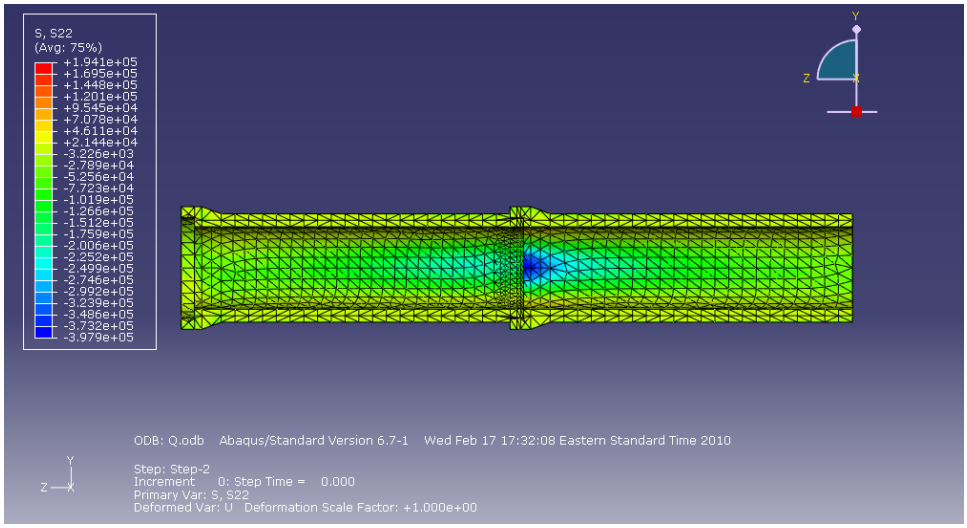

Figure J.40 Stress σ_{yy} for the poor burial condition at 4 ft of cover (1000 Pa = 0.14 psi)

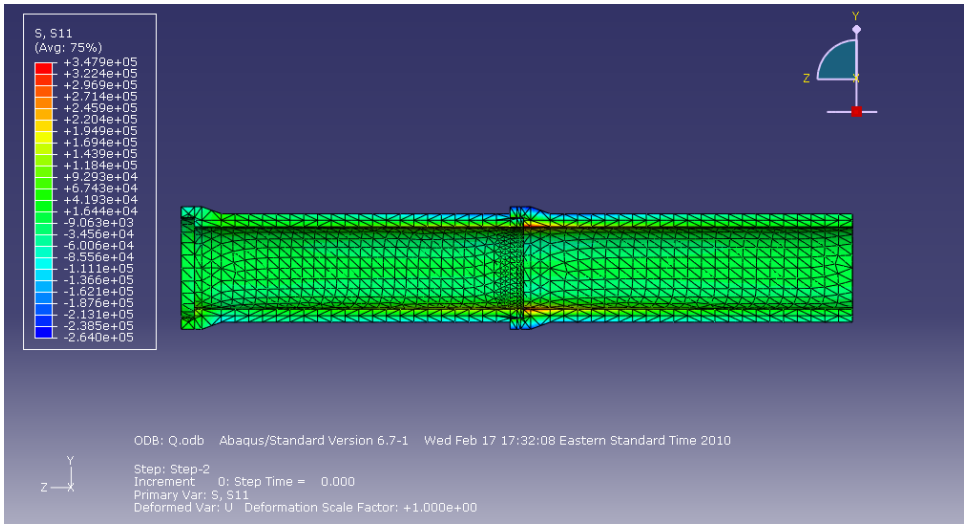

Figure J.41 Stress σ_{xx} for the poor burial condition at 4 ft of cover (1000 Pa = 0.14 psi)

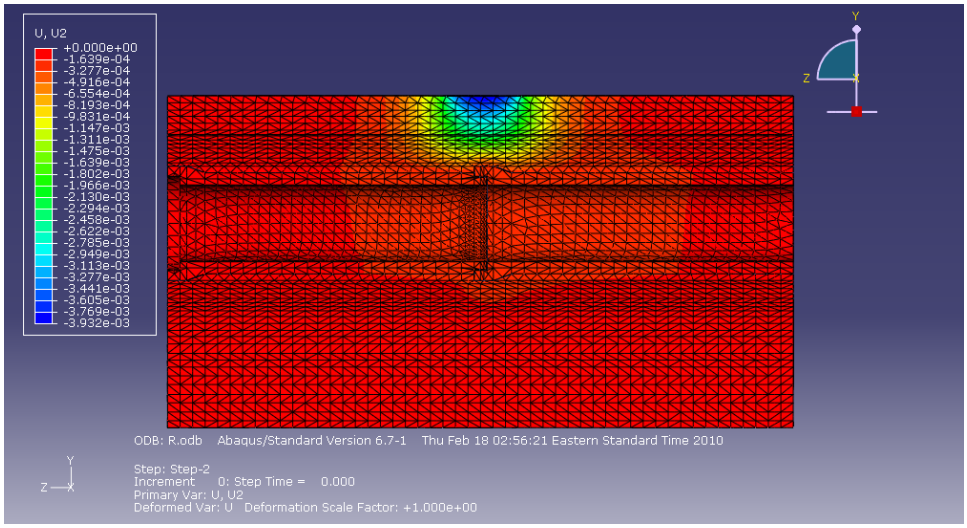

Figure J.42 Vertical displacement for the poor burial condition at 2 ft of cover (1m = 39.4 in.)

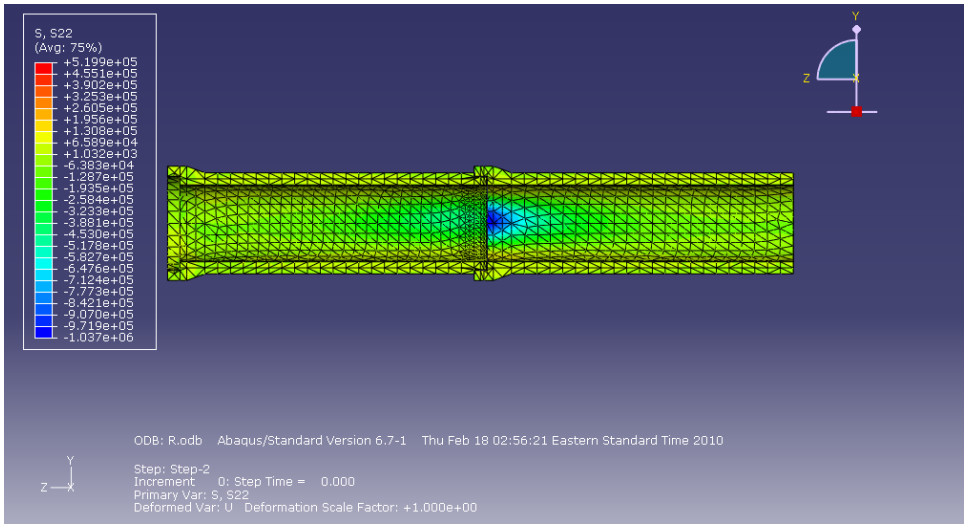

Figure J.43 Stress σ_{yy} for the poor burial condition at 2 ft of cover (1000 Pa = 0.14 psi)

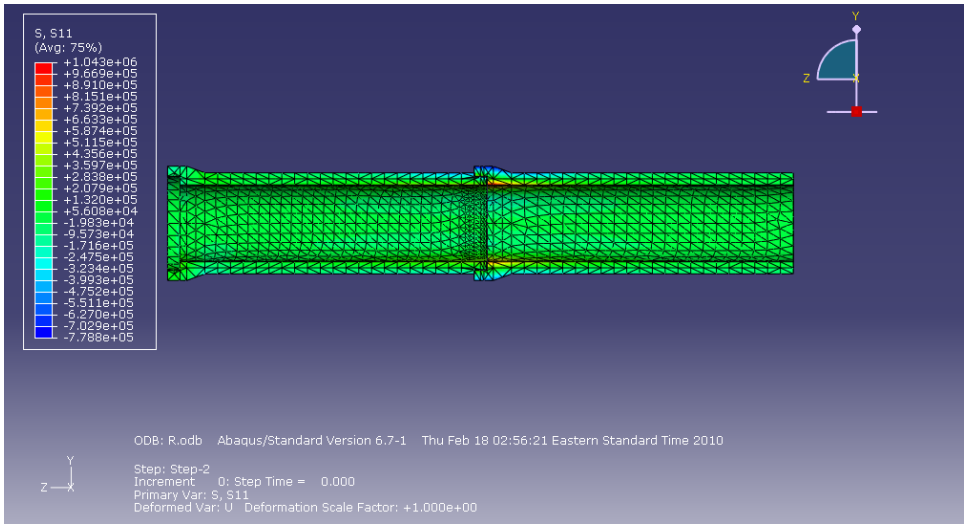

Figure J.44 Stress σ_{xx} for the poor burial condition at 2 ft of cover (1000 Pa = 0.14 psi)

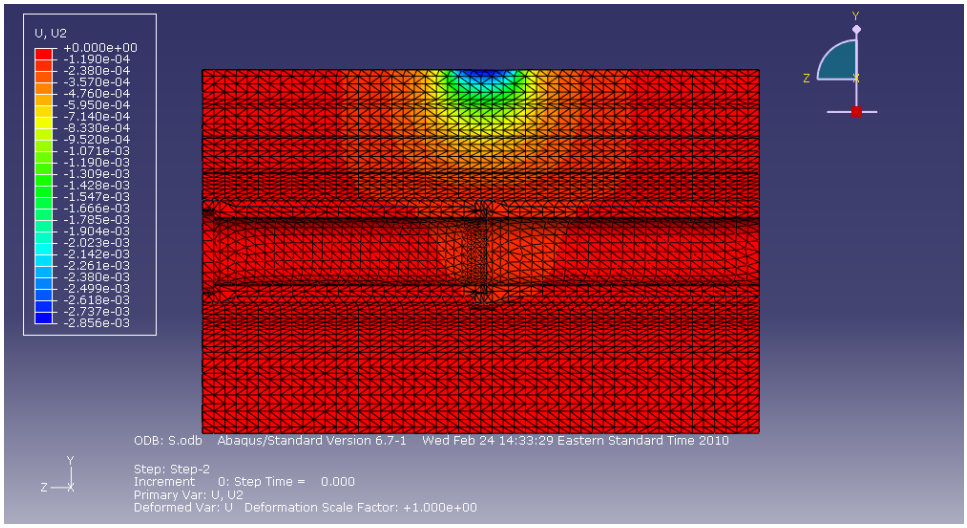

Figure J.45 Vertical displacement for the good burial condition at 2 ft of cover (1m = 39.4 in.)

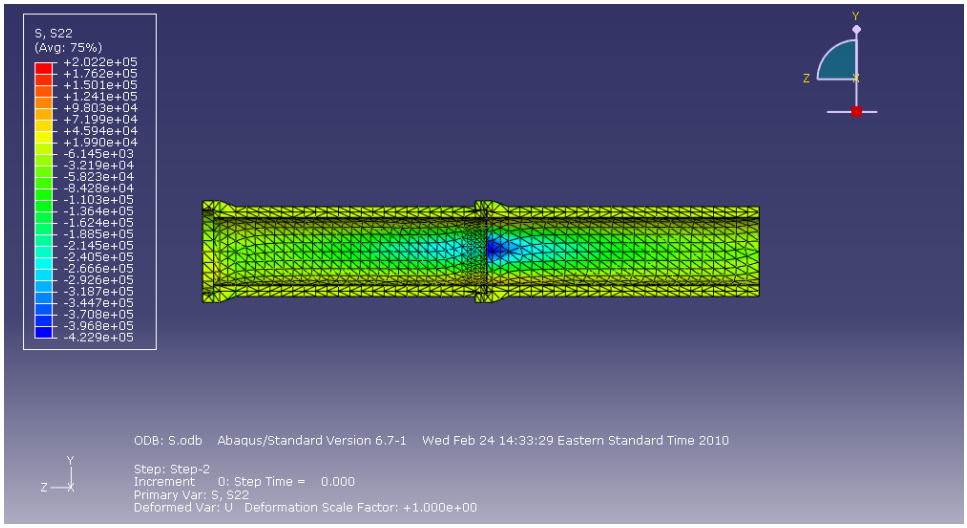

Figure J.46 Stress σ_{yy} for the good burial condition at 4 ft of cover (1000 Pa = 0.14 psi)

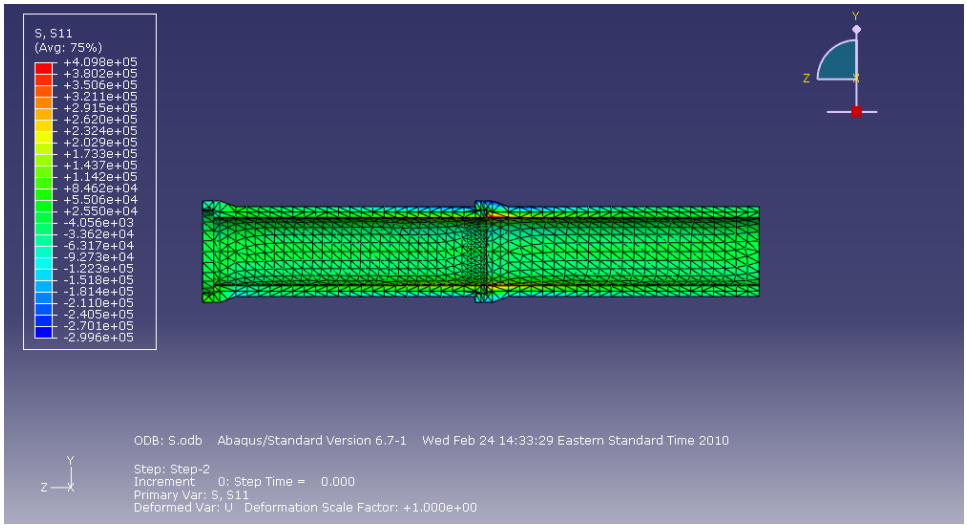

Figure J.47 Stress σ_{xx} for the good burial condition at 4 ft of cover (1000 Pa = 0.14 psi)

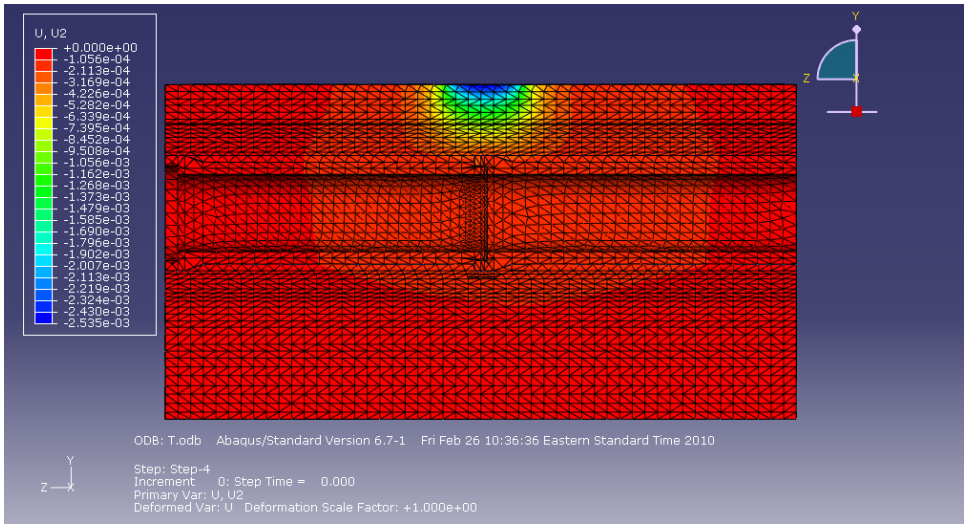

Figure J.48 Vertical displacement for the good burial condition at 2 ft of cover (1m = 39.4 in.)

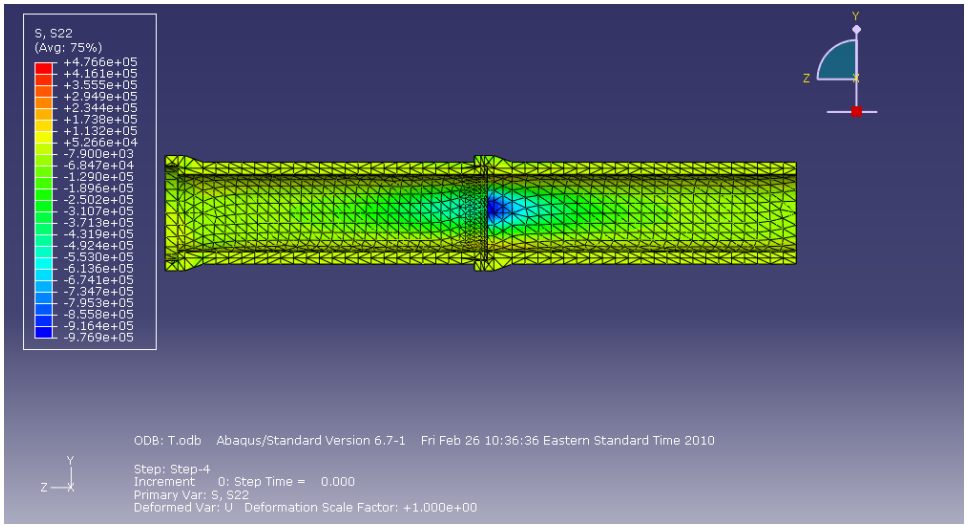

Figure J.49 Stress σ_{yy} for the good burial condition at 2 ft of cover (1000 Pa = 0.14 psi)

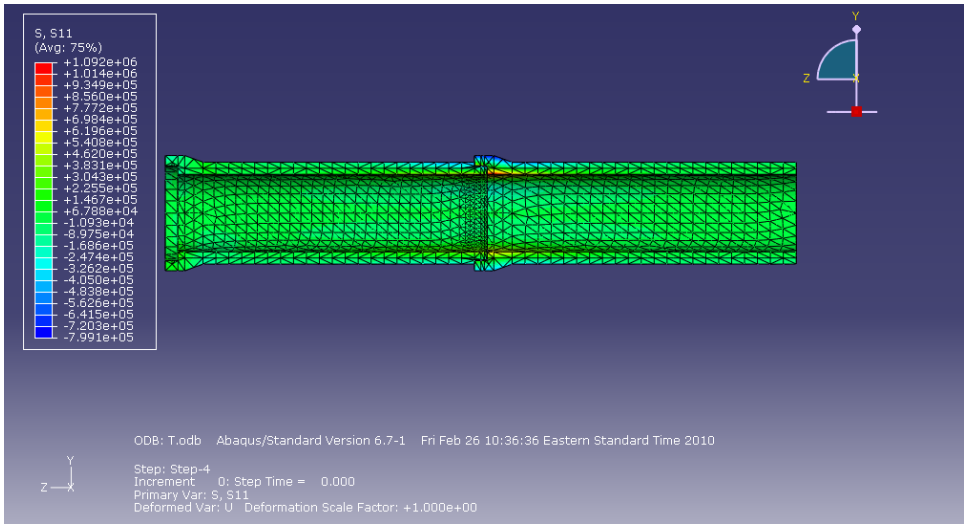

Figure J.50 Stress σ_{xx} for the good burial condition at 2 ft of cover (1000 Pa = 0.14 psi)

Comparison of analyses using "expected" soil moduli with experimental data

In this section, the calculated results are compared with experimental data to evaluate performance of the computer models. The test pipes were instrumented with electrical strain gages in regions of interest in the joint elements and in some locations through the barrels. These measurements of strain are shown in the following tables and compared with the strains calculated in the finite element simulations. Figure J.51 shows locations in the bell and in the spigot where measurements were taken and used in these comparisons.

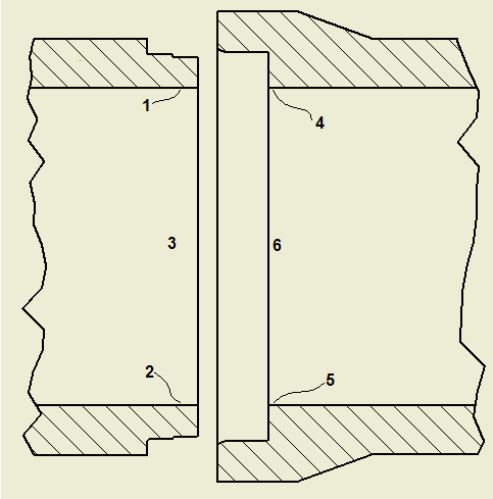

Figure J.51. Comparison points in the bell and spigot

Table J.15 Comparison of experimental results and calculations for the poor burial case at 4 ft

Point ID	Location/description	Experimental result με	Simulation result με
1	Spigot region, inside the pipe, Crown location, hoop direction	7	5
2	Spigot region, inside the pipe, Invert location, hoop direction	6	5
3	Spigot region, inside the pipe, Springline location, hoop direction	-4	-5
4	Bell region, inside the pipe, Crown location, hoop direction	12	11
5	Bell region, inside the pipe, Invert location, hoop direction	21	10
6	Bell region, inside the pipe, Springline location, hoop direction	-14	-13

Table J.16 Comparison of experimental results and calculations for the poor burial case at 2 ft

Point ID	Location/description	Experimental result με	Simulation result με
1	Spigot region, inside the pipe, Crown location, hoop direction	14	13
2	Spigot region, inside the pipe, Invert location, hoop direction	12	13
3	Spigot region, inside the pipe, Springline location, hoop direction	-12	-11
4	Bell region, inside the pipe, Crown location, hoop direction	38	34
5	Bell region, inside the pipe, Invert location, hoop direction	40	26
6	Bell region, inside the pipe, Springline location, hoop direction	-35	-34

Table J.17 Comparison of experimental results and calculations for the good burial case at 4 ft

Point ID	Location/description	Experimental result με	Simulation result με
1	Spigot region, inside the pipe, Crown location, hoop direction	7	7
2	Spigot region, inside the pipe, Invert location, hoop direction	3	6
3	Spigot region, inside the pipe, Springline location, hoop direction	-5	-7
4	Bell region, inside the pipe, Crown location, hoop direction	3	13
5	Bell region, inside the pipe, Invert location, hoop direction	4	10
6	Bell region, inside the pipe, Springline location, hoop direction	-10	-14

Table J.18 Comparison of experimental results and calculations for the good burial case at 2 ft

Point ID	Location/description	Experimental result με	Simulation result με
1	Spigot region, inside the pipe, Crown location, hoop direction	10	14
2	Spigot region, inside the pipe, Invert location, hoop direction	8	12
3	Spigot region, inside the pipe, Springline location, hoop direction	-8	-13
4	Bell region, inside the pipe, Crown location, hoop direction	13	36
5	Bell region, inside the pipe, Invert location, hoop direction	12	23
6	Bell region, inside the pipe, Springline location, hoop direction	-25	-32

Tables J.15 and J.16 providing results for the poor burial condition indicate that the simulations at both burial depths provide very effective estimates of the local strain values measured in the experiments; not only are the patterns of strain captured in the analysis, but most magnitudes of these strains were close. Only strains calculated at point 5 (circumferential strain on the inside of the bell at the invert) showed any significant difference; the sign at this location was correct, but the calculated strain 50-65% of the measured value; this is the location most likely to be influenced by the specific geometry where the bell rests directly on the compacted foundation; appears support in the tests was over a narrower zone of the circumference than what was assumed in the analysis (90 degrees). It appears that the modeling of the pipe, the bell-gasket-spigot interaction and the ground support associated with the poor burial case were all being represented very effectively.

Tables J.17 and J.18 provide results for the good burial condition. Again, the analysis largely captures the patterns of strain distribution observed in the tests. For this burial case, the magnitudes of strain at points 1, 2, 3 and 6 were close to those observed, while there was a greater discrepancy of strain magnitude for points 4 and 5 (where calculated strains were from two to three times the observed values). Points 4 and 5 are both on the inside of the pipe directly adjacent to the bell. It is clear that the analysis of the good burial case features soil support in the vicinity of the bell that is more severe than that experienced by the pipe. Perhaps when modeling the region of low stiffness soil under the bell, it should have extended further away from the bell under the invert. Alternatively the modulus in the tests was less than that modeled.

Table J.19 Vertical displacements in the joint at the crown

	4 ft poor burial
Bell– analysis	-0.15 mm
Spigot– analysis	-0.15 mm
Bell – test	-1.2 mm
Spigot – test	-1.3 mm
	2 ft poor burial
Bell – analysis	-0.27 mm
Spigot – analysis	-0.23 mm
Bell – test	-0.93 mm
Spigot – test	-1.1 mm
	4 ft good burial
Bell– analysis	-0.14 mm
Spigot– analysis	-0.13 mm
Bell – test	-0.37 mm
Spigot – test	-0.38 mm
	2 ft good burial
Bell– analysis	-0.21 mm
Spigot– analysis	-0.18 mm
Bell – test	-0.38 mm
Spigot – test	-0.39 mm

Table J.19 provides calculated values of vertical deflection in the bell and spigot of the central joint (at the pipe crown). These reveal that:

- movements observed for poor soil support were much higher than those calculated
- movements observed for good soil support were about double those calculated

If moduli used in the analysis were set to the design modulus values (about half the expected moduli), crown deformations for the case of good soil support would have doubled – giving much closer to the observed values. Deflection calculations for the poor burial condition need additional changes to the modeling to obtain effective calculations.

Analyses based on "design" moduli

Table J.20 demonstrates that the soil properties have only a modest effect on the strains calculated in the pipe. This is because for a rigid pipe, the pipe has high stiffness relative to the soil, for both sets of soil properties. The loads that develop on the outside of the pipe are then almost unaffected by modulus choice.

Table J.20 Influence of soil moduli ("expected" versus "design"; poor burial condition at 2 ft (0.6 m) cover

Point ID	Location/description	Experimental result με	Analysis – expected modulus με	Analysis – design modulus με
1	Spigot region, inside the pipe, Crown location, hoop direction	14	13	10
2	Spigot region, inside the pipe, Invert location, hoop direction	12	13	13
3	Spigot region, inside the pipe, Springline location, hoop direction	-12	-11	-9
4	Bell region, inside the pipe, Crown location, hoop direction	38	34	33
5	Bell region, inside the pipe, Invert location, hoop direction	40	26	26
6	Bell region, inside the pipe, Springline location, hoop direction	-35	-34	-33

Effect of gasket modulus

Table J.21 provides values of pipe strain calculated after changing the characteristics of the gasket (and thereby the resistance to rotation across the joint). Moduli for the 'harder' gasket case were three times more those for the case considered earlier. Moduli for the 'softer' gasket case were three times less those for the case considered earlier.

These results demonstrate that these changes in the gasket stiffness have no significant impact on calculated response. It appears that the resistance to rotation is low relative, and it remains so regardless of which of these choices are made. This implies that effort need not be expended characterizing the resistance to rotation, since provided that resistance is low, it has little impact on pipe strain (and therefore stress).

Table J.21 Strains at 4 ft of cover and poor burial

	Test 4 ft of Central joint με	**Simulation Central loading με**	**Harder Gasket με**	**Softer Gasket με**
S06-Cro-Ins-θ	7	5	5	5
S06-Sp1-Ins-θ	-4	-5	-5	-6
S06-Inv-Ins-θ	6	5	6	5
S06-Sp2-Ins-θ	N/A	-5	5	-6
S10-Cro-Ins-θ	12	11	11	11
S10-Sp1-Ins-θ	-14	-13	-13	-13
S10-Inv -Ins-θ	21	10	10	10
S10-Sp2-Ins-θ	-12	-13	-13	-13

Table J.22 Strains at 2 ft of cover and poor burial

	Test 2 ft of Central joint με	**Simulation Central loading με**	**Harder Gasket με**	**Softer Gasket με**
S06-Cro-Ins-θ	14	13	12	13
S06-Sp1-Ins-θ	-12	-11	-11	-12
S06-Inv-Ins-θ	12	13	14	12
S06-Sp2-Ins-θ	N/A	-11	-11	-12
S10-Cro-Ins-θ	38	34	34	34
S10-Sp1-Ins-θ	-35	-34	-35	-34
S10-Inv -Ins-θ	40	26	26	27
S10-Sp2-Ins-θ	-33	-34	-35	-34